Unravelling the roles of a small membrane protein in DNA-damage repair and tolerance in *Caulobacter crescentus*

By

Alejandro Carrion Sanabria

31/01/2023

A thesis submitted to the University of East Anglia, Norwich, for the Degree of Doctor of Philosophy

Abstract

Antibiotic resistance has become a major concern in public health in recent years. Bacteria harbour numerous mechanisms to bypass and resist antimicrobial compounds. DNA damage response in bacteria has been widely studied in species such as *Escherichia coli* but poorly investigated in other bacterial species. We aimed to study the DNA damage response in a different class of alphaproteobacteria with a distinct chromosome organisation and segregation pattern than *E. coli*. In this study, we report the discovery of a novel 37-amino-acid protein with an essential effect on maintaining cell fitness under DNA-damaging conditions in *C. crescentus*. CalP is a small amphipathic transmembrane protein with N_{out}-C_{in} topology that polymerises, generating a homooligomer in the inner cell membrane. Sensitivity assays confirmed the Δ*calP* deficient phenotype in antibiotic-treated cells such as mitomycin C (MMC), norfloxacin, ciprofloxacin, or MMS. Complementation analysis confirmed the restoration of the WT phenotype in MMC or norfloxacin-exposed cells. DNA damage-induced cells with MMC caused *calP* downregulation in Δ*recA*. In contrast, the *calP* expression in WT upregulated *calP* following the induction of DNA damage with MMC. Immunoblot assays showed that CalP production increased following cellular DNA damage with MMC, norfloxacin, or MMS. Nevertheless, despite MMC-induced DNA damage in the mutant cells, CalP production did not increase in Δ*recA*. Δ*calP* mutants were more permeable to MMC-TRC (MMC linked to the Texas Red Cadaverine fluorophore) than WT, suggesting that CalP may have an efflux pump-like function in the cell. Our results indicate that CalP could be involved in DNA damage tolerance/response in *C. crescentus*. However, elucidating the role and molecular mechanisms of CalP requires further investigation.

Table of contents

Index

List of figures

Appendix of figures

List of tables

Appendix of tables

List of abbreviations

Alternative end-joining (A-EJ)

Amino acids (aa)

Antimicrobial resistance (AMR)

Antimicrobial peptides (AMPs)

Autoinducers (AI)

Bacterial two-hybrid (BACTH)

Base excision repair (BER)

Base pair(s) (bp)

Benzo(a)pyrene diolepoxide (BPDE)

Caulobacter crescentus (*C. crescentus*)

Caulobacter little protein (CalP)

Catabolite activator protein (CAP)

Cell fractionation resuspension buffer (CFRB)

Cyclic AMP (cAMP)

Distilled water (dH_2O)

DNA adenine methylase (Dam)

DNA-damage response (DDR)

DNA damaging agents (DDAs)

DNA polymerase I (Pol I)

DNA polymerase II (Pol II)

DNA single-strand break (DSB)

DNA single-strand break repair (DSBR)

DNA single-strand gap (SSG)

DNA single-strand gap repair (SSGR)

Escherichia coli (*E. coli*)

Ethanol (EtOH)

Extracytoplasmic function sigma factors (σ^{ECF})

Global-genome mechanism (GG-NER)

High-performance liquid chromatography (HPLC)

Holliday junction (HJ)

Homologous recombination (DNA adenine methylase)

Hydroxyurea (HU)

Hydrogen peroxide (H_2O_2)

Hydroxyl radicals (OH)

Horizontal gene transfer (HGT)

Hour(s) (hr(s))

Interstrand crosslinks (ICLs)

Interstrand crosslink repair (ICLR)

Ionising radiation (IR)

Isopropyl β-d-1-thiogalactopyranoside (IPTG)

John Innes Centre (JIC)

Kanamycin resistant (Kan^R)

Kilodaltons (KDa)

Base pairs (bp)

lexA (locus for X-ray sensitivity A)

Luria Bertani (LB)

Mass photometry (MP)

Methanol (MeOH)

Methyl methanesulfonate (MMS)

Sub-inhibitory concentration (SIC)

Millisecond(s) (ms)

Minute(s) (min)

Mismatch repair (MMR)

Mitomycin A (MMA)

Mitomycin C (MMC)

Multidrug efflux pumps (MDEPs)

Mycobacterium smegmatis (*M. smegmatis*)

Non-coding RNAs (ncRNAs)

Non-homologous end joining (NHEJ)

Nucleotides (nt)

Nucleotide excision repair (BER)

Overnight (ON)

PafBC (proteasome accessory factor B and C)

Penicillin-binding proteins (PBPs)

Peptone-yeast extract (PYE)

Phosphate-buffered saline (PBS)

Polycyclic aromatic hydrocarbons (PAHs)

Pseudomonas aeruginosa (*P. aeruginosa*)

Pup-proteosome system (PPS)

Quinolones (QLs)

Quorum sensing (QS)

Reactive oxygen species (ROS)

Recombinase A (RecA)

Recombinational repair (RR)

Relative centrifuge force (RCF)

Ribonucleotide reductase class I (RNRs)

RNA polymerase (RNAP)

Room temperature (RT)

scrambled calP (*scr calP*)

Seconds (sec)

SidA (SOS-induced inhibitor of cell division A)

Signal recognition protein (SRP)

Single-stranded DNA (ssDNA)

Small membrane proteins (SMPs)

Small open reading frames (smORFs)

Small protein(s) (SPs)

Small transmembrane proteins (STPs)

smORF-encoded polypeptides (SEPs)

Sodium dodecyl sulphate (SDS)

Sodium dodecyl sulphate-polyacrylamide gel electrophoresis (SDS-PAGE)

Sodium hypochlorite (NaClO)

Superoxide anion (O_2^-)

Tandem mass spectrometry (MS/MS)

Tetracycline resistant (Tet^R)

Texas Red Cadaverine (TRC)

Toxin-antitoxin (TA)

Transcription-coupled NER (TC-NER)

Transcription start sites (TSS)

Translesion synthesis (TLS)

Transmembrane (TM) domain

Transposon mutagenesis (Tn5-seq)

Triethylamine (TEA)

Trifluoroacetic acid (TFA)

Ultraviolet radiation (UV)

Wild type (WT)

Chapter 1. General introduction

1.1 *Caulobacter crescentus*

1.1.1 Organism

Cells of the genus *Caulobacter* are elongated and curved with rounded ends, as described by A. T. Henrici and D. E. Johnson in 1935 [1]. However, J. Stove and R. Stanier in 1962 affirmed that some species of the genus also showed straight forms [2]. *Caulobacter* is a genus of strict aerobic unicellular free-living bacteria that live in diverse environments such as freshwater (rivers, ponds, wells, canals, tap water), seawater, soil, and even the intestinal tract of millipedes (an arthropod of the subphylum myriapod) [1, 2]. Bacteria of the genus *Caulobacter* are Gram-negative α-proteobacteria that, at each cell cycle can differentiate and divide symmetrically or asymmetrically, depending on the species [3]. Asymmetric *Caulobacter* divides into two different morphologies and physiologies: swarmer and stalk cells [2, 4]. Both cell types are vibrioid rod-shaped bacteria of similar size and shape [2, 5]. Swarmer cells have a single polar flagellum that is used for motility [2, 4]. Stalk cells are not motile and do not have a flagellum but an outgrowth extension of the cell, the stalk, which is continuous along the cytoplasm [2, 6, 7]. This appendix is composed of swelling at the distal part of the stalk, which secretes a substance called the holdfast that allows stalk cells to adhere to surfaces [2, 5]. *Caulobacter crescentus* (*C. crescentus* hereafter) is a fresh-water bacterium with asymmetric cell division. In *C. crescentus,* following the asymmetric cell division, stalk cells stay adhered to a surface and swarmer cells swim to disseminate the species. Swarmer cells are unable to replicate DNA and remain in the G1 phase with a single chromosome. At some point, swarmer cells transition to stalk cells, losing the flagellum and retracting the polar pili [4]. At the pole of the excised flagellum and pili, cells develop the stalk and initiate the conversion to the S phase to start DNA replication. DNA replication ends with the G2 phase and the segregation of the two copies of the chromosomes and separation of the two differentiated cells, the swarmer and the stalked, reinitiating the cycle [2, 4]. *C. crescentus* can be easily synchronised, enabling accurate temporal analysis of the cell cycle [4]. *C.*

crescentus is used as a model organism to study how it establishes and maintains cellular asymmetry, chromosome segregation, and cell division, because of its ease of being genetically manipulated [3]. Likewise, *Bacillus subtilis* has an asymmetric cell division under starving conditions that trigger the formation of a spore. Other bacteria such as *Escherichia coli* (*E. coli*), *Pseudomonas aeruginosa* (*P. aeruginosa*), *Listeria monocytogenes*, and *Shigella flexneri* which seem to have symmetric cell division, also have asymmetric poles on a closer view. α-proteobacteria species such as *Brucella abortus*, *Agrobacterium tumefaciens*, *Sinorhizobium meliloti*, or *Rickettsia prowazekii* share common features that were discovered in *C. crescentus* [8-14]. These bacterial species have implications in medical, biowarfare protection, and environmental applications. Therefore, the study of mechanisms related to cell division in *C. crescentus* can have broader importance and be used to identify new targets and design novel antimicrobial drugs [4]. Currently, the most common *C. crescentus* used in laboratory research is NA1000, derived from the strain CB15 [15]. Marks et al. (2010) [15] found differences between the two strains in growth rate, mucoidy, adhesion, sedimentation, phage susceptibility, and stationary phase due to 50 years of culturing in laboratories.

1.1.2 History

The first bacterium of the genus *Caulobacter* was described as early as 1905 by M. Jones [1]. However, the genus *Caulobacter* was not created until 1935 by Henrici and Johnson, who categorised previously unrecognised stalked bacteria [2]. They discovered these organisms by microscopy examination of submerged slides left in fresh water to allow stalked bacteria to settle onto the slide (slide culture technique) [3]. However, Henrici and Johnson failed to isolate species of this genus and maintained these bacteria along with other organisms in crude liquid cultures supplemented with lake water and cellulose or chitin [4, 5]. In 1950, Houwink and van Iterson found stalked bacteria in their electron microscopy samples, whose source was the water used to prepare slides [6]. Houwink further isolated various strains of stalked bacteria from the tap and canal water and was the first to study the structure of these bacteria by electron microscopy [7, 8]. Bowers isolated

stalked bacteria from wells and named it *Caulobacter vibroides* Henrici and Johnson [9]. In 1964, Poindexter isolated and characterised several species of *Caulobacter* from a wide variety of sources, such as freshwater environments, seawater, soil, and the intestinal tract of millipedes. He also reviewed previous investigations of the genus *Caulobacter* [5]. In 2001, *C. crescentus* was the first free-living α-class proteobacterium to be sequenced [10].

1.2 DNA damage

Maintaining genomic information is crucial for the viability of living organisms [11]. Multiple DNA sequence modifications are usual in living organisms and can alter genomic information if left unrepaired. Mutagenesis can act as an evolutionary force and generate cancer, ageing or apoptosis in eukaryotic cells [12]. Accumulated mutations can trigger apoptosis as a protective strategy to prevent transmitting defective genomes to offspring [13, 14].

1.2.1 Sources of DNA damage

Agents from various sources can cause DNA damage that is classified into two categories: endogenous and exogenous. Endogenous or exogenous agents can trigger chemical or physical alterations of the genuine DNA sequence [12]. Endogenous sources can occur because of errors produced during DNA replication by DNA polymerases that insert wrong nucleotides in nascent DNA chains [15]; or by chemical or physical agents, which are compounds produced as subproducts of cellular metabolisms, such as reactive oxygen species (ROS) [16-18] or reactive nitrogen species (RNS) [16]. Exogenous agents are those compounds generated naturally or synthetically from environmental, physical, or chemical nature, that cause harmful effects on DNA, such as antimicrobial agents [12].

1.2.2 Endogenous sources of DNA damage

1.2.2.1 Errors generated during replication

High-fidelity polymerases generally amplify the DNA of cells in the absence of severe DNA damage. The proofreading activity of DNA polymerases in all domains

of life sometimes overlooks DNA replication errors. Bacterial transcriptases generate mismatches every 15.5 rounds of replication, or in other words, every 59 million replicated bases [19]. High-fidelity DNA polymerases have effective proofreading systems (exonuclease activity) that minimise errors. Replication errors caused by DNA polymerases are the primary source of mutations in cells, ahead of any other source of mutations [20]. The ratio of base substitution, single base insertion, or deletion frequency without DNA mismatch repair or environmental stress ranges from 10^{-6} to 10^{-8} [21, 22]. Several low-fidelity polymerases replicate DNA in eukaryotic cells in (non-severe) DNA damage conditions [23]. In the presence of DNA damage, cells trigger the translesion synthesis (TLS) mechanism that activates error-prone low-fidelity DNA polymerases to bypass unrepairable DNA lesions [24-26]. TLS is the main source of point mutations in the cell [27]. Low-fidelity DNA polymerases have a higher error ratio per base than high-fidelity polymerases. Low-fidelity polymerases can contribute to inserting mistaken nucleotides during replication, especially during DNA damage conditions [11, 23]. Some low-fidelity DNA polymerases even lack proofreading activity (e.g., DnaE in *E. coli*), which can be a source of genetic diversity and promote evolution under stress conditions [20, 27].

Mutations can arise from DNA strand slippage, mis-insertions, strand misalignments (that create unpaired bases), or nucleotide misalignment at the polymerase active site [22]. Another event causing mutations is the addition of uracil, which causes alterations in the relative ribonucleotide triphosphate (rNTPs)-deoxyribonucleotide diphosphate (dNTPs) ratio [28-33]. Topoisomerases can cause permanent double-strand breaks (DSBs) after nicking DNA if they do not re-ligate each end of a duplex DNA during replication or transcription [34, 35]. Quinolones, a type of topoisomerase inhibitor, can prevent DNA re-joining originating DSBs in *E. coli* [36-42]. Furthermore, DNA adducts and other abnormal DNA configurations, such as mismatches, nicks, or abasic sites, can block the topoisomerase-DNA complex [43, 44].

1.2.2.1.1 Spontaneous base deamination

Base deamination, which consists of removing the exocyclic amine from nucleotides, is the most frequent source of mutation in human cells [12]. The loss of exocyclic amines of cytosine (C), adenine (A), guanine (G), and 5-methyl cytosine (5mC) converts them into uracil (U), hypoxanthine, xanthine, and thymine (T), respectively [12]. Single-stranded DNA (ssDNA) is more susceptible to undergoing base deamination processes. The frequency of base deamination increases during replication, transcription, or recombination when double-strand DNA separates into ssDNA [45-47]. Cytosine and 5-methyl cytosine are the two most frequent alterations, with 5-methyl cytosine approximately 3 to 4-fold more susceptible to going through this modification [48]. AID enzymes (activation-induced deaminases) use cytosine deamination to edit mRNA, immunoglobulin gene class switching, and immunoglobulin gene hypermutation [49, 50]. Additionally, cytosine deamination is an immune protective mechanism that deaminates viral cytosines in virus-infected cells to prevent the synthesis of new proviruses [49]. Other mutagenesis sources, such as UV radiation, sodium bisulphite, nitrous acid, and intercalating agents, can boost base deamination frequency in DNA [45, 51-53].

1.2.2.1.2 Abasic sites

Abasic or AP (apyrimidic/apurinic) sites form when DNA glycosylases spontaneously cleave the N-glycosyl bond joining the sugar-phosphates and nitrogenous bases of nucleotides [54]. Uracil-DNA glycosylases remove uracil when inserted into DNA [54]. High temperatures and elevated pH concentrations enhance the likelihood of undergoing abasic sites, which in human cells can occur around 10,000 daily and easily create single-strand gaps (SSGs) [46, 55-58]. Base-excision repair (BER) and TLS are known pathways to repair abasic sites [58].

1.2.2.1.3 Oxidative DNA damage

ROS arise in cells as by-products of the electron transport chain and as a consequence of catabolic oxidases, anabolic processes, and peroxisomal metabolism [59]. ROS are necessary at appropriate concentrations for cellular

functions such as redox signalling reactions or immune responses against pathogens [60-62]. Nonetheless, ROS become toxic when exceeding a certain threshold, causing about 100 distinct oxidative lesions and DNA alterations [63-68]. The most common ROS are superoxide anion (O_2^-), hydrogen peroxide (H_2O_2), and hydroxyl radical (OH). OH, is the most harmful ROS, capable of damaging DNA, proteins, and lipids [55, 69, 70]. Electrophilic OH radicals can react with nucleotides in three different ways (ordered from higher to lower frequency): (i) fusing to the base double bonds, (ii) removing hydrogen atoms from their methyl groups, and (iii) reacting with phosphate groups [71, 72]. ROS can also attack the DNA backbone, causing SSGs (approximately 2300 per cell per hour in mammalian cells) [73-75]. Lipid peroxidation (oxidation of lipids by electrophilic OH) also creates aldehyde molecules such as malondialdehyde and 4-hydroxynonenal, which can alter cytosine, adenine, and guanine to generate mutagenic adducts [76-78].

1.2.2.1.4 DNA methylation

S-adenosylmethionine (SAM), which is used by methyl transferases as a co-substrate to transfer methyl groups, generates strongly mutagenic nucleotide-methylated derivatives [12, 79]. A highly mutagenic product is the derivative O^6-methylguanine (and its related residues O^4-methylthymine and O^4-ethylthymine), produced 10 to 30 times per cell per day in mammalian cells [80-84]. Mammals create the DNA-synthesis inhibitor N3-methyladenine (medium-toxicity) 600 times per cell and day [80, 85, 86]. Finally, mammalian cells also generate (the low toxicity compound) N7-methylguanine 4000 times per cell per day [80, 87-89]. Methylated agents include choline, betaine, endogenous nitrosated bile salts, environmental compounds such as pollution or derivatives of N-nitroso molecules, and tobacco smoke [90, 91]. Two mechanisms repair the DNA damage in methylated nucleotides. The first mechanism consists of removing the injured DNA base by O^6-methylguanine DNA methyltransferase or via oxidation using an AlkB homolog of α-ketoglutarate-dependent dioxygenase. The second mechanism is the BER system, which eliminates the glycosidic bonds of methylated bases with DNA glycosylases [89, 92-95].

1.2.2.2 Exogenous sources of DNA damage

1.2.2.2.1 Exogenous physical agents

1.2.2.2.1.1 Ionising radiation

Ionising radiation (IR) is a highly energetic radiation comprised of X-rays, alpha, beta, gamma, and neutrons, categorised according to their direct or indirect effect and ionisation density (low or high linear energy transferred to matter) [12]. Rocks, soil, radon, cosmic radiation, or medical devices emit IR. IR can damage DNA directly or indirectly by converting surrounding water into OH by radiolysis or potentiating oxygen or ROS to generate other DNA-reactive free radicals [60, 96, 97]. Indirect lesions produced on DNA by IR are highly similar to DNA damage produced by ROS and entail approximately 65% of all IR-induced DNA damage [98]. IR also causes SSGs due to the formation of 3′-phosphate or 3′-phosphoglycolate, a characteristic lesion generated by IR [75, 99, 100]. IR also creates DSBs when multiple damages accumulate in both strands. The recombinational repair (RR) pathway repairs this type of lesion in the DNA [98, 101-103].

1.2.2.2.1.2 Ultraviolet radiation

Ultraviolet radiation (UV) is medium-intensity radiation situated between the wavelength of the ionising radiation spectra (<190 nm) and visible light (>320 nm). UV radiation is divided into three categories according to wavelength: UV-C (190–290 nm), UV-B (290–320 nm), and UV-A (320–400 nm). The UV-radiation absorption peak of DNA is at 260 nm, and absorption markedly decreases proportionally to the distance to the peak [104]. UV light affects DNA directly by absorbing energy and exciting DNA molecules, causing photochemical alteration, or indirectly by receiving energy from surrounding excited molecules (photosensitisers) [12]. The main consequence of UV radiation on DNA is the creation of covalent linkages between two adjacent pyrimidines. UV light generates two main photoproducts in bacterial and eukaryotic DNA: cyclobutane pyrimidine dimers and pyrimidine-pyrimidone (6–4) photoproducts ((6-4) PP), with two

adjacent pyrimidines covalently bound [104-107]. UV radiation also creates less frequent products such as dipurines and pyrimidine hydrates in eukaryotes [108-111]. In bacteria, the saturation of the 5,6 double bond of pyrimidines generates damaged bases such as thymine glycol and cytosin hydrate [107]. Mammalian cells undergo DNA protein crosslinking as an effect of UV radiation, and UV-A explicitly causes DNA strand breaks [60, 112]. UV-produced lesions are repaired by interstrand crosslink repair (ICLR), nucleotide excision repair (NER), a direct reversal of UV-damaged bases, recombinational repair (RR), or TLS pathways that repair DNA damage [57, 60, 113, 114]. Numerous repair mechanisms have evolved in bacteria to repair UV-induced damage. These mechanisms comprise the excision of the injured oligonucleotides (nucleotide excision repair, NER), the fixation of the damaged bases by photolyases (photoreactivation), the removal of the injured base by DNA glycosylase (base excision repair, BER), and the cutting of the DNA adjacent to the damage by endonucleases (UV damage endonuclease, UVDE) [107].

1.2.2.2.2 Exogenous chemical agents

1.2.2.2.2.1 Alkylating agents

Alkylating agents are compounds that interact with the oxygens of ring bases especially with their reactive nucleophilic nitrogens (mainly with N7 of guanine and N3 of adenine). Some frequent nucleotide modifications are N3, N^4, and O^2 in cytosine; N1, N^2, N3, N7 and O^6 in guanine; N3, O^2 and O^4 in thymine; and N1, N3, N^6 and N7 in adenine [60, 115, 116]. The mode of action of alkylating agents consists of inserting an alkyl group into the base via S_N1 or S_N2 mode. The S_N1 method is a substitution reaction performed through the first order of kinetics and uses a carbonium ion intermediate (although not all compounds of S_N1 use this intermediate) [117]. The S_N2 method acts through the second order of kinetics and creates less mutagenic and carcinogenic adducts than the S_N1 mode [118]. The most important alkylated agents are: O^4-methylthymine (O^4meT), O^6-methylguanine (O^6meG), N^1-methyladenine (1meA), N^3-methyladenine (3meA), N^3-methylcytosine (3meC), and N^7-methylguanine (7meG). Among these products, the

most cytotoxic and mutagenic derivatives are O^6-methylguanine (O^6meG) and N^3-methyladenine (3meA) [119]. Examples of alkylating agents are methyl methanesulfonate (MMS) (Fig. 1), ethyl methanesulfonate (EMS), N-methyl -N′–nitro-N-nitrosoguanidine (MNNG), and methylnitrosourea (MNU). These compounds are used in labs to induce mutagenesis and carcinogenesis [81, 120, 121]. Other examples of alkylating agents are tobacco smoke, chemotherapeutic agents, biomass processing, dietary components or sulphur, and nitrogen mustards used in wars (that combine S_N1 and S_N2 modes) [122, 123]. In many bacteria, such as *E. coli*, the BER, ICLR, direct damage reversal, and Ada response mechanisms repair alkylating-agent lesions in DNA [119, 121, 124].

1.2.2.2.2.2 Aromatic amines

The potentially carcinogenic P450 monooxygenase system converts aromatic amines into alkylating agents that alter the C8 carbon of guanine [117, 125]. The most common examples of aromatic amines are 2-aminofluorene (AF) and its acetylated derivative, N-acetyl-2-aminofluorene (AAF) [126]. Aminofluorenes cause C8-guanine lesions, leading to permanent substitutions and frameshift mutations [127-129]. C8-guanine shows two different conformations (internal and external) that can disturb the geometry of the DNA helix [126, 130, 131]. In humans, the NER system repairs DNA lesions provoked by alkylating aromatic amines [132]. Examples of compounds, including aromatic amines, are fuel, industrial dyes, coal, pesticides, or insecticides (ultimately banned because of their carcinogenic attributes) [126, 133, 134].

1.2.2.2.2.3 Polycyclic aromatic hydrocarbons

Polycyclic aromatic hydrocarbons (PAHs) are nonpolar and inert compounds made of carbon with two or more aromatic rings [135]. They are DNA intercalators and carcinogens in humans, first documented as early as 1775 and isolated from coal tar in 1982 [136-138]. Reactions such as nitrogen reduction, one electron oxidation, photo-oxidation, multiple ring oxidation, or the human P-450 system of the liver create PAH [137, 139-145]. Interaction of PAHs with intermediate molecules of P-450 generates benzo(a)pyrene diolepoxide (BPDE), which intercalates into DNA,

followed by the formation of adducts (upon the interaction of the C10 carbon of BPDE with the N_2 exocyclic position of guanine) [146, 147]. Examples of PAHs are pyrene, anthracene, naphthalene, dibenzo[a,l]pyrene, 1-nitropyrene, 1-hydroxypyrene, and benzo(a)pyrene [148]. Substances containing PAHs are fossil fuels, incomplete combustion of organic matter, tobacco smoke, or carbonised food [145, 149]. NER, BER, or TLS systems repair DNA damage caused by PAHs [150, 151].

1.2.2.2.2.4 Toxins

Toxins produced by microorganisms can be genotoxic and potentially carcinogenic to mammals [152]. Humans and animals can be intoxicated with toxins in vegetables, fruits, or dairy products, such as the liver carcinogenic aflatoxin B1 from *Aspergillus flavus* and *Aspergillus parasiticus* [120, 153]. The P-450 complex metabolises B1 in the liver and causes depurination upon converting B1 into the active form (B1-8,9-epoxide). B1-8,9-epoxide reacts with guanine N7 generating potential mutations and tumours [154, 155].

1.2.2.2.2.5 Environmental stresses

Some physical environmental factors can provoke DNA damage, such as oxidative stress, hypoxia, heat or cold in humans [156-160]. These factors can generate mutations in trinucleotide repeats, triggering neurogenerative disorders via the alt-non-homologous end joining (NHEJ) repair pathway [161, 162].

1.2.2.2.2.6 Cytotoxic agents

Cytotoxic agents are compounds that are toxic to cells, and many of them affect eukaryotic and bacterial cells [12]. Antibiotics are cytotoxic agents produced naturally in certain organisms as antimicrobials to defend themselves or generate a competitive advantage over other organisms in the environment [163]. Antibiotics, such as quinolones or tetracyclines, can be artificially synthesised or semi-synthesised, respectively (the tetracyclic core of *Streptomyces*-extracted tetracyclines can be artificially modified to potentiate their effect) [36, 164]. Two main types of antibiotics are categorised according to the effect generated in the

target cell: bacteriostatic or bactericidal [165]. Bacteriostatic agents prevent the growth of bacteria in a "frozen state," while bactericidal agents are those that kill bacteria [165-167]. Bactericidal antibiotics are supposed to be more potent at eliminating bacteria, whereas bacteriostatic antibiotics are usually less powerful and require the host immune system to phagocyte bacteria to eliminate them [167]. However, a given antibiotic can be bacteriostatic or bactericidal depending on its effectivity on killing bacteria, which depends on many factors such as concentration, temperature, phase, exposition time, growth medium, inoculum level, or incubation period [166, 168]. The degradation of the antibiotic is also an element to consider when measuring its effectiveness [169]. Likewise, categorising an antimicrobial as bacteriostatic or bactericidal is species-dependent and even strain-dependent [166]. The antibiotics listed below were used in various experiments for this project or other studies referred to in this manuscript.

1.2.2.2.2.6.1 Mitomycin C

Mitomycin C (MMC) is a natural antibiotic and antitumor compound produced by *Streptomyces caespitosus* that belongs to the mitomycins group [170, 171]. Bacterial flavoreductases convert MMC into a potent bifunctional DNA-alkylating agent [171]. The oxidation-reduction activation process generates ROS that can damage the cell. The converted MMC forms monoadducts and crosslinked monoadducts in complementary CpG sequences by N-alkylating guanine nucleosides at the 2-amino group of the base [171]. Thus, MMC causes SSGs and DSBs, leading to mutagenesis and inhibition of DNA synthesis in bacteria. Bacteria activate the SOS-dependent and SOS-independent systems in response to DNA lesions provoked by MMC [172, 173] (Fig. 1). MMC is widely used in lab assays to induce DNA damage conditions *in vivo* and *in vitro* [171]. MMC is commonly used as a chemotherapeutic agent to treat different types of cancer [174] and as a treatment for eye glaucoma [175].

1.2.2.2.2.6.2 Quinolones

Quinolones (QLs) are synthetic antimicrobials based on the 4-oxo-1,4-dihydroquinolone skeleton [36]. Their structure derives from the heterobicyclic

aromatic compound quinoline, whose name originates from the oily substance arising upon alkaline distillation of quinine [39]. Nalidixic acid (NA) belongs to the first generation of QLs, along with oxolinic acids. NA is effective against Gram-negative bacteria, and it used to be commonly employed to treat urinary tract infections [36, 39]. The clinical use of quinolones (e.g., nalidixic acid) in the European Union has been suspended because of serious side effects in patients [176]. Norfloxacin (Fig. 1) and ciprofloxacin are grouped in the second generation of QLs and include a fluorine atom at position six and cumbersome piperidine at position seven. This modification increases the efficiency of the antimicrobial activity against Gram-positive bacteria such as *Staphylococcus aureus* and some Gram-negative species such as *Pseudomonas spp.* [36]. The bacteriostatic or bactericidal action of ciprofloxacin is concentration-dependent in *E. coli* [168]. The clinical use of fluoroquinolones (e.g., norfloxacin or ciprofloxacin) has been restricted and is only allowed in certain cases of severe infections when no other alternatives are available [176]. QLs target the type IIA topoisomerases: DNA topoisomerase IV and DNA gyrase [36-38, 40-42]. DNA gyrase introduces negative supercoils into DNA by creating DSBs to pass one of the strands around the second strand to relax topological stress arising while transcribing or replicating DNA [36-38, 42]. This process is ATP hydrolysis-driven, and the absence of ATP reverses the mechanism, introducing gyrase-positive supercoiling [36, 37, 40, 42]. Topoisomerase IV decatenates DNA following replication and conducts a similar function to DNA gyrase by relaxing supercoiled DNA (although it cannot supercoil it, unlike gyrase) [177-182]. QLs function by trapping the DNA cleavage site of bacterial topoisomerases type IIA, inhibiting their action, and thus preventing them from re-joining broken DSBs [42, 180, 183]. Consequently, replication forks get blocked, as do replication and transcription, leading to bacteriostasis [36, 40]. Gyrase is the primary target of QLs in Gram-negative bacteria, while topoisomerase IV is the main target of QLs in Gram-positive bacteria [184-186].

1.2.2.2.2.6.3 Methyl methane sulphonate

Methyl methane sulphonate (MMS) is an alkylating DNA-damage inducer in bacterial cells (Fig. 1). MMS is a typical SN2-type alkylating agent that primarily

methylates nitrogen atoms in purines, causing mutations and stalling replication [124]. MMS causes replication blocks by mispairing bases and changing guanines to 7meG and adenine to 3-meA [187]. The BER system, oxidative DNA demethylation, and alkyltransferases often repair alkylating-agent-induced DNA damage [124, 188]. In *E. coli*, the oxidative methylase AlkB and the alkyltransferases OgT and Ada substitute alkyl groups with the original DNA bases [124].

1.2.2.2.2.6.4 Cisplatin

Cisplatin is a crosslinking alkylating DNA damage inducer based on platinum and is commonly used in cancer treatment [189]. Cisplatin mainly produces intra-strand crosslinks between consecutive adenines (~65%), adjacent adenines and guanines (~25%), and guanines separated by a base (~5-10%) [190]. It also generates inter-strand crosslinks in about 2% of cases. The intra-strand crosslinks (ICLs) produce adducts that block the progression of the DNA polymerase *in vitro* and *in vivo* [191]. The NER pathway repairs cisplatin-alkylated bases in *E. coli* [192].

1.2.2.2.2.6.5 Hydroxyurea

Hydroxyurea (HU) is an antineoplastic drug proven to inhibit ribonucleotide reductase class I (RNRs) in prokaryotes and eukaryotes *in vitr*o [193, 194] (Fig. 1). RNR inhibition can deplete dNTPs, causing replication fork arrest and replication inhibition that leads to DNA DSBs [195, 196]. RNR converts rNDPs into dNDPs by using a tyrosyl free radical [197]. HU can also be toxic to the cell via the non-RNR pathway [198].

1.2.2.2.2.6.6 Hydrogen peroxide

H_2O, OH, and O_2^- are ROS. The cellular respiratory chain produces ROS when single electrons interact with oxygen [199]. *E. coli* controls ROS homeostasis with the enzymes Ahp [200], KatE [18, 200, 201], superoxide dismutase [202], and glutathione [203]. In *C. crescentus*, the regulator OxyR controls the homeostasis of ROS, inducing transcription of genes *katG*, *ahpC*, and *ahpF* when the ROS concentrations are high [199]. ROS cause oxidative stress to DNA, inducing the

transcription of genes of the SOS response, such as *imuA*, which is also regulated by OxyR [199].

1.2.2.2.2.6.7 Novobiocin

Novobiocin targets the B protein of DNA gyrase and inhibits gyrase-catalysed DNA supercoiling *in vitro* [204]. More specifically, the drugs are competitive inhibitors of the ATPase reaction catalysed by GyrB [204]. Novobiocin has been described as cytotoxic against Gram-positive bacteria and effectively inhibits the DNA damage response [38, 205]. The toxic effect is less potent against Gram-negative bacteria because of a lower membrane permeability [38]. However, novobiocin was demonstrated to inhibit TLS, by preventing the potential acquisition of antimicrobial resistance (AMR) generated through DNA damage-induced mutagenesis [206].

1.2.2.2.2.6.8 Sodium hypochlorite

Sodium hypochlorite (NaClO) is a chlorine-based agent with a strong oxidising capacity [207]. In high electron density situations, the CI atom dissociates, combining with a pair of electrons and behaving as Cl^+, a potent electrophile [208]. NaClO attacks the electron-rich core of biomolecules like peptides, enzymes, lipids, or DNA through the one-electron transfer mechanism [209]. NaClO shows broad-spectrum antimicrobial activity and is an efficient disinfectant against biofilms and planktonic cells in Gram-positive [210] and Gram-negative bacteria [211].

1.2.2.2.2.6.9 Gentamicin

Gentamicin is an aminoglycoside (AG) antibiotic with a high affinity for the 30S and 50S bacterial ribosomal subunit, that leads to the inhibition of protein synthesis [212]. AGs have a bactericidal effect and are commonly used to treat infections of Gram-negative bacteria, some Gram-positive infections, and particularly, multidrug-resistant tuberculosis [212, 213]. It has been described that gentamicin inhibits swarming motility in *E. coli* by lowering the expression of the gene encoding for the succinate dehydrogenase enzyme [214]. Exposure to this class of antibiotics generates bacterial mechanisms of AG resistance. The most common

mechanism is the inactivation of the compound by AG-modifying enzymes, which makes it harmless or reduces its toxicity [213]. The ribosomal modification by methyltransferases is a mechanism that modifies the target of AGs, impeding the recognition of the targeted ribosomal structures and preventing their inhibition. The modification and overexpression of efflux pumps contribute to expelling AGs out of the cell. The modification of the cell membrane elements reduces the uptake of AGs into the cell because of a lower permeability and a change in electrochemical properties and polarity [213].

1.2.2.2.2.6.10 Tetracycline

Tetracyclines are broad-spectrum antibiotics effective against various gram-positive and gram-negative bacteria and some single-cell eukaryotic organisms [164]. Tetracycline belongs to the tetracycline family of antibiotics with a tetracyclic nucleus, from which the group's name derives [164]. The different derivatives of the family differentiate from each other, with distinct functional groups attached to the core [164]. Some family members are chemically synthesised, such as methacycline and doxycycline, and some are naturally synthesised by species of the genus *Streptomyces* [164]. *Streptomyces rimosus* and *Streptomyces aureofaciens* are the species from which oxytetracycline and chlorotetracycline were first extracted in the 1940s, respectively [164]. The tetracycline family of drugs prevents aminoacyl-tRNA from binding to the ribosomal acceptor (A), inhibiting protein synthesis [215, 216].

1.2.2.2.2.6.11 Spectinomycin

Spectinomycin is an aminoinositol drug that inhibits protein translation. Spectinomycin interacts with RpsE at the minor groove of helix-34 of the 16S ribosomal RNA blocking the amino acid elongation process [217, 218]. It has been shown that spectinomycin has a moderate effect on Gram-positive and Gram-negative bacteria in broad-spectrum infections. The most prevalent spectinomycin resistance mechanisms are target modification [219], enzymatic inactivation by nucleotidyltransferases [219-221], and native efflux pumps [222, 223].

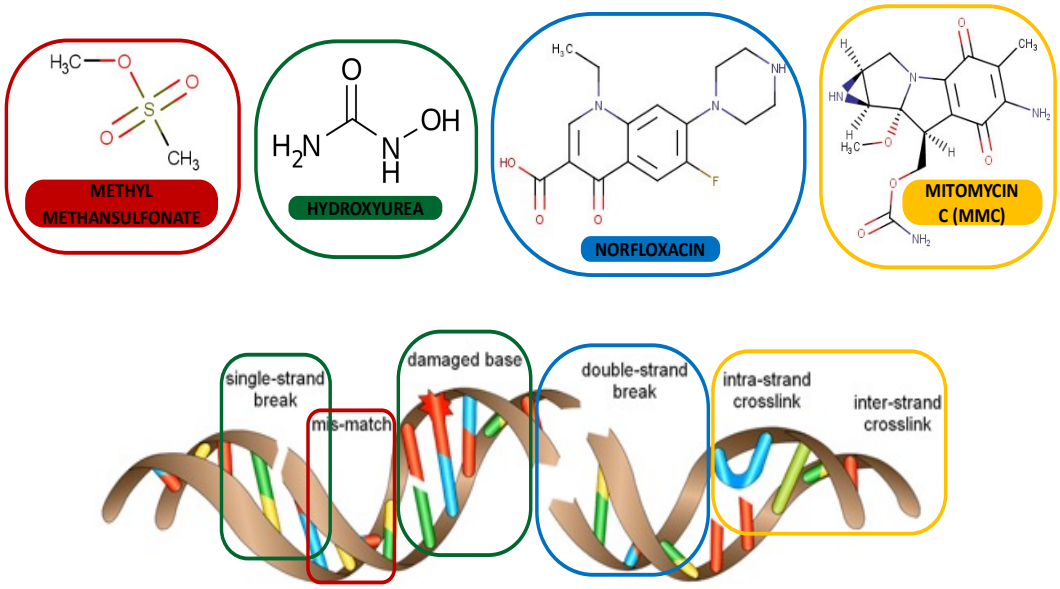

Fig. 1. Scheme shows different DNA damage types produced by various DNA-damaging agents. The colour of circles links the kind of compound with the type of damage they can provoke.

1.2.3 Types of DNA damage

1.2.3.1 Damaged base

DNA bases can be damaged in a wide variety of ways, from endogenous to exogenous sources, that alter and destabilise the nucleotide structure (Fig. 1). UV light [52], ROS [71], IR [75], or alkylating agents [115, 116] are among the most common damage-base inducers. Examples of damaged bases are the removal of the exocyclic amine of the nucleotide (spontaneous base deamination) [47, 51], loss of the nitrogen ring (abasic sites) [54], alterations at the C8 carbon of guanine (aromatic rings) [117, 125], or O^6-methylguanine (DNA methylation) [79, 81, 84]. NER and BER are DNA repair mechanisms to substitute damaged bases [224].

1.2.3.2 Mismatches

Nucleotide misincorporation or mismatches occur during DNA synthesis resulting in noncomplementary base pairs that must be corrected to prevent coping mutations in subsequent replication steps [225] (Fig. 1). Mismatch nucleotides in DNA can be caused by mistakes during the replication process that incorporate errors, recombination between heteroallelic parental DNA, and physical or chemical-damaging agents [226]. Repetitive sequences can provoke the formation of unusual secondary structures after aberrant DNA repair, causing mismatches. Another source of mismatches comes with the misincorporation of damaged bases [225]. Bacterial species such as *Pseudomonas spp.* (HexA), and *E. coli* (MutSLH complex) harbour mismatch repair mechanisms [227-229].

1.2.3.3 Intrastrand crosslinks

Intrastrand crosslinks are produced when a strand of DNA crosslinks with itself [230] (Fig. 1). Platinum drugs (carboplatin and cisplatin), widely used as antitumor treatments, create intrastrand crosslinks [230]. The adducts generated with these compounds are between purines at neighbour guanines (~54-65%), at 5'AG sequences (~17-19%), and GNG sequences in which the nucleotide in the middle can be any random nucleotide (<8%) [231]. ROS, such as the 5-(uracyl) methyl radical, can react with nearby adenines and guanines to create intrastrand crosslinks [232, 233]. UV radiation also causes intrastrand crosslinks [192]. Crosslinks, which

cause DSBs and SSGs, are repaired in *E. coli* by combining RecBCD and RecF repair pathways [234].

1.2.3.4 Interstrand crosslinks

Interstrand crosslinks (ICLs) are created when two complementary strands of DNA crosslink [230] (Fig. 1). ICLs are one of a cell's most deleterious DNA lesions. Repair-deficient bacteria can die because of only a single ICL; a mammalian cell would need approximately 40 ICLs to succumb. Indeed, the mode of action for most anticancer agents is ICL, which constitutes the most cytotoxic lesion for many drugs. Moreover, ICL can promote other types of mutations and DNA rearrangements. ICLs alter the DNA structure and provoke devastating effects in numerous cellular processes if left unrepaired, as DNA strands cannot separate to replicate or transcribe [230]. ICLs are repaired in *E. coli* and other bacteria by excision repair and RR pathways [235]. MMC is used as an anticancer treatment that generates ICL [192].

1.2.3.5 DNA single-strand gap

DNA single-strand gaps (SSGs), single-strand breaks, or daughter strand gaps are three terms to name a lesion in which one of the DNA strands is discontinuous [234] (Fig. 1). IR and UV light [74, 75, 99], ROS [63, 66], crosslinking agents [73, 236] and high temperature or extreme pH concentration [46, 55] cause abasic sites that lead to SSGs [58]. A pyrimidine dimer or abasic site that cannot be bypassed by the replisome can block it and ultimately cause SSGs. As the replication is discontinuous, other replisomes continue replicating the DNA strand beyond the lesion, rendering a gap from the stalled site to the newly synthesised DNA site [234]. The RecF system, or in minor cases, RecBCD repairs DSGs in bacteria [237].

1.2.3.6 DNA double-strand break

A DNA double-strand break (DSB) occurs when a gap in the DNA interrupts the continuity of the chain, creating a division with a length of a few base pairs [238] (Fig. 1). Different factors cause this type of DNA damage, such as DNA-damaging agents (DDAs) or replication past single-strand nicks [239]. The repair of DSB is

essential to preserve genomic integrity and prevent situations of fork collapse [240]. In bacteria, two main pathways for DSB repair are known: RR and NHEJ.

1.2.4 Types of DNA damage repair mechanisms

The preservation of genome integrity is important to perpetuate life, and only minor mutations contribute to genetic diversity and evolution [12]. Major changes usually lead to cell malfunction and cell death in bacteria. Unrepaired DNA damage is a very serious challenge to cells and can cause harmful mutations and produce cell death. Exogenous and endogenous DNA damaging agents represent a source of potential threats to genome integrity [241]. The recognition of the DNA damage occurs with an appropriate response triggered according to the class of lesion suffered by the DNA [242]. Following the recognition of the lesion, to repair the DNA and maintain genome integrity, organisms have developed diverse mechanisms to cope with DNA damage in an error-free and error-prone manner [241]. DNA repair, damage tolerance, cell cycle checkpoints, or cell death pathways are the resources that cells possess to combat DNA damage and prevent transmitting errors to the offspring [12].

1.2.4.1 DNA excision repair pathways

1.2.4.1.1 Base excision repair

Base excision repair (BER) is the most critical DNA repair pathway to fix single-base lesions in DNA [243, 244]. BER is found in all domains of life, highlighting its importance as a DNA damage repair mechanism [245]. BER fixes DNA damage such as alkylated bases, oxidative DNA base lesions, deaminated bases, UV-induced cyclopyrimidine dimers, or oxidised pyrimidines [124, 243]. DNA glycosylases recognise DNA damage initially and extract the damaged base by cleaving N-glycosidic bonds between the 2′-deoxyribose and the injured nucleotide [246]. Different glycosylases specialise in specific types of damaged bases and can recognise subtle differences compared to undamaged bases [246]. Two main groups of DNA glycosylases, monofunctional or bifunctional, are classified depending on the reaction mechanism [247]. Monofunctional glycosylases disrupt the anomeric

carbon of the injured base through an activated water molecule that generates an AP site and a free base [247]. The abasic site is cleaved by AP endonucleases or AP lyases, and a phosphodiesterase removes the aromatic ring-phosphate from the DNA chain [224, 248]. Eventually, DNA polymerase and DNA ligase add a new nucleotide and seal the strand [249]. Bifunctional DNA glycosylases incorporate lyase activity that cuts the DNA strand at the abasic site [246]. Bifunctional DNA glycosylase cleaves the damaged base's N-glycosidic bond, generating an abasic site [224, 243]. The lyase activity of the glycosylase through ß-elimination cuts the bond that links the backbone and the phosphate group, separating both molecules [224, 249]. The 3´unsaturated aldehyde abasic fragment is removed by the AP endonuclease, and DNA polymerases fill the gap left in the DNA strand [249].

1.2.4.1.1.1 Ada response

In *E. coli*, the Ada response system overcomes DNA damage generated by cytotoxic and mutagenic DNA alkylation. Ada is a regulon controlled by the Ada protein that regulates the expression of four genes, *ada, alkA, alkB, and aidB* [119, 121]. The methyltransferase Ada is involved in repairing O^6meG. The glycosylase AlkA repairs 3meA and initiates the BER pathway [250, 251]. The dioxygenase AlkB catalyses oxidative DNA demethylation to fix 1meA and 3meC lesions [252, 253]. Additionally, the constitutively expressed alkyltransferase Ogt, which has a similar function to Ada, repairs O^6meG and O^4meT and induces the Ada response [254-256]. The Ada response is a widely conserved mechanism across the bacterial domain, although the substrate specificity of specific proteins varies depending on species [119, 256]. The Ada response fixes alkylation damage induced by MMS. A deficient BER system and functional AlkB response induce the SOS response, increase the number of spontaneous mutations, and cause a growth-deficient phenotype [124, 257].

1.2.4.1.2 Nucleotide excision repair

The nucleotide excision repair (NER) system is present in all domains of life and can repair various types of DNA lesions [258]. NER divides into two distinct pathways, categorised according to the type of modification generated in the DNA

[259]. The first sub-pathway is the global-genome mechanism (GG-NER), which recognises significant alterations of the DNA that modify the structure and, in humans, are sensed by the XPC protein [260]. The second sub-pathway is RNA polymerase (RNAP) mediated, as the blockage of these enzymes triggers the second transcription-coupled NER (TC-NER) mechanism [261]. GG-NER is mainly active in inactive transcription sites, and TC-NER acts primarily in active transcription sites [262]. NER was first discovered in studies of UV-induced DNA lesions in bacteria [263-265]. Bacterial NER comprises four main proteins: UvrA, UvrB, UvrC, and UvrD [266]. Dimeric UvrA is a DNA-damage tracker that binds alone or in conjunction with UvrB to injured DNA and is ATP-driven [267-269]. UvrB binds to the UvrA-DNA complex by directly interacting with UvrA, and then UvrA dissociates from the complex [267]. UvrC, which possesses two nuclease domains, is recruited to the UvrB-DNA complex (directly binding UvrB) to cut damaged bases at each side of the lesion [265, 266]. Finally, UvrD helicase removes the damaged sequence and polymerase I fill the gap with new nucleotides [270]. In *E. coli*, one of the mechanisms to counteract the effect of DNA damage caused by cisplatin is NER [192]. NER mutants are highly sensitive to cisplatin, unlike WT cells [190]. Similarly, the RR mechanisms are equally important to overcome the DNA damage produced by cisplatin. Recombination-deficient mutants, with knockouts in *recA*, *recBCD*, *uvrABC,* or *priA*, show impairment in growth upon treatment with cisplatin [190].

1.2.4.1.3 Mismatch repair

Mismatch repair (MMR) primarily detects two types of DNA errors: single base mismatches and insertion or deletion events [60]. Certain mismatches, like G-T, naturally occur at a higher frequency than others, like C-C mismatches [271]. Consequently, mismatch-sensing proteins like MutS are adapted to detect frequent-occurring mismatches and overlook rare-occurring mismatches [272]. In bacteria, the mismatch repair mechanism can be either methyl-dependent or methyl-independent according to the organism [273, 274]. The best-well-studied bacterium for mismatch repair is *E. coli*, which harbours the methyl-dependent system, that is also present in other closely related bacteria [275]. This mechanism has two

principal proteins: DNA adenine methylase (Dam) and the hemi-methylation-specific endonuclease MutH [275]. MutH nicks unmethylated, newly synthesised DNA strands to rectify incorrect bases [273]. In most bacteria, the methyl-directed pathway (Dam and MutH) is absent [275]. However, it is replaced by other methylation-independent mismatch repair proteins, such as MutS in *B. subtilis*, or MutS and MutL in *C. crescentus* [276, 277]. DnaN, which forms a replication sliding clamp, recruits DNA repair proteins to the replisome [278, 279]. MutS, which has a DnaN binding motif, is recruited to the active transcription site to contribute to finding DNA mismatches [280]. Likewise, the endonuclease mismatch-specific protein EndoMS (or NucS) is an alternative to Dam and MutH in certain archaea and Actinobacteria, such as Mycobacterium [281, 282]. NucS, which possesses a mismatch-specific RecB-like nuclease domain, associates with DnaN to form a non-conventional mismatch repair complex [281-285].

1.2.4.2 Recombinational repair pathways

DNA damage repair by homologous recombination (HR) requires a previous preparatory process called pre-synapsis or pre-synaptic single-strand gap repair (SSGR). The pre-synapsis mechanism consists of the unwinding and degradation of the injured DNA to prepare the lesion for a later binding of RecA, that initiates the recombinational repair (RR) or HR repair. Following this presynaptic phase, the synaptic step consists of the alignment of the injured sequence with an intact homologous sequence. The third and final step, post-synapsis, is the resolution of the DNA junctions. The preliminary step differs depending on whether the lesion is an SSG or a DSB [234].

1.2.4.2.1 Pre-synaptic single-strand gap repair

1.2.4.2.1.1 RecF

E. coli repairs DNA SSGs with the RecF pathway. The study and characterisation of the RecF system have been mainly done in *E. coli* [234]. The RecA pathway involves several proteins: RecA, RecF, RecG, RecJ, RecN, RecO, RecQ, RecR, RuvA, RuvB, RuvC, single-strand DNA binding (SSB) proteins, UvrD, and HelD

[286-292]. RecF is widely conserved across bacteria, and so are its constituent elements [293]. The pre-synaptic repair process starts with RecQ or RecJ. Depending on the type of DSB end (5′-ssDNA overhang, 3′-ssDNA overhang, or blunt end), either the exonuclease RecJ or the helicase RecQ start the pre-synaptic DSB repair [294]. RecQ is a 3′ to 5′ helicase that initiates the pre-synaptic repair process before RR and participates in later recombination steps [295, 296]. The exonucleolytic degradation of ssDNA by RecJ requires interaction with SSB proteins [294]. RecJ degrades dsDNA (100-200 nt) from the strand terminating with a 5′-ssDNA overhang [297, 298]. The resultant 3′-ssDNA overhang (or a 3′-ssDNA overhang caused by the DSB) is unwound by the helicase RecQ, which can also unwind blunt ends [294, 299, 300]. Additionally, RecQ can decatenate DNA duplexes in conjunction with Topoisomerase III [296, 301]. Following DNA unwinding, the 5′-ssDNA strand is again available to be the substrate for the exonuclease activity of RecJ [294]. Although the function of RecN is unknown in *E. coli*, *B. subtilis* RecN is one of the first proteins to appear in the DSB end. It is thought that RecA promotes the re-joining of both strands by recruiting other repair proteins to the site of the lesion [302-304]. The SSB proteins bind the ssDNA generated by the action of RecJ and RecQ to protect it from nuclease degradation [237]. RecF, RecO, and RecR form the RecFOR complex to bind to the 5′-end of an ssDNA gap and load RecA onto SSB-coated ssDNA [305]. The combination of RecO and RecR is sufficient for the efficient loading of RecA into the SSB-ssDNA complex and expelling SSB proteins from the ssDNA [306, 307]. However, the presence of RecF increases the loading efficiency since RecF participates in SSB displacement [234]. RecA finishes the pre-synaptic process and initiates the RR of the SSG [234, 237]. The RuvABC complex is a Holliday junction (HJ) resolvase that acts at the RR process, catalysing migration, and cleavage of HJs [308, 309]. RecG is a multifunctional helicase that works during the RR as a DNA translocator at HJs and drives their branch migration, contributing to DNA repair [234, 310].

1.2.4.2.1.2 RecBCD

The RecBCD is a pre-synaptic system coupled to RR, mainly described for DSB repair (described below) [234, 237, 311]. Nevertheless, recent investigations

revealed that a *recB* deficient strain showed a decrease in SSG DNA repair. This deficient phenotype suggests the involvement of RecBCD in SSG repair (although to a much lesser extent than the RecF pathway) [312].

1.2.4.2.2 Pre-synaptic double-strand break repair

RR is, along with NHEJ, the mechanism to repair pre-synaptic double-strand break repair (DSB) in bacterial cells [313] (Fig. 2A). RR requires a homologous sequence that is used as a template for repairing the injured DNA sequences [239]. However, before the pre-synaptic stage [296], cells developed certain mechanisms to prepare DNA strands to be suitable for RR. In bacterial cells, this RR pre-processing event is performed by three multiunit enzymatic complexes: RecBCD, AddAB and AdnAB [239, 313].

1.2.4.2.2.1 RecBCD

RecBCD, present in *E. coli,* is the most well-studied and characterised member of the RecBCD and AddAB enzyme families [239, 313]. They differ primarily in the combination of nuclease and helicase activity used to resect DNA strands [239]. Bacterial genomic DNA contains preferred binding site sequences (Chi sites) to which RR enzymes bind to fix DNA lesions [314, 315]. The first step of RecBCD is binding to the end of the damaged fragment, followed by DNA unwinding [316] (Fig. 2B). RecBCD slides from the lesion towards the Chi site, powered by RecB in one strand (3′-5′direction) and RecD in the opposite strand (5′-3′direction) [317, 318] (Fig. 2BC). While moving towards the Chi site, the magnesium-dependent nuclease domain of RecB degrades both strands [319] (Fig. 2C). The translocation and degradation continue until the RecBCD complex reaches the Chi site in the 3′-terminated strand, which is recognised by RecC [320] (Fig. 2D). Once on the Chi site, RecBCD undergoes conformational changes and chews only the 5′-terminated strand, rendering a 3′overhang in the complementary strand [319] (Fig. 2E). The last common step for the three pathways of RR is the loading of the recombinase RecA to the Chi site, creating nucleoprotein filaments [321] (Fig. 2F). Following RecA loading, the RecBCD complex dissociates, and RecA starts the strand invasion of the intact homologous DNA sequence [322-324] (Figs. 4A4, A5).

1.2.4.2.2.2 AddAB

AddAB is a DSB repair complex found in *B. subtilis* like RecBCD. The overall mechanism of both complexes is very similar, although remarkable dissimilarities exist. The lack of a RecD helicase subunit homolog is the most striking difference between both systems [325]. The AddA subunit shares the same folding as RecB, but the AddB subunit differs from RecC in essential features. For example, in the amino-terminal helicase-like fold, AddB conserves more vestigial amino acids surrounding the nucleotide binding sites than RecC [239]. Furthermore, unlike RecC, AddB possesses an additional nuclease domain with a putative structural role in a 4Fe-4S iron-sulphur cluster. Hence, AddAB has two nucleases and one helicase, while RecBCD displays two helicases and one nuclease [326]. In contrast to RecBCD, which recognises the Chi binding site, the recognition motif of AddAB only detects 5 nt. However, AddAB is more stable than the RecBCD-Chi complexes [327].

1.2.4.2.2.3 AdnAB

Mycobacterium spp. harbours AdnAB, a member of the RecBCD/AddAB family [328]. Following a DSB and without ssDNA, AdnAB unwinds dsDNA from the DSB ends [329]. AdnAB is composed of two subunits that are, in turn, formed by two heterodimers, a nuclease and a helicase [330]. The helicase of each subunit unwinds both strands by hydrolysing ATP to translocate the AdnAB complex along the same 3′-5′strand, analogous to AddAB [330, 331]. The AdnB helicase is the major translocator of AdnAB and plays a more critical role in powering the complex along the 3′-5′ ssDNA [331]. The nuclease AdnB degrades ssDNA in 3′-5′direction, while AdnA is the lagged helicase, whose nuclease heterodimer degrades ssDNA in the opposite 5′-3′ strand [329, 332]. As opposed to AddAB and RecAB, no Chi site has been identified in AdnAB to assist in the polymerisation of RecA [332]. Functionally, AdnAB is more similar to AddAB than RecBCD [313]. However, the structural complexity of AdnAB is halfway through the evolution of repair mechanisms from simple helicases to more complex RecBCD systems [332].

1.2.4.2.2.4 RecF

Recombination was considered for many years dependent on the RecBCD pathway. The RecBCD pathway initiates following DSBs in biological processes such as phage crosses, conjugation, and transduction. Thus, the RecF pathway was thought to be a minor system [234, 237]. However, RecF is involved in all RR of ssDNA gaps, like the repair of strand gaps resulting from inefficient DNA replication from imperfect templates [234, 311]. The absence of RecBCD in certain bacteria or the inhibition of this system demonstrates that the RecF pathway, which has been mainly described for repairing SSGs, is also involved in DNA DSB repair [234, 312]. The capability of the exonuclease RecJ to resect dsDNA allows the RecF pathway to repair DSGs [295]. *E. coli* deficient RecBC, induced by *sbcC* and *sbcD* (suppressors of RecCD) mutations, repairs DNA DSBs via the RecF pathway [234, 333, 334]. Likewise, *Deinococcus radiodurans*, a highly radiation-resistant bacteria, repairs numerous DSBs with the RecF pathway, given the absence of RecBCD in this species [335-337].

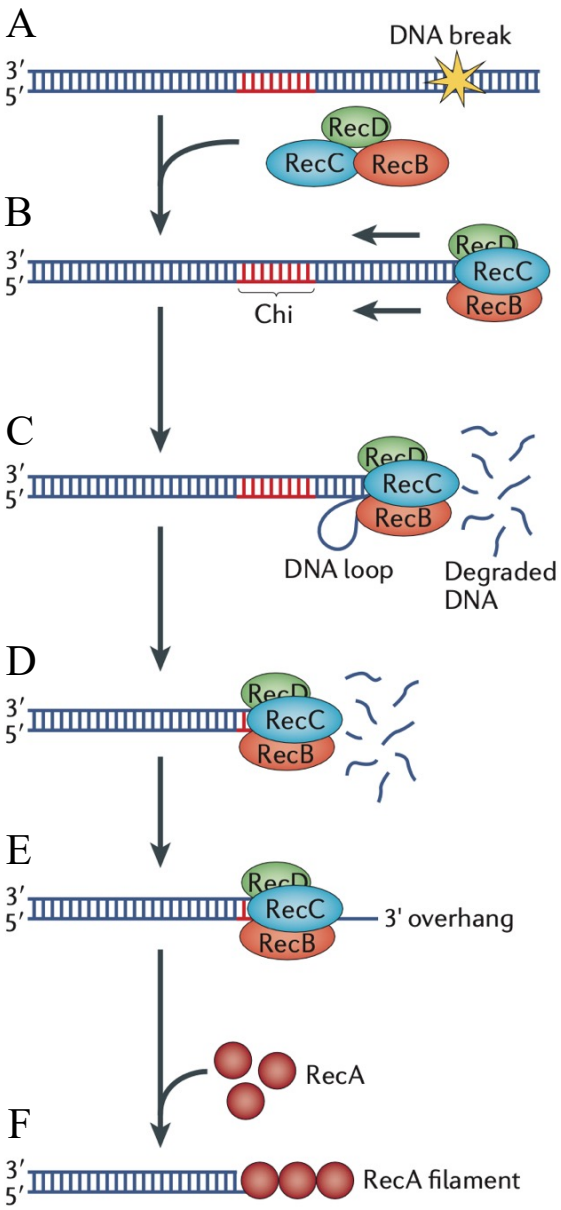

Fig. 2. Diagram of the RecBCD pathway. (A) DSB is caused by DNA damage. (B) RecBCD binding to the end of a duplex DNA upon DSB, unwinding, and translocation along the DNA duplex. The Chi sequence (red colour) is a stop signal for the RecBCD translocation. (C) RecB (3′ to 5′) and RecD (5′ to 3′) parallelly advance over complementary strands. RecB runs faster than RecD, resulting in a ssDNA loop ahead of the complex. The nuclease activity of RecB degrades both DNA strands, which is concomitant to the progress of the complex. (D) RecBCD stops and settles at the Chi site. (E) RecBCD undergoes conformational changes that accelerate the degradation of the 5′-end, leaving a 5′-end overhang. (F) RecBCD loads RecA to the 3′-overhanging DNA and dissociates [239].

1.2.4.2.3 Recombinational repair mechanism (synapsis)

A pre-synaptic preparation of damaged sequences precedes the RR synaptic repair. The repair process finishes when the RecF or RecBCD pathways load RecA into SSB-coated ssDNA to initiate the RR [234, 237, 305, 338]. Following RecA loading onto SSB-coated ssDNA by RecFOR or RecBCD, RecA forms a nucleoprotein filament to link the ssDNA to one of the strands of homologous dsDNA sequences [234, 305, 339]. The nucleoprotein filament is formed by the polymerisation of RecA monomers in a right-handed helix conformation around the DNA (with approximately six monomers per turn). This quaternary conformation allows the filament to acquire catalytic properties [321, 340]. RecA searches for dsDNA homologous to ssDNA through the nucleoprotein filaments [339]. The RecA-ssDNA twosome displaces one of the strands of the intact homologous sequence dsDNA and aligns with the other strand, creating a displacement loop (D-loop) [341, 342] (Fig. 4A4). The effectivity of the pairing relies on homology, with the possibility of reverting the pairing if homology is low [343, 344]. A DNA polymerase is recruited to extend the stable D-loop by using the complementary homologous DNA strand as a template and the ssDNA as an oligo [339]. The risk of D-loop disassembly remains feasible until no ssDNA is available, although this possibility lowers with each nucleotide synthesised, which increases sequence homology [345, 346].

The postsynaptic process is the resolution of the four-strand junctions, or HJs, formed due to the two exchanged DNA strands (Fig. 4A5). In *E. coli,* junction removal is catalysed by the RecG and RuvABC resolvasomes. RecG is a potent monomeric DNA helicase that regresses the three-strand HJs and dissociates to allow RuvABC to bind the fork [347]. The RuvABC enzymatic complex translocates four-strand HJs and cuts DNA strands symmetrically at suitable resolution sites. The damaged strand is then repaired after copying the sequence of another undamaged homologous dsDNA and the resolution of the four-strand junctions [234].

1.2.4.2.3.1 RecA

RecA is an ATP-dependent multifunctional protein with ss/dsDNA binding activity. RecA plays a crucial role in two central DNA damage repair and response pathways: the recombinational repair system (as described above) and the SOS response [338, 340]. For the RR mechanism, RecA is involved in three main functions: creating the nucleoprotein filament on ssDNA, searching homologous dsDNA to initiate homologous synaptic repair, and managing strand exchange activity by the invasion of the intact homologous dsDNA [321, 346, 348, 349] (Fig. 4A4). RecA is one of the crucial components of the SOS-dependent response [350] (and the SOS-independent response in some bacterial species [351]) (described below). RecA has two main functions in the SOS-response pathway. The first role is the co-protease activity to stimulate the autocleavage of the LexA repressor, which regulates the expression of diverse genes involved in the DNA damage repair system [352, 353]. The second function is the induction of translesion synthesis to bypass unrepairable DNA lesions by facilitating the DNA autocatalytic cleavage of UmuD, which stimulates DNA synthesis with polymerase V [24-26, 338].

RecA is a powerful ATPase with a catalytic rate constant (K_{at}) of ~30 min^{-1} if attached to a ssDNA or ~20 min^{-1} if bound to a dsDNA [354]. RecA hydrolyses ATP at least in three steps of presynaptic homologous recombination. The first occurs during the early stages of the homology search of the intact homologous dsDNA [341]. The second case of ATP hydrolysis is triggered to disassemble RecA from the nucleoprotein filament once strand invasion is accomplished [355]. Finally, the third ATP hydrolysis occurs when RecA bypasses non-homologous sequences during strand invasion [346, 356]. Before the action of RecA, the RecBCD complex hydrolyses ~3 ATP per bp/s and unwinds 930 bp/s of dsDNA in the presynaptic preparation before the recombinational repair [357, 358]. *E. coli* consumes an average of 0.8 million and 6.4 million ATP per second in the stationary phase and the exponential phase, respectively [359]. Another example of ATP hydrolysis in a DNA damage repair mechanism is the *Mycobacterium smegmatis* AdnAB, a helicase-nuclease complex that hydrolyses 5 ATP per bp unwound of at least 11.2 kilo bp of linear duplex DNA (the maximum unwound plasmid DNA tested in

Mihaela-Carmen Unciuleac and Stewart Shuman in 2010) [329]. A homologous DNA repair mechanism found in the *B. subtilis* AddAB helicase-nuclease hydrolyses two ATP per bp [360]. The superfamily 1 helicase only consumes one ATP per bp, being far more efficient than any of the mentioned helicases [361-363]. These cases show the variability of energy consumption among similar processes in different species of bacteria. These are only a few examples of an extensive network that bacteria display to address the vital aspect of DNA damage repair, whose energy cost is probably low in comparison to the high benefit of maintaining genome integrity. However, the energy cost greatly depends on factors such as the species, environment, growth phase, or nutrient availability [359].

1.2.4.3 Alternative repair pathways

1.2.4.3.1 Non-homologous end joining

Non-homologous end joining (NHEJ) is a DSB repair mechanism that mainly differentiates from RR because it does not need a DNA strand template to recombine to repair DNA damage [364]. NHEJ bypasses the limitation of requiring an intact DNA template that is only available in certain phases of the life cycle [364]. NHEJ is advantageous over RR because it is a more straightforward mechanism that can be performed at any time during the life cycle. Nevertheless, NHEJ has the drawback of being a low-fidelity repair system [239]. NHEJ processes DSB ends to make them suitable for subsequent ligation of both ends [239]. Although a standard model for the bacterial NDEJ system can be outlined, other accessory proteins participate in the mechanism and are species-dependent [364]. The model for the NHEJ system consists of a Ku dimer, which is recruited to the DSB lesion and attaches to the end of the chain [365] (Fig. 3A). Ku recruits and directly interacts with the ATP-dependent ligase LigD (or LigC, LigD2, or LigD4, depending on the bacterial species), probably via the polymerase domain of the holoenzyme (PolDom) [365] (Fig. 3A). LigD processes unligatable DSB ends with the PolDom, the nuclease domain (NucDom), or both, before the ligation process by the ligase domain (LigDom) [365] (Fig. 3A). NHEJ competes with RR for fixing DSBs during replicating phases in certain bacterial species, but not in all

of them. Following the deletion of two *ku* genes in *S. avermitilis* and *ku*, *ligC*, or *ligD* in *S. ambofaciens*, the RR system compensates for the lack of DSBR in NHEJ [366, 367]. In contrast, NHEJ and RR do not compete to repair dsDNA ends in *B. subtilis*, since the NHEJ mechanism inhibits RecJ and AddAB nucleases in germinating spores [322, 368]. NHEJ system is triggered in *S. meliloti* by the entry into the stationary phase and the exposition to thermic stress, which causes the upregulation of *ku* [369]. ~90% of α-proteobacteria species have at least one binding site for a type of sigma factor (σ) called extracytoplasmic function sigma factor G (σ^{ECFG}) in at least one *ku* gene, suggesting that σ^{ECF} often regulates the transcription of *ku* [370, 371]. Homolog and ortholog screening studies revealed that ~25% of prokaryotes encoded *ku*-like genes, suggesting a remarkable dissemination of the NHEJ mechanism [372]. More than ~70% of *Streptomyces* species encode more than one *ku* gene, and more than ~50% of α-proteobacteria, which encode at least one *ku* gene, harbour two or more genes [367, 372]. The NHEJ system is widely present in plasmids and bacteriophages, suggesting their incorporation through horizontal gene transfer (HGT) [364]. This, together with the fact that NHEJ can link unrelated non-homologous DNA ends, potentiates genomic diversity [373]. *ku* and *ligD* are essential for logarithmic growth in *Mycobacteria spp.* or *S. meliloti* to repair linearised plasmids after transformation [369, 374-376]. Likewise, *ligD* and *ku are* necessary for circularising mycobacteriophages Omega and Corndog to infect *M. smegmatis* [377].

1.2.4.3.2 Alternative end-joining

Alternative end-joining (A-EJ) is an alternative non-templated mechanism for repairing DSBs discovered in pathogenic *E. coli* [373]. *E. coli* is an NHEJ-free bacterium that lacks Ku and LigD proteins and has even been used as a negative control in NHEJ experiments with other bacteria [378, 379]. The A-EJ repair pathway relies on the use of the nuclease/helicase RecBCD complex to detect DSBs and degrade the ends of two strands [373] (Fig. 3B). Ligase A (LigA), an enzyme involved in the ligation of Okazaki fragments for joining DNA breaks, links both DNA ends in the microhomology regions (1-9 nt) [373] (Fig. 3B). The microhomology between both strands is essential for their synapsis and is strongly

dependent on the stickiness of their ends [373]. Therefore, A-EJ is likely a mechanism specific for DSBs in sequences with high homology with compatible ends [373]. The process is finished with an uncommon DNA synthesis event [373] (Fig. 3B). A-EJ in pathogenic bacteria shows a high-fidelity repair pathway rather than other common repair mechanisms involving microdeletions or more extensive deletion processes [373]. The fidelity rate is species-dependent and is determined by the short- or long-range exonuclease activity [373]. *E. coli* can incorporate unrelated exogenous non-homologous DNA sequences via A-EJ [373]. Similar to NHEJ, A-EJ can contribute to bacterial HGT and promote gene evolution in bacteria to acquire new traits for adapting to changing environmental conditions [373].

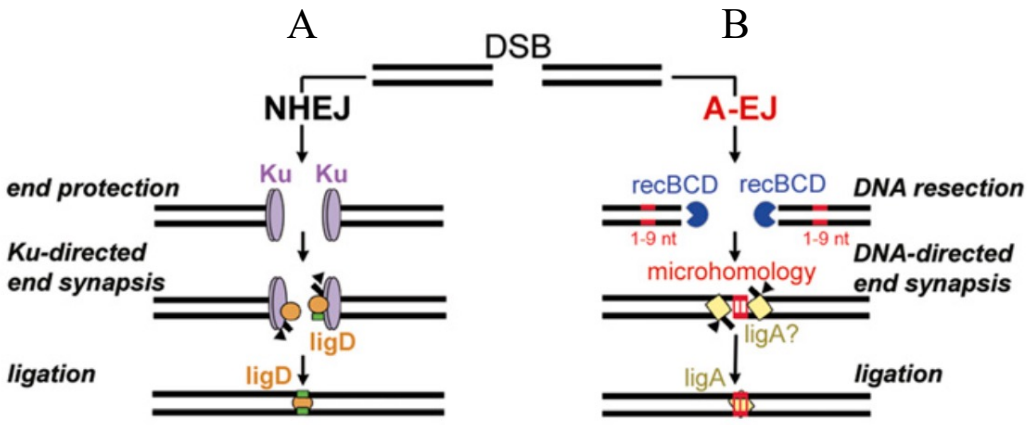

Fig. 3. Diagram of the putative model of A-EJ. (A) The Ku (ellipse) homodimer protects DSB ends and recruits LigD for processing and ligation of duplex DNA for synapsis in the NHEJ pathway. (B) In A-EJ, the helicase/nuclease RecBCD complex (dark-blue incomplete circle) degrades overhanging or blunt-end sequences that pair by microhomology (red square in the middle of DNA sequences). LigA (yellow rhombus) seals the ends completing the synapsis [373].

1.2.4.3.3 Interstrand crosslink repair

1.2.4.3.3.1 RecA-dependent interstrand crosslink repair pathway

The interstrand crosslink repair (ICLR) pathway in *E. coli* is the best-characterised ICLR system in bacteria. It implies the conjunction of the NER and RR pathways working together to remove a crosslinked DNA lesion [235, 380] (Fig. 4A). After the introduction of an ICL (Fig. 4A1), the NER enzymes UvrABC cut one of the strands at both sides of the lesion, at the ninth phosphodiester bond 5′ and the third bond 3′ to the ICL [235] (Fig. 4A2). The 5′-exonuclease activity of DNA polymerase I (Pol I) excises nucleotides from the 3′ side of the ICL to create a gap [381, 382] (Fig. 4A3). This gap creates a ssDNA that RecA needs to form a nucleoprotein filament and ultimately perform RR [348, 381] (Fig. 4A4). The RecA nucleoprotein binds to the damaged strand with the ICL oligonucleotide (the injured fragment of DNA cut at both sides to be excised). The RecA-ssDNA twosome starts the strand invasion by exchanging the injured strand with the intact homologous ssDNA duplex and displacing the complementary intact ssDNA [383] (Fig. 4A4). The resolution of the resulting HJ separates dsDNA [384, 385] (Fig. 4A5). Two more incisions of UvrABC at each side of the crosslinked oligonucleotide remove the complementary damaged strand of the ICL dsDNA [381, 383, 386] (Fig. 4A5). DNA Pol I fill the gaps of the ssDNA, and ligase seals the gaps between nucleotides [381] (Fig. 4A6).

1.2.4.3.3.2 RecA-independent ICL repair pathway

RecA-deficient strains possess an alternative system to repair the ICL that employs NER and DNA polymerase II (Pol II) [387] (Fig. 4B). After a DNA ICL (Fig. 4B1), UvrABC starts cutting one of the DNA strands like in the ICLR RecA-dependent pathway [381, 386] (Fig. 4B2). However, since the RR system is absent in this independent ICLR, RecA does not participate. Pol II synthesises bases directly along the gap left by the oligonucleotide (Fig. 4B3). The damaged oligonucleotide moves apart, and UvrABC cuts it to remove it completely [387] (Fig. 4B4). Finally, Pol II finishes synthesising complementary bases on the homologous non-crosslinked template, and ligase sealing the gaps [381, 386] (Fig. 4B5).

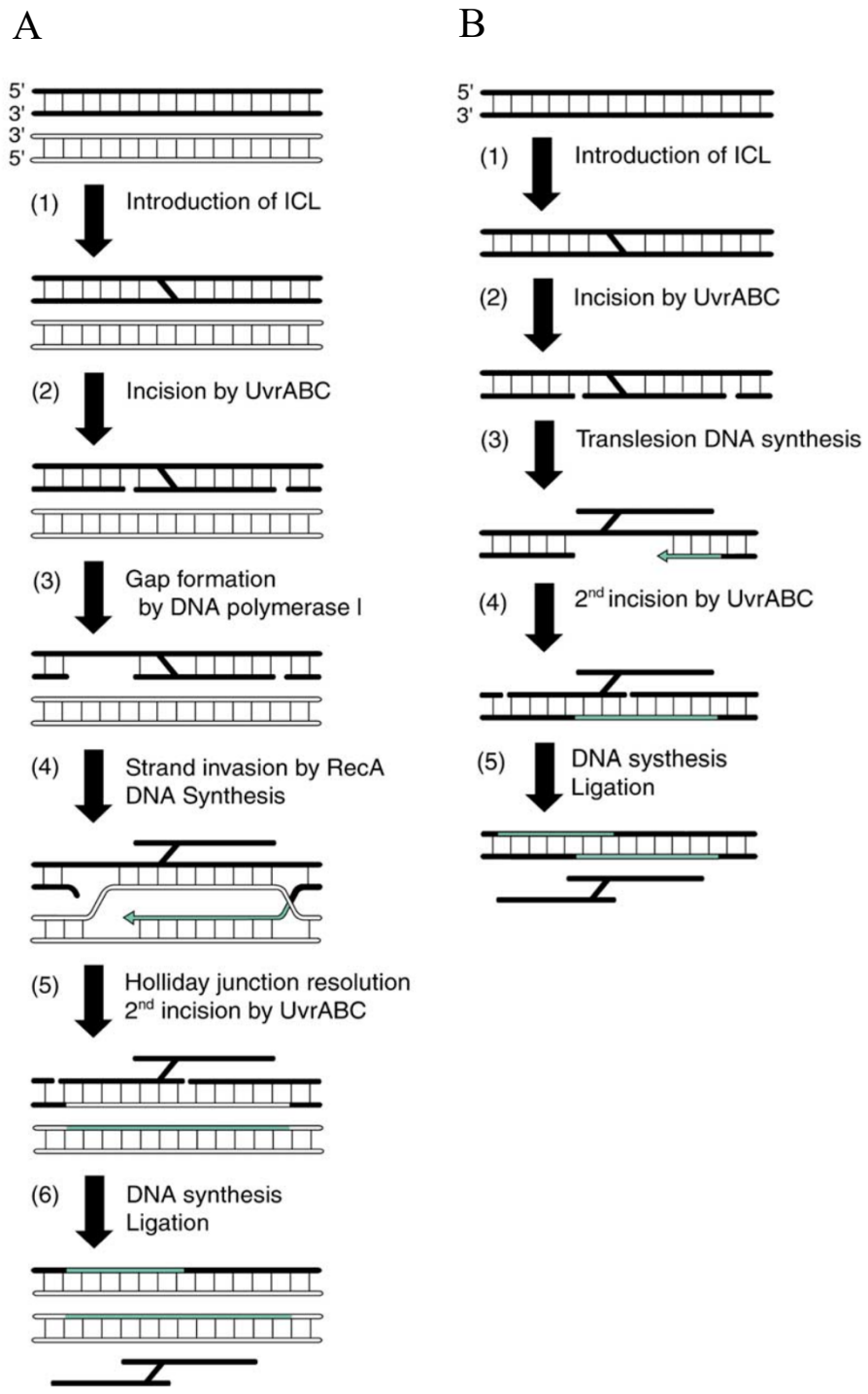

Fig. 4. Diagram illustrating ICLR and alternative ICLR in RecA deficient strains. (A) The black and white DNA duplexes represent homologous DNA sequences, and the vertical lines represent nucleotide pairing. *De novo* synthesised DNA is represented in green. The ICL is represented by the black diagonal line. (A) RecA-dependent ICL system via recombinational repair. (A1) ICL is generated in the

DNA. (A2) The endonuclease UvrABC cleaves DNA on both sides of an ICL. (A3) The exonuclease activity of Pol I produces an ssDNA gap on the 3′-end of the ICL that allows RecA to polymerise on the ssDNA, forming a nucleoprotein filament. (A4) The RecA-ssDNA twosome invades an intact homologous dsDNA (to the damaged sequence) and starts strand invasion, followed by DNA synthesis. (A5) The HJs formed during the strand invasion are resolved by specialised helicases. The ICL-damaged strand is cut at both sides by UvrABC. (A6) Pol I fills the gap between the newly synthesised DNA and the non-damaged DNA ends (eventually ligated), removing the crosslinked damaged sequence. (B) RecA-independent ICLR system via NER and TLS. (B1) Insertion of an ICL within DNA bases. (B2) The NER endonuclease UvrABC cleaves at both sides of an ICL. (B3) Pol II synthesise DNA in a TLS-induced response. (B4) UvrABC cuts at both sides of the ICL damage on the complementary ssDNA. (B5) Pol I fills the gap between the newly synthesised DNA and the non-damaged DNA ends (eventually ligated), removing the crosslinked damaged sequence [172].

1.2.4.3.4 Translesion synthesis

NER and RR pathways could fail to repair DNA under severe DNA damage or during life cycle stages without homologue sequences (RR) [339, 388, 389]. Many bacteria harbour an alternative backup mechanism to bypass the replication blockage caused by unrepairable DNA damage [234]. Translesion synthesis (TLS) is an error-prone system that uses specialised low-fidelity polymerases to synthesise bases at the site of the lesion. This mechanism is the primary source of point mutations and promotes genetic diversity [24]. TLS is a repair system widely distributed across all domains of life. In higher eukaryotes, the DNA polymerases REV1, POL ζ, POL η, POL κ and POL ι are part of the TLS, bypassing DNA damage to continue the replication. These error-prone polymerases could insert incorrect bases that, if uncorrected, persist in the genome [12]. TLS is present in many bacteria under the regulation of the SOS response, which induces the expression of error-prone polymerases in DNA damage conditions [390-392]. Although this alternative mechanism is not involved in recombinational repair, it is controlled by RecA and requires its direct collaboration [393, 394]. When a lesion is detected and the TLS is induced, RecA dissociates from the site of the lesion, and the replisome changes the conformation to bypass the damage [234]. In *E. coli,* the highly conserved TLS DNA polymerase PolIV (DinB) and PolV (UmuDC) are responsible for the TLS DNA synthesis in conditions of unrepairable DNA [395]. RecA regulates TLS in two ways: indirect activation of UmuC and UmuD via LexA (SOS response) and direct activation of UmuD. The first regulation is triggered upon prolonged activation of the SOS response, upregulating the expression of *umuC* and *umuD* [396, 397]. The second level of regulation activates UmuD through binding RecA filament for auto-cleavage [398]. This cleavage requires high concentrations of magnesium, likely to modulate a late response of TLS in the late stages of the SOS response [234]. The auto-cleaved UmuD links to UmuC to form the UmuDC active complex to catalyse DNA TLS [399, 400]. DinB is also SOS response regulated and markedly upregulates upon DNA damage [60], becoming the most abundant polymerase in the cell (~2500 molecules) [401]. This fact indicates the importance of polymerase IV in overcoming cellular DNA damage. DinB can act alone or form a binary complex with RecA, indeed the efficiency of repairing

alkylated damaged bases is higher if partnered with RecA [402]. DinB can bypass N_2-deoxyguanosine adducts [403-406] and lesions derived from alkylation [402, 403, 407, 408]. DinB can bypass damaged bases thanks to a broader active site than other high-fidelity polymerases. However, this active site prevents DinB from proofreading synthesised bases, unlike high-fidelity polymerases [409, 410]. Thus, low-fidelity polymerases cause frameshift mutations and nucleotide misincorporation if the proofreading activity is poor or absent [411, 412]. The TLS repair pathway in *B. subtilis* is performed by the polymerases YqjH and YqjW [413, 414]. *yqjH* is independent of the SOS-dependent response, as it is constitutively transcribed during vegetative growth. Meanwhile, *yqjW* is controlled by the SOS-dependent response and is tightly repressed during vegetative growth, but it is induced under DNA-damaging conditions [413]. Novobiocin was demonstrated to inhibit translesion synthesis (TLS), preventing the potential acquisition of AMR generated through DNA damage-induced mutagenesis [206]. *imuABC* (an *umuDC* homolog) is the system controlling TLS-induced mutagenesis in *C. crescentus*, *M. tuberculosis*, and other bacteria devoid of *umuDC* [415, 416]. *imuABC* is an SOS-dependent regulon that, unlike u*muDC*, it does not require the mediation of RecA to activate [417]. *C. crescentus* also harbours a DinB homolog but not a *polB* homolog, unlike *E. coli* [418]. ImuA is an SOS-response-regulated protein and cell-division-blockage inducer, and ImuB is a member of the Y polymerase family. ImuC is a polymerase III (Pol III) that efficiently participates in error-prone TLS, bypassing persistent DNA damage [418-420]. TLS is highly regulated as a security measure to avoid error-prone transcription-induced mutations without previous unrepairable lesions in the DNA. TLS does not induce mutagenesis even when it is engineered to be expressed constitutively [173, 417].

1.2.5 DNA damage response

Bacteria possess complex systems to cope with environmental changes [421]. Antibiotic resistance is one of the main concerns for public health. Mutations in critical bacterial genes confer bacteria with the capacity to tolerate higher doses of antibiotics [422]. Persistent bacteria, which are populations of highly stress-resistant bacteria, create chronic infections due to antibiotic resistance [422-424]

through various complex and redundant molecular mechanisms [425, 426]. Critical systems to generate antibiotic resistance are translesion synthesis (TLS) [173], HGT [427], quorum sensing, oxidant tolerance, toxin-antitoxin system (TA), energy metabolism, global stress response, multidrug efflux pumps (MDEPs) and DNA damage responses (DDR) like the SOS response [424, 425, 428, 429].

1.2.5.1 SOS response

The SOS response is an inducible system evolved in bacteria to survive DNA damage conditions. The SOS response enables the orchestrated induction of several proteins that contribute to protecting the integrity of the DNA [241]. The SOS response is triggered by different types of DNA damage that are recognised by different mechanisms and specific proteins. The regulation of this system is very complex given the high probability of mutagenesis in cases of severe DNA damage in the genome that can induce error-prone polymerases to bypass unrepairable lesions [241]. The SOS response is divided into the SOS-dependent and SOS-independent responses.

1.2.5.1.1 SOS-dependent response

The SOS-dependent response is a global transcriptional stress response regulon that controls several genes involved in DNA damage tolerance and repair [430] (Fig. 5). It was first described in the 1970s in *E. coli*, where most research has been done, and first named by Miroslav Radman in 1974 [352]. The SOS response pathway is widely conserved across bacterial species and the best-characterised DNA-damage response system [431]. This system requires *recA* (recombinase A) and *lexA* (locus for X-ray sensitivity A) [352] (Fig. 5). The SOS response comprises several genes (more than 50 genes in *E. coli*) that, under non-stress conditions, are repressed by the LexA dimer, which binds to the promoter region of target genes (SOS boxes) [353, 432, 433] (Fig. 5). DNA damage causes DNA polymerases to stall due to the lesion, while helicases continue to unravel DNA, and ssDNA levels increase [25]. Following DNA-damage induction, RecA, the central member of RR (described above), binds to the 3´-end of ssDNA, forming a nucleoprotein filament around it. The co-protease activity of the RecA-ssDNA stimulates the autocleavage of the

repressor LexA [338, 352] (Fig. 5). LexA derepresses the transcription of various genes of the SOS response involved in error-prone replication, base-excision repair, cell cycle, and chromosome segregation [388] (Fig. 5). This is a reversible system that regresses to its initial state once RecA is inactivated after DNA damages have been repaired. The LexA dimer is restored and returns to repress its target genes [431, 434]. The SOS response is sequentially executed and depends on the strength of the LexA-binding sites. For example, *sulA* or *umuDC* genes with powerful LexA-binding sites are de-repressed late and only in the presence of a high level of DNA damage [27]. High-fidelity repair mechanisms act primarily, followed by low-fidelity repair mechanisms (such as TLS), which activate when DNA damage persists [435]. The SOS response upregulates the transcription of three error-prone DNA polymerases (*polB, dinB, and umuDC*) to overcome the DNA-repair stalls when the damages persist [241, 436]. In *C. crescentus*, the *imuABC-dnaE2* operon is responsible for SOS-induced TLS mutagenesis [417]. Many genes involved in the SOS response are conserved genes such as *lexA, recA, ssb, uvrA,* and *ruvCAB* [437]. However, some other genes involved in the SOS response vary between different species and their LexA binding site, which regulates their transcription [433, 438-440]. This SOS-regulated operon is conserved in bacteria and is part of the SOS-mediated response to the antibiotic ciprofloxacin in *P. aeruginosa* (11). ROS causes DNA oxidative stress, inducing the transcription of genes in the SOS response [199]. Another component of the SOS system is SulA, a protein that delays cell division during DNA damage in *E. coli* by disrupting the polymerisation of FtsZ to prevent septation. This mechanism prevents the cell from segregating a damaged chromosome and gives cells more time to repair the damage [441].

1.2.5.1.1.1 SOS-dependent response in C. crescentus

C. crescentus has a similar LexA binding motif to *E. coli*. The *C. crescentus* LexA binding motif has direct nucleotide repeats ($GTTCN_7GTTC$) that bind and repress genes involved in the SOS-mediated response [431]. This binding sequence and conserved genes such as *lexA, recA, ssb, uvrA* and *ruvCAB* are part of the *C. crescentus* SOS regulon and are considered universal among the α-proteobacteria class [437]. Site-directed mutagenesis studies on the *imuA* promoter of *C.*

crescentus demonstrated that at least 37 genes are LexA-regulated [431]. The *C. crescentus imuABC,* a three-gene operon ortholog of the *E. coli umuDC*, is responsible for the SOS-inducible mutagenesis or TLS [442]. MmcB is a putative endonuclease specific for MMC-induced mutagenesis, that acts on the same pathway as *imuC* and is under the ImuABC regulon that controls the TLS-dependent pathway [173]. The transmembrane protein SidA (SOS-induced inhibitor of cell division A) directly inhibits FtsW, a late cell division protein of *C. crescentus* [443] (Fig. 5). SidA and FtsW, which also interact with FtsI (another component of the cell divisome), cause cell division blockage under DNA-damaging conditions by preventing the final constriction of the cytokinetic ring [443] (Fig. 5). SidA overproduction is sufficient to cause cell division blockage, but cell elongation is not inhibited, and cells show an elongated phenotype [443]. The *sidA* promoter region contains a LexA-binding motif, indicating that SidA is controlled by the LexA regulon and thus is part of the SOS-dependent response system [443]. BapE is an endonuclease activated under extensive DNA damage conditions to induce apoptotic-like cell death in *C. crescentus* [13]. BapE induces supercoiled DNA fragmentation in a nonspecific-sequence manner and does not participate in DNA damage repair [13]. By triggering cell apoptosis, cells can avoid disseminating defective genomes to offspring [13]. Furthermore, this mechanism may prevent the activation of lysogenic bacteriophages or the release of death factors into the extracellular medium that may influence its peers [13]. In addition to proteins, non-coding RNAs (ncRNAs) were also found to play a role in DNA damage response and repair in *C. crescentus*. These are post-transcriptional regulators that target mRNA. For example, the ncRNA ChvR is expressed in response to DNA damage, low pH, or growth in a minimal medium, and it targets the mRNA of the TonB-dependent receptor ChvT [444]. Dozens of genes in the SOS response are not yet studied but are important for the survival of *C. crescentus* in DNA-damaging conditions. This emphasises the need for further investigation to elucidate the entire SOS pathway [431].

1.2.5.1.2 SOS-independent response

The SOS-independent system is a cellular response to manage DNA damage that is different from the canonical SOS-dependent response that uses RecA and LexA as central regulators [445] (Fig. 5). The SOS-independent system reacts to specific types of DNA damage or redundantly to the SOS-dependent system [441]. The SOS-dependent response is highly conserved in different bacterial species. However, it is a very heterogeneous and species-dependent mechanism, except for some elements that are conserved across different species [445]. Nonetheless, little is known about the SOS-independent response, which requires further investigation. In species such as *Mycobacterium tuberculosis*, most DNA-damage repair inducible genes are transcribed independently of the SOS-dependent system, and 140 genes are upregulated upon exposure to MMC in SOS-deficient mutants [170]. *Mycobacterial smegmatis* has an SOS-independent response system controlled by the master transcriptional regulator PafBC (proteasome accessory factor B and C), which controls the RecA/LexA-independent pathway [170]. PafBC is encoded in the Pup-proteosome system (PPS) gene locus, and PPS degrades SOS-independent RecA once DNA damage has been repaired [170]. In *E. coli*, RecBCD and RecF repair pathways act independently of the SOS response [339], stimulating recombination between divergent sequences after the induction of DNA damage by fluoroquinolones [446]. RecBCD and RecF increase mutagenicity, promoting genomic variability and thus antibiotic resistance, acting as an SOS-dependent TLS-like pathway [446]. Ada is an *E. coli* alkyltransferase that activates the transcription of *ada* and the three downstream genes *alkA, alkB,* and *aidB* involved in alkylated DNA repair. Furthermore, Ada repairs alkylated DNA through alkyltransferase activity [441]. *Deinococcus spp.* are extremely resistant bacteria to radiation that deploy a specific system to manage DNA damage produced by such high energy [351]. *Deinococcus spp.* activates an SOS-independent response to transcribe various DNA damage repair genes, such as *recA* [351]. This specific mechanism called the radiation/desiccation response, is regulated by the metallopeptidase IrrE and the repressor DdrO, remarkably conserved in *Deinococcus spp.* [351]. Species such as *Helicobacter pylori* and *Streptococcus*

pneumoniae, which lack any LexA homolog but retain RecA, induce cell competence to uptake exogenous DNA after DNA damage [447, 448].

1.2.5.1.2.1 SOS-independent response in C. crescentus

C. crescentus possesses mechanisms such as *mmcA,* specific to DNA-damage repair generated by MMC but not to MMS or UVC light [173]. MmcA is part of the glyoxalase/dioxygenase protein family involved in the SOS-independent response [173]. DidA acts as an SOS-independent cell division inhibitor at a later stage upon DNA damage in *C. crescentus* [449] (Fig. 5). The lack of DidA and SidA in the cell provokes premature cell division following DNA damage [449]. DidA constitutes a second layer for cell division delay under DNA-damage conditions, representing a redundancy of DNA-damage checkpoints along with SidA [449]. Similar to SidA, DidA does not disrupt the assembly of the divisome machinery but interacts with FtsW and FtsI, in addition to interacting with the essential division protein FtsN [449] (Fig. 5). The DriD transcription factor (TF) controls DidA expression after DNA damage induction [449] (Fig. 5). DriD is a DNA-damage-induced transcription activator that senses ssDNA and binds to a specific gene promoter in *C. crescentus* [450]. DriD binds ssDNA through its C-terminal region between the WYL domain and the WYL-C-terminal extension dimerisation domain (WCX) [450]. The binding of ssDNA to DriD stabilises the WYL domain to which the HTH domain is linked to [450]. On the N-terminal HTH domain, DriD binds to the promoter region of genes, such as the DidA promoter, to which it is the only known activator [450].

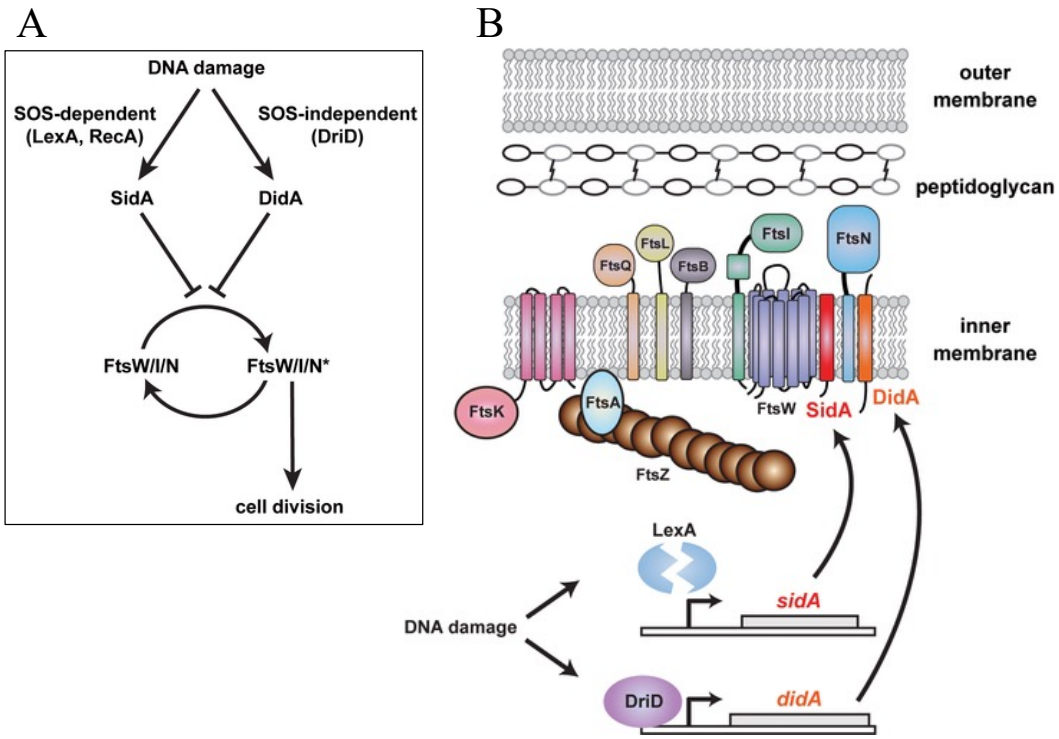

Fig. 5. The *E. coli* SOS response in *C. crescentus*. (A) SOS-dependent and SOS-independent responses activate the production of proteins such as SidA and DidA, respectively, that block cell division. (B) Under DNA-damaging conditions, the universal repressor of SOS LexA activates self-cleavage upon induction of the coprotease complex RecA protein-DNA filaments. The self-cleavage of LexA derepresses several genes of the SOS-dependent response involved in DNA repair, damage tolerance, and checkpoints [443, 449].

1.3 Small proteins in bacteria

Prokaryotic and eukaryotic genomes contain many small open reading frames (smORFs). Some smORFs encode small proteins (smORF-encoded small proteins) that play essential roles in cellular physiology and adaptation [451]. According to Storz and colleagues, a small bacterial protein is "a protein with less than 50 amino acids, which directly results from the translation of a small ORF, excluding post-translationally modified peptides with less than 50 amino acids" [452]. Therefore, Storz and colleagues exclude peptides from ribosome-independent systems and prominent precursors that need cleavage for maturation (e.g., leader peptides) [452, 453]. As a result of their small size, proteins usually fold into their unique native structures since the presence of multiple weak interactions overcomes the folding energy barrier. Small proteins (SPs) can only fold into a limited number of three-dimensional structures. Thus, SPs need the plasma membrane as a scaffold to acquire stability. Consequently, most SPs are membrane proteins anchored to the cell membrane or inserted in the membrane (small transmembrane proteins) [451, 452]. Therefore, SPs perform a limited number of functions, mainly restricted to modulating the activity of larger proteins and stabilising protein assemblies [452]. Membrane proteins containing fewer than 50 amino acids usually consist of an amphipathic polypeptide with a single transmembrane domain (TM) [451]. However, in other cases, like AzuC, the hydrophobic section is probably too short to span the cell membrane entirely; thus, AzuC is likely attached but not embedded into the inner membrane [454, 455]. Cells usually produce SPs in response to stress or environmental changes to modulate the metabolism according to internal and external conditions [451]. SPs participate in various cellular processes, including transport, enzymatic activity, regulatory networks, stress responses, morphogenesis, and cell division [452]. *E. coli* produces more than 60 tiny proteins with fewer than 50 amino acids that have been barely characterised. ~65% of these polypeptides are membrane-localised and possess a projected α-helical transmembrane (TM) domain [454]. *E. coli* is the organism in which small membrane proteins (SMPs) have been more extensively studied and characterised and show evidence of the numerous distinct functions and protein interactions they can perform [456]. A common characteristic among numerous small membrane

proteins in *E. coli*, besides the hydrophobicity, is the positive net charge that results in high pI values in proteins such as YohP (9.3), AzuC (10.3), and YkgR (8.14) (except in some cases like YshB (4.35). The pI values of SPs are generally higher than the pI of the antimicrobial peptides (AMPs). The low arginine and lysine contents of SPs compared to AMPs likely prevent membrane destabilisation [451]. The amphiphilic AzuC is an exception since bioinformatics tools predicted this protein to be an AMP [457, 458]. The interaction of SMPs with phospholipids is influenced by the position of positively charged residues at the carboxylic or amino termini, which determines the membrane topology [454, 455]. Lpt is a toxin SMP from *Lactobacillus rhamnosus* whose accumulation alters cell membrane integrity, causing growth impairment when heterologously expressed in *E. coli*, underscoring the capability of SMPs to modify the plasma membrane [459]. Positively charged residues also promote binding with other proteins, especially in highly charged protein oligomers in the membrane [455]. The positive net charge of SPs may also promote contact with DNA bases, such as the SMP Lpt, which promotes nucleoid condensation when it is heterologously expressed in *E. coli* [459].

1.3.1 Outlook of SPs

SPs were overlooked in the past due to conventional annotation pipelines that usually excluded smORF and the low cut-off set to detect and annotate proteins [452]. Genomic research established a cut-off of 50 amino acids in prokaryotes and 100 amino acids in eukaryotes since shorter proteins were considered too small to play any role in the cell [460]. Indeed, SPs are difficult to identify because mutants sometimes do not show an apparent phenotype or the cut-off for the co-purification procedure is set for polypeptides longer than 5 KDa in size. Furthermore, the prediction and detection of SPs have been challenging because of the limitations in bioinformatics and biochemical resources. Recently, two publications described the development of bioinformatics pipelines (smORFer and sPepFinder) to ease the identification of smORFs in bacteria [461, 462]. In previous years, several studies with SPs shed light on the crucial role of a wide variety of small polypeptides involved in many different biological processes. New techniques like ribosome profiling, COFRADIC, and poly-ribo-seq made the detection of SPs easier [463-

468]. Also, creating an SP database was the starting point for the officialisation of this new field [469]. In terms of SP nomenclature, no consensus exists about the different denominations like micro-peptides [470, 471], micro-proteins [472], mini-proteins [473], smORF-encoded polypeptides (SEPs) [474], or small single transmembrane domain proteins [475]. Besides, SPs seem to be a better alternative for referring to ribosome-generated products than micro-peptide, which is more accurate for defining proteolytic cleavages. The common trend in these terms is the emphasis on reduced size. Nonetheless, this classification fails to describe SPs' vast functional diversity [451]. The term peptide is sometimes used as a synonym for an SP, although standardisation will be needed in the future since AMPs meet the criteria for being considered an SP [476]. A function-based classification for SPs would be ideal for sorting them into categories according to their activity. However, the information needed to create such types is scarce, given the insufficiency of functional studies. Therefore, the investigation of SP folding, targeting, and transport is needed [458] (Fig. 6). SPs presumably function similarly to larger proteins, but specific functional studies for SPs are required to pinpoint their mechanisms [477-479].

1.3.2 Categories of SPs

SPs can be classified into two big groups: the first group comprises non-secreted proteins, usually membrane-associated or, less commonly, cytoplasmic [476]. These proteins are frequently associated with sensing stress conditions and, less regularly, cellular metabolism [476]. The second group comprises secreted proteins, whose primary function is bacterial and bacteriophage communication or competition [476].

1.3.2.1 Non secreted SPs

1.3.2.1.1 Stress response and metabolic regulation of SPs

E. coli has approximately 150 catalogued SPs in its genome, but others were likely not yet identified [480, 481]. Several stress-associated SPs localise at the inner membrane and comprise a single TM domain with uniquely few amino acids facing

the periplasm or cytoplasm [451, 452, 454]. Exposure to oxidative stress or temperature increases the production of SPs in *E. coli* [456]. A similar increase in protein production occurs in the impasse from rich to minimal medium or when they enter the stationary phase [482]. Cytoplasmic SPs have many functions in several cellular pathways like cell division (e.g., MciZ, SidA, and Blr), transport (e.g., KdpF, AcrZ, and SgrT), regulation of membrane-bound enzymes (e.g., CydX, PmrR, and MgtR), regulation of protein kinases, signal transduction (e.g., MgrB and Sda), and spore formation (e.g., SpoVM and CmpA). SPs can also act as chaperones (e.g., MntS, FbpB and, FbpC) to promote or prevent interactions between cell components or anchor proteins at the membrane [452, 456, 483].

1.3.2.1.1.1 The role of SPs as metabolic regulators

The limited size of SPs confers on this class of polypeptides the characteristic of mainly performing regulatory functions (rather than a catalytic role on their own). For example, SgrT, a 43-amino-acid protein, blocks glucose uptake by inhibiting the transport activity of the major glucose permease, PtsG. This function is part of a stress response to maintain glucose-phosphate homeostasis. The accumulation of sugar phosphates because of a disrupted glycolytic flux triggers a mechanism to inhibit cell growth [484]. Another small-protein regulator of transportation is KdpF in *E. coli*. This hydrophobic 29-amino-acid protein binds to a high-affinity potassium transporter (switched on only under K^+-limiting conditions) to stabilise the KdpABC transporter complex [485]. Another small membrane protein, MgrB (47-amino acid), represses the two-component signalling system PhoQ/PhoP upon associating with PhoQ in the membrane [486, 487]. Sda, a 46-amino-acid polypeptide, inhibits various kinases and, thus, sporulation in *B. subtilis* [488]. YbhT [489], a 49-amino acid protein, controls the AcrA-AcrB-TolC efflux pumps. SPs typically work mechanically rather than enzymatically. Thus, they act as a facilitator of protein-protein or protein-molecule interaction [452], as in the case of MgtR [490] and MntS [491]. SPs can act as inhibitors of protein-protein interactions; e.g., Sda [488] or MgrB [486] in *B. subtilis* or SulA in *E. coli* prevent the polymerisation of FtsZ [441]. In another example, Blr, a 41 amino-acid SP component of the *E. coli* divisome, interacts with FtsL, FtsI, FtsK, and FtsN [452].

1.3.2.1.1.2 SPs involved in DNA-damage response

A few SPs are involved in DNA-damage tolerance repair in *C. crescentus*. The 29-amino-acid transmembrane polypeptide SidA inhibits cell division by binding FtsW, preventing the final constriction of the cytokinetic ring following treatment with a DNA-damaging agent [443]. The 70-amino-acid membrane protein DidA is a cell division inhibitor at a later stage than SidA. DidA binds FtsZ following DNA damage, which causes a cytokinesis blockage in *C. crescentus* [449]. The deletion of DidA and SidA in *C. crescentus* with DNA damage conditions provokes premature cell division and aberrant elongated cells [449]. *sidA* is SOS-regulated in *C. crescentus*, unlike *didA,* which is SOS-independent [443]. BapE is an apoptotic-like cell death protein induced under extensive DNA damage conditions in *C. crescentus* [13]. Lastly, SPs are implicated in antibiotic resistance in bacteria. For example, an *E. coli* 49-amino-acid AcrZ protein enhances the efflux activity of a wide range of different toxic and antibiotic compounds [492].

1.3.2.1.1.3 Type I toxin/antitoxins

Type 1 toxins have an α-helical domain and are usually hydrophobic [493, 494]. They play essential roles in bacterial growth control, cell death, persistence during antibiotic treatment, infection, and defence against infection [493, 495, 496]. Type I toxins mainly function in two different ways: the induction of nucleoid condensation (e.g., the 33 aa Fst toxin) or the ATP synthesis and membrane potential decrease, for example, Hok (52 aa), TisB (29 aa), and PepA1 (30 aa) toxins provoked by membrane permeation via pore-formation [493].

1.3.2.1.2 SPs involved in folding and transport

SPs may find difficulties fitting intracellular trafficking and protein folding machinery, given their short size. Nevertheless, recent studies showed that SPs use alternative trafficking pathways [451].

1.3.2.1.2.1 Folding of SPs

The SP research field is accelerating its discoveries, although folding and transport are areas that need further investigation. The presence of multiple weak interactions is stronger than the folding barrier, so proteins fold into their unique native structures [497]. The reduced number of intramolecular interactions in SPs generates folding instability *in vitro,* so they require stabilisation by oligomerisation, metal chelation, or disulphide bridges [498-500]. The nuclear magnetic resonance spectroscopy analysis of 27 proteins of 9 different bacteria and archaea revealed that the native state of a considerable number of proteins was partially folded or unstructured [501]. Intramolecular interactions induce folded conformation, according to bioinformatic predictions [501]. Most AMPs may acquire their α-helical structure when interacting with the hydrophobic lipid environment or the anionic membrane surface [502-504]. The antimicrobial activity of the Australian *toadlet Uperoleia mjobergii* AMP Uperin 3.5 depends on the secondary structure conformational change when exposed to membranes [505]. The lipidic membrane constitutes a scaffold for protein folding, like YohP, an *E. coli* SP that is a monomer in solution but dimerises in the membrane [458]. A single glycine residue and its correct orientation in the cell membrane are essential for YohP dimerisation [458].

1.3.2.1.2.2 Transport of SPs

The small size and the lack of secondary structure are challenges for transporting proteins that have to be inserted into the membrane or secreted across the membrane [451]. Integral membrane proteins lack the signal sequence cleavage site and have an uncleavable N-terminal target motif called the signal anchor sequence or signal sequence. This anchor sequence functions as a transmembrane domain [506]. Signal sequences direct proteins to protein transport channels in the endoplasmic reticulum membrane of eukaryotes or the cytoplasmic membrane of bacteria [477, 507, 508]. Thus, signal sequences serve as tags and gate openers for protein transport channels, providing a dual purpose for protein targeting factors [509-513]. Signal sequences usually have a length of 25-30 amino acids and a tripartite structure. Bacterial AMP utilises different transport systems, such as the SecYEG translocon [514] or the ABC transporter [515, 516]. The activation of inactive AMP

precursors occurs upon protein cleavage [517]. Furthermore, post-translational modifications add thioether-based ring structures to some AMPs, like lantibiotics, before they are transported via the ABC transporter LanT [518]. Proteins like YshB, which are produced during stress conditions or stationary phases, might probably require specific transport systems [457]. A significant issue is the reduced size of bacterial SPs, which could prevent co-translational recognition by the signal recognition protein (SRP). Hence, alternative mechanisms to transport SPs constitute the central transport system for secretory proteins in bacteria [519, 520]. As an example, the ATPase SecA delivers SPs to the receptor system SecYEG for translocation [509] (Fig. 6). SecA mainly acts post-translationally [521, 522], although it can also interact with RNCs [523-525]. So far, only a few studies have addressed the involvement of SecA in SP targeting. Bacteria possess two known Sec-dependent pathways to transport and translocate proteins to and across the cell membrane [455, 477, 526-528]. The first mechanism is a translationally coupled system where the SRP binds to the newly synthesised polypeptide and drives it to the membrane to find the ATPase SecA translocase. This pathway requires the attachment of the ribosome to the membrane-bound SecAEG translocase to directly synthesise the nascent protein across the membrane or insert it directly into it [455, 477, 526-528]. SRP identifies an N-terminal recognition site in the target protein called the signal sequence (or signal anchor sequence for transmembrane proteins) that carries polypeptides to protein transport channels in the cell membrane of bacteria [477, 507]. SMP's small size makes it unlikely that they can co-translationally bind to SRP, as they would have been synthesised and released from the peptidyl transferase core of the ribosome before being exposed to the ribosomal surface for SRP identification [529]. Unlike the first transportation and translocation pathway, the second mechanism is specific to bacteria. The second pathway is uncoupled from protein synthesis [530-532]. SecA is the protein that recognises and drives the nascent protein to the cytoplasmic membrane to bind to the SecYEG translocon or the YidC insertase [455, 477, 526-528, 533, 534]. Most outer membrane proteins and soluble periplasmic proteins in *E. coli* rely on the SecA-mediated route for localisation [535-538]. The almost universal conservation of SecA in other bacteria shows that this mechanism is vital for all bacteria [539].

Otherwise, it was discovered in *E. coli* that the 27-amino-acid YohP and the 33-amino-acid YkgR follow an alternative pathway for the insertion of SMPs into the cell membrane [482] (Fig. 1). YohP and YkgR post-translationally bind to SRP, which carries them to the membrane to be inserted by the SecYEG translocon or YidC insertase [454, 528] (Fig. 6). Due to their high hydrophobicity and the tendency for aggregation of SMPs, targeting the membrane without assistance is unlikely. Interestingly, ribosome-uncoupled *yohP* mRNAs were found primarily in the cytoplasmic membrane and may play some regulatory function [455] (Fig. 6).

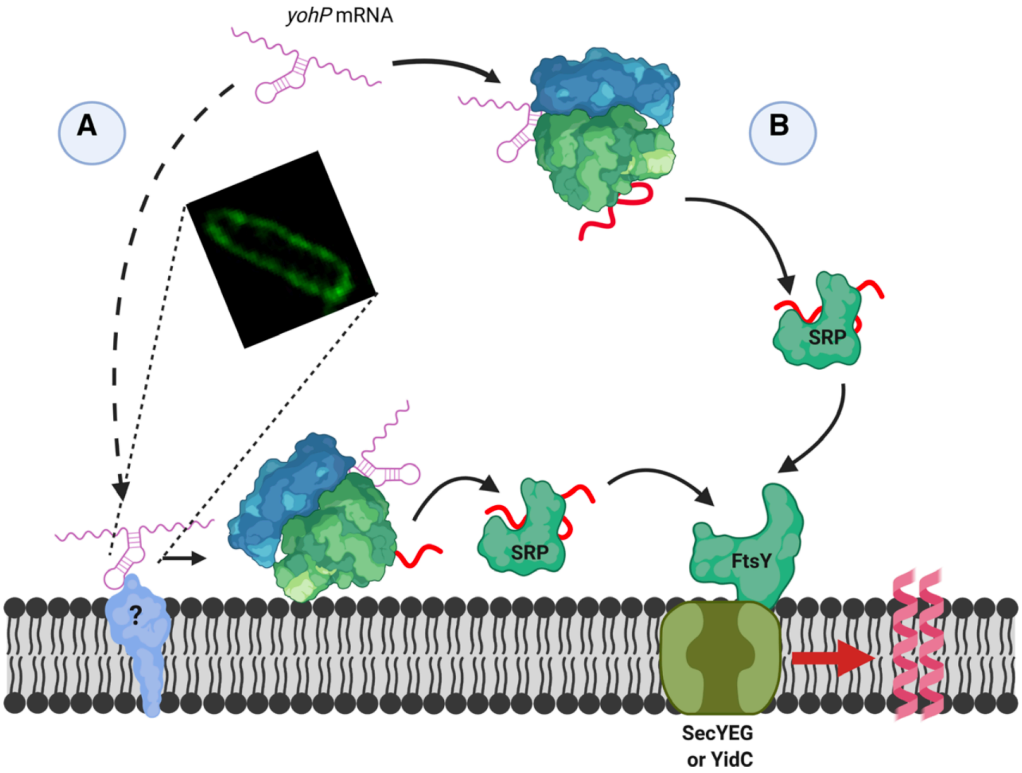

Fig. 6. Transport of small membrane proteins in bacteria [451]. YohP, a 27-amino acid *E. coli* membrane protein, has been the subject of most research on targeting and transporting small membrane proteins. (A) *yohP* mRNA binds to the *E. coli* plasma membrane in a translation-independent manner. The phage MS2 fluorescent protein was used to visualise the *yohP* mRNA, whose 3'-end was fused to the MS2 recognition particle [455]. The identity of the putative mRNA receptor remains undiscovered. The mRNA is transcribed through membrane-bound ribosomes and released from the ribosome following the mRNA binding process. SRP post-translationally interacts with the newly synthesised YohP to deliver it to the SRP receptor FtsY, which can interact with the SecYEG translocon or YidC insertase. YohP dimerises upon being inserted into the cell membrane by SecYEG or YidC. (B) *yohP* mRNA may be captured and translated into YohP by cytoplasmic ribosomes before attaching SecYEG- or YidC-bound FtsY for insertion [451].

1.3.2.2 Secreted SPs

1.3.2.2.1 Auto-inducing peptides and quorum sensing

Bacteria can communicate through signal peptides (autoinducers, AI), which they release into the environment. AIs trigger the simultaneous expression of specific genes when a particular concentration is reached to provoke a collective response in a bacterial population [540-542]. This communication within bacterial populations is called quorum sensing (QS) and is characteristic of processes like virulence, antibiotic production, competence, biofilm formation, or sporulation [476]. Gram-negative and Gram-positive bacteria produce different types of AI. AIs are classified into four groups according to their characteristics and receptors: the first group is from the RNPP family (Rap, NprR, PlcR, and PrgX), the second group is Agr-type cyclic pheromones, the third group is Rgg-family regulators, and the fourth group is double glycine (Gly-Gly) processing motifs [543]. Most AI precursors undergo posttranslational maturation processes and are transported to the membrane to be secreted. AIs are usually cyclic or linear, and their size ranges from 5 to 17 amino acids [542].

1.3.2.2.2 Bacteriocins, antimicrobial peptides, and toxins

AMPs are secreted by prokaryotic and eukaryotic cells to combat pathogens and competitors. AMPs encompass a significant group of small secreted proteins targeting the bacterial membrane preferentially [544] and intracellular targets, like the ribosome [545]. Different eukaryotic and prokaryotic cells and viruses secrete AMPs to kill pathogens or as a defence mechanism to inhibit or control the proliferation of competitors [502, 517, 546]. Approximately 3000 peptides are recorded in the AMP Database, and more than 2.700 are ribosomally synthesised. Furthermore, around 13000 synthetic peptides were demonstrated to target Gram-negative or Gram-positive bacteria [451]. Bacteria produce approximately 8% of all known AMPs, and fungi around 2%. The classification of AMPs can be done according to several criteria, spanning from the mode of action to the secretion mechanism, to the producing strain [547]. AMPs cause inhibition of gene expression, protein production, and disruption of the bacterial cell envelope (by the

direct interaction of AMPs with the cell envelope) [548]. The destabilisation effect of the cytoplasmic membrane occurs because AMPs possess a cationic and amphipathic nature [549, 550]. The AMP's pI values are generally lower than the pI of SPs, and their high lysine and arginine content probably promotes membrane destabilisation [451]. A membrane destabilisation probably causes inhibition of cell wall synthesis [551, 552] and divalent cation displacement [553, 554]. The amphipathic and cationic nature of most AMPs is essential for their membrane-destabilising effect on the cytoplasmic membrane [64, 65]. The effect of AMPs on the outer membrane and the peptidoglycan layer is generally less explored, but AMPs are assumed to cross the outer membrane and the cell wall spontaneously. Another distinction among AMPs is that some are non-ribosomally synthesised. Other AMPs, such as bacteriocins, are ribosomally synthesised SPs subjected to substantial post-translational modifications in some cases [548, 555].

Bacteriocins are a different group of small peptides, referred to as bacterial AMPs, with a larger size, structure, and other modes of action [517]. Bacteria of the microbiota produce phenol-soluble modulins, or microcins, two types of bacteriocins essential to defend their host against infection and combat pathogens [556, 557]. Pathogenic bacteria can use bacteriocins to alter the bacterial fitness of the microbiota and thus originate an infection in the host, such as BacSp222 from *Staphylococcus pseudintermedius* and Listeriolysin S from *L. monocytogenes* [558-560]. Gram-negative bacteria produce tailocins and microcins, two types of bacteriocins. Tailocins are large peptides composed of several subunits and related to the tail proteins of bacteriophages [561]. Microcins are colicin-like bacteriocins synthesised as precursor peptides with (class I) or without (class II) post-translational modifications like the 626 amino acid colicin 1a [562, 563]. Microcins hijack nutrient uptake systems, especially iron, to get into cells [564]. Once they are in the cell, they can alter the normal function of the cell by impairing ATP production [565] or protein translation [566]. Only microcins from Gram-negative bacteria and Class I and II bacteriocins of Gram-positive bacteria meet the criteria to be SPs despite sharing an antimicrobial activity with other bacteriocins [451].

1.4 Objectives of this project

I. To characterise CalP through genetic modification of *C. crescentus* and *E. coli*, and biophysical methods.

II. To investigate the role of CalP in the DNA-damage tolerance/response of C. crescentus.

III. To investigate potential protein interacting partners of CalP in *C. crescentus* that could interplay in a DNA-damage tolerance/response pathway.

Chapter 2. Characterisation of CalP, a small protein involved in the response/tolerance to DNA damage in *C. crescentus*

2.1 Introduction

2.1.1 DNA-damaging agents

Norfloxacin and ciprofloxacin are fluoroquinolones that target two essential bacterial enzymes, DNA topoisomerase IV and DNA gyrase, generating DSB [40, 41]. MMS is an alkylating agent that methylates DNA in the nitrogen atoms of purines, causing mutations and stalling replication [124]. MMC crosslinks DNA strands that cause DBS through the repair of damaged bases or chemically modified nucleotides that provoke replication fork failure [567, 568]. Cisplatin creates intra-strand (~98%) and inter-strand (~2%) crosslinks that block the progression of DNA polymerase, leading to the formation of DSB [191, 569, 570].

2.1.2 Cytotoxic compounds

A myriad of compounds affects the sensitivity of bacteria and may indirectly alter the integrity of the genome. Hydroxyurea (HU) is an antineoplastic drug that has been shown to inhibit ribonucleotide reductase class I (RNRs) in prokaryotes [193, 194]. This inhibition of RNR can cause depletion in the production of deoxyribonucleotide triphosphate, inducing replication inhibition and DNA double-strand breaks by causing replication fork arrest [195, 196]. Novobiocin targets the B protein of DNA gyrase and inhibits gyrase-catalysed DNA supercoiling *in vitro* [204]. More specifically, drugs are competitive inhibitors of the ATPase reaction catalysed by GyrB [204]. H_2O_2 is a reactive oxygen species, as are OH and O_2^-. These species are generated when single electrons are added to oxygen in the respiratory chain of the cell [199]. ROS are potent oxidising agents that can create free radicals and damage numerous biomolecules, inducing a cellular stress response [17, 199]. NaClO is a chlorine-based agent with a strong oxidising capacity [207]. NaClO attacks the electron-rich core of biomolecules such as

peptides, enzymes, lipids, or DNA through the one-electron transfer mechanism [209]. Gentamicin is an aminoglycoside antibiotic with a high affinity for the 30S and 50S bacterial ribosomal subunits, which provokes protein synthesis inhibition [212]. The tetracycline family of drugs prevents aminoacyl-tRNA from binding to the ribosomal acceptor (A) site, inhibiting protein synthesis [215, 216]. Spectinomycin is an aminoinositol drug that inhibits protein translation by interacting with the RpsE protein in the minor groove of helix-34 of 16S ribosomal RNA [217, 218].

2.1.3 Genes encoding ncRNA

Small RNAs (sRNAs) in bacteria are a diverse class of post-transcriptional regulators that frequently work by base-pairing with their target mRNAs. The conserved ChvI-ChvG is a two-component system that regulates *chvR* transcription in *C. crescentus*. Transcription of *chvR* is triggered by DNA damage, low pH, and growth in an insufficient medium. *chvR* mRNA posttranscriptionally represses the mRNA of the TonB-dependent receptor ChvT by directly binding to it to prevent its translation [444].

2.1.4 Small membrane proteins

Bacterial SPs are those with 50 or fewer amino acids, which get their short size by directly translating a small open reading frame (smORF) instead of longer proteins through proteolytic cleavage or ribosome-independent synthesis [451-453, 571]. Membrane proteins of fewer than 50 amino acids usually have a single transmembrane domain (TM) [451]. As a result of their small size, proteins typically fold into their distinctive native structures due to numerous weak interactions, which are not strong enough to promote folding [497]. SPs usually obtain stabilisation by disulphide bridges, metal ion chelation, oligomerisation, or binding to the plasma membrane [498-500]. Most SPs are membrane proteins anchored to the cell membrane or inserted in the membrane [451-455]. The cytoplasmic membrane is a scaffold for SMPs to fold and interact with other polypeptides [451, 452, 455]. These transmembrane proteins are amphipathic polypeptides with a unique transmembrane domain and a short number of amino

acids that point to the periplasm or cytoplasm [451]. The fact that a substantial fraction of the entire protein is the TM domain embedded in the membrane contributes to its high hydrophobicity [455]. SMP topology in the membrane is determined by the location of positively charged residues at the N or C termini, enabling interactions with the polar head groups of phospholipids [454, 455]. Positive charges may also facilitate connections with nucleotides and other polypeptides, especially when oligomerisation produces highly charged groups within the phospholipid bilayer [173, 455].

2.1.5 Protein oligomerisation

Oligomer formation is a way to gain stability for SPs [571]. Many proteins exist in a multimeric or polymeric form, consisting of many repeating units, and are regarded as a crucial biological process [572]. Two types of multimeric proteins are homomultimeric and heteromultimeric, whose differences are determined by the protein sequence. The same protein units stand for homomultimeric proteins, whereas heteromultimeric proteins have different units [573]. The *E. coli* SMP YohP is a monomer in the cytoplasm and a dimer in the plasma membrane (PM), YohP links a glycine from each monomer and forms a homooligomer through a helix-helix connection [455]. A higher similarity in the sequence of two polypeptides strengthens their interaction [574, 575] and increases coaggregation efficiency between different protein domains [576], likely due to the greater stability or foldability [577, 578]. Protein oligomerisation can control the function of numerous SPs such as enzymes, ion channel proteins, receptors, transcription factors, and cell-cell adhesion processes [579, 580]. Substitutions or deletions of single amino acids may significantly impact the specificity or stability of a complex [581]. Functional activity can be altered if amino acid changes occur at homo-oligomer interfaces [573]. The association or dissociation of homo-oligomers may result from amino acid changes applied to the protein surface or interface [573]. Hashimoto et al. (2010) [581] investigated the oligomeric state of homologous proteins in different organisms and found that 25% of all proteins investigated and 40% of enzymes include areas that promote or disrupt the formation of oligomers. They demonstrated that the addition of large nonpolar side chains, such as

phenylalanine or tryptophan, promoted complex formation in some of these proteins, which only required a single amino acid alteration to boost oligomerisation [582]. Moreover, equilibrium may change in favour of the generation of oligomers if solvent-exposed amino acids are substituted with more hydrophobic and prominent residues [583]. Furthermore, another specific mechanism for dimer formation is translationally driven, binding the two nascent monomers concurrently with releasing both strands from the ribosome [584].

2.1.6 Background

As a first approach to this project, Rosaria Campilongo performed a Tn5-seq screen to find DNA damage tolerance/repair genes in *C. crescentus* NA1000 (hereafter *C. crescentus*). To select genes involved in DNA damage, cells were treated with several compounds that affect DNA in different ways. Before the addition of the drug, cells were mixed with transposons. Cells were left untreated or treated with the following MICs of cytotoxic compounds: 0.25 μg/mL MMC, 4 μg/mL norfloxacin, 1 μg/mL MMC, 3 μg/mL hydroxyurea, and 0.5 μg/mL novobiocin. Cultures were incubated for 20 hrs at 30ºC in a liquid medium. Cells were also streaked on an agar plate and incubated at 30ºC for 48 hrs. Cells were collected from the liquid and the solid medium and genomic DNA was extracted to be deep-sequenced. The number of read-outs of transposon insertions at each gene is compared under different conditions in drug-treated and drug-free cells. Under certain conditions, cells having transposon insertions in the genomic DNA that truncate an essential gene or genes causing lethality do not survive. Hence, during genomic DNA sequencing, cells with transposon insertions in essential genes do yield transposon reads, whereas cells lacking transposon insertions in these genes produce readable genomic DNA. Therefore, the overall count of transposon insertions is reduced in populations that have insertions in essential genes, particularly when treated with a compound which is lethal in the absence of those specific genes. In contrast, cells facing challenging conditions, whether with transposon insertions in non-essential genes or in conditions with or without transposon insertions but under less challenging circumstances, showed an increased number of sequencing counts. Deep sequencing of transposon-

mutagenised *C. crescentus* cells revealed a low number of reads when the transposon insertion occurred in *CCNA_03982*, particularly in cells treated with MMC, MMS, norfloxacin, and novobiocin in both solid and liquid medium. Conversely, untreated cells with transposon insertions in *CCNA_03982* showed much more reads than drug-treated cells. This suggested that *C. crescentus* cells with transposon insertions in *calP* were less viable under DDA conditions. In other words, *calP* might be important for *C. crescentus* to survive under DNA-damaging conditions. The gene *CCNA_03982* has been renamed *calP,* and it encodes a SP now named CalP (*Caulobacter* little protein). Particularly, the number of reads of transposon insertions in MMC-treated cells remained remarkably low in solid and liquid media (Table 1). Because of this consistency, I selected MMC to graphically represent the sequencing panel of transposon insertions in *wild-type* (WT) *C. crescentus* (Fig. 7). Cells treated with novobiocin showed a lower number of transposon insertions reads in the locus of *CCNA_02151* during the deep sequencing compared to untreated cells both in the liquid and the solid media (Table 1). Similarly, transposon insertions in *CCNA_02329* showed a reduction in the number of counts when cells were treated with MMS in both liquid and solid media (Table 1).

Gene	Liq. PYE	Liq. MMC	Liq. MMS	Liq. NOV	Liquid HU	Sol. MMC	Sol. MMS	Sol. NOV	Sol. HU	Sol. NORF
CCNA_02151	2707	2921	2508	1926	2236	1466	2593	908	2670	1056
CCNA_02329	3500	4772	2678	3010	3356	1191	2914	680	2180	276
CCNA_03982	5519	2062	496	0	4578	318	3063	6724	1252	21

Table 1. *C. crescentus CCNA_02151*, *CCNA_02329*, and *CCNA_03982* exhibited a reduced number of transposon insertions in the drug-treated cells compared to the untreated cells. Deep sequencing analysis of the genomic DNA of *C. crescentus* WT. The table summarises the count transposon insertions in cells incubated in either liquid or solid peptone yeast extract (PYE) medium supplemented with MMC, MMS, novobiocin, HU, or norfloxacin as necessary. The sequencing reads from cells grown in a solid medium with norfloxacin failed, and consequently, are not included in the table. The values highlighted in green indicate that, in both liquid and solid media the number of reads from drug-treated cells is lower than untreated cells. A gene is deemed a potential candidate for causing lethality if there is a minimum 15% in counts between treated and untreated cells.

Fig. 7. Transposon mutagenesis revealed that the deletion of *calP* affects the capacity of *C. crescentus* to survive in the presence of MMC. Transposon insertion profiles in *C. crescentus* NA1000 are depicted in the upper panel for the PYE medium and in the lower panel for the PYE medium with 0.25 μg/mL MMC. The red vertical strip shows the *calP* (*CCNA_03982*) locus on the genome. Horizontal green bars show the positions of deep-sequencing reads.

2.2 *calP* is important for survival in the presence of DNA-damaging agents

Previous results from the Tn5-seq analysis in *C. crescentus* found that the candidate gene *CCNA_3982* (renamed as *calP*) was essential for the cell viability of *C. crescentus* after MMC treatment (Fig. 7). I wanted to test whether *calP* was the gene responsible for counteracting the toxic effect of MMC or whether it was a polar effect of knocking out other genes(s) nearby. To do so, I deleted *calP* from a *C. crescentus* WT background and performed sensitivity assays with the subinhibitory concentrations (SIC) of DDAs in solid and liquid media. I evaluated the effect of DDAs on *ΔcalP* to determine if *calP* was important for DNA damage repair/tolerance and whether the phenotype observed in the Tn5-seq analysis result was reproducible. WT and Δ*recA* were also included as control strains for the sensitivity assay in a solid medium. Δ*recA* is a strain commonly used as a positive control for DNA-damage-sensitive cells. Cultures were serially diluted ten times and spotted from right to left on plain agar (Fig. 8A). Additionally, agar plates were supplemented with each of the following concentrations of DDA: 6 μg/mL norfloxacin (Fig. 8B), 2 μg/mL ciprofloxacin (Fig. 8C), 0.25 μg/mL MMC (Fig. 8D), and 1 mM MMS (Fig. 8E). Plates were incubated at 30ºC for 48 hrs. In this experiment, I compared the differences in spot densities of WT, Δ*recA*, and Δ*calP*. A lower cell density of spots indicates that the strain has a higher sensitivity to the compound it was exposed to. Cells in the drug-free agar plate did not show any difference between the density of the cell spots of WT, Δ*recA*, or Δ*calP* (Fig. 8A). Following norfloxacin treatment, *ΔcalP* showed cell spots with a lower density than WT, which exhibited much denser cell spots (Fig. 8B). *ΔrecA* cells were more sensitive to norfloxacin than *ΔcalP* or WT. *ΔrecA* cells could grow when cultures were diluted up to 10^{-4}-fold compared to *ΔcalP* or WT, which formed cell spots up to the 10^{-6}-fold dilution (Fig. 8B). Cells treated with ciprofloxacin showed that *ΔcalP* cell spots had a lower cell density compared to WT (Fig. 8C). Indeed, *ΔcalP* and WT formed colonies at the 10^{-6}-fold dilution (Fig. 8C). Cell spots of *ΔcalP* or WT were denser than *ΔrecA* spots in the presence of ciprofloxacin (Fig. 8C). *ΔrecA* cell spots only formed colonies up to the 10^{-4}-fold serial dilution (Fig. 8C). When *ΔcalP* cells were exposed to MMC, the resulting spots showed lower density compared to the WT, indicating increased sensitivity in *ΔcalP* due to the presence

of MMC (Fig. 8D). *ΔrecA* only formed some spontaneous mutants in the 10 and 10^{-1}-fold-dilution cell spots, indicating a higher sensitivity than *ΔcalP* or WT with MMC (Fig. 8D). *ΔcalP* or WT could form colonies up to 10^{-4} and 10^{-5}-fold-dilutions in the presence of MMC (Fig. 8D). The presence of norfloxacin or MMC produced a substantial reduction in the cell spot density of *ΔcalP* in comparison to WT. This phenotype suggests that *ΔcalP* is more sensitive than WT to norfloxacin or MMC (Figs. 8B, D). Following the treatment with MMS, *ΔcalP* cells showed cell spots with a lower cell density than WT, indicating more sensitivity to MMS than WT cells (Fig. 8E). *ΔrecA* showed cell spots with a lower cell density than WT or *ΔcalP*. *ΔrecA* could only form cell spots up to the 10^{-1}-fold dilution with MMS, but WT or *ΔcalP* could form cell spots up to the 10^{-4} dilution (Fig. 8E). *ΔcalP* cells treated with ciprofloxacin or MMS showed cell spots with a lower cell density than WT (Figs. 8C, E). However, the difference in the cell spot density was not as marked as the density between *ΔcalP* and WT in the presence of norfloxacin or MMC (Figs. 8B, D). Δ*recA* was more sensitive in the presence of every tested compound than WT or Δ*calP*, proving the toxic effect of DDAs on cells hypersensitive to DNA damage. To summarise, Δ*calP* showed cell sports with a lower cell density than WT when exposed to every tested antibiotic, suggesting a greater sensitivity to DDA. Therefore, Δ*calP* and Δ*recA* exhibited a higher sensitivity to norfloxacin, ciprofloxacin, MMC, or MMS compared to WT in a solid medium (Figs. 8B-E).

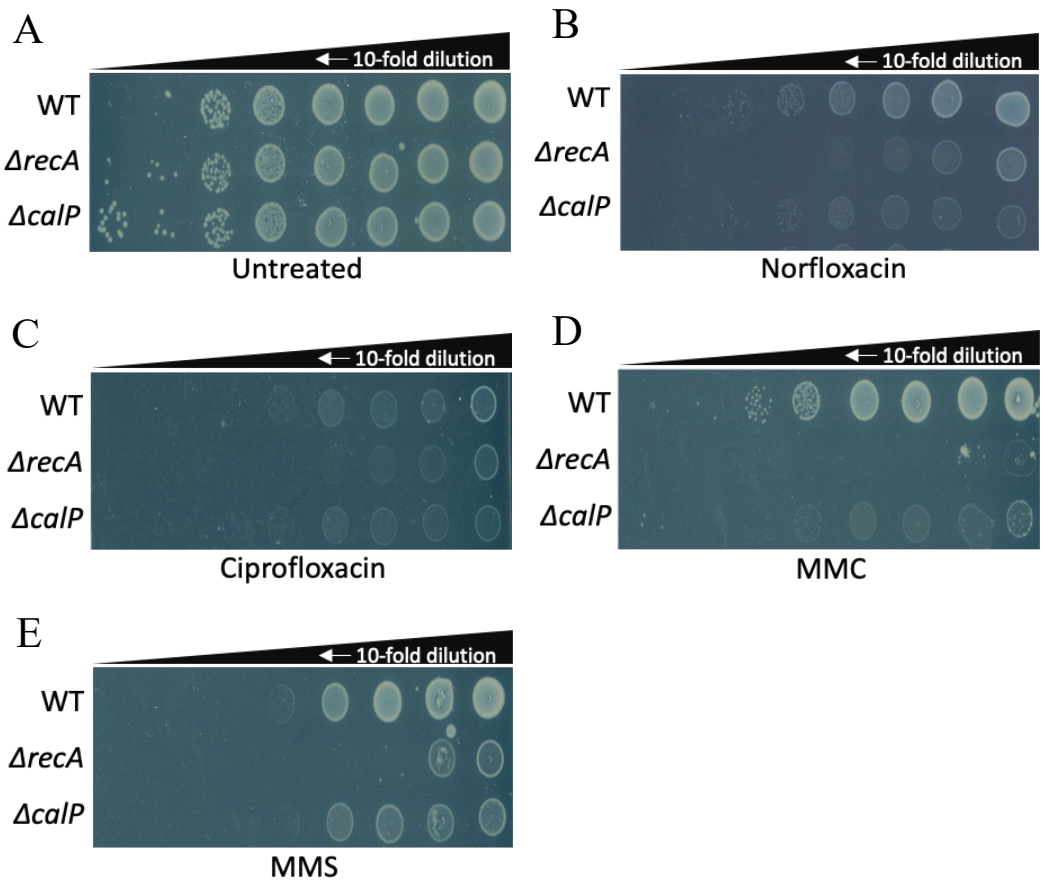

Fig. 8. *ΔcalP* shows spots with a lower cell density than WT when exposed to norfloxacin, ciprofloxacin, MMC, or MMS in a solid medium. Spotting assay of WT, *ΔrecA*, and *ΔcalP* cells growing on a PYE agar medium with or without DNA-damaging agents. Cells were initially grown to mid-exponential phase and subsequently diluted to an OD_{600}=0.1. Then, 10-fold serially diluted (represented by the wedge on top of each image) were prepared to plate the cells. Agar plates were incubated for at 30°C 48 hrs before capturing the images. The plates shown correspond to media with (A) no additives, (B) 6 μg/mL norfloxacin, (C) 2 μg/mL ciprofloxacin, (D) 0.25 μg/mL MMC, and (E) 1 mM MMS.

To test Δ*calP* sensitivity in a liquid medium, I inoculated WT, Δ*recA*, and Δ*calP* in an untreated medium (Fig. 9A) or a medium treated with the SIC of one of the following antibiotics: 4 μg/mL norfloxacin (Fig. 9B), 1 μg/mL ciprofloxacin (Fig. 9C), 0.25 μg/mL MMC (Fig. 9D), or 1 mM MMS (Fig. 9E). Cultures were incubated for 48 hrs at 30°C, and the optical density (OD_{600}) was monitored hourly. The measurement of the OD_{600} compares the absorbance of the cell culture with the absorbance of the medium without cells (used as a reference). I employed the mean of the optical densities of three technical replicates per strain to make a plot line. The optical density can be taken as a pattern to evaluate the sensitivity of cells for a given compound supplemented in the medium. A low optical density of the target strain compared to a control (a few hrs after inoculation) usually indicates a high sensitivity, and vice versa. The exponential phase is defined as the point on the plot where the curve starts to exhibit an exponential tendency in the early stages of the growth curve. The stationary phase is defined as the point of the plot where the curve levels off horizontally after the exponential growth, indicating a plateau or equilibrium in cell numbers. The transition from the exponential to the stationary phase occurs at different time points for each population under different conditions. The comparison of the growth curves of different strains and conditions is done by dividing their OD_{600} values. The result of this division determines the quantitative difference between the optic densities of two different cell cultures. Untreated WT, *ΔrecA*, and *ΔcalP* entered the stationary phase 21 hrs after inoculation (Fig. 9A). WT, *ΔrecA*, and *ΔcalP* reached a maximum $OD_{600}\approx0.5$ in the drug-free medium (Fig. 9A). The liquid medium test showed a sensitivity of *ΔcalP* compared to WT when challenged with norfloxacin, ciprofloxacin, MMC, or MMS (Figs. 9B-9E). The lower optical density of *ΔcalP* compared to WT was caused by the early entry of Δ*calP* into the stationary phase when treated with every DDA (Figs. 9B-9E). The $OD_{600}\approx0.4$ of Δ*calP* was 1.5-fold lower than the $OD_{600}\approx0.6$ observed in WT when both strains were treated with norfloxacin, suggesting that Δ*calP* is more sensitive than WT to norfloxacin (Fig. 9B). Following the treatment with norfloxacin, the optical density of Δ*calP* was 1.44-fold delayed compared to WT (from 18 to 26 hrs) when entering the stationary phase (Fig. 9B). In the presence of ciprofloxacin, the $OD_{600}\approx0.55$ observed in Δ*calP* was reduced by 1.35-fold compared to the

OD_{600}≈0.75 of WT, indicating that Δ*calP* was more sensitive than WT to ciprofloxacin (Fig. 9C). *ΔcalP* cells challenged with ciprofloxacin reached the stationary phase 1.33-fold earlier than WT (15 and 20 hrs after inoculation, respectively) (Fig. 9C). After treatment with MMC, the optical density of Δ*calP* decreased by 1.85-fold compared to WT, from an OD_{600}≈0.48 to an OD_{600}≈0.26, respectively (Fig. 9D). After inoculation, MMC-treated Δ*calP* reached the stationary phase 18 hours later, which was 1.22-fold earlier than WT, taking 22 hours to reach the same phase (Fig. 9D). After MMS treatment, the OD_{600}≈0.34 observed in Δ*calP* was 1.5-fold lower than the OD_{600}≈0.5 of WT, indicating that Δ*calP* exhibited higher sensitivity compared to WT (Fig. 4E). After MMS exposure, Δ*calP* reached the stationary phase 1.24 times earlier than WT, doing so after 17 hours compared to WT's entry into the stationary phase at 22 hours post-inoculation (Fig. 9E). The optical density of WT increased for a longer period than *ΔcalP* in the exponential phase when challenged with MMS (Fig. 9E). During the stationary phase, the optical density of *ΔcalP* remained relatively unchanged, leading to an increased disparity between the optic densities of WT and *ΔcalP* (Fig. 9E). *ΔcalP* displayed a different sensitivity phenotype depending on the DNA-damaging agent supplied, probably because their modes of action are different. However, the *ΔcalP* phenotype when challenged with norfloxacin or ciprofloxacin was very similar since both quinolones have a similar toxicity pattern (Fig. 9). The sensitivity test results demonstrated that cells prematurely entered the stationary phase when *calP* was absent. This phenotype might have been caused by accumulated DNA damage preventing cells from thriving or by a programmed growth-stall pathway induced by DNA damage. *ΔrecA* showed a lagged growth curve compared to WT or *ΔcalP* in the presence of norfloxacin (Figs. 9B). After 20 hours with norfloxacin, *ΔrecA* exhibited an OD_{600}≈0.15, which was lower than the OD_{600}≈0.30 observed in WT and the OD_{600}≈0.4 of *ΔcalP* in the exponential phase (Figs. 9B). However, *ΔrecA* surpassed the OD_{600}≈0.4 of *ΔcalP* and reached a similar OD_{600}≈0.62 to WT in the stationary phase after 46 hrs with norfloxacin (Figs. 9B). Cells exposed to ciprofloxacin showed a similar but smoother delay of the growth curve of *ΔrecA* in comparison to WT or *ΔcalP* with norfloxacin in the exponential phase (Fig. 9C). A hypothesis to explain the early delay in the rise of the optical density of *ΔrecA* with

norfloxacin or ciprofloxacin might be an initial cell division arrest when DNA damage was detected. After the cell division arrest, mutations in the DNA gyrase (the target of QLs) may potentially alleviate the cell division block, cells to resume division. *ΔrecA* had a very low or zero OD_{600} when challenged with MMC or MMS, indicating that the inoculated cells were unable to grow when exposed to this compound (Figs. 9D, E). Δ*recA,* a defective-DNA-damage-repair genotype strain, confirmed the reliability of our sensitivity assays, showing a low optical density when exposed to each DDA. Our results suggest that *calP* is important for *C. crescentus* survival under DNA damage conditions and may be involved in the cell stress response pathway. *ΔcalP* sensitivity in a liquid medium was consistent with results obtained from the assay in a solid medium (Figs. 8A-E).

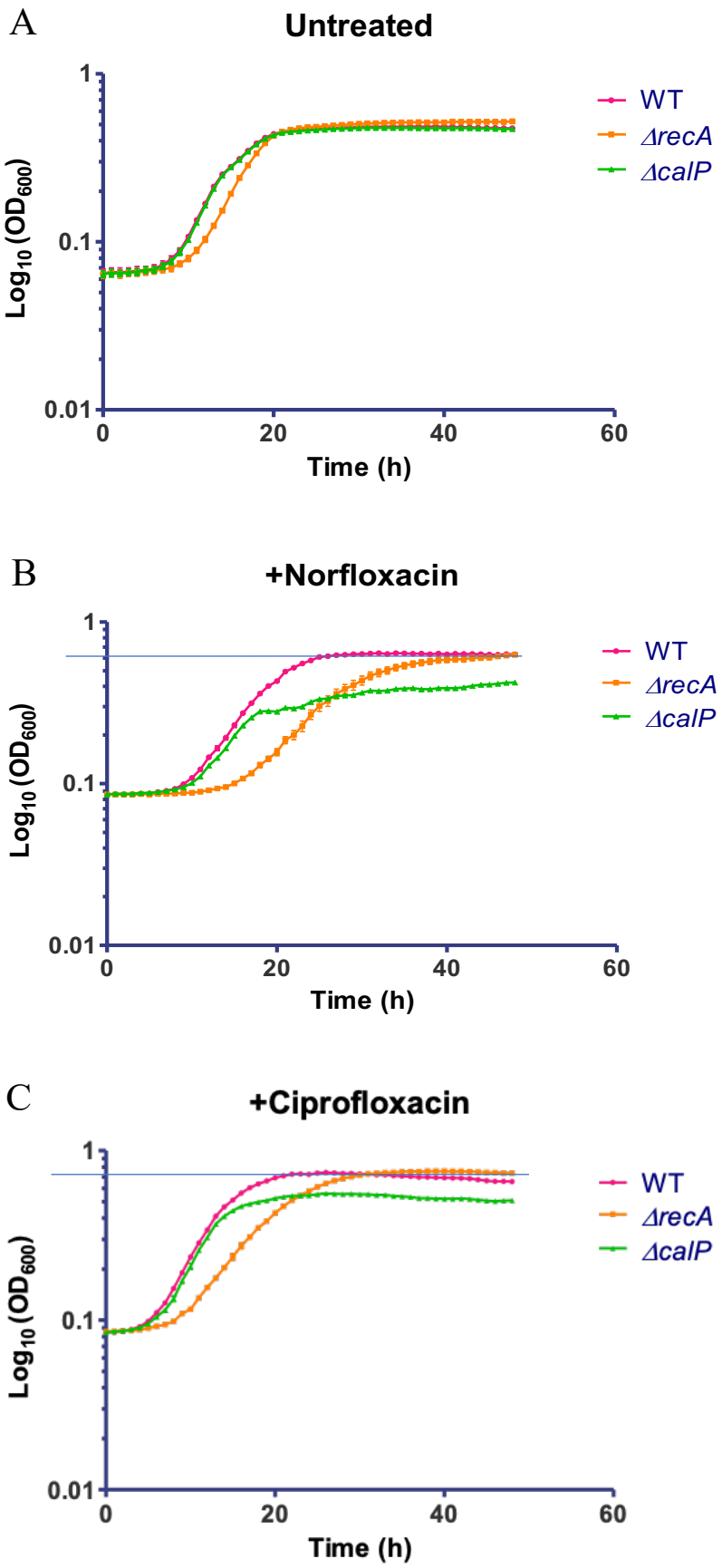
A
Untreated
1
0.1
0.01
Log10 (OD600)
0
20
40
60
Time (h)
WT
ΔrecA
ΔcalP
B
+Norfloxacin
1
0.1
0.01
Log10 (OD600)
0
20
40
60
Time (h)
WT
ΔrecA
ΔcalP
C
+Ciprofloxacin
1
0.1
0.01
Log10 (OD600)
0
20
40
60
Time (h)
WT
ΔrecA
ΔcalP

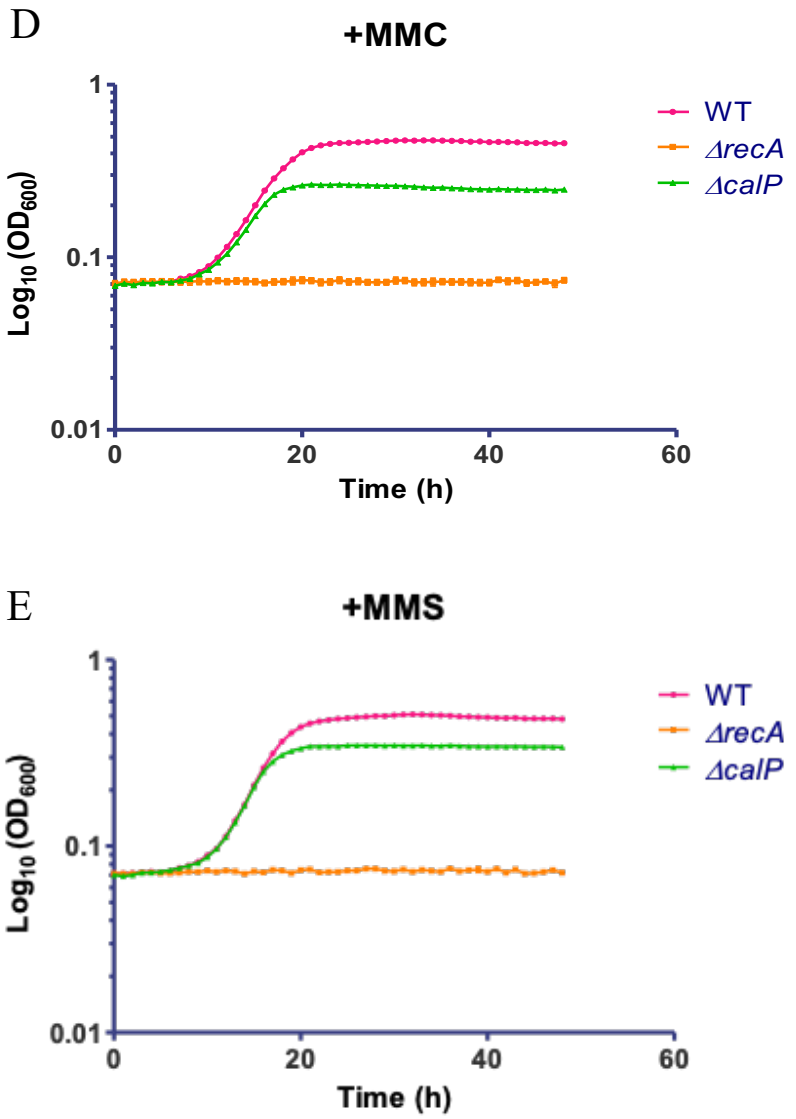

Fig. 9. The optical density of *ΔcalP* was lower than that of WT when exposed to norfloxacin, ciprofloxacin, MMC, or MMS in a liquid medium. Growth curves were generated for the evaluation of *ΔcalP* sensitivity in a liquid medium, with WT and *ΔrecA* serving control strains. Cells were cultivated to mid-exponential phase and subsequently diluted to an $OD_{600}=3.3\cdot10^{-4}$. Cells were mixed with the appropriate DDA and incubated for 48 hrs at 30°C. Hourly OD_{600} measurements were taken, and the mean OD_{600} value was calculated using three technical replicates. PYE medium was supplemented with (A) no additives, (B) 4 µg/mL norfloxacin, (C) 1 µg/mL ciprofloxacin, (D) 0.12 µg/mL MMC, and (E) 1 mM MMS.

2.3 *ΔcalP* showed a similar phenotype to WT when exposed to several non-DNA-damaging agents

Sensitivity assays of *C. crescentus in vivo* demonstrated that *calP* is important to maintain proper cell fitness in the presence of DDA and might be involved in DNA damage tolerance/repair. We wondered whether *calP* is specific for DNA damage/tolerance repair, so it is only affected by DDAs or whether it plays a more generalist role in stress response and is also affected by non-DDAs. To answer this question, I performed sensitivity assays with HU, novobiocin, H_2O_2, and NaClO, which have different modes of action and generate distinct types of cellular stress. For the analysis of the results of this experiment, I followed the same criteria I followed in the assays from section 2.2. Similarly, I employed the same strains (WT, Δ*recA*, and Δ*calP*) as in the previous tests from section 2.2. Strains were cultivated to mid-exponential phase in unsupplemented medium (Fig. 10A) or medium supplemented with 9 µg/mL HU (Fig. 10B), 0.5 µg/mL novobiocin (Fig. 10C), 0.15% H_2O_2 (Fig. 10D), and 15 µL 6-14% NaClO (Fig. 10E). Cultures were incubated at 30ºC for 48 hrs and the OD_{600} was monitored hourly. The drug-free medium did not show any difference in the sensitivity of WT, Δ*recA,* or Δ*calP* (Fig. 10A). In the presence of hydroxyurea, the WT, Δ*recA,* and Δ*calP* strains showed a similar $OD_{600}\approx0.7$ in the stationary phase (Fig. 10B). Thus, Δ*calP* was not sensitive to HU and exhibited a WT-like phenotype (Fig. 10B). After exposure to novobiocin, both Δ*calP* and WT exhibited nearly zero optical density for the initial 20 hours, marking the onset of their exponential growth phase (Fig. 10C). After 30 hrs of inoculation, the $OD_{600}\approx0.2$ observed in both WT and Δ*calP* (Fig. 10C) was reduced by 3.5-fold compared to the $OD_{600}\approx0.7$ of the same strains in the drug-free medium at the same time point (Fig. 10A). Both strains reached the exponential phase with a similar $OD_{600}\approx0.7$ approximately 45 hrs post-inoculation in the presence of novobiocin (Fig. 10C). While in a drug-free medium, both WT and Δ*calP* took approximately 25 hours to reach a similar $OD_{600}\approx0.7$ (Fig. 10A), indicating a sensitivity of both strains only when exposed to DDA. Surprisingly, Δ*recA* entered the stationary phase approximately 15 hours earlier than WT or Δ*calP*, reaching an $OD_{600}\approx0.7$ after 30 hours of inoculation in the novobiocin-supplemented medium

(Fig. 10C). After 48 hours of novobiocin exposure, WT, Δ*recA*, and Δ*calP* displayed a similar OD_{600}≈0.7 (Fig. 10C). Upon entering the stationary phase 30 hours after inoculation, Δ*calP* exhibited an optical density of approximately 0.65 when exposed to H_2O_2 or NaClO (Figs. 10D, E). In comparison, WT displayed an optical density of OD_{600}≈0.5 under the same conditions (Figs. 10D, E). In the presence of H_2O_2 and NaClO, Δ*recA* displayed an initial lag in the OD_{600} compared to WT or Δ*calP*, which subsequently increased to OD_{600}≈0.75 48 hrs after incubation (Fig. 10D, E). In summary, Δ*calP* showed no sensitivity compared to WT when exposed to novobiocin, HU, H_2O_2, NaClO, or when left untreated (Fig. 10A, B, C, D, and E).

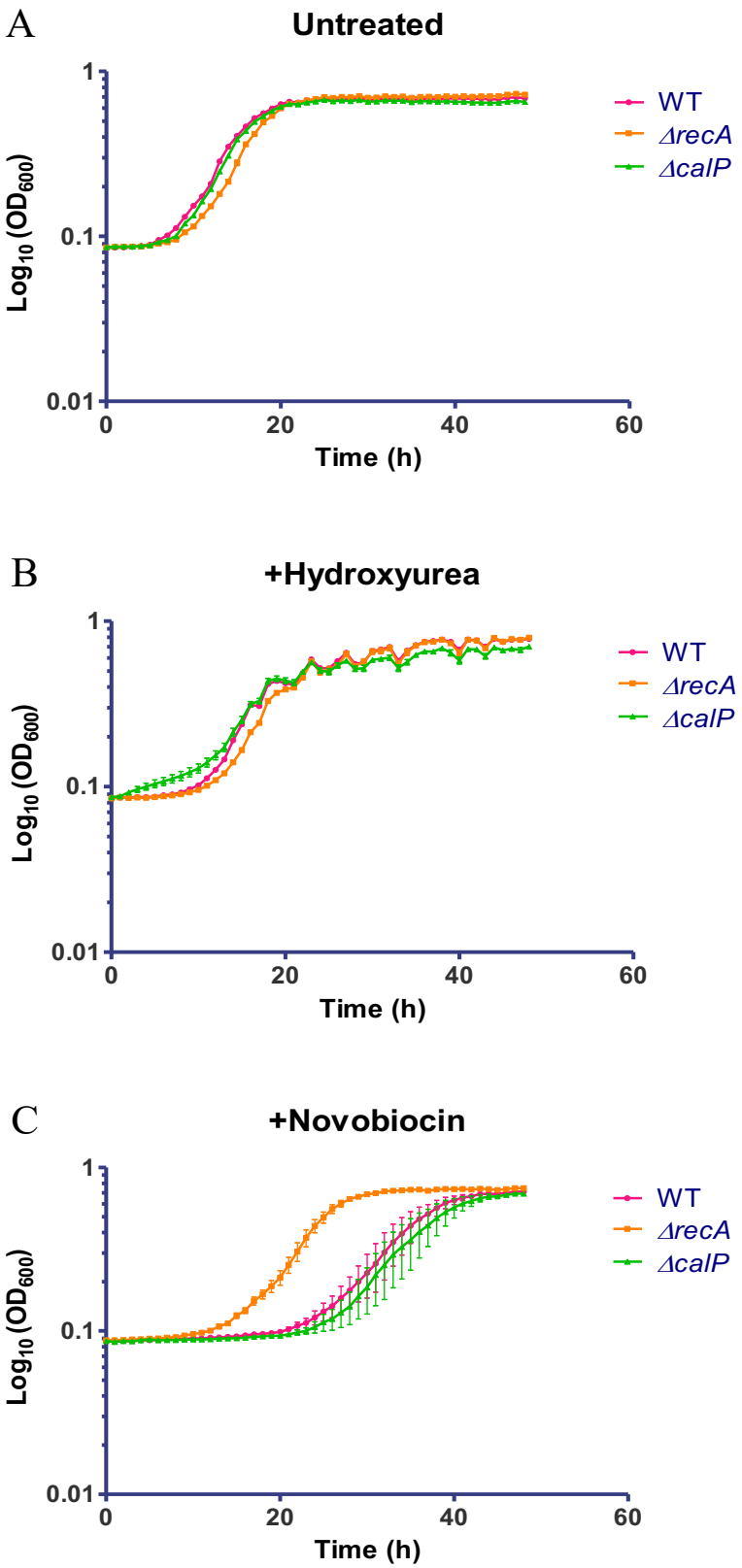
A
Untreated
1
0.1
0.01
Log10 (OD600)
0
20
40
60
Time (h)
WT
ΔrecA
ΔcalP
B
+Hydroxyurea
1
0.1
0.01
Log10 (OD600)
0
20
40
60
Time (h)
WT
ΔrecA
ΔcalP
C
+Novobiocin
1
0.1
0.01
Log10 (OD600)
0
20
40
60
Time (h)
WT
ΔrecA
ΔcalP

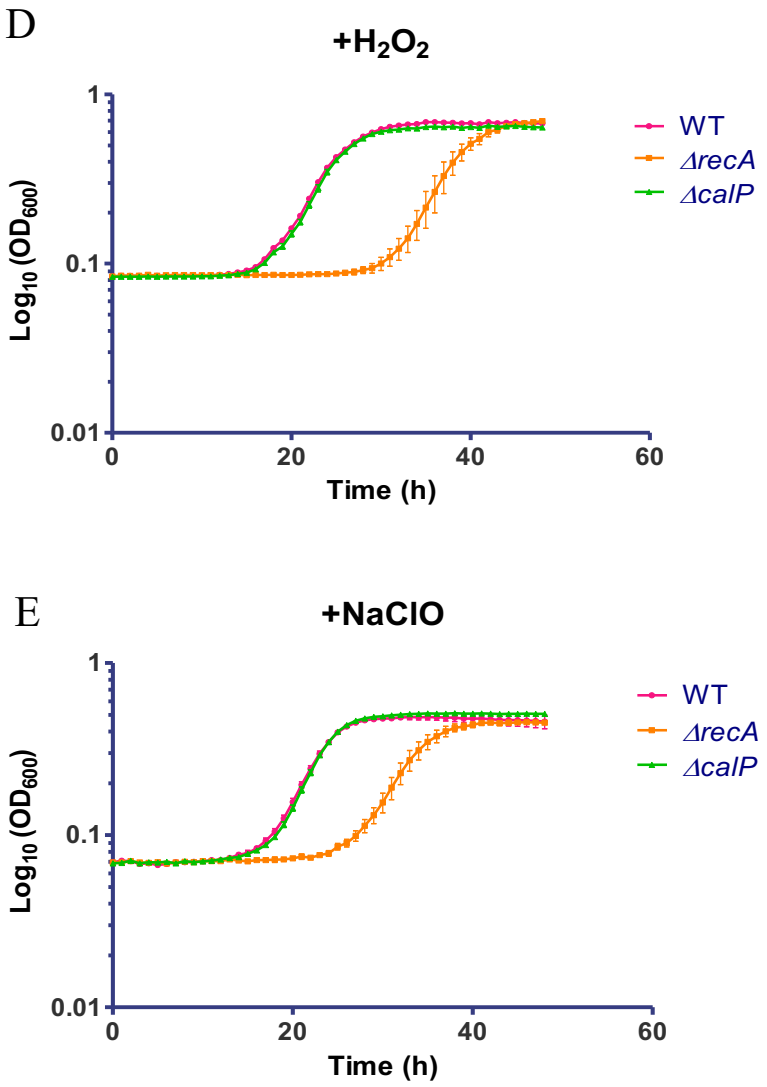

Fig. 10. *ΔcalP* is not sensitive to the non-DNA damaging agents HU, novobiocin, H_2O_2, or NaCl in a liquid medium. Growth curves were plotted to evaluate the sensitivity of *ΔcalP* in a liquid medium under the influence of various non-DNA damaging compounds, including HU, novobiocin, H_2O_2, or NaClO. Control strains included WT and *ΔrecA*. Cells were grown to mid-exponential phase and then diluted to $OD_{600}=3.3\cdot10^{-4}$. Cells were incubated with the respective compound for 48 hrs at 30°C and OD_{600} measurements were recorded hourly. Three technical replicates were used to calculate the OD_{600} mean. The liquid PYE medium was prepared in the following variations: (A) unsupplemented; or supplemented with (B) 9 µg/mL HU, (C) 0.5 µg/mL novobiocin, (D) 0.15% H_2O_2, and (E) 15 µL 6-14% NaClO.

Price et al. (2018) performed a high-throughput transposon mutagenesis of thousands of bacterial genes [585]. To do so, they tested the sensitivity of cells carrying mutations in single genes by treating cells with hundreds of compounds of different natures. Among these genes, they tested Δ*calP* in *C. crescentus,* which exhibited consistent sensitivity across various compounds, including carbon and nitrogen sources, variation in pH, and antibiotics. Antibiotics like tetracycline, spectinomycin, gentamicin, or nalidixic acid are cytotoxic compounds that do not directly impact DNA integrity and do not induce sensitivity in *ΔcalP*. In contrast, cisplatin (2.5 and 5 µg/mL) reduced Δ*calP* sensitivity [585] (Fig. 11). Fig. 11 displays the most toxic compounds on the bottom left side and the less harmful compounds on the top right side. The two blue dots corresponding to 5 µg/mL of cisplatin are located at the bottom left corner close to the Y-axis. The leftmost dot represents *ΔrecA*, indicating sensitivity, while the rightmost dot represents *ΔcalP*). The two blue dots corresponding to 2.5 µg/mL of cisplatin are positioned closer to the middle of the X-axis. The left dot represents *ΔrecA,* while the right dot represents *ΔcalP*. Hence, apart from Cisplatin, no other compound tested by Price et al. (2018), seemed to impact the viability of *C. crescentus* Δ*calP* [585]. These results are consistent with previous assays in which only DNA-damaging agents showed toxicity to Δ*calP* (Figs. 8-10). These results, together with DDAs sensitivity tests, in which Δ*calP* showed altered sensitivity in the presence of DDAs, suggest that *calP* may have a specific role related to DNA-damage tolerance/repair in *C. crescentus*.

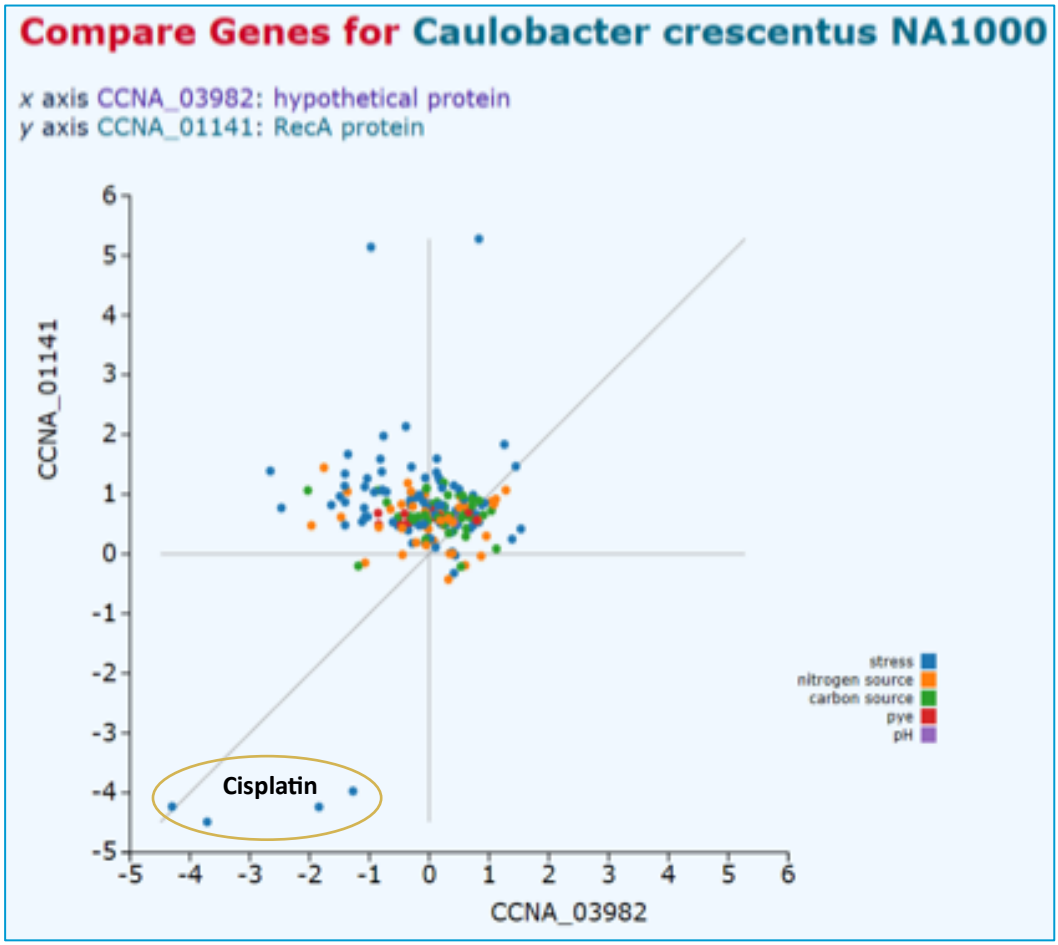

Fig. 11. *ΔcalP* showed a sensitivity similar to WT when exposed to several non-DNA damaging agents but exhibits sensitivity only with the DNA-damaging agent cisplatin [585]. Plot comparing *C. crescentus ΔcalP* and *ΔrecA* sensitivity following treatment with different types of compounds. Compounds are categorised into five groups based on their impact on the cell, represented by different colour dots: stress (blue), nitrogen source (orange), carbon source (green), PYE medium (red (for control)), and pH (purple). The X-axis indicates the sensitivity of *ΔcalP (CCNA_03982)*, while the Y-axis indicates the sensitivity of *ΔrecA (CCNA_01141)*. Dots closer to the bottom left corner indicate compounds that induced a greater toxicity compared to those located above closer to the right side of the table. The yellow circle highlights the most sensitive area caused by the compound.

2.4 Complementation of Δ*calP* successfully rescues the WT phenotype in the presence of MMC

Previous results showed that the deletion of *calP* negatively affected *C. crescentus* fitness in the presence of DDA. To validate whether *calP* is the gene responsible for causing the sensitivity in previous assays, I performed a complementation assay and challenged *ΔcalP* cells with MMC. I inserted *calP* under a xylose-inducible promoter (P_{xyl}) at the *xylX* locus in a *C. crescentus ΔcalP* background (*ΔcalP*::P_{xyl}-*calP*). I included WT, *ΔrecA*, and *ΔcalP*::P_{xyl}-*ø* as control strains. I grew cells to mid-exponential phase and incubated cultures at 30ºC for 48 hrs in a solid or liquid medium. To test the phenotype of the complemented strain and the controls I streaked cells on a solid agar medium supplemented with 0.3% xylose (to induce *calP* expression) and 0.25 µg/mL MMC when necessary. The addition of xylose induces the expression of *calP,* which was ectopically inserted under the P_{xyl} promoter. The P_{xyl} promoter allows the controlled expression of any gene inserted downstream of its sequence [586], like *calP* in this case. We observed that WT, *ΔrecA*, *ΔcalP*, or *ΔcalP*::P_{xyl}-*calP* were not sensitive in the xylose-supplemented medium (Fig. A1A). However, Δ*calP* showed a clear reduction in the size and number of isolated colonies in the presence of norfloxacin or MMC (Figs. A1B, C). In contrast, *ΔcalP*::P_{xyl}-*calP* displayed a phenotype that resembles the WT control strain in the presence of norfloxacin or MMC, forming thick isolated colonies (Figs. A1B, C). The similarity between the phenotypes observed in WT and *ΔcalP*::P_{xyl}-*calP* suggests that the insertion of *calP* back into the *C. crescentus* genome notably increased cell resistance to norfloxacin or MMC (Figs. A1B, C). *ΔrecA* exhibited very small-sized colonies when exposed to norfloxacin (Fig. A1B) and no colonies when exposed to MMC (Figs. A1B, C). On the contrary, *ΔrecA* in the antibiotic-free medium exhibited a similar colony size compared to WT (Fig. A1A). The fact that the *ΔrecA* control strain had a reduced colony size in the presence of norfloxacin or MMC confirmed that DNA-damage deficient cells were sensitive when exposed to both compounds (Figs. A1B, C). The strains did not show any sensitivity in the drug-free medium supplemented with xylose, indicating that the reduction in the colony size of cells was caused by the presence of antibiotics (Figs. A1A, B, C). Thus, our observations indicate that *calP* is important for survival in

the presence of DNA-damaging agents. Restoration of *C. crescentus* sensitivity by ectopically expressing *calP* in a *ΔcalP* background when challenged with norfloxacin or MMC in a solid medium suggests that the phenotype was not caused by a polar effect on genes downstream of *calP* (Figs. A1B, C).

For the complementation assay in a liquid medium, I used the target strain *ΔcalP*::P_{xyl}-*calP* alongside WT, *ΔrecA*, and *ΔcalP* as control strains (Fig. 7). Additionally, I inserted the empty vector pXYFPC-2 into the *ΔcalP* background of *C. crescentus* to add it as a control strain. I analysed the results by applying the same criteria for the exponential and stationary phases and comparing two strains with the ratio of optical densities as in the experiments from section 2.2. I grew cells to mid-exponential phase in a liquid medium. I challenged cells with 0.4 μg/mL norfloxacin, 0.12 μg/mL MMC, or 0.1% xylose (to induce *calP* expression) when necessary. Cultures were incubated at 30ºC for 48 hrs in an automated plate reader and the OD_{600} was monitored hourly. All strains exhibited a WT phenotype in the unsupplemented (Fig. 12A; Fig. A2A) and xylose-supplemented media (Fig. 12B; Fig. A2B). Following norfloxacin exposure, *ΔcalP, ΔcalP*::*ø,* and *ΔcalP*::P_{calP}-*calP* showed a maximum OD_{600}≈0.23 at the beginning of the stationary phase 15 hrs after inoculation. However, WT appeared unaffected by norfloxacin, reaching a maximum OD_{600}≈0.4 after 22 hours upon entering the stationary phase (Fig. A2, C). The optical density of WT upon norfloxacin exposure was 1.74-fold higher than that of *ΔcalP, ΔcalP*::*ø,* and *ΔcalP*::P_{calP}-*calP* (Fig. A2, C). This discrepancy arose from the distinct timing of entry into the stationary phase between *ΔcalP, ΔcalP*::*ø,* and *ΔcalP*::P_{calP}-*calP* at 16 hours post-inoculation and WT, which entered at 22 hours post-inoculation (Fig. A2C). Intriguingly, at 45 hours, *ΔrecA* displayed a peak OD_{600}≈0.35, similar to WT, and notably higher than *ΔcalP, ΔcalP*::*ø,* and *ΔcalP*::P_{calP}-*calP* during the exponential phase under norfloxacin exposure (Fig. A2C). However, when exposed to xylose and norfloxacin combined, *ΔcalP*::P_{calP}-*calP* also reached the maximum OD_{600}≈0.4 observed in *ΔrecA* (Fig. A2C). The treatment with xylose allowed *ΔcalP*::P_{calP}-*calP* to restore the WT phenotype when exposed to norfloxacin and reached an OD_{600}≈0.45 comparable to that of WT (Fig. A2D). This occurred because the supplementation with xylose induced the

expression of *calP*, which was under the xylose-inducible promoter P_{xyl}. *ΔcalP* and *ΔcalP*::*ø* could not rescue the WT phenotype despite the addition of xylose when exposed to norfloxacin, likely because of the absence of *calP* in the genome (Fig. A2D). The OD_{600}≈0.32 observed in *ΔcalP* and *ΔcalP*::*ø* was 1.4-fold lower than the OD_{600}≈0.45 of WT and *ΔcalP*::P_{calP}-*calP* when exposed to norfloxacin and xylose after 45 hrs (Fig. A2D). Hence, the *C. crescentus* strains expressing *calP* exhibited an optical density 1.4-fold higher than the strains lacking *calP* expression in the presence of both norfloxacin and xylose (Fig. A2D).

After exposure to MMC, WT reached an OD600≈0.7 at the 40-hour mark post-inoculation (Fig. 12A). WT exhibited an OD600≈0.7 in the presence of MMC (Fig. 12C), resembling its behaviour in the drug-free medium (Fig. 12A). *ΔcalP*, *ΔcalP*::*ø*, and *ΔcalP*::P_{calP}-*calP* exhibited an OD_{600}≈0.43 40 hours post-inoculation in the presence of MMC, representing a reduction of 1.63-fold compared to the OD_{600}≈0.7 observed in WT (Fig. 12C). *ΔcalP*::P_{calP}-*calP* did not show sensitivity to MMC upon addition of xylose (Fig. 12D). Xylose induced the expression of *calP* and rescued the WT phenotype. WT and *ΔcalP*::P_{calP}-*calP* were unaffected when treated with the combination of xylose and MMC compared to WT and *ΔcalP*::P_{calP}-*calP* in the untreated medium (Figs. 12A, D). WT and *ΔcalP*::P_{calP}-*calP* exhibited overlapping plot lines (OD_{600}≈0.75) during the stationary phase when exposed to xylose and MMC combined (Fig. 12D). They displayed a phenotype similar to that observed in the compound-free medium (Fig. 12A, D). Nevertheless, both *ΔcalP* and *ΔcalP*::*ø* exhibited an OD_{600}≈0.5 when exposed to a combination of xylose and MMC after 30 hrs (Fig. 12D). The OD_{600}≈0.5 observed in both *ΔcalP* and *ΔcalP*::*ø* represented a reduction of 1.6-fold compared to the OD_{600}≈0.75 seen in WT or *ΔcalP*::P_{calP}-*calP* when exposed to the combined challenge of xylose and MMC (Fig. 12D). The lower optical density observed in populations of *ΔcalP* and *ΔcalP::ø* compared to WT or *ΔcalP*::P_{calP}-*calP* suggests that the absence of *calP* negatively impacts *C. crescentus* when exposed to MMC (Fig. 12D). The OD_{600} value observed in *ΔcalP* and *ΔcalP*::*ø* with MMC (OD_{600}≈0.5) differs from that of both strains in the free-antibiotic medium (OD_{600}≈0.7). This contrast suggests that the sensitivity observed with MMC

resulted from the exposure to this compound (Fig. 12A, D). *ΔcalP* and *ΔcalP*::*ø* initiated an early stationary phase after 19 hours under MMC challenge, whereas WT and *ΔcalP*::P_{calP}-*calP* entered this phase after 27 hours (Fig. 12D). The early entry of *ΔcalP* and *ΔcalP*::*ø* in the stationary phase when exposed to norfloxacin or MMC caused a stall in the exponential phase (Fig. 12C, D; Fig. A2C, D). This phenotype may have arisen due to DNA damage-induced cell growth arrest, preventing the transmission of DNA errors to subsequent generations. *ΔrecA* exhibited high sensitivity to MMC, displaying no net increase in optical density whether exposed or not to xylose (Figs. 12C, D). This indicates that the drug actively affected DNA-damage-sensitive cells. The complementation of *ΔcalP* with calP successfully restored the WT phenotype, equipping the cells with the ability to withstand both MMC and norfloxacin. This evidence confirms that *calP* is the gene accountable for counteracting the effects of DDAs, rather than being a consequence of genes downstream of *calP* in the genome causing a polar effect. Hence, our findings suggest that *calP* contributes to DNA damage tolerance/repair in *C. crescentus*, playing a vital role in survival when exposed to DNA-damaging agents in a liquid medium. These results are consistent with those obtained in the sensitivity assays in a solid medium.

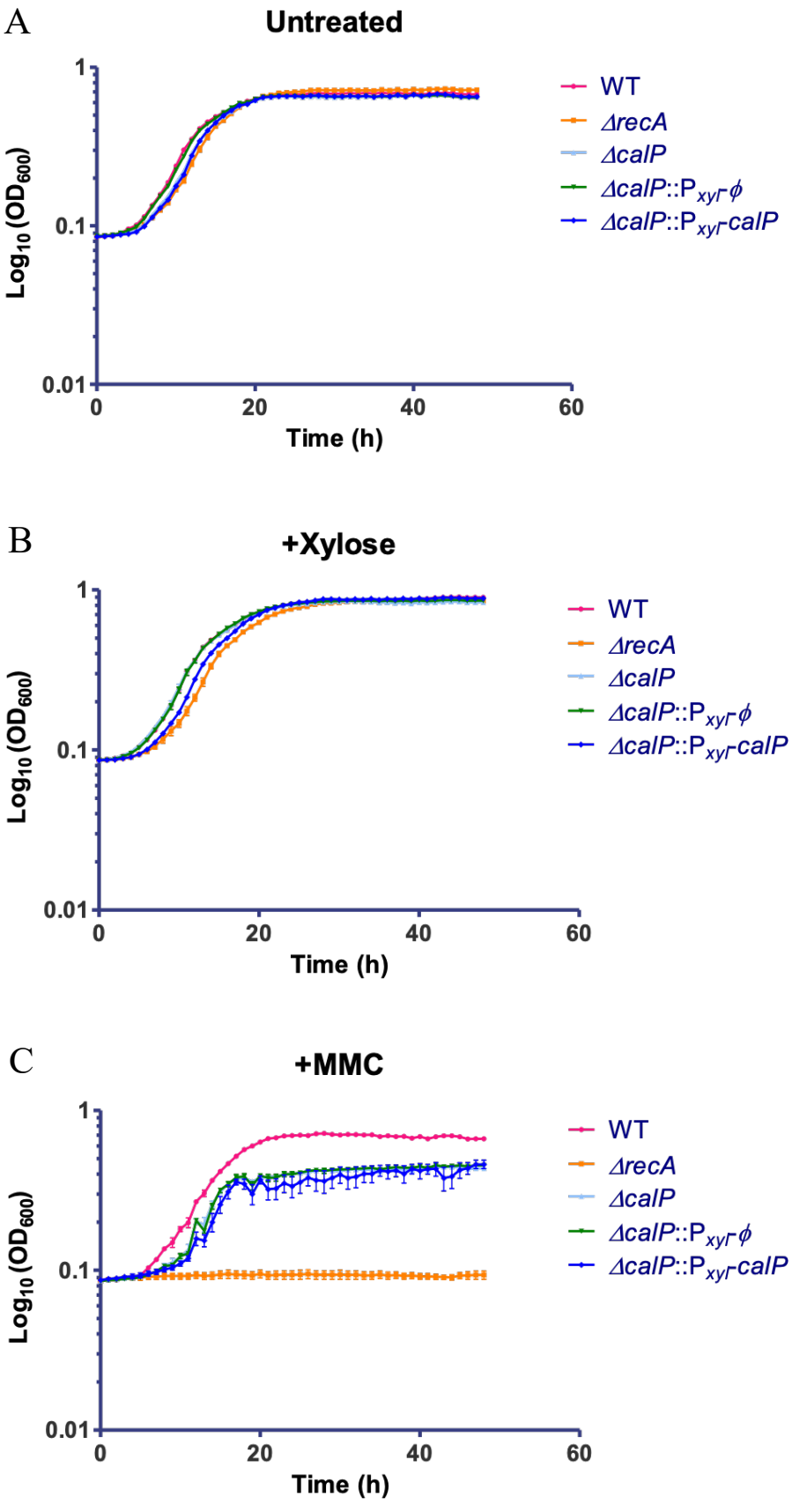
A
Untreated
Log10 (OD600)
1
0.1
0.01
0
20
40
60
Time (h)
WT
ΔrecA
ΔcalP
ΔcalP::Pxyl-ϕ
ΔcalP::Pxyl-calP
B
+Xylose
Log10 (OD600)
1
0.1
0.01
0
20
40
60
Time (h)
WT
ΔrecA
ΔcalP
ΔcalP::Pxyl-ϕ
ΔcalP::Pxyl-calP
C
+MMC
Log10 (OD600)
1
0.1
0.01
0
20
40
60
Time (h)
WT
ΔrecA
ΔcalP
ΔcalP::Pxyl-ϕ
ΔcalP::Pxyl-calP

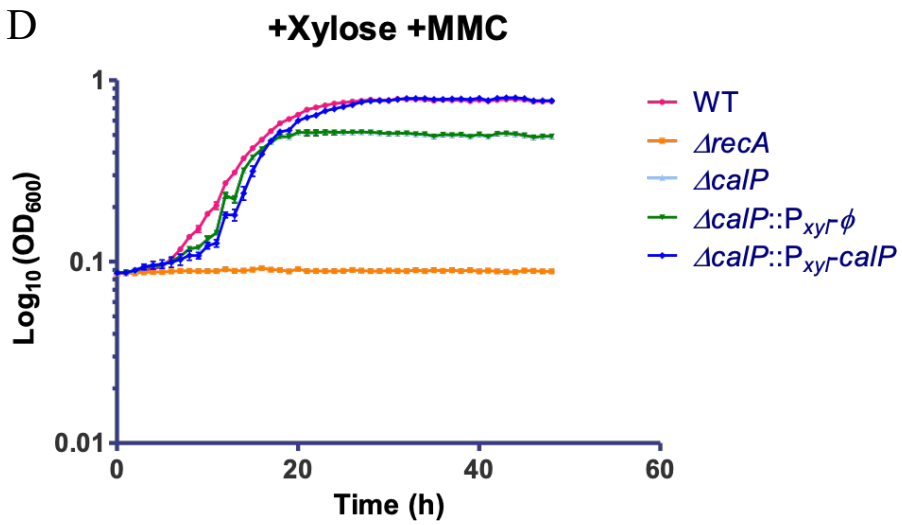

Fig. 12. Ectopic expression of *calP* increases *ΔcalP* tolerance to MMC. Growth curve analysis conducted to evaluate the complementation of *ΔcalP::*P_{xyl}*-calP*, both in the presence and absence of 0.12 µg/mL MMC in a liquid medium. WT, *ΔrecA, ΔcalP,* and *ΔcalP::*P_{xyl}*-ø* were used as control strains. *calP* expression in strains carrying the xylose-inducible promoter pXYFPC-2 vector was induced by supplementing the medium with 0.1% xylose when necessary. Cells were grown to mid-exponential phase in a PYE medium to an OD_{600}≈0.5, and cultures were diluted to an $OD_{600}=3.3\cdot10^{-4}$. Cells were mixed with 0.12 µg/mL MMC when needed and incubated for 48 hrs at 30°C before measuring OD_{600} hourly. Three technical replicates were used to calculate the OD_{600} mean. The medium contained (A) no additives, (B) 0.1% xylose, (C) 0.12 µg/mL MMC, and (D) 0.1% xylose and 0.12 µg/mL MMC.

2.5 The complementation of Δ*calP* with *scrambled calP* successfully restores the WT phenotype in the presence of MMC

RNAs do not always translate to proteins; occasionally, ORFs encode ncRNAs that play regulatory roles rather than proteins. An ncRNA may play an active role in the DNA damage response system in *C. crescentus* [444]. To distinguish between these two possibilities, I chemically synthesised the *scrambled calP* (*scr calP*), in which its original nucleotide sequence was scrambled while maintaining the original codons (Fig. 13A). Because of the redundancy in the genetic code, a different combination of nucleotides in the codon sequence can translate the same amino acid. In this way, the amino acid sequence remains unchanged (Fig. 13A). Nonetheless, a different nucleotide sequence originates an altered secondary structure of a putative ncRNA (Fig. 13B) different from the original *calP* (Fig. 13C). I reason that in a scenario where *ΔcalP*::P_{calP}-*scr calP* successfully complemented Δ*calP* in a medium supplemented with MMC, *calP* would encode a protein. On the contrary, in a scenario in which *ΔcalP*::P_{calP}-*scr calP* did not complement *ΔcalP* when challenged with MMC, *calP* would encode a putative ncRNA. This second scenario may occur because changing the nucleotide sequence could disrupt the ncRNA's putative secondary structure, which is required for its function. I inserted *scrambled calP* at the *C. crescentus xylX* locus under the xylose-inducible promoter P_{xyl} (*ΔcalP*::P_{calP}-*scr calP*). I tested the complementation of *ΔcalP* in a sensitivity assay in a liquid medium treated with 0.12 μg/mL MMC or left untreated. I supplemented the medium with xylose when necessary to induce the expression of *scrambled calP*. WT, *ΔrecA, ΔcalP*, and *ΔcalP*::P_{calP}-*ø* were included in the sensitivity assay as control strains. To analyse the results, I proceeded the same way as in section 2.2 to define the exponential and stationary phases and to compare the ratio of optical densities between the two strains. WT, Δ*recA*, Δ*calP*, Δ*calP*::P_{calP}-*ø* and *ΔcalP*::P_{calP}-*scr calP* in the compound-free medium exhibited no sensitivity, showing all overlapping curves (Fig. 14B). In the presence of MMC, both WT and *ΔcalP*::P_{calP}-*scr calP* strains showed a doubling in the OD_{600} to approximately 0.46 during the stationary phase after 20 hrs, whereas *ΔcalP* and *ΔcalP*::P_{calP}-*ø* strains maintained an OD_{600} approximately 0.23 (Fig. 14C). *ΔcalP* and *ΔcalP*::P_{calP}-*ø* prematurely entered the stationary phase when treated with MMC after 18 hrs (Fig.

14C). This drop in the optical density increase of *ΔcalP* and *ΔcalP*::P_{calP}-*ø* may occur because the *calP* absence allows the accumulation of DNA damage followed by cell arrest (Fig. 14C). Conversely, *ΔcalP*::P_{calP}-*scr calP* did not show sensitivity when challenged with MMC, showing an OD_{600}≈0.46 similar to WT and successfully complementing the *ΔcalP* background with *scr calP* (Fig. 14C). *ΔcalP*::P_{calP}-*scr calP* showed the same phenotype as WT when exposed to MMC, even though no xylose was supplemented to the medium to promote the *scr calP* expression (Fig. 14C). This phenotype occurred likely due to a leaky expression of the P_{xyl} promoter that led to the *scr calP* transcription (Fig. 14C). All strains in the MMC medium without xylose and the MMC medium with xylose exhibited a similar phenotype (Figs. 14C, D). In summary, *ΔcalP*::P_{calP}-*scr calP* could successfully complement *ΔcalP* in the presence of MMC despite having a nucleotide sequence other than *calP* (Figs. 14C, D). Therefore, the restoration of the WT phenotype occurred due to the invariable codon sequence of *calP*, demonstrating that *calP* encodes a protein instead of an ncRNA (Figs. 14C, D). Δ*recA* was hypersensitive to MMC and did not increase the optical density, proving the toxic effect of MMC on DNA-damage-sensitive strains (Figs. 14C, D).

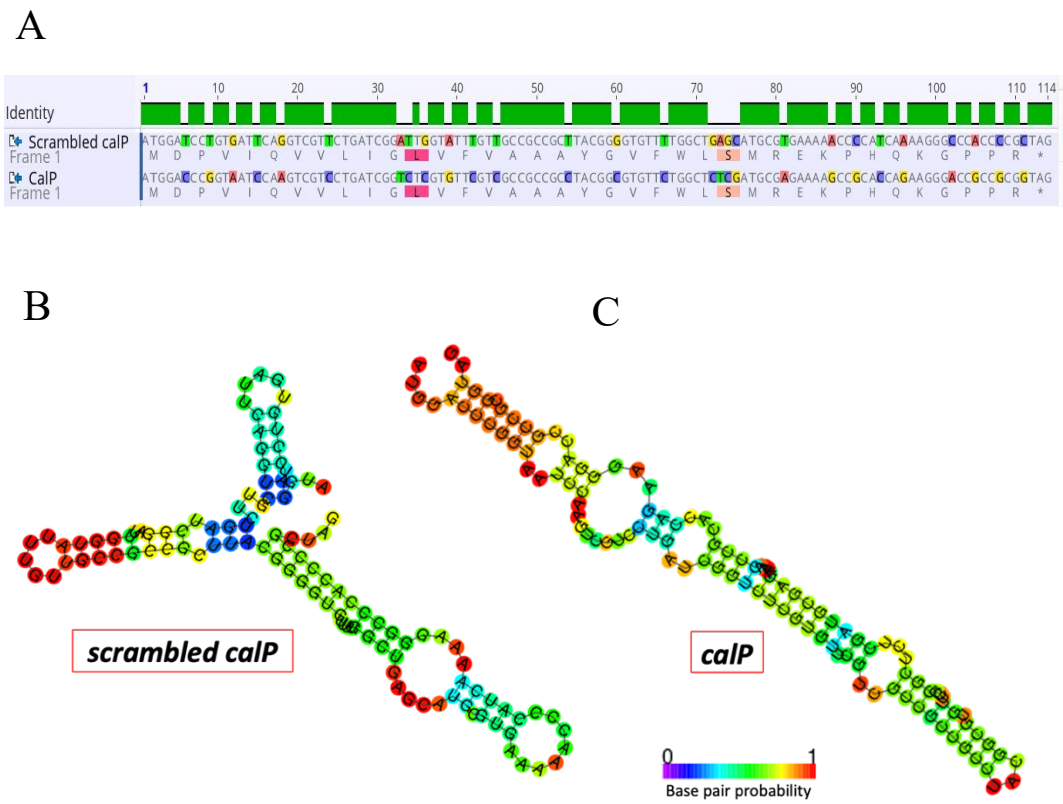

Fig. 13. The predicted secondary structure of a putative ncRNA was compared with the sequence of *calP,* which had been scrambled. This comparison aimed to assess whether *calP* encodes a non-coding RNA instead of a signal peptide (SP). The predictions were generated using Geneious Prime v. 2019 (Biomatters Inc.), a bioinformatic software for sequencing data analysis. (A) Pairwise alignment between the *scr calP* sequence (top) and the original *calP* sequence (bottom). (B) The predicted secondary structure of a putative ncRNA from the *scr calP* sequence. (C) The predicted secondary structure of a putative ncRNA from the original *calP* sequence. The base pair probability indicates the likelihood of a certain nucleotide being the correct one according to the prediction. The legend is represented from zero to one with a rainbow-colour range.

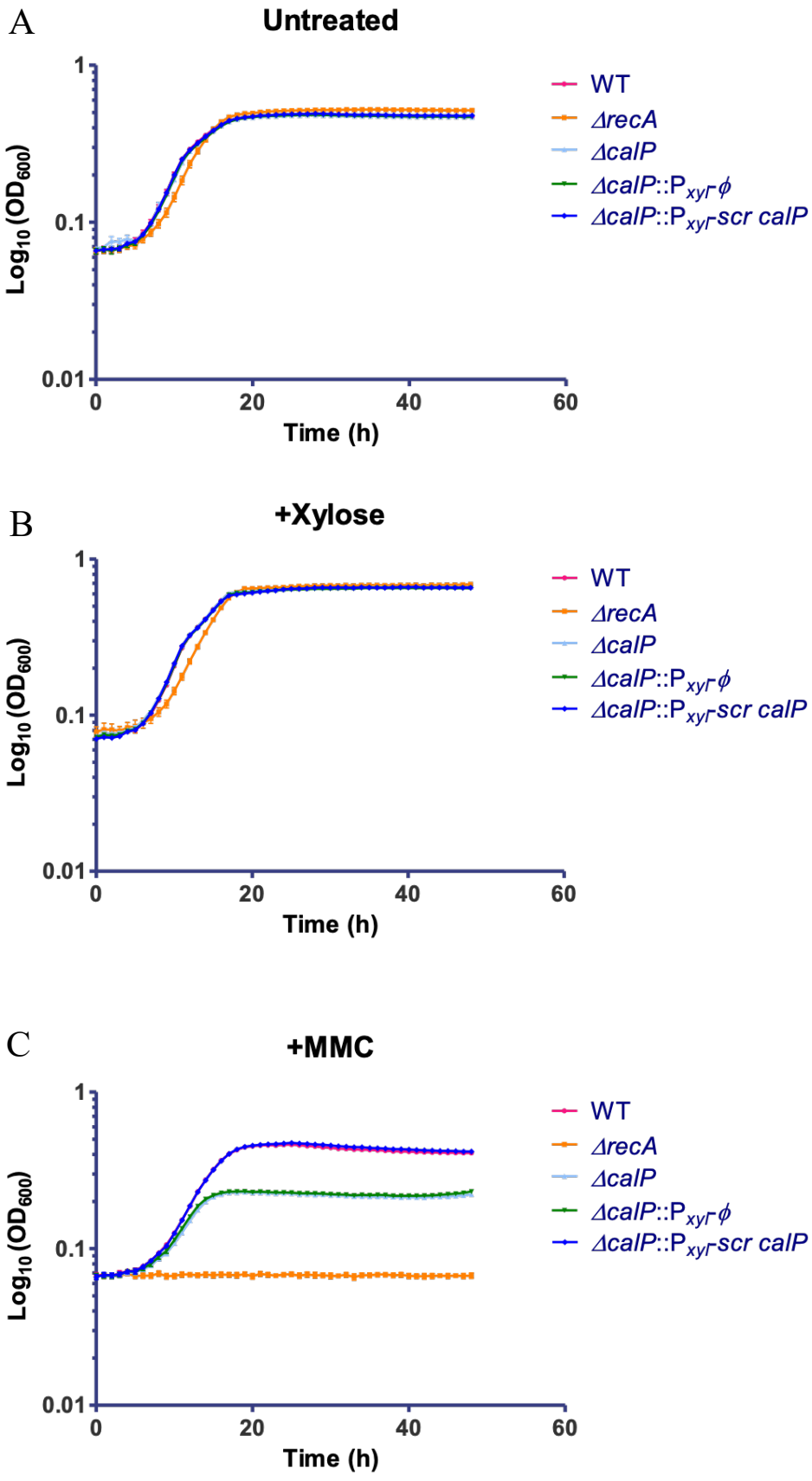
A
Untreated
Log10 (OD600)
1
0.1
0.01
0
20
40
60
Time (h)
WT
ΔrecA
ΔcalP
ΔcalP::Pxyl-ϕ
ΔcalP::Pxyl-scr calP
B
+Xylose
Log10 (OD600)
1
0.1
0.01
0
20
40
60
Time (h)
WT
ΔrecA
ΔcalP
ΔcalP::Pxyl-ϕ
ΔcalP::Pxyl-scr calP
C
+MMC
Log10 (OD600)
1
0.1
0.01
0
20
40
60
Time (h)
WT
ΔrecA
ΔcalP
ΔcalP::Pxyl-ϕ
ΔcalP::Pxyl-scr calP

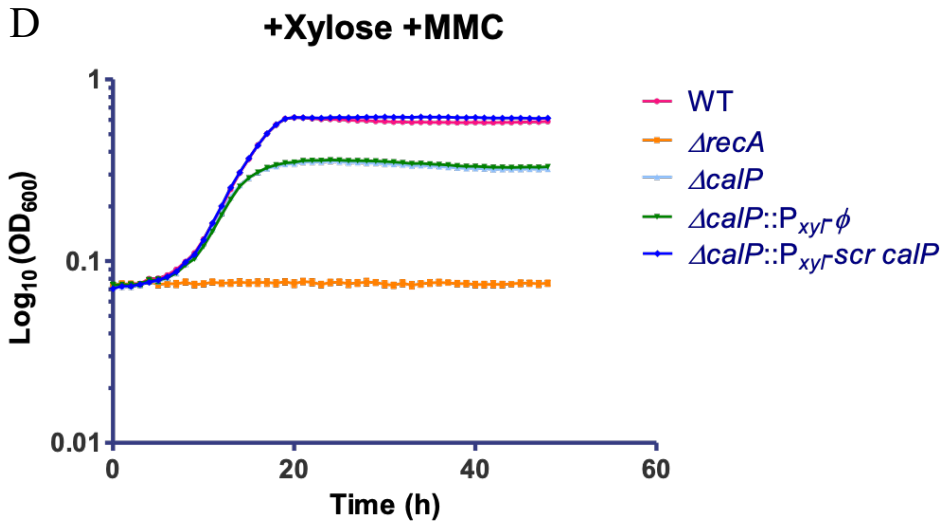

Fig. 14. *scrambled calP* cells do not show sensitivity in the presence of MMC. Analysis of the complementation of *ΔcalP*::P_{calP}-*scr calP* (blue line) in the presence and absence of 0.12 µg/mL MMC in a liquid medium. WT (magenta line), *ΔrecA* (orange line), *ΔcalP* (blue light line), and *ΔcalP*::P_{calP}-*calP* (green line) were used as control strains. The medium was supplemented with 0.1% xylose when necessary to induce *calP* expression, which was under the xylose-inducible promoter P_{xyl} carried in the plasmid pXYFPC-2. Cells were grown in a liquid PYE medium to mid-exponential phase and cultures were diluted to an $OD_{600}=3.3\cdot10^{-4}$. Cells were supplemented with MMC when needed and incubated for 48 hrs at 30°C. The OD_{600} was measured hourly and the results of the OD_{600} of three technical replicates were used to calculate the OD_{600} mean. Cells were grown in a medium with (A) no additives, (B) 0.1% xylose, (C) 0.12 µg/mL MMC, or (D) 0.12 µg/mL MMC and 0.1% xylose.

Complementation analysis with *scr calP* in a *C. crescentus* Δ*calP* background successfully restored the WT phenotype, suggesting that *calP* encodes a protein instead of an ncRNA. To further confirm that *calP* is transcribed and *calP* mRNA translated into CalP protein, I performed immunoblot assays to visualise CalP when cells were treated with MMC or left untreated (Fig. 15). For this analysis, I C-terminally *flag*-tagged *calP* and *scr calP.* Each variant was inserted under the native P_{calP} promoter (*ΔcalP*::P_{calP}-*calP-flag* and *ΔcalP*::P_{calP}-*scr calP-flag*) or at the *xylX* locus under the P_{xyl} promoter (*ΔcalP*::P_{xyl}-*calP-flag* and *ΔcalP*::P_{xyl}-*scr calP-flag*) in a *C. crescentus ΔcalP* background. I also included native *calP* under the P_{xyl} or P_{calP} promoter (*ΔcalP*::P_{calP}-*calP-flag* and *ΔcalP*::P_{xyl}-*calP-flag*) as complemented control strains, and WT and the empty plasmid strain *ΔcalP*::P_{xyl}-*ø* as untagged control strains. I grew cells to mid-exponential phase in a medium treated with 0.12 µg/mL MMC or left untreated. When necessary, strains with *calP* variants under the xylose-inducible promoter were supplemented with 0.1% xylose. Cells were homogenised, and lysates were run in a 4-20% Tris-glycine SDS-PAGE. Membranes were blotted against the α-FLAG/M2 antibody. The percentage shown on top of each bar is the relative value of brightness intensity of each band after normalisation compared to the brightness intensity of the protein band isolated from untreated cells (Figs 15B, D). The difference between the percentages of two band intensities of CalP was obtained by dividing the value of percentages of the strains treated with xylose and MMC combined, and the strains only treated with xylose. Native *calP* (*ΔcalP::*P_{xyl}-*calP-flag*) and *scr calP* (*ΔcalP::*P_{xyl}-*scr calP-flag*) expressed from P_{xyl} showed CalP bands when cells were exposed solely to xylose or xylose and MMC combined (Fig. 15A). Meanwhile, neither *ΔcalP*::P_{xyl}-*calP-flag* nor *ΔcalP*::P_{xyl}-*scr-calP-flag* showed CalP bands when exposed to MMC or left unexposed (Fig. 15A). MMC alone could not stimulate CalP production, a phenotype that was expected given the lack of xylose in the medium (Fig. 15B). After exposure to a combination of xylose and MMC, CalP production increased 8.69-fold in *ΔcalP::*P_{xyl}-*calP-flag* and 36.6-fold in *ΔcalP::*P_{xyl}-*scr calP-flag* compared to CalP production in both strains in the drug-free medium (Fig. 15B). Surprisingly, CalP production increased 2.18-fold in *ΔcalP::*P_{xyl}-*calP-flag* when MMC was added to the xylose-containing medium (Fig. 15B). Similarly, after

addition of MMC to the xylose-containing medium, CalP production increased by 4.96-fold (Fig. 15B). Intriguingly, CalP production increased by 4.21-fold when *ΔcalP::*P_{xyl}*-scr calP-flag* was treated with a combination of xylose and MMC in comparison to *ΔcalP::*P_{xyl}*-scr calP-flag* (Fig. 15B). MMC enhanced CalP production even though *calP* was inserted at the *xylX* locus. MMC should not play a role in the *calP* regulation since this expression takes place in a distinct genomic context other than the native *calP* locus. The increase in CalP production may occur because the CalP regulation with MMC might not just occur at the transcription level but at the translation level instead. This hypothesis would explain why *calP* expressed under a xylose-inducible promoter was found to enhance CalP production when exposed to a compound other than xylose. The untagged WT control strain showed no protein bands, confirming that the bands observed in the blot correspond to FLAG-tagged CalP (Fig. 15A). *calP* expressed from the native *calP* promoter (P_{calP}) produced CalP when cells were treated with MMC or left untreated (Fig. 15C). Indeed, MMC-treated cells exhibited a 4-fold increase in the band intensity of CalP and a 3.55-fold increase in scr CalP compared to the same proteins from untreated cells (Fig. 15D). Interestingly, there was only a 1.13-fold difference in the production of CalP and scr CalP between MMC-treated cells (Fig. 15D). This small difference in the CalP production indicates that the scrambling of *calP* did not affect CalP production even though the nucleotide sequence was shuffled. WT did not show any band in any condition since it was an untagged strain, confirming that the bands observed in the immunoblot correspond to CalP (Fig. 15C). In summary, the *calP* or *scr calP* production did not differ from each other regardless the treatment or not with MMC, suggesting that shuffling *calP* nucleotides while preserving the codon sequence did not affect the *C. crescentus* sensitivity (Fig. 15). Moreover, *calP* ectopically expressed from the *xylX* locus was induced by the xylose-inducible promoter (P_{xyl}). However, CalP production was higher when cells were exposed to xylose and MMC combined compared to the sole addition of xylose (Figs. 10A, B). Therefore, the CalP production was not only dependent on the xylose induction of P_{xyl} to express *calP* but was also influenced by MMC. This phenotype indicates that the CalP activation was MMC-dependent and possibly occurred in a posttranslational level (Figs. 15A, B). scr CalP produced in *ΔcalP*::P_{xyl}*-scr-calP-*

flag showed a band 4.21-fold more intense than CalP produced in *ΔcalP::*P_{xyl}*-calP-flag* following the exposition of cells to both xylose and MMC (Fig. 15B). The higher production of scr CalP when *scr calP* was expressed from the P_{xyl} promoter, may suggest deregulation of *calP* at the RNA level since the nucleotide scrambling may alter the correct regulation of *scr calP* (Fig. 15B). However, when exposed to the combination of xylose and MMC, the production of scr CalP decreased by 1.27-fold compared to CalP when both were expressed under the native *calP* promoter (Fig. 15B). Therefore, this phenotype does not correlate with the scr CalP production of *ΔcalP*::P_{xyl}*-scr-calP-flag*, indicating that the difference could have occurred at the transcriptional level (Figs. 15B, D). Alternatively, this phenotype could be an artefact caused by a higher induction of the xylose-inducible promoter P_{xyl} (Figs. 15A, B).

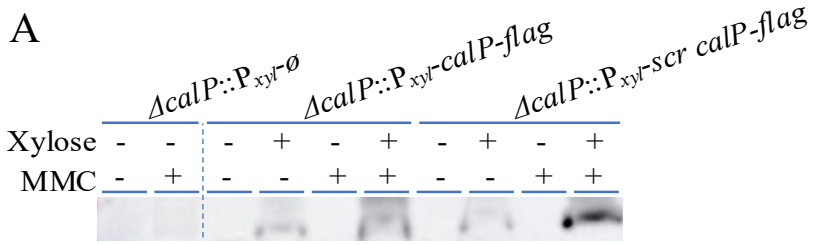
A
ΔcalP::P xyl-ø
ΔcalP::P xyl-calP-flag
ΔcalP::P xyl-scr calP-flag
Xylose - - - + - + - + - +
MMC - + - - + + - - + +

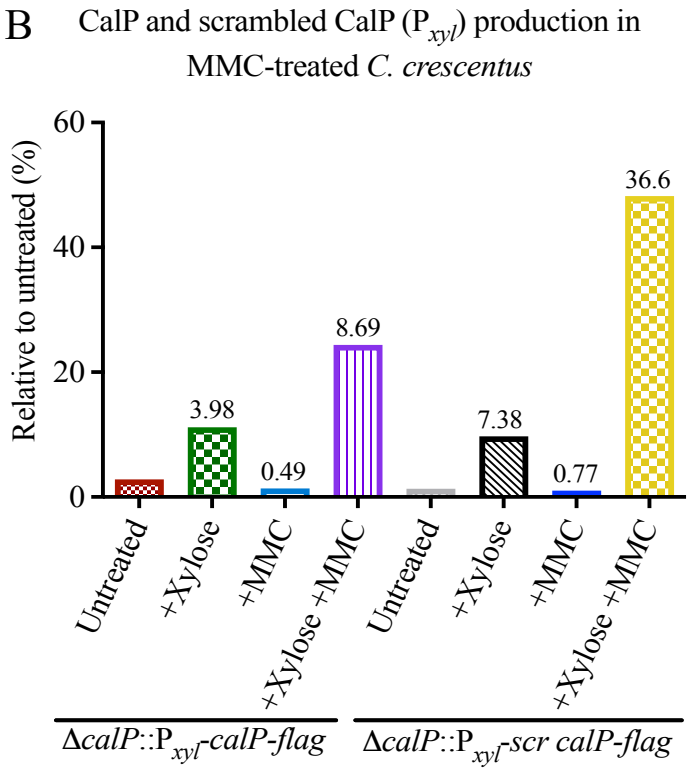
B
CalP and scrambled CalP (P xyl) production in
MMC-treated C. crescentus
Relative to untreated (%)
60
40
20
0
3.98
0.49
8.69
7.38
0.77
36.6
Untreated
+Xylose
+MMC
+Xylose +MMC
Untreated
+Xylose
+MMC
+Xylose +MMC
ΔcalP::P xyl-calP-flag
ΔcalP::P xyl-scr calP-flag

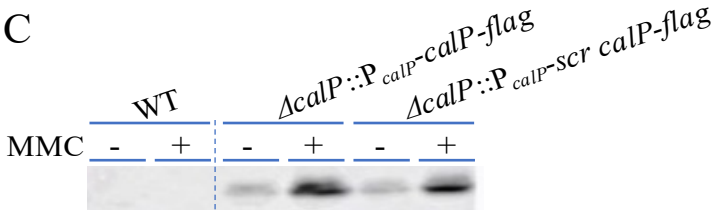
C
WT
ΔcalP::P calP-calP-flag
ΔcalP::P calP-scr calP-flag
MMC - + - + - +

D

CalP and scrambled CalP (P_{calP}) production in MMC-treated *C. crescentus*

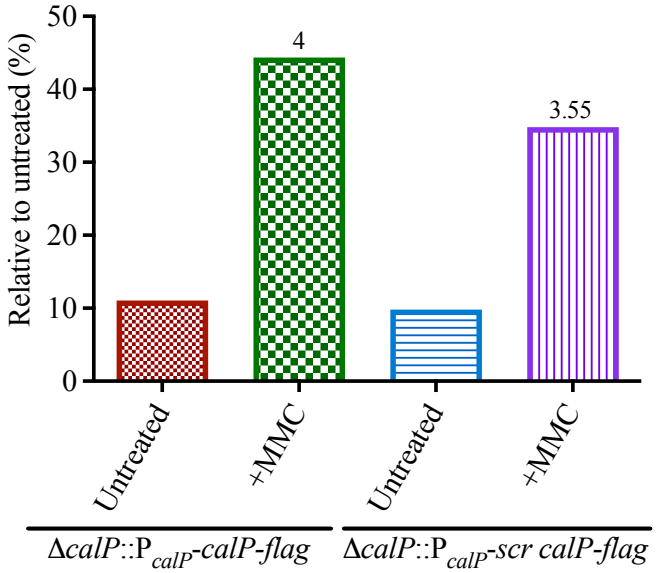

Fig. 15. *calP* shows a different polymerisation pattern expressed under different promoters. Different western blots assessing *C. crescentus* strains under different conditions. Cells were grown in a PYE medium to mid-exponential phase at 30ºC and exposed to 0.12 µg/mL MMC or unexposed. Samples were run in a 4-20% Tris-Glycine SDS-PAGE, and membranes were blotted against the α-FLAG antibody. (A) Immunoblot comparing *ΔcalP*::P_{xyl}-*ø* (Δ*calP* background complemented with empty vector pXYFPC-2), *ΔcalP*::P_{xyl}-*calP-flag* (Δ*calP* background complemented with *calP*), and *ΔcalP*::P_{xyl}-*scrambled calP-flag* (Δ*calP* background complemented with *scrambled calP*). These samples were expressed from the P_{xyl} promoter and arranged from left to right for comparison. Xylose-inducible strains *ΔcalP::*P_{xyl}-*calP-flag* and *ΔcalP::*P_{xyl}-*scrambled calP-flag* were treated with 0.1% xylose. (B) Column bar graph showing the relative percentage of CalP production in *C. crescentus* when exposed to MMC (Fig. A3A). The numbers on top of the bars indicate the relative difference compared to the drug-free control. The Y-axis displays the relative percentage of CalP production (%) out of 100%. The X-axis shows bars with untreated, xylose-treated, and/or MMC-treated *ΔcalP*::P_{xyl}-*calP-flag* and

ΔcalP::P_{xyl}-*scrambled calP-flag*. (C) Immunoblot comparing WT, *ΔcalP*::P_{calP}-*calP-flag* (Δ*calP* background complemented with *calP*), and *ΔcalP*::P_{calP}-*scrambled calP-flag* (Δ*calP* background complemented with *scrambled calP*). These samples were expressed from the native P_{calP} promoter and arranged from left to right for comparison. (D) Column bar graph showing the relative percentage of CalP production in *C. crescentus* when exposed to MMC (Fig. S3B). The numbers on top of the bars indicate the relative difference compared to the drug-free control. The Y-axis displays the relative percentage of CalP production (%) out of 100%. The X-axis shows bars of MMC-treated or untreated *ΔcalP*::P_{calP}-*calP-flag* and *ΔcalP*::P_{calP}-*scrambled calP-flag*.

2.6 CalP production increases upon treating cells with DNA-damaging agents in *C. crescentus*

Previous *in vivo* assays showed a sensitivity of *C. crescentus ΔcalP* in the presence of DDA, while other *in vivo* assays demonstrated that the sensitivity of *ΔcalP* did not decrease when exposed to non-DDA. Thus, CalP plays an important role in the tolerance/repair of DNA damage in *C. crescentus*. I hypothesised that the CalP production would rise when cells are challenged with DDA but would remain low when exposed to non-DDA. To test CalP production when exposed to distinct DDAs, I immunoblotted a C-terminally FLAG-tagged CalP (Δ*calP*::P_{calP}-*calP-flag*) (Fig. 16). Mid-exponential phase cultures expressing a chromosomally encoded *calP* from its native locus and WT (control) were left unexposed to drugs, or exposed to 0.12 µg/mL MMC, 1.5 µg/mL MMS, 4 µg/mL norfloxacin, 15 µg/mL HU, or 0.5 µg/mL novobiocin. I homogenised cells and denatured proteins with an SDS/β-mercaptoethanol-containing buffer. I ran samples in a 4-20% Tris-Glycine SDS-PAGE for immunoblotting and incubated the membrane with an anti-FLAG antibody.

C-terminally FLAG-tagged CalP showed intense bands when cells were exposed to MMC, MMS, or norfloxacin (Fig. 16A). Δ*calP*::P_{calP}-*calP-flag* showed 8 KDa CalP monomeric bands and 60 KDa CalP polymeric bands when cells were in the presence or absence of each DDA (Fig. 16A). Furthermore, the 75 KDa CalP polymeric bands appeared only when cells were exposed to MMC, MMS, or norfloxacin. Nonetheless, these bands were absent when challenged with HU or novobiocin (Fig. 16A). As opposed to untreated cells, the brightness intensity of the 8 kDa monomeric CalP was only increased by a 1.34-fold when cells were treated with HU and 1.06-fold when treated with novobiocin (Fig. 16B). Meanwhile, compared to untreated cells, the 8 KDa monomeric CalP production increased by 3.08-, 3.94- and 2.3-fold in cells exposed to MMC, MMS, and norfloxacin, respectively (Fig. 16B). MMS was the antibiotic that provoked *C. crescentus* to produce the highest proportion of monomeric CalP. When *C. crescentus* was challenged with MMC and norfloxacin, CalP production was 1.28-fold and 1.71-fold lower, respectively, compared to CalP production induced by

MMS (Fig. 16B). Differential CalP production between cells exposed to distinct DDAs was greater with 60 KDa multimers. The CalP multimers showed an 8.13-, 7.23-, and 5.82-fold increase in brightness intensity with MMC, MMS, and norfloxacin, respectively, compared to untreated cells (Fig. 16C). However, the difference in CalP production of HU- or novobiocin-treated cells in comparison to untreated cells was 1.15- and 1.64-fold, respectively (Fig. 16C). The 75 KDa CalP multimeric band produced from cells challenged with MMC was the protein band with the highest intensity (Fig. 16C). The 75 KDa CalP multimeric band from MMC-treated cells was only 1.12- and 1.4-fold higher than CalP produced from cells challenged with MMS and norfloxacin, respectively (Fig. 16C). As opposed to untreated cells, the 75 KDa multimers showed greater production when generated from cells exposed to MMC, MMS, or norfloxacin (5.3-, 6.13-, and 3.52-fold increase, respectively), in comparison to HU or novobiocin (1.15- and 1.64-fold increase, respectively) (Fig. 16D). Proteins produced in cells exposed to HU or novobiocin had fewer bright bands than proteins isolated from cells exposed to MMC, MMS, or norfloxacin (Figs. 16A, B, C, D). This phenotype indicates that CalP production in cells challenged with HU or novobiocin resembled CalP production in an unsupplemented medium. These results suggest that HU and novobiocin did not promote CalP production, probably because they were not DDAs (Figs. 16). CalP isolated from untreated cells generated low-intensity bands (Fig. 16). Low-intensity CalP bands barely increased their intensity from the 8 KDa monomers (36.9%) to the 60 KDa polymers (42.2%) or the intensity was even reduced in the 75 KDa multimers (20.8%) (Fig. 16E). The band intensity in the monomer or multimers produced from cells exposed to novobiocin or HU- was similar to the intensity of CalP isolated from untreated cells (Figs. 16A, E). Nevertheless, multimeric CalP bands isolated from cells exposed to MMC increased their intensity in the 75 KDa multimer (28.8%) compared to the CalP monomeric bands (16.6%); especially in the 60 KDa multimer (54.6%) (Fig. 11F). Following exposition of cells to MMC, the 60 KDa CalP multimer increased brightness in a greater proportion than the 75 KDa multimer or the 10 KDa CalP monomer (Fig. 16A). This phenotype suggests that multimeric CalP may be the active form of CalP under DNA damage conditions. CalP monomeric and

multimeric bands isolated from MMC-treated cells showed an intensity similar to CalP isolated from cells exposed to MMS or norfloxacin (Figs. 16A-F). However, CalP produced in MMC-treated cells exhibited the brightest bands (Figs. 16A-F). Therefore, the production of 10, 60, and 75 KDa CalP multimers increased when cells were challenged with MMC, MMS, or norfloxacin (Figs. 16A-D, F). Thus, it is likely that the rise in CalP production is a cellular response to the presence of DDA. The untagged WT control did not show any band with the same size as CalP-tagged strains but only some unspecific bands of 18 and 42 KDa with every condition (Fig. 16A). The WT phenotype proves that the CalP-FLAG bands correspond to Δ*calP*::P_{calP}-*calP-flag* since they were the only FLAG-tagged strains in the immunoblot (Fig. 16A).

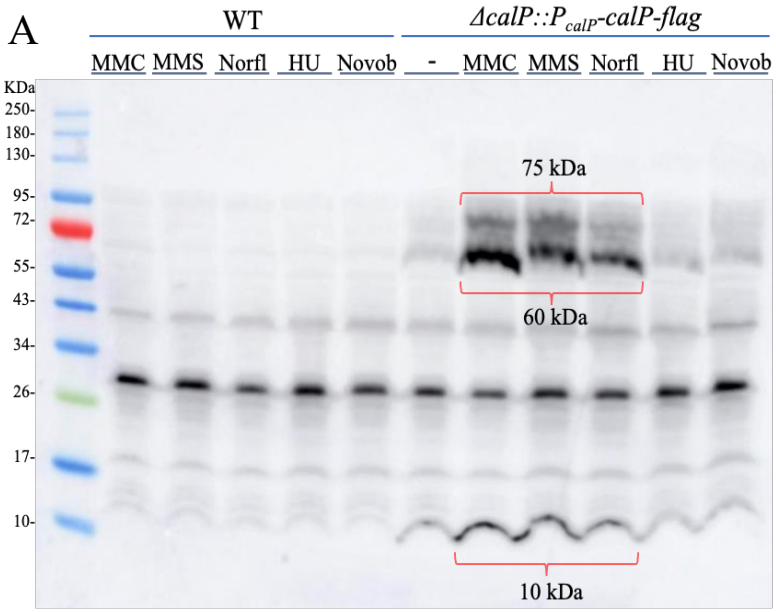

B

8 KDa monomeric CalP production in *C. crescentus* with DDAs

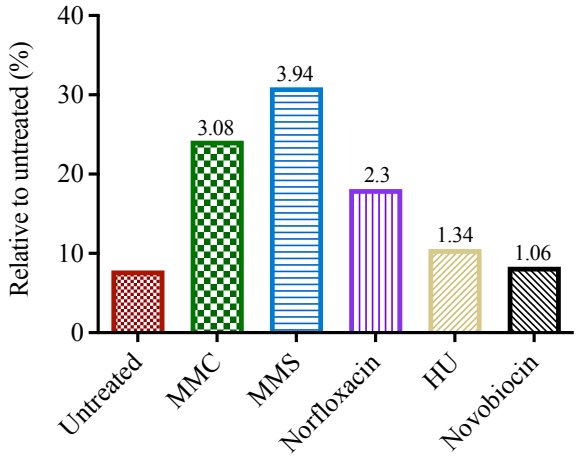

C

60 KDa multimeric CalP production in *C. crescentus* with DDAs

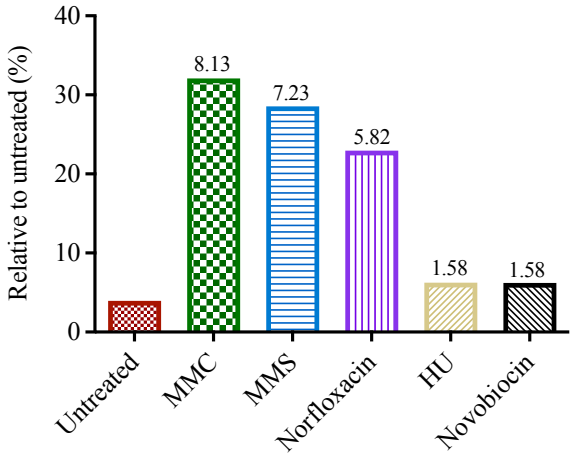

D

75 KDa multimeric CalP production in *C. crescentus* with DDAs

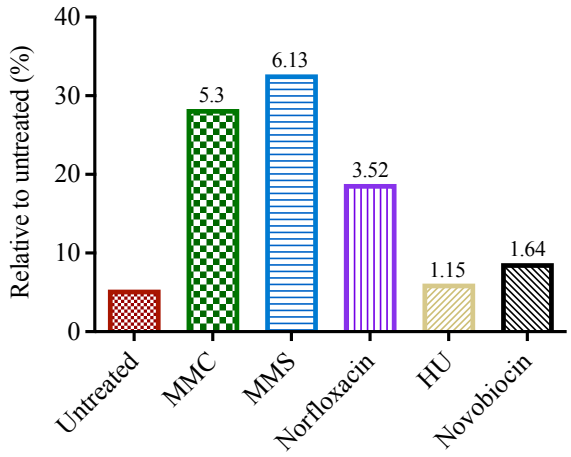

E

Comparison of CalP forms production in untreated *C. crescentus*

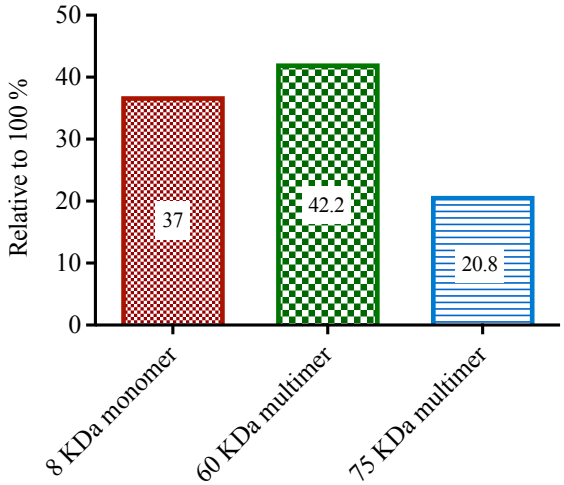

F

Comparison of CalP forms production in *C. crescentus* with MMC

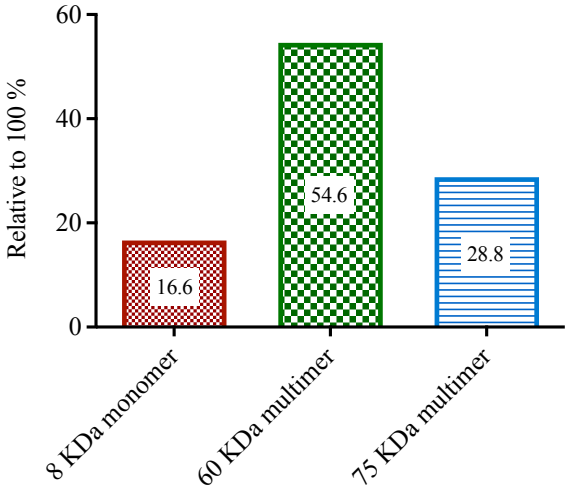

Fig. 16. *C. crescentus* increases CalP production when exposed to DDA. Immunoblots showing CalP production in *C. crescentus* exposed to different cytotoxic compounds. C-terminally *calP* was inserted at the native *calP* locus encoded from the chromosomal P_{calP} promoter of *C. crescentus ΔcalP* cells (Δ*calP*::P_{calP}-*calP-flag*). WT was included as an untagged control strain. Cells were grown to mid-exponential phase and diluted to an OD_{600}=0.1. Cultures were incubated for 3 hrs at 30°C. Cells were centrifuged and resuspended in a Triton-X-containing buffer. Cells were homogenised and run in a 4-20% SDS-PAGE. The polyacrylamide gel was immunoblotted with a 1:10000 α-FLAG/M2 antibody to highlight the desired bands. (A) Western blot comparing CalP-FLAG production when cells were treated with DDA or left untreated. Cells were exposed to each of the following compounds: 0.12 μg/mL MMC, 1.5 mM MMS, 4 μg/mL norfloxacin, 15 mM HU, or 0.5 μg/mL novobiocin. (B) Column bar graph showing the relative percentage of the production of 8 KDa CalP monomers in *C. crescentus* when exposed to different compounds. The numbers on top of the bars indicate the relative difference compared to the drug-free control. The Y-axis displays the relative percentage of CalP production (%) out of 100%. The X-axis shows bars with the name of each compound used to treat cells. The peak area calculating the band intensity is shown in Fig. A4A. (C) As in B, the production of 60 KDa CalP multimers. The peak area calculating the band intensity is shown in Fig. A4B. (D) As in B and C, the production of 75 KDa CalP multimers. The peak area calculating the band intensity is shown in Fig. A4C. (E) Column bar graph showing the relative percentage in the production of the different forms of CalP from *C. crescentus* in an unsupplemented medium. The numbers on the bars indicate the relative percentage of band intensity in the immunoblot out of 100%. The Y-axis displays the relative percentage of CalP production (%) out of 100% (the sum of the three bars is 100%). The X-axis shows the bars, which represent the intensity of each CalP form. The peak area calculating the band intensity is shown in Fig. A4D. (F) As in E, different forms of CalP from *C. crescentus* challenged with MMC. The peak area calculating the band intensity is shown in Fig. A4E.

I observed that the presence of MMC with specific concentrations increased CalP production. However, I wanted to analyse whether this increase was dependent or independent of the quantity of DDA supplemented to the medium. To answer this question, I challenged *C. crescentus* Δ*calP*::P_{calP}-*calP-flag* with increasing MMC concentrations and performed an immunoblot assay to assess whether the CalP production also increased (Fig. 17A). Cells were grown to mid-exponential phase were treated with 0.05, 0.1, 0.25, 0.5 µg/mL MMC, or left untreated. Cells were homogenised, and lysates were run in a 4-20% Tris-Glycine SDS-PAGE to resolve protein bands. Gels were blotted with an anti-FLAG antibody to probe for CalP-FLAG.

Results showed visible CalP-FLAG bands for each concentration from zero to 0.5 µg/mL MMC (Fig. 17A). A CalP band was observed even though no MMC was added to the culture growing medium, suggesting that *calP* is constitutively expressed at a low level even when no DNA damage was induced (Fig. 17A, B). The immunoblot showed that CalP production increased when treated with 0.05 (1.1-fold), 0.25 (1.44-fold), and 0.5 (1.73-fold) µg/mL MMC compared to the CalP production in untreated cells (Fig. 17B). The CalP production gradually increased proportional to the rise in the MMC concentration (Fig. 17B). However, CalP production did not increase when cells were challenged with 0.1 µg/mL MMC compared to CalP produced in cells unexposed to drugs (Fig. 17B). Omitting the results of CalP production with 0.1 µg/mL MMC, the rest of the bars on the graph showed a correlation between MMC concentration and CalP production (Fig. 17B). Therefore, CalP production is DNA-damage dependent and rise with increasing DNA damage. Hence, it may play a role in DNA damage tolerance and/or repair in *C. crescentus*. No other bands of similar size in untagged WT lanes were detected, indicating that bands from *ΔcalP::*P_{calP}*-calP-flag* lanes were genuine CalP-FLAG bands (Fig. 17A).

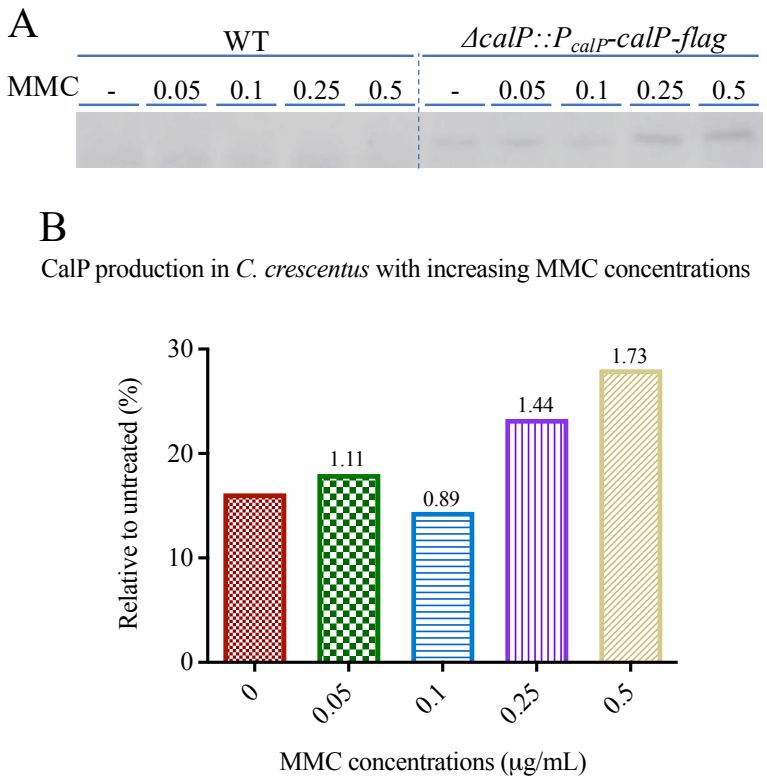

Fig. 17. CalP production in *C. crescentus* increases proportionally to the MMC concentration. (A) Immunoblot showing CalP production when *C. crescentus* was treated with increasing concentrations of MMC or left untreated. *calP* was C-terminally *flag* tagged and transcribed under the P_{calP} promoter at the *C. crescentus* *ΔcalP* native locus (Δ*calP*::P_{calP}-*calP-flag*). WT was also used as an untagged control strain. Cells were grown to mid-exponential phase and cultures were diluted to an OD_{600}=0.1 and incubated at 30°C. Cultures were grown in a medium treated with 0.05, 0.1, 0.25, or 0.5 µg/mL MMC or untreated. Cells were resuspended in a Triton-X-containing buffer. Cells were homogenised, run in a 4-20% SDS-PAGE and immunoblotted with a 1:10000 α-FLAG antibody. (B) Column bar graph showing the relative percentage of CalP production in *C. crescentus* when exposed to increasing concentrations of MMC (0.05, 0.1, 0.25, or 0.5 µg/mL MMC) (Fig. A5). The numbers on top of each bar indicate the relative difference compared to the drug-free control. The Y-axis displays the relative percentage (%) of 100%. The X-axis shows a range of MMC concentrations in µg/mL, ranging from no additive (leftmost bar) to 0.5 µg/mL MMC (rightmost bar) added to the medium.

Previous immunoblot assays showed that CalP displayed several bands of distinct molecular weights (MW). This result did not coincide with the predicted size of 3.7 KDa for CalP (4.2 KDa for CalP-FLAG), nor for the number of bands observed in the blot (Fig. 17A). To test whether the bands shown in the western blot in Fig. 17A correspond to different CalP polymers or whether they belong to different proteins, I analysed CalP in a MP assay. Mass photometry (MP) measures the size and concentration of molecules in a solution. I grew Δ*calP*::P_{calP}-*calP-flag* to mid-exponential phase in a liquid medium supplemented with 0.12 µg/mL MMC or without MMC. I homogenised cells and purified CalP-FLAG with columns containing anti-FLAG antibody. MP results showed an enriched 69 KDa CalP polymer when *C. crescentus* grew in an MMC-supplemented (282 counts) or unsupplemented media (507 counts) (Fig. 18). Surprisingly, the number of counts was higher when CalP-FLAG cells were untreated in comparison to CalP-FLAG cells challenged with MMC (Fig. 18). This result differs from the results shown in the previous immunoblot in Figs. 15, 16, 17, where the presence of DDAs increased the CalP production compared to CalP-FLAG from cells grown in a drug-free medium. The 69 KDa CalP-FLAG multimer detected in the MP assay (Fig. 18) could be the same 60 KDa CalP-FLAG multimer observed in the previous immunoblot in Fig. 17, which was isolated from DDA-treated or untreated cells (Fig. 17A). The presence of molecules with a size greater than the predicted size of CalP suggests that CalP polymerises and shows a wider variety of isoforms other than monomers. The MP analysis also detected a second group of 156 KDa CalP-FLAG (377 counts) when cells were exposed to MMC. Intriguingly, after cells were challenged with MMC, the number of counts of the 156 KDa CalP-FLAG multimer (377 counts) was greater than the 69 KDa CalP multimer (282 counts) (Fig. 18). Nevertheless, the number of counts of the 156 KDa CalP-FLAG multimer (377 counts) produced in MMC-treated cells was lower than the 69 KDa CalP-FLAG isolated from untreated *C. crescentus* (507 counts) (Fig. 18). MMC influences the formation of high-MW polymers (over 69 KDa), which shows a greater number of counts than CalP-FLAG from untreated cells (light green bars in the graph from 69 to 400 KDa) (Fig. 18). This 156 KDa CalP-FLAG multimer was not visible in the previous immunoblot assay, probably because the quantity was not high enough or

because it was too unstable and got disrupted when run in an SDS-PAGE (Fig. 17A). The MP analysis did not show any compound with a size smaller than 40 KDa because this is the minimum MW that the instrument can detect (Fig. 18). Therefore, it could not detect CalP-FLAG in the monomeric state (Fig. 18). Results showed that CalP was present in more than one isoform (Fig. 18), supporting the previous western blot results in which several CalP-FLAG bands were visible (Fig. 17A).

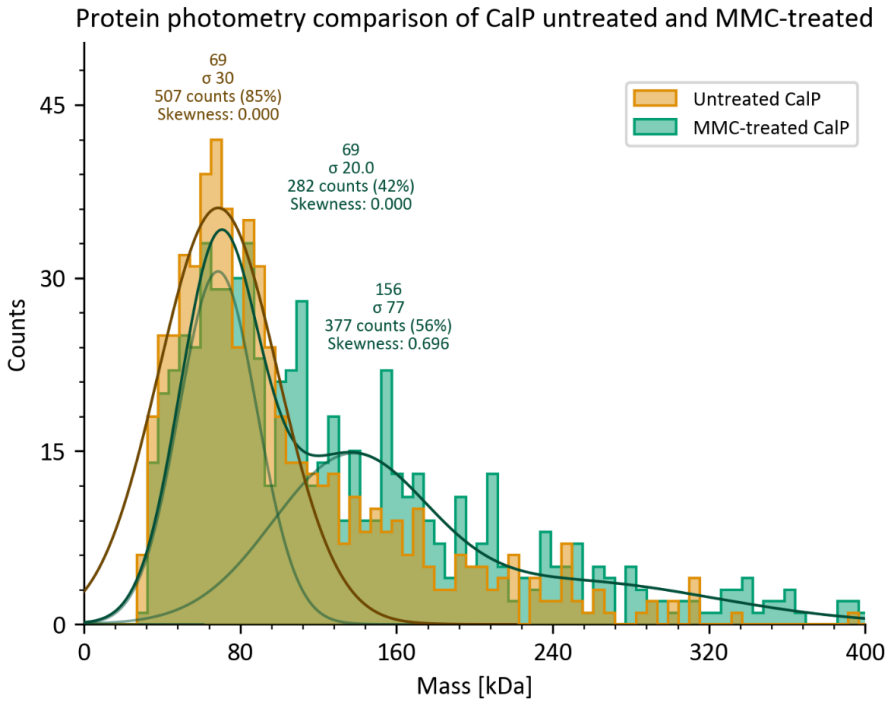

Fig. 18. Most CalP multimers in *C. crescentus* are 69 KDa on average. MP comparison of CalP-FLAG from MMC-treated or untreated *C. crescentus*. The MP instrument emits a laser that impacts the protein surface, scatters light, and records the detected signal variation. The Y-axis indicates the number of times (counts) that the multimeric CalP is detected. The X-axis represents the mass (in KDa) corresponding to each bar, which is determined by the number of counts. CalP from untreated *C. crescentus* is shown with yellowish colour bars, CalP from MMC-treated cells is represented with green colour bars.

2.7 The size of CalP-FLAG significantly decreases upon *in vitro* incubation at 100 degrees

The size of different CalP-FLAG bands from previous immunoblot assays was always larger than the predicted 4.6 KDa size. Detergents such as SDS or β-mercaptoethanol could not denature CalP to disrupt the high-MW bands. It is still unclear whether those bands correspond to CalP-FLAG self-polymers or whether they were interactions between CalP-FLAG and some other proteins. I aimed to elucidate why the CalP-FLAG size on previous western blots was larger than the predicted CalP-FLAG size. To address this question, I heated samples at 100°C for 5 min to try to disrupt the protein-protein bonds. I ran samples in an SDS-PAGE to further immunoblot the heated proteins and unheated control proteins. The high temperature must disrupt bonds in a self-interaction or an interaction with other proteins. CalP was C-terminally FLAG-tagged and produced from a *C. crescentus* Δ*calP* background (Δ*calP*::P_{calP}-*calP-flag*). Cells were exposed to MMC to evaluate whether the DDA had an impact on the CalP polymerisation pattern. Cells expressing CalP-FLAG and the untagged WT control strain were grown to mid-exponential phase in a medium supplemented with 0.12 µg/mL MMC or unsupplemented. I homogenised cells in a Triton-X-containing buffer to enhance CalP solubilisation. I heated a duplicate of the cell lysate at 100 °C for 5 min and left the other duplicate at RT. Cell lysates were loaded in the automated western blot, WES, with an anti-FLAG antibody for analysis. CalP-FLAG showed an 8 KDa band in the blot when the cell lysate was unheated and treated with MMC or left untreated (Fig. 19A). The blot with unheated samples showed an additional multimeric 65 KDa CalP-FLAG band that was only visible when cells were exposed to MMC (Fig. 19A). On the contrary, the CalP-FLAG band was not found in the drug-free medium when unheated (Fig. 19A), supporting previous results in which CalP production increased upon cell exposure to DDA (Figs. 15, 16, 17). The rest of the CalP-FLAG bands were also visible in the WT control strain from unheated samples, so they must be non-specific bands of untagged proteins (Fig. 19A). The immunoblot with the cell lysate heated at 100°C showed a very different CalP-FLAG band pattern, with most of the proteins on top of the lanes of the MMC treated and untreated samples (Fig. 19B). These heated proteins did not enter the

gel lanes, probably because they denatured and became too hydrophobic to migrate into the gel. The bottom of the lane containing heated samples from MMC-treated cells showed a smeary 15 KDa band (Fig. 19B). Unheated CalP-FLAG from the free-drug medium cells showed a low brightness 13 KDa band (Fig. 19B). When samples were heated, the WT control exhibited faint 8 KDa bands in the presence or absence of MMC, although these must be non-specific bands since WT was untagged (Fig. 19B).

Considering the CalP aggregation on top of the WES immunoblot from the heated cell lysate, I wondered whether the purification of CalP would prevent CalP from aggregating when it was incubated at a high temperature. Hence, I purified a C-terminally FLAG-tagged CalP and ran it in an acrylamide gel to visualise CalP-FLAG. To do so, Δ*calP*::P_{calP}-*calP-flag* and the untagged WT control strain were grown to mid-exponential phase and homogenised. I mixed cell lysates with anti-FLAG-conjugated magnetic beads and incubated one sample duplicate at 100ºC for 5 min. I ran the mixture through the column to retain C-terminally FLAG-tagged CalP, ran the elution in a 4-20% Tris-Glycine SDS-PAGE, and stained the gel with Blue Coomassie afterwards. The Coomassie-stained gel only showed CalP-FLAG bands in lanes from heated/unheated samples in which cells were challenged with MMC (Fig. 19C). Surprisingly, the heated sample only showed a 10 KDa CalP-FLAG band, and the unheated sample solely exhibited a 55 KDa CalP-FLAG band (Fig. 19C). Heating purified CalP-FLAG at 100°C disrupted protein bonds that detergents could not disrupt. Hence, the absence of other proteins in the gel, characterised by diverse protein sizes compared to CalP-FLAG, indicates the exclusive presence of CalP-FLAG in the sample (Fig. 19C). This result dismisses the possibility that the large band size of CalP-FLAG is due to an interaction between CalP-FLAG and another protein partner.

The Coomassie-stained polyacrylamide gel may have contained CalP-FLAG bands that were not visibly bright enough to be seen. To investigate whether these bands were present in the gel, I immunoblotted purified CalP-FLAG (from Δ*calP*::P_{calP}-*calP-flag*) and WT strains. The bands shown in the immunoblot were comparable

to the bands observed in the Coomassie-stained polyacrylamide gel. Additionally, the immunoblot showed bands that were invisible in the previous gel (Figs. 19C, D). The immunoblot showed an additional 10 and 55 KDa CalP-FLAG bands at RT corresponding to untreated cells (Figs. 19C, D). Furthermore, two 10 KDa CalP-FLAG bands were visible in the western blot, the first band at RT with MMC and the second band after heating proteins from untreated cells at 100ºC (Fig. 19C, D). These bands were not visible on the Coomassie-stained gel, probably because they were not bright enough, in contrast to CalP-FLAG from cells exposed to MMC, which showed brighter bands in the gel (Figs. 19C, D). The other two bands found in the immunoblot were the 55 KDa CalP-FLAG band from the unheated proteins and the 10 KDa CalP-FLAG band from proteins heated at 100ºC, both isolated from cells exposed to MMC (Figs. 19C, D).

In summary, no additional protein monomers with a distinct size other than the heated CalP in the Coomassie-stained gel were found. The presence of other protein monomers with distinct size in the gel could indicate the existence of additional proteins besides CalP, suggesting the interaction of CalP-FLAG with a protein partner. Nevertheless, after samples were heated, the CalP-FLAG multimer was completely disassembled into single monomers, supporting the possibility that CalP self-polymerises.

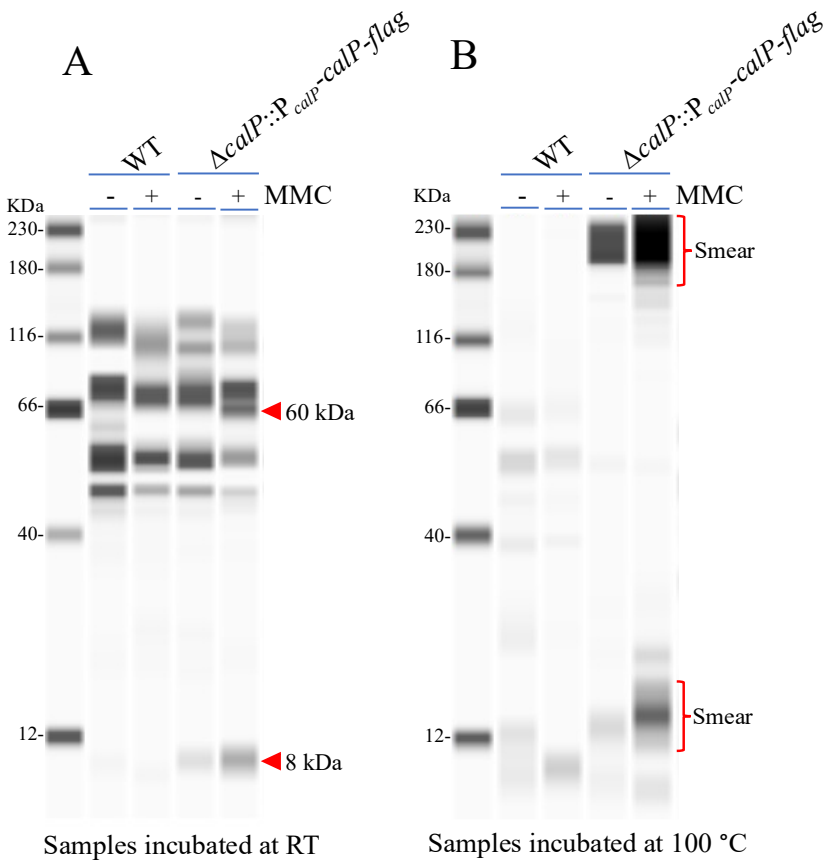
A
B
WT
ΔcalP::P calP-calP-flag
MMC
KDa
230-
180-
116-
66-
40-
12-
60 kDa
8 kDa
Smear
Smear
Samples incubated at RT
Samples incubated at 100 °C

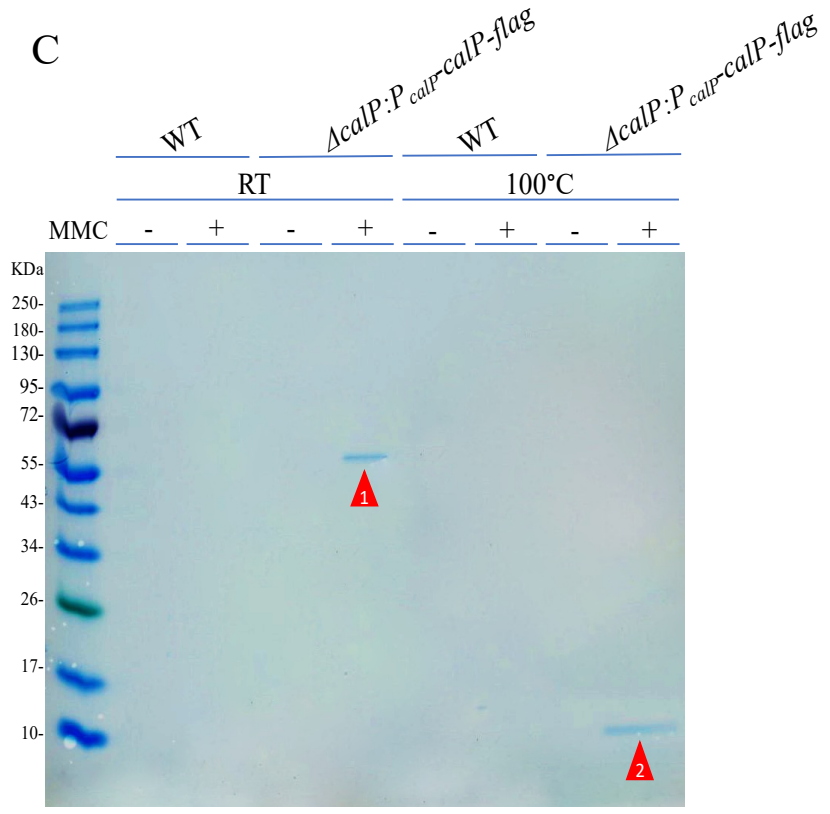
C
WT
ΔcalP:P calP-calP-flag
RT
100°C
MMC
KDa
250-
180-
130-
95-
72-
55-
43-
34-
26-
17-
10-
1
2

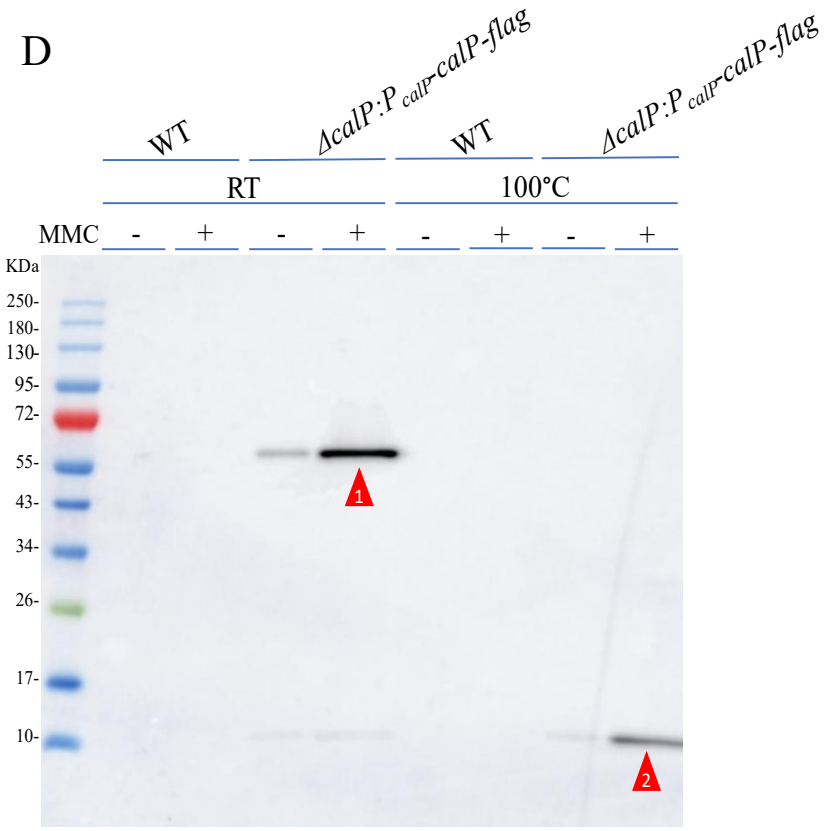

Fig. 19. CalP polymers disassemble at high temperatures in *C. crescentus*. Immunoblot showing the difference between the size of CalP at RT and after exposure at 100ºC. *calP-flag* was chromosomally encoded in the native *calP* locus of *ΔcalP* in *C. crescentus* under the P_{xyl} promoter (Δ*calP*::P_{calP}-*calP-flag*). WT was used as an untagged control strain. Cells were grown to mid-exponential phase in a medium supplemented with 0.12 µg/mL MMC or unsupplemented. (A) Cells were broken and resuspended in a TE buffer, and RT cell lysates were run in the WES automated western blot, or (B) incubated at 100°C for 5 min and run in the WES automatic western blot. (C) Cells were broken and resuspended in CFRB. To purify CalP, cell lysates with anti-FLAG antibody conjugated with magnetic beads were passed through a column under a magnetic field. Eluates were incubated at RT or 100ºC for 5 min. Samples were run in a 4-20% SDS-PAGE, and the polyacrylamide gel was stained with Instant Blue Coomassie before visualisation. (1) 60 KDa multimeric CalP with MMC. (2) 8 KDa monomeric CalP with MMC. (D) As in (C), the gel was not stained but blotted with a 1:10000 α-FLAG antibody.

2.8 CalP self-interacts *in vivo*

The Coomassie-stained gel and immunoblot assay indicated that CalP was self-polymerised *in vitro.* To cross-validate these results, I aimed to perform a bacterial two-hybrid (BACTH) assay to check for CalP self-interaction. To do so, *calP* was heterologously co-expressed in *E. coli* alongside a protein subunit that generates a measurable phenotypic trait *in vivo* (Fig. 20A). *calP* was N-terminally fused to the T25 or T18 subunit of the adenylate cyclase enzyme (CyaA) carried in pKNT25 and pUT18 plasmids, respectively (Fig. 20A). If CalP self-interacts, both CyaA subunits are reconstituted to produce cyclic AMP (cAMP), which is used as a cofactor of the catabolite activator protein (CAP) (Fig. 15A). CAP associates with certain promoters to activate transcription of reporter genes such as *lac* and *mal* operons, which are involved in lactose and maltose catabolism (Fig. 20A). Lactose and maltose production can be used by *E. coli* as the only carbon source. The production of these compounds generates phenotypic traits in the cell that can be distinguished on MacConkey agar plates [587]. The change in the colony colour from white to magenta means an interaction between target proteins [587]. *calP-T25* or *calP-T18* were transcribed from the isopropyl β-d-1-thiogalactopyranoside (IPTG)-inducible promoter P_{lac} in both plasmids. The assay included ZIP N-terminally fused to T18/T25 as a positive control strain, which indicates a protein-protein interaction [587] (Fig. 20B). As a negative control strain, I used pKNT25::*ø* and pUT18::*ø* vectors with no fusion with T18 or T25 subunits (Fig. 20B). These unfused subunits were tested against CalP (CalP-T18+T25 and CalP-T25+T18), and between each other (T18+T25) (Fig. 15B). The two negative control strains did not show an interaction between CalP or the T18/T25 portion of CyaA (Fig. 20B). In contrast, ZIP fusions with both CyaA subunits showed an intense magenta colour, indicating a strong interaction, as expected (Fig. 20B). When vectors carrying *calP*-T25 and *calP*-T18 were co-transformed into *cya*$^-$ cells, the resulting colonies exhibited a strong red colour on a MacConkey agar like ZIP, suggesting that CalP self-interacts (Fig. 20B). These results further confirm that CalP self-interacts *in vivo* and support previous results in which CalP self-interacts *in vitro*. Predictions of bioinformatic tools made in AlphaFold2 also indicated that CalP self-interacts and proposed a circle-like shape multimer (Fig. 20C).

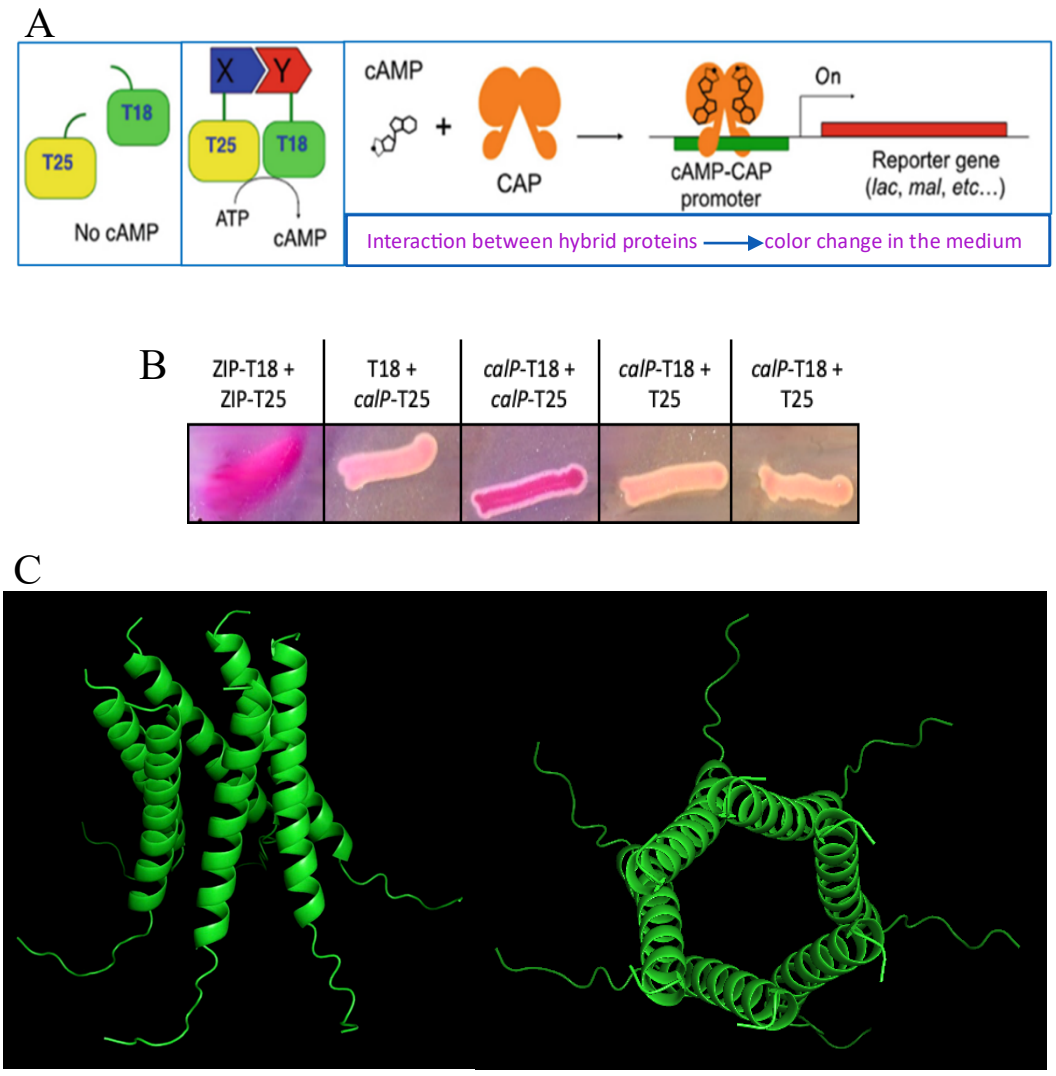

Fig. 20. CalP self-interacts. (A) Schematic of a BACTH assay [587] displaying interactions between T25 and T18 (negative control) on the left image. On the right image of the schematic, T25 and T18 are fused to proteins X and Y respectively. The restoration of adenylate cyclase activity after the interaction of the X and Y proteins enables cAMP production. cAMP associates with the CAP cofactor, and both together bind to *lac, mal,* and other gene promoters to induce transcription. Enzymes catalysed the cleavage of certain metabolites, such as lactose or maltose, which provokes a colour change in MacConkey plates. (B) A BACTH analysis evaluating interactions between T18/T25-CalP. As a negative control, empty vectors pUT18C (T18) and pKT25 (T25) were tested with the two strains mentioned previously and against each other. Also, ZIP/ZIP interactions were used

as a positive control strain. The *E. coli* strains that harbour each pair of vectors were streaked on MacConkey plates (1% maltose, 0.5 mM IPTG, 50 μg/mL kanamycin, 100 μg/mL carbenicillin) and incubated for 48 hrs at 30°C. Magenta colonies indicate interaction and white colonies indicate lack of interaction. Plasmid combinations are shown on top of the image. (C) Bioinformatics prediction using the AlphaFold2 platform suggested that CalP is a multimer formed by the interaction of six monomers [588, 589].

2.9 CalP is a transmembrane protein with the N-terminus in the periplasm and the C-terminus in the cytoplasm

In vitro and *in vivo* experiments confirmed that CalP is a self-polymerising protein, but it remains unclear whether CalP is a membrane or a cytoplasmic protein. SPs are more often localised in the membrane, which acts as a scaffold since the short number of amino acids limits the number of possible structures and decreases their stability [452, 454]. Elucidating CalP localisation in the membrane or cytoplasm can also shed light on its function in *C. crescentus* [452]. To investigate this, I performed a cell fractionation assay in which I separated soluble (cytoplasmic) and membrane fractions from *C. crescentus* cell lysates and visualised them in a western blot. To do so, I expressed *calP* from a chromosomally encoded *calP-flag* inserted at the native *calP* locus in *C. crescentus* (Δ*calP*::P_{calP}-*calP-flag*). I also included WT as an untagged control strain. I cultured cells until they reached mid-exponential phase and exposed them to 0.12 µg/mL MMC or left them untreated. I homogenised cells in the CFRB to promote CalP solubilisation and ultracentrifuged cell lysates at 194000 RCF to separate membrane and soluble fractions. I ran both fractions alongside the whole-cell extract (the pre-ultracentrifuged cell lysate with the membrane and soluble fractions) in a 4-20% Tris-Glycine SDS-PAGE. I immunoblotted the membranes with α-FLAG antibody. If CalP is a membrane protein, the membrane fraction must have CalP bands with a higher intensity. The immunoblot showed 60, 80, and 95 KDa-multimeric CalP-FLAG bands from the whole-cell extract and from the membrane fraction with and without MMC (Fig. 21). However, only the multimeric 60 KDa band was present in the soluble fraction under either condition (Fig. 21). Additionally, the 10 KDa CalP-FLAG bands were present in the membrane fraction and the whole-cell extract with or without MMC (Fig. 21). Monomeric CalP did not appear in the soluble fraction under either condition (Fig. 21). The CalP-FLAG band intensity also increased when cells were challenged with MMC in all three fractions (except monomeric CalP-FLAG challenged with MMC in the membrane fraction that was not visible) (Fig. 21). CalP was more enriched in the membrane fraction than in the soluble fraction, suggesting that CalP is a membrane protein (Fig. 21). The presence of faint CalP-FLAG bands in the soluble fraction may be caused by nascent CalP translated by

ribosomes just before being transported and inserted into the cell membrane (Fig. 21).

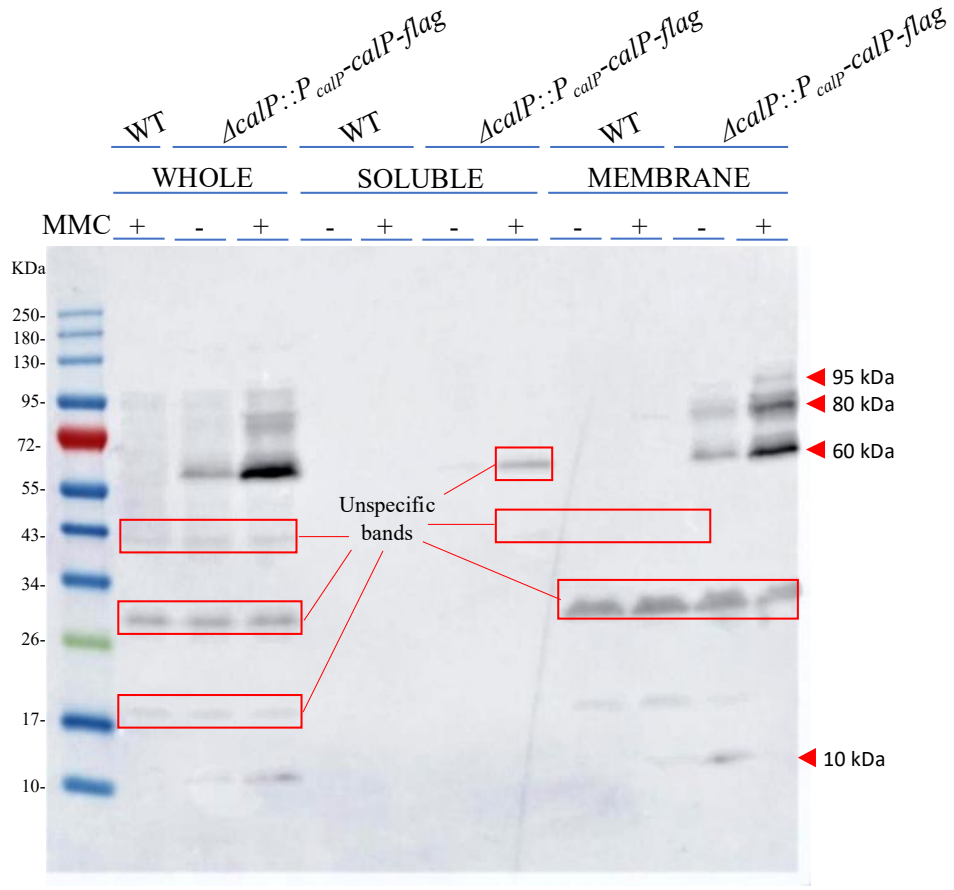

Fig. 21. CalP multimers localise in the *C. crescentus* membrane. A western blot displaying the separation of *C. crescentus* whole-cell lysate into soluble and membrane fractions. *ΔcalP* background with a chromosomally encoded *calP-flag* from the native *calP* locus under the *calP* native promoter P_{calP}. WT was added as an untagged control strain. Cells were grown to mid-exponential phase in a PYE medium supplemented with 0.12 µg/mL MMC or unsupplemented for 2 hrs at 30 ºC. Cells were broken, and cell lysates were ultracentrifuged at 194000 RCF to separate fractions. The soluble fraction was run in a 4-20% Tris-Glycine SDS-PAGE and blotted using the α-FLAG/M2 antibody.

The membrane fractionation assay suggested that CalP is localised in the membrane. However, this experiment did not give any clue about the possible anchorage or insertion into the membrane and, if so, the topology of the protein. Thus, as a first step to determine whether CalP is a transmembrane protein and, if so, the orientation of the protein, I performed a bioinformatic prediction using the TMHMM web server (DTU Health Tech) [590, 591] (Fig. 22A). TMHMM predicted that CalP is a transmembrane protein (transmembrane helix: AA 4 to 26) with the amino terminus in the periplasm and the carboxylic terminus in the cytoplasm (N_{out}-C_{in} topology) (Fig. 22A). To verify this prediction experimentally, I employed a *phoA-lacZ* reporter system that uses proteins which are solely active in the cytoplasm (LacZ) or the periplasm (PhoA) [592]. When PhoA is active, the selective medium turns blue, and when LacZ is active, the medium turns purple. This system can be employed to elucidate whether the orientation of proteins in the membrane is N_{in}-C_{out} or N_{out}-C_{in}. To investigate the CalP topology, I fused the C-terminus of *calP* in-frame to a PhoA-LacZα chimaera (pKTOP plasmid system) (Fig. 22B). I did the same fusion with *rsbN,* a known membrane protein with N_{in}-C_{out} topology used as a control strain (Fig. 22B) [593]. I also employed the empty plasmid pKTOP as a control strain that remains in the cytoplasm so LacZ would constantly be active, and the medium would turn purple (Fig. 22B). I transformed *E. coli* DH5α with the cloned plasmids, and the resulting colonies were streaked on an indicator medium. Plates showed that only the N_{in}-C_{out} control strain (carrying the pKTOP::*rsbN* plasmid) turned blue (Fig. 22C). Meanwhile, strains carrying either the empty vector pKTOP (Fig. 22C) or pKTOP::*calP* (Fig. 22C) turned purple. This phenotype suggests that CalP may have a N_{out}-C_{in} topology or may be entirely in the cytoplasm. Bioinformatics prediction indicated that CalP is a transmembrane protein with a N_{out}-C_{in} topology.

Similarly, the cell fractionation analysis suggested that CalP is a membrane protein (Fig. 22D). Together with previous results and the Pho/LacZ test, it is likely that CalP is a transmembrane protein with a N_{out}-C_{in} orientation (Figs. 22A, C, D). Indeed, it is likely that CalP is an inner transmembrane protein since a putative outer transmembrane protein would have turned blue as RsbN did in the topology assay (Fig. 22C). However, it turned purple, indicating that the C-terminus of CalP is

situated in the cytoplasm. To further support the previous results, I performed a prediction in the Alpha-fold bioinformatics tool to visualise the putative insertion into the transmembrane CalP domain and confirm its N_{out}-C_{in} topology. The AlphaFold2 prediction also indicated that CalP is a transmembrane protein with an N_{out}-C_{in} topology. The CalP C-terminus section had a longer domain in the cytoplasm than the N-terminus in the periplasm (Fig. 22E). These results are consistent with the previous prediction on the TMHMM platform, in which it was estimated that CalP had three amino acids in the periplasm and eleven in the cytoplasm (Fig. 22A).

A

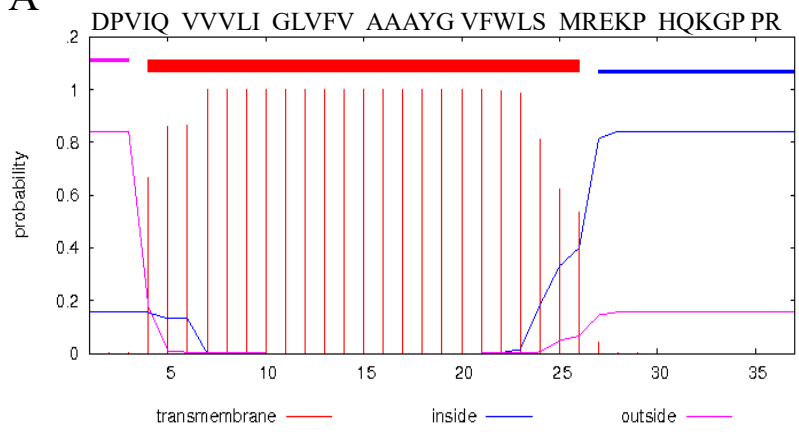
DPVIQ VVVLI GLVFV AAAYG VFWLS MREKP HQKGP PR
probability
transmembrane
inside
outside

B

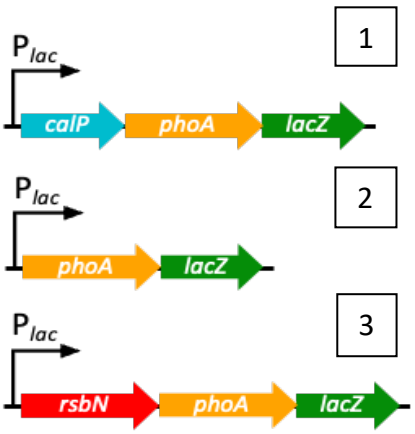
P lac
calP
phoA
lacZ
1
P lac
phoA
lacZ
2
P lac
rsbN
phoA
lacZ
3

C

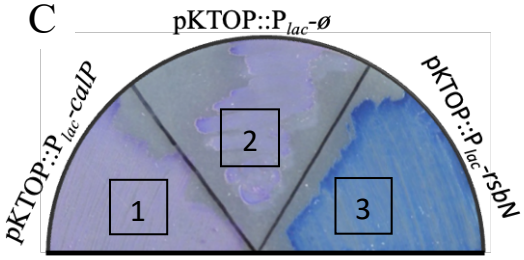
pKTOP::P lac-ø
pKTOP::P lac-calP
pKTOP::P lac-rsbN
1
2
3

D

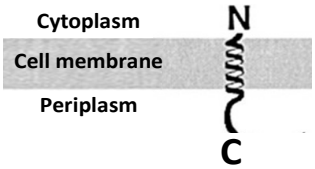
Cytoplasm
Cell membrane
Periplasm
N
C

E

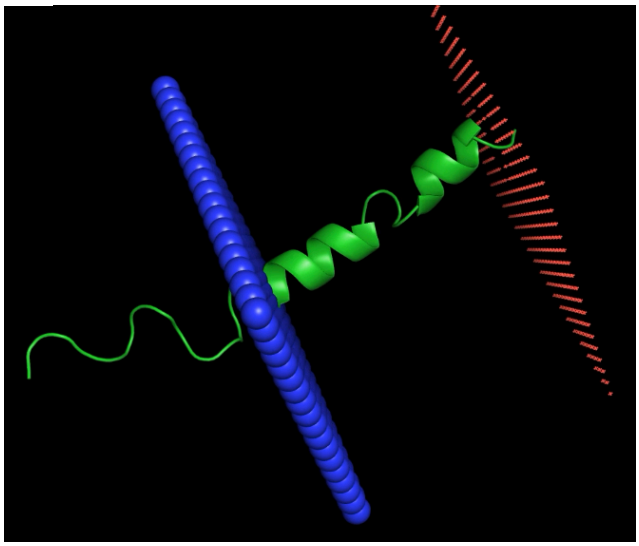

Fig. 22. CalP is a transmembrane protein with a N_{out}-C_{in} topology. Bioinformatics predictions and laboratory experiments assessing the cellular CalP localisation and putative topology in the case of a transmembrane protein. (A) Prediction of transmembrane helices in CalP with the TMHMM bioinformatics prediction tool [590, 591]. On top of the image is the CalP amino acid sequence. (B) Assay testing CalP topology (orientation in the membrane). CalP was fused with a chimaera protein (PhoA-LacZα), which produces a different compound depending on the orientation of the membrane that results in a colour change when cells grow in a selective medium. Colonies turned blue when the periplasmic alkaline phosphatase was active and purple when the cytoplasmic β-galactosidase was active. The indicator plate contained 80 µg/mL magenta-gal, 100 µg/mL X-Pho, 1 mM IPTG, and 50 µg/mL kanamycin. Plates were incubated at 30°C for 24 hrs. (C) Strains used in the PhoA-LacZα assay were pKTOP::P_{lac}-*calP*, pKTOP::P_{lac}-*ø*, and pKTOP::P_{lac}-*rsbN*. (D) Illustration summarising CalP topology results. (E) Image representing the N_{out}-C_{in} orientation of CalP in the cell membrane obtained with the bioinformatics prediction platform AlphaFold2. The results were visually represented with the molecular visualisation system PyMOL. C-ter is represented on the left side of the image and N-ter on the right of the image. The blue layer represents the cytosolic side of the bilayer, and the red layer represents the periplasmic side.

2.10 Microscopy observations of CalP in the outer part of *C. crescentus* indicate membrane localisation

To further determine the subcellular localisation of CalP in *C. crescentus*, I employed epifluorescence microscopy. To do so, I fused *yfp*, which encodes the fluorescent protein YFP, to the C-terminus of *calP*. I inserted *calP-yfp* at the native locus of *calP* in a *C. crescentus ΔcalP* background (*ΔcalP::*P_{calP}*-calP-yfp*). The much larger size of the YFP epitope could affect CalP activity because it was 6-fold larger than CalP itself. To determine whether fusion with YFP affected CalP activity, I performed a complementation assay. I conducted the assay similarly to previous complementation assays in a liquid medium in the absence and presence of 0.12 µg/mL MMC. As control strains, I employed WT, *ΔrecA,* and *ΔcalP*. I incubated cultures at 30ºC for 48 h. Restoration of a WT phenotype should indicate that the YFP tag did not affect CalP function. The experiments showed that *ΔcalP::*P_{calP}*-calP-yfp* successfully restored the WT phenotype in the absence (Fig. 23A) and presence of MMC (Fig. 23B). Therefore, the complementation of *ΔcalP* with *calP-yfp* rescued the WT phenotype when challenged with MMC (Fig. 23B). In contrast, cells exposed to MMC exhibited an OD_{600}≈0.4 for *ΔcalP* after 30 hours post-inoculation (Fig. 23B). This value was 1.75-fold lower compared to the OD_{600}≈0.7 observed in the complemented *ΔcalP*::P_{calP}*-calP-yfp* and WT (Fig. 23B). These phenotypes suggest that the absence of *calP* affected the sensitivity of *C. crescentus* in MMC (Fig. 23B). *ΔrecA* showed no growth throughout 48 hrs, indicating hypersensitivity to MMC and proving the toxic effect of the drug (Fig. 23B). In the absence of the antibiotic, all strains showed normal growth, indicating that MMC specifically induced sensitivity in *ΔcalP* and *ΔrecA* cells (Fig. 23A). These results indicated that the functionality of CalP remained unaltered even upon fusion with a significantly larger YFP tag.

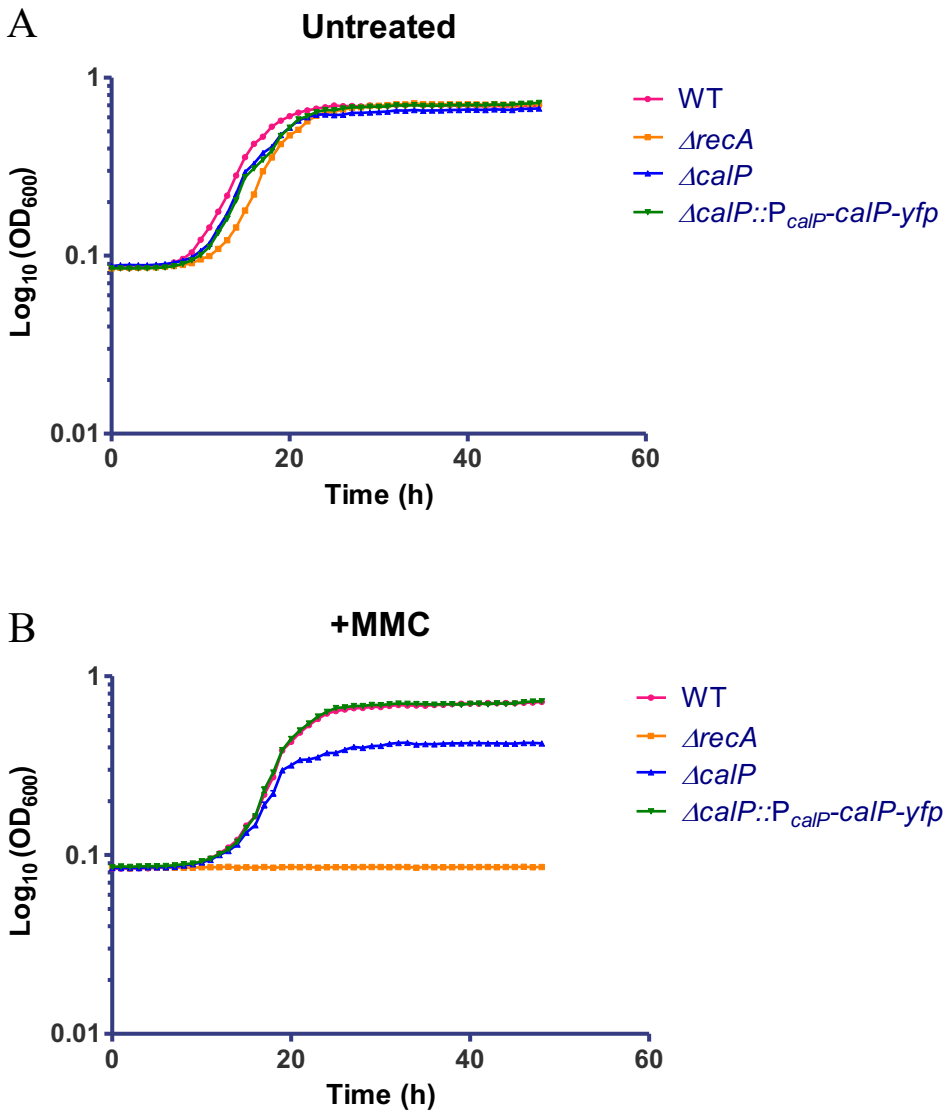

Fig. 23. The fusion of *yfp* to the C-terminus of *calP* did not hinder the complementation of *ΔcalP* in a liquid medium even in the presence of MMC**.** Growth curves comparing *ΔcalP::P$_{calP}$-calP-yfp* complementation in liquid medium with and without MMC. Successful complementation suggests that the fusion of *yfp* to the C-terminus of *calP* did not hinder CalP function in the presence of MMC. Control strains used were WT, *ΔrecA,* and *ΔcalP*. Cells were grown to mid-exponential phase in a PYE medium and subsequently diluted to an $OD_{600}=3.3\cdot10^{-4}$. Cells were treated with 0.12 µg/mL MMC or left untreated and incubated for 48 hrs at 30°C. The OD_{600} was measured hourly. The OD_{600} mean of three technical replicates was used to generate the plot. Strains were grown in a media (A) unsupplemented or (B) supplemented with 0.12 µg/mL MMC.

The subcellular localisation of CalP in the cell can shed light on its putative function and categorise it as a membrane or cytoplasmic protein. Furthermore, treatment with and without MMC may be useful to compare the production, localisation, and distribution of CalP under both conditions. To further examine the subcellular localisation of CalP by epifluorescence microscopy, I tested the construct *ΔcalP::*P_{calP}*-calP-yfp* in a drug-free medium (Fig. 24A) or challenged it with 0.12 µg/mL MMC (Fig. 24B). CalP-YFP exhibited fluorescent spots when *C. crescentus* was treated with MMC (Fig. 19A) or untreated (Fig. 24B). *ΔcalP::*P_{calP}*-calP-yfp* cells challenged with MMC showed brighter dots than cells in the antibiotic-free medium (Fig. 24A, B). This result suggests a higher CalP production when cells were challenged with MMC (Fig. 24A, B). Indeed, dots were mainly localised in the outer part of the cell grown in an MMC-supplemented or unsupplemented media, indicating a membrane localisation of CalP (Figs. 24A, B). These results correlate with previous results in which CalP production raised after exposure to MMC (Figs. 15, 16, 17) or other DDAs (Fig. 21). These findings align with previous results that demonstrated CalP as a transmembrane protein primarily localised in the cell membrane (Fig. 22).

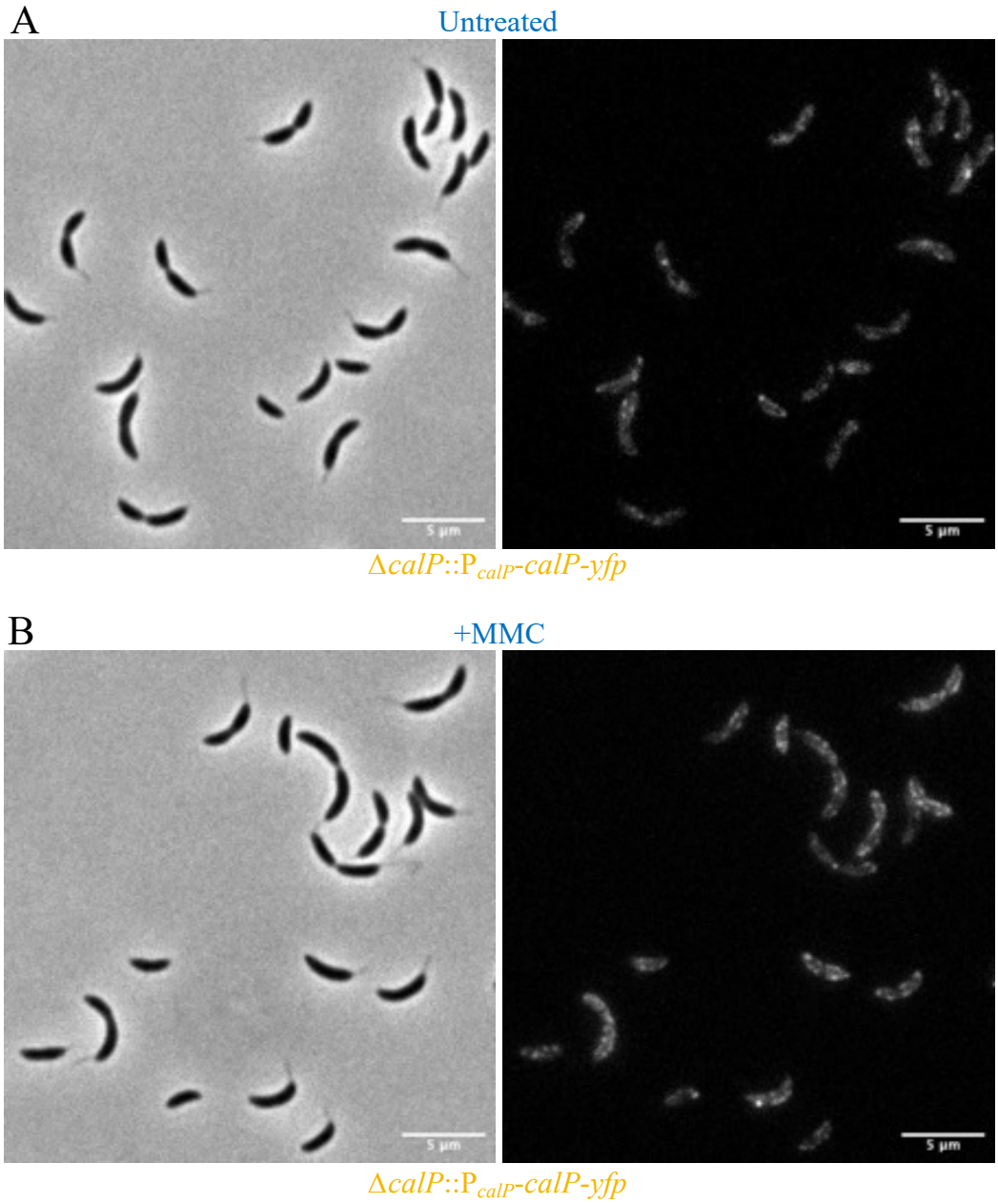

Fig. 24. CalP-FLAG is localised throughout the cell in a patchy distribution with or without MMC. Microscopy visualisation of the fluorescence intensity of CalP-FLAG produced in *ΔcalP::PcalP-calP-yfp* treated with MMC or left untreated. The brighter signal indicates a higher expression of *calP*. Exponential phase cultures grown in a PYE medium were diluted to an OD_{600}=0.1 and incubated for 1 hr at 30°C. Cells were treated with 0.12 µg/mL MMC or left untreated and incubated for 2 hrs before being visualised.. The bright-field microscopy images are situated on the left side of the figure and the phase contrast microscopy images are placed on the right side of the figure. (A) Untreated cells and (B) MMC-treated cells.

2.11 The amino acid residues 9th, 16th, 18th, and 22nd are important for the function of CalP

Previous immunoblot assays showed that CalP forms multimers, which are the functional form of the protein and get activated upon DNA damage induction. To understand which of the 37 amino acids was critical for CalP function *in vivo*, I individually mutagenised the entire CalP amino-acid sequence to alanine. Additionally, I replaced the 16th, 17th, and 18th alanine residues with prolines to investigate their specific impact, in the presence or absence of MMC. The sequence of each *calP* derivative mutant was C-terminally *flag*-tagged for subsequent immunoblot analysis. These mutants were ectopically expressed from the xylose-inducible promoter P_{xyl} at the *xylX* locus in a *C. crescentus ΔcalP* background. As a control strain exhibiting WT phenotype, I utilised *C. crescentus* Δ*calP*, which was complemented with the native *calP* inserted at the *xylX* locus (Δ*calP::*P_{xyl}*-calP flag*). As a negative control strain, I used *C. crescentus* Δ*calP* containing the empty plasmid pXYFPC-2 (*ΔcalP::*P_{xyl}*-ø*). This vector backbone was used for inserting derivative *calP* mutants at the *xylX* locus. As an untagged control strain for subsequent immunoblot assays, I generated a variant of *calP* fused to a truncated *flag* sequence. This variant contains specific deletions in the nucleotide sequence, whose translation results in a non-functional FLAG epitope. I evaluated the sensitivity of *C. crescentus in vivo* after mutating specific nucleotides of *calP*. I analysed whether the *calP* complementation with 36 *calP* derivative mutants (start and stop codon constructs were omitted) could restore the WT phenotype when challenged with MMC in a solid or liquid medium. To analyse the results, I followed the procedure outlined in section 2.2 to establish the boundaries between the exponential and the stationary phases. Additionally, I compared two strains using the ratio of optical densities, as described. I grew cells to mid-exponential phase in a liquid medium. For the sensitivity assay in a liquid medium, cells were treated with xylose, 0.12 µg/mL MMC, both compounds combined or left untreated. Cultures were incubated at 30ºC for 48 hrs and the OD_{600} was monitored hourly in an automated plate reader. The sensitivity assay in the liquid medium showed that none of the strains was sensitive in the drug-free medium (Figs. 25A, E, I; Figs.

A6A-A15A) or after xylose addition (Figs. 25B, F, J; Figs. A6B-A15B). All *calP* derivative mutants exhibited sensitivity when challenged with MMC. However, the native *calP* strain did not show sensitivity and had a WT-like phenotype comparable to the phenotype from cells grown in the unsupplemented medium (Figs. 25C, G, K; Figs. A6C-A15C). Following MMC treatment, *calP* derivative mutants did not exhibit a WT phenotype because the *calP* derivative was under a xylose-inducible promoter and the medium was xylose deficient (Figs. 25C, G, K; Figs. A6C-A15C). After exposure to the combination of xylose and MMC, *calP* mutants (*L9A*), *calP* (*A16P*), *calP* (*A18P*), and *calP* (*F22A*) could not restore the WT phenotype (Figs. 25D, H, L). In contrast, the other 33 *calP* mutants successfully complemented Δ*calP* in the liquid medium with xylose and MMC together (Figs. 25D, H, L; Figs. A6D-A15D). The *calP* (*L9A*) mutant showed sensitivity to MMC despite the treatment with xylose to induce the expression of the *calP* derivative mutant (Fig. 25D). "In the stationary phase after 48 hours, the OD_{600}≈0.4 was observed in *calP* (L9A) when treated with Xylose and MMC (Fig. 25D). This value was 1.25-fold lower than the OD_{600}≈0.5 observed in the strain complemented with native *calP* when exposed to the combination of xylose and MMC (Fig. 25D). However, the OD_{600}≈0.4 observed in *calP* (*L9A*) doubled the OD_{600}≈0.2 of the control strain harbouring the empty plasmid when exposed to xylose and MMC combined (Fig. 25D). The OD_{600}≈0.35 observed in *calP* (*A16P*) and the OD_{600}≈0.3 observed in *calP* (*A18P*) were lower than the OD_{600}≈0.5 measured in native *calP* strain when challenged to the combination of xylose and MMC (Fig. 25H). The optical density of *calP* (*A16P*) and *calP* (*A18P*) was 1.43-fold and 1.66-fold lower, respectively, compared to the native *calP* strain in the stationary phase after 48 hrs (Fig. 25H). Thus, this phenotype denotes a higher sensitivity in *calP* (*A16P*) and *calP* (*A18P*) compared to the native *calP* when challenged with MMC despite the presence of xylose in the medium (Fig. 25H). *calP* (*A17P*) successfully complemented Δ*calP* and mimicked the OD_{600}≈0.5 of the strain complemented with the native *calP* (Fig. 25H). *calP* (*A18P*) resembled the OD_{600}≈0.2 of the strain harbouring the empty plasmid control (*ΔcalP::*P_{xyl}*-ø*), which could not restore the WT phenotype because it lacked *calP* (Fig. 25H). Similarly, *calP (F22A)* was sensitive to MMC and the WT phenotype could not be rescued with the addition of xylose (Fig. 25L). The

OD_{600}≈0.4 of *calP* (*F22A*) was 1.37-fold lower than the OD_{600}≈0.55 of the native *calP* strain, *calP* (*V7A*), and *calP* (*V8A*) when exposed to both xylose and MMC combined (Fig. 25L). However, the OD_{600}≈0.4 of *calP (F22A)* was 1.33-fold greater than the OD_{600}≈0.3 of *ΔcalP::*P_{xyl}*-ø* when exposed to the combination of xylose and MMC (Fig. 25L). The optical density of *calP (F22A)*, which was halfway between the native *calP* and *calP* mutant, suggests that the truncated CalP is perhaps semi-functional or tries to perform its native role to counteract the DNA crosslinking of MMC. In summary, mutations of CalP residues *L9A*, *A16P*, *A18P*, and *F22A* caused sensitivity that impeded Δ*calP* from restoring the WT phenotype in the presence of MMC (Figs. 25D, H, L). This phenotype could be caused by the inability of the protein to properly perform its function due to a mutation in an essential amino acid.

To further assess mutant sensitivity, I performed a sensitivity assay in a solid medium. Mid-exponential phase cultures were streaked on an agar medium supplemented with 0.3% xylose, 0.25 μg/mL MMC, both compounds combined, or left unsupplemented. Additionally, I tested WT, *ΔrecA*, and *ΔcalP* as control strains. WT, *ΔrecA*, and *ΔcalP* cells showed no sensitivity when treated with xylose or left untreated, and all their colonies exhibited similar densities (Fig. A16A, B). The xylose-supplemented plates showed a similar phenotype in all strains and colonies were thicker than colonies in the unsupplemented medium (Fig. A16A, B). The WT sensitivity was not diminished after MMC treatment, whereas *ΔrecA* and *ΔcalP* exhibited a reduced sensitivity (Fig. A16C). Intriguingly, the supplementation of the medium with xylose and MMC combined reduced the *ΔcalP* sensitivity by forming more isolated colonies than in the MMC-supplemented medium. Conversely, *ΔrecA* could not grow in the presence of MMC despite xylose was supplemented to the medium (Fig. A16D). I tested the complementation of 36 *calP* derivative mutants under different conditions, showing restoration of the WT phenotype in the drug-free medium (Figs. A17A, E) or the xylose-supplemented medium (Figs. A17B, F). Following MMC treatment, all mutants showed sensitivity comparable to *ΔcalP* (Figs. A17C, G). Following the supplementation with a combination of xylose and MMC, 33 mutants could rescue the WT phenotype (Figs. A17D, H). However, *calP (A16P)*, *calP (A18P)*, and *calP (F22P)* mutants still exhibited sensitivity to MMC (Figs. A17D, H). Xylose was required

to induce the expression of each mutant (under the P_{xyl} promoter) to restore the WT phenotype in MMC-treated cells (Figs. A17D, H). The control, consisting of the native *calP* fused to the *flag*-truncated derivative of *calP* (*K45A*), displayed a comparable number and size of colonies to WT and the other 33 derivative mutants when both xylose and MMC were supplemented to the medium (Figs. A17D, H). *calP (A16P)*, *calP (A18P)*, and *calP (F22P)* mutants exhibited smaller colonies than WT with the combination of both xylose and MMC (Figs. A17D, H). The colony size of 33 *calP* derivative mutants that rescued the WT phenotype was similar in the presence of MMC (Figs. A17C, G) or in its absence (Figs. A17A, E). *calP (A16P)* and *calP (A18P)* proline substitution mutants caused a stronger sensitivity than the *F22P* alanine substitution mutant when exposed to both xylose and MMC combined (Figs. A17D, H). In conclusion, the *ΔcalP* complementation with *calP (L9A), calP (A16P)*, *calP (A18P),* and *calP (F22A)* could not rescue the WT phenotype in *C. crescentus* upon MMC exposure in a solid medium.

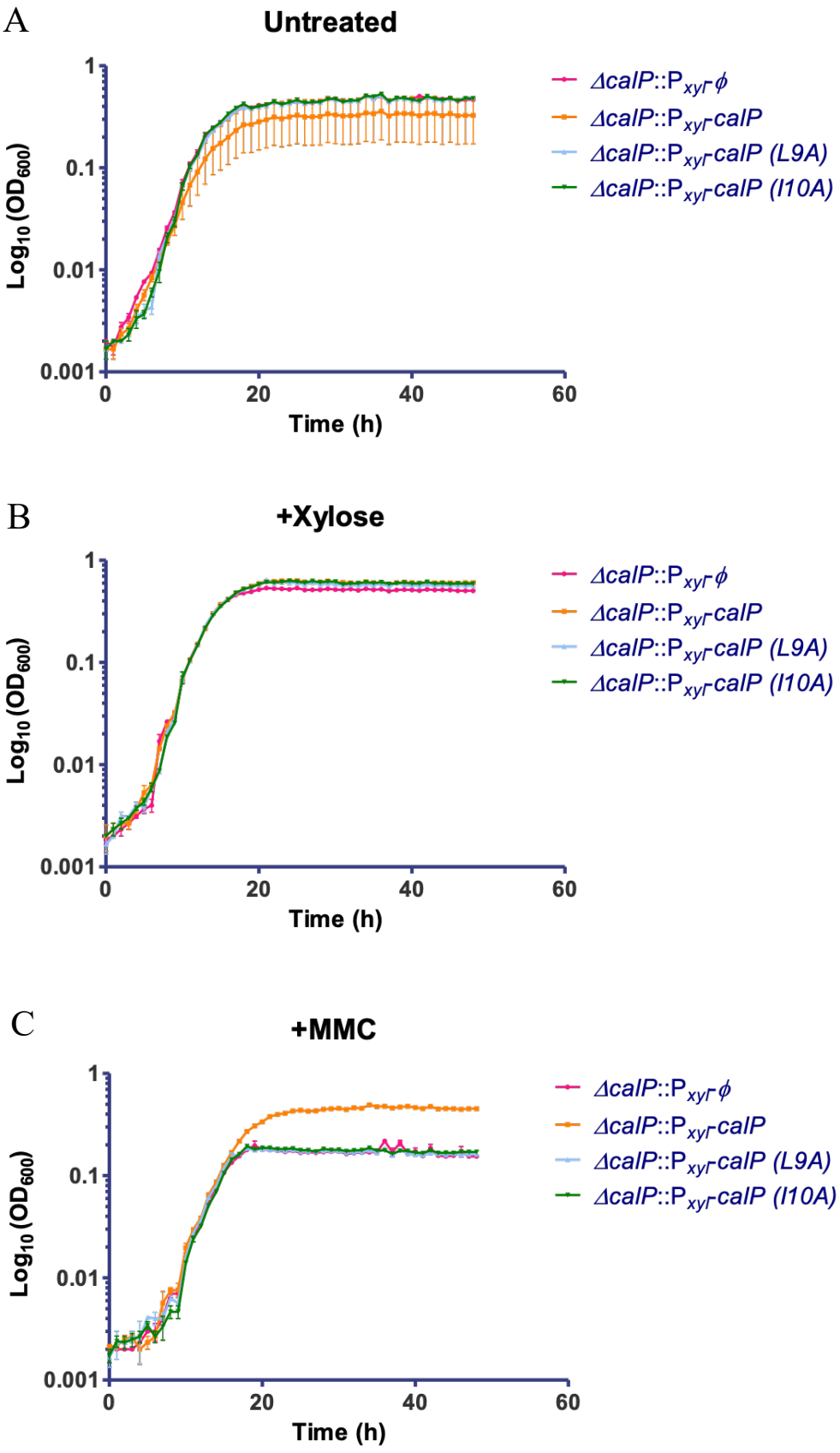
A
Untreated
Log10 (OD600)
1
0.1
0.01
0.001
0
20
40
60
Time (h)
ΔcalP::Pxyl-ϕ
ΔcalP::Pxyl-calP
ΔcalP::Pxyl-calP (L9A)
ΔcalP::Pxyl-calP (I10A)
B
+Xylose
Log10 (OD600)
1
0.1
0.01
0.001
0
20
40
60
Time (h)
ΔcalP::Pxyl-ϕ
ΔcalP::Pxyl-calP
ΔcalP::Pxyl-calP (L9A)
ΔcalP::Pxyl-calP (I10A)
C
+MMC
Log10 (OD600)
1
0.1
0.01
0.001
0
20
40
60
Time (h)
ΔcalP::Pxyl-ϕ
ΔcalP::Pxyl-calP
ΔcalP::Pxyl-calP (L9A)
ΔcalP::Pxyl-calP (I10A)

D

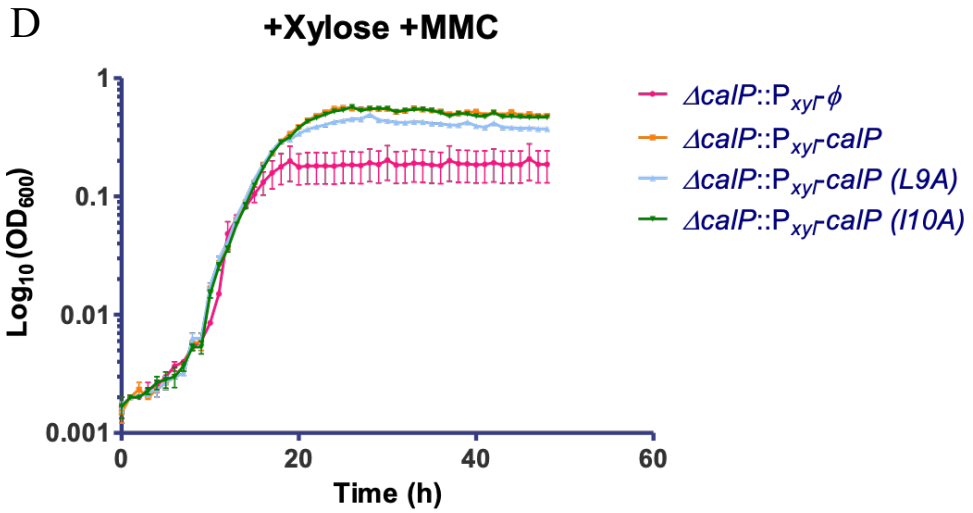
+Xylose +MMC
Log10 (OD600)
1
0.1
0.01
0.001
0
20
40
60
Time (h)
ΔcalP::Pxyl-ϕ
ΔcalP::Pxyl-calP
ΔcalP::Pxyl-calP (L9A)
ΔcalP::Pxyl-calP (I10A)

E

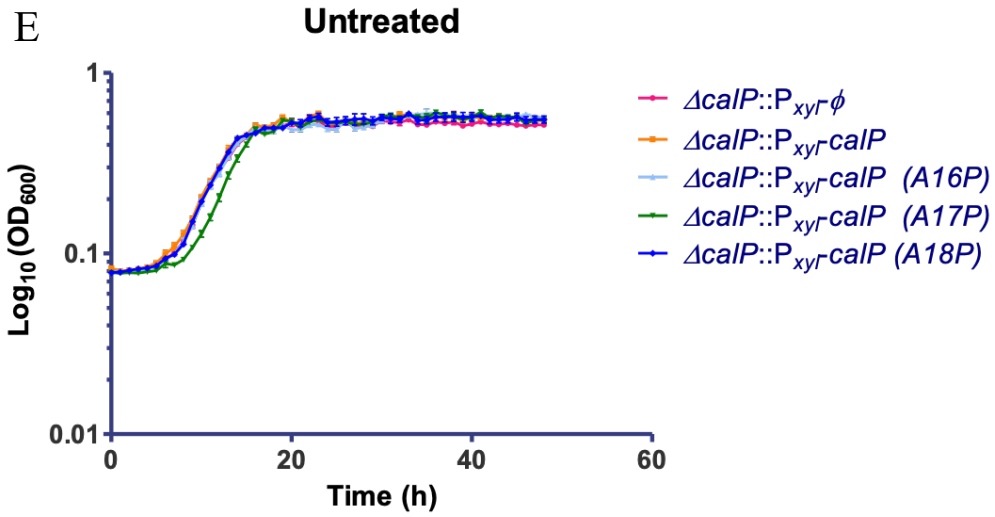
Untreated
Log10 (OD600)
1
0.1
0.01
0
20
40
60
Time (h)
ΔcalP::Pxyl-ϕ
ΔcalP::Pxyl-calP
ΔcalP::Pxyl-calP (A16P)
ΔcalP::Pxyl-calP (A17P)
ΔcalP::Pxyl-calP (A18P)

F

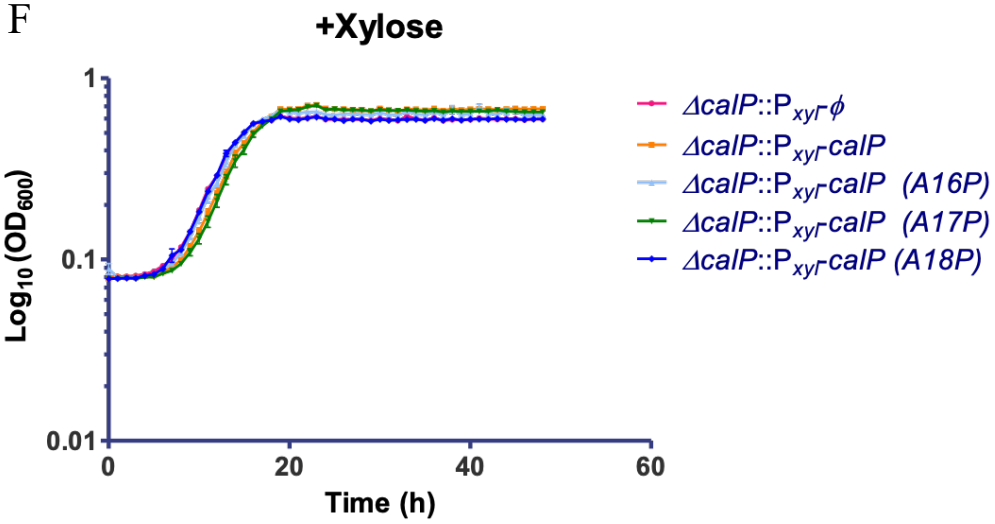
+Xylose
Log10 (OD600)
1
0.1
0.01
0
20
40
60
Time (h)
ΔcalP::Pxyl-ϕ
ΔcalP::Pxyl-calP
ΔcalP::Pxyl-calP (A16P)
ΔcalP::Pxyl-calP (A17P)
ΔcalP::Pxyl-calP (A18P)

G

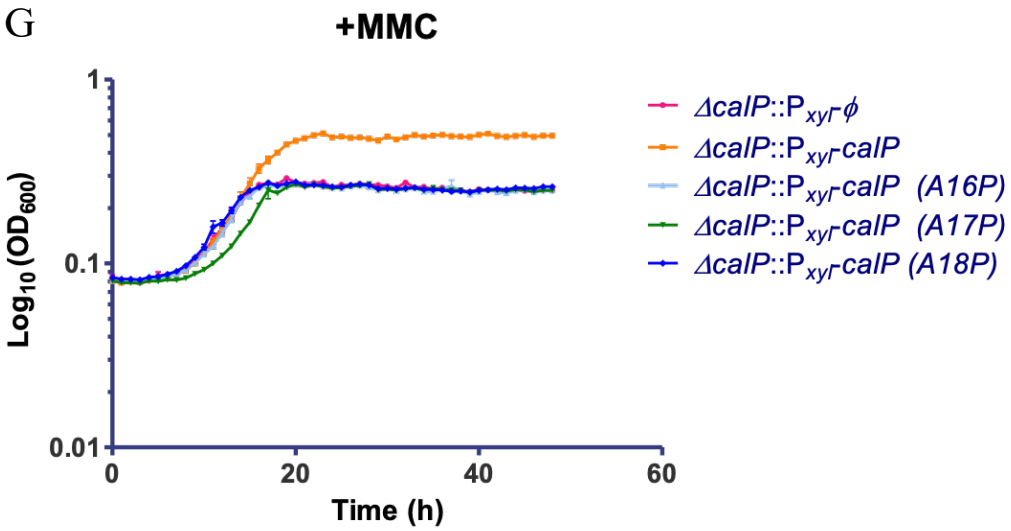
+MMC
Log10 (OD600)
1
0.1
0.01
0
20
40
60
Time (h)
ΔcalP::Pxyl-ϕ
ΔcalP::Pxyl-calP
ΔcalP::Pxyl-calP (A16P)
ΔcalP::Pxyl-calP (A17P)
ΔcalP::Pxyl-calP (A18P)

H

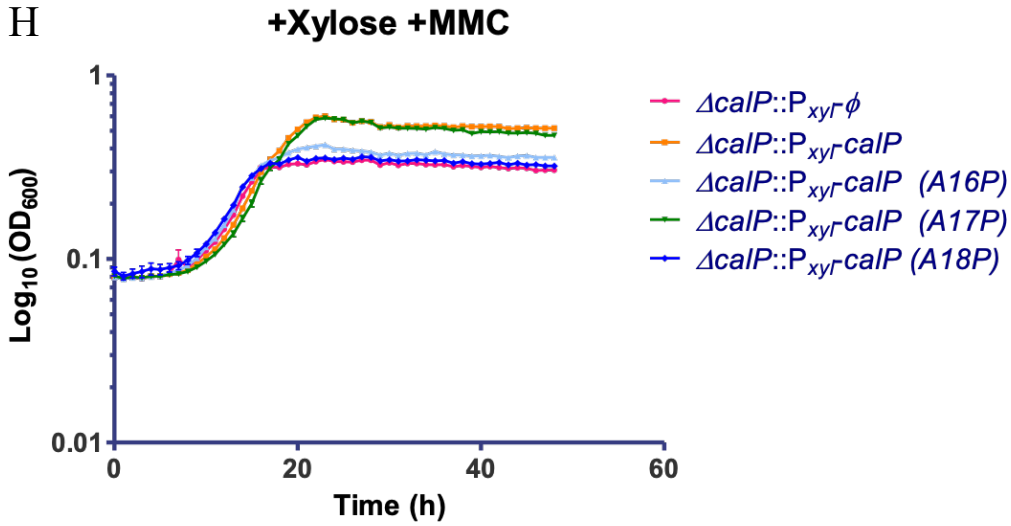
+Xylose +MMC
Log10 (OD600)
1
0.1
0.01
0
20
40
60
Time (h)
ΔcalP::Pxyl-ϕ
ΔcalP::Pxyl-calP
ΔcalP::Pxyl-calP (A16P)
ΔcalP::Pxyl-calP (A17P)
ΔcalP::Pxyl-calP (A18P)

I

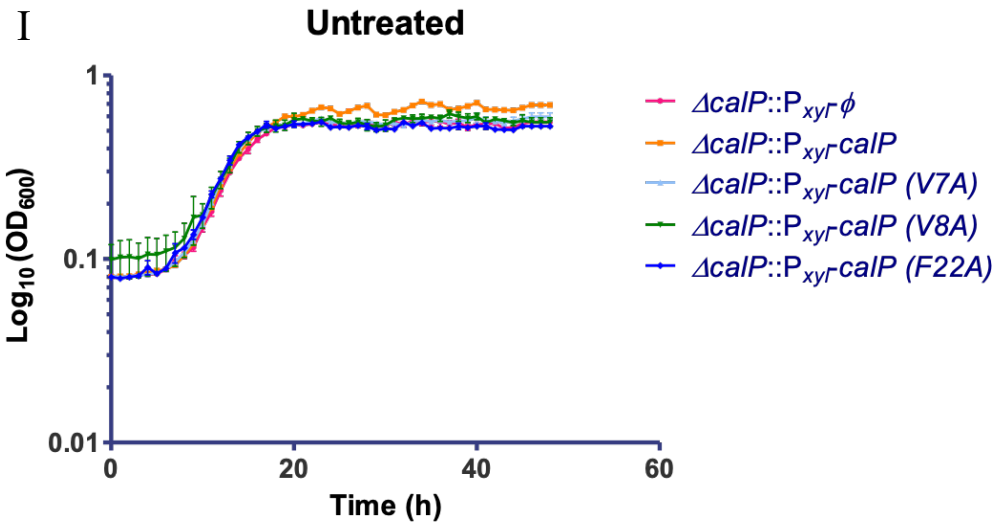
Untreated
Log10 (OD600)
1
0.1
0.01
0
20
40
60
Time (h)
ΔcalP::Pxyl-ϕ
ΔcalP::Pxyl-calP
ΔcalP::Pxyl-calP (V7A)
ΔcalP::Pxyl-calP (V8A)
ΔcalP::Pxyl-calP (F22A)

J

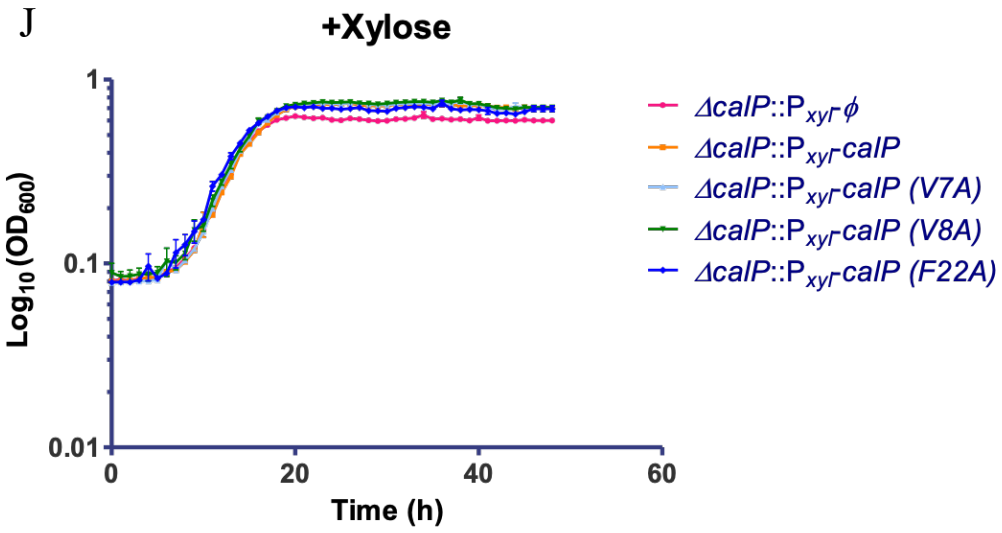
+Xylose
Log10 (OD600)
1
0.1
0.01
0
20
40
60
Time (h)
ΔcalP::Pxyl-ϕ
ΔcalP::Pxyl-calP
ΔcalP::Pxyl-calP (V7A)
ΔcalP::Pxyl-calP (V8A)
ΔcalP::Pxyl-calP (F22A)

K

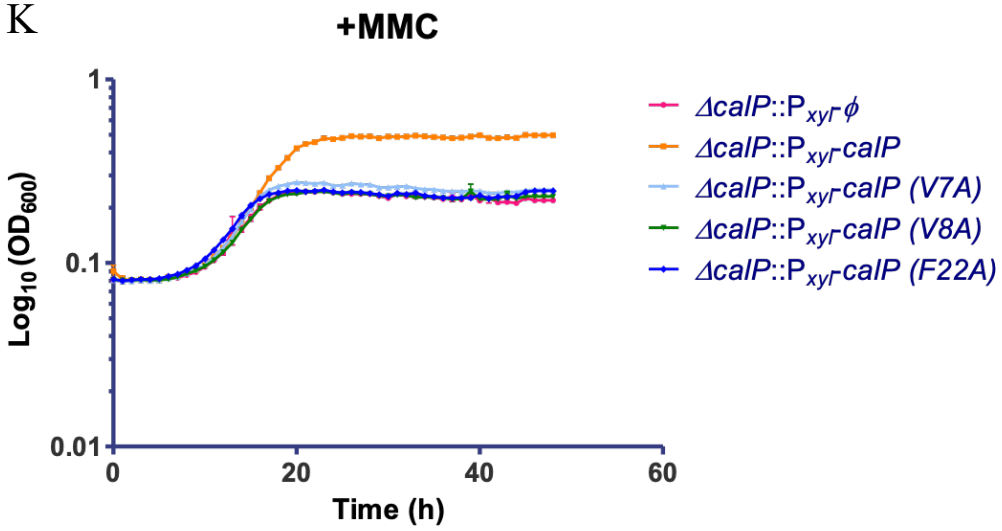
+MMC
Log10 (OD600)
1
0.1
0.01
0
20
40
60
Time (h)
ΔcalP::Pxyl-ϕ
ΔcalP::Pxyl-calP
ΔcalP::Pxyl-calP (V7A)
ΔcalP::Pxyl-calP (V8A)
ΔcalP::Pxyl-calP (F22A)

L

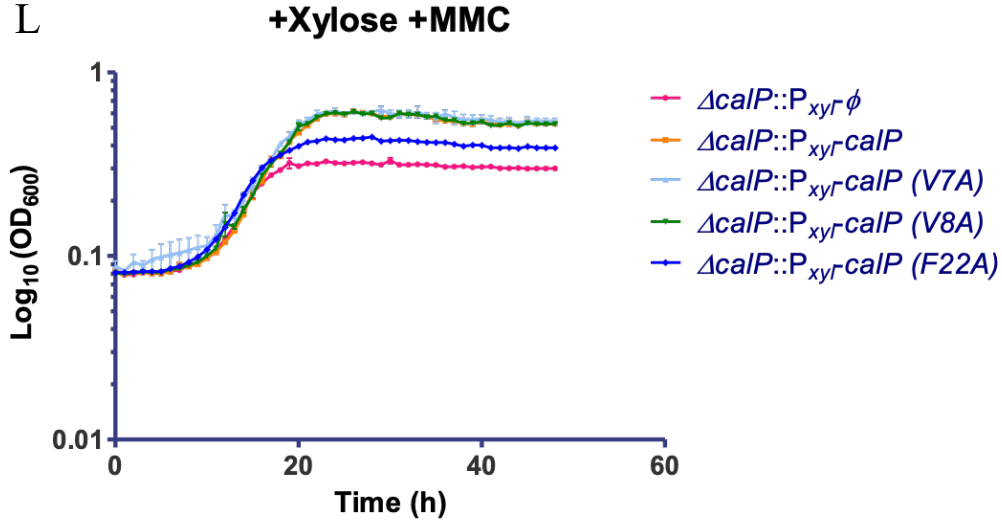
+Xylose +MMC
Log10 (OD600)
1
0.1
0.01
0
20
40
60
Time (h)
ΔcalP::Pxyl-ϕ
ΔcalP::Pxyl-calP
ΔcalP::Pxyl-calP (V7A)
ΔcalP::Pxyl-calP (V8A)
ΔcalP::Pxyl-calP (F22A)

Fig. 25. Substitutions at residues 9, 16, 18, and 22 in CalP result in increased sensitivity of *C. crescentus* when exposed to MMC. Plot displaying the phenotypes of *calP* derivative mutants when exposed to MMC. The *calP* derivative mutants were ectopically expressed using a xylose-inducible promoter (P_{xyl}) in the *ΔcalP* background of *C. crescentus*. Cells were cultured in a PYE medium until reaching mid-exponential phase, approximately at an OD_{600}≈0.5. The cultures were diluted to an $OD_{600}=3.3\cdot10^{-4}$ and then incubated at 30°C for 48 hrs. The OD_{600} of cultures was measured hourly and the average OD_{600} of three cultures was taken for the data analysis. Each plate contained no additives (A, E, I), 0.1% xylose (B, F, J), 0.12 µg/mL MMC (C, G, K), or 0.1% xylose and 0.12 µg/mL MMC combined (D, H, L). Strains included in the test were: *ΔcalP::*P_{xyl}*-ø*, *ΔcalP::*P_{xyl}*-calP-flag, ΔcalP::*P_{xyl}*-calP (V7A)-flag, ΔcalP::*P_{xyl}*-calP (V8A)-flag*, and *ΔcalP::*P_{xyl}*-calP (F22A)-flag* (A-D); *ΔcalP::*P_{xyl}*-ø*, *ΔcalP::*P_{xyl}*-calP-flag, ΔcalP::*P_{xyl}*-calP (A16P)-flag*, *ΔcalP::*P_{xyl}*-calP (A17P)-flag*, and *ΔcalP::*P_{xyl}*-calP (A18P)-flag* (E-H); *ΔcalP::*P_{xyl}*-ø*, *ΔcalP::*P_{xyl}*-calP-flag, ΔcalP::*P_{xyl}*-calP (L9A)-flag*, and *ΔcalP::*P_{xyl}*-calP (I10A)-flag* (I-L).

2.12 CalP (A16P), CalP (A18P), and CalP (F22A) are unable to self-polymerise *in vitro*

C. crescentus increases CalP production when exposed to DDA such as MMC, MMS, norfloxacin, or ciprofloxacin (Fig. 9). Additionally, CalP forms multimers, whose intensity increases in the presence of DDA, suggesting that CalP multimers are the active forms of the protein (Figs. 16A, 19, 21). CalP appeared as a 10 KDa monomer exclusively when heated at boiling temperature. No other high MW band was visible, suggesting that no additional protein was present in the sample (Figs. 19B, D). Therefore, CalP must self-interact to form multimers, as demonstrated in previous BACTH assays (Fig. 20B). Furthermore, previous sensitivity assays with derivative *calP* mutants showed that substitutions in CalP residues 9th, 16th, 18th, and 22nd reduced *C. crescentus* fitness when exposed to MMC. I hypothesised that single-point mutations of the entire CalP amino acid sequence might result in defective mutants that could not polymerise due to changes in the protein-binding residues. To investigate the effect on the size and polymerisation capability of CalP mutants, I performed immunoblot assays using C-terminally FLAG-tagged derivative mutants (Figs. S18A-M). Additionally, I selected those *calP* mutant strains that exhibited the lowest optical density in previous sensitivity assays when challenged with MMC. To do so, I purified *calP (L9A), calP (A16P)*, *calP (A18P),* and *calP (F22A)* to achieve immunoblots with bands of higher resolution (Fig. 26B). These *calP* derivatives were ectopically inserted at the *xylX* locus of *C. crescentus* Δ*calP* under the xylose-inducible promoter P_{xyl}. As a WT phenotype control strain, I included *C. crescentus* Δ*calP* complemented the with native *calP* at the *xylX* locus (*ΔcalP::*P_{xyl}*-calP-flag*), and as a negative control strain, I used *C. crescentus* WT. Mid-exponential phase cultures were treated with xylose, MMC, both compounds combined or left untreated. Cells were homogenised and resuspended in a Triton-X lysis buffer to solubilise CalP. Cell lysates were incubated with microbeads and conjugated with a monoclonal anti-FLAG antibody. Cell lysates were applied to a column containing magnetic beads to retain C-terminally FLAG-tagged CalP. Proteins were run in a 4-20% Tris-Glycine SDS-PAGE and analysed by immunoblotting with a monoclonal anti-FLAG antibody. The immunoblot results showed that native CalP displayed 8 KDa monomeric

bands and 60 KDa multimeric bands in samples from cells treated with MMC or left untreated (Fig. 26B). However, both polymers showed bands with higher intensity when coming from MMC-treated cells compared to CalP bands that were extracted from untreated cells (Fig. 26B). This intensity increases when *C. crescentus* is exposed to the drug, suggesting that CalP production was greater with MMC than in the free-drug medium (Figs. 16, 21, 26B). CalP (L9A) showed low-intensity monomeric bands of 8 KDa when proteins were isolated from MMC-treated or untreated cells (Fig. 26B). This phenotype indicates a reduction in protein production compared to the native CalP-FLAG control (Fig. 26B). Following MMC exposure, CalP (L9A) exhibited a faint 17 KDa band that did not appear in the CalP control strain (Fig. 26B). CalP (L9A) probably failed to form a complete multimer due to the mutation in the 9th leucine (Fig. 26B). CalP (L9A) also showed a 63 KDa multimer under both conditions (-/+ MMC) with a higher protein size than native CalP (Fig. 26B). CalP (A16P) and CalP (A18P) showed strong monomer production, with no difference in the protein intensity with or without MMC (Fig. 26B). Indeed, these monomers exhibited a lower size than native CalP with and without MMC (Fig. 26B). CalP (A16P) and CalP (A18P) bands had a size of 18, 22, 26, and 38 KDa (Fig. 26B). The size of these bands is halfway between the 8 KDa of the monomeric native CalP and 60 KDa of the multimeric native CalP when exposed or not to MMC (Fig. 26B). *calP* derivative mutants formed truncated multimers with approximately one-third the size of the native CalP multimer (Fig. 26B). In summary, CalP (A16P) and CalP (A18P) could not polymerise nor form multimers with a size comparable to the native CalP (Fig. 26B). Eventually, CalP (F22A) exhibited a WT-like phenotype in the monomeric form, showing an 8 KDa band when cells were treated with MMC or untreated (Fig. 26B). CalP (F22A) could not form any multimer but only a smear in the upper half of the lane when exposed or not to MMC (Fig. 26B). Therefore, CalP (F22A) showed the strongest phenotype compared to the rest of CalP mutants (Fig. 26B). These smears may occur due to the breakage of weak interactions between proteins of a multimer that eventually disassemble while running along the gel. Intriguingly, the band intensity of each defective polymer of CalP (A16P) and CalP (A18P) did not increase upon exposure to MMC, suggesting the deregulation in the production of CalP (Fig. 26B).

Meanwhile, the protein production of the CalP (F22A) monomer increased after exposure to MMC, showing a phenotype comparable to the native CalP monomer (Fig. 26B). Previous Coomassie-stained polyacrylamide gels and immunoblot assays showed that heating samples at boiling temperature disrupted CalP self-interaction and disaggregated protein multimers to monomers (Fig. 19C, D). To investigate whether defective multimers of CalP mutants get destabilised and disassemble into monomers, I heated proteins at 100°C and blotted them in a membrane (Fig. 26C). The blot showed that native CalP, CalP (A16P), and CalP (A18P) only showed 8 KDa monomers with or without MMC (Fig. 26C). Therefore, exposure to high temperatures may have disassembled multimers into monomers, since multimers were no longer visible in the blot when proteins were previously incubated at 100°C (Fig. 26C). Intriguingly, the 63 KDa CalP (L9A) multimers became smeary and disassembled into three new 18, 22 and, 26 KDa multimers (Fig. 26C). The smeary multimers of CalP (F22A) were brighter in the heated samples than in the unheated samples of the previous immunoblot (Fig. 26C). CalP (A16P) and CalP (A18P) also showed smears, although they had a lower intensity than the smeary CalP (F22A) (Fig. 26C). Monomers of the native CalP, CalP (A16P), and CalP (A18P) remained unchanged after exposure to high temperatures (Fig. 26C). Nonetheless, monomers of CalP (L9A) and CalP (F22A) surprisingly disappeared after exposure to high temperatures (Fig. 26C). Native CalP production from MMC-treated or untreated cells did not show any difference after heating samples (Fig. 26C). Whereas the unheated native CalP markedly increased multimer intensity with MMC (Fig. 26C). In summary, multimers of CalP derivative mutants disassembled into monomers after exposure to high temperatures, comparable to the phenotype of the native CalP. However, CalP (L9A) was the exception, showing multimers with a lower size than the other multimers with or without MMC (Fig. 26C). Multimeric CalP must establish strong interactions with solid bonds since the detergents used to denature proteins in the preparation of samples for immunoblot assays could not disrupt their connections (Figs. 14C, D). However, high temperatures could break CalP-self-interaction that detergents could not (Figs. 14C, D). Truncating the amino acid sequence of CalP derivative mutants L9A, A16P, A18P, and F22A prevented CalP-FLAG from

multimerising (Fig. 26B). These results are consistent with previous results in which only the derivative mutant *calP (L9A), calP (A16P)*, *calP (A18P),* and *calP (F22A)* showed sensitivity to MMC (Figs. 25D, H, L). In conclusion, CalP polymerisation is likely important to counteract DNA damage in *C. crescentus*.

A

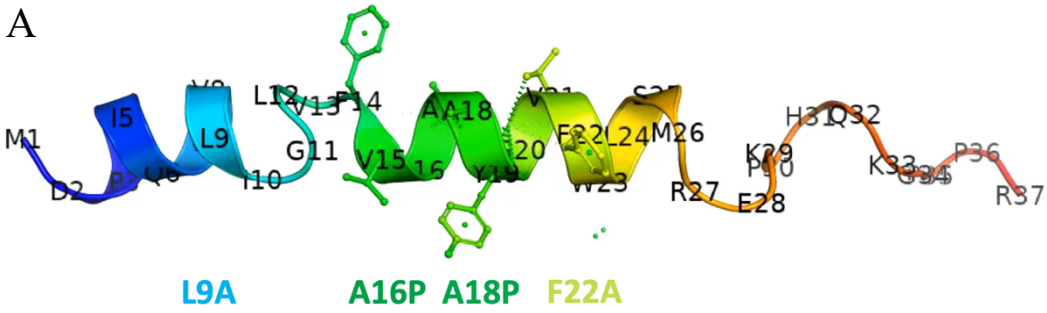
M1
I5
L9
G11
I10
V15
A18
F22
L24
M26
R27
E28
H31
Q32
P36
R37
L9A
A16P
A18P
F22A

B

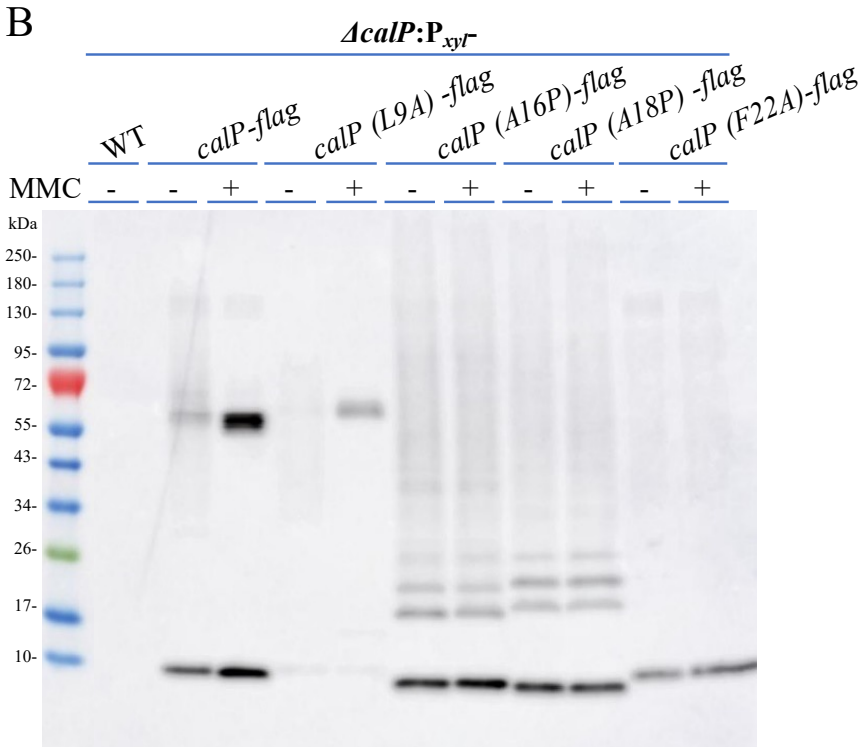
ΔcalP:P xyl-
WT
calP-flag
calP (L9A) -flag
calP (A16P)-flag
calP (A18P) -flag
calP (F22A)-flag
MMC
- - + - + - + - + - +
kDa
250-
180-
130-
95-
72-
55-
43-
34-
26-
17-
10-

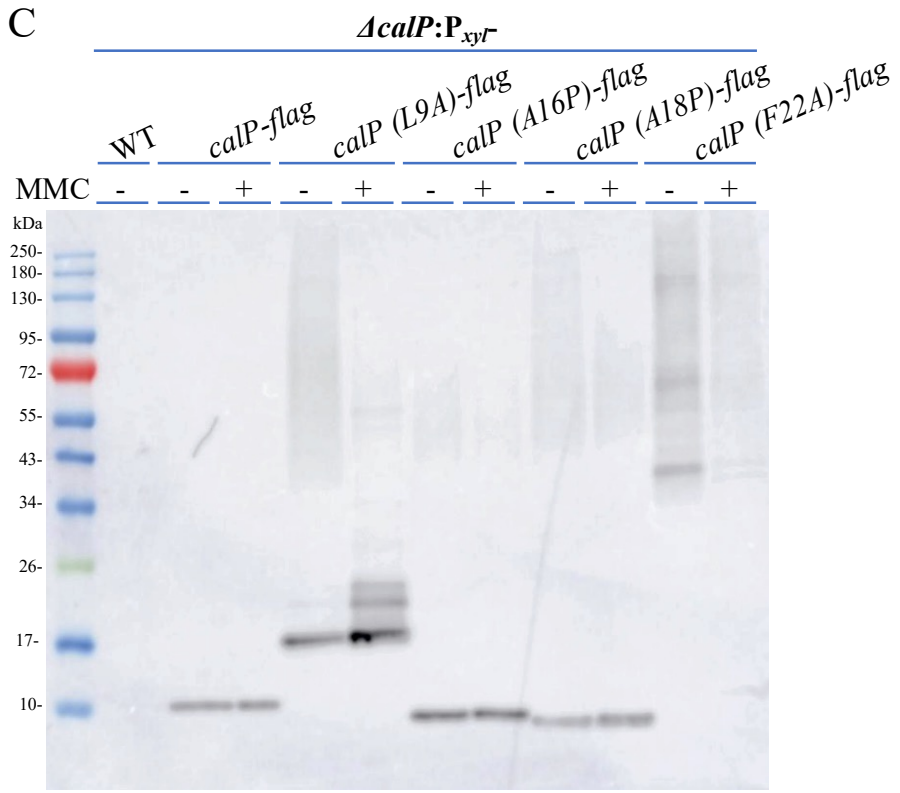

Fig. 26. CalP (A16P), CalP (A18P), and CalP (F22A) cannot form stable multimers. (A) Image of the CalP structure highlighting the substituted residues that exhibit the most affected phenotype. The image was generated using protein bioinformatic software for structure prediction and visualised using PyMOL, a molecular visualisation system. (B) Western blot assays showing truncated versions of CalP when cells were treated with MMC or left untreated. *calP* mutants were ectopically expressed from the xylose-inducible promoter P$_{xyl}$ in a *C. crescentus ΔcalP* background. Cells were grown in a PYE medium until reaching mid-exponential phase and were subsequently treated with either 0.1% xylose, 0.12 µg/mL MMC, both combined or left untreated. Cell lysates were mixed with anti-FLAG antibody conjugated with magnetic beads and passed through a purification column to retain C-terminally FLAG-tagged CalP. Eluates were run in a 4-20% SDS-PAGE and blotted with a 1:10000 α-FLAG antibody to highlight the desired bands. Strains used in the immunoblot: WT (only exposed to MMC but not xylose), *ΔcalP*::P$_{xyl}$-*calP-flag, ΔcalP*::P$_{xyl}$-*calP (L9A)-flag, ΔcalP*::P$_{xyl}$-*calP (A16P)-flag*, *ΔcalP*::P$_{xyl}$-*calP (A18P)-flag* and *ΔcalP*::P$_{xyl}$-*calP (F22A)-flag* incubated at RT for 30 min. (C) The same samples as in (B) with an additional incubation step at 100°C for 5 min.

To confirm the loss of interaction among truncated CalP mutants incapable of forming multimers, I conducted a BACTH assay *in vivo* using the *calP* derivative mutants that exhibited the most pronounced phenotypes. For this test, I used *calP (L9A)*, *calP (L12A)*, *calP (A16P)*, *calP (A17P)*, *calP (A18P),* and *calP (A22P)* strains. To achieve this, I fused each *calP* derivative mutant in-frame with the C-terminus of either the T18 (pUT18C) or T25 (pKT25) subunits of *E. coli* adenylate cyclase (CyaA) [587] (Fig. 20A). If two units of a derivative CalP interact with each other, both CyaA subunits fused to each protein also interact. This synthesis leads to the creation of a compound that manifests a phenotypic trait *in vivo* [587] (Fig. 20A). I performed a transformation of *E. coli cya*$^{-}$ using plasmids pUT18C and pKT25, which contain fusions of *calP* derivative mutants to the CyaA subunits. I also included both empty vectors as control strains for non-interaction. I conducted tests to assess interactions between a *calP* derivative mutant fused to T18 and the identical derivative mutant fused to T25. I evaluated the interaction of each *calP* derivative mutant fused to T18/T25 with the empty vectors containing fusion-less T18/T25 subunits. Additionally, I assessed the interaction between both empty subunits as a control for non-interaction. As a self-interaction control, I conducted tests using the T18/T25 subunit fused separately to the native *calP* and fused to ZIP [587] (Fig. 20B). I streaked the strains onto a selective MacConkey agar medium and incubated them at 30ºC for 48 hrs. The magenta colour may indicate that the adenylate cyclase subunits of each plasmid interact, indicating that *calP* derivatives also interacted. Strains harbouring plasmids carrying *calP (A17P)* and *calP (A18P)* showed white colonies, indicating no self-interaction (Fig. 27). In contrast, *E. coli* strains expressing native *calP* and *calP (L12A)* had a strong magenta colour like the ZIP positive control strain, which indicates protein self-binding (Fig. 27). Meanwhile, *calP (L9A)* and *calP (A16P)* strains exhibited a light magenta colour that indicates a weak protein self-interaction (Fig. 27). This weak protein-protein interaction may imply the inability of *calP (L9A)* and *calP (A16P)* to establish robust bonds within key residues. Assays assessing the interactions between strains carrying a *calP* derivative mutant and strains with the empty vector control T18/T25 showed white colonies, indicating no binding between T18 and T25 subunits (Fig.

27). *E. coli* AB1157, a negative control, did not form colonies because it was not transformed with any plasmid, so it lacked antibiotic-resistance cassettes. This phenotype demonstrates that all other strains thrived despite having antibiotics in the medium. The plasmid-containing strains could form colonies because they harboured the vectors pKT25 and PUT18C that confer them resistance to antibiotics (Fig. 27). The results of this BACTH assay support the observations seen in previous immunoblot assays in which proteins with substitutions in key residues could not polymerise (Figs. 26B, 27). In conclusion, this test confirms that CalP self-binding is essential for protein polymerisation and switching to the active form.

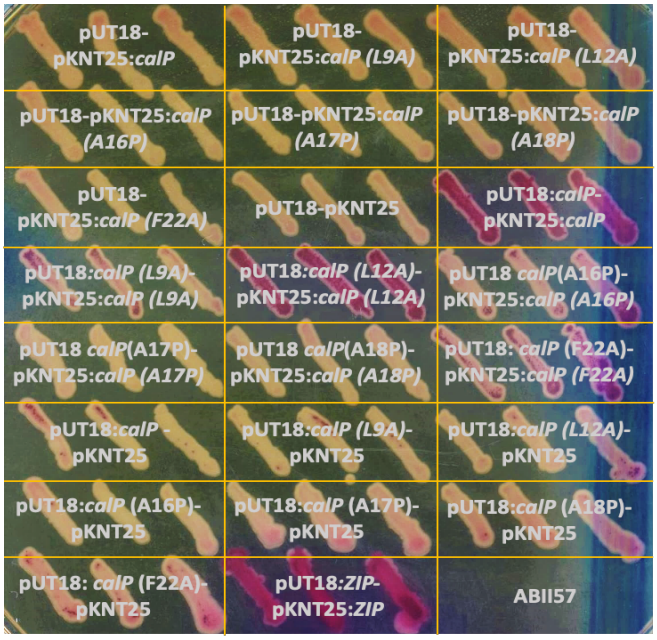

Fig. 27. CalP does not interact with itself in *E. coli* when some key residues are mutated. BACTH assay testing the self-interaction of CalP derivatives L9A, L12A, A16P, A17P, A18P, and F22A fused to the T18 or T25 subunit of *E. coli* adenylate cyclase. As a negative control, strains harbouring empty vectors pUT18C (T18) and pKT25 (T25) were tested against different CalP derivative strains and between each other. As a positive control strain, CalP-CalP and ZIP-ZIP interactions were also tested. *E. coli* strains harbouring each pair of modified vectors were streaked on MacConkey plates (1% maltose, 0.5 mM IPTG, 50 µg/mL kanamycin, 100 µg/mL carbenicillin) and incubated at 30°C for 48 hrs. Magenta colonies indicate interaction and white colonies show no interaction.

2.13 CalP cannot be inserted into the membrane when key residues are mutated

Previous sensitivity assays showed that the presence of MMC caused sensitivity in *C. crescentus* derivative mutants with substitutions in the CalP residues 9th, 16th, 18th, and 22nd in comparison to WT (Fig. 25). Additionally, western blot results indicated that mutating certain CalP amino acids became essential for self-interaction and thus CalP polymerisation (Fig. 26). Indeed, membrane fractionation analysis suggested that CalP is a membrane protein, and polymeric CalP was more enriched in the membrane than monomeric CalP (Fig. 21). I demonstrated in previous immunoblot assays that the multimeric state is active form of CalP because it was produced more abundantly after DNA damage induction (Figs. 16, 19, 21). I believe that the insertion of CalP in the membrane is a *sine qua non* condition for the correct function of the protein. Hence, I hypothesise that the inability of CalP to form multimers after mutating certain residues may affect its membrane insertion. To investigate how substitutions of certain amino acids can affect CalP insertion in the cell membrane, I performed a cell fractionation assay by separating the cytoplasmic and membrane fractions of *C. crescentus*. To do so, I evaluated the capacity to insert into the cell membrane of CalP derivative mutants, which showed the strongest sensitivity following MMC treatment and were incapable of self-polymerising. As a native CalP-FLAG control strain, I included *C. crescentus* Δ*calP* complemented with native *calP* in *trans* in the *xylX* locus under the P_{xyl} promoter. As a negative control strain, I inserted the empty plasmid pXYFPC-2 (used to insert genes at the *xylX* locus) into a Δ*calP* background. As an untagged control strain, I included WT. I grew cells to mid-exponential phase in a medium supplemented with 0.12 µg/mL MMC or left unsupplemented. The medium was additionally supplemented with 0.1% xylose to induce the expression of genes under the xylose-inducible promoter $P_{xyl.}$ I homogenised and ultracentrifuged cell lysates at 194000 RCF to separate the membrane from the cytoplasmic fraction. I ran both fractions alongside the whole-cell extract (before ultracentrifugation) that contains the membrane and soluble fractions in a 4-20% Tris-Glycine SDS-PAGE. I immunoblotted the gel and highlighted CalP-FLAG with an anti-FLAG antibody. In the scenario where CalP is a membrane protein, the membrane fraction must

contain the brightest bands. Western blot showed non-specific protein bands in the WT and Δ*calP*::P_{calP}-*ø* untagged control strains in each fraction (Fig. 28A). CalP bands were more abundant in the whole cell extract and membrane fraction than in the soluble fraction (Fig. 28B). This result indicated that CalP is mainly localised in the membrane, as demonstrated in previous results of membrane fractionation assays (Fig. 28B, 21). All fractions exhibited non-specific bands that were also visible in the untagged control strains (Figs. 28A, B). CalP (L9A) bands showed a WT phenotype comparable to the native *calP* strain (positive control) (Fig. 28B). CalP (L9A) also showed protein bands in the whole-cell extract and membrane fraction but barely in the soluble fraction (Fig. 28B). CalP (L9A) bands in the membrane fraction indicate that CalP (L9A) could be inserted into the membrane-like native CalP (Fig. 28B). The CalP (L9A) band intensity was lower than the native CalP band intensity (Fig. 28B). Following exposure to MMC, the intensity of CalP (L9A) monomers remained unchanged, so MMC treatment did not enhance CalP (L9A) production (Fig. 28B). The phenotype of this CalP (L9A) mutant is consistent with the phenotypes observed in previous sensitivity assays or blots assessing the polymerisation pattern of *calP* derivative mutants. The phenotype of CalP (L9A) resembles more the phenotype of WT than the phenotype of CalP (A16P/A18P/F22A) (Figs. 25D, H, L, 26B, 28B). Otherwise, CalP (A16P) showed monomers brighter with higher intensity in the whole cell extract and soluble fraction in comparison to the membrane fraction with or without MMC (Fig. 28C). These results suggest that CalP (A16P) might have had difficulty inserting into the membrane due to the mutation in this critical residue, as it remained predominantly in the soluble fraction (Fig. 28C). CalP (A16P) did not increase band intensity after MMC treatment (Fig. 28C), resembling the CalP (A16P) phenotype from the immunoblot assay in Fig. 26B. However, the native *calP* strain also did not increase band intensity, showing a phenotype that was sometimes observed in CalP monomers (Fig. 19D). Similarly, CalP (A17P) exhibited bands with a higher intensity in the soluble fraction compared to the membrane fraction. These results indicate that CalP (A17P) remained in the cytoplasm and did not insert into the membrane (Fig. 28C). Intriguingly, CalP (A17P) was not sensitive to MMC in competition assays and successfully complemented Δ*calP* (Fig. 25H), even though

it could not insert into the cell membrane (Fig. 26C). The whole-cell extract was strangely fainter than the soluble or membrane fractions, considering that the whole-cell extract consists of both the soluble and membrane fractions combined (Fig. 28C). CalP (A18P) showed a different phenotype in which soluble and membrane fractions had an equal amount of protein (Fig. 28D). The whole-cell extract exhibited a reduced amount of CalP (A18P) (Fig. 28D), like the whole-cell extract of CalP (A17P) (Fig. 28C). CalP (A18P) apparently struggled to insert into the cell membrane but succeeded approximately half of the time (Fig. 28D). CalP (F22A) showed only two bands in the whole-cell extract, but nothing in the soluble or membrane fractions (Fig. 27D). Therefore, since CalP (F22A) did not appear in the soluble or membrane fractions, we cannot conclude whether this derivative mutant protein could insert or not in the cell membrane (Fig. 28D). The size of the bands of CalP (F22A) were slightly higher compared to other *calP* derivative mutant bands such as CalP (A18P) or native *calP* (Fig. 28D). These higher-size bands were comparable to the size of CalP (F22A) monomers observed in the immunoblot assessing the polymerisation pattern of *calP* derivative mutants in Fig. 26B. The exposure of CalP derivatives to MMC did not increase band intensity, which remained unaltered and showed proteins with the same band intensity as in the drug-free medium (Fig. 28B, C, D). In summary, CalP (L9A) was inserted into the membrane as native CalP did and CalP (A16P) and CalP (A17P) could not be inserted into the membrane and remained in the cytoplasm (Fig. 28B, C, D). CalP (A18P) could insert partially into the membrane, and CalP (F22A) did not show a clear phenotype (Fig. 28). To conclude, the incapability of some CalP derivative mutants to insert into the cell membrane may have prevented them from polymerising and get activated to play an important role in the DNA-damage tolerance/repair (Fig. 28C).

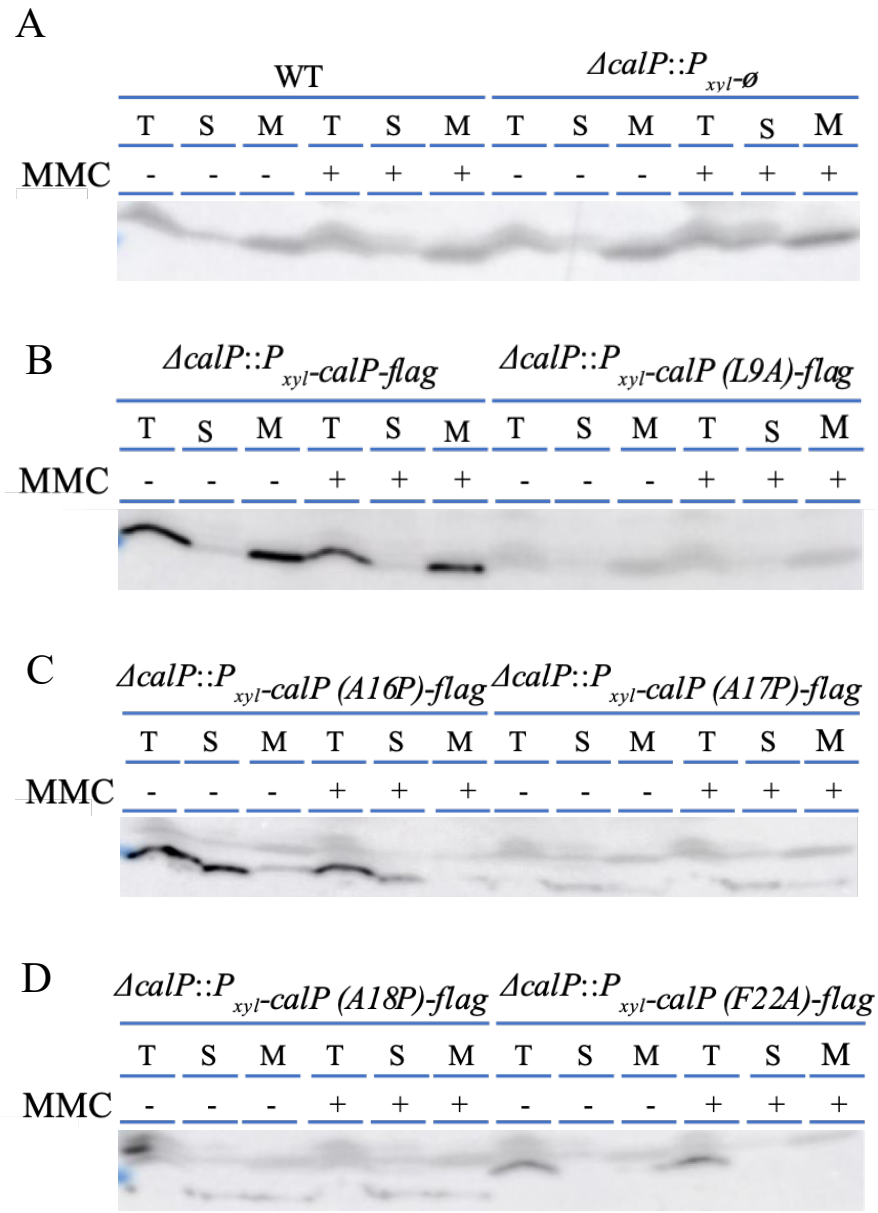

Fig. 28. The mutation of key CalP amino acids prevents it from being inserted into the cell membrane. Western blotting showing CalP isolated from the total cell lysate (T), the cytoplasmic or soluble fraction (S), or the cell membrane fraction (M). Cells were grown in a PYE medium to mid-exponential phase and were treated with 0.1% xylose, 0.12 µg/mL MMC, both compounds combined, or left untreated. *calP* mutants were ectopically expressed from a xylose-inducible promoter (P_{xyl}) in a *C. crescentus ΔcalP* background. Cell fractions were separated by ultracentrifugation, run in a 4-20% SDS-PAGE, and immunoblotted with an α-FLAG antibody. Strains used in each immunoblot were: (A) WT and *ΔcalP*::P_{xyl}-*ø* (untagged control

strains), (B) *ΔcalP*::P_{xyl}-*calP-flag* and *ΔcalP*::P_{xyl}-*calP (L9A)-flag,* (C) *ΔcalP*::P_{xyl}-*calP (A16P)-flag* and *ΔcalP*::P_{xyl}-*calP (A17P)-flag,* and (D) *ΔcalP*::P_{xyl}-*calP (A18P)-flag* and *ΔcalP*::P_{xyl}-*calP (F22A)-flag*. The immunoblot was cropped because several non-specific bands and smears appeared. The only portion of each blot shown in the figure is the region corresponding to the size range from 10 to 17 KDa where CalP monomers are found (according to its predicted size).

2.14 Overproduction of CalP in *C. crescentus* does not promote tolerance to MMC

In previous experiments, we demonstrated that *calP* deletion raised the *C. crescentus* sensitivity in the presence of DDA (Figs. 8-12). *C. crescentus* increases CalP production when exposed to DDAs, especially the 60 KDa polymers. We demonstrated that this 60 KDa multimer is the active form of CalP when cells are challenged with DDA (Fig. 16). Therefore, we theorised that the CalP production increase could enhance the *C. crescentus* tolerance to MMC. I wanted to investigate whether CalP overproduction could enhance and influence the CalP polymerisation pattern and whether this could protect *C. crescentus* from DNA-damaging effects. To answer the first question, I visualised CalP overproduction in MMC-treated or untreated cells in a western blot. To do so, I transformed *C. crescentus* WT cells with a high-copy plasmid harbouring *calP* from the xylose-inducible promoter P_{xyl} (WT+pBXMCS-2::P_{xyl}-*calP-flag*). Cells were cultured to mid-exponential phase in a medium supplemented with 0.1% xylose, 0.12 µg/mL MMC, a combination of both compounds or in the absence of either. I homogenised cells and immunoprecipitated CalP-FLAG with an anti-FLAG antibody. I ran the overproduced purified CalP-FLAG in a 4-20% Tris-Glycine SDS-PAGE and immunoblotted it with an α-FLAG antibody. 8 KDa monomeric CalP-FLAG bands were strongly produced and accumulated at the bottom of the immunoblot when treated with xylose, MMC, both compounds combined, or left untreated (Fig. 29). The intensity and so the production of the 8 KDa CalP monomer was invariable across all conditions (Fig. 29). CalP also showed 55 KDa multimeric bands under all conditions. However, as opposed to the monomeric bands, the multimeric bands increased their brightness only upon exposure to xylose or with the combination of xylose and MMC (Fig. 29). Monomeric CalP showed higher intensity bands than multimeric CalP in all tested conditions (Fig. 29). I hypothesised that the accumulation of monomeric CalP could have overloaded the transport system that delivers CalP to the cell membrane, where it polymerises (Fig. 29). Hence, CalP could not be delivered and remained accumulated in the cytoplasm in a monomeric form. This accumulation was particularly unusual when cells were challenged with MMC, as evidenced by the significant increase in multimeric CalP band intensity,

as shown in previous immunoblots (Figs. 16, 19, 21). Intriguingly, each lane corresponding to a different condition displayed a smear from 30 KDa to 130 KDa, likely indicating a failed attempt of CalP to polymerise (Fig. 29). Similar to the observations in the earlier western blot depicted in Fig. 26, where CalP derivative mutants were assessed, each protein displayed an inability to polymerise. This resulted in a smear spanning the upper half of the lane (Fig. 26). Perhaps the accumulation of monomeric CalP impedes the formation of multimers. Therefore, incomplete multimers may be too unstable to resist the tension of running across the gel and eventually disassemble. To summarise, despite CalP overproduction, it predominantly persisted in the monomeric state, with only a fraction undergoing polymerisation (Fig. 29).

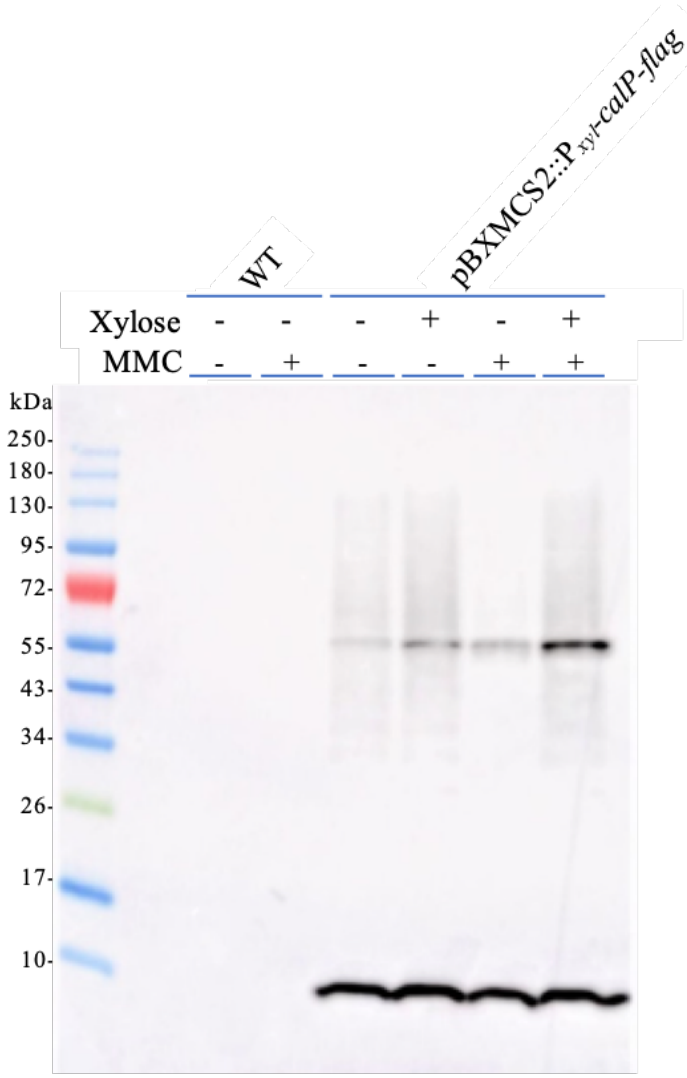

Fig. 29. CalP accumulates in monomeric form when is overproduced in *C. crescentus*. CalP polymerisation rose when *calP* expression from pBXMCS::P_{xyl}-*calP-flag* was induced with the combination of xylose and MMC. Western blot analysis was performed on overproduced CalP purified from the *C. crescentus* strain. The strain expressed *calp-flag* from the xylose-inducible promoter (P_{xyl}) on the non-integrative plasmid pBXMCS-2. WT was included in the assay as control strain without any tag. Cells were grown to mid-exponential phase in a liquid medium and cells and exposed to either 0.1% xylose, 0.12 µg/mL MMC, both compounds, or left untreated. Cultures were incubated 30 °C for 2 hrs. Proteins were denatured with SDS and β-mercaptoethanol, loaded in a 4-20% Tris-Glycine SDS-PAGE, and detected using an anti-FLAG antibody. On the two left lanes of the Western blot are the bands of the untagged WT. On the four right lanes are the bands of the overproduced CalP (pBXMCS-2::*calP-flag*).

To test whether a higher CalP production improves *C. crescentus* tolerance to DDA, I tested pBXMCS-2::*calP-flag* in a sensitivity assay to analyse cell tolerance in a liquid medium with MMC. As control strains, I included WT, the empty overexpression plasmid pBXMCS-2, and the plasmid pBXMCS-2 carrying the untagged *calP* (pBXMCS-2::*calp*). I grew cells to mid-exponential phase in a liquid medium and treated cultures with 0.1 % xylose, 0.75 µg/mL MMC, both compounds combined, or left untreated. The OD_{600} was measured hourly in a 96-well plate incubated for 48 hrs at 30°C in an automated plate reader. I established the same definition for the limits of the exponential and stationary phases and the same ratio to compare the optic densities of two different strains, as described in section 2.2. All strains in the free-antibiotic medium showed a similar sensitivity compared to WT, which reached an $OD_{600}\approx0.7$ in the stationary phase 40 hrs after inoculation (Fig. 30A). Every strain in the xylose-supplemented medium also exhibited overlapping growth curves that reached an $OD_{600}\approx0.9$ in the stationary phase after incubation for 40 hrs (Fig. 30B). Xylose- or xylose- and MMC-treated strains harbouring the vector showed marked difficulty increasing the cell optical density and reaching an $OD_{600}\approx0.08$ after 35 hrs (Fig. 30C, D). Interestingly, WT started the exponential phase 5 hrs after inoculation in the medium with MMC or xylose and MMC combined. This entry into the exponential phase occurred 7-fold earlier than the strains harbouring the pBCMCS-2 vector (Fig. 30B). Strains expressing pBCMCS-2 started a late and short exponential phase that reached an $OD_{600}\approx0.2$ after approximately 48 hrs, which was 1.5-fold lower than the $OD_{600}\approx0.3$ of WT (Figs. 30C, D). The growth curves for all tested strains remained very similar irrespective of treatment with MMC alone or in combination with xylose (Figs. 30C, D). This result suggests that the addition of xylose did not influence the phenotype of any strain (Figs. 30C, D). The late increase in the optical density observed in strains harbouring the overexpression plasmid when exposed to MMC alone or in combination with xylose was significantly reduced (Figs. 30A, C, D). This reduction amounted to 3.5-fold compared to the $OD_{600}\approx0.7$ observed in the same strains in the untreated medium (Figs. 30A, C, D). Similarly, the $OD_{600}\approx0.9$ of the strains with pBCMCS-2 was reduced by 4.5-fold when exposed to the xylose-

supplemented medium compared to the supplementation to the medium with a combination of xylose and MMC (Figs. 30B, C, D). In summary, WT showed the highest optical density compared to the strains harbouring the empty plasmid with MMC or the combination of xylose and MMC together (Figs. 30C, D). Even the strain that only contained the empty plasmid exhibited a significant sensitivity compared to WT when challenged with MMC or both xylose and MMC combined (Fig. 30C, D). Therefore, the presence of the plasmid seemed to be detrimental to the sensitivity of *C. crescentus* and diminished the ability of the cell to cope with DNA damage. To conclude the analysis, which compares the strains harbouring the overexpression vector, the insertion or not of *calP* or *calP-flag* did not confer any advantage to *C. crescentus* to resist or minimise the effect of MMC. Therefore, the *calP* expression was insufficient to counteract the effect of DNA damage in conjunction with the expression of a high-copy number plasmid. *C. crescentus* might have been overwhelmed in the presence of MMC, the sensitivity rose considerably compared to cells unexposed to DDA or cells not harbouring the high-copy plasmid.

A

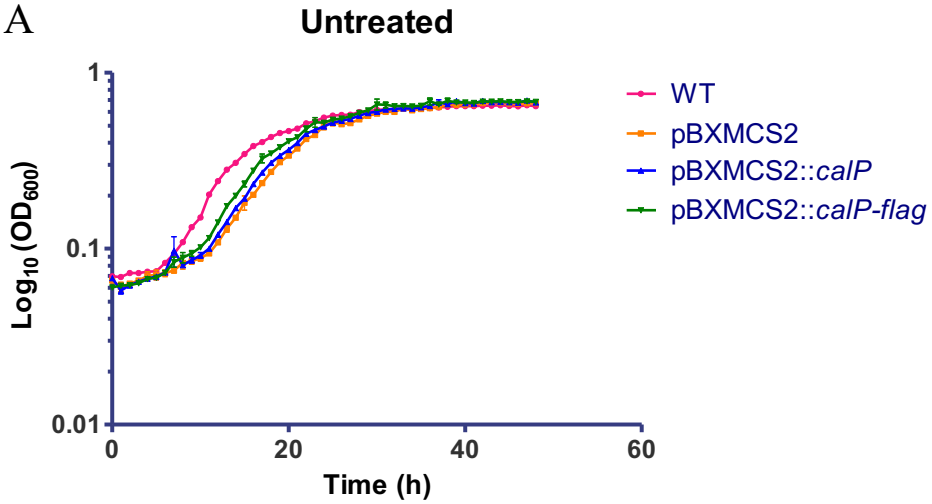
Untreated
1
0.1
0.01
Log10(OD600)
0
20
40
60
Time (h)
WT
pBXMCS2
pBXMCS2::calP
pBXMCS2::calP-flag

B

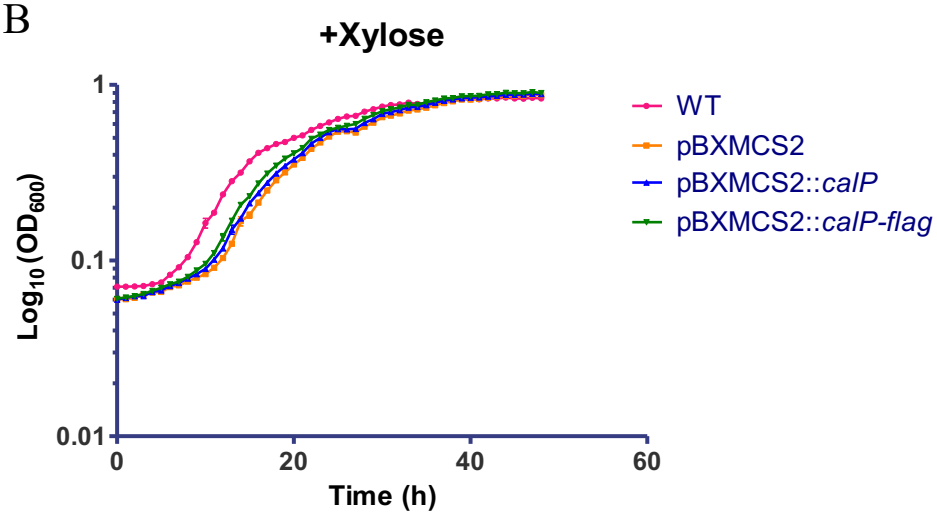
+Xylose
1
0.1
0.01
Log10(OD600)
0
20
40
60
Time (h)
WT
pBXMCS2
pBXMCS2::calP
pBXMCS2::calP-flag

C

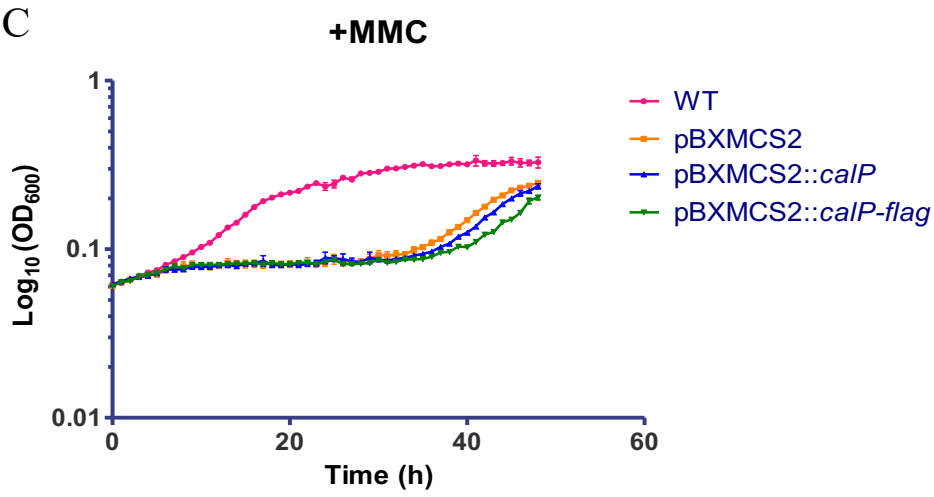
+MMC
1
0.1
0.01
Log10(OD600)
0
20
40
60
Time (h)
WT
pBXMCS2
pBXMCS2::calP
pBXMCS2::calP-flag

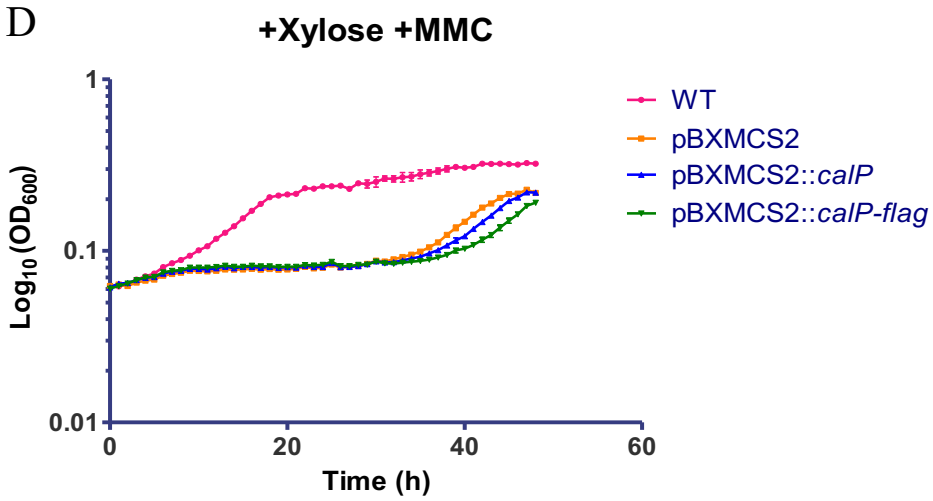

Fig. 30. *calP* overexpression in a liquid medium does not increase *C. crescentus* resistance to MMC. Plot showing *calP* overexpression in a liquid medium. *calP* was expressed from the xylose-inducible promoter (P_{xyl}) of the non-integrative expression plasmid pBXMCS-2 in a *C. crescentus* WT background. Cells were grown in a PYE medium to mid-exponential phase and cultures were diluted to an $OD_{600}=3.3\cdot10^{-4}$. Cells were treated with 0.1% xylose, 0.12 µL MMC, both compounds combined, or left untreated. Plates were incubated at 30°C for 48 hrs in an automated plate reader. The OD_{600} was measured at the indicated times, and the average of three cultures was taken to make the plot. WT, *ΔrecA, ΔcalP,* WT+PBXMCS-2, and WT+PBXMCS-2::*calP* strains were tested on a plate with (A) no additives, (B) 0.1% xylose, (C) 0.75 µg/mL MMC, or (D) 0.1% xylose and 0.75 µg/mL MMC combined.

2.15 CalP cannot form stable multimers when it is heterologously produced in *E. coli*

CalP forms multimers that localise in the *C. crescentus* cell membrane. The truncation of key residues causes the inability of CalP to insert into the membrane. I wanted to investigate whether CalP could also self-polymerise when it is heterologously produced in *E. coli*. To do so, I transformed *E. coli* AB1157 with the high-copy plasmid pUT18C (-T18) expressing *calP-flag* from the IPTG-inducible promoter P_{lac} (AB1157::P_{lac}-*calP-flag*). As a negative control strain, I transformed AB1157 with the high-copy plasmid expressing untagged *calP* from P_{lac} (AB1157::P_{lac}-*calP*). I grew cells to mid-exponential phase in a liquid medium supplemented with 0.1 mM IPTG, 0.25 µg/mL MMC, both compounds combined or left unsupplemented. I homogenised cells and purified CalP-FLAG by immunoprecipitation using an anti-FLAG antibody. Proteins were run in a 4-20% Tris-glycine SDS-PAGE and immunoblotted with α-FLAG/M2. The immunoblot showed two bright 8 KDa CalP-FLAG monomeric bands when challenged or not with MMC (Fig. 31). The other two fainter 13 KDa bands were visible under both conditions (Fig. 31). The upper half of the blot showed two CalP-FLAG smears, spanning from 29 KDa to approximately 180 KDa when proteins were isolated from cells treated with MMC or left untreated (Fig. 31). However, the 60 and 72 KDa multimeric CalP bands observed when CalP-FALG was produced in *C. crescentus* (Figs. 16, 19, 21) did not appear in *E. coli* whether with or without MMC treatment (Fig. 31). The untagged CalP control strain produced two distinct 120 KDa bands, irrespective to MMC exposure, with no evidence of any other CalP-like bands (Fig. 31). However, given that the *calP* strain was tag-free, those two bands were likely non-specific and unrelated to the CalP protein (Fig. 31). The CalP-FLAG polymerisation pattern in *E. coli* (Fig. 31) was different from CalP-FLAG in *C. crescentus* (Figs. 16, 19, 21). The *E. coli* polymerisation pattern resembles previous phenotypes of truncated CalP derivative mutants which failed to polymerise in *C. crescentus* (Fig. 26). In this assay, *E. coli* produced native C-terminally tagged CalP-FLAG but did not exhibit polymerisation either (Fig. 31). As I demonstrated previously, CalP may need to insert into the cell membrane to polymerise. The absence of a *calP* homolog in the *E. coli* genome, could potentially lead to

inefficient transportation of CalP to the cell membrane for polymerisation. CalP may necessitate specific element absent in *E. coli* for proper transport, membrane insertion, or polymerisation.

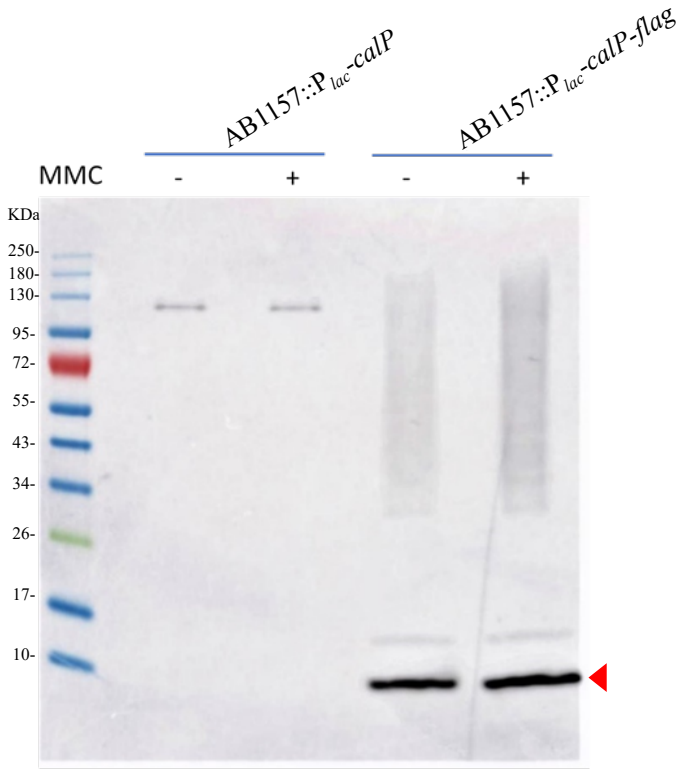

Fig. 31. CalP does not stably polymerise when it is heterologously produced in *E. coli*. Immunoblot showing CalP production in *E. coli* and its polymerisation pattern when exposed to MMC. c*alP* was expressed from the lactose-inducible promoter P_{lac} in the non-integrative plasmid pUT18C, replacing the T18 subunit with either *calP* or *calP-flag*. The *E. coli* AB1157 strain was transformed with AB1157::P_{lac}-*calP* and AB1157::P_{lac}-*calP-flag*. Strains were exposed to IPTG to induce the expression of *calP* and *calP-flag*. Cells were grown to mid-exponential phase in a liquid medium at 30°C. Cells were treated with 0.25 µg/mL MMC, 0.1 mM IPTG, both compounds combined or left untreated. I performed co-immunoprecipitation using anti-FLAG resin columns with magnetic beads to isolate proteins. Samples were run in a 4-20% Tris-Glycine SDS-PAGE and detected using an anti-FLAG antibody. Untagged CalP (AB1157::P_{lac}-*calP*) was used as a control strain in the left lanes of the Western blot, while CalP (AB1157::P_{lac}-*calP-flag*) was placed in the right lane.

2.16 CalP forms defective multimers in the membrane when heterologously produced in *E. coli*

I demonstrated that CalP was unable to self-polymerise in *E. coli*. However, we wondered whether this inability to polymerise was caused by the incapacity of CalP to insert into the cell membrane and, as a result, was unable to polymerise. To investigate this possibility, I performed a cell fractionation test by separating the cytoplasmic and membrane fractions to discover in which fraction CalP was found. To do so, I assayed the *E. coli* strains AB1157::P_{lac}-*calP-flag* and AB1157::P_{lac}-ø (a vector-less AB1157 strain used as a negative control). I grew cells to mid-exponential phase and treated cultures with 0.1 mM IPTG, 0.25 µg/mL MMC, both compounds combined or left untreated. I homogenised cells in a Triton-X-containing buffer to solubilise membranes and ultracentrifuged at 194000 RCF. The pre-centrifuged fraction was saved to be used as a whole-cell extract control. I ran the three fractions in a 4-20% Tris-Glycine SDS-PAGE and immunoblotted with a FLAG-tag antibody. CalP-FLAG showed 10 KDa bands in each fraction when cells were unexposed to DDA, exposed to IPTG, MMC, or both (Fig. 32A). Additionally, a 12 KDa CalP band appeared in the membrane fraction in every condition (Fig. 32A). These 12 KDa bands were not visible in the soluble fraction but were evident in the membrane and whole-cell extract (Fig. 32). The whole cell extracts only showed a single thick band, probably because the 10 and 12 KDa bands merged due to the large wideness of both multimers (Fig. 32A). CalP-FLAG was produced even in the absence of IPTG, possibly due to the IPTG-inducible promoter (P_{lac}) being activated by endogenous metabolites, causing the expression of *calP-flag* (Fig. 32A). Expression of *calP* under the P_{lac} promoter remained consistent across all conditions and was not influenced by exposure to MMC (Fig. 32A). In contrast, CalP production increased in *C. crescentus* in the presence of MMC when *calP* was ectopically expressed (Fig. 15). This suggest that *C. crescentus* likely employs a specific posttranslational pathway that activate CalP during the DNA-damage stress response.

Nevertheless, *E. coli* lacks this posttranslational activation system for CalP due to its absence in the bacterium´s native protein repertoire. CalP was fully polymerised

in *C. crescentus*, especially in the presence of MMC (Figs. 16, 19, 21). On the contrary, CalP was unable to form full multimers under any conditions, but only a 12 KDa band in the membrane fraction (Fig. 32A). Therefore, these results support the fact that CalP is localised in the membrane fraction and suggest that CalP needs the membrane as a scaffold to form multimers (Fig. 32A). Faint 25 KDa bands observed in both the *E. coli* strain expressing *calP* (Fig. 32A) and the vector-less control strain *E. coli* (Fig. 32B), were likely non-specific (boxed in red squares).

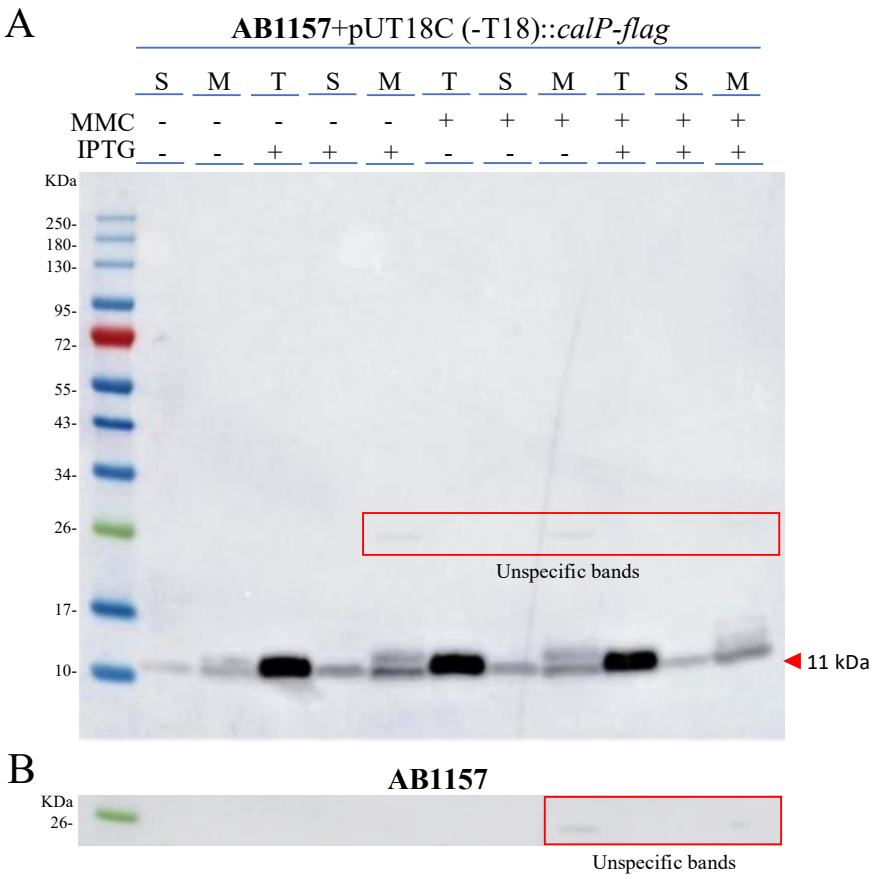

Fig. 32. CalP cannot fully polymerise in *E. coli*. Western blot showing cell fractions with C-terminally FLAG-tagged CalP heterologously produced in *E. coli*. Cells were standardised to a starting OD_{600}=0.1 and grown to mid-exponential phase in a PYE medium. Cultures were treated with 0.1 mM IPTG, 0.25 µg/mL MMC, both compounds combined or left untreated. Cells were homogenised and cell lysates were ultracentrifuged at 194000 RCF to separate the soluble, membrane and whole cell fractions. The three fractions were run in a 4-20% Tris-Glycine SDS-PAGE and blotted with an α-FLAG/M2 antibody. (A) *E. coli* AB1157 strain carrying the plasmid pUT18C (-T18) expressing *calP-flag* from the P_{lac} promoter (A1157::P_{lac}-*calP-flag*). This strain was supplemented with 1 mM IPTG for 3 hrs when necessary to induce *calP-flag* expression. (B) *E. coli* AB1157 was employed as an empty vector control strain. Unspecific bands in the control strain are boxed in red squares and pointed with red arrowheads.

2.17 Heterologous expression of *calP* in *E. coli* does not enhance tolerance to MMC

As I demonstrated in previous sensitivity assays, CalP confers tolerance to DNA-damaging agents in *C. crescentus*. The substitution of certain CalP residues caused the inability of CalP to polymerise and insert into the *C. crescentus* cell membrane, so mutants became sensitive to DDAs. The previous immunoblot assay showed that CalP could not polymerise when it was heterologously produced in *E. coli.* My objective was to investigate whether CalP enhances tolerance to DDA when exposed to MMC. Conversely, I aimed to explore if CalP does affect sensitivity to MMC due to its inability to polymerise and insert into the cell membrane. To do so, I transformed *E. coli* AB1157 with the empty plasmid pUT18C (-T18) as a control strain (AB1157::P_{lac}-ø). Additionally, I used the plasmid expressing *calP* or *calP-flag* from the IPTG-inducible promoter P_{lac} (AB1157::P_{lac}-*calP* or AB1157::P_{lac}-*calP-flag*). I included AB1157 and DH5α (*recA*$^-$) as control without the vector. I grew cells to mid-exponential phase in a liquid medium and incubated cultures at 30°C for 24 hrs. I treated cells with 0.1 mM IPTG, 0.75 µg/mL MMC, both compounds combined or left untreated. The explanation for the definition of the exponential and stationary phases and the comparison between the optical densities of the two strains was described in section 2.2. Strains in the free-drug medium or in the presence of IPTG exhibited a comparable OD_{600}≈1, showing overlapping plot lines (Fig. 33A). However, DH5α entered the stationary phase 4 hrs after inoculation, which was 2-fold earlier than the other strains (Fig. 33B). These strains entered the stationary phase after 8 hrs, whether treated with IPTG or left untreated (Fig. 33B). Following MMC treatment, the optical density of DH5α remained close to zero, likely due to the lack of *recA*, which made this strain hypersensitive to DDA (Fig. 33C). AB1157::P_{lac}-ø, AB1157::P_{lac}-*calP*, and AB1157::P_{lac}-*calP-flag* when challenged with MMC, entered the stationary phase 7 hrs after inoculation at OD_{600}≈0.3, decreasing to an OD_{600}≈0.2 after 13 hrs (Fig. 33C). Whereas the plot line of AB1157 showed a distinct tendency, maintaining the OD_{600}≈0.05 up to the 13th hr when it started the exponential phase, which reached an OD_{600}≈0.5 after 24 hrs (Fig. 33C). The phenotype shown by the strains exposed to with MMC (Fig. 33C) was very similar to the phenotype of the strains exposed to IPTG+MMC,

suggesting that the addition or not of IPTG to the medium does not make any difference (Fig. 33D). *calP* and *calP-flag* strains exhibited the same sensitivity as the empty vector strain in all plot lines (Fig. 33). This suggests that the presence or absence of *calP* or *calP-flag* did not have an impact on *E. coli* sensitivity to the tested conditions (Fig. 33). Indeed, the presence of the plasmid was detrimental to the survival of *E. coli* when challenged with MMC. All strains harbouring plasmids had a reduced optical density and increased sensitivity compared to the free-plasmid strain (Figs. 33C, D). I can conclude that the production of CalP in *E. coli* did not contribute to lower cell sensitivity in the presence of MMC. These results correlate with previous results where CalP could not polymerise and thus did not configure the active form of the protein. Hence, CalP could not perform its regular activity to reduce the stress generated by the DNA-damaging agent MMC.

A

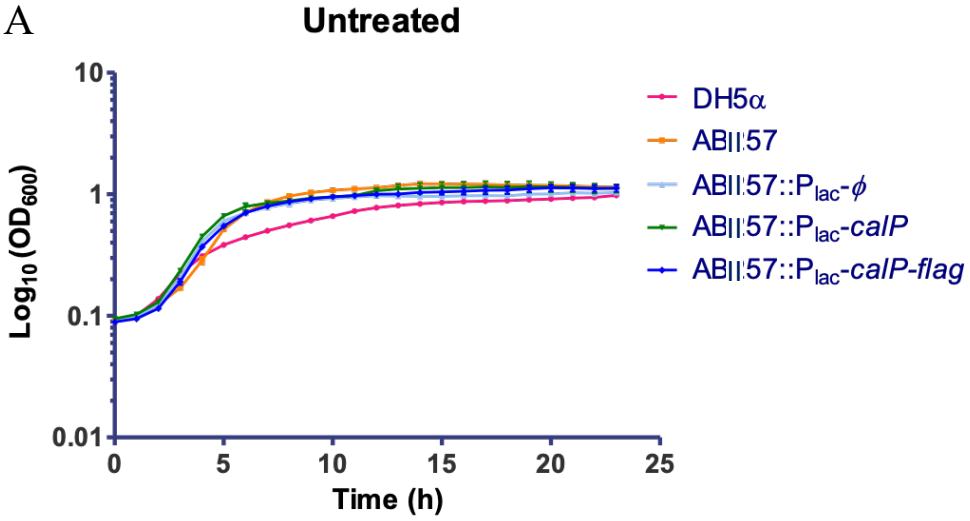
Untreated
Log10 (OD600)
10
1
0.1
0.01
0
5
10
15
20
25
Time (h)
DH5α
ABII57
ABII57::Plac-ϕ
ABII57::Plac-calP
ABII57::Plac-calP-flag

B

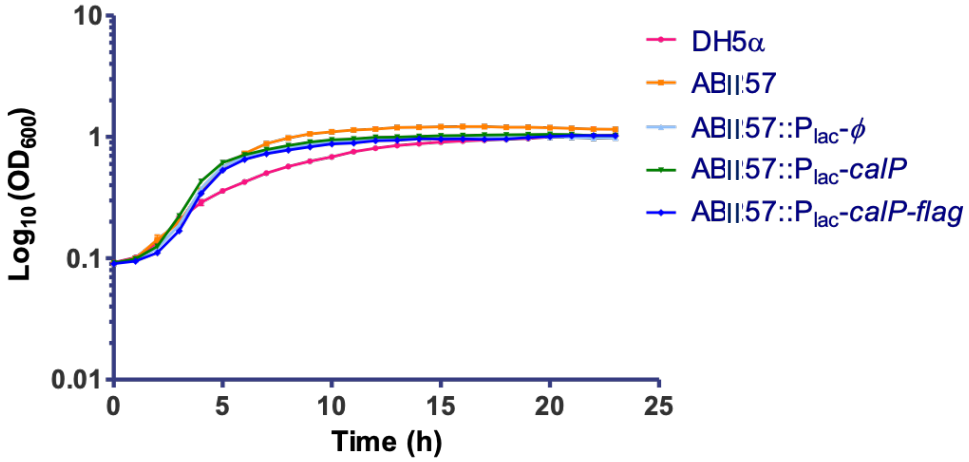
+IPTG
Log10 (OD600)
10
1
0.1
0.01
0
5
10
15
20
25
Time (h)
DH5α
ABII57
ABII57::Plac-ϕ
ABII57::Plac-calP
ABII57::Plac-calP-flag

C

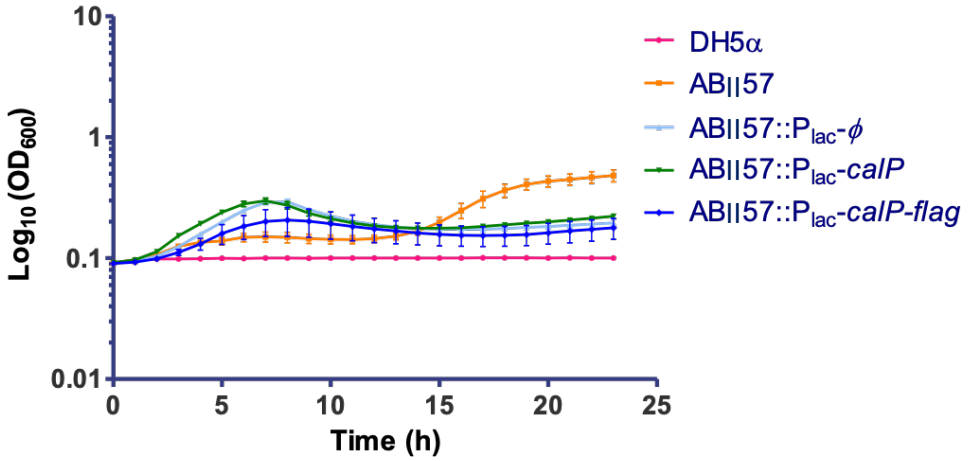
+MMC
Log10 (OD600)
10
1
0.1
0.01
0
5
10
15
20
25
Time (h)
DH5α
ABII57
ABII57::Plac-ϕ
ABII57::Plac-calP
ABII57::Plac-calP-flag

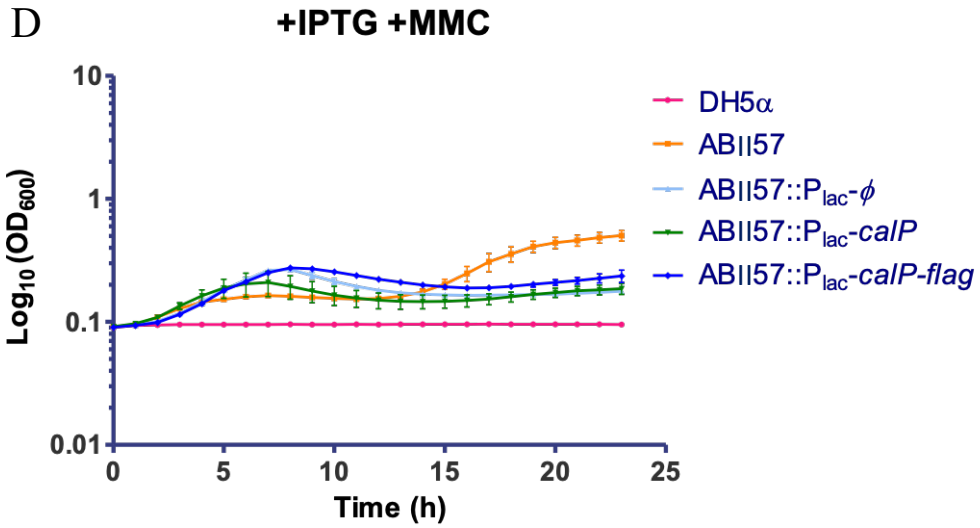

Fig. 33. *calP* heterologous expression does not increase *E. coli* tolerance to MMC. A plot showing the effect of the heterologous expression of *calP* in *E. coli* AB1157 when cells were challenged with MMC. c*alP* was expressed from a lactose-inducible promoter (P_{lac}) in the non-integrative plasmid pUT18C by substituting the T18 subunit for *calP* (untagged control strain) or *calP-flag*. Cells were grown to mid-exponential phase in a PYE medium. Cultures were diluted to an $OD_{600}=3.3\cdot10^{-4}$ and treated with 0.1 mM IPTG, 0.75 µg/mL MMC, both compounds combined or left untreated. *E. coli* strains DH5α, AB1157, AB1157::P_{lac}-ø, AB1157::P_{lac}-*calP*, and AB1157::P_{lac}-*calP-flag* were incubated at 30°C for 24 hrs. The mean of three technical replicates was used to make the plot. The plots correspond to (A) no additives, (B) 1 mM IPTG (to induce *calP* expression from P_{lac}), (C) 0.75 µg/mL MMC, and (D) 1 mM IPTG and 0.75 µg/mL MMC combined.

2.18 Discussion

In this study, I report the discovery of a novel ORF that encodes an SP with an important effect on cell tolerance against DNA-damaging agents. Results indicated that CalP is an amphipathic small transmembrane protein with N_{out}-C_{in} topology. CalP forms a homooligomer in the cell membrane and increases its production upon DNA damage induction in *C. crescentus*.

2.18.1 CalP is involved in DNA damage tolerance/repair in *C. crescentus*

DNA damage repair is a system that specifically fixes damaged DNA caused by distinct agents of different natures, like antibiotics, reactive oxygen species, or UV light [594]. In this work, I report how CalP is required to maintain proper fitness in *C. crescentus* in the presence of DDAs such as MMC, MMS, norfloxacin, and ciprofloxacin. *C. crescentus* possesses other mechanisms, such as *mmcA* and *mmcB,* that are exclusively involved in DNA damage repair when exposed to MMC but not MMS [173]. MmcA is a member of the glyoxalase/dioxygenase protein family that works independently of known DNA damage repair pathways. MmcB is an endonuclease that generates substrates for imuABC-mediated TLS patches [173]. MmcA and MmcB are cytoplasmic proteins targeted to DNA damage produced by MMC [173], suggesting that it is a very specific pathway for repairing the damage caused by double-strand breaks [173]. However, CalP is more generalist and affects the tolerance of a wider range of antibiotics that create distinct types of DNA damage to the cell, such as norfloxacin, ciprofloxacin, MMC, and MMS (Fig. 9).

2.18.2 *calP* encodes a protein

Certain genes are subjected to post-transcriptional regulation by mRNA or ncRNA. The mRNA ChvR represses the TonB-dependent receptor mRNA ChvT by direct base-pairing in *C. crescentus* [444]. In *E. coli,* the *yohP* mRNA accumulates in the vicinity of the plasma membrane and may play some regulatory function in the insertion of YohP into the membrane [455]. It was proposed that *calP* was an ncRNA instead of a protein. The successful complementation suggested that *calP* encoded a protein instead of an ncRNA. Alternatively, the alteration in the nucleotide sequence might affect protein optimisation, resulting in the production

of a defective protein. However, Zhou et al. (2016) demonstrated that codon optimisation has an impact on transcription, but does not affect mRNA translation or stability [595]. I showed that complementation of the *calP* mutant with *scrambled calP* mRNA did not have any effect on the *C. crescentus* phenotype in the presence of MMC or norfloxacin (Fig. 15). Therefore, a putative mRNA transcribed from *calP* is unlikely to perform post-transcriptional regulation, since *scrambled calP* did not increase CalP production after MMC treatment (Fig. 15). However, the regulation of *calP* insertion in the membrane has not yet been tested.

2.18.3 Multimeric CalP

CalP monomeric (or single) form is approximately 8 KDa in size (Figs. 16, 19, 21). However, CalP was predicted to be 3.7 KDa (4.2 KDa for CalP-FLAG). Therefore, three possible theories were feasible for the unexpectedly larger size of CalP in immunoblot assays. The first hypothesis represents a different running pattern between the protein ladder and CalP-FLAG, resulting in deflected values. The second hypothesis is the possibility that two co-translationally nascent CalP dimerise, as demonstrated by Bertolini et al. (2021) and Shieh et al. (2015) [584, 596]. A third option may be a posttranslational modification that enlarges CalP [597-599]. We could not distinguish between these three possibilities by analysing CalP in MP or cryo-electron microscopy assays because of the small size of CalP. Nevertheless, boiling the samples to denature CalP-FLAG resulted in bands with an 8 KDa size, comparable to the size of untreated CalP-FLAG (Fig. 19). Multimers were disrupted into monomers after boiling proteins, so it is likely that putative dimers also get disrupted. A putative posttranslational modification must be very stable for the protein to resist boiling temperatures. However, some modifications like phosphorylation, acetylation, and succinylation could resist such a high temperature but would not double CalP size to that extent. Therefore, the CalP-FLAG size observed in the SDS-PAGEs or immunoblots might not be CalP´s real size but a deviation provoked by a different running pattern compared to the protein ladder.

Changes or deletions of single amino acids can substantially affect homooligomer stability, particularly if the protein interface is altered [573, 581]. Hashimoto et al. (2010) discovered that 25% of homologs had regions that either enhance or inhibit the formation of multimers [581]. They revealed that removing large non-polar side groups, such as phenylalanine or tryptophan, was important to forming protein interactions. A single amino acid replacement was enough to raise polymerisation [582]. I demonstrated that the active conformation of CalP is the multimeric form. The stability of the CalP multimer is compromised by substituting certain residues crucial for the self-interaction that allows polymerisation (Figs. 26B, C). The substitution of the CalP 22nd phenylalanine provoked the total inability of the CalP mutant to polymerise *in vitro* (Figs. 26B, C). Furthermore, this substitution caused one of the sickest phenotypes in *C. crescentus* CalP derivative mutants *in vivo* in the presence of MMC (Figs. 25K, L). Interestingly, other amino acid substitutions that alter CalP stability and interfere with multimerisation causing sensitivity, also occurred in the transmembrane domain (Figs. 22A, E, 25, 26). The substitution of CalP 16th alanine caused multimer destabilisation that impeded correct CalP insertion in the membrane, causing a loss of CalP function (Fig. 27C).

2.18.4 Transport and insertion of CalP

SMPs such as *E. coli* YohP are inserted into the *E. coli* cytosolic membrane through an alternative SRP-mediated recruitment pathway. This pathway transports YohP to be inserted in the membrane by the SecYEG or YidC mechanisms [455]. Nonetheless, whether this system exists in other proteobacteria, such as *C. crescentus,* remains unexplored. CalP was accumulated in a high proportion in the *C. crescentus* membrane after DNA damage (Fig. 21). Nonetheless, CalP heterologously produced in *E. coli* was equally found in the membrane and cytoplasm when DNA damage occurred (Fig. 32A). This phenotype indicates a defective delivery or insertion of CalP into the *E. coli* cell membrane (Fig. 32A). A hypothesis to explain the similarity in the amount of CalP in the cytoplasm and membrane in *E. coli* may be that *C. crescentus* lacks post-transcriptional SRP-mediated transport of SMPs to the *E. coli* cell membrane. Hence, CalP might not be recognised by SRP and may remain in the *E. coli* cytoplasm. Alternatively, CalP

may be delivered to the *C. crescentus* membrane via direct recognition by SecA [458]. Therefore, SRP-independent targeting may not be the optimum option for SMPs in *E. coli,* so the efficiency in recognising and transporting CalP might be quite low. A tripartite motif determines the identification tags for protein targeting factors and is also necessary to recognise and open protein transport channels in the cell membrane [509, 510, 513, 600]. These recognition motifs span the entire length of SPs [451]. CalP might have a different recognition site that is identified by the SRP-mediated transport system of *E. coli.* Alternatively, the impossibility of inserting into the membrane might be due to CalP being residually recognised with low affinity and inefficiently delivered to the cell membrane.

Bertolini et al. (2021) [584] demonstrated that the assembly of homodimers was machine- and species-independent (and even kingdom-independent), and they successfully expressed a nuclear lamin from human cells heterologously in *E. coli*. However, heterologously expressed CalP in *E. coli* could not fully polymerise (Fig. 31). This phenotype was like CalP mutants with single mutations in essential amino acids, resulting in a defective CalP polymerisation in *C. crescentus* (Figs. 26B, C). CalP, as a transmembrane protein, likely needs the membrane scaffold to multimerise, unlike lamin C, which is a non-transmembrane nuclear protein that could successfully dimerise without a membrane insertion. When heterologously produced in *E. coli*, CalP only formed defective multimers in the membrane fraction but remained in monomeric form in the soluble fraction (Fig. 32A). The fact that CalP could only polymerise in the membrane fraction reinforces the hypothesis that CalP needs the membrane as a scaffold to form multimers (Fig. 32A). According to Kukatsky et al. (2007) and Andre et al. (2008) [574, 575], a higher similarity in the amino acid sequence fosters multimers formation. However, the same CalP sequence was not enough to polymerise CalP in a bacterium different from *C. crescentus*. Although we cannot yet answer the reason why CalP cannot fully polymerise in *E. coli*, we speculate that SecYEG or YidC insertase were unsuccessful in promoting the CalP multimerisation in the *E. coli* cell membrane (Fig. 32A). These results suggest that CalP requires specific assembly machinery to

form CalP multimers because it is unable to do so when it is heterologously produced in *E. coli*.

Several questions still await an answer, such as the function of CalP in the membrane, other proteins that may regulate CalP or the origin of CalP and why it is not conserved in other bacteria. CalP will contribute to shedding light on the barely known field of SPs, which is rapidly expanding and helping to solve biological questions that have been undefined so far. More concretely, the information provided about the characterisation of CalP will expand our knowledge about the stress response system in *C. crescentus* and bacteria in general. Eventually, understanding the mechanisms that bacteria possess to defend themselves from external agents is essential to antimicrobial control and public health. Therefore, each contribution may help shed light on the bacterial resistance mechanisms and find the best tools to combat them.

Chapter 3. Defining the function of CalP, a RecA-dependent protein related to DDA export in the *C. crescentus* inner membrane

3.1 Introduction

Bacteria possess complex systems to cope with environmental changes [421]. Antibiotic resistance is one of the main concerns for public health. Mutations in critical bacterial genes confer bacteria with the capacity to tolerate higher doses of antibiotics [422]. Persistent bacteria, which are populations of highly stress-resistant bacteria, create chronic infections due to antibiotic resistance [422-424] through various complex and redundant molecular mechanisms [425, 426]. Important systems to generate antibiotic resistance are TLS [173], HGT [427], quorum sensing, oxidant tolerance, TA systems, energy metabolism, global stress response, MDEPs, and SOS response [424, 425, 428, 429].

3.1.1 TonB-dependent receptors

Iron is one of the essential cofactors for bacteria and is crucial in metabolic pathways such as oxidative phosphorylation, electron transport, and deoxyribonucleotide synthesis [601]. Bacteria employ two central systems to uptake extracellular iron into the cell. The first system is passive diffusion through porins in favour of the concentration gradient [602]. The second system uses siderophores as ion chelators, which are imported against a concentration gradient using energy-dependent transport mechanisms [602]. Siderophores are low-molecular-weight molecules (500-1500 Da) secreted under iron-limiting conditions to bind iron [603]. TonB-dependent proteins are a family of proteins responsible for transporting siderophores from the extracellular environment across the outer membrane and periplasm to the cytoplasm [604]. Three cytoplasmic proteins, TonB, ExbB, and ExbD, form a complex that spans the entire periplasm and reaches the outer membrane [604]. These proteins are coupled to a proton gradient and are responsible for transporting siderophores through the periplasm to the cytoplasm [604]. The outer membrane proteins that recognise and translocate iron-bound

siderophores across the outer membrane are called TonB-dependent receptors [605]. These protein receptors depend on the energy of the cytoplasmic protein complex and physically bind to TonB [605-607]. This interaction requires that the receptor has a TonB box, which consists of six semi-conserved amino acids close to the N-terminus of the protein [608].

3.1.2 Multidrug efflux pumps

Bacteria display several mechanisms to resist the effects of antibiotics [609]. These effects can be divided into intrinsic causes of antibiotic resistance and acquired antibiotic resistance. Among the intrinsic antibiotic resistance are the export of toxic compounds by multidrug efflux pumps, outer membrane permeability, drug inactivation, alteration or destruction through enzyme modification, and biofilm formation. Acquired antibiotic resistance mechanisms are resistance by mutations, acquisition of resistance genes by HGT (e.g., transformation, transduction, conjugation), and metabolic bypass: camouflaging the target through changing antibiotic affinity modifying antibiotic targets (e.g., modification of topoisomerases to prevent QLs recognition or the alteration of penicillin-binding proteins (PBPs) to prevent the recognition of ß-lactams), target protection (e.g., the addition of methyl groups), modification of drug permeability by changing cell surface, and expressing alternative proteins that are less recognisable by certain antibiotics (e.g., *mecA* encodes an alternative PBP in *S. aureus*) [610-612]. Efflux pumps like MDEPs are transmembrane transporters responsible for expelling poisonous compounds out of the cell [613, 614] that contribute to multidrug resistance in bacteria [609, 615]. MDEPs are a family of ubiquitous proteins conserved in many organisms, including bacteria and mammals [616, 617]. Species such as *E. coli* have up to 37 efflux-pumps-encoding genes [618] and *Salmonella enterica* has ten [619, 620]. MDEPs of *Salmonella enterica* serovar Typhimurium can distinguish between different cytotoxic compounds from a wide range of unrelated categories [621]. MDEPs detect antibiotics such as quinolones (norfloxacin, ciprofloxacin, or nalidixic acid), ß-lactams (carbenicillin, penicillin G, or ampicillin), macrolides (erythromycin or spiramycin), tetracycline, or chloramphenicol [621]. They can recognise compounds such as detergents (sodium dodecyl sulphate or deoxycholic

acid), dyes (ethidium bromide, crystal violet, rhodamine 6G, or acriflavine), or antiseptics (benzalkonium or triclosan) [621]. Efflux pumps are part of a multisystemic bacterial stress response element. Efflux pumps can be the most efficient and fastest defensive mechanism for exporting compounds that can be harmful to the cell. [622]. The presence of antibiotics can trigger transcriptomic changes that cause the expression of several transporter genes [623]. The simultaneous expression of different efflux pumps can activate a coordinated response with redundant functionality to combat the drug threat [624, 625]. In *Salmonella enterica* serovar *typhimurium*, the MDEP response is the primary mechanism to prevent antibiotic accumulation in the exponential phase, and lower membrane permeability is the primary system in the stationary phase [626]. In addition, efflux pumps participate in mechanisms other than exporting antibiotics, such as biofilm formation, transport of virulence factors, proteinaceous toxins and lipids, and cell communication [622, 627, 628]. Efflux pumps can be divided into six families according to their structure, coupling energies, and characteristically conserved amino acid sequence [629-632]. The ATP-binding cassette (ABC) family employs ATP as the driving force to transport compounds across the lipid bilayer [632]. The other efflux pump families are electrochemically powered by the energy produced in the membrane during ion exchange gradients. These other five efflux pump families are the major facilitator superfamily (MFS), multidrug and toxin extrusion (MATE), small multidrug resistance (SMR), resistance-nodulation-cell division (RND), and proteobacterial antimicrobial compound efflux (PACE) [631, 633]. One of the best-studied efflux pumps is AcrAB-TolC in *E. coli,* which belongs to the RND family [634]. This protein set comprises the RND-type inner membrane protein AcrB, the periplasmic protein AcrA, and the outer membrane protein TolC [635, 636]. These tripartite complexes span the periplasmic space and connect the inner and outer membranes to transport compounds bidirectionally [636, 637]. In *C. crescentus*, the AcrAB2-NodT efflux pump has an antibiotic export function and an intricate function as a regulator of the cell polarity protein TipN [638]. During cell division, the TipN function directs the flagellum to its target in the new cell pole [638]. TipN acts in *C. crescentus* as a misregulation controller for the AcrAB2-

NodT efflux pump, preventing toxicity to nalidixic acid when AcrAB2-NodT is overproduced [638].

3.1.3 RNA polymerase sigma and anti-sigma factors

The transcription of bacterial genes is regulated by biomolecules called sigma factors, which are proteins that undergo modifications according to internal and external conditions [639, 640]. Sigma factors bind RNAP reversibly to induce gene transcription in bacteria [639, 640]. These factors have three different functions to initiate transcription: binding to the RNAP core to form the "holoenzyme" and carrying it to the correspondent promoter region forming the close complex (RP_c) [641, 642]; stabilisation of the open complex (RP_o), in which double-stranded DNA nearby the transcription start site melts and converts to single-stranded DNA [643-645]; and interaction of the complex with other transcription activators to add an extra layer of regulation [640, 646]. Two main sigma factor families are classified according to their structure and evolutionary origin: σ^{54} (sometimes referred to as RpoN) [647] and σ^{70} (also called RpoD or σ^{A}) [642, 648]. Several bacterial species, but not all, produce σ^{54}, induced by environmental signals and regulation of nitrogen metabolism genes [640, 646] and require enhancer proteins and ATP hydrolysis to promote transcription [649]. Nevertheless, at least one member of the σ^{70} family is present in all bacterial species [640, 648]. σ^{70} is the responsible factor for vegetative bacterial growth and is responsible for the expression of essential genes (for this reason, it is also known as the housekeeping sigma factor) [640, 648]. σ^{70} is categorised into four structurally and phylogenetically distinct groups, starting with the essential primary group (or Group I) and followed by the other three groups (Group II, III, and IV), comprised of alternative sigma factors with specialised functions [650-652]. Sigma factors of Groups II and III are involved in the transcription control of many genes involved in chemotaxis, flagellum structure and function, general stress response, and other processes related to cell development, such as endospore formation [640]. Group IV of sigma factors is also known as σ^{ECF} and is the most numerous group of the σ^{70} family specialised in sensing environmental stimuli and generating a sufficient gene expression response [646]. σ^{ECF} factors are divided into two different groups depending on whether the

signal that triggers the anti-sigma factor release mechanism is solely extracytoplasmic (canonical σ^{ECF}) or, in addition to this signal, requires an additional cytoplasmic signal (non-canonical σ^{ECF}) [639]. 93% of regular bacterial promoters in *C. crescentus* have binding sites for sigma factors upstream of the transcription start sites (TSS) between positions [-34 to -37] and -10 [653]. The most abundant housekeeping sigma factor in *C. crescentus* is σ^{73} (RpoD) [654]. The binding sites of the TFs RpoD, SigT, and RpoN comprise 63% (1725/2726) of all regions upstream of TSS in *C. crescentus,* and the other 13 TFs known in this bacterium can activate the other 37% of binding motifs upstream of TSS [653]. A high-throughput analysis of TSS and promoter binding sites in *C. crescentus* revealed that *calP* is regulated by σ^{73} (RpoD), with a binding site at position -36 upstream of the *calP* TSS, and is not cell-cycle regulated [653].

Bacteria deploy an extra layer of regulation with antagonists of sigma factors called anti-sigma factors. Alternative sigma factors control transcription via anti-sigma factors. Anti-sigma factors sequester sigma factors to prevent them from binding RNA polymerase to the gene promoter region [655]. Anti-sigma factors undergo specific regulatory systems to release sigma factors, usually after a proteolytic process when a signal is perceived either directly by the anti-sigma factor or by an associated signalling system [639, 655]. These mechanisms can be triggered by intracellular or extracellular signals transduced to the cytoplasm [646]. Unlike sigma factors, anti-sigma factors have little primary sequence homology and are often co-transcribed with sigma factors [656]. Anti-sigma factors of distinct σ^{ECF} families have periplasmic domains with high variability as an adaptation, allowing them to recognise diverse signals [657, 658]. Most anti-sigma factors are predicted to have a unique transmembrane domain with the N-terminal anti-sigma domain in the cytoplasm [657].

3.1.4 Small peptides can alter membrane properties

Small membrane proteins can influence membrane thickness and fluidity [659], a key factor for stress tolerance [660]. A change in membrane fluidity can trigger stress signalling pathways and induce chaperone activity [661]. Some SPs provoke

membrane destabilisation, such as TA proteins, which are made up of a stable toxin and an unstable RNA or protein antitoxin, blocking the toxic effect of the toxin, such as the TisB/IstR1 TA system [662, 663]. TisB is an SOS-regulated 29-amino-acid small membrane protein involved in the DNA-damage response [664, 665] and whose accumulation decreases membrane fluidity [659] and causes membrane depolarisation that reduces cellular ATP levels [666]. TisB also contributes to the generation of persisting cells [665] and chronic infections [429, 451].

De novo emergence peptides acquired through HGT [667], gene duplication [668], or non-coding regions of the genome [669, 670] can be transcribed and produce small peptides [671-673]. Occasionally, highly hydrophobic peptides with specific sequences can be inserted into the membrane, reducing the membrane potential and decreasing drug uptake to confer antibiotic resistance [674].

3.1.5 Detection of small proteins

Tandem mass spectrometry (MS/MS) is one of the most widely used approaches for detecting new proteins in living organisms, and bottom-up proteomics is the most widely used technique [675]. This technique consists of proteolytic digestion of proteins into peptides before LC-MS analysis, characterisation of the resulting peptides, and bioinformatics of spectral information analysis to infer the identity of peptides and determine the original proteins [675, 676]. The detection by bottom-up proteomics of SEPs lower than 10-15 KDa is inefficient and has limitations such as incomplete sequence coverage, difficulties with protein deduction, and recognition of posttranslational modifications [676]. This occurs because only a limited number of proteolytic peptides are formed with the bottom-up technique, which hinders the detection of SEP given the complex background, which is mainly made up of peptides derived from large proteins of high MW [599, 677]. The use of trypsin to digest peptides is inefficient for detecting SPs because it only generates a limited number of proteolytic peptides that can be taken as false positives if the unique count of peptides is less than one [678]. Hence, detecting SEP requires different or unique approaches, such as the enrichment of SPs or the depletion of larger proteins using differential solubilities to increase the proportion of SEP [679-

681]. The combination of multiple proteases has also been demonstrated to increase the number of detected SPs [678].

Furthermore, detection of SEP requires techniques such as MW cut-off filters [676, 682], enrichment of SPs (by the Gel-Free system) [683], size exclusion chromatography [684] or solid phase extraction (SPE) [685-688], reduction of high MW proteins (by precipitation of acetonitrile) [689], or precipitation of acetic acid [680]. However, these procedures may be beneficial or detrimental for specific proteins and would not be desirable in some other cases [679]. The use of top-down proteomics improves the performance of bottom-up proteomics for SEP detection, as it measures compounds in their intact form [599]. Top-down proteomics generates a much higher level of characterisation information, which is very precious if protein products are alternatively encoded [599, 690]. The complete molecular information is recorded from the accurate intact mass at MS and the sequence at the MS/MS level [599, 690].

Moreover, it allows the detection of full-length SEP, the identification of disulphide bonds in SEP, and the recognition of potential posttranslational modifications [599, 690]. Bottom-up MS detection has some drawbacks, such as the need for efficient separation before analysis due to lower sensitivity, challenging data interpretation, and limited protein solubility [599, 675]. The best results are achieved by combining the techniques of both methods, the top-down approach to analyse samples and the bottom-up approach to confirm results [599]. To optimise efficiency when using both techniques, SEP is enriched by SPE, and robust cation exchange is used to minimise the proportion of low-charged ions [599].

3.2 Protein-protein interaction assays *in vivo* indicated CalP binding to different polypeptides

SPs are usually too small to perform complex actions on their own, such as performing catalytic reactions as larger enzymes do [452]. Therefore, they usually act as regulatory elements in larger protein processes [456]. SPs are usually integral pieces of higher complexes or systems, especially SMPs [452, 456]. CalP is a small

transmembrane protein that self-interacts, forming a multimer whose mechanism is still unknown (Figs. 19-22). In previously stained polyacrylamide gels, I showed that heating CalP could disrupt its stable self-interactions that were resistant to detergent treatment (Fig. 19). Furthermore, no other proteins were present after heating the samples, suggesting that the multimer shown on the polyacrylamide gel was only formed by CalP monomers (Fig. 19). Nonetheless, this result does not prove that CalP does not interact with other proteins in the membrane. The search for protein partners for CalP may shed light on the function of CalP and a putative system in which CalP might be involved. To further investigate a possible interaction of CalP with other protein partners, I screened for potential binding proteins of CalP in *C. crescentus*. To do so, I tested the interaction between CalP and other proteins by C-terminally fusing CalP to the T25 subunit of adenylate cyclase (CyaA). Additionally, I C-terminally fused sonicated fragments of the *C. crescentus* genome to the T18 Cya (Figs. 20A, 34). The sonicated fragments were random pieces of the genome that could harbour the ORF of a gene (Fig. 34). Each chimaera of CalP-T25 and the sonicated fragment-T18 were carried in a plasmid to be transcribed. If a gene in the sonicated fragment, which is fused to T18, encodes a protein, the translated protein may interact with CalP (fused to T25). In the scenario where T25 and T18 subunits bind and restore CyaA activity (Fig. 20A), cAMP synthesis is triggered, and it is used as a cofactor for the catabolite activator protein (CAP). CAP binds to promoters of genes involved in the catalysis of carbon sources to induce the transcription of genes whose enzymatic activity can be used as a measurable phenotypic trait (Fig. 20A) [587]. These genes encode enzymes that catalyse the cleavage of certain carbohydrates. The products of these carbohydrates generate a measurable phenotypic trait when they are in contact with an indicator substance in a selective medium [587] (Figs. 20A, 34). An *E. coli cya-* strain was co-transformed with the medium-copy plasmid pKT25 carrying *calP-T25* and the high-copy plasmid pUT18C carrying a *C. crescentus* genome fragment N-terminally fused to *T18* (Fig. 34). These strains were spread onto a minimum selective medium with lactose and X-gal. Cells would use the compounds as the only carbon sources if T25 and T18 bind and reconstitute CyaA, which turns the cells blue (Fig. 34). If T18 and T25 did not re-bind, *mal and lac* operons would not

activate and could not use lactose and X-gal as carbon sources, and colonies would not grow (Figs. 20A, 34). Plates showed several blue colonies growing on the selective medium, and colonies were picked and sent for sequencing to retrieve the gene sequences encoding the proteins that interacted with CalP-T25 (Fig. 34). Sequencing results demonstrated that CalP potentially interacted with several proteins. However, most of them showed interactions in a BACTH assay only once or twice (Table 1). Such a low number of interactions may be because the potential CalP binding proteins were not genuine interactive partners of CalP but were false positives. Therefore, we rejected potential binding partners of CalP that only interacted once or twice. I selected seven proteins that interacted with CalP at least four times in a BACTH screen (Table 1). The main CalP binding partners consisted mainly of transmembrane proteins (Table 1). Most of these proteins were metabolite transporters such as MalY (maltose transporter), Slc5-6 (sodium/glucose transporter), or UhpB (specific micronutrients like sugars or phosphates) (Table 1). A translocase protein (T2SS) and a protein of unknown function (CCNA_03673) were also detected in the BACTH assay (Table 1). Additionally, the RNA sigma factor (CCNA_02837) was found to be the only cytoplasmic protein at first glance (Table 1). However, after a deeper analysis of the sequencing results of the vector carrying the *C. crescentus* fragment, I discovered that the fragment contained two genes instead of a single gene (Table 1). The second gene in the fragment was a gene upstream of *CCNA_02837* that was annotated as *CCNA_02836* and is predicted to be a transmembrane anti-sigma factor (Table 1).

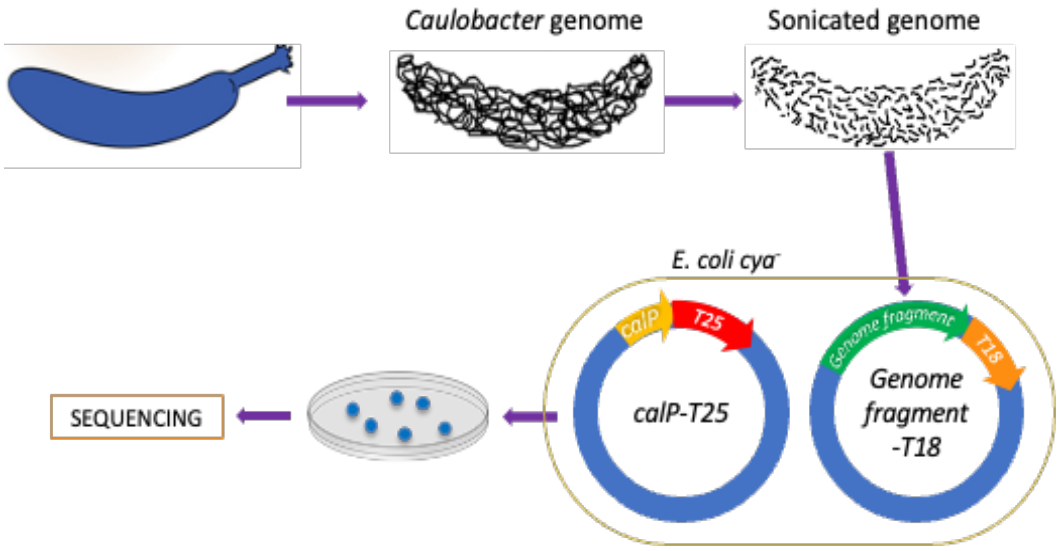

Fig. 34. BACTH screen contributes to finding potential interacting partners for CalP. Diagram summarising the cloning process of the *C. crescentus* BACTH library. Sonicated fragments of *C. crescentus* genomic DNA were cloned at the SmaI site of the plasmid pUT18C. *E. coli* BTH101 was co-transformed with the plasmid pUT18C carrying random sonicated fragments of the *C. crescentus* genome along with *calP* C-terminally fused to *T25* in the vector pKT25. Cells were streaked on minimal medium plates (0.3% lactose, 0.5 mM IPTG, 50 µg/mL kanamycin, 100 µg/mL carbenicillin, and 40 µg/mL X-Gal) and incubated for 4-6 days at 30°C. Blue colonies were picked, and plasmids were extracted for sequencing to determine which gene from the *C. crescentus* library was inserted into the vector.

BACTH CalP binding partners			
Gene name	**Predicted function**	**Localisation**	**#Hits**
CCNA_02366 (malY)	Maltose transporter	Transmembrane	x18
CCNA_03673	Unknown function	Cytoplasmic transmembrane	x16
CCNA_02089 (slc5-6)	Sodium/glucose transporter	Cytoplasmic transmembrane	x7
CCNA_02837	RNA pol. sigma factor	Cytoplasmic	x7
CCNA_00182 (T2SSN)	Type II secretion system	Transmembrane	x3
CCNA_01007 (uhpB)	ABC transporter permease	Transmembrane	x4
CCNA_02836	RNA pol. anti-sigma factor	Transmembrane	-

Table 2. *calP* presumably interacts with other protein partners in *C. crescentus*. BACTH screening candidates from the *C. crescentus* library, using CalP-T25 as bait. This table summarises the top hit proteins found in the CalP binding partner screening. The predicted function and localisation information were retrieved from the Uniprot bioinformatics protein database.

To investigate whether CalP interacted with CCNA_02837 or CCNA_02836, I performed a one-to-one protein interaction assessment in a BACTH assay. To do so, I fused T25 to the N-terminus of *CCNA_02837* and T18 to the N-terminus of *CCNA_02836*. Additionally, I fused T25 to the retrieved fragment CCNA_02837-CCNA_02836 from the BACTH screen to confirm its direct one-to-one interaction with CalP (Fig. 35A). I co-transformed *E. coli cya*- with the cloned vectors and streaked the cells on MacConkey agar medium. *E. coli* cells carrying *calP-T18* and *T25-CCNA_02836* exhibited a magenta colour, suggesting a direct interaction between CalP and the anti-sigma factor (CCNA_02836) (Fig. 35A). In contrast, *E. coli* exhibited white colonies when expressing plasmids containing *calP* and *CCNA_02837,* indicating a lack of interaction between CalP and CCNA_02837 (Fig. 35A). The strain carrying plasmids expressing *calP* and the *CCNA_02837/CCNA_02836* fragment exhibited magenta-coloured colonies. This colour indicates an interaction of CalP with CCNA_02837/6, validating the result observed in the BACTH screening assay (Table 1, Fig. 35A). Therefore, the false interaction of CalP with CCNA_02837 may have occurred via CCNA_02836. Thus, we assume that CCNA_02837 and CCNA_02836 interact. To verify this hypothesis, I tested the direct interaction of CCNA_02837 with CCNA_02836 in a BACTH assay (Fig. 35B). Cells harbouring vectors carrying *CCNA_02837* and *CCNA_02836* exhibited an intense magenta colour, indicating that sigma and anti-sigma factors also interact with each other (Fig. 35B). Additionally, I tested the CalP interaction with the other proteins found in the BACTH screening (Table 1). I N-terminally fused genes selected from the BACTH screening to *T25*. I co-transformed cells with the plasmid carrying the *T25* fusion and the plasmid carrying *calP-T18* and streaked them on a MacConkey agar medium. All strains producing proteins that interacted with CalP in the BACTH screening, except CCNA_02837, exhibited a magenta colour. This phenotype indicates that CalP also bound to them in a BACTH one-to-one interaction assay (Fig. 35A). Control strains producing ZIP and CalP fused to both T25 and T18 CyaA subunits also displayed a vivid magenta colour, validating the observed phenotype in other strains (Fig. 35A). In summary, the BACTH screening and one-to-one BACTH interaction demonstrated that CalP presumably binds to other membrane proteins.

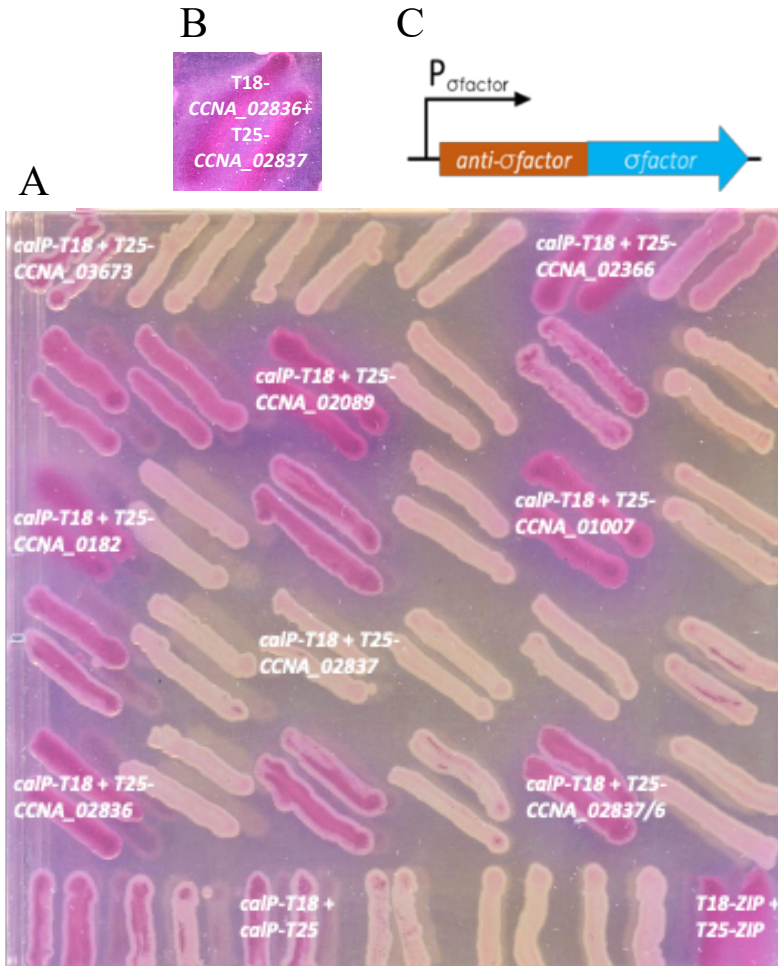

Fig. 35. *C. crescentus* proteins heterologously expressed in *E. coli* interact with CalP. MacConkey agar plates were used to evaluate protein-protein interactions of top-hit CalP binding candidates detected in screening against the *C. crescentus* two-hybrid library with CalP as bait. Strains were streaked on MacConkey plates (1% maltose, 0.5 mM IPTG, 50 µg/mL kanamycin, 100 µg/mL carbenicillin) and incubated for 48 hrs at 30°C. (A) Evaluation of binding between CalP and the main proteins found during BACTH screening in a one-to-one BACTH interaction assay. The proteins assayed in this assay were initially identified as CalP binding partners during the BACTH screening. (B) The image shows a cropped section of a MacConkey agar plate showing the interaction between T25-CCNA_2837 (sigma factor) and T18-CCNA_2836 (anti-sigma factor). (C) Illustration of two neighbour genes, *CCNA_02836* (anti-sigma factor) and *CCNA_02837* (sigma factor), which could co-transcribe [31].

3.3 Mutants of *C. crescentus* genes encoding putative CalP interacting partners are not sensitive to MMC

I hypothesised that a protein interacting with CalP might be involved in DNA damage tolerance/response. Hence, to further confirm the connection of CalP with proteins found in the BACTH screening, I knocked out various *C. crescentus* genes found in the BACTH screening. These genes are *CCNA_02366* (*malY*), *CCNA_03673*, *CCNA_02089* (*slc5-6*), *CCNA_02837*, *CCNA_00182* (*T2SSN*), *CCNA_01007* (*uhpB*), and *CCNA_02836* (see their description in Table 2). I tested the sensitivity of the mutant strains of these genes with MMC. WT, Δ*recA*, and Δ*calP* were included in the experiment as control strains. Cells were streaked on a solid agar medium and incubated at 30ºC for 48 hrs. Results showed that cells in the drug-free medium showed a phenotype comparable to WT, Δ*recA* and Δ*calP* (Figs. 36A, B, C). Following MMC treatment, mutants showed small-sized colonies similar to WT (Figs. 36D, E, F). Whereas Δ*calP* did not show any isolated colony, and Δ*recA* did not show any colony when exposed to MMC (Figs. 36D, E, F). The reduction in colony size observed in WT and the mutants with MMC was not as pronounced as the colony size reduction seen in Δ*recA* and Δ*calP* (Figs. 36D, E, F). These results suggest that the genes identified in the BACTH screening may not be directly involved in DNA damage repair/response mechanisms. Another hypothesis is that these genes may have redundant functions and consequently did not exhibit any adverse phenotype in the presence of DDA. However, the predicted function of these genes does not inherently suggest involvement in DNA damage repair or related mechanism. Hence, it is likely that these genes were false positives and do not have any direct connection to CalP.

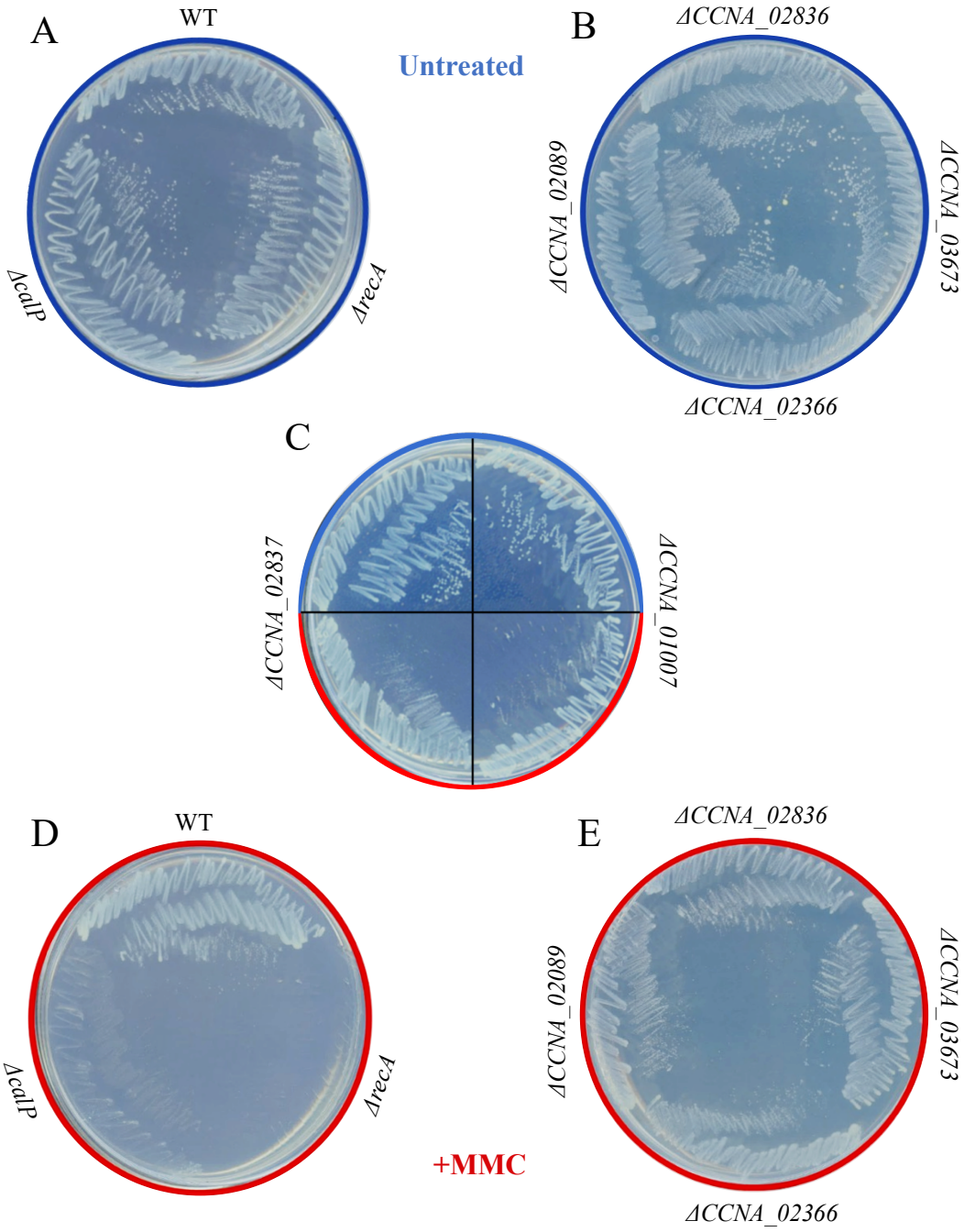

Fig. 36. Deletion of CalP interacting genes resulted in a WT phenotype under MMC conditions on solid medium. MMC sensitivity assay in a solid medium with the mutants of putative CalP binding proteins *ΔCCNA_02366, ΔCCNA_03673, ΔCCNA_02836, ΔCCNA_02089, ΔCCNA_02837*, and *ΔCCNA_01007*. WT, *ΔrecA*, and *ΔcalP* were included as control strains. Cells were streaked on a PYE agar medium without drugs (A, B, C; blue circled plates) or with 0.12 µg/mL MMC (C, D, E; red circled plates). Plates were incubated for 48 hrs at 30°C.

To further analyse the sensitivity of the mutants in a liquid medium in the presence of MMC, cells were grown for 48 hrs at 30ºC. WT, Δ*recA*, and Δ*calP* were included in the assay as control strains. The OD_{600} was monitored hourly in an automated plate reader. The definition of the exponential and stationary phases and the comparison between two optical densities from distinct strains were explained in section 2.2. Results showed that mutants were not sensitive in the unsupplemented medium, showing all a WT phenotype (Figs. 37A, C, E, G, I, K, M). Mutants were also not sensitive in comparison to the WT phenotype in the MMC-supplemented medium (Figs. 37B, D, F, H, J, L, N). However, Δ*recA* and Δ*calP* showed sensitivity in the presence of MMC, as was also demonstrated in previous experiments (Figs. 8, 9). On the contrary, none of the mutants of the BACTH screening candidates were sensitive to MMC, suggesting that they are not involved in DNA damage repair/tolerance. In the drug-free medium, all mutants showed a similar sensitivity, displaying overlapping plot lines comparable to WT, Δ*recA*, or Δ*calP* (Fig. 37). The mutants did not exhibit sensitivity to MMC similarly to the WT phenotype (Fig. 37B, D, F, H, J, L). However, the mutants of CalP-binding protein candidates were not sensitive compared to Δ*recA* or Δ*calP*, which struggled to form colonies (Fig. 37 B, D, F, H, J, L). The results of sensitivity assays in the liquid PYE medium in the presence of MMC were consistent with the results of sensitivity assays in the solid medium under the same conditions (Fig. 36, 37). In summary, mutant strains of CalP-interacting partner candidates from the BACTH screening did not show sensitivity when challenged with MMC. This suggests that they are probably not involved in the DNA-damage tolerance repair system, and thus they are not involved in the same pathway as CalP (Figs. 36, 37). The interactions between CalP and the putative CalP-interactive partners seen in the BACTH screening assessment occurred in *E. coli* but probably did not occur in the native *C. crescentus*. Therefore, this result could be an artefact of producing CalP heterologously in *E. coli*. It may also be likely that CalP interacted with other membrane proteins because they were in the vicinity of the same 2D plane on the cell membrane. Therefore, T25 and T18 could have bound to each other, even

though CalP did not truly interact with the other protein fused to T25 or T18 in a biologically meaningful way.

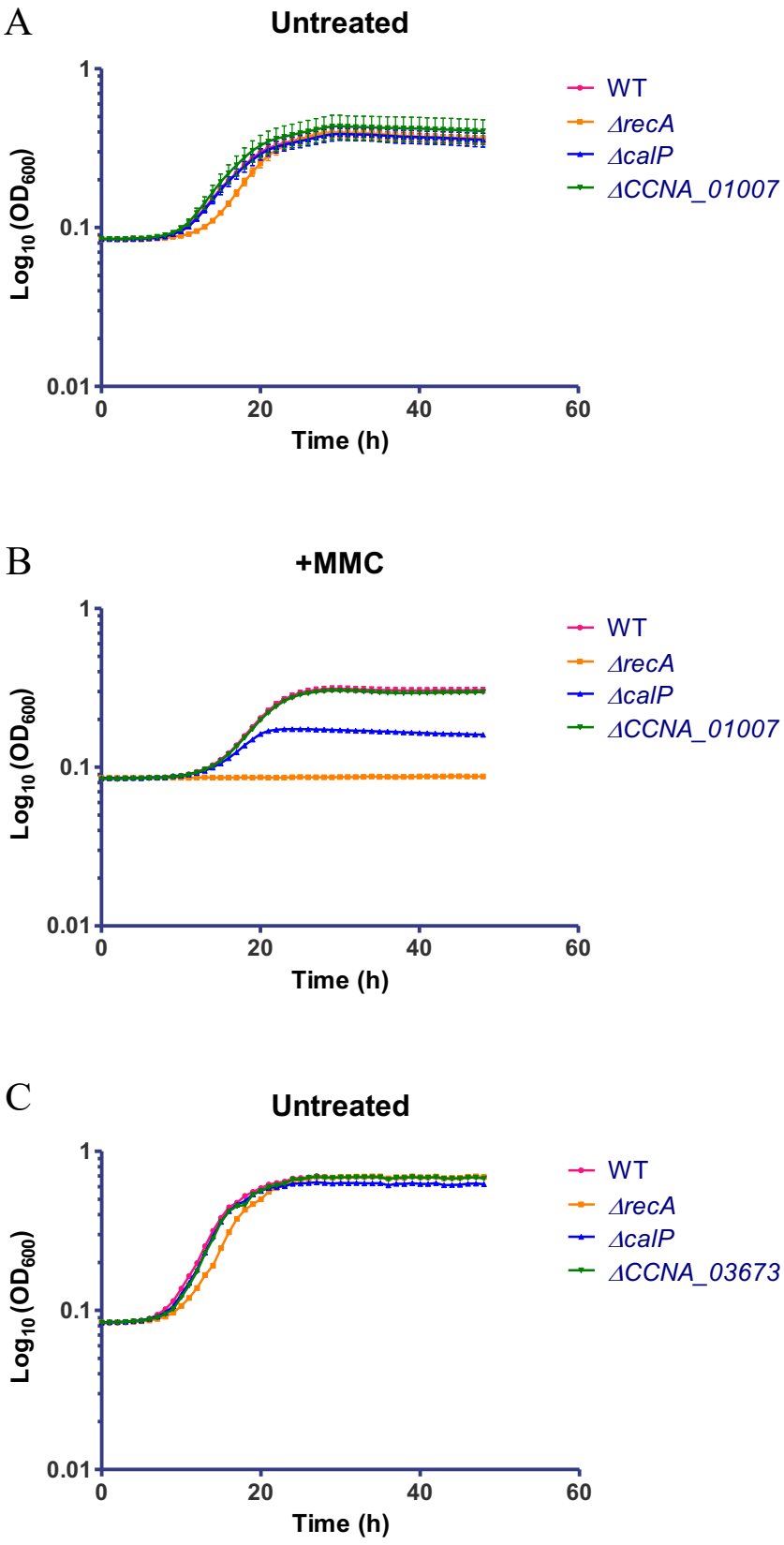
A
Untreated
1
0.1
0.01
Log10 (OD600)
0
20
40
60
Time (h)
WT
ΔrecA
ΔcalP
ΔCCNA_01007
B
+MMC
1
0.1
0.01
Log10 (OD600)
0
20
40
60
Time (h)
WT
ΔrecA
ΔcalP
ΔCCNA_01007
C
Untreated
1
0.1
0.01
Log10 (OD600)
0
20
40
60
Time (h)
WT
ΔrecA
ΔcalP
ΔCCNA_03673

D

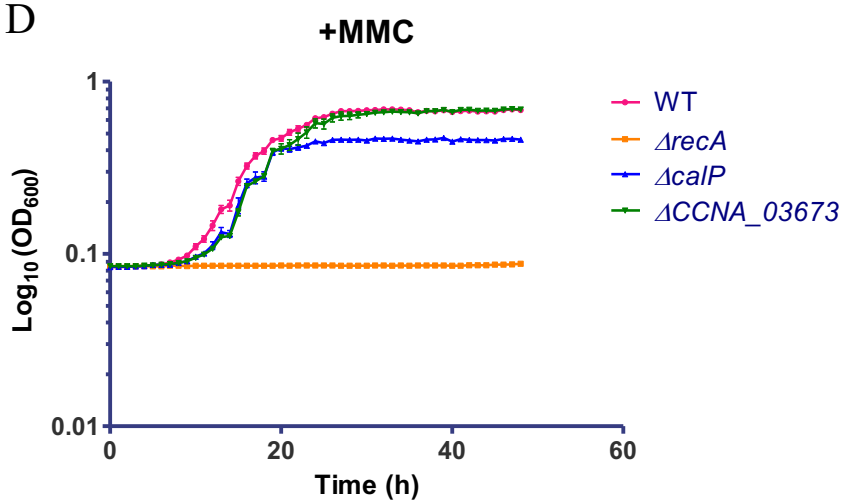
+MMC
1
0.1
0.01
Log10 (OD600)
0
20
40
60
Time (h)
WT
ΔrecA
ΔcalP
ΔCCNA_03673

E

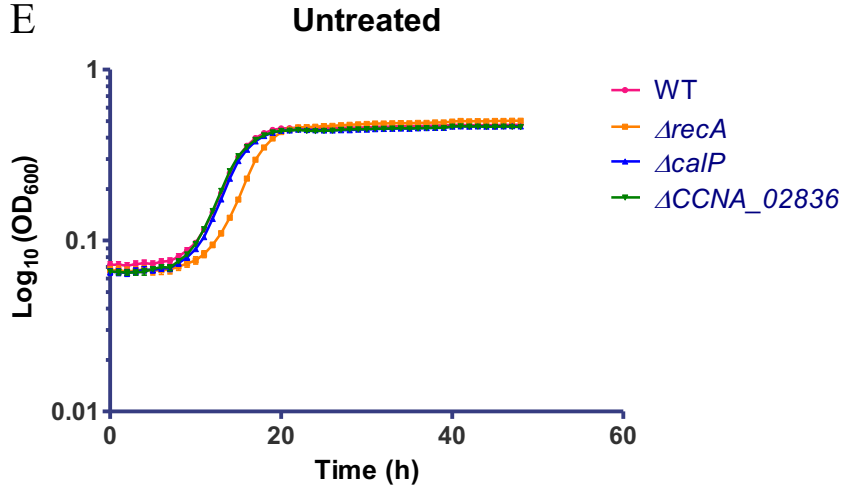
Untreated
1
0.1
0.01
Log10 (OD600)
0
20
40
60
Time (h)
WT
ΔrecA
ΔcalP
ΔCCNA_02836

F

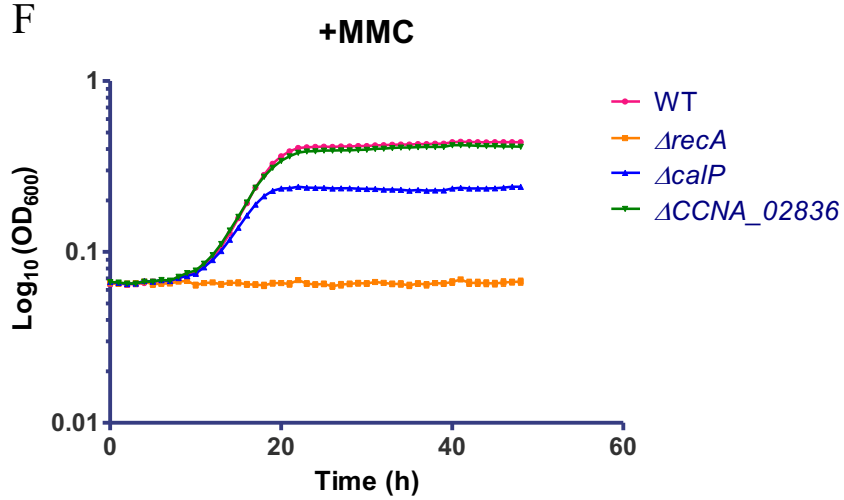
+MMC
1
0.1
0.01
Log10 (OD600)
0
20
40
60
Time (h)
WT
ΔrecA
ΔcalP
ΔCCNA_02836

G

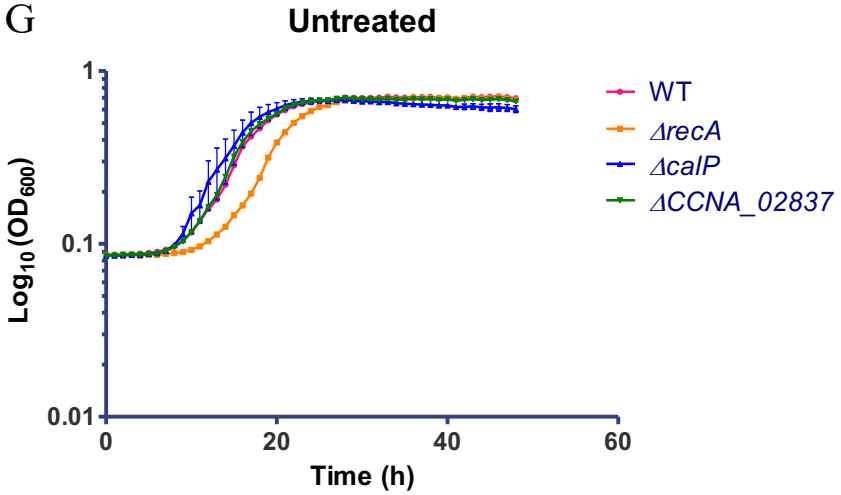
Untreated
1
0.1
0.01
Log10(OD600)
0
20
40
60
Time (h)
WT
ΔrecA
ΔcalP
ΔCCNA_02837

H

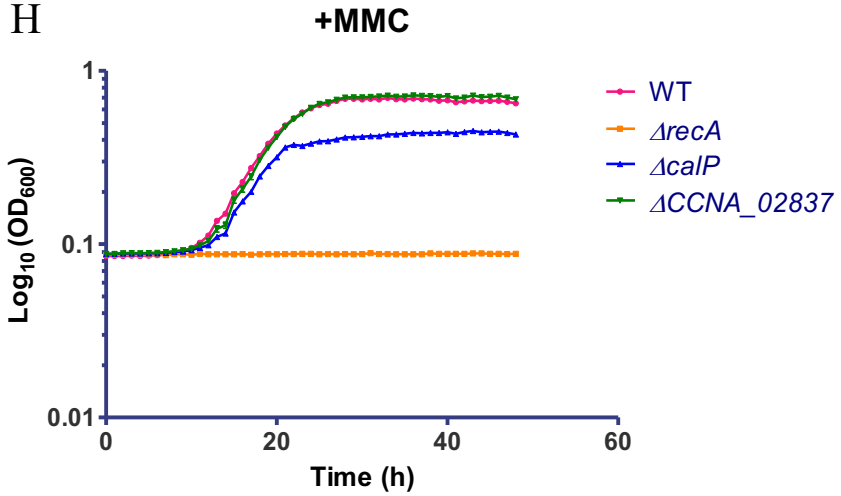
+MMC
1
0.1
0.01
Log10(OD600)
0
20
40
60
Time (h)
WT
ΔrecA
ΔcalP
ΔCCNA_02837

I

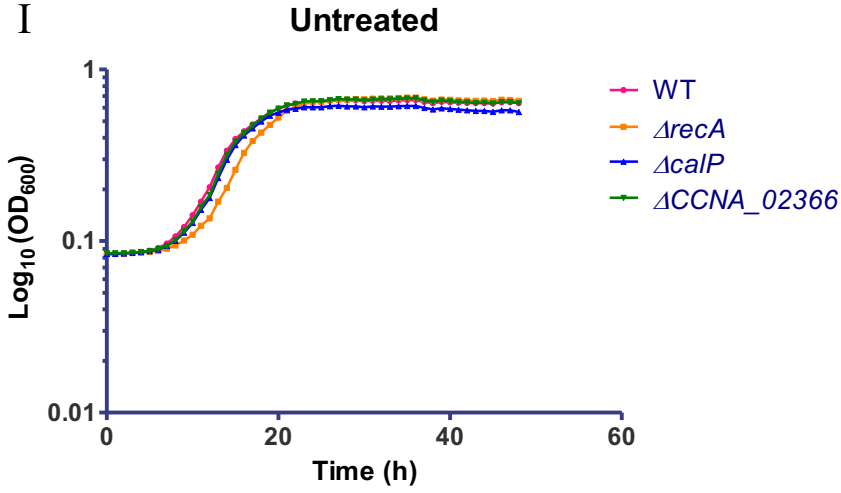
Untreated
1
0.1
0.01
Log10(OD600)
0
20
40
60
Time (h)
WT
ΔrecA
ΔcalP
ΔCCNA_02366

J

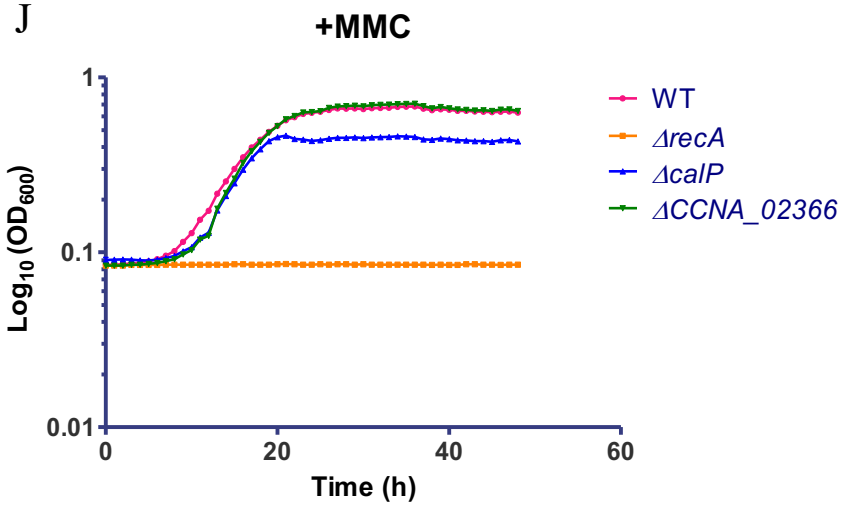
+MMC
1
0.1
0.01
Log10(OD600)
0
20
40
60
Time (h)
WT
ΔrecA
ΔcalP
ΔCCNA_02366

K

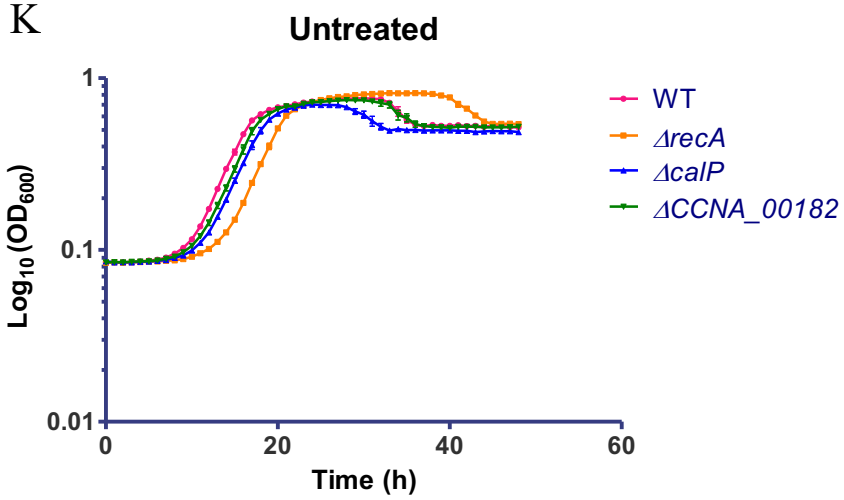
Untreated
1
0.1
0.01
Log10(OD600)
0
20
40
60
Time (h)
WT
ΔrecA
ΔcalP
ΔCCNA_00182

L

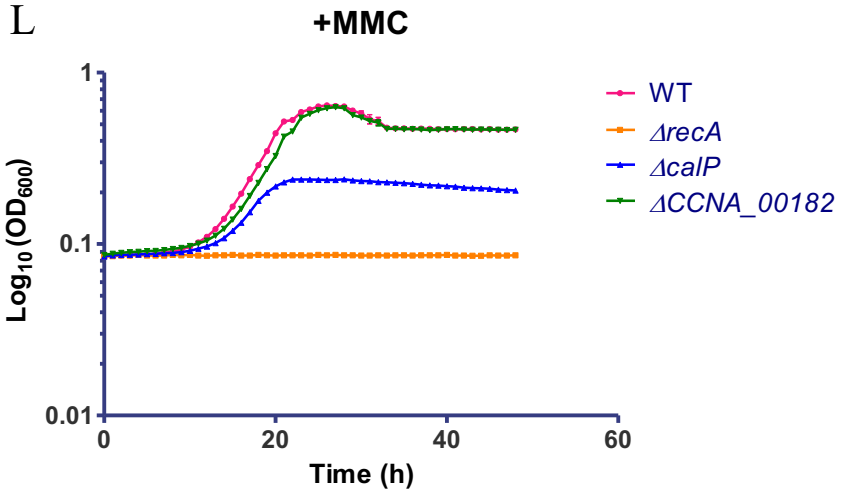
+MMC
1
0.1
0.01
Log10(OD600)
0
20
40
60
Time (h)
WT
ΔrecA
ΔcalP
ΔCCNA_00182

Fig. 37. The sensitivity of mutants harbouring mutations in genes encoding proteins that possibly interact with CalP is not reduced with MMC. Sensitivity assessment of CalP interacting partner mutants in the presence of MMC (*ΔCCNA_01007, ΔCCNA_03673*, *ΔCCNA_02836, ΔCCNA_02837, ΔCCNA_02366*, *ΔCCNA_00182*, and *ΔCCNA_03981*). WT, *ΔrecA,* and *ΔcalP* were used as control strains. Cells were grown exponentially to an OD_{600}=0.5 and diluted to an OD_{600}=$3.3 \cdot 10^{-4}$. Cultures were mixed with or without 0.12 μg/mL MMC and incubated for 48 hrs at 30°C. OD_{600} measurements were taken hourly in an automated plate reader. Three technical replicates were used to calculate the mean of the OD_{600}. (A) Untreated *ΔCCNA_01007,* (B) MMC-treated *ΔCCNA_01007*, (C) untreated *ΔCCNA_03673,* (D) MMC-treated *ΔCCNA_03673*, (E) untreated *ΔCCNA_02836,* (F) MMC-treated *ΔCCNA_02836*, (G) untreated *ΔCCNA_02837,* (H) MMC-treated *ΔCCNA_02837*, (I) untreated *ΔCCNA_02366*, (J) MMC-treated *ΔCCNA_02366*, (K) untreated *ΔCCNA_00182,* and (L) MMC-treated *ΔCCNA_00182*.

3.4 Deleting an MMC-upregulated gene upstream of CalP did not show sensitivity to MMC in *C. crescentus*

A transcriptomics study conducted by Frohlich et al. (2018) reported that after exposure of *C. crescentus* to MMC, *CCNA_03981*, the gene upstream of *calP* was upregulated [444]. *CCNA_03981* was 2.94-fold upregulated when cells were challenged with MMC in comparison to the same strain grown in a drug-free medium [444]. According to the same study, *calP* was 2.02-fold upregulated when cells were treated with MMC compared to *calP* isolated from untreated cells [444]. *CCNA_03981* is predicted to encode a hypothetical protein whose function is unknown. *CCNA_03981* is located upstream of *calP* and is upregulated under DNA damage conditions. This fact suggests that *CCNA_03981* could be a DNA damage repair/response-associated gene and perhaps related to CalP. To determine whether *CCNA_03981* was involved in DNA damage tolerance/response in *C. crescentus*, I performed a sensitivity assay with Δ*CCNA_03981* in a liquid medium with MMC. To do so, cells were grown to mid-exponential phase and treated with 0.12 μg/mL or left untreated. Cultures were incubated at 30ºC for 48 hrs and the OD_{600} was monitored hourly in an automated plate reader. WT, Δ*recA,* and Δ*calP* were included as control strains. The criteria followed to determine the entry into the exponential and stationary phases and the comparison of optic densities from two distinct strains was detailed in section 2.2. Results showed that all strains in the drug-free medium had a similar phenotype (Fig. 38A). These untreated strains exhibited overlapping curves with an $OD_{600}\approx0.65$ in the transition from the exponential to the stationary phase after 20 hrs (Fig. 38A). Δ*CCNA_03981* exhibited a WT phenotype when challenged with MMC, displaying curves that overlapped with those of the WT (Fig. 38B). Following treatment with MMC, Δ*CCNA*_03981 and WT exhibited an $OD_{600}\approx0.6$ in the transition from the exponential to the stationary phase after 20 hrs (Fig. 38B). Whereas Δ*calP*, with an $OD_{600}\approx0.45$, exhibited sensitivity in the exponential phase after 20 hrs in the presence of MMC (Fig. 38B). After 20 hrs of MMC exposure, the $OD_{600}\approx0.45$ observed in Δ*calP* was 1.33-fold lower than the $OD_{600}\approx0.6$ measured in Δ*CCNA*_03981 (Fig. 38B). Therefore, Δ*CCNA_03981* exhibited less sensitivity to MMC than Δ*calP* (Fig. 38B). Following exposure to MMC, Δ*recA* exhibited an

optical density close to zero (Fig. 38B). These results showed that deletion of *CCNA_03981* did not affect *C. crescentus* sensitivity to MMC. This outcome was not correlated with the upregulation of *CCNA_03981* observed in the study of Frohlich et al. (2018). Therefore, I determined that a mutant with a phenotype different from Δ*calP* in the presence of MMC may not be involved in the same pathway as CalP. Hence, I excluded *CCNA_03981* as a potential CalP-binding partner candidate.

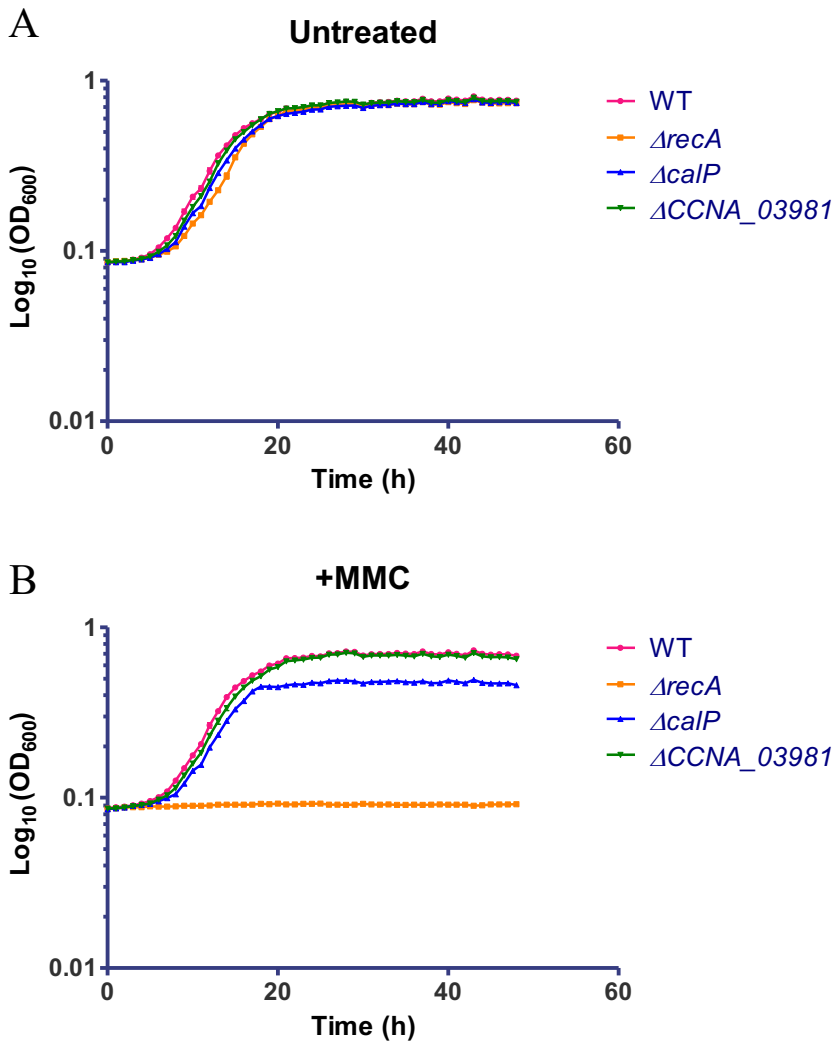

Fig. 38. Deletion of genes encoding interacting partners of CalP shows a WT phenotype when exposed to MMC in a solid medium. Sensitivity test measuring the optical density over 48 hrs of *ΔCCNA_03981* (the gene upstream of *calP*) when exposed to MMC. Cells were grown in a PYE medium to mid-exponential phase and cultures were diluted to an $OD_{600}=3.3\cdot10^{-4}$ before the addition of 0.12 µg/mL MMC or left the medium drug-free. Cultures were incubated at 30ºC for 48 hrs, and the OD_{600} was measured hourly in an automated plate reader. The OD_{600} mean of three replicates was selected to represent each point of the plot line. (A) Untreated *ΔCCNA_03981* and (B) MMC-treated *ΔCCNA_03981*.

3.5 Mass-spectrometry (MS) analysis found several putative CalP-binding partners

MS/MS is probably the most widely used method for detecting new proteins when coupled with co-immunoprecipitated protein samples, as well as detecting interacting protein partners [675]. The search for CalP-binding partners in *E. coli in vivo* through BACTH screening found several membrane proteins. To further test if the putative candidates interacting with CalP were genuine proteins, I performed an *in vitro* screening assay directly with the purified CalP. To do this, I used an MS/MS approach to screen for CalP binding partners that were previously co-immunoprecipitated alongside CalP. To this end, I C-terminally *flag*-tagged *calP* and inserted it into a *C. crescentus* Δ*calP* background (Δ*calP*::P_{calP}-*calP-flag*). Cells grew to mid-exponential phase in a liquid medium. Cultures were supplemented with 0.12 µg/mL MMC or left untreated. Cells were homogenised and passed through a column containing FLAG antibody to retain CalP-FLAG. Samples were loaded in a Tris-Glycine SDS-PAGE and the stained bands were cut into slices. Bands were cleaned of loading dye and impurities and dehydrated. CalP-FLAG and putative co-immunoprecipitated proteins were digested with trypsin and analysed by bottom-up MS/MS analysis. Results showed that CalP-FLAG coimmunoprecipitated with several proteins (Fig. 39A). The TonB-dependent receptor CCNA_00028 was 3.63-fold more abundant (159 hits) than the other ten proteins represented on the right side of the graph (an average of 43.7 hits) (Fig. 39A). The three proteins with the highest number of hits were TonB-dependent receptors (159, 136, and 113 hits, respectively) (Fig. 39A). Six TonB-dependent receptors were found in the top eighth position (on the left side of the graph) (Fig. 39A). Conversely, among the ten proteins that were more underrepresented (on the right side of the graph), only one TonB-dependent receptor (42 hits) was found (Fig. 39A). In addition to the TonB-dependent receptors, both the iron receptor CCNA_01856, with 90 hits, and the polar localisation protein TipN, with 90 hits, were among the top eight proteins with the highest hits (Fig. 39A). The group of TonB-dependent receptors constituted the most represented proteins among all CalP coimmunoprecipitated proteins, with seven distinct receptors accounting for 38.89% of the total (Fig. 39B). The remaining proteins, belonging to diverse protein

families, collectively accounted for a smaller proportion (5.56%) of the total protein amount in the sample (Fig. 39B). The majority of proteins identified in the coimmunoprecipitated sample were membrane proteins, consistent with the findings from the BACTH results (Figs. 34B, 39). The proteins identified in this MS/MS screening analysis did not correspond to any of the proteins identified in the BACTH screening as potential CalP binding partners (Figs. 34B, 39). As a result, I faced challenges in validating any of the proteins identified through the BACTH screening. Given that all proteins discovered in the MS/MS analysis were newly identified, it led to uncertainty regarding whether these proteins truly interacted with CalP or if they were false positive candidates. There is a chance that these proteins could be randomly interacting with CalP, potentially due to their shared characteristic of being membrane proteins and their proximity in location. The frequency of recurrence among TonB-dependent receptors warrants consideration, particularly because certain proteins within this group were found multiple times. CalP coimmunoprecipitated with various proteins, notably showing a significant enrichment of TonB-dependent receptors (Fig. 39).

A

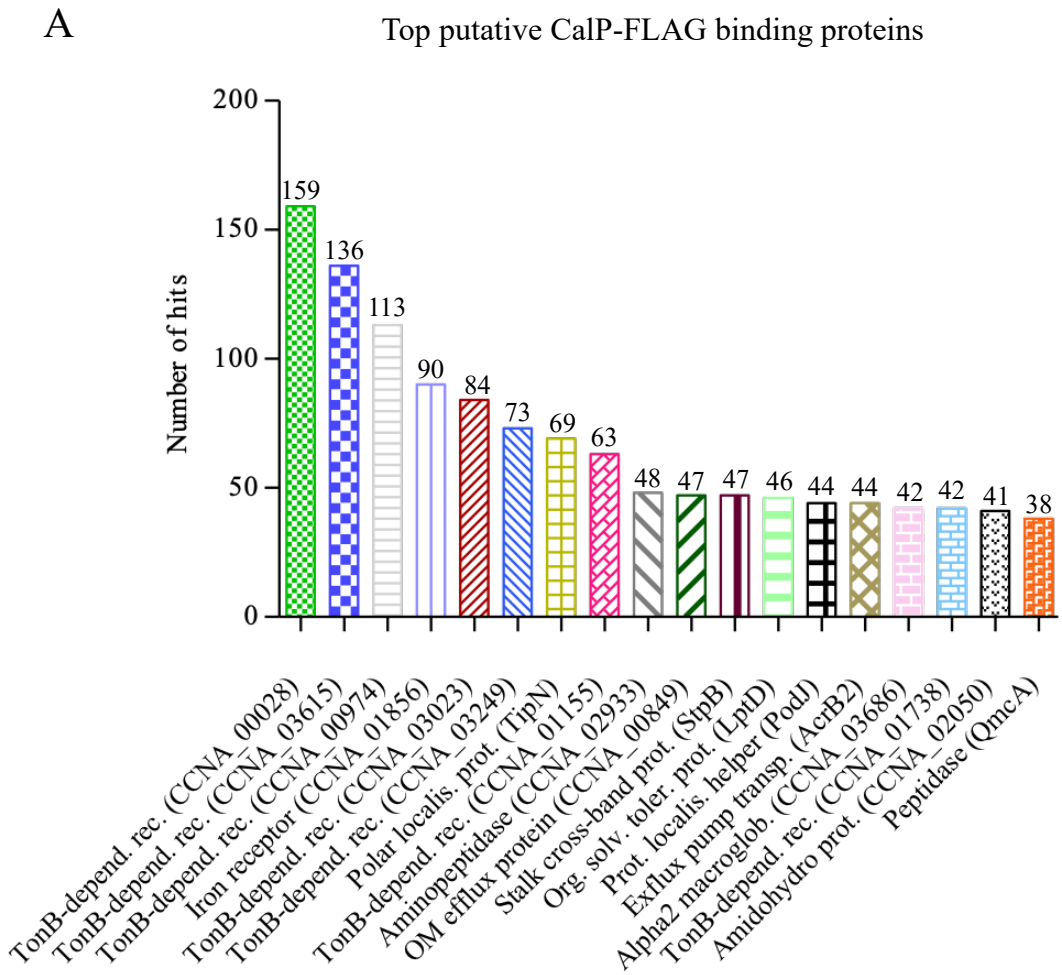
Top putative CalP-FLAG binding proteins
Number of hits
200
150
100
50
0
159
136
113
90
84
73
69
63
48
47
47
46
44
44
42
42
41
38
TonB-depend. rec. (CCNA_00028)
TonB-depend. rec. (CCNA_03615)
TonB-depend. rec. (CCNA_00974)
Iron receptor (CCNA_01856)
TonB-depend. rec. (CCNA_03023)
TonB-depend. rec. (CCNA_03249)
Polar localis. prot. (TipN)
TonB-depend. rec. (CCNA_01155)
Aminopeptidase (CCNA_02933)
OM efflux protein (CCNA_00849)
Stalk cross-band prot. (StpB)
Org. solv. toler. prot. (LptD)
Prot. localis. helper (PodJ)
Exflux pump transp. (AcrB2)
Alpha2 macroglob. (CCNA_03686)
TonB-depend. rec. (CCNA_01738)
Amidohydro prot. (CCNA_02050)
Peptidase (QmcA)

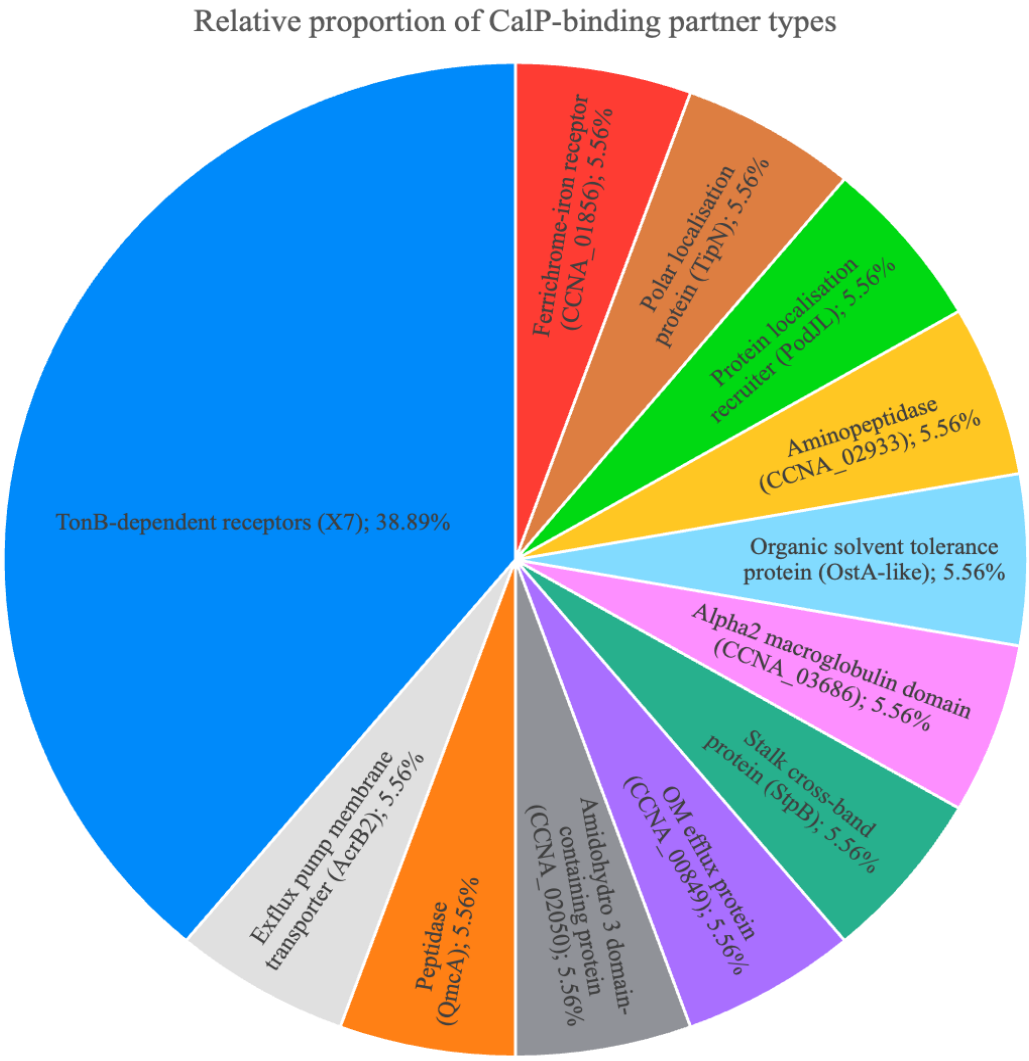

Fig. 39. All identified CalP binding partners correspond to the category of membrane proteins. The graphs summarise the enrichment and proportion of CalP-binding proteins found in MS/MS analysis. Cells were grown to mid-exponential phase and treated with 0.12 µg/mL MMC or left untreated. Cell homogenisation was followed by the purification of CalP-FLAG using columns packed with anti-FLAG antibodies The elution of samples was performed with a buffer containing Triton-X. Samples were loaded onto a Tris-Glycine polyacrylamide gel without the utilisation of a stacking gel. Bands were excised from the gel, cleaned, and dehydrated. The CalP-FLAG slices underwent trypsin digestion before being subjected to analysis in the MS/MS equipment. (A) The bar graph illustrates the number of hits for each putative CalP-binding protein identified in the MS/MS analysis. Hits of MMC-treated and untreated samples were mixed and are represented on top of each bar (-/+MMC). Proteins are arranged from left to right

in descending order, with the highest number of hits on the left and the lowest on the right. (B) Pie chart displaying the proportion of CalP-binding partners.

3.6 The deletion of *recA* downregulates *calP* expression in *C. crescentus*

In prior sensitivity assays, I illustrated that *calP* contributes to tolerance against DDAs and potentially plays a role in DNA damage response or tolerance mechanisms in *C. crescentus*. The SOS-dependent response serves as the primary mechanism for detecting and responding to DNA damage in bacteria, with RecA and LexA acting as the two main regulators of this system [422]. RecA serves as the initial protein to detect DNA damage in bacteria, triggered by evaluated intracellular ssDNA, and is frequently utilised in experiments as a hallmark of the SOS-dependent response [26, 691]. Interestingly, RecA has also been reported to be a key part of the SOS-dependent system in some species, such as *Mycobacterial smegmatis, Deinococcus spp., Helicobacter pylori,* and *Streptococcus pneumoniae* [170, 351, 447, 448]. I proposed a potential connection between CalP and RecA as a fundamental regulator of the DNA damage response. Consequently, modifications in this pathway may influence the expression of *calP*. To test this hypothesis, I quantitatively measured the differential transcription of *calP* in a WT background compared to a Δ*recA* background when *C. crescentus* cells were treated with MMC or left untreated. Cells were grown to an OD_{600}=0.15 and cultures were incubated at 30°C. Cells were treated with 3 μg/mL MMC or left untreated and incubated for 1 hr at 30ºC. I extracted the RNA, converted it to cDNA and measured the expression of *calP* using RT-qPCR. Results indicated that *calP* was downregulated by 1.4-fold in Δ*recA* (relative normalised expression (RNE)=0.32)) in comparison to *calP* in WT (RNE=0.45) in the drug-free medium (Fig. 40A). After exposure to MMC, the *calP* expression in Δ*recA* (RNE=0.47) was downregulated by 2.28-fold compared to *calP* in WT (RNE=1.07) (Fig. 40A). These results suggest that *recA* knockout alters *calP* expression when exposed to MMC (Fig. 40A). *calP* was 2.38-fold upregulated in WT when treated with MMC compared to *calP* in an antibiotic-free medium (Fig. 40A). *calP* was 1.47-fold upregulated in the Δ*recA* background when cells were challenged with MMC compared to *calP* from cells grown in the drug-free medium (Fig. 40A). Thus, the differential expression of calP under ΔrecA in both conditions was 1.62-fold lower than that observed for calP in WT when challenged with MMC or in its absence (Fig. 40A). Therefore, deletion of *recA*, a crucial regulator in the bacterial DNA-damage response, resulted in a

downregulation in *calP* expression, suggesting a possible connection of *calP* with the SOS response.

The differential expression analysis sheds light on the expression of *calP* at the transcriptional level. To validate if the phenotype aligns with the expression outcome, I conducted an immunoblot assay to assess CalP production specifically in a Δ*recA* background. To achieve this, I introduced a chromosomally encoded C-terminally *flag*-tagged *calP* into the native locus of *calP* in a double mutant (Δ*calP* and Δ*recA*) of *C. crescentus* (Δ*recA-tetR*::Δ*calP*::P_{calP}-*calP-flag*). I included in the assay the strains Δ*calP*::P_{calP}-*calP-flag* (as a FLAG-tagged control for CalP production in WT) and WT (as an untagged control). Cells were grown to mid-exponential phase and cultures were treated with 0.12 µg/mL or left untreated. After two-hrs incubation at 30ºC, cells were homogenised. The cell lysate was run in a 4-20% Tris-Glycine SDS-PAGE and blotted with an anti-FLAG antibody. The western blot showed that Δ*recA-tetR*::Δ*calP*::P_{calP}-*calP-flag* produced CalP. However, when exposed to MMC, it exhibited diminished protein production, displaying fainter bands compared to Δ*calP*::P_{calP}-*calP-flag* (Fig. 40B). Unlike the Δ*recA* background strain, the control strain Δ*calP*::P_{calP}-*calP-flag* demonstrated an augmented production of *calP* when exposed to MMC, showcasing a higher band intensity (Fig. 40B). Both Δ*recA-tetR*::Δ*calP*::P_{calP}-*calP-flag* and Δ*calP*::P_{calP}-*calP-flag* showed monomeric and multimeric CalP bands (Fig. 40B). However, following exposure of cells to MMC, the monomeric CalP produced in the Δ*recA* background strain was also unable to increase CalP production compared to the monomeric CalP produced in WT (Fig. 40B). Even in the drug-free medium, CalP production was more significantly reduced in the Δ*recA* background than in the WT phenotype strain, displaying bands with greater intensity (Fig. 40B). The untagged WT control strain showed no bands, indicating that that the bands observed in the CalP-FLAG lanes were genuine (Fig. 40B). In summary, CalP production could not increase when *C. crescentus* was exposed to MMC in a Δ*recA* background. The incapacity of Δ*recA* to enhance CalP production correlates with the downregulated expression of *calP* in the differential expression analysis (Fig. 40). These results support the implication of CalP in the DNA damage response of *C. crescentus.*

A

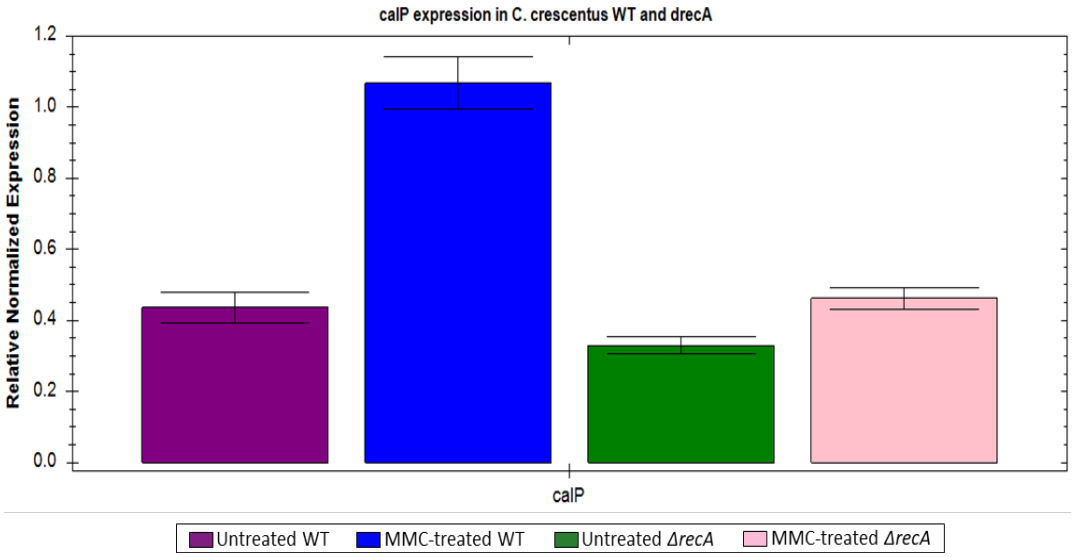
calP expression in C. crescentus WT and drecA
Relative Normalized Expression
1.2
1.0
0.8
0.6
0.4
0.2
0.0
calP
Untreated WT
MMC-treated WT
Untreated ΔrecA
MMC-treated ΔrecA

B

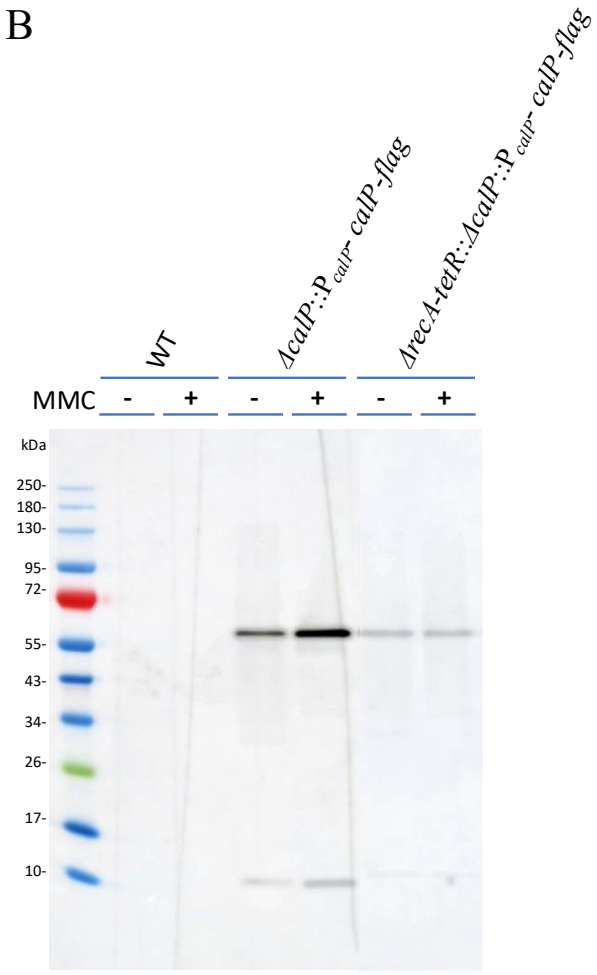
WT
ΔcalP::P calP- calP-flag
ΔrecA-tetR::ΔcalP::P calP- calP-flag
MMC - + - + - +
kDa
250-
180-
130-
95-
72-
55-
43-
34-
26-
17-
10-

Fig. 40. *C. crescentus* Δ*recA* cannot elevate *calP* expression or CalP production in response to MMC. (A) Assay comparing the differential expression of *calP* before and after MMC treatment in the WT and Δ*recA* background strains of *C. crescentus.* The WT strain served as a control for assessing the baseline expression level of *calP. rpoD* was used as a normalisation control and selected as a gene with unaltered expression. Cells were cultivated to an $OD_{600=}$0.15 either with 3 µg/mL MMC or in a drug-free medium and were incubated at 30°C. Cell lysis was performed to extract RNA, followed by its conversion into cDNA. cDNA was used for measuring the differential expression between *calP* in MMC-treated and untreated cells in an RT-qPCR thermocycler. Each coloured bar on the X-axis represents the relative expression levels (as indicated on the Y-axis) of WT or Δ*recA* strains, both treated with or without MMC. The X-axis legend denotes the name of each strain represented by the corresponding bar. The error bars on top of each bar indicate the standard deviation derived from three biological replicates. (B) Western blot analysis for the analysis of CalP production in a *C. crescentus* Δ*recA* background (Δ*recA-tetR*::Δ*calP*::P_{calP}-*flag*) (right lanes). WT was utilised as an untagged control strain (left lanes) while Δ*calP*::P_{calP}-*flag* (middle lanes) served as the CalP control strain for standard protein production. Cells were grown in a PYE medium to mid-exponential phase and treated with 0.12 µg/mL MMC or left untreated. Proteins were purified and run in a 4-20% Tris-Glycine SDS-PAGE and were detected in an immunoblotted membrane using an anti-FLAG antibody.

I demonstrated that the absence of *recA* in *C. crescentus* Δ*recA* influenced the expression level of *calP* and, thus, CalP production (Fig. 40). However, it is still unknown whether a connection between CalP and RecA exists. To further investigate this association, I tested whether CalP and RecA directly interact with each other *in vivo*. To do so, I performed a bacterial-two hybrid (BACTH) assay with CalP and RecA co-expressed in *E. coli*. I streaked *E. coli* cells on a MacConkey selective medium that generates a measurable phenotypic trait to assess whether both proteins interact with each other. I fused each protein to one of the two subunits of the adenylate cyclase (CyaA), T18 or T25, which re-bind if proteins interact with each other (Fig. 20A). I fused *calP* or *recA* to *T25* in the low-copy plasmid pKT25, being both genes expressed under the IPTG-inducible promoter (P_{lac}). Additionally, I fused *calP* or *recA* (under P_{lac}) to *T18* in the high-copy plasmid pUT18C. I included C-terminally fused *calP* to *T25* and *T18*. I used commercially made N-terminally fused ZIP to *T25* and *T18* as positive interaction control plasmids. I co-transformed *E. coli cya*$^{-}$ cells using the previously described combination of constructs. Additionally, I employed combinations of these constructs with empty vectors carrying *T25* or *T18*, which were utilised as negative control strains. The results indicated no interaction between CalP-T25 and T18-RecA, and between CalP-T18 and T25-RecA (Fig. 41). The combination of the aforementioned constructs with empty plasmids solely carrying the T18 or T25 subunits similarly displayed no interaction (Fig. 41). The observed interactions were limited to the self-binding positive control T18-ZIP and T25-ZIP, in addition to those between CalP-T18 and CalP-T25 (Fig. 41). These BACTH results indicate an absence of interaction between CalP and RecA (Fig. 41). However, the potential interaction of CalP with other constituents of the SOS-dependent system cannot be dismissed. However, the precise mechanism through which the absence of *recA* influences the expression of *calP* remains unclear. The potential involvement of CalP in the SOS-dependent system aligns with its recognition as the most well-characterised DNA-damage response/repair pathway in bacteria. This association correlates with the compromised phenotype observed in Δ*calP* when exposed to DDAs (Figs. 8, 9).

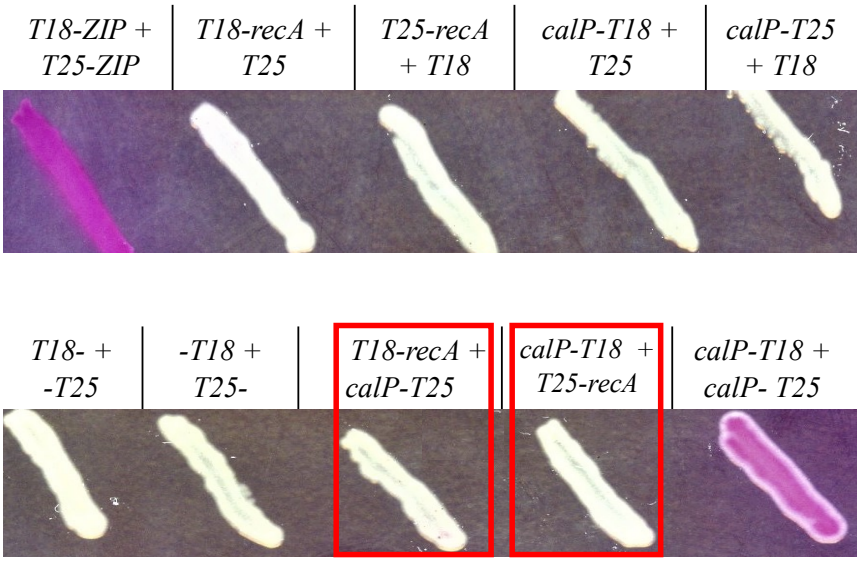

Fig. 41. CalP does not interact with RecA in *E. coli in vivo*. BACTH analysis of interactions between T18/T25-RecA and CalP-T18/T25. The BACTH assay was conducted to assess the potential interaction between T18-RecA and CalP-T25, in addition to between T25-RecA and CalP-T18. As negative control strains, empty vectors pUT18C (T18) and pKT25 (T25) were examined in comparison to the two aforementioned vectors and in mutual interaction with each other. Furthermore, interactions involving ZIP/ZIP complexes were used as a positive control strain. *E. coli* strains harbouring each pair of vectors were streaked on MacConkey agar plates. Plates contained 1% maltose, 0.5 mM IPTG, 50 µg/mL kanamycin, and 100 µg/mL carbenicillin. Plates were incubated at 30°C for 48 hrs. Colonies coloured in magenta indicate interaction, while white colonies denote the absence of interaction.

3.7 *ΔcalP* is more sensitive to membrane depolarisation than WT

CalP is a transmembrane protein that polymerises in the cell membrane. Hence, CalP may potentially influence membrane fluidity and polarity, as suggested by Knopp et al. (2019) in their findings regarding other transmembrane peptides [674]. To further examine the impact of CalP on the membrane, I conducted sensitivity assays with WT and Δ*calP*. To do so, I challenged cells with 1.5 µg/mL of the SIC of carbonyl cyanide 3-chlorophenylhydrazone (CCCP). CCCP acts as an uncoupler of oxidative phosphorylation, disrupting the ionic gradient across bacterial membranes [692]. To evaluate the impact of CCCP on Δ*calP*, I performed sensitivity assays in a solid and liquid media. WT and Δ*recA* were also included as control strains. In this assay, I evaluated the spot densities of WT, Δ*recA*, and Δ*calP* under CCC exposure. Spots displaying a greater cell density indicate reduced sensitivity to CCCP. For the sensitivity assay in a solid medium, cultures were diluted ten times and spotted from right to left (Fig. 42A) on the agar medium supplemented with CCCP or unsupplemented (Fig. 42B). Results demonstrated that the cell spots of WT, Δ*recA*, and Δ*calP* had a similar size in the drug-free medium (Fig. 42A). WT, Δ*recA*, and Δ*calP* formed cell spots in the drug-free medium up to the 10^{-4}-fold dilution and exhibited isolated colonies beyond this dilution (Fig. 42A). After exposure to CCCP, WT formed a cell spot in the undiluted drop (rightmost spot) and isolated colonies in the 10^{-1} and 10^{-2}-fold dilution cell spots. However, no colonies were observed with higher dilutions after MMC exposure (Fig. 42B). Δ*calP* was more sensitive to CCCP than WT or Δ*recA* (Fig. 42B). Despite the inability to form distinct cell spots in the undiluted drops, Δ*calP* demonstrated the formation of a pseudo-spot through the agglomeration of isolated colonies (Fig. 42B). The 10^{-1}-fold and 10^{-2}-fold dilution drops of Δ*calP* exhibited significantly fewer isolated colonies compared to the equivalent dilutions of WT. This suggests a higher sensitivity to CCCP in comparison to WT (Fig. 42B). Unexpectedly, Δ*recA* displayed reduced sensitivity to CCCP compared to WT, forming cell spots in both the undiluted drop and the 10^{-2}-fold dilution (Fig. 42B). Δ*recA* displayed isolated colonies in the 10^{-2}- and 10^{-3}-fold dilutions, yet no colony were observed beyond these dilutions (Fig. 42B). The reduced sensitivity of Δ*recA* to CCCP compared to Δ*calP* suggests that CCCP, as a membrane decoupler,

primarily impacts membrane proteins such as CalP rather than cytoplasmic proteins such as RecA. In summary, Δ*calP* showed higher sensitivity to CCCP exposure compared to both WT and Δ*recA*.

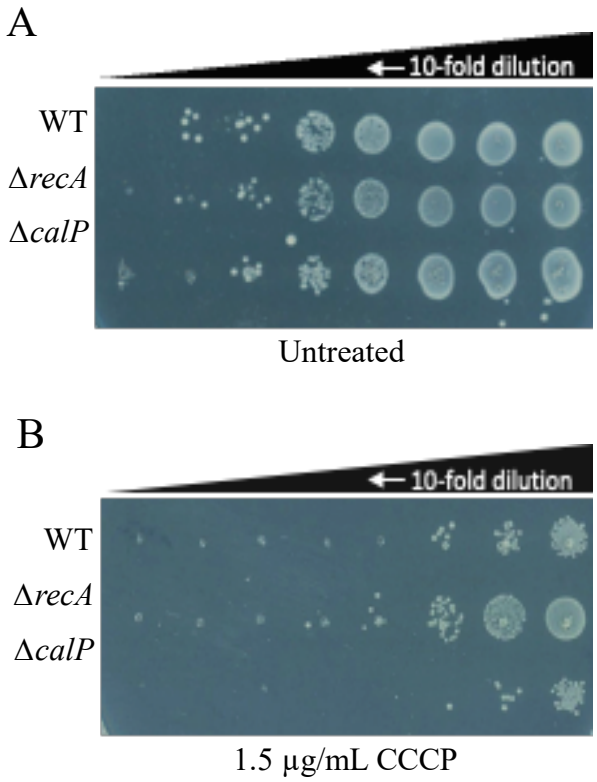

Fig. 42. *ΔcalP* shows a lower cell density in cell spots than WT when exposed to CCCP in a solid medium. Cell spotting assays involved WT, *ΔrecA*, and *ΔcalP* cells cultured on a solid medium with or without CCCP. Cells were grown to mid-exponential phase and cultures were initially diluted to an OD_{600}=0.1. Following this, the culture of each strain was 10-fold serially diluted (represented with the wedge on top of each image) for spotting onto a plate. Agar plates were incubated for 48 hrs at 30°C before images were taken. The displayed plates consist of either (A) unsupplemented medium or (B) a medium supplemented with 1.5 µg/mL CCCP (SIC).

To further investigate the impact of CCCP on WT, Δ*recA*, and Δ*calP*, I conducted a sensitivity assay in a liquid medium. Cells were grown in a liquid medium until reaching mid-exponential phase. Cultures were supplemented with 1.5 or 2 µg/mL CCCP or left unsupplemented. Cells were incubated at 30ºC for 48 hrs and the OD_{600} was monitored hourly. The transition into both the exponential and stationary phases, along with the computation of the optical density ratio between two strains, was detailed in section 2.2. Results indicated comparable optical densities among WT, Δ*recA*, and Δ*calP* in the drug-free medium (Fig. 43A). In the exponential phase after 32 hrs of incubation and following treatment with 1.5 µg/mL CCCP, the OD_{600}≈0.15 observed in Δ*calP* was 1.33-fold lower than the OD_{600}≈0.2 measured in WT and 2.66-fold lower than the OD_{600}≈0.4 observed in Δ*recA* (Fig. 43B). In the stationary phase after 48 hrs of treatment with 1.5 mg/mL CCCP, Δ*recA* also showed the highest optical density (OD_{600}≈0.68) followed by WT (OD_{600}≈0.58), and Δ*calP* (OD_{600}≈0.49) (Fig. 43B). The optical density measured in Δ*calP* was 1.33-fold lower than the optical density observed in WT and 1.33-fold lower than Δ*recA* in the stationary phase in the medium supplemented with 1.5 µg/mL CCCP (Fig. 43B). The difference in the optical density between strains decreased from the exponential to the stationary phase. The higher sensitivity of the three strains when exposed to CCCP compared to the untreated medium indicates that 1.5 µg/mL CCCP causes a toxic effect in *C. crescentus* (Fig. 43B). WT, Δ*recA*, and Δ*calP* exhibited similar phenotypes in sensitivity assays in a liquid and solid medium when challenged with 1.5 µg/mL CCCP (Figs. 43A, B). After 40 hours of exposition to 2 µg/mL CCCP, WT and Δ*recA* exhibited a similar OD_{600}≈0.45 (Fig. 43C However, the optical density of Δ*calP* was close to zero in the whole line plot, indicating a severe sensitivity when exposed to 2 µg/mL CCCP) (Fig. 43C). Therefore, Δ*calP* could not tolerate concentrations greater than 1.5 µg/mL CCCP, whereas WT and Δ*recA* could grow at least at concentrations of 2 µg/mL CCCP (Figs. 43B, C). The high tolerance to CCCP of Δ*recA* in a liquid medium was likely because the depolarisation effect of CCCP did not affect RecA. Overall, these results suggest that the effect of membrane depolarisation when CalP was absent was higher than the effect of membrane depolarisation when CalP was present. CalP may play some role in stabilising membrane polarity, so its absence causes an

impact when the ionic gradient of the membrane is disrupted. Alternatively, CalP may act as an exporter of toxic compounds that contribute to pumping CCCP out of the cell to prevent membrane depolarisation. In this case, the absence of CalP might negatively affect cell fitness since CCCP would accumulate intracellularly and would generate a toxic effect on *C. crescentus*.

A

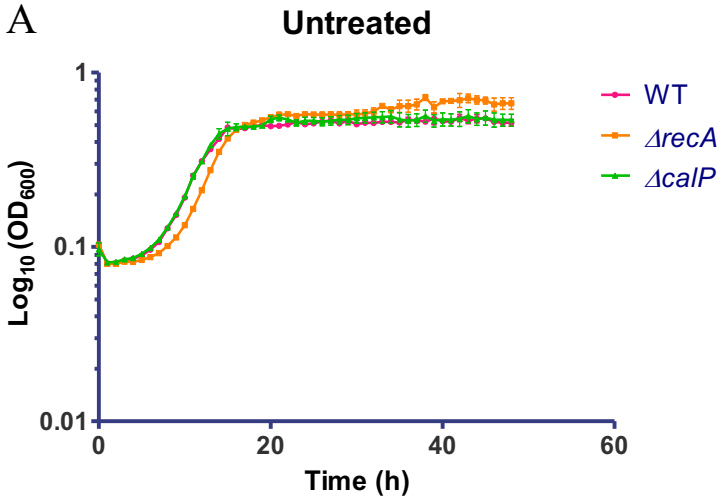
Untreated
WT
ΔrecA
ΔcalP
Log10(OD600)
1
0.1
0.01
0
20
40
60
Time (h)

B

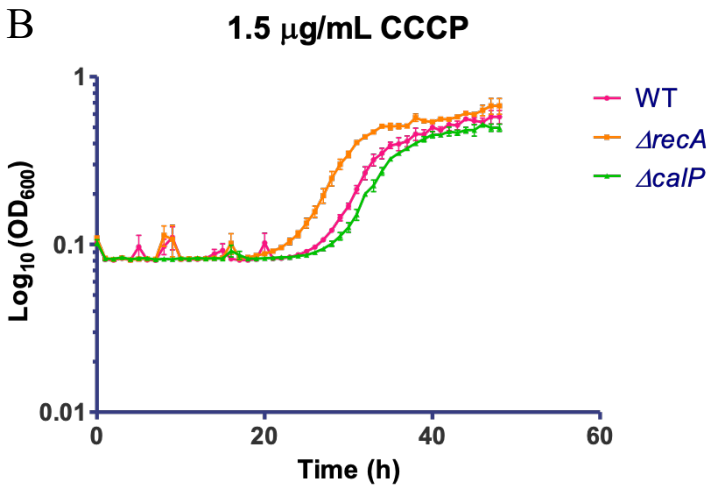
1.5 μg/mL CCCP
WT
ΔrecA
ΔcalP
Log10(OD600)
1
0.1
0.01
0
20
40
60
Time (h)

C

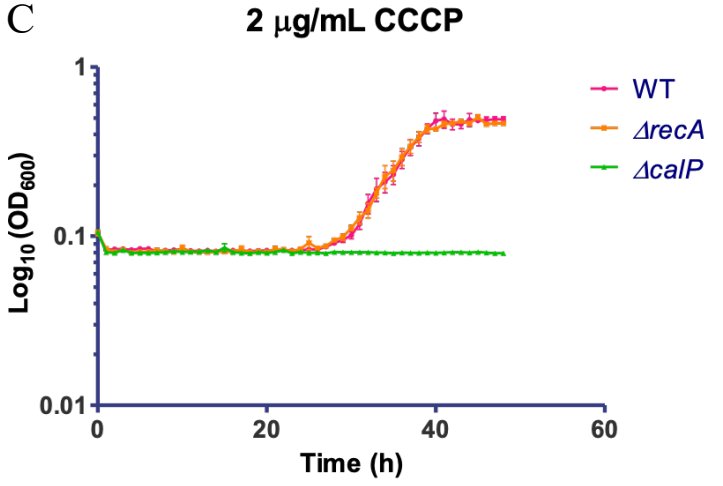
2 μg/mL CCCP
WT
ΔrecA
ΔcalP
Log10(OD600)
1
0.1
0.01
0
20
40
60
Time (h)

Fig. 43. *ΔcalP* shows lower optical density than WT when treated with CCCP in a liquid medium. Growth curves testing the sensitivity of *ΔcalP* in a liquid medium with CCCP. WT and *ΔrecA* were included as control strains. Cells were grown in a PYE medium to mid-exponential phase and cultures were diluted to an $OD_{600}=3.3\cdot10^{-4}$. Cells were challenged with 1.5 µg/mL CCCP, 2 µg/mL CCCP or left untreated. Cultures were incubated for 48 hrs at 30°C. OD_{600} measurements were taken hourly, and three technical replicates were used to calculate the OD_{600} mean. Each medium contained (A) no additives, (B) 1.5 µg/mL CCCP (MIC), or (C) 2 µg/mL CCCP.

3.8 Δ*calP* cells accumulate more MMC-TRC than WT in *C. crescentus*

The mechanisms underlying the role of CalP in DNA damage tolerance/repair in *C. crescentus* remains unclear. The likelihood of CalP engaging in DNA damage repair is low, given its limited size with only eleven or twelve amino acids in the cytoplasm. It is improbable for such. A short domain to perform a repairing function. As a multimeric transmembrane protein, CalP may potentially be involved in activities associated with the detection or extrusion of DDAs from the cell, resembling the function of efflux pumps [638]. CalP might function within a larger system similar to an MDEP, akin to the AcrAB-TolC system observed in *E. coli*, where small membrane protein like AcrZ play pivotal roles [492]. According to predictions from AlphaFold2, the multimeric structure of CalP appears to adopt a hexamer-cylindric model, potentially indicating compatibility with an efflux pump system (Fig. 20C). To investigate whether the absence of CalP leads to an intracellular accumulation of MMC, I compared MMC uptake between WT and Δ*calP* strains. To do so, it was necessary to have a traceable DDA whose amount could be quantified and mimicked the effect of DNA damage on cells. As MMC displayed the most promising performance in sensitivity assays, we conjugated mitomycin A (MMA) with the fluorophore Texas Red Cadeverine (TRC) to form MMC-TRC. Therefore, I aimed to quantify the cytoplasmic accumulation of this compound by fluorescence, comparing its levels in *C. crescentus* WT with that of Δ*calP* (Fig. 44). The newly conjugated compound was chemically synthesised and could be isolated by high-performance liquid chromatography (HPLC) (Fig. 44A). The correct isoform was analysed and selected by high-resolution mass spectrometry (HR-MS) analysis (Fig. 44B). The conjugation project was performed by Dr Martin Rejzek at the Chemistry Platform at the John Innes Centre (JIC).

To evaluate the toxicity of the newly created compound, I conducted a sensitivity assay using MMC-TRC on WT, Δ*recA*, and Δ*calP* strains. This experiment aimed to assess the efficacy of MMC-TRC as a DDA compared to the original MMC. I grew cells to mid-exponential phase in a liquid medium, supplementing the media with 0.8 µg/mL MMC-TRC (SIC) or leaving it unsupplemented. I incubated cultures at 30ºC for 48 hrs. Instructions for defining entry into exponential and

stationary phases and calculating the difference in the optical densities between the strains were provided in section 2.2. WT, Δ*recA*, and *calP* exhibited a comparable OD_{600}≈0.75 after 30 hrs in the unsupplemented medium (Figs. 44A). WT in the MMC-TRC-supplemented medium showed an OD_{600}≈0.75 similar to that of the WT under the same conditions (Figs. 44A, B). However, Δ*calP* exhibited sensitivity when exposed to MMC-TRC, showing an OD_{600}≈0.5 after 30 hrs (Figs. 45A, B). In comparison, Δ*calP* in the drug-free medium was reduced by 1.5-fold, exhibiting an OD_{600}≈0.75 after 30 hrs (Figs. 45A, B). After 30 hours, Δ*recA* exhibited an OD_{600}≈0.45, which decreased by 1.66-fold when exposed to MMC-TRC compared to the unexposed Δ*recA* (Figs. 45A, B). However, the optical density of Δ*recA* when challenged with MMC-TRC was markedly different compared to Δ*recA* when exposed to MMC, in which the plot line was flat and close to zero (Figs. 45B, 4E). The OD_{600}≈0.75 observed in Δ*calP* after 30 hrs with MMC-TRC was 1.85-fold lower than the OD_{600}≈0.27 measured in Δ*calP* after 30 hrs of MMC-treatment (Figs. 45B, 4D). The SIC of 0.8 µg/mL MMC-TRC used to treat Δ*calP* was 6.6-fold higher than the SIC used for Δ*calP* with MMC (Figs. 45B, 9E). This difference in the SIC of both compounds indicates a reduction in the toxicity caused by the loss of potency of MMC-TRC (Figs. 45B, 9E). This decrement may occur due to modifications in the MMC chemical structure, which could hinder MMC-TRC from adequately accessing or binding DNA to effectively crosslink it. Alternatively, chemical modifications might alter the charges and polarities of the compound, resulting in reduced permeability that diminishes the compound's efficiency in passing through the cell membrane.

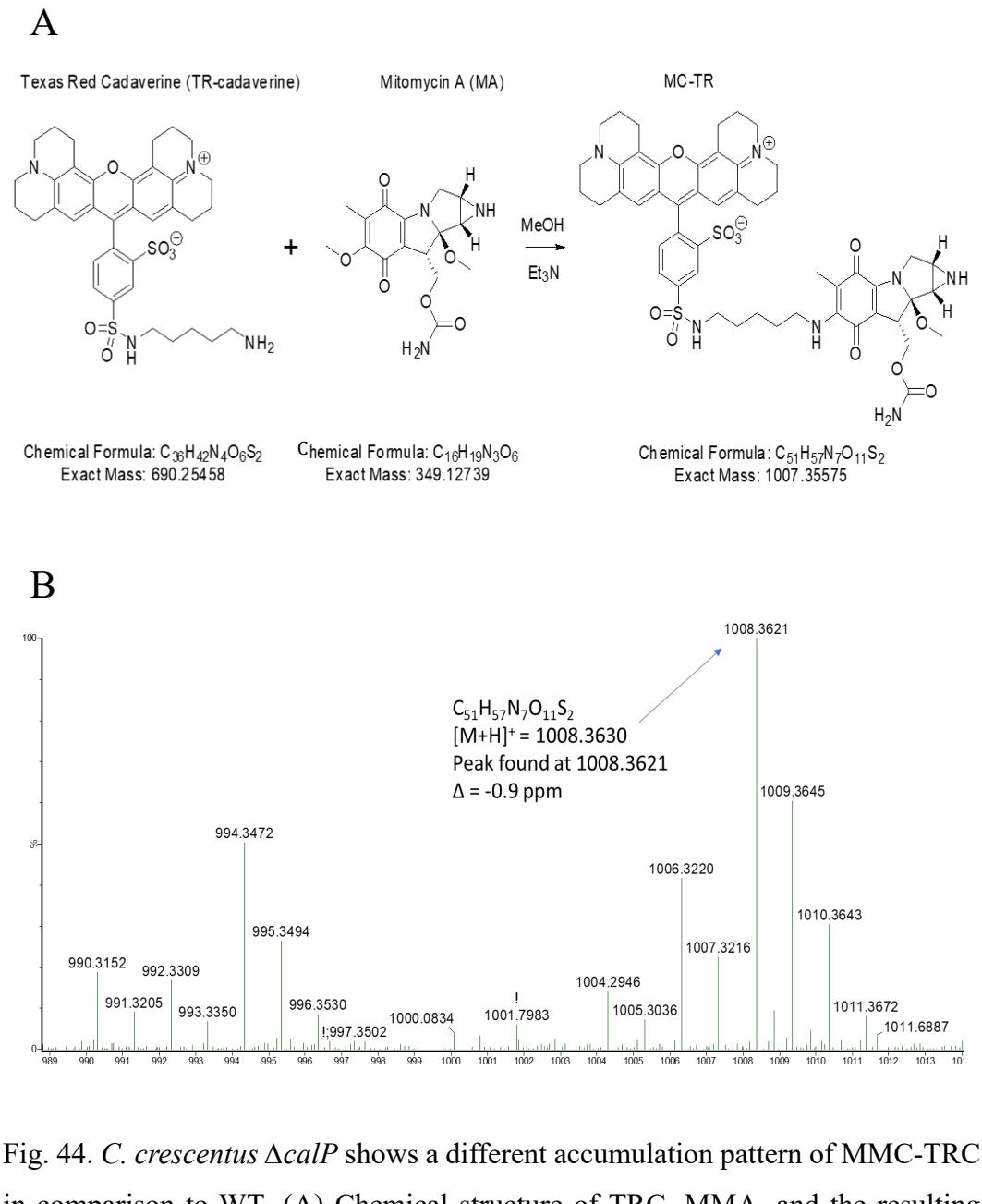

Fig. 44. *C. crescentus* Δ*calP* shows a different accumulation pattern of MMC-TRC in comparison to WT. (A) Chemical structure of TRC, MMA, and the resulting conjugated compounds MMC-TRC. Conjugation with TRC causes MMA to lose a methanol (MeOH) group, transforming it into MMC. The chemical formula and molar mass are displayed at the bottom of the image. (B) HR-MS spectra of MMC-TRC. Each peak in the HR-MS analysis represents a detected substance, and its height indicates the relative amount compared to a standard compound. The number on top of each peak specifies the exact mass detected for each compound. The Y-axis represents the percentage scale for comparing sample peaks, while the X-axis denotes the mass of the compound. The highest peak corresponding on the right

side of the image represents MMC-TRC and details various parameters. From top to bottom, it delineates the chemical formula, anticipated mass, detected mass in the HR-MS analysis, and deviation value between the predicted and detected masses. Dr Martin Rejzek performed this work at the Chemistry Platform of the JIC.

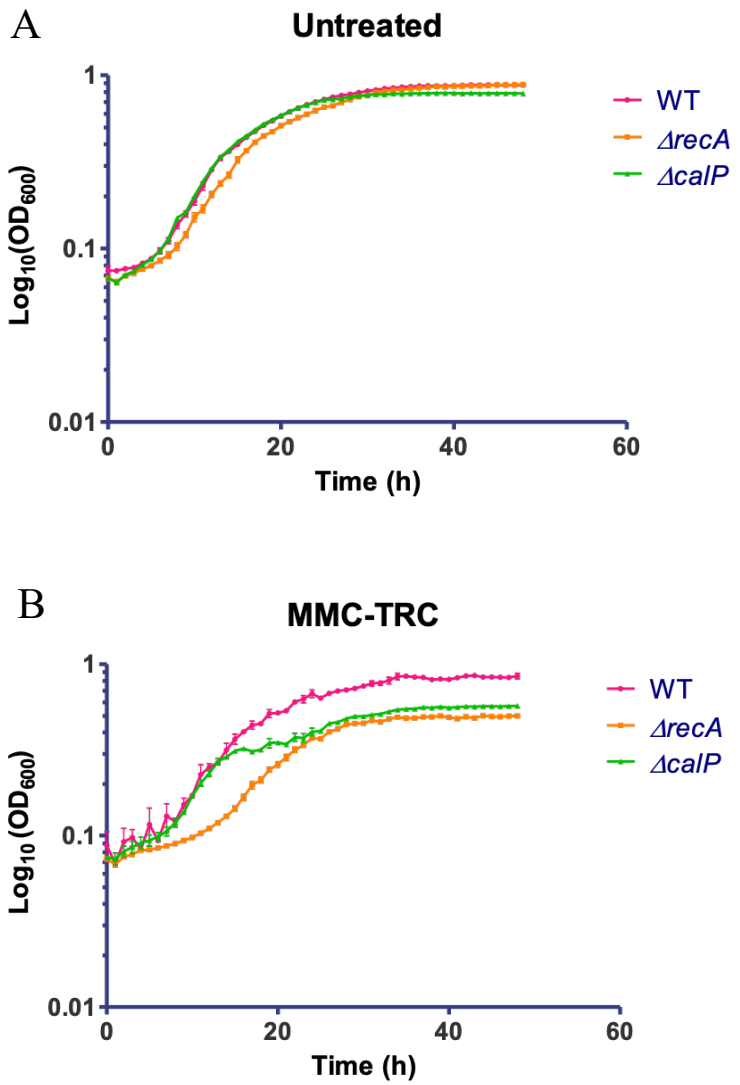

Fig. 45. MMC-TRC exhibits lower toxicity than MMC against Δ*calP*. *ΔcalP* was more sensitive when challenged with MMC than when challenged with MMC-TRC in a liquid medium. Growth curves were used to evaluate the sensitivity of Δ*calP* when exposed to the newly conjugated compound MMC-TRC. WT and *ΔrecA* were included as control strains. Cells were grown to mid-exponential phase in a PYE liquid medium and cultures were diluted to an $OD_{600}=3.3\cdot10^{-4}$. Cultures were treated with 0.8 µg/mL MMC-TRC or left untreated and incubated at 30°C for 48 hrs. OD_{600} measurements were taken hourly, and three technical replicates were used to calculate the OD_{600} mean. Each medium contained (A) no additives, and (B) 0.8 µg/mL MMC-TRC.

I theorised that if the amount of MMC-Texas Red Cadaverine (MMC-TRC) in the WT or Δ*calP* cytoplasm differed from each other, the lack of *calP* may have an impact on MMC uptake or export in *C. crescentus*. A defect in the uptake or export can influence the intracellular accumulation of compounds. Therefore, to determine the accumulation of compounds in WT compared to Δ*calP*, I treated *C. crescentus* with a spectrophotometrically measurable MMC-TRC. To do so, I grew cells to mid-exponential phase in a liquid medium and treated cultures with MMC-TRC or left them untreated. Cells, whether MMC-treated or untreated, were incubated for 2 hrs at 30ºC and then washed to remove the media and MMC-TRC. After washing, cells were placed in a 96-well plate to quantify MMC-TRC accumulation in the cytoplasm. I did so in the cytoplasms of both WT and Δ*calP* by assessing fluorescence intensity using a plate reader. The mean of the fluorescence values of MMC-TRC in WT and Δ*calP* was compared. Results of the unsupplemented control medium showed that WT and Δ*calP* did not emit any signal and were slightly negative below zero compared to the buffer control (Fig. 46). WT treated with MMC-TRC showed a mean fluorescence intensity of 61077 (Fig. 46). Meanwhile, Δ*calP* exhibited a mean fluorescence intensity of 77841, which was 1.28-fold higher than the mean fluorescence intensity of WT (Fig. 46). The unpaired T-test with Welch correction determined a p-value of 0.0017 for the fluorescence intensity means of WT and Δ*calP* (Fig. 46, Table A2, Fig. A19). The mean of both values is significantly different since the p-value of 0.0017 is below the threshold of $P<0.05$ (Fig. 46, Table A2, Fig. A19). The fact that Δ*calP* showed a higher fluorescence intensity than WT suggests that the absence of CalP in the membrane caused a higher cellular uptake and accumulation of MMC-TRC (Fig. 46). The lack of signal in untreated samples indicates that the fluorescence intensity observed in MMC-TRC-treated cells was not due to a signal emitted by the cells, medium, or plate in which samples were analysed. Whereas MMC-TRC emitted a signal detected by the spectrophotometer (Fig. 46). Therefore, CalP could play a role in the membrane as a DDA exporter and contribute to mitigating the toxic effects of such compounds. The rise of CalP production induced by the SOS response system may be one of the multiple resources that *C. crescentus* displays to counteract DNA damage.

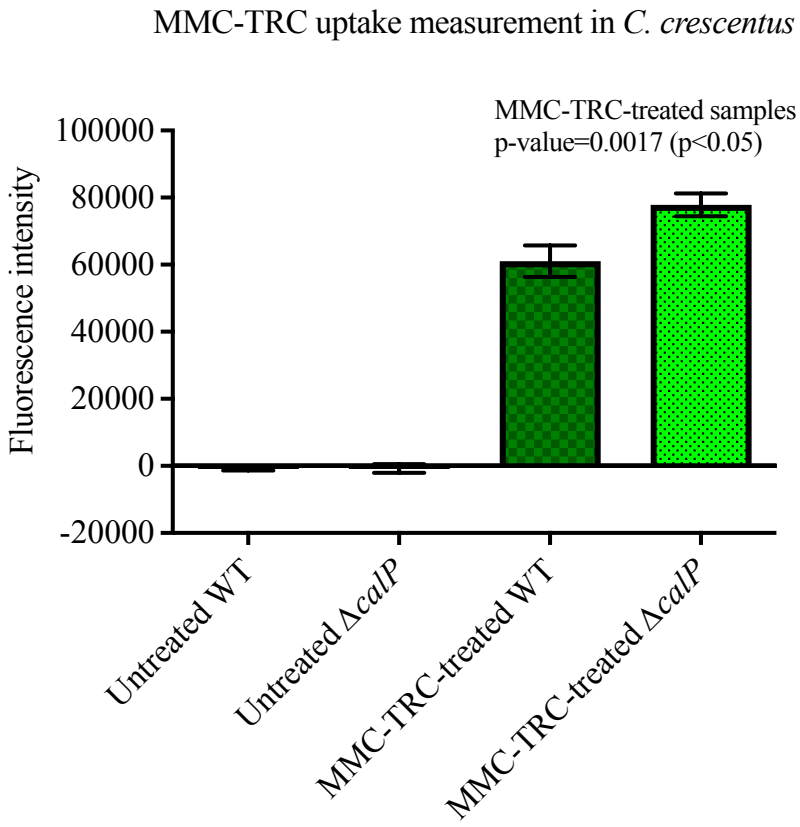

Fig. 46. The deletion of *calP* boosts the accumulation of MMC-TRC in *C. crescentus*. A graph depicting the fluorescence intensity comparison between *C. crescentus* WT and Δ*calP in vivo* before and after exposition to MMC-TRC. The Y-axis indicates the fluorescence intensity in absolute values. The X-axis shows untreated WT and Δ*calP* before exposure to MMC-TRC (time zero) and both strains after 2 hrs of exposure to MMC-TRC. WT was used as a reference control for the accumulation of MMC-TRC. Cells were grown to mid-exponential phase and treated with 0.8 µg/mL MMC-TRC or left untreated. Cultures were incubated for 2 hrs at 30ºC and washed to remove the medium and MMC-TRC. The fluorescence intensity was measured at 470-20 and 630-40 nm. The error bars on top of each bar represent the standard deviation of four biological replicates. The p-value indicates whether the difference between the means of WT and Δ*calP* treated with MMC-TRC is statistically significant.

3.9 Δ*calP* is not conserved and shows residual homology to membrane proteins

Conserved protein domains can shed light on the evolution and origin of a certain protein. Hence, a bioinformatics analysis to assess CalP's conservation in other organisms could help elucidate its function, based on the activity of similar proteins. To do so, I performed homology analysis using a genomic database from the National Library of Medicine belonging to the National Center for Biotechnology Information (NCBI). The BLASTP homology analysis of the CalP amino acid sequence revealed that only four proteins exhibited an identity of at least 50% similarity to the CalP sequence. All four of these proteins were associated with four distinct species of the genus *Caulobacter*. More specifically, *Caulobacter sp. SL161* exhibited a 37-amino-acid protein sharing an identity of 35 out of 37 (95%) amino acids with CalP (Fig. 47A). Furthermore, an unclassified *Caulobacter* displayed a 31-amino-acid protein, demonstrating an identity of 18 out of 29 (62%) amino acids similarity to CalP (Fig. 47A). A 37-amino-acid protein found in *Caulobacter sp. RHG1* demonstrated an identity of 18 out of 33 (55%) amino acids when compared to the CalP amino acid sequence (Fig. 47A). Finally, *Caulobacter sp.* 602-1 showcased a protein with an identity of 16out of w33 (48%) amino acids compared to the CalP amino acid sequence (Fig. 47A).

The NCBI bioinformatics analysis indicated that the sequence of CalP, specifically from the 5th isoleucine to the 37th arginine, shares similarities with the DUF6479 superfamily, characterised as a protein family of unknown function (Fig. 47B). This domain family, commonly present in bacteria, typically ranges between 39 and 51 amino acids in length (Fig. 47B). Furthermore, I conducted another BLASTP analysis in the Kyoto Encyclopedia of Genes and Genomes (KEGG) [693, 694] to explore potential homologues of CalP (Fig. 47C). The results indicated that CalP displayed 36% identity with a small section of the complete amino acid sequence (366 aa) of Hhal_1739. This protein belongs to the RND family and functions as an MDEP transporter in the bacterium *Halorhodospira halophila* (Fig. 47C). Although these results are inconclusive on their own because the genes found only showed homology with *calP* in a limited section of the sequence, they can serve as valuable

supplementary data. Combining these findings with others may contribute to unravel the role of CalP.

A

hypothetical protein [Caulobacter sp. SL161]

Sequence ID: WP_268068497.1 **Length:** 37 **Number of Matches:** 1

Score	Expect	Method	Identities	Positives	Gaps
73.6 bits(179)	4e-16	Compositional matrix adjust.	35/37(95%)	35/37(94%)	0/37(0%)

```
CalP    MDPVIQVVLIGLVFVAAAYGVFWLSMREKPHQKGPPR  37
        MDPVIQVVLIGLVFVAA YGVFWLSMR KPHQKGPPR
Query   MDPVIQVVLIGLVFVAAGYGVFWLSMRAKPHQKGPPR  37
```

MULTISPECIES: hypothetical protein [unclassified Caulobacter]

Sequence ID: WP_235519293.1 **Length:** 31 **Number of Matches:** 1

Score	Expect	Method	Identities	Positives	Gaps
42.7 bits(99)	7e-04	Compositional matrix adjust.	18/29(62%)	22/29(75%)	0/29(0%)

```
CalP    MDPVIQVVLIGLVFVAAAYGVFWLSMREK  29
        MD +++  L+ LVF AAAYGVFWLSMR
Query   MDFLLRATLLSLVFAAAAYGVFWLSMRSD  29
```

hypothetical protein [Caulobacter sp. RHG1]

Sequence ID: WP_241736135.1 **Length:** 37 **Number of Matches:** 1

Score	Expect	Method	Identities	Positives	Gaps
41.2 bits(95)	0.003	Compositional matrix adjust.	18/33(55%)	23/33(69%)	0/33(0%)

```
CalP    MDPVIQVVLIGLVFVAAAYGVFWLSMREKPHQK  33
        MDPV Q +LI LVF+A+A+GV W  MR+    K
Query   MDPVFQSMLICLVFIASAFGVHWFFMRDYNRAK  33
```

hypothetical protein [Caulobacter sp. 602-1]

Sequence ID: WP_233586413.1 **Length:** 39 **Number of Matches:** 1

Score	Expect	Method	Identities	Positives	Gaps
38.5 bits(88)	0.033	Compositional matrix adjust.	16/33(48%)	23/33(69%)	0/33(0%)

```
CalP    MDPVIQVVLIGLVFVAAAYGVFWLSMREKPHQK  33
        M P+ Q +LI LVF+A+A+GV W  MR+   +K
Query   MAPIFQSMLICLVFIASAFGVHWFFMRDYNREK  33
```

B

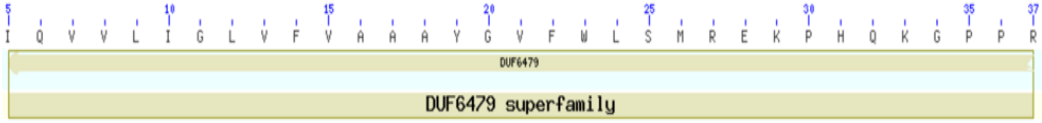

C

	CalP	*Caulobacter crescentus*	37 aa	114 nt	
DBHit(Length)	**Over-lap**	**Ident. (%)**	**Score**	**margin**	**Para-log**	**Cont.**	**KO**	**Orth**
> hha:Hhal_1739(366)	36	36.1	103	()	8	--	K03585	acrA
hypothetical protein	*Halorhodospira halophila*		366 aa	1101 nt				

Current Annotation
efflux transporter, RND family, MFP subunit; K03585 membrane fusion protein, multidrug efflux system

Fig. 47. CalP is conserved across species within the genus *Caulobacter* but shows minimal homology with proteins of other species. Figures presenting alignments of both amino acid and nucleotide sequences of CalP with proteins demonstrating relative sequence similarity. (A) Amino acid homology test of CalP using the compositional matrix adjustment method through BLASTP on the NCBI platform. Hits are arranged from top to bottom, listed in descending order based on identity percentage. The name of each *Caulobacter* species is written in bold letters at the top of each letterbox. The CalP sequence (aa sequence on top), the protein query sequence of the *Caulobacter* species (bottom aa sequence) and the consensus sequence are situated at the bottom of each letterbox. (B) Protein family test (Pfam) from the KEEG platform. The segment of the CalP amino acid sequence spanning from the 5^{th} to the 37^{th} amino acid exhibits conservation within the DUF6479 superfamily. (C) BLASTP analysis on the KEEG platform. Comparative data displaying amino acid and nucleotide sequences, along with the identity percentage, between CalP and Hhal_1739. Hhal_1739 is a multidrug efflux pump transporter of the RND family from the bacterium *Halorhodospira halophila*.

Furthermore, I conducted a nucleotide alignment (BLASTN) on the NCBI platform to explore nucleotide homology within the genomic sequences of other species. Among the identified gene candidates, I specifically chose 14 genes from various bacterial species that displayed identities ranging between 95 and 100% similarity with *calP* (Table 2). The nucleotide alignments revealed minimal homology between *calP* and various genes encoding membrane proteins of diverse functions. Only 21 to 24 nt coincided with the *calP* nucleotide sequence (Table 2). These nucleotides constituted roughly 18 to 21% of the complete 114 nt sequence of *calP*, indicating a minor segment within the entire *calP´s* nucleotide sequence (Table 2). However, the nucleotide sequences of the 14 identified genes from the alignment ranged from as little as 585 nt to as large as 1653 nt (Table 2). Therefore, in relative terms, *calP* accounted for approximately 7% to 19% of the overall nucleotide sequence among the 14 genes selected in the nucleotide alignment. All identified genes encoded membrane proteins, with the majority being membrane transporters or signal transducers (Table 2). Among the 11 genes displaying 100% identity with a segment of the nucleotide sequence of *calP*, 6 genes encoded stress membrane proteins and metal-sensing proteins. Notably, these proteins are engaged in signal transduction across different *Streptomyces* species (Table 2). A single gene exhibited 100% identity with *calP*, while two other displayed 96% identity, and all three encoded different types of MDEP (Table 2). The identified MDEPs consisted of the ABC permease from *Streptomyces sp. CNQ-509,* and an MFS transporter found in *Cellulomonas dongxiuzhuiae* (Table 2). Additionally, an efflux transporter belonging to the MATE family was identified from *Halolamina sp. CBA1230* (Table 2). Among the remaining identified genes were those encoding a peptidase, fusaric acid resistance protein (FUSC family), a methyl-accepting chemotaxis protein, and an RNA-splicing ligase (RtcB) (Table 2). All shared 100% identity with *calP*, except for RtcB, which displayed 96% identity (Table 2). The sequence and length variability observed between CalP and proteins displaying homology from the *genus Caulobacter* was moderate (Table 2). However, outside the genus *Caulobacter* the sequence identity in other genes was notably low, and the sequences displaying homology were notably short. The identified gene candidates exhibiting homology to *calP* were 5.13 to 14.5 times larger than *calP* (Table 2).

Conversely, proteins homologous to CalP within the *Caulobacter* genus demonstrated a comparable number of amino acids to CalP (Table 2). Collectively, these findings indicate the presence of CalP-like homologues in other members of the genus *Caulobacter*. With limited conservation observed beyond this specific genus. Therefore, based on the results, it is reasonable to hypothesise that the origin of CalP potentially emerged in a common ancestor of the genus *Caulobacter*. Exploring beyond the genus *Caulobacter* for a common ancestor is feasible, as evolutionary imprint might have left traceable sequence footprints. Furthermore, the presence of higher similarity homologs in other species supports this exploration. Substantial variability is evident in three of the four species within the genus *Caulobacter* (62, 55, and 48% amino acid identity). This suggests the possibility of a common ancestor of CalP in species outside of the genus *Caulobacter*. While the sequence divergence might suggest it has become untraceable, this hypothesis is less likely as evolutionary divergence typically leaves a discernible footprint. Examining the anticipated functions of proteins linked to genes sharing identity with *calP* could offer valuable insights. This exploration remains significant despite the observed variability in these genes. The top hits included genes encoding proteins related to signal transduction, while the remaining three genes encoded MDEPs. These and other findings offer opportunities for a discussion on the potential role of CalP within *C. crescentus.*

Gene name	Predicted protein function	Organism	Gene length (bp)	Identity (nt)
CP969_20525	Stress protein	*Streptomyces viridosporus*	585	23/23 (100%)
CP972_05265	Stress protein	*Streptomyces prasinus*	585	23/23 (100%)
CNQ36_18160	Stress protein	*Streptomyces fungicidus*	585	23/23 (100%)
SPA2297_30475	Stress protein	*Streptomyces parvulus*	585	23/23 (100%)
SACTE_0325	Stress protein	*Streptomyces sp. SirexAA-E*	585	23/23 (100%)
DMB37_09820	Peptidase	*Nocardia sp. CS682*	525	23/23 (100%)
AA958_27815	ABC transporter permease	*Streptomyces sp. CNQ-509*	1326	22/22 (100%)
DSYM_14180	RNA-splicing ligase RtcB	*Candidatus Desulfobacillus denitrificans*	1428	22/22 (100%)
C5746_41955	Stress protein	*Streptomyces atratus*	585	21/21 (100%)
NFX46_23040	TerD family- metal sensing	*Streptomyces phaeoluteigriseus*	585	21/21 (100%)
H9L06_07705	FUSC family- fusaric acid resist.	*Leucobacter denitrificans*	1059	21/21 (100%)
KKR89_16740	MFS transporter	*Cellulomonas dongxiuzhuiae*	1263	24/25 (96%)

B4589_008335	MATE family efflux transporter	*Halolamina sp. CBA1230*	1398	24/25 (96%)
ACMV_17410	Methyl-accepting chemotaxis protein	*Acidiphilium multivorum*	1653	24/25 (96%)

Table 3. Small amino acid sequences of CalP are conserved in genes from species other than the genus *Caulobacter*. A table summarising identified proteins in a nucleotide homology test (BLASTN) of *calP* conducted on the NCBI platform. The genes are listed in descending order of similarity with *calP* (represented in percentage). The rightmost column displays number of amino acids sharing the nucleotide sequence with *calP* and the corresponding percentage ratio (identity). Only proteins exhibiting an identity greater than 95% were selected and presented in the table. The comprehensive data and alignment of nucleotide sequences for the genes highlighted in this table are detailed in Table A1.

3.10 Discussion

In this chapter, I demonstrated that CalP possibly interacts with several proteins in BACTH screening (Table 1) and in MS/MS analysis of co-immunoprecipitated CalP samples (Fig. 39). BACTH screening found membrane proteins, and the top hits found in MS/MS were mainly composed of TonB-dependent receptors (Fig. 39B). Moreover, induction of DNA damage using MMC led to a downregulation of *calP* in the Δ*recA* background strain. Conversely, *calP* demonstrated upregulation in WT *C. crescentus* when exposed to MMC, triggering the DNA damage response (Fig. 40A). The alteration in *calP* expression due to *recA* deletion strongly suggest a probable interconnection between *calP* and *recA* within the shared regulatory pathway of DNA damage tolerance/response. Furthermore, immunoblot assays showed that CalP production remained unchanged despite DNA damage caused by MMC (Fig. 40B). Meanwhile WT clearly showed higher CalP production in the presence of MMC (Fig. 40B). This phenotype at the translational level confirms the previous phenotype at the transcriptional level. The absence of *calP* is detrimental to *C. crescentus* when the membrane depolarises and could play a role in maintaining the membrane potential (Figs. 42, 43). Lastly, Δ*calP* was more permeable for absorbing MMC-TRC than WT, suggesting that CalP could be important in keeping toxic compounds out of the cell or exporting them once they enter the cell (Fig. 46).

3.10.1 DNA damage

The deletion of a key component in the SOS-dependent system, such as RecA, impacts both *calP* transcription and CalP production. This suggests that CalP may be regulated through the SOS-dependent response, as shown in Figure 40A. However, it's worth noting that RecA is also involved in the SOS-independent response in certain species, like Mycobacterium smegmatis, where RecA/LexA is controlled by the SOS-independent master transcriptional activator PafBC [170]. *Deinococcus spp.* triggers an SOS-independent response called the radiation/desiccation response, in which various DNA damage repair genes are transcribed, such as *recA* [351]. Furthermore, *Helicobacter pylori* and *Streptococcus pneumoniae* do not have any *lexA* homolog in their genome but

conserve *recA*, whose protein induces cell competence to import extracellular DNA under DNA damage conditions [447, 448]. Therefore, considering the involvement of RecA in the SOS-independent response in other species, it is feasible that CalP could participate in the SOS-independent response. This hypothesis is further supported by the fact that *calP* lacks a LexA-binding promoter, as demonstrated by da Rocha et al. (2008) in screening to search for SOS box sequences in promoter regions of *C. crescentus* [431]. Despite my demonstration that CalP is downregulated in Δ*recA* in the presence of MMC, the regulation of CalP in *C. crescentus* could be RecA-dependent but LexA-independent (Fig. 40A). However, it is not yet clear whether this regulation is controlled via the SOS-dependent or SOS-independent pathway, or even both, as in *Deinococcus spp.* [351]. The other two SPs of the SOS-dependent response in *C. crescentus*, SidA (involved in cell division arrest) [443] and BapE (controls cell apoptosis after irreversible DNA damage), had SOS boxes [13], according to da Rocha et al. (2008) [431]. In contrast, DidA (involved in cell division arrest) and DriD (an activator of the SOS-independent response) are SPs involved in the SOS-independent system in *C. crescentus* that do not have SOS boxes. An SOS box sequence in the promoter site is often an unequivocal sign of participation in the SOS-dependent response. Considering the regulation of CalP through RecA, the likelihood that CalP is part of the SOS-dependent system is significant, especially considering that the SOS-dependent system is well conserved and present across different species, regulating a wide set of genes related to DNA damage response. Nevertheless, CalP could even participate in both systems, the SOS-dependent and SOS-independent responses, like *Deinococcus spp*. [351].

3.10.2 Detection of CalP-binding partners

Identifying interacting protein partners for CalP is a conventional approach to contextualising the protein within the cell and uncovering its role in *C. crescentus*. BACTH screening found several membrane protein candidates that interacted with CalP (Table 1). However, none of these binding partners showed sensitivity to MMC (Figs. 36, 37). One of the main concerns of two-hybrid assays (bacterial/yeast two-hybrid) is the number of cases of false positives [695]. In our BACTH results,

all the proteins found were transmembrane proteins primarily involved in solute transport (Table 1). As CalP seems to be involved in the DNA-damage response and none of the candidates is sensitive to MMC, it is plausible that most of the candidates found in the BACTH screening were false positives. However, one of the binding protein candidates detected in the CalP BACTH screening, the anti-sigma factor (CCNA_02836), could be truly related to CalP (Table 1). This protein is the cognate anti-sigma factor of the σ^{70} factor (CCNA_02837), and both are presumably co-transcribed and interacted *in vivo* in BACTH assays (Figs. 35A, B). σ^{70} factor is an extracytoplasmic function sigma factor (σ^{ECF}) part of the sigma factor group IV, the most numerous group of σ^{70} family specialised in sensing environmental stimuli and generating an adequate gene expression response [646]. Therefore, the anti-sigma factor of σ^{70} may be a genuine regulator of CalP that sequesters σ^{70} in the membrane, preventing its binding to the RNA polymerase that transcribes *calP*. The anti-sigma factor could release σ^{70} upon interaction with CalP or after sensing some extracytoplasmic stimuli [646, 648, 655]. Therefore, σ^{70} as an σ^{ECF} might be involved in sensing extracytoplasmic conditions and may regulate *calP* transcription in response to potential DNA damage generated by DDA. In addition to that, Zhou et al. (2015) discovered that the promoter binding site of numerous genes in *C. crescentus* showed that *calP* had a σ^{73} (RpoD) binding site [653]. RpoD is considered the housekeeping sigma factor in *C. crescentus* [654] and probably regulates *calP* transcription under non-stress conditions; as I demonstrated in previous immunoblot assays, *C. crescentus* produces CalP even though no DNA damage was induced in the cell (Figs. 16, 17).

SPs are challenging to detect in standard MS analysis, and poor results are sometimes achieved [599, 676, 677]. Sample preparation is also crucial for the later detection of SPs and for detecting binding proteins [599, 675, 678, 681, 689]. MS/MS analysis to screen for CalP interacting partners found several potential binding proteins. However, none of these candidates matched with protein candidates previously found in the BACTH protein partners screening (Table 1). Numerous proteins were found in the coimmunoprecipitated CalP samples, and it is unlikely that such a high number of proteins interacted with CalP (Fig. 39). TonB-

dependent receptors represent nearly 39% of all proteins found to interact with CalP (Fig. 39A). The other 61% of proteins found were comprised of membrane proteins, with a proportion slightly higher than 5.5% each (Fig. 39). TonB-dependent receptors are the outermost element of the siderophore uptake system to import extracellular iron [604]. In *E. coli,* TonB, ExbB, and ExbD form the siderophore import system and span the entire periplasm to connect with TonB-dependent receptors. The fact that CalP is an inner transmembrane protein could cause TonB-periplasmic spanning proteins to interact with CalP serendipitously. Alternatively, CalP could play a role in the *C. crescentus* TonB system and contribute to the import of siderophores into the inner membrane. Nevertheless, our experiments have consistently suggested the connection of CalP with DNA damage response and never indicated the involvement of CalP in iron uptake, although it is something to further investigate in future experiments. Ultimately, the use of bottom-up standard proteomics procedures and the lack of sample optimisation for the detection of CalP and its binding partners could have caused unconvincing results (Fig. 39). However, previously stained polyacrylamide gels showed that after heating CalP samples at 100ºC, no other proteins were found in the sample besides CalP (Fig. 19C). Therefore, the possibility of CalP not interacting with other proteins is also feasible. Alternatively, CalP could be indirectly regulated by other proteins that are controlled by the SOS-dependent response.

3.10.3 CalP function

Bacteria possess several systems to counteract the effects of drugs [609], such as MDEPs, which are membrane transporters that transport cytotoxic compounds out of the cell [613, 614]. Antibiotics can trigger the expression of several genes that encode membrane metabolite transporters [623]. Simultaneous activation of numerous MDEPs in the cell can generate multiple redundant responses to block antibiotic uptake and initialise antibiotic export [624, 625]. We hypothesised that CalP could be an MDEP because data obtained in previous results may suggest that: (i) CalP contributes to maintaining lower intracellular levels of MMC-TRC, (ii) CalP is a transmembrane protein, that forms homomers in the membrane, and (iii) CalP has efflux pump orthologs in other bacterial species. I showed that the absence

of CalP increased intracellular levels of MMC-TRC in *C. crescentus* (Fig. 46). The slight increase in the uptake of MMC-TRC observed in Δ*calP* compared to WT may be a consequence of redundancy in the elements destined to protect the bacterium from cytotoxic substances (Fig. 46). CalP probably forms a single homomeric structure comprised of six or eight monomers that insert into the inner membrane, forming a pore-like structure that could pump toxic compounds out of the cell (Figs. 19-21).

The inner membrane proteins of efflux pumps are often medium- to large proteins with multiple transmembrane domains that translocase solutes across the lipid bilayer [622]. In *E. coli*, the homo-trimeric inner membrane protein AcrB interacts with AcrA and TolC to form the tripartite AcrB-AcrA-TolC efflux pump that spans from the inner membrane to the outer membrane [492]. Previous experiments with stained polyacrylamide gels with heated CalP suggest the absence of proteins other than CalP in the sample (Fig. 19C). Additionally, BACTH and MS/MS analysis showed inconclusive interactions of CalP with other proteins (Table 1, Fig. 39). Therefore, if CalP did not interact with other proteins, it would not form a pump-like tripartite AcrB-AcrA-TolC efflux complex. Nevertheless, other efflux pumps could be feasible CalP orthologs, such as the non-tripartite ABC superfamily or the MATE family, which are inner membrane proteins [622]. Homodimers form the (non-tripartite) ABC superfamily in Gram-negative bacteria, which bind and hydrolyse ATP to power the transport mechanism [696, 697], like McjD, which exports antibacterial peptides [698]. The DinF subfamily belonging to the MATE family of proteins is inducible by DNA damage [699]. PfMATE, a member of the DinF subfamily, has a N_{out}-C_{in} topology (like CalP) and uses the electrochemical gradient of H^+ or Na^+ across the membrane as a driving force to export compounds such as the norfloxacin-derivative substrate Br-NRF [699-701].

In *E. coli*, the same transcriptional regulator (MarA) regulates genes encoding efflux pumps (*acrAB* and *tolC*), DNA damage repair, and transport proteins [702]. Hence, these mechanisms demonstrate examples of connections between DNA damage response/repair and efflux pumps. A bioinformatics screening for CalP

homologs (BLASTP) found an efflux pump with 36% identity (only in a small domain that comprised a tiny portion of the entire amino acid sequence of the protein) in the bacterium *Halorhodospira halophila* (Fig. 47C). Although this homology was low, it was the only CalP ortholog found outside of the genus *Caulobacter*. Similarly, *calP* nucleotide alignments (BLASTN) showed 96 to 100% identity with small fragments of 21-24 nt from 14 different genes (with length ranges between 585 and 1653 nt) (Table 2). Three of these 14 genes were MDEPs, such as the ABC permease of *Streptomyces sp. CNQ-509,* the MFS transporter from *Cellulomonas dongxiuzhuiae,* and the efflux transporter from the MATE family (Table 2). Despite the identity between *calP* and the candidate genes being high, the sequence coverage was low, and so was the fidelity of the homology. Hence, considering the low fidelity of these data, these results are not conclusive but support the hypothesis that CalP may be an efflux pump. In contrast, I showed in previous experiments that Δ*calP* was more sensitive to the membrane depolariser CCCP than WT (Figs. 42, 43). This phenotype could be caused by the destabilisation of the membrane potential upon deletion of *calP*. Alternatively, it could be possibly due to the loss of the CCCP extrusion capacity because of the absence of CalP, which enhances the sensitivity of Δ*calP* to CCCP. CCCP is also known to be a potent inhibitor of efflux pumps [692, 703]. Therefore, if CalP functioned as an efflux pump, its inhibition by CCCP in the WT strain would display a phenotype akin to Δ*calP*. In such a scenario, both the WT and Δ*calP* strains would exhibit identical phenotypes. However, considering the optical density observed in Δ*calP* compared to WT, it is plausible that CalP might not function as an efflux pump (Figs. 42, 43). Previous data suggested that CalP may be a specific efflux pump transporter that exports DNA-damaging compounds, but the latter result suggested that CalP is not an efflux pump. Hence, given the inconclusive and contradictory results, the hypothesis that CalP is an MDEP will need further investigation.

3.10.4 CalP origin

Bioinformatics analysis showed that CalP is not conserved beyond the genus *Caulobacter*, except for a few exceptions showing low homology and poor identity.

Nonetheless, the poor SEP annotations in genomes still make possible the existence of CalP-like proteins with high homology in other species [463, 673, 704]. Thus, if we consider CalP to only be present in the genus *Caulobacter*, an evolutionary divergence from common ancestors may not answer the question of its origin. However, other hypotheses based on previous studies could explain the origin of CalP, such as Boto L. (2010) and Nasvall et al. (2012), which theorised the origin of new genes acquired by HGT and gene duplication, respectively [667, 668]. Other studies, such as B. A. Wilson and J. Masel (2011) and Ruiz-Orera et al. (2018), showed that previous non-coding ORFs were transcribed and subsequently translated [669, 670]. Grage et al. (2016) showed that small membrane proteins could influence membrane thickness and fluidity [659]. Knopp et al. (2019) demonstrated that synthetic-made peptides produced in *E. coli* could reduce membrane potential and decrease drug uptake to confer antibiotic resistance [674]. CalP shares properties such as short ORF and high hydrophobicity with peptides mentioned in Knopp et al. (2019), that confer antibiotic resistance. I showed in previous experiments that Δ*calP* was more sensitive than WT in the presence of CCCP (Fig. 43), suggesting that CalP may be important in maintaining the ionic gradient of the cell membrane. Perhaps CalP affects membrane potential and/or fluidity and prevents the entrance of antibiotics. Nevertheless, I demonstrated that CalP is regulated by RecA, so *calP* expressed in a Δ*recA* background was unable to upregulate upon MMC-induced DNA damage in the differential expression assay (Fig. 40A). Therefore, an unresolved question is how RecA could associate with and regulate a *de novo* generated *calP* [353]. All these questions require further investigation to elucidate the origin and role of CalP in *C. crescentus*.

Chapter 4. General Discussion

4.1 Outlook of bacterial resistance

Antibiotic resistance is one of the major concerns in public health and has been estimated to cause millions of human and livestock deaths over the next decades [164, 705-708]. The mode of action of antibiotics is very diverse and positively impacts their capacity to treat a wide variety of bacterial species. However, this diversity negatively affects the rapid adaptation of bacteria to different types of antibiotics [709]. Although multi-resistant bacteria usually have fast and developed systems to bypass the harmful effects of antibiotics on cells, many of these mechanisms are conserved across bacteria [609]. Distinct bacterial mechanisms contribute to creating AMR, such as membrane permeability, efflux pumps [619, 632, 710], DNA damage repair pathways [417, 702], antibiotic degradation pathways [709], or a combination of these mechanisms [609]. Bacteria rapidly adapt to resist new antibiotics with error-prone mutagenesis systems like TLS [24, 26]. HGT also plays a crucial role in exchanging genetic information intra- and inter-species to foster AR. The acquisition of new traits through HGT is common during antibiotic-treated infections [427]. Bacteria often trigger apoptotic-like systems that release cellular components into the extracellular medium, causing irreversible DNA damage [13]. Conjugation mechanisms [446] and cell damage-induced prophage pathways also enhance genetic variability via active genetic transference [433, 711]. Understanding the new methods bacteria develop to create AR is necessary to establish new strategies to overcome this evolving threat.

The multifunctional SOS-response system is ubiquitous in bacteria and contributes to creating AR [422, 430]. The SOS-dependent response was discovered in 1970 and was well-characterised, especially in *E. coli* [234, 352]. However, the SOS-independent response is still very unknown in many bacteria [351, 446, 450]. Some of the most striking SOS-independent systems are the *M. smegmatis* PafBC [170, 712, 713], Irre and DdrO in *Deinococcus spp*. [351], or the Ada system in *E. coli* [119]. Surprisingly, in *C. crescentus*, the SOS-independent response and SPs converge with at least three known proteins: DriD [450], DidA [449], and MmcA

[173]. A further understanding of SOS-independent systems in bacteria can shed light on unknown systems that can contribute to an effective AR [422]. The ubiquity of many AR systems in many classes of pathogenic and non-pathogenic bacteria enables the study of these pathways in non-pathogenic organisms. Thus, many discoveries in non-pathogenic model organisms can establish versatile models valid for numerous classes of bacteria. This insight can be ultimately transferred to studying pathogenic species.

The current bacterial resistance situation requires new strategies to stop this increasing problem. The development of new-generation antibiotics has increased substantially in recent years, given the increase in bacterial resistance [714-718]. New techniques such as genome mining and editing allow the development of several antibiotics. Nowadays, numerous antibiotics, some with novel modes of action, are in advanced phase trials [718]. An interesting and promising strategy to treat bacterial infections is using engineered bacteriophages to target specific populations of pathogenic bacteria. This method can limit the damage to commensal bacteria in the microbiota to maintain eubiosis. It can also reduce the side effects of certain antibiotics that affect eukaryotic cells [715, 719, 720]. Lastly, AMPs can be an alternative technique against AMR (described below) [517].

4.2 Overview of SPs

The investigation of SPs in different organisms has been scarce in recent years. The SPs scope is a growing scientific field that emerged a few years ago with the dedication of SPs specialist researchers such as Gisela Storz, Kai Papenfort, Joe Wade, and Todd Gray. In 2020, the mentioned researchers organised the first international Congress about SPs to gather scientists to present the latest discoveries in SPs investigations [451]. The Congress was eventually postponed because of the COVID-19 pandemic and reorganised as a virtual Congress in 2021. For many decades, SPs were considered too small to be functional, leading to an incomplete interpretation of pathways in which SPs play an important role [452]. The study of SPs can shed light on completing the puzzle that the biomolecules of an organism constitute. SPs are important in many regulatory processes and are integral parts of

several complexes in different bacteria, like photosynthetic machinery [721, 722] or efflux pumps, such as AcrB [492, 638]. Detecting SPs is more challenging than detecting bigger ones because the annotation of SPs was overlooked (due to a minimum cut-off of 50 KDa in bacteria), and far fewer annotations are available in genomic data [451, 452, 723]. In addition, SPs do not always show an apparent phenotype and are detected via mutagenesis, and if so, they may run off when copurified if the gel system is not optimised to detect proteins smaller than 5 KDa [452, 724]. Laboratory work with SPs is also more complicated than managing larger proteins with specific protocols, materials, and facilities optimised for them. The minimum detection threshold for proteins by MP analysis is 40 KDa [725]. Similarly, SPs (fewer than 50 aa) are not large enough to be analysed in electron microscopy or crystallography. Other detection assays, like MS/MS, struggle to detect SPs because the number of residues these devices can detect is often too scarce and does not reach the necessary amount to be sensed [675, 676, 678]. Usually, immune or fluorescence tags are far more prominent than the protein of the study itself, making it harder to discern whether the results are a genuine observation or an artefact of the fusion tag [451, 452, 724].

Understanding the functions of SPs, their conformation, and their structure can provide useful insight into developing anti-SP weapons to attack bacteria. The simplicity of SPs, with a short amino acid sequence and a single TM domain, makes them accessible for the action of potential drugs. Nonetheless, once SMPs are embedded in the membrane, they might be relatively inaccessible, especially for more hydrophilic compounds. In a reverse way, small peptides, like AMPs, can destabilise membrane integrity when the net charge is low and they have a high lysine and arginine content [451]. Small peptides can destroy cell envelopes by inhibiting cell wall synthesis and/or pore formation [517, 549]. Hence, engineering SPs to destabilise bacterial membranes could be an option to use as an antimicrobial strategy [717]. Furthermore, this method can work alongside conventional antibiotic and/or phage therapy treatments. A higher effectivity in treatments can allow the use of lower doses of antibiotics and, thus, reduce the propensity to create bacterial resistance.

CalP did not have any high-identity homologues in other organisms, according to BLAST screenings (Fig. 47). However, bioinformatics predictions showed several proteins of unknown function with domains like CalP. Therefore, a myriad of proteins whose genes are annotated require ribosome profiling to prove their translation and further characterisation and categorisation. By doing this, we will keep creating data libraries that will pave the way for future discoveries that will walk over previous discoveries. It will be like a puzzle in which several pieces are completed, and the setting process already speeds up. Sequencing and newer bioinformatics tools play a crucial role in this development, and machine automation in the future will likely be vital for completing laborious tasks and accelerating the process.

Chapter 5. Materials and methods

5.1 Bioinformatics procedures

The design and analysis of the constructs (oligo design, sequencing analysis, fragment synthesis design) were performed using Geneious Prime version 2019 (Biomatters, inc.). The DNA sequence annotator, visualiser, and analyser software Artemis (version 17.0.1) were used to analyse sequences like the BACTH fragments and visualise the genome of *C. crescentus* NA1000. The scrambling of the *calP* nucleotide sequence was done through the bioinformatic portal Expasy. The analysis of the *C. crescentus* genome and BACTH data was done in Geneious and Artemis. The BLAST analysis of the binding partners of CalP was done with the portal of the National Centre for Biotechnology Information (NCBI) from the US National Library of Medicine (NIH). For predicting the CalP structure, the bioinformatics platform AlphaFold2 and the molecular visualisation system PyMOL (Schrödinger/version 2.4.1) were used to represent the images. The information about *C. crescentus* genes and proteins was retrieved from the Uniprot and Caulobrowser databases [726].

5.2 Experimental procedures

5.2.1 Growth and storage conditions

5.2.1.1 Growth conditions

E. coli and *C. crescentus* were grown in LB or PYE media, respectively. *C. crescentus* cells were incubated at 30ºC and *E. coli* cells at 37ºC. *C. crescentus* cells with genes expressed under the P_{xyl} locus (ectopically inserted in the *xylX* locus) were treated with 0.1% xylose in a liquid PYE medium and 0.3% xylose in a solid medium. *E. coli* cells harbouring plasmids with the P_{lac} promoter were exposed to 0.1 mM IPTG.

5.2.1.2 Storage of strains

E. coli and *C. crescentus* strains, plasmids, and DNA fragments were stored at -20ºC for short- and mid-term storage and at -80ºC for long-term storage. *E. coli and C. crescentus* strains were preserved in 900 µL of LB and PYE cell cultures, respectively, with the addition of 100 µL of DMSO to prevent cell breakage during freezing.

5.2.2 Media, antibiotics, and buffers

5.2.2.1 Media

1.4.1.1.1.1 C. crescentus

PYE

Peptone yeast extract (PYE) is a complex medium rich in amino acids commonly employed as the standard medium to grow *C. crescentus* in laboratories. The high amino acid content provides the bacterium with a carbon source that can be used by the cell via amino acid degradation pathways as an energy source [727]. The standard recipe (for 1 L) of PYE medium was: 2 g/L bactopeptone, 1 g/L yeast extract, 1 mM $MgSO_4$ (0.3 g/L), 0.5 mM $CaCl_2$ (0.0735 g/L) (Ca is required for growth) [728].

Solid medium (standard recipe for 1 L): addition of 1.5% Bacto Agar (15 g/L) and fill to 1 L with liquid PYE. The mixture was boiled to dissolve the Bacto Agar.

Sterilisation: autoclave for 20 min.

1.4.1.1.1.2 E. coli

LB

JIC media service

Lysogeny broth, also known as LB, is a nutritionally rich medium used to grow *E. coli* and many other types of bacteria. The general composition for 1 L is:

10 g/L tryptone
5 g/L yeast extract
10 g/L NaCl

Components were dissolved in dH_2O [729, 730]. Solid medium: for the LB agar, a final concentration of 1.5% of the agar was added and filled up to 1 L. The mixture was boiled to dissolve the agar. The mixture was sterilised and autoclaved for 15 min at 15 psi, from 121 to 124°C [731].

SOC

(JIC media service)
The components for 1 L of SOC medium are:

5 g yeast extract
20 g tryptone
0.584 g NaCl
0.186 g KCl
2.4 g MgSO4
20 mL 20% glucose

All components except the glucose were mixed. The solution was autoclaved and let cool down below 50ºC. 20 ml of 20% glucose was sterilised by passing it through a 0.2 μm filter, added to the solution, and mixed.

MacConkey agar

(Millipore/cat. no. 70143)

40 g/L MacConkey agar
20% glucose-free maltose
1 mM IPTG

The MacConkey agar powder was dissolved in dH_2O and autoclaved. The glucose-free maltose was sterilised by filtration and added to the dissolved MacConkey agar medium. Antibiotics (carbenicillin and kanamycin) were added to the autoclaved MacConkey medium just before pouring plates. IPTG was included in the medium to induce protein expression [587].

M63

The components for 1 L of M63 medium are:

2 g/L $(NH_4)_2SO_4$
13.6 g/L KH_2PO_4
0.5 mg/L $FeSO_4 \cdot 7H_2O$
15 g/L agar per L of dH_2O
0.3% lactose
0.5 mM IPTG
40 µg/mL X-Gal

After autoclaving, the following reagents were added to the mixture, and the pH was adjusted to 7.0 with KOH. [587]:

1M MgSO4·7H2O
10 mL 20% maltose
2 mL 0.05 % vitamin B1 (thiamin)

Dual-indicator medium

The LB agar was mixed with:
80 µg/mL Magenta-gal
100 µg/mL X-Pho
1 mM IPTG

One single plate was poured with ~12.5 ml of medium to make it as thin as possible to distinguish the colours [592].

5.2.2.2 Antibiotics used for trait selection

To select antibiotic-resistant cells, cultures were treated with the appropriate antibiotic when required in a solid or liquid PYE medium. The antibiotics, which depended on the strain (Table 5) and the plasmid (Table 6), had the following concentrations (liquid/solid medium (µg/mL)):

PYE

- Kanamycin (5/25) for the *C. crescentus* strains transformed with the plasmids pXYFPC-2 and pBXMCS-2.
- Oxytetracycline (1/2) for the *C. crescentus* strain transformed with the plasmid Δ*recA-tetR*::Δ*calP*::P_{calP}-*calP-flag*.

LB

- Kanamycin (30/50), for the *E. coli* cells harbouring the plasmid(s) pK(N)T25.
- Carbenicillin (50/100), for the *E. coli* cells harbouring the plasmid(s) pUT18(C).
- Oxytetracycline (12/12) for the *E. coli* strain harbouring the plasmid Δ*recA-tetR*::Δ*calP*::P_{calP}-*calP-flag*.

MacConkey

- Kanamycin (-/50) for the *E. coli* cells harbouring the plasmid(s) pK(N)T25.
- Carbenicillin (-/100) for the *E. coli* cells harbouring the plasmid(s) pUT18(C).

M63

- Kanamycin (-/25) for the *E. coli* cells harbouring the plasmid(s) pK(N)T25.
- Carbenicillin (-/50) for the *E. coli* cells harbouring the plasmid(s) pUT18(C).

Dual-indicator medium

- Kanamycin (-/50) for the *E. coli* cells harbouring the plasmid(s) pK(N)T25.

Table 4. SIC of the stress inducer agents used in sensitivity assays in *C. crescentus* WT

Compound	SIC (µg/mL) of liquid PYE	Manufacturer/source
MMC	0.12/0.75 (overexpression)/ 3 (RT-qPCR)	Sigma-Aldrich. M4287
Norfloxacin	4	Merck/cat. no. N9890
MMS	1	Merck/cat. no. 129925
Ciprofloxacin	1	Merck/cat. no. 17850
Novobiocin	0.5	Merck/cat. no. N6160
HU	9	Merck/cat. no. H8627
CCCP	2	Sigma-Aldrich/cat. no. 215911
MMC-TRC	0.75	This study
Compound	**MIC (%)**	
H_2O_2	0.15%	Sigma-Aldrich/cat. no. H1009
NaClO	15 µL 6-14% stock	JIC media service

Table 4.1. SIC of the stress inducer agent used in sensitivity assays in *E. coli* BTH101

Compound	SIC (µg/mL) of liquid PYE	Manufacturer/source
MMC	0.75	Sigma-Aldrich. M4287

5.2.2.3 Buffers

Phosphate-buffered saline

Buffer from the JIC media service

0.8 g/L NaCl (Sigma-Aldrich/cat. no. S3014)

0.2 g/L KCl (Sigma-Aldrich/cat. no. P9541)

1.44 g/L Na_2HPO_4 Sigma-Aldrich/cat. no. S9763)

0.24 g/L KH_2PO_4 (Sigma Aldrich/cat. no. E6635)

0.133 g/L $CaCl_2 \cdot 2H_2O$ (Sigma Aldrich/cat. no. C3306)

0.10 g/L $MgCl_2 \cdot 6H_2O$ Sigma Aldrich/cat. no. M2393)

* pH was adjusted to 7.4 (or 7.2, if required) with HCl

Cell fractionation resuspension buffer

Buffer modified from Modell et al. (2011) [443]

1 M Tris-HCl (pH8) (Merck/cat. no. 648317)

250 mM EDTA (Sigma Aldrich/cat. no. E6635)

0.3 M sucrose (Sigma Aldrich/cat. no. S0389)

200 µg/mL lysozyme (Sigma-Aldrich/cat. no. L6876)

2 U/mL DNAse I (Invitrogen/cat. no. 10694233).

Protein lysis buffer

Buffer modified from the manufacturer (Miltenyi Biotec/cat. no. 130-101-591)

50 mM Tris-HCl pH8 (Merck/cat. no. 648317)

150 mM NaCl (Sigma-Aldrich/cat. no. S3014)

1%Triton-X (Merck/cat. no. 1086031000)

1x protease inhibitor (per 10 mL) (Merck/cat. no. P8849)

200 µg/mL lysozyme (Sigma-Aldrich/cat. no. L6876)

TE buffer

0.75 M Tris-HCl (Merck/cat. no. 648317)

0.5 M EDTA (Sigma Aldrich/cat. no. E6635)

pH 8

TBST

Tris-buffered saline (TBS) (Severn Biotech/cat. no. 20-7301-10)

0.1% Tween (Promega/cat. no. H5151)

5% skimmed dehydrated milk (Tesco)

Uptake assay lysis buffer

Buffer modified from **A.** E. Asuquo and L. J. Piddock (1993) [732]

0.05 M Tris-HCl pH8 (Merck/cat. no. 648317)

0.150 M NaCl (Sigma-Aldrich/cat. no. S3014)

0.1 M glycine (Sigma-Aldrich/cat. no. G8898)

5.2.3 Biological material

All the biological materials used for this study are listed in the following tables: strains (Table 5), plasmids (Table 6), synthesised DNA fragments (Table 7), and oligonucleotides (Table 8).

Notes:

- I deleted genes uniquely in *C. crescentus* and only used *E. coli* for heterologous expression of *calP.* Hence, all gene deletion mutants correspond to *C. crescentus* mutants.
- For the oligo names, I used indistinctly *CCNA_03982* or *calP*.

Table 5. Strains

Strains	Description	Source
C. crescentus		
NA1000	Synchronisable derivative of WT CB15	Laboratory stock
	NA1000+pBXMCS-*2*, Kan^R	This study
	NA1000+pBXMCS-*2::calP*, Kan^R	This study
	NA1000+pBXMCS-*2::calP-flag*, Kan^R	This study
	ΔcalP	Laboratory stock
	ΔcalP::P_{calP}*-calP-flag*	This study
	ΔcalP::P_{calP}*-scr calP-flag*	This study
	ΔcalP::P_{calP}*-calP-yfp*	This study
	ΔcalP::P_{calP}*-Φ*	This study
	ΔcalP::P_{calP}*-calP*	This study
	ΔcalP::P_{xyl}*-calP-flag,* Kan^R	This study
	ΔcalP::P_{xyl}*-calP (D2A)-flag*, Kan^R	This study
	ΔcalP::P_{xyl}*-calP (P3A)-flag*, Kan^R	This study
	ΔcalP::P_{xyl}*-calP (V4A)-flag*, Kan^R	This study
	ΔcalP::P_{xyl}*-calP (I5A)-flag*, Kan^R	This study
	ΔcalP::P_{xyl}*-calP (Q6A)-flag*, Kan^R	This study
	ΔcalP::P_{xyl}*-calP (V7A)-flag*, Kan^R	This study
	ΔcalP::P_{xyl}*-calP (V8A)-flag*, Kan^R	This study
	ΔcalP::P_{xyl}*-calP (L9A)-flag*, Kan^R	This study
	ΔcalP::P_{xyl}*-calP (I10A)-flag*, Kan^R	This study
	ΔcalP::P_{xyl}*-calP (G11A)-flag*, Kan^R	This study
	ΔcalP::P_{xyl}*-calP (L12A)-flag*, Kan^R	This study
	ΔcalP::P_{xyl}*-calP (V13A)-flag*, Kan^R	This study
	ΔcalP::P_{xyl}*-calP (F14A)-flag*, Kan^R	This study
	ΔcalP::P_{xyl}*-calP (V15A)-flag*, Kan^R	This study
	ΔcalP::P_{xyl}*-calP (A16P)-flag*, Kan^R	This study

NA1000	*ΔcalP*::P_{xyl}-*calP (A17P)-flag*, Kan^R	This study
	ΔcalP::P_{xyl}-*calP (A18P)-flag*, Kan^R	This study
	ΔcalP::P_{xyl}-*calP (Y19A)-flag*, Kan^R	This study
	ΔcalP::P_{xyl}-*calP (G20A)-flag*, Kan^R	This study
	ΔcalP::P_{xyl}-*calP (V21A)-flag*, Kan^R	This study
	ΔcalP::P_{xyl}-*calP (F22A)-flag*, Kan^R	This study
	ΔcalP::P_{xyl}-*calP (W23A)-flag*, Kan^R	This study
	ΔcalP::P_{xyl}-*calP (L24A)-flag*, Kan^R	This study
	ΔcalP::P_{xyl}-*calP (S25A)-flag*, Kan^R	This study
	ΔcalP:: P_{xyl}-*calP (M26A)-flag*, Kan^R	This study
	ΔcalP::P_{xyl}-*calP (R27A)-flag*, Kan^R	This study
	ΔcalP::P_{xyl}-*calP (E28A)-flag*, Kan^R	This study
	ΔcalP::P_{xyl}-*calP (K29A)-flag*, Kan^R	This study
	ΔcalP::P_{xyl}-*calP (P30A)-flag*, Kan^R	This study
	ΔcalP::P_{xyl}-*calP (H31A)-flag*, Kan^R	This study
	ΔcalP::P_{xyl}-*calP (Q32A)-flag*, Kan^R	This study
	ΔcalP::P_{xyl}-*calP (K33A)-flag*, Kan^R	This study
	ΔcalP::P_{xyl}-*calP (G34A)-flag*, Kan^R	This study
	ΔcalP::P_{xyl}-*calP (P35A)-flag*, Kan^R	This study
	ΔcalP::P_{xyl}-*calP (P36A)-flag*, Kan^R	This study
	ΔcalP::P_{xyl}-*calP (K45A)-flag*, Kan^R	This study
	ΔcalP::P_{xyl}-*calP*, Kan^R	This study
	ΔcalP::P_{xyl}-*calP-flag*, Kan^R	This study
	ΔcalP::P_{xyl}-*scr calP*, Kan^R	This study
	ΔcalP::P_{xyl}-*scr calP-flag*, Kan^R	This study
	Δ*recA*	This study
	Δ*recA-tetR*::Δ*calP*::P_{calP}-*calP-flag,* Kan^R, Tet^R	This study
	ΔCCNA_03981	This study
	ΔCCNA_02836	This study
	ΔCCNA_03673	This study
	ΔCCNA_02366	This study

	ΔCCNA_02837	This study
	ΔCCNA_02089	This study
	ΔCCNA_00182	This study
	ΔCCNA_01007	This study
E. coli		
DH5α	General host for DNA cloning (F^- φ80*lac*ZΔM15 Δ(*lac*ZYA-*arg*F) U169 *rec*A1 *end*A1 *hsd*R17(r_K^-, m_K^+) *pho*A *sup*E44 λ^-*thi*-1 *gyr*A96 *rel*A1)	Laboratory stock
	DH5α+pXYFPC-2::*Φ*, Kan^R	This study
	DH5α+pXYFPC-2::*calP,* Kan^R	This study
	DH5α+pXYFPC-2::*calP-flag,* Kan^R	This study
	DH5α+pXYFPC-2::P_{xyl}-*calP (D2A)-flag*, Kan^R	This study
	DH5α+pXYFPC-2::P_{xyl}-*calP (P3A)-flag*, Kan^R	This study
	DH5α+pXYFPC-2::P_{xyl}-*calP (V4A)-flag*, Kan^R	This study
	DH5α+pXYFPC-2::P_{xyl}-*calP (I5A)-flag*, Kan^R	This study
	DH5α+pXYFPC-2::P_{xyl}-*calP (Q6A)-flag*, Kan^R	This study
	DH5α+pXYFPC-2::P_{xyl}-*calP (V7A)-flag*, Kan^R	This study
	DH5α+pXYFPC-2::P_{xyl}-*calP (V8A)-flag*, Kan^R	This study
	DH5α+pXYFPC-2::P_{xyl}-*calP (L9A)-flag*, Kan^R	This study
	DH5α+pXYFPC-2::P_{xyl}-*calP (I10A)-flag*, Kan^R	This study
	DH5α+pXYFPC-2::P_{xyl}-*calP (G11A)-flag*, Kan^R	This study
	DH5α+pXYFPC-2::P_{xyl}-*calP (L12A)-flag*, Kan^R	This study
	DH5α+pXYFPC-2::P_{xyl}-*calP (V13A)-flag*, Kan^R	This study
	DH5α+pXYFPC-2::P_{xyl}-*calP (F14A)-flag*, Kan^R	This study
	DH5α+pXYFPC-2::P_{xyl}-*calP (V15A)-flag*, Kan^R	This study
	DH5α+pXYFPC-2::P_{xyl}-*calP (A16P)-flag*, Kan^R	This study
	DH5α+pXYFPC-2::P_{xyl}-*calP (A17P)-flag*, Kan^R	This study
	DH5α+pXYFPC-2::P_{xyl}-*calP (A18P)-flag*, Kan^R	This study
	DH5α+pXYFPC-2::P_{xyl}-*calP (Y19A)-flag*, Kan^R	This study
	DH5α+pXYFPC-2::P_{xyl}-*calP (G20A)-flag*, Kan^R	This study
	DH5α+pXYFPC-2::P_{xyl}-*calP (V21A)-flag*, Kan^R	This study

DH5α	DH5α+pXYFPC-2::P$_{xyl}$-*calP (F22A)-flag*, Kan^R	This study
	DH5α+pXYFPC-2::P$_{xyl}$-*calP (W23A)-flag*, Kan^R	This study
	DH5α+pXYFPC-2::P$_{xyl}$-*calP (L24A)-flag*, Kan^R	This study
	DH5α+pXYFPC-2::P$_{xyl}$-*calP (S25A)-flag*, Kan^R	This study
	DH5α+pXYFPC-2:: P$_{xyl}$-*calP (M26A)-flag*, Kan^R	This study
	DH5α+pXYFPC-2::P$_{xyl}$-*calP (R27A)-flag*, Kan^R	This study
	DH5α+pXYFPC-2::P$_{xyl}$-*calP (E28A)-flag*, Kan^R	This study
	DH5α+pXYFPC-2::P$_{xyl}$-*calP (K29A)-flag*, Kan^R	This study
	DH5α+pXYFPC-2::P$_{xyl}$-*calP (P30A)-flag*, Kan^R	This study
	DH5α+pXYFPC-2::P$_{xyl}$-*calP (H31A)-flag*, Kan^R	This study
	DH5α+pXYFPC-2::P$_{xyl}$-*calP (Q32A)-flag*, Kan^R	This study
	DH5α+pXYFPC-2::P$_{xyl}$-*calP (K33A)-flag*, Kan^R	This study
	DH5α+pXYFPC-2::P$_{xyl}$-*calP (G34A)-flag*, Kan^R	This study
	DH5α+pXYFPC-2::P$_{xyl}$-*calP (P35A)-flag*, Kan^R	This study
	DH5α+pXYFPC-2::P$_{xyl}$-*calP (P36A)-flag*, Kan^R	This study
	DH5α+pXYFPC-2::P$_{xyl}$-*calP (K45A)-flag*, Kan^R	This study
	DH5α+pXYFPC-2::*scrambled calP,* Kan^R	This study
	DH5α+pBXMCS-*2*::*Φ,* Kan^R	This study
	DH5α+pBXMCS-*2::calP,* Kan^R	This study
	DH5α+pBXMCS-*2::calP-flag,* Kan^R	This study
	DH5α+pUT18C (-T18)::*Φ,* Kan^R	This study
	DH5α+pUT18C (-T18)::*calP,* Kan^R	This study
	DH5α+pUT18C (-T18)*::calP-flag,* Kan^R	This study
	DH5α+pNPTS138::*calP-flag,* Kan^R	This study
	DH5α+pNTPS138::*scr calP-flag,* Kan^R	This study
	DH5α+pNTPS138::*calP-yfp,* Kan^R	This study
	DH5α+pNTPS138::*(FS1-FS2) CCNA_02836,* Kan^R	This study
	DH5α+pNTPS138::*(FS1-FS2) CCNA_03673,* Kan^R	This study

DH5α	DH5α+pNTPS138::*(FS1-FS2) CCNA_02366,* Kan^R	This study
	DH5α+pNTPS138::*(FS1-FS2) CCNA_02837,* Kan^R	This study
	DH5α+pNTPS138::*(FS1-FS2) CCNA_02089,* Kan^R	This study
	DH5α+pNTPS138::*(FS1-FS2) CCNA_00182,* Kan^R	This study
	DH5α+pNTPS138::*(FS1-FS2) CCNA_01007,* Kan^R	This study
	DH5α+pNTPS138::*(FS1-FS2)CCNA_03981,* Kan^R	This study
	DH5α+pNTPS138::Δ*recA-tetR*::Δ*calP*::P_{calP}-*calP-flag,* Kan^R, Tet^R	This study
	DH5α+pXYFPC-2::*scr calP-flag,* Kan^R	This study
	DH5α+pNKT25, Kan^R	This study
	DH5α+pUT18, Amp^R	This study
	DH5α+pNKT25::*calP,* Kan^R	This study
	DH5α+pUT18::*calP,* Amp^R	This study
	DH5α+pKTN25::*calP,* Kan^R	This study
	DH5α+pUT18::*calP,* Amp^R	This study
	DH5α+pKT25::*calP,* Kan^R	This study
	DH5α+pUT18C::*calP,* Amp^R	This study
	DH5α+pKT25::*CCNA_02837,* Kan^R	This study
	DH5α+pUT18C::*CCNA_02837,* Amp^R	This study
	DH5α+pKT25::*CCNA_02836,* Kan^R	This study
	DH5α+pUT18C::*CCNA_02836,* Amp^R	This study
	DH5α+pKT25::*CCNA_02837-CCNA_02836,* Kan^R	This study
	DH5α+pUT18C::*CCNA2837-CCNA_02836,* Amp^R	This study

DH5α	DH5α+pKT25::*CCNA_02366,* Kan^R	This study
	DH5α+pUT18C::*CCNA_02366,* Amp^R	This study
	DH5α+pKT25::*CCNA_02089* Kan^R	This study
	DH5α+pUT18::*CCCNA_02089,* Amp^R	This study
	DH5α+pKT25::*CCNA_0182,* Kan^R	This study
	DH5α+pUT18C::*CCNA_0182,* Amp^R	This study
	DH5α+pKT25::*CCNA_01007,* Kan^R	This study
	DH5α+pUT18C::*CCNA_01007,* Amp^R	This study
	DH5α+pKT25::*CCNA_03673,* Kan^R	This study
	DH5α+pUT18C::*CCNA_03673,* Amp^R	This study
	DH5α+pKNT25::*calP (L9A)-flag,* Kan^R	This study
	DH5α+pUT18::*calP (L9A)-flag,* Amp^R	This study
	DH5α+pKNT25::*calP (L12A)-flag,* Kan^R	This study
	DH5α+pUT18::*calP (L12A)-flag,* Amp^R	This study
	DH5α+pKNT25::*calP (A16P)-flag,* Kan^R	This study
	DH5α+pUT18::*calP (A16P)-flag,* Amp^R	This study
	DH5α+pKNT25::*calP (A17P)-flag,* Kan^R	This study
	DH5α+pUT18::*calP (A17P)-flag,* Amp^R	This study
	DH5α+pKNT25::*calP (A18P)-flag,* Kan^R	This study
	DH5α+pUT18::*calP (A18P)-flag,* Amp^R	This study
	DH5α+pKNT25::*calP (F22A)-flag,* Kan^R	This study
	DH5α+pUT18::*calP (F22A)-flag,* Amp^R	This study
	DH5α+pKTop::*Φ,* Kan^R	Laboratory stock
	DH5α+pKTop::*calP,* Kan^R	This study
	DH5α+pKTop::*rsbN,* Kan^R	This study
	DH5α+pUT18C (-T18), Kan^R	This study
	DH5α+pUT18C (-T18)::*calP,* Kan^R	This study
	DH5α+pUT18C (-T18)*::calP-flag,* Kan^R	This study
	Δ*cya* used for BACTH assays (BTH101: F_, cya-99, araD139, galE15, galK16, rpsL1 (Strr), hsdR2,	(Laboratory stock)

BTH101	*mcrA1*, *mcrB1*; DHM1: F-, *cya*-854, *recA1*, *endA1*, *gyrA96* (NalR), *thi1*, *hsdR17*, *spoT1*, *rfbD1*, *glnV44*(AS)))	[733]
	BTH101+pKT25::*zip*+pUT18C::*zip,* Kan^R, Amp^R	This study
	BTH101+pKT25::*Φ*+pUT18C::*Φ,* Kan^R, Amp^R	This study
	BTH101+pKT25::*Φ*+pUT18C::*calP,* Kan^R, Amp^R	This study
	BTH101+pKT25::*Φ*+pUT18::*calP,* Kan^R, Amp^R	This study
	BTH101+pKT25::*calP*+pUT18C::*Φ,* Kan^R, Amp^R	This study
	BTH101+pKT25::*calP*+pUT18C::*calP,* Kan^R, Amp^R	This study
	BTH101+pKT25::*calP*+pUT18::*calP,* Kan^R, Amp^R	This study
	BTH101+pKNT25::*calP*+pUT18C::*Φ,* Kan^R, Amp^R	This study
	BTH101+pKNT25::*calP*+pUT18C::*calP,* Kan^R, Amp^R	This study
	BTH101+pKNT25::*calP*+pUT18::*calP,* Kan^R, Amp^R	This study
	BTH101+pKT25::*Φ*+pUT18C::*CCNA_02837,* Kan^R, Amp^R	This study
	BTH101+pKT25::*Φ*+pUT18C::*CCNA_02836,* Kan^R, Amp^R	This study
	BTH101+pKT25::*Φ*+pUT18C::*CCNA_02837*+*CCNA_02836,* Kan^R, Amp^R	This study
	BTH101+pKT25::*calP*+pUT18C::*Φ,* Kan^R, Amp^R	This study
	BTH101+pKT25::*calP*+pUT18C::*CCNA_02837,* Kan^R, Amp^R	This study
	BTH101+pKT25::*calP*+pUT18C::*CCNA_02836,* Kan^R, Amp^R	This study

BTH101	BTH101+pKT25::*calP*+ pUT18C::*CCNA_02837*+ *CCNA_02836,* Kan^R, Amp^R	This study
	BTH101+pKNT25::*calP*+ pUT18C::*Φ,* Kan^R, Amp^R	This study
	BTH101+pKNT25::*calP*+pUT18C::*CCNA_02837* , Kan^R, Amp^R	This study
	BTH101+pKNT25::*calP*+pUT18C::*CCNA_02836* , Kan^R, Amp^R	This study
	BTH101+pKNT25::*calP*+ pUT18C::*CCNA_02837*+ *CCNA_02836,* Kan^R, Amp^R	This study
	BTH101+pKT25::*CCNA_02837*+pUT18C::*Φ,* Kan^R, Amp^R	This study
	BTH101+ pKT25::*CCNA_02837*+ pUT18C::*CCNA_02837,* Kan^R, Amp^R	This study
	BTH101+pKT25::*CCNA_02837*+ pUT18C::*CCNA_02836,* Kan^R, Amp^R	This study
	BTH101+ pKT25::*CCNA_02837*+ pUT18C::*CCNA_02837*+ *CCNA_02836,* Kan^R, Amp^R	This study
	BTH101+pUT18::*Φ*+BTH101+pKNT25::*calP (L9A)-flag,* Kan^R, Amp^R	This study
	BTH101+pUT18::*calP (L9A)-flag*+BTH101+pKNT25::*Φ,* Kan^R, Amp^R	This study
	BTH101+pUT18::*calP (L9A)-flag*+BTH101+pKNT25::*calP (L9A)-flag,* Kan^R, Amp^R	This study
	BTH101+pUT18::*Φ*+ BTH101+pKNT25::*calP (L12A)-flag,* Kan^R, Amp^R	This study
	BTH101+pUT18::*calP (L12A)-flag*+BTH101+pKNT25::*Φ,* Kan^R, Amp^R	This study

BTH101	BTH101+pUT18::*calP (L12A)-flag*+BTH101+pKNT25::*calP (L12A)-flag,* Kan^R, Amp^R	This study
	BTH101+pUT18::*Φ*+ BTH101+pKNT25::*calP (A16P)-flag,* Kan^R, Amp^R	This study
	BTH101+pUT18::*calP (A16P)-flag* +BTH101+pKNT25::*Φ,* Kan^R, Amp^R	This study
	BTH101+pUT18::*calP (A16P)-flag*+BTH101+pKNT25::*calP (A16P)-flag,* Kan^R, Amp^R	This study
	BTH101+pUT18::*Φ*+BTH101+pKNT25::*calP (A17P)-flag,* Kan^R, Amp^R	This study
	BTH101+pUT18::*calP (A17P)-flag*+BTH101+pKNT25::*Φ,* Kan^R, Amp^R	This study
	BTH101+pUT18::*calP (A17P)-flag* +BTH101+pKNT25::*calP (A17P)-flag,* Kan^R, Amp^R	This study
	BTH101+pUT18::*Φ*+BTH101+pKNT25::*calP (A18P)-flag,* Kan^R, Amp^R	This study
	BTH101+pUT18::*calP (A18P)-flag*+BTH101+pKNT25:*Φ,* Kan^R, Amp^R	This study
	BTH101+pKNT25::*calP (A18P)-flag*+ BTH101+pUT18::*calP (A18P)-flag,* Kan^R, Amp^R	This study
	BTH101+pUT18::*Φ*+ BTH101+pKNT25::*calP (F22A)-flag,* Kan^R, Amp^R	This study
	BTH101+pUT18::*calP (F22A)-flag* BTH101+pKNT25::*Φ*	This study
	BTH101+pUT18::*calP (F22A)-flag*+BTH101+pKNT25::*calP (F22A)-flag,* Kan^R, Amp^R	This study
	$RecA^+$ host used for heterologous expression of *calP* (*F-, thr-1*, *araC14*, *leuB6*(Am), *Δ(gpt-*	Laboratory stock

AB1157	*proA)62*, *lacY1*, *tsx-33*, *qsr'-0*, *glnX44*(AS), *galK2*(Oc), *λ⁻*, *Rac-0*, *hisG4*(Oc), *rfbC1*, *mgl-51*, *rpoS396*(Am), *rpsL31*(StrR), *kdgK51*, *xylA5*, *mtl-1*, *argE3*(Oc), *thiE1I*)	[734]
	AB1157+pUT18C (-T18)::*Φ,* Kan^R	This study
	AB1157+pUT18C (-T18)::*calP,* Kan^R	This study
	AB1157+pUT18C (-T18)*::calP-flag,* Kan^R	This study

Table 6. Plasmids

Plasmid	Description	Reference
pXYFPC-2	Integrative vector for generating C-terminal protein fusions encoded at the *xylX* locus, Kan^R	[586]
pXYFPC-2::*calP*	Integrative vector carrying *calP* encoded at the *xylX* locus, Kan^R	This study
pXYFPC-2::*calP-flag*	Integrative vector carrying *calP-flag* encoded at the *xylX* locus, Kan^R	This study
pXYFPC-2::*scr calP*	Integrative vector carrying *scrambled calP* encoded at the *xylX* locus, Kan^R	This study
pXYFPC-2::*scr calP-flag*	Integrative vector carrying *scrambled calP-flag* encoded at the *xylX* locus, Kan^R	This study
pXYFPC-2::P$_{xyl}$-*calP (D2A)-flag*, Kan^R	*calP* derivative carrying substitution of aspartic acid in position 2nd for alanine, Kan^R	This study
pXYFPC-2::P$_{xyl}$-*calP (P3A)-flag*, Kan^R	*calP* derivative carrying substitution of proline in position 3rd for alanine, Kan^R	This study
pXYFPC-2::P$_{xyl}$-*calP (V4A)-flag*, Kan^R	*calP* derivative carrying substitution of valine in position 4th for alanine, Kan^R	This study

pXYFPC-2::P*xyl*-*calP (I5A)-flag*, Kan^R	*calP* derivative carrying substitution of isoleucine in position 5th for alanine, Kan^R	This study
pXYFPC-2::P*xyl*-*calP (Q6A)-flag*, Kan^R	*calP* derivative carrying substitution of glutamine in position 6th for alanine, Kan^R	This study
pXYFPC-2::P*xyl*-*calP (V7A)-flag*, Kan^R	*calP* derivative carrying substitution of valine in position 7th for alanine, Kan^R	This study
pXYFPC-2::P*xyl*-*calP (V8A)-flag*, Kan^R	*calP* derivative carrying substitution valine acid in position 8th for alanine, Kan^R	This study
pXYFPC-2::P*xyl*-*calP (L9A)-flag*, Kan^R	*calP* derivative carrying substitution leucine in position 9th for alanine, Kan^R	This study
pXYFPC-2::P*xyl*-*calP (I10A)-flag*, Kan^R	*calP* derivative carrying substitution of isoleucine in position 10th for alanine, Kan^R	This study
pXYFPC-2::P*xyl*-*calP (G11A)-flag*, Kan^R	*calP* derivative carrying substitution of glycine in position 11th for alanine, Kan^R	This study
pXYFPC-2::P*xyl*-*calP (L12A)-flag*, Kan^R	*calP* derivative carrying substitution of leucine in position 12th for alanine, Kan^R	This study
pXYFPC-2::P*xyl*-*calP (V13A)-flag*, Kan^R	*calP* derivative carrying substitution of valine in position 13th for alanine, Kan^R	This study
pXYFPC-2::P*xyl*-*calP (F14A)-flag*, Kan^R	*calP* derivative carrying substitution of phenylalanine in position 14th for alanine, Kan^R	This study

pXYFPC-2::P*xyl*-*calP (V15A)-flag*, Kan^R	*calP* derivative carrying substitution of valine in position 15th for alanine, Kan^R	This study
pXYFPC-2::P*xyl*-*calP (A16P)-flag*, Kan^R	*calP* derivative carrying substitution of alanine in position 16th for proline, Kan^R	This study
pXYFPC-2::P*xyl*-*calP (A17P)-flag*, Kan^R	*calP* derivative carrying substitution of alanine in position 17th for proline, Kan^R	This study
pXYFPC-2::P*xyl*-*calP (A18P)-flag*, Kan^R	*calP* derivative carrying substitution of alanine in position 18th for proline, Kan^R	This study
pXYFPC-2::P*xyl*-*calP (Y19A)-flag*, Kan^R	*calP* derivative carrying substitution of tyrosine in position 19th for alanine, Kan^R	This study
pXYFPC-2::P*xyl*-*calP (G20A)-flag*, Kan^R	*calP* derivative carrying substitution of glycine in position 20th for alanine, Kan^R	This study
pXYFPC-2::P*xyl*-*calP (V21A)-flag*, Kan^R	*calP* derivative carrying substitution of valine in position 21st for alanine, Kan^R	This study
pXYFPC-2::P*xyl*-*calP (F22A)-flag*, Kan^R	*calP* derivative carrying substitution of phenylalanine in position 22nd for alanine, Kan^R	This study
pXYFPC-2::P*xyl*-*calP (W23A)-flag*, Kan^R	*calP* derivative carrying substitution of tryptophan acid in position 23rd for alanine, Kan^R	This study
pXYFPC-2::P*xyl*-*calP (L24A)-flag*, Kan^R	*calP* derivative carrying substitution of leucine in position 24th for alanine, Kan^R	This study

pXYFPC-2::P_{xyl}-*calP (S25A)-flag*, Kan^R	*calP* derivative carrying substitution of serine in position 25th for alanine, Kan^R	This study
pXYFPC-2:: P_{xyl}-*calP (M26A)-flag*, Kan^R	*calP* derivative carrying substitution of methionine in position 26th for alanine, Kan^R	This study
pXYFPC-2::P_{xyl}-*calP (R27A)-flag*, Kan^R	*calP* derivative carrying substitution of arginine in position 27th for alanine, Kan^R	This study
pXYFPC-2::P_{xyl}-*calP (E28A)-flag*, Kan^R	*calP* derivative carrying substitution of glutamic acid in position 28th for alanine, Kan^R	This study
pXYFPC-2::P_{xyl}-*calP (K29A)-flag*, Kan^R	*calP* derivative carrying substitution of lysine in position 29th for alanine, Kan^R	This study
pXYFPC-2::P_{xyl}-*calP (P30A)-flag*, Kan^R	*calP* derivative carrying substitution of proline in position 30th for alanine, Kan^R	This study
pXYFPC-2::P_{xyl}-*calP (H31A)-flag*, Kan^R	*calP* derivative carrying substitution of histidine in position 31st for alanine, Kan^R	This study
pXYFPC-2::P_{xyl}-*calP (Q32A)-flag*, Kan^R	*calP* derivative carrying substitution of glutamine in position 32nd for alanine, Kan^R	This study
pXYFPC-2::P_{xyl}-*calP (K33A)-flag*, Kan^R	*calP* derivative carrying substitution of lysine in position 33rd for alanine, Kan^R	This study
pXYFPC-2::P_{xyl}-*calP (G34A)-flag*, Kan^R	*calP* derivative carrying substitution of glycine in position 34th for alanine, Kan^R	This study

pXYFPC-2::P$_{xyl}$-*calP (P35A)-flag*, Kan^R	*calP* derivative carrying substitution of proline in position 35th for alanine, Kan^R	This study
pXYFPC-2::P$_{xyl}$-*calP (P36A)-flag*, Kan^R	*calP* derivative carrying substitution of proline in position 36th for alanine, Kan^R	This study
pXYFPC-2::P$_{xyl}$-*calP (K45A)-flag*, Kan^R	*calP* derivative carrying substitution of lysine in position 45th for alanine, Kan^R	This study
pBXMCS-*2*	Non-integrative high-copy number plasmid for overexpression in *C. crescentus*, Kan^R	[586]
pBXMCS-*2*::*calP*	Non-integrative high-copy number plasmid for overexpression carrying *calP*, Kan^R	This study
pBXMCS-*2*::*calP-flag*	Non-integrative high-copy number plasmid for overexpression carrying *calP-flag*, Kan^R	This study
pUT18C (-T18)	T18-less high-copy number plasmid used as an empty vector control for the heterologous expression of *calP* in *E. coli,* Amp^R	This study
pUT18C (-T18)::*calP*	T18-less high-copy number plasmid used for the heterologous expression of *calP* in *E. coli*, Amp^R	This study
pUT18C (-T18)::*calP-flag*	T18-less high-copy number plasmid used for the heterologous expression of *calP-flag* in *E. coli,* Amp^R	This study
pUT18	High copy number plasmid for generating C-terminal protein fusions expressing CyaA$_{225-339}$, Amp^R	BioBasics [587]

pKNT25	Low copy number plasmid for generating C-terminal protein fusions expressing $CyaA_{1-224}$, Kan^R	BioBasics [587]
pUT18::*zip*	High-copy number plasmid producing *zip* cloned at the N-terminus domain of $CyaA_{225-339}$, Amp^R	BioBasics [587]
pKNT25::*zip*	Low-copy number plasmid producing *zip* cloned at the N-terminus domain of $CyaA_{1-224}$, Kan^R	BioBasics [587]
pUT18::*calP*	High-copy number plasmid producing *calP* cloned at the N-terminus domain of $CyaA_{225-339}$, Amp^R	This study
pKNT25::*calP*	Low-copy number plasmid producing *calP* cloned at the N-terminus domain of $CyaA_{1-224}$, Kan^R	This study
pUT18::*C. crescentus library*	Library cloned by the insertion of random sonicated fragments of the *C. crescentus* genome in the SmaI site of pUT18 at the N-terminus of $CyaA_{225-339}$, Amp^R	Laboratory stock /BioS&T
pUT18C	High copy number plasmid for generating N-terminal protein fusions expressing $CyaA_{225-339}$, Amp^R	BioBasics [587]
pKT25	Low copy number plasmid for generating N-terminal protein fusions expressing $CyaA_{1-224}$, Kan^R	BioBasics [587]
pUT18C::*calP*	High-copy number plasmid producing *calP* cloned at the C-terminus domain of $CyaA_{225-339}$, Amp^R	This study
pKT25::*calP*	Low-copy number plasmid producing *calP* cloned at the C-terminus domain of $CyaA_{1-224}$, Kan^R	This study

pUT18C::*CCNA_02837*	High-copy number plasmid producing *CCNA_02837* cloned at the C-terminus domain of $CyaA_{225-339}$, Amp^R	This study
pKT25::*CCNA_02837*	Low-copy number plasmid producing *CCNA_02837* cloned at the C-terminus domain of $CyaA_{1-224}$, Kan^R	This study
pUT18C::*CCNA_02836*	High-copy number plasmid producing *CCNA_02836* cloned at the C-terminus domain of $CyaA_{225-339}$, Amp^R	This study
pKT25::*CCNA_02836*	Low-copy number plasmid producing *CCNA_02836* cloned at the C-terminus domain of $CyaA_{1-224}$, Kan^R	This study
pUT18C::*CCNA_02837-CCNA_02836*	High-copy number plasmid producing *CCNA_02837-CCNA_02836* cloned at the C-terminus domain of $CyaA_{225-339}$, Amp^R	This study
pKT25::*CCNA_02837-CCNA2836*	Low-copy number plasmid producing *CCNA_02837-CCNA_02836* cloned at the C-terminus domain of $CyaA_{1-224}$, Kan^R	This study
pUT18C::*CCNA_02366*	High-copy number plasmid producing CCNA_02366 cloned at the C-terminus domain of $CyaA_{225-339}$, Amp^R	This study
pKT25::*CCNA_02366*	Low-copy number plasmid producing *CCNA_02366* cloned at the C-terminus domain of $CyaA_{1-224}$, Kan^R	This study
pUT18::*CCNA_02089*	High-copy number plasmid producing *CCNA_02089* cloned at the C-terminus domain of $CyaA_{225-339}$, Amp^R	This study
pKT25::*CCNA_02089*	Low-copy number plasmid producing *CCNA_02089* cloned at the C-terminus domain of $CyaA_{1-224}$, Kan^R	This study

pUT18C::*CCNA_00182*	High-copy number plasmid producing *CCNA_00182* cloned at the C-terminus domain of $CyaA_{225-339}$, Amp^R	This study
pKT25::*CCNA_00182*	Low-copy number plasmid producing *CCNA_00182* cloned at the C-terminus domain of $CyaA_{1-224}$, Kan^R	This study
pUT18C::*CCNA_01007*	High-copy number plasmid producing *CCNA_01007* cloned at the C-terminus domain of $CyaA_{225-339}$, Amp^R	This study
pKT25::*CCNA_01007*	Low-copy number plasmid producing *CCNA_01007* cloned at the C-terminus domain of $CyaA_{1-224}$, Kan^R	This study
pUT18C::*CCNA_03673*	High-copy number plasmid producing *CCNA_03673* cloned at the C-terminus domain of $CyaA_{225-339}$, Amp^R	This study
pKT25::*CCNA_03673*	Low-copy number plasmid producing *CCNA_03673* cloned at the C-terminus domain of $CyaA_{1-224}$, Kan^R	This study
pUT18::*calP (L9A)-flag*	High-copy number plasmid producing *calP (L9A)-flag* cloned at the C-terminus domain of $CyaA_{225-339}$, Amp^R	This study
pKNT25::*calP (L9A)-flag*	Low-copy number plasmid producing *calP (L9A)-flag* cloned at the C-terminus domain of $CyaA_{1-224}$, Kan^R	This study
pUT18::*calP (L12A)-flag*	High-copy number plasmid producing *calP (L12A)-flag* cloned at the C-terminus domain of $CyaA_{225-339}$, Amp^R	This study

pKNT25::*calP (L12A)-flag*	Low-copy number plasmid producing *calP (L12A)-flag* cloned at the C-terminus domain of $CyaA_{1-224}$, Kan^R	This study
pUT18::*calP (A16P)-flag*	High-copy number plasmid producing *calP (A16P)-flag* cloned at the C-terminus domain of $CyaA_{225-339}$, Amp^R	This study
pKNT25::*calP (A16P)-flag*	Low-copy number plasmid producing *calP (A16P)-flag* cloned at the C-terminus domain of $CyaA_{1-224}$, Kan^R	This study
pUT18::*calP (A17P)-flag*	High-copy number plasmid producing *calP (A17P)-flag* cloned at the C-terminus domain of $CyaA_{225-339}$, Amp^R	This study
pKNT25::*calP (A17P)-flag*	Low-copy number plasmid producing *calP (A17P)-flag* cloned at the C-terminus domain of $CyaA_{1-224}$, Kan^R	This study
pUT18::*calP (A18P)-flag*	High-copy number plasmid producing *calP (A18P)-flag* cloned at the C-terminus domain of $CyaA_{225-339}$, Amp^R	This study
pKNT25::*calP (A18P)-flag*	Low-copy number plasmid producing *calP (A18P)-flag* cloned at the C-terminus domain of $CyaA_{1-224}$, Kan^R	This study
pUT18::*calP (F22A)-flag*	High-copy number plasmid producing *calP (F22A)-flag* cloned at the C-terminus domain of $CyaA_{225-339}$, Amp^R	This study
pKNT25::*calP (F22A)-flag*	Low-copy number plasmid producing *calP (F22A)-flag* cloned at the C-terminus domain of $CyaA_{1-224}$, Kan^R	This study
pNTPS138::*(FS1-FS2) calP-flag*	Integrative vector carrying *calP* fused to a C-terminal FLAG tag epitope tag	

	transcribed from its native promoter, Kan^R	This study
pNTPS138::*scr calP-flag*	Integrative vector carrying *scrambled calP* fused to a C-terminal FLAG tag epitope tag transcribed from its native promoter, Kan^R	This study
pNTPS138::*calP-yfp*	Integrative vector carrying *calP* fused to a C-terminal YFP epitope tag transcribed from its native promoter, Kan^R	This study
pNTPS138::*(FS1-FS2) CCNA_02836*	Vector used to create a markerless in-frame *CCNA_02836* deletion, Kan^R	This study
pNTPS138::*(FS1-FS2) CCNA_03673*	Vector used to create a markerless in-frame *CCNA_03673* deletion, Kan^R	This study
pNTPS138::*(FS1-FS2) CCNA_02366*	Vector used to create a markerless in-frame *CCNA_02366* deletion, Kan^R	This study
pNTPS138::*(FS1-FS2) CCNA_02837*	Vector used to create a markerless in-frame *CCNA_02837* deletion, Kan^R	This study
pNTPS138::*(FS1-FS2) CCNA_02089*	Vector used to create a markerless in-frame *CCNA_02089* deletion, Kan^R	This study
pNTPS138::*(FS1-FS2) CCNA_00182*	Vector used to create a markerless in-frame *CCNA_00182* deletion, Kan^R	This study
pNTPS138::*(FS1-FS2) CCNA_001007*	Vector used to create a markerless in-frame *CCNA_01007* deletion, Kan^R	This study
pNTPS138::*(FS1-FS2) CCNA_03981*	Vector used to create a markerless in-frame *CCNA_03981* deletion, Kan^R	This study
pNTPS138::Δ*recA-tetR*::Δ*calP*::P_{calP}-*calP-flag*	Vector used to create a *tetR* marker in-frame *recA* deletion in a Δ*calP* background, Kan^R, Tet^R	This study
pNPTS138::*ΔrogA*::*tetR*	Vector used to amplify a *tetR* marker, Kan^R, Tet^R	Lab stock

pKTop::*Φ*	Vector expressing dual reporter $Pho_{A22-472}/LacZ_{4-60}$, p15 ori; Kan^R	[592]
pKTop::*calP*	*calP* cloned at the N-terminus domain of $Pho_{A22-472}/LacZ_{4-60}$, p15 ori; Kan^R	This study
pKTop::*rsbN*	*rsbN* cloned at the N-terminus domain of $Pho_{A22-472}/LacZ_{4-60}$, p15 ori; Kan^R	Gifted by Felix Ramos-Leon [593]

Table 7. Synthesised fragments

DNA fragments	Description	Source
calP-flag	*flag tag* fused to the C terminus of *calP*	Integrated DNA Technologies
scr calP	*Scrambled calP* sequence keeping the amino acid sequence	Integrated DNA Technologies
calP (D2A)-flag	*calP* derivative carrying substitution of aspartic acid in position 2nd for alanine, Kan^R	Novogene
calP (P3A)-flag	*calP* derivative carrying substitution of proline in position 3rd for alanine, Kan^R	Novogene
calP (V4A)-flag	*calP* derivative carrying substitution of valine in position 4th for alanine, Kan^R	Novogene
calP (I5A)-flag	*calP* derivative carrying substitution of isoleucine in position 5th for alanine, Kan^R	Novogene

calP (Q6A)-flag	*calP* derivative carrying substitution of glutamine in position 6th for alanine, Kan^{R}	Novogene
calP (V7A)-flag	*calP* derivative carrying substitution of valine in position 7th for alanine, Kan^{R}	Novogene
calP (V8A)-flag	*calP* derivative carrying substitution valine acid in position 8th for alanine, Kan^{R}	Novogene
calP (L9A)-flag	*calP* derivative carrying substitution leucine in position 9th for alanine, Kan^{R}	Novogene
calP (I10A)-flag	*calP* derivative carrying substitution of isoleucine in position 10th for alanine, Kan^{R}	Novogene
calP (G11A)-flag	*calP* derivative carrying substitution of glycine in position 11th for alanine, Kan^{R}	Novogene
calP (L12A)-flag	*calP* derivative carrying substitution of leucine in position 12th for alanine, Kan^{R}	Novogene
calP (V13A)-flag	*calP* derivative carrying substitution of valine in position 13th for alanine, Kan^{R}	Novogene
calP (F14A)-flag	*calP* derivative carrying substitution of phenylalanine in position 14th for alanine, Kan^{R}	Novogene

calP (V15A)-flag	*calP* derivative carrying substitution of valine in position 15th for alanine, Kan^{R}	Novogene
calP (A16P)-flag	*calP* derivative carrying substitution of alanine in position 16th for proline, Kan^{R}	Novogene
calP (A17P)-flag	*calP* derivative carrying substitution of alanine in position 17th for proline, Kan^{R}	Novogene
calP (A18P)-flag	*calP* derivative carrying substitution of alanine in position 18th for proline, Kan^{R}	Novogene
calP (Y19A)-flag	*calP* derivative carrying substitution of tyrosine in position 19th for alanine, Kan^{R}	Novogene
calP (G20A)-flag	*calP* derivative carrying substitution of glycine in position 20th for alanine, Kan^{R}	Novogene
calP (V21A)-flag	*calP* derivative carrying substitution of valine in position 21st for alanine, Kan^{R}	Novogene
calP (F22A)-flag	*calP* derivative carrying substitution of phenylalanine in position 22nd for alanine, Kan^{R}	Novogene
calP (W23A)-flag	*calP* derivative carrying substitution of tryptophan acid in position 23rd for alanine, Kan^{R}	Novogene

calP (L24A)-flag	*calP* derivative carrying substitution of leucine in position 24th for alanine, Kan^{R}	Novogene
calP (S25A)-flag	*calP* derivative carrying substitution of serine in position 25th for alanine, Kan^{R}	Novogene
calP (M26A)-flag	*calP* derivative carrying substitution of methionine in position 26th for alanine, Kan^{R}	Novogene
calP (R27A)-flag	*calP* derivative carrying substitution of arginine in position 27th for alanine, Kan^{R}	Novogene
calP (E28A)-flag	*calP* derivative carrying substitution of glutamic acid in position 28th for alanine, Kan^{R}	Novogene
calP (K29A)-flag	*calP* derivative carrying substitution of lysine in position 29th for alanine, Kan^{R}	Novogene
calP (P30A)-flag	*calP* derivative carrying substitution of proline in position 30th for alanine, Kan^{R}	Novogene
calP (H31A)-flag	*calP* derivative carrying substitution of histidine in position 31st for alanine, Kan^{R}	Novogene
calP (Q32A)-flag	*calP* derivative carrying substitution of glutamine in position 32nd for alanine, Kan^{R}	Novogene

calP (K33A)-flag	*calP* derivative carrying substitution of lysine in position 33rd for alanine, Kan^R	Novogene
calP (G34A)-flag	*calP* derivative carrying substitution of glycine in position 34th for alanine, Kan^R	Novogene
calP (P35A)-flag	*calP* derivative carrying substitution of proline in position 35th for alanine, Kan^R	Novogene
calP (P36A)-flag	*calP* derivative carrying substitution of proline in position 36th for alanine, Kan^R	Novogene
calP (K45A)-flag	*calP* derivative carrying substitution of lysine in position 45th for alanine, Kan^R	Novogene

Table 8. Oligonucleotides

*The manufacturer of all oligonucleotides was Sigma-Aldrich

Oligo ID	Description	Sequence (5´to 3´)
P1-pXYFPC2-CCNA_03982F	Complementation of *ΔcalP* with *calP*	GAGTTTTGGGGAGACGAC CATATGGACCCGGTAATCC AAGTCGTCCTGATC
P2-pXYFPC2-CCNA_03982R		CTAGTGGATCCCCCGGGC TGCAGCTACCGCGGCGGT CCCTTCTGGTGC GGC
P5-pBXMCS2-CCNA_03982F	Primers for the amplification of *calP* to insert it in the overexpression plasmid pBXMCS-2	CGCTCGAGTTTTGGGGAG ACGACCAATGGACCCGGT AATCCAAGTCGTC
P6-pBXMCS2-CCNA_03982R		CGACTCACTATAGGGCGA ATTGGAGCTCTACCGCGG CGGTCCCTTCTGGT

P9-pKNT25/pUT18-CCNA3982F	BACTH CalP-self interaction test	AAACAGCTATGACCATGATTACGCCAATGGACCCGGTAATCCAAGTCGTC
P10-pKNT25-CCNA3982R		TTGAATTCGAGCTCGGTACCCGGGGCCGCGGCGGTCCCTTCTGGTGCGGC
P11-pUT18-CCNA3982R		AATTCGAGCTCGGTACCCGGGGCCGCGGCGGTCCCTTCTGGTGCGGCTTTTC
P12-CCNA3982-FS1-F	Construction of *ΔcalP*::P_{calP}-*scr calP-flag* for western blot analysis	CAATTGAAGCCGGCTGGCGCCACGGCCAAGGCGCCGACCGAAGCCGCCGCGC
P15-CCNA3982-FS2-R		CGCGTCACGGCCGAAGCTAGCGGGCGCTGACGGTGCGCATCTGATCAATGG
P16-pKT25_calPF1	BACTH: One-to-one interaction analysis of CalP against putative binding partners candidates detected during the screening of CalP with *C. crescentus* binding protein candidates in a	GCGGGCTGCAGGGTCGACTCTAGAGATGGACCCGGTAATCCAAGTCGTC
P17-pKT25_calPR2		TCACGACGTTGTAAAACGACGGCCGCTACCGCGGCGGTCCCTTCTGGTG
P18-pUT18C-calPF1		CGCCACTGCAGGTCGACTCTAGAGATGGACCCGGTAATCCAAGTCGTC
P19-pUT18C-calPR2		CACCATATTACTTAGTTATATCGATGCTACCGCGGCGGTCCCTTCTGGTG
P20-pUT18C-CCNA_02837F1		CGCCACTGCAGGTCGACTCTAGAGTTGGTCTCCGACGGGAACGATC

P21-pUT18C-CCNA_02837R2	two-hybrid assay in *E. coli*.	CCATATTACTTAGTTATATCGATGTCACGCTTCGCCTCGCGTCAGATC
P22-pUTC18-CCNA_02836F1		CGCCACTGCAGGTCGACTCTAGAGATGACGGCGGCCGGCATGTCTGTG
P23-pUTC18-CCNA_02836R2		CCATATTACTTAGTTATATCGATGTCATAGCGCGGAAGACTCCTCAAG
P24-pNTPS138-FS1-calP-F	Construction of *ΔcalP*::P_{calP}-*calP-flag* for western blot analysis	GTGCAATTGAAGCCGGCTGGCGCCACGGCCAAGGCGCCGACCGAAG
P25-calP-(FS1)-FLAGTAG-R		GACTACAAGGATGACGATGACAAGTAAGCGTCGGACCCGTTTCCCCAAAAGGTCTCGTG
P26-FLAGTAG-FS2(calP)-F		TTACTTGTCATCGTCATCCTTGTAGTCCCGCGGCGGTCCCTTCTGGTGCGGCTTTTCTC
P27-555bpupstcalPF	Verification of the genotype of mutants of *C. crescentus*	GTGGAGAAGGCAAAGGCGAAG
P28-617bpdowncalPR		CGCGAGTGTCAGCCGATTTTC
P29.pUT18C.CCNA2366F		CGCCACTGCAGGTCGACTCTAGAGATGGCCAGGCAAAGGCTCAGTTTC
P30.pUT18C.CCNA2366R		CCATATTACTTAGTTATATCGATGTCAGGCGGGGGCGCCGGCGACGCGGTC

P31.pKT25.CCNA2366F	BACTH: One-to-one interaction analysis of CalP against putative binding partners candidates detected during the screening of CalP with *C. crescentus* binding protein candidates in a two-hybrid assay in *E. coli*.	GCGGGCTGCAGGGTCGACTCTAGAGATGGCCAGGCAAAGGCTCAGTTTC
P32.pKT25.CCNA2366R		CACGACGTTGTAAAACGACGGCCGTCAGGCGGGGGCGCCGGCGAC
P33.pUT18C.CCNA2089F		CCACTGCAGGTCGACTCTAGAGTTGACGGCTCCAAGGTGCGGCGGGAG
P34.pUT18C.CCNA2089R		GCACCATATTACTTAGTTATATCGATGTCAGACCGGCACGAACTGCAGAAG
P35.pKT25.CCNA2089F		GGCTGCAGGGTCGACTCTAGAGTTGACGGCTCCAAGGTGCGGCGGGAG
P36.pKT25.CCNA2089R		CACGACGTTGTAAAACGACGGCCGTCAGACCGGCACGAACTGCAGAAG
P37.pUT18C.CCNA0182F		GCCACTGCAGGTCGACTCTAGAGATGAGCCATCGCCTTCTCCTGGTGATC
P38.pUT18C.CCNA0182R		CCATATTACTTAGTTATATCGATGCTAGCGCGACGTCAGCCGACCGGCGAC
P39.pKT25.CCNA0182F		CGGGCTGCAGGGTCGACTCTAGAGATGAGCCATCGCCTTCTCCTGGTGATC
P40.pKT25.CCNA0182R		CACGACGTTGTAAAACGACGGCCGCTAGCGCGACGTCAGCCGACCGGCGAC

P41.pUT18C.CCNA1007		CCACTGCAGGTCGACTCTAGAGATGACCGTCGCCTCGCAGACCCGTTC
P42.pUT18C.CCNA1007		CCATATTACTTAGTTATATCGATGTCACAAACTCAGGAAGACCTTCGCCAC
P43.pKT25.CCNA1007F		GGGCTGCAGGGTCGACTCTAGAGATGACCGTCGCCTCGCAGACCCGTTC
P44.pKT25.CCNA1007R		CACGACGTTGTAAAACGACGGCCGTCACAAACTCAGGAAGACCTTCGCCAC
p45-pUT18::calP**R		GAATTCGAGCTCGGTACCCGGGGTTACTACCGCGGCGGTCCCTTCTGGTG
P46.pUT18C.CCNA3673F		CGCCACTGCAGGTCGACTCTAGAGGTGATGTTCGAAAAAACTCTGATG
P47.pUT18C.CCNA3673R		CACCATATTACTTAGTTATATCGATGTCAGCGTTCTGGCGGCTTGGGATC
P48.pUT25.CCNA3673F		GCGGGCTGCAGGGTCGACTCTAGAGGTGATGTTCGAAAAAACTCTGATG
P49.pUT25.CCNA3673R		CACGACGTTGTAAAACGACGGCCGTCAGCGTTCTGGCGGCTTGGGATC
P56.calPFS1(pNTPS.YFP)R		GAACAGCTCCTCGCCCTTGCTCACCCGCGGCGGTCCCTTCTGGTG

P57.YFP(calPFS1/2)F	Construction of *ΔcalP*+pNTPS138::*calP-yfp* for visualising the subcellular localisation of CalP	CCGCACCAGAAGGGACCGCCGCGGGTGAGCAAGGGCGAGGAGCTGTTC
P58.YFP(calPFS1/2)R		CCTTTTGGGGAAACGGGTCCGACGCTTACTTGTACAGCTCGTCCATGCCGAG
P59.calPFS2(YFP.pNTPS)F		CGGCATGGACGAGCTGTACAAGTAAGCGTCGGACCCGTTTCCCCAAAAGG
P60.pKT25.CCNA2837F	Construction of *C. crescentus ΔCCNA_02837*	GCGGGCTGCAGGGTCGACTCTAGAGTTGGTCTCCGACGGGAACGATC
P61.pKT25.CCNA2837R		CACGACGTTGTAAAACGACGGCCGTCACGCTTCGCCTCGCGTCAGATC
P62.pKT25.CCNA2836F	Construction of *C. crescentus ΔCCNA_02836*	GGGCTGCAGGGTCGACTCTAGAGATGACGGCGGCCGGCATGTCTGTG
P63.pKT25.CCNA2836R		GTCACGACGTTGTAAAACGACGGCCGTCATAGCGCGGAAGACTCCTCAAG
P66.UpS.xylocus.F	Verification of the genotype of mutants of *C. crescentus* with insertions in *xylX*	CGGGCTGGAAGGCGTTCATC
P67.DwS.xylocus.R		GTCAGGTCGGTCATGGGCAAG
P68.UpS.calP.Cau.F		CGGCGCAGATGTTCTTGCAATG
P69.DwS.calP.Cau.R		GACAGCAGCGAAGAGCGCTAG
P70.p138.FS1.CCNA2836.F		GCAATTGAAGCCGGCTGGCGCCACCTGCTGGACCGACGCTTGCCGCGCATTC

P71.FS1.FS2CCNA2836.F	Construction of *C. crescentus ΔCCNA_02836*	CCGATCAGCAGCGGACGCGGAAGACCAGCAGACCTCCTTCATCACGCTTC
P72.FS1.FS2CCNA2836.F		GCGTGATGAAGGAGGTCTGCTGGTCTTCCGCGTCCGCTGCTGATC
P73.FS2.CCNA2836.p138.R		GACGCGTCACGGCCGAAGCTAGCGCGCCTGGATTTCCAGATCGCGCGCCGTC
P74.p138.FS1.CCNA3673.F	Construction of *C. crescentus ΔCCNA_03673*	GTGCAATTGAAGCCGGCTGGCGCCAACCTTAGCCTCGCTTCGCGCATTG
P75.FS1.FS2CCNA3673.F		TCGGCTGACAACACAACGCGCGACGGTTGTGACGGCTGCCGCCGGCGATG
P76.FS1.FS2CCNA3673.F		CGCCGGCGGCAGCCGTCACAACCGTCGCGCGTTGTGTTGTCAGCCGAAAG
P77.FS2.CCNA3673.p138.R		CGCGTCACGGCCGAAGCTAGCGGGCGGCCAGTTCGGCGCCCGGCGCGGTC
P78.p138.FS1.CCNA2366.F	Construction of *C. crescentus ΔCCNA_02366*	GCAATTGAAGCCGGCTGGCGCCAGGGCCGGCGGGCATGTAGCGACGGAAC
P79.FS1.FS2CCNA2366.F		CGTCAGGCTTGAAGGAAAAGGACGATCCTCCGCCACTCCGACCACCGGTTG
P80.FS1.FS2CCNA2366.F		CGGTGGTCGGAGTGGCGGAGGATCGTCCTTTTCCTTCAAGCCTGACGAG

P81.FS2.CCNA2366.p138.R		GACGCGTCACGGCCGAAGCTAGCGAGGGCCGTCACCGTCACGCGCACGAAC
P82.p138.FS1.CCNA2837.F	Construction of *C. crescentus ΔCCNA_02837*	GTGCAATTGAAGCCGGCTGGCGCCAGACGGAAACGTTTGCCCGCATCGTTC
P83.FS1.FS2CCNA2837.F		CGCCGTCATCAGCAGACCTCCTTCAAACTCAGCTCGCCGCGCACGTCGTC
P84.FS1.FS2CCNA2837.F		CGACGACGTGCGCGGCGAGCTGAGTTTGAAGGAGGTCTGCTGATGAC
P85.FS2.CCNA2837.p138.R		GACGCGTCACGGCCGAAGCTAGCGATGAGCCCGATCAGCAGCGGACGCG
P86.p138.FS1.CCNA2089.F	Construction of *C. crescentus ΔCCNA_02089*	GTGCAATTGAAGCCGGCTGGCGCCAGGCCTGCGGGTTGGCGACGTCCTC
P87.FS1.FS2CCNA2089.F		GGCGTCAGCTTCTCGATCTGAACCGTGCGTATCGCCACCTGGAACGTC
P88.FS1.FS2CCNA2089.F		GACGTTCCAGGTGGCGATACGCACGGTTCAGATCGAGAAGCTGAC
P89.FS2.CCNA2089.p138.R		GACGCGTCACGGCCGAAGCTAGCGGAACCGACGCCCCTTCGATTTG
P90.p138.FS1.CCNA0182.F		GTGCAATTGAAGCCGGCTGGCGCCACAGCGATCTCATCATCAGGAGAAAG

P91.FS1.FS2CCNA0182.F	Construction of *C. crescentus ΔCCNA_00182*	CGGATCCACTTCGTCGGAAAATGCTGGGGCGGCGCGCGCGAAGGTGATC
P92.FS1.FS2CCNA0182.F		CGAGATCACCTTCGCGCGCGCCGCCCCAGCATTTTCCGACGAAGTGGATC
P93.FS2.CCNA0182.p138.R		GACGCGTCACGGCCGAAGCTAGCGTCCCGACAGGCTGACCCTGCCCTTC
P94.p138.FS1.CCNA1007.F	Construction of *C. crescentus ΔCCNA_01007*	GTGCAATTGAAGCCGGCTGGCGCCAGCCGATCGTCATCGGCCGCGATC
P95.FS1.FS2CCNA1007.F		GGAGAAGTACGAAACGCTTACGCGAAACGCTCCTTAACCATGACCCCATG
P96.FS1.FS2CCNA1007.F		GGGGTCATGGTTAAGGAGCGTTTCGCGTAAGCGTTTCGTACTTCTC
P97.FS2.CCNA1007.p138.R		GACGCGTCACGGCCGAAGCTAGCGCTACGAAGCCAACCTCAATGTCATC
P98.SeqFS1CCNA2836F	Verification of the genotype of *C. crescentus ΔCCNA_02836*	GAGTTTTGGTCTCCGACGGGAAC
P99.SeqFS2CCNA2836R		GCGGCTGCTTTGGCGCATAG
P100.SeqFS1CCNA3673F	Verification of the genotype of *C. crescentus ΔCCNA_03673*	CAGTCCCCGCACAGCTTCAAG
P101.SeqFS2CCNA3673R		CGTCGTGGGTCGAGATGATCTTC
P102.SeqFS1CCNA2366F		CCGGCCAACAGTTCCAGGAAG

P103.SeqFS2CCNA2366R	Verification of the genotype of *C. crescentus ΔCCNA_02366*	CTGGCCTTCAGGCTGAGGAAC
P104.SeqFS1CCNA2837F	Verification of the genotype of *C. crescentus ΔCCNA_02837*	CCTCATCCTGAGCTTGTCGAAG
P105.SeqFS2CCNA2837R		TGGCGGGCGGAGTCGATAG
P106.SeqFS1CCNA2089F	Verification of the genotype of *C. crescentus ΔCCNA_02089*	CGCCGTCGGCCTGCATATAG
P107.SeqFS2CCNA2089R		GTCGCCTTCATGAGCGACGAAG
P108.SeqFS1CCNA0182F	Verification of the genotype of *C. crescentus ΔCCNA_00182*	CCGGTCGACCATCGTCTACAAC
P109.SeqFS2CCNA0182R		CAGGCGCTACCCTCTCCTTG
P110.SeqFS1CCNA1007F	Verification of the genotype of *C. crescentus ΔCCNA_01007*	GCCGGCCAGAAGATCAGGTTC
P111.SeqFS2CCNA1007R		CCGAGTACGATCCCGGCAAC
P112.FS1.scrcalPR	Construction of *ΔcalP*::P_{calP}-*scr calP-flag* for western blot	GAACGACCTGAATCACAGGATCCATTCAATCCTCCACGCGCGACAAGATG
P113.scrcalP.FS1F		CATCTTGTCGCGCGTGGAGGATTGAATGGATCCTGTGATTCAGGTCGTTC
P114.scrcalP.FLAGTR	Construction of *ΔcalP*::P_{xyl}-*scr calP-flag* for western blot	CTTGTCATCGTCATCCTTGTAGTCGCGGGGTGGGCCCTTTTGATG
P115.scr calP.pXYFPC2F		GCTCGAGTTTTGGGGAGACGACCATATGGATCCTGTGATTCAGGTCGTTC

P116.pXYFPC2.FLAGTF		CTACAAGGATGACGATGACAAGTAACTGCAGCCCGGGGGATCCACTAG
P117.fdsmcs.pXYFPC2R		CTAGTGGATCCCCCGGGCTGCAGTTACCGCCTTTGAGTGAGCTGATAC
P122.calP-FT.pUT18CF	Forward primer for amplification of *calP* from genomic DNA (NA1000) and *calP-flag* from pNTPS138::*calP-flag*	CAGCTATGACCATGATTACGCCAATGGACCCGGTAATCCAAGTCGTC
P123.calP-FT.pUT18CR	Reverse primer for amplification of *calP-flag* from pNTPS138::*calP-flag* for the construction of pUT18C (-T18)::*calP*	GATGAATTCGAGCTCGGTACCCGGGTTACTTGTCATCGTCATCCTTGTAG
P128.CCNA3981FS1.p138F	Amplification of *CCNA_03981* flanking sequences for deletion of *CCNA_03981*	GCAATTGAAGCCGGCTGGCGCCAAGTTCCGCCTGTTCCACGAGGAG
P129.CCNA3981FS1.FS2R		CCCTGCAAGACAACGAAGCCGATCATGGCGCGAACATTGCAAGAAC
P130CCNA3981FS2.FS1R		CTTGCAATGTTCGCGCCATGATCGGCTTCGTTGTCTTGCAGGGGCTTC
P131.CCNA3981FS2.p138R		CGCGTCACGGCCGAAGCTAGCGAAACTTGTAGGCGCGCTGGTTC
P132.calP.pUT18CR	Reverse primer for amplification of *calP* from genomic DNA (NA1000)	GATGAATTCGAGCTCGGTACCCGGGCTACCGCGGCGGTCCCTTCTGGTG

	for the construction of pUT18C (-T18)::*calP*	
P133.US3981FS1F	Verification of the genotype of *ΔCCNA_03981*	CGGCAGCCTCTTGATGACCTTC
P134.IntraCCNA3981F		GAACTCCGATGGATCAGCTTCTTG
P135.IntraCCNA3981R		CAGCAGAGCCGAAACCAGGAAAG
138.calP-flag.pBXMCS2R	Amplification of *calP-flag* with flanking sequences of the vector pBXMCS-2 for Gibson cloning	CACTATAGGGCGAATTGGAGCTTTACTTGTCATCGTCATCCTTGTAGTC
139.calP-yfp.pBXMCS2R		GACTCACTATAGGGCGAATTGGAGCTTTACTTGTACAGCTCGTCCATG
P145.*recA*.pNTPS138F	Deletion of *recA* in a Δ*calP*-P_{calP}-*calP-flag* background	GCAATTGAAGCCGGCTGGCGCCAGCGGATGTGCTTGTCGGCAGGTTC
P146.pNTPS138F.*recA*.R		GACGCGTCACGGCCGAAGCTAGCGAGCGAGGGGTGGTGAGTTGCCTTC
4029	Forward oligo to delete *recA*	GCAATTGAAGCCGGCTGGCGCCACAGCACGACAGGGCCGCGCCGCACG
4032	Reverse oligo to delete *recA*	CGGCCGAAGCTAGCGAATTCGTGAGAGGGGAGCAGAATCTGTGAGCGTC
4080F	Oligos to construct *recA*::*tetR* in pNPTS138	GGACCGAGAAAGGGTGACGATTGAACTTGTCATTGTTGATCCGCCTTC
4081R		GCAGGGCAACGAGCCGATCGCTGAGAGGACTAGATCCAGGCGCTCAAG

2303	Forward oligo to amplify *tetR* cassette	TCAATCGTCACCCTTTCTCGG
2304	Reverse oligo to amplify *tetR* cassette	TCAGCGATCGGCTCGTTGCCC
P973F	Sequencing of the region downstream of P_{xyl}	ATGCCGTTTGTGATGGCTTCCATGTCG
P975R	Test for integration into the *xylX* locus	TCTTCCGGCAGGAATTCACTCACGCC
P977	Sequencing of the region downstream of P_{xyl}	CCCACATGTTAGCGCTACCAAGTGC
1411	Reverse sequencing from pUT18C	CCTCTGACACATGCAGCTCCCGG
1412	pUT18C-read from T18	CGCCGGATGTACTGGAAACG
1413	Reverse sequencing from pKT25	TTCGGTGACCAGCGGCGATT
3058	Reverse sequencing from pUT18	CTCGGTGCCCACTGCGGAAC
1372 (M13F (-47))	Forward sequencing from pNTPS138	CGCCAGGGTTTTCCCAGTCACGAC
1708 (M13R)	Reverse sequencing from pNTPS138	CAGGAAACAGCTATGAC
q141.calPF1	Amplification of *calP* in RT-qPCR	GTAATCCAAGTCGTCCTGATCG
q142.calPR1		CCTTCTGGTGCGGCTTT
2740F	Amplification of the housekeeping *rpoD* as a control gene in RT-qPCR	TCAGGCCAAGAAGGAAATGG
2741R		GCCTTCATCAGGCCGATATT

5.2.4 Genetic manipulations

5.2.4.1 Plasmid construction

The procedure for the construction of the plasmids used in this work is explained below. A brief description of these plasmids is shown in Table 6. The chemically synthesised fragments are shown in Table 7. The sequences and information about the oligonucleotides used to amplify DNA fragments cloned in these plasmids are shown in Table 8 (the manufacturer of all oligonucleotides). The concentration of antibiotics used in the plasmid construction is described in section 5.2.2.1.2.

pXYFPC-2::*calP*

The *calP* sequence (114 bp) was amplified by PCR using Phusion polymerase (Thermo-Fisher Scientific/F630S) with the oligos P1-pXYFPC2-CCNA_03982F and P2-pXYFPC2-CCNA_03982R. The PCR product was run in a 2% agarose gel and the DNA fragment was extracted from the agarose gel with the isolation kit Qiagen/cat. no. 28706. The *calP* fragment and the plasmid pXYFPC2 were each double-digested with NdeI (NEB/R0111S) and NheI (NEB/R3131S). The cleaving of the DNA with restriction enzymes excised a region of the multi-cloning site (MCS) of the plasmid. The digested *calP* fragment and the plasmid pXYFPC2 were run in a 2% agarose gel to separate them from the cleaved bases. The DNA bands corresponding with the expected bases of *calP,* and the plasmid were extracted from the agarose gel with the kit Qiagen/cat. no. 28706. 2.5µL of the PCR-amplified fragment and 2.5µL of the plasmid pXYFPC2 were assembled by mixing them with 5µL of the Gibson assembly master mix. Gibson assembly was possible due to a 25 bp sequence homology shared between the PCR fragment and the NdeI-NheI digested pXYFPC-2 vector backbone. The assembly aims to insert the DNA fragment of *calP* into the gap left by the excised MCS. The mixture was incubated for 1 hr at 50 °C and then used to transform chemically competent *E. coli* DH5α by heat shock. The culture was incubated for 1 hr with a rotatory shake at 37°C. Cells were plated onto LB agar plates treated with kanamycin (see antibiotic concentrations in section 5.2.2.1.2) and incubated at 37°C ON. Colonies from the successful transformants had the plasmids extracted (Qiagen/cat. no. 27104) and

sent for sequencing with the oligonucleotides P973F and P975R to Eurofins Genomics. P973F binds a DNA sequence on the left flanking side of the MCS of the plasmid pXYFPC2 and starts the amplification direction to the MCS. P975R binds a DNA sequence on the right flanking side of the MCS of the plasmid direction to the MCS.

pXYFPC-2::*calP-flag*

The *calP-flag* fragment was chemically synthesised by Integrated DNA Technologies (IDT) with 25 bp homology with the vector pXYFPC2 for Gibson assembly cloning. The plasmid pXYFPC-2 was digested with NdeI (NEB/R0111S) and NheI (NEB/R3131S) and assembled with the DNA fragment *calP-flag* by Gibson assembly.

pXYFPC-2::*scr calP*

The fragment *scrambled calP* was chemically synthesised by IDT with 25 bp homology with the vector pXYFPC2 for Gibson assembly cloning. The plasmid pXYFPC-2 was digested with NdeI (NEB/R0111S) and NheI (NEB/R3131S) and assembled with the DNA fragment *scrambled calP* by Gibson assembly.

pXYFPC-2::*scr calP-flag*

The sequence of *calP* was PCR amplified using a template genomic DNA of *C. crescentus* with the oligos P114.scr calP.FLAGTR and P115.scr calP.pXYFPC2F (Sigma-Aldrich). The oligo P115 had 25 bp homology with the plasmid pXYFPC-2, and the oligo P114 had 25 bp homology with the *flag tag* sequence. A sequence of 200 bp downstream of the HindIII (NEB/ R3104S) site of the plasmid pXYFPC2F was PCR amplified using as a template the plasmid pXYFPC2F with the oligos P116.pXYFPC2.FLAGTF and P117.fdsmcs.pXYFPC2R (Sigma-Aldrich). The oligo P116 had 25 bp homology with the *flag* tag sequence, and the oligo P117 had 25 bp homology with the plasmid pXYFPC-2 for Gibson assembly cloning. The plasmid pXYFPC-2 was digested with NdeI (NEB/R0111S) and NheI (NEB/R3131S) and cloned alongside the PCR fragments by Gibson assembly. The

rest of the steps were performed as described above for the construct of pXYFPC-2-*calP.*

pXYFPC-2::*calP (XNA)/(ANP)-flag*

X=original CalP residue substituted

N=position of the CalP residue substituted

A=alanine

P=proline

36 *calP* derivatives carrying an alanine substitution (*XNA*) in each amino acid, or a proline substitution if it was originally an alanine *(ANP)*, were chemically synthesised by Invitrogen. Each derivative was cloned into the vector pXYFPC-2 by Gibson assembly through microhomology between the flanking sequences of each fragment and the edges in the backbone of the plasmid. pXYFPC-2 was previously digested with NdeI (NEB/R0111S) and NheI (NEB/R3131S), and the gel was digested to separate the backbone and the MCS.

pBXMCS-2::*calP*

The calP sequence was PCR-amplified using *C. crescentus* genomic DNA as a template with the P5-pBXMCS-2-CCNA_03982F and P6-pBXMCS-2-CCNA_03982R oligos (Sigma-Aldrich). Both oligos had 25 bp homology with the plasmid pBXMCS-2. The plasmid pBXMCS-2 was digested with NdeI (NEB/R0111S) and SacI (NEB/R3156S) and cloned alongside the PCR fragments by Gibson assembly. The rest of the steps were performed as described above for the construct of pXYFPC-2-*calP.*

pBXMCS-2::*calP-flag*

The sequence of *calP-flag* was PCR amplified using a template pXYFPC-2::*calP-flag* with the oligos P5-pBXMCS-2-CCNA_03982F and 138.calP-flag.pXBMCS2R (Sigma-Aldrich). Both oligos had 25 bp homology with the plasmid pBXMCS-2. The plasmid pBXMCS-2 was digested with NdeI (NEB/R0111S) and SacI (NEB/R3156S) and cloned alongside the PCR fragments

by Gibson assembly. The rest of the steps were performed as described above for the construct of pXYFPC-2-*calP.*

pUT18C (-T18)::*calP*

The plasmid pUT18C was digested with BamHI (NEB/R3136S) and HindIII (NEB/ R3104S) to excise the *T18* fragment. *calP* was PCR amplified using as a template genomic DNA of *C. crescentus* WT with the oligos P122.calP-FT.pUT18CF and P132.calP.pUT18CR (Sigma-Aldrich). Both oligos had 25 bp homology with the vector pUT18C (-T18) for Gibson assembly cloning. The rest of the steps were performed as described above for the construct of pXYFPC-2-*calP,* except that plates were supplemented with carbenicillin instead of kanamycin. The reverse oligo 1411 was used to verify the insertion of *calP* in pUT18C (-T18) by Sanger sequencing with Genewiz.

pUT18C (-T18)::*calP-flag*

The plasmid pUT18C was digested with BamHI (NEB/R3136S) and HindIII (NEB/ R3104S) to excise the *T18* fragment. The sequence of *calP-flag* was PCR amplified using as a template pXYFPC-2::*calP-flag* with the oligos P122.calP-FT.pUT18CF and P123.calP-FT.pUT18CR. Both oligos had 25 bp homology with the vector pUT18C (-T18) for Gibson assembly cloning. The rest of the steps were performed as described above for the construct of pXYFPC-2-*calP,* except that plates were supplemented with carbenicillin instead of kanamycin. The reverse oligo 1411 was used to verify the insertion of *calP-flag* in pUT18C (-T18) by Sanger sequencing with Genewiz.

pKNT25::*calP*

calP was PCR amplified using a template genomic DNA of *C. crescentus* with the oligos P9-pKNT25/pUT18-CCNA3982F and P10-pKNT25-CCNA3982R (Sigma-Aldrich). Both oligos had 25 bp homology with the vector pKNT25 for Gibson assembly cloning. The plasmid pKNT25 was digested with BamHI (NEB/R3136S) and HindIII (NEB/ R3104S). The rest of the steps were performed as described above for the construct of pXYFPC-2-*calP.* The reverse oligo 1490 was used to

verify the insertion of *calP* derivatives in pKNT25 by Sanger sequencing with Eurofins Genomics.

pKNT25::*calP (L9A/L12A/A16P/A17P/A18P/F22A)-flag*

calP derivatives were PCR amplified using as a template synthesised fragments of DNA (Invitrogen) (Table 7) with the oligos P9-pKNT25/pUT18-CCNA3982F and P10-pKNT25-CCNA3982R (Sigma-Aldrich). Both oligos had 25 bp homology with the vector pKNT25 for Gibson assembly cloning. The plasmid pKNT25 was digested with BamHI (NEB/R3136S) and HindIII (NEB/ R3104S). The rest of the steps were performed as described above for the construct of pXYFPC-2-*calP.* The reverse oligo 1490 was used to verify the insertion of *calP* derivatives in pKNT25 by Sanger sequencing with Genewiz.

pKT25::*calP*

calP was PCR amplified using as a template genomic DNA of *C. crescentus* with the oligos P16-pKT25_calPF1 and P17-pKT25_calPR2 (Sigma-Aldrich). Both oligos had 25 bp homology with the vector pKT25 for Gibson assembly cloning. The plasmid pKT25 was digested with BamHI (NEB/R3136S) and HindIII (NEB/ R3104S). The rest of the steps were performed as described above for the construct of pXYFPC-2-*calP.* The reverse oligo 1413 was used to verify the insertion of *calP* derivatives in pKT25 by Sanger sequencing with Eurofins Genomics.

pUT18::*calP*

calP was PCR amplified using as a template genomic DNA of *C. crescentus* with the oligos P9-pKNT25/pUT18-CCNA3982F and P11-pUT18-CCNA3982R (Sigma-Aldrich). Both oligos had 25 bp homology with the vector pUT18 for Gibson assembly cloning. The plasmid pUT18 was digested with BamHI (NEB/R3136S) and HindIII (NEB/ R3104S). The rest of the steps were performed as described above for the construct of pXYFPC-2-*calP,* except that plates were supplemented with carbenicillin instead of kanamycin. The reverse oligo 3058 was used to verify the insertion of *calP* in pUT18 by Sanger sequencing with Eurofins Genomics.

pUT18::*calP (L9A/L12A/A16P/A17P/A18P/F22A)-flag*

calP derivatives were PCR amplified using as a template the synthesised fragments of DNA (Invitrogen) (Table 7) with the oligos P9-pKNT25/pUT18-CCNA3982F and P11-pUT18-CCNA3982R (Sigma-Aldrich). Both oligos had 25 bp homology with the vector pUT18 for Gibson assembly cloning. The plasmid pUT18 was digested with BamHI (NEB/R3136S) and HindIII (NEB/ R3104S). The rest of the steps were performed as described above for the construct of pXYFPC-2-*calP,* except that plates were supplemented with carbenicillin instead of kanamycin. The reverse oligo 3058 was used to verify the insertion of *calP* derivatives in pUT18 by Sanger sequencing with Genewiz.

pUT18C::*calP*

calP was PCR amplified using as a template genomic DNA of *C. crescentus* with the oligos P18-pUTC18-calPF1 and P19-pUTC18-calPR2 (Sigma-Aldrich). Both oligos had 25 bp homology with the vector pUT18C for Gibson assembly cloning. The plasmid pUT18C was digested with BamHI (NEB/R3136S) and EcoRI (NEB/R3101S). The rest of the steps were performed as described above for the construct of pXYFPC-2-*calP,* except that plates were supplemented with carbenicillin instead of kanamycin. The reverse oligo 1411 was used to verify the insertion of *calP* in pUT18C by Sanger sequencing with Eurofins Genomics.

pUT18C::*CCNA_02837*

CCNA_02837 was PCR amplified using a template genomic DNA of *C. crescentus* with the oligos P20-pUT18C-CCNA_02837F1 and P21-pUT18C-CCNA_02837R2 (Sigma-Aldrich). Both oligos had 25 bp homology with the vector pUT18C for Gibson assembly cloning. The plasmid pUT18C was digested with BamHI (NEB/R3136S) and EcoRI (NEB/R3101S). The rest of the steps were performed as described above for the construct of pXYFPC-2-*calP,* except that plates were supplemented with carbenicillin instead of kanamycin. The reverse oligo 1411 was used to verify the insertion of *CCNA_02837* in pUT18C by Sanger sequencing with Eurofins Genomics.

pKT25::*CCNA_02837*

CCNA_02837 was PCR amplified using a template genomic DNA of *C. crescentus* with the oligos P60.pKT25.CCNA2837F and P61.pKT25.CCNA2837R (Sigma-Aldrich). Both oligos had 25 bp homology with the vector pKT25 for Gibson assembly cloning. The plasmid pKT25 was digested with BamHI (NEB/R3136S) and EcoRI (NEB/R3101S). The rest of the steps were performed as described above for the construct of pXYFPC-2-*calP.* The reverse oligo 1413 was used to verify the insertion of *CCNA_02837* in pKT25 by Sanger sequencing with Eurofins Genomics.

pUT18C::*CCNA_02836*

CCNA_02836 was PCR amplified using a template genomic DNA of *C. crescentus* with the oligos P22-pUT18C-CCNA_02836F1 and P23-pUT18C-CCNA_02836R2 (Sigma-Aldrich). Both oligos had 25 bp homology with the vector pUT18C for Gibson assembly cloning. The plasmid pUT18C was digested with BamHI (NEB/R3136S) and EcoRI (NEB/R3101S). The rest of the steps were performed as described above for the construct of pXYFPC-2-*calP,* except that plates were supplemented with carbenicillin instead of kanamycin. The reverse oligo 1411 was used to verify the insertion of *CCNA_02837* in pUT18C by Sanger sequencing with Eurofins Genomics.

pKT25::*CCNA_02836*

CCNA_02836 was PCR amplified using as a template genomic DNA of *C. crescentus* with the oligos P62.pKT25.CCNA2836F and P63.pKT25.CCNA2836R (Sigma-Aldrich). Both oligos had 25 bp homology with the vector pKT25 for Gibson assembly cloning. The plasmid pKT25 was digested with BamHI (NEB/R3136S) and EcoRI (NEB/R3101S). The rest of the steps were performed as described above for the construct of pXYFPC-2-*calP.* The reverse oligo 1413 was used to verify the insertion of *CCNA_02836* in pKT25 by Sanger sequencing with Eurofins Genomics

pUT18C::*CCNA_02837-CCNA_02836*

CCNA_028367 and *CCNA_02836* were PCR amplified using as a template genomic DNA of *C. crescentus* with the oligos P20-pUT18C-CCNA_02837F1 and P23-pUT18C-CCNA_02836R2 (Sigma-Aldrich). Both oligos had 25 bp homology with the vector PUT18C for Gibson assembly cloning. The plasmid pUT18C was digested with BamHI (NEB/R3136S) and EcoRI (NEB/R3101S). The rest of the steps were performed as described above for the construct of pXYFPC-2-*calP,* except that plates were supplemented with carbenicillin instead of kanamycin. The reverse oligo 1411 was used to verify the insertion of *CCNA_02836* in pUT18C by Sanger sequencing with Eurofins Genomics.

pKT25::*CCNA_02837-CCNA2836*

CCNA_028367 and *CCNA_02836* were PCR amplified using as a template genomic DNA of *C. crescentus* with the oligos P60.pKT25.CCNA2837F and P63.pKT25.CCNA2836R (Sigma-Aldrich). Both oligos had 25 bp homology with the vector pKT25 for Gibson assembly cloning. The plasmid pKT25 was digested with BamHI (NEB/R3136S) and EcoRI (NEB/R3101S). The rest of the steps were performed as described above for the construct of pXYFPC-2-*calP.* The reverse oligo 1413 was used to verify the insertion of *CCNA_02836-CCNA_02836* in pKT25 by Sanger sequencing with Eurofins Genomics.

pUT18C::*CCNA_02366*

CCNA_02366 was PCR amplified using as a template genomic DNA of *C. crescentus* with the oligos P29.pUT18C.CCNA2366F and P30.pUT18C.CCNA2366R (Sigma-Aldrich). Both oligos had 25 bp homology with the vector PUT18C for Gibson assembly cloning. The plasmid pUT18C was digested with BamHI (NEB/R3136S) and EcoRI (NEB/R3101S). The rest of the steps were performed as described above for the construct of pXYFPC-2-*calP,* except that plates were supplemented with carbenicillin instead of kanamycin. The reverse oligo 1411 was used to verify the insertion of *CCNA_02366* in pUT18C by Sanger sequencing with Eurofins Genomics.

pKT25::*CCNA_02366*

CCNA_02366 was PCR amplified using as a template genomic DNA of *C. crescentus* with the oligos P31.pKT25.CCNA2366F and P32.pKT25.CCNA2366R (Sigma-Aldrich). Both oligos had 25 bp homology with the vector pKT25 for Gibson assembly cloning. The plasmid pKT25 was digested with BamHI (NEB/R3136S) and EcoRI (NEB/R3101S). The rest of the steps were performed as described above for the construct of pXYFPC-2-*calP.* The reverse oligo 1413 was used to verify the insertion of *CCNA_02366* in pKT25 by Sanger sequencing with Eurofins Genomics.

pUT18C::*CCNA_02089*

CCNA_02089 was PCR amplified using as a template genomic DNA of *C. crescentus* with the oligos P33.pUT18C.CCNA2089F and P34.pUT18C.CCNA2089R (Sigma-Aldrich). Both oligos had 25 bp homology with the vector PUT18C for Gibson assembly cloning. The plasmid pUT18C was digested with BamHI (NEB/R3136S) and EcoRI (NEB/R3101S). The rest of the steps were performed as described above for the construct of pXYFPC-2-*calP,* except that plates were supplemented with carbenicillin instead of kanamycin. The reverse oligo 1411 was used to verify the insertion of *CCNA_02089* in pUT18C by Sanger sequencing with Eurofins Genomics.

pKT25::*CCNA_02089*

CCNA_02089 was PCR amplified using as a template genomic DNA of *C. crescentus* with the oligos P35.pKT25.CCNA2089F and P36.pKT25.CCNA2089R (Sigma-Aldrich). Both oligos had 25 bp homology with the vector pKT25 for Gibson assembly cloning. The plasmid pKT25 was digested with BamHI (NEB/R3136S) and EcoRI (NEB/R3101S). The rest of the steps were performed as described above for the construct of pXYFPC-2-*calP.* The reverse oligo 1413 was used to verify the insertion of *CCNA_02089* in pKT25 by Sanger sequencing with Eurofins Genomics.

pUT18C::*CCNA_00182*

CCNA_00182 was PCR amplified using as a template genomic DNA of *C. crescentus* with the oligos P37.pUT18C.CCNA0182F and P38.pUT18C.CCNA0182R (Sigma-Aldrich). Both oligos had 25 bp homology with the vector PUT18C for Gibson assembly cloning. The plasmid pUT18C was digested with BamHI (NEB/R3136S) and EcoRI (NEB/R3101S). The rest of the steps were performed as described above for the construct of pXYFPC-2-*calP,* except that plates were supplemented with carbenicillin instead of kanamycin. The reverse oligo 1411 was used to verify the insertion of *CCNA_00182* in pUT18C by Sanger sequencing with Eurofins Genomics.

pKT25::*CCNA_00182*

CCNA_00182 was PCR amplified using as a template genomic DNA of *C. crescentus* with the oligos P39.pKT25.CCNA0182F and P40.pKT25.CCNA0182R (Sigma-Aldrich). Both oligos had 25 bp homology with the vector pKT25 for Gibson assembly cloning. The plasmid pKT25 was digested with BamHI (NEB/R3136S) and EcoRI (NEB/R3101S). The rest of the steps were performed as described above for the construct of pXYFPC-2-*calP.* The reverse oligo 1413 was used to verify the insertion of *CCNA_00182* in pKT25 by Sanger sequencing with Eurofins Genomics.

pUT18C::*CCNA_01007*

CCNA_01007 was PCR amplified using as a template genomic DNA of *C. crescentus* with the oligos P41.pUT18C.CCNA1007 and P42.pUT18C.CCNA1007 (Sigma-Aldrich). Both oligos had 25 bp homology with the vector PUT18C for Gibson assembly cloning. The plasmid pUT18C was digested with BamHI (NEB/R3136S) and EcoRI (NEB/R3101S). The rest of the steps were performed as described above for the construct of pXYFPC-2-*calP,* except that plates were supplemented with carbenicillin instead of kanamycin. The reverse oligo 1411 was

used to verify the insertion of *CCNA_01007* in pUT18C by Sanger sequencing with Eurofins Genomics.

pKT25::*CCNA_01007*

CCNA_01007 was PCR amplified using as a template genomic DNA of *C. crescentus* with the oligos P43.pKT25.CCNA1007F and P44.pKT25.CCNA1007R (Sigma-Aldrich). Both oligos had 25 bp homology with the vector pKT25 for Gibson assembly cloning. The plasmid pKT25 was digested with BamHI (NEB/R3136S) and EcoRI (NEB/R3101S). The rest of the steps were performed as described above for the construct of pXYFPC-2-*calP.* The reverse oligo 1413 was used to verify the insertion of *CCNA_01007* in pKT25 by Sanger sequencing with Eurofins Genomics.

pUT18C::*CCNA_03673*

CCNA_03673 was PCR amplified using as a template genomic DNA of *C. crescentus* with the oligos P46.pUT18C.CCNA3673F and P47.pUT18C.CCNA3673R (Sigma-Aldrich). Both oligos had 25 bp homology with the vector PUT18C for Gibson assembly cloning. The plasmid pUT18C was digested with BamHI (NEB/R3136S) and EcoRI (NEB/R3101S). The rest of the steps were performed as described above for the construct of pXYFPC-2-*calP,* except that plates were supplemented with carbenicillin instead of kanamycin. The reverse oligo 1411 was used to verify the insertion of *CCNA_03673* in pUT18C by Sanger sequencing with Eurofins Genomics.

pKT25::*CCNA_03673*

CCNA_03673 was PCR amplified using as a template genomic DNA of *C. crescentus* with the oligos P48.pKT25.CCNA3673F and P49.pKT25.CCNA3673R (Sigma-Aldrich). Both oligos had 25 bp homology with the vector pKT25 for Gibson assembly cloning. The plasmid pKT25 was digested with BamHI (NEB/R3136S) and EcoRI (NEB/R3101S). The rest of the steps were performed as described above for the construct of pXYFPC-2-*calP.* The reverse oligo 1413 was

used to verify the insertion of *CCNA_03673* in pKT25 by Sanger sequencing with Eurofins Genomics.

pNTPS138::(*FS1-FS2*) *calP-flag*

500 bp upstream of *calP* plus *calP* were PCR amplified using as a template genomic DNA of *C. crescentus* with the oligos P12-CCNA3982-FS1-F and P26-FLAGTAG-FS2 (calP)-F. The oligo P12 had 25 bp homology with the plasmid pNTPS138, and the oligo P26 had 25 bp homology with a *flag tag*. The sequence 500 bp downstream of *calP* was PCR amplified using as a template genomic DNA of *C. crescentus* with the oligos P25-calP-(FS1)-FLAGTAG-R and P15-CCNA3982-FS2-R (Sigma-Aldrich). The oligo P25 had 25 bp homology with *flag tag,* and the oligo P26 had 25 bp homology with the plasmid pNTPS138. The plasmid pNTPS138 was digested with EcoRI (NEB/R3101S) and HindIII (NEB/ R3104S). The rest of the steps were performed as described above for the construct of pXYFPC-2-*calP.* The oligos 1372 and 1708 were used to verify the insertion of *(FS1-FS2) calP-flag* in pNTPS138 by Sanger sequencing with Eurofins Genomics.

pNTPS138::*scrambled calP-flag*

500 bp upstream of *calP* was PCR amplified using as a template genomic DNA of *C. crescentus* with the oligos P12-CCNA3982-FS1-F and P112.FS1.scr calPR. The oligo P12 had 25 bp homology with the plasmid pNTPS138, and the oligo P112 had 25 bp homology with the *scrambled calP* sequence. The sequence *scrambled calP* was PCR amplified using as a template the plasmid pXYFPC-2::*scrambled calP* with the oligos P113.scr calP.FS1F and P114.scr calP.FLAGTR. The oligo P113 had 25 bp homology with the flanking sequence upstream *calP,* and the oligo P114 had 25 bp homology with the *flag* tag sequence. The sequence 500 bp downstream of *calP* was PCR amplified using as a template genomic DNA of *C. crescentus* with the oligos P25-calP-(FS1)-FLAGTAG-R and P15-CCNA3982-FS2-R (Sigma-Aldrich). The oligo P25 had 25 bp homology with the *flag* tag sequence, and the oligo P15 had 25 bp homology with the plasmid pNTPS138. The plasmid pNTPS138 was digested with EcoRI (NEB/R3101S) and HindIII (NEB/ R3104S). The rest of the steps were performed as described above for the construct of

pXYFPC-2-*calP.* The oligos 1372 and 1708 were used to verify the insertion of *scrambled calP-flag* in pNTPS138 by Sanger sequencing with Eurofins Genomics.

pNTPS138::*calP-yfp*

500 bp upstream of *calP* plus *calP* were PCR amplified using as a template genomic DNA of *C. crescentus* with the oligos P12-CCNA3982-FS1-F and P56.calPFS1(pNTPS.YFP)R. The oligo P12 had 25 bp homology with the plasmid pNTPS138, and the oligo P56 had 25 bp homology with *yfp*. The sequence of *yfp* was PCR amplified using as a template the plasmid pXYFPC-2 with the oligos P57.YFP(calPFS1/2)F and P58.YFP(calPFS1/2)R. The oligo P57 had 25 bp homology with *calP,* and the oligo P54 had 25 bp homology with the flanking sequence downstream *calP*. The sequence 500 bp downstream of *calP* was PCR amplified using as a template genomic DNA of *C. crescentus* with the oligos P59.calPFS2(YFP.pNTPS)F and P15-CCNA3982-FS2-R (Sigma-Aldrich). The oligo P55 had 25 bp homology with *yfp,* and the oligo P15 had 25 bp homology with the plasmid pNTPS138. The plasmid pNTPS138 was digested with EcoRI (NEB/R3101S) and HindIII (NEB/ R3104S). The rest of the steps were performed as described above for the construct of pXYFPC-2-*calP.* The oligos 1372 and 1708 were used to verify the insertion of *calP-yfp* in pNTPS138 by Sanger sequencing with Eurofins Genomics.

pNTPS138::*(FS1-FS2) CCNA_02836*

500 bp upstream of *CCNA_02836* was PCR amplified using as a template genomic DNA of *C. crescentus* with the oligos P70.p138.FS1.CCNA2836.F and P71.FS1.FS2CCNA2836.R. The oligo P70 had 25 bp homology with the plasmid pNTPS138, and the oligo P71 had 25 bp homology with *CCNA_02836.* The sequence 500 bp downstream of *CCNA_02836* was PCR amplified using as a template genomic DNA of *C. crescentus* with the oligos P72.FS1.FS2CCNA2836.F and P73.FS2.CCNA2836.p138.R (Sigma-Aldrich). The oligo P72 had 25 bp homology with the *CCNA_02836,* and the oligo P73 had 25 bp homology with plasmid pNTPS138. The plasmid pNTPS138 was digested with EcoRI (NEB/R3101S) and HindIII (NEB/ R3104S). The rest of the steps were performed

as described above for the construct of pXYFPC-2-*calP.* The oligos P70.p138.FS1.CCNA2836.F and P73.FS2.CCNA2836.p138.R were used to verify the insertion of *CCNA_02836* in pNTPS138 by Sanger sequencing with Eurofins Genomics.

pNTPS138::*(FS1-FS2) CCNA_03673*

500 bp upstream of *CCNA_03673* was PCR amplified using as a template genomic DNA of *C. crescentus* with the oligos P74.p138.FS1.CCNA3673.F and P75.FS1.FS2CCNA3673. The oligo P74 had 25 bp homology with the plasmid pNTPS138, and the oligo P75 had 25 bp homology with *CCNA_03673.* The sequence 500 bp downstream of *CCNA_03673* was PCR amplified using the oligos P76.FS1.FS2CCNA3673.F and P77.FS2.CCNA3673.p138.R (Sigma-Aldrich). The oligo P76 had 25 bp homology with the *CCNA_03673,* and the oligo P77 had 25 bp homology with plasmid pNTPS138. The plasmid pNTPS138 was digested with EcoRI (NEB/R3101S) and HindIII (NEB/ R3104S). The rest of the steps were performed as described above for the construct of pXYFPC-2-*calP.* The oligos P74.p138.FS1.CCNA3673.F and P77.FS2.CCNA3673.p138.R were used to verify the insertion of *CCNA_03673* in pNTPS138 by Sanger sequencing with Eurofins Genomics.

pNTPS138::*(FS1-FS2) CCNA_02366*

500 bp upstream of *CCNA_02366* was PCR amplified using as a template genomic DNA of *C. crescentus* with the oligos P78.p138.FS1.CCNA2366.F and P79.FS1.FS2CCNA2366.F. The oligo P78 had 25 bp homology with the plasmid pNTPS138, and the oligo P79 had 25 bp homology with *CCNA_02366.* The sequence 500 bp downstream of *CCNA_02366* was PCR amplified using the oligos P80.FS1.FS2CCNA2366.F and P81.FS2.CCNA2366.p138.R (Sigma-Aldrich). The oligo P80 had 25 bp homology with the *CCNA_02366,* and the oligo P81 had 25 bp homology with plasmid pNTPS138. The plasmid pNTPS138 was digested with EcoRI (NEB/R3101S) and HindIII (NEB/ R3104S). The rest of the steps were performed as described above for the construct of pXYFPC-2-*calP.* The oligos

P78.p138.FS1.CCNA2366.F and P81.FS2.CCNA2366.p138.R were used to verify the insertion of *CCNA_02366* in pNTPS138 by Sanger sequencing with Eurofins Genomics.

pNTPS138::*(FS1-FS2) CCNA_02837*

500 bp upstream of *CCNA_02837* was PCR amplified using as a template genomic DNA of *C. crescentus* with the oligos P82.p138.FS1.CCNA2837.F and P83.FS1.FS2CCNA2837.F. The oligo P82 had 25 bp homology with the plasmid pNTPS138, and the oligo P83 had 25 bp homology with *CCNA_028367.* The sequence 500 bp downstream of *CCNA_02837* was PCR amplified using the oligos P84.FS1.FS2CCNA2837.F and P85.FS2.CCNA2837.p138.R (Sigma-Aldrich). The oligo P84 had 25 bp homology with the *CCNA_02837,* and the oligo P85 had 25 bp homology with plasmid pNTPS138. The plasmid pNTPS138 was digested with EcoRI (NEB/R3101S) and HindIII (NEB/ R3104S). The rest of the steps were performed as described above for the construct of pXYFPC-2-*calP.* The oligos P82.p138.FS1.CCNA2837.F and P85.FS2.CCNA2837.p138.R were used to verify the insertion of *CCNA_02837* in pNTPS138 by Sanger sequencing with Eurofins Genomics.

pNTPS138::*(FS1-FS2) CCNA_02089*

500 bp upstream of *CCNA_02089* was PCR amplified using as a template genomic DNA of *C. crescentus* with the oligos P86.p138.FS1.CCNA2089.F and P87.FS1.FS2CCNA2089.F. The oligo P86 had 25 bp homology with the plasmid pNTPS138, and the oligo P87 had 25 bp homology with *CCNA_02089.* The sequence 500 bp downstream of *CCNA_02089* was PCR amplified using the oligos P88.FS1.FS2CCNA2089.F and P89.FS2.CCNA2089.p138.R (Sigma-Aldrich). The oligo P88 had 25 bp homology with the *CCNA_02089,* and the oligo P89 had 25 bp homology with plasmid pNTPS138. The plasmid pNTPS138 was digested with EcoRI (NEB/R3101S) and HindIII (NEB/ R3104S). The rest of the steps were performed as described above for the construct of pXYFPC-2-*calP.* The oligos P86.p138.FS1.CCNA2089.F and P89.FS2.CCNA2089.p138.R were used to verify

the insertion of *CCNA_02089* in pNTPS138 by Sanger sequencing with Eurofins Genomics.

pNTPS138::*(FS1-FS2) CCNA_00182*

500 bp upstream of *CCNA_00182* was PCR amplified using as a template genomic DNA of *C. crescentus* with the oligos P90.p138.FS1.CCNA0182.F and P91.FS1.FS2CCNA0182.F. The oligo P90 had 25 bp homology with the plasmid pNTPS138, and the oligo P91 had 25 bp homology with *CCNA_00182.* The sequence 500 bp downstream of *CCNA_00182* was PCR amplified using the oligos P92.FS1.FS2CCNA0182.F and P93.FS2.CCNA0182.p138.R (Sigma-Aldrich). The oligo P92 had 25 bp homology with the *CCNA_0018,2,* and the oligo P93 had 25 bp homology with plasmid pNTPS138. The plasmid pNTPS138 was digested with EcoRI (NEB/R3101S) and HindIII (NEB/ R3104S). The rest of the steps were performed as described above for the construct of pXYFPC-2-*calP.* The oligos P90.p138.FS1.CCNA0182.F and P93.FS2.CCNA0182.p138.R were used to verify the insertion of *CCNA_00182* in pNTPS138 by Sanger sequencing with Eurofins Genomics.

pNTPS138::*(FS1-FS2) CCNA_01007*

500 bp upstream of *CCNA_01007* was PCR amplified using as a template genomic DNA of *C. crescentus* with the oligos P94.p138.FS1.CCNA1007.F and P95.FS1.FS2CCNA1007.F. The oligo P94 had 25 bp homology with the plasmid pNTPS138, and the oligo P95 had 25 bp homology with *CCNA_1007.* The sequence 500 bp downstream of *CCNA_01007* was PCR amplified using the oligos P96.FS1.FS2CCNA1007.F and P97.FS2.CCNA1007.p138.R (Sigma-Aldrich). The oligo P96 had 25 bp homology with the *CCNA_1007,* and the oligo P97 had 25 bp homology with plasmid pNTPS138. The plasmid pNTPS138 was digested with EcoRI (NEB/R3101S) and HindIII (NEB/ R3104S). The rest of the steps were performed as described above for the construct of pXYFPC-2-*calP.* The oligos P94.p138.FS1.CCNA1007.F and P97.FS2.CCNA1007.p138.R were used to verify the insertion of *CCNA_01007* in pNTPS138 by Sanger sequencing with Eurofins Genomics.

pNTPS138::*(FS1-FS2) CCNA_03981*

500 bp upstream of *CCNA_03981* was PCR amplified using as a template genomic DNA of *C. crescentus* with the oligos P128.CCNA3981FS1.p138F and P129.CCNA3981FS1.FS2R. The sequence 500 bp downstream of *CCNA_03981* was PCR amplified using the oligos P130CCNA3981FS2.FS1R and P131.CCNA3981FS2.p138R (Sigma-Aldrich). The oligos P128.CCNA3981FS1.p138F and P131.CCNA3981FS2.p138R had 25 bp homology with the plasmid pNTPS138 and the oligo P129.CCNA3981FS1.FS2R and P128.CCNA3981FS1.p138F had 25 bp homology with *CCNA_03981.* The plasmid pNTPS138 was digested with EcoRI (NEB/R3101S) and HindIII (NEB/ R3104S). The rest of the steps were performed as described above for the construct of pXYFPC-2-*calP.* The oligos 1372 and 1708 were used to verify the insertion of *(FS1-FS2) CCNA_03981* in pNTPS138 by Sanger sequencing with Eurofins Genomics.

pNTPS138::Δ*recA-tetR*::Δ*calP*::P_{calP}-*calP-flag*

500 bp upstream of *recA* was PCR amplified using as a template the *C. crescentus* strain *ΔcalP::*P_{calP}-*calP-flag* with the oligos 4029 and 4080. The sequence 500 bp downstream of *CCNA_03981* was PCR amplified using the oligos 4081 and 4032 (Sigma-Aldrich). The *tetR* cassette was PCR amplified from the plasmid pNPTS138::*ΔrogA*::*tetR* using the oligos 2303 and 2304. The oligos 4029 and 4032 had 25 bp homology with the plasmid pNTPS138, and the oligos 4080 and 4081 had 25 bp homology with the *tetR* cassette. The plasmid pNTPS138 was digested with BamHI (NEB/R3136S) and HindIII (NEB/R3104S) and gel purified to remove the cleaved fragments. The upstream flanking sequence, downstream flanking sequence, *tetR* cassette, and the backbone of pNTPS138 were ligated by homology (Gibson cloning). The rest of the steps were performed as described above for the construct of pXYFPC-2-*calP.* The oligos 1372 and 1708 were used to verify the insertion of Δ*recA-tetR::*Δ*calP::*P_{calP}-*calP-flag* in pNTPS138 by Sanger sequencing with Eurofins Genomics.

pKTOP::*calP*

The sequence of *calP* was PCR amplified using oligos P3-pKTop-CCNA_03982F and P4-pKTop-CCNA_03982R (Sigma-Aldrich). The resulting DNA fragments were digested with HindIII (NEB/R3104S) and SacI (NEB/R3156S). The rest of the steps were performed as described above for the construct of pXYFPC-2-*calP.* The oligo P3-pKTop-CCNA_03982F was used to verify the insertion of *CCNA_03982* in pKTOP by Sanger sequencing with Eurofins Genomics.

5.2.4.2 Preparation of competent cells

5.2.4.2.1 Preparation of chemically competent *E. coli*

E. coli DH5α cells (see information about the strains in Table 5) were made competent via the calcium chloride method. A single colony was inoculated in LB (media service of the JIC) and incubated at 37ºC ON. 1 mL of culture was sub-inoculated in 100 mL of fresh LB and incubated at 37ºC for 3 hrs or until reaching an. OD_{600}≈0.4. Cells were transferred to a pair of 50 mL tubes that were put on ice for 10 min. Tubes were centrifuged at 5000 RCF at 4ºC for 3 min. Supernatants were discarded, and pellets were gently resuspended in 10 mL of cold 0.1 M $CaCl_2$ (Sigma-Aldrich/cat. no. 21108) and put on ice for 20 min. Cells were centrifuged at 5000 RCF for 3 min and the supernatant was discarded. Cell pellets were gently resuspended in 5 mL of cold 0.1 M $CaCl_2$/15% glycerol and aliquoted in 50 µL per microfuge tube. Tubes were frozen at -80ºC.

5.2.4.2.2 Preparation of electrocompetent cells

1.4.1.1.1.3 Preparation of electrocompetent E. coli

The *E. coli* strain BT101 (see information about the strains in Table 5) was inoculated in LB with the corresponding antibiotic and incubated ON at 37 °C. Cultures were sub-inoculated to OD=0.1 in LB and were grown till the OD_{600}=0.4 was reached. The culture was transferred to two precooled 50 mL tubes and centrifuged at 3500 RCF for 10 min at 4°C. Cultures were kept always on ice to enhance the electrocompetent efficiency of cells. The supernatant was discarded, and the tubes were put upside down to let the remaining liquid drain out. Pellets

were resuspended in 1mL of ice-cold 10% glycerol and the tubes were filled up to 50 mL with ice-cold 10% glycerol (Sigma-Aldrich/cat. no. G5516). The washing step was repeated twice and the pellet was resuspended in 400 µL of ice-cold 10% glycerol. The electrocompetent cells were aliquoted in 50 µL microfuge tubes and used directly for electroporation or frozen in liquid nitrogen and stored at -80°C.

1.4.1.1.1.4 Preparation of electrocompetent *C. crescentus*

C. crescentus WT and Δ*calP* (see information about the strains in Table 6) were grown ON in PYE at 30ºC. Cultures were sub-inoculated in PYE to an OD_{600}=0.1 and incubated at 30ºC until each culture reached the OD_{600}=0.1. Cells were centrifuged at 6500 RCF for 10 min at 4ºC. Pellets were resuspended in 50 ml of ice-cold 10% glycerol. Cells were centrifuged at 8000 RCF for 10 min at 4ºC and the washing step was repeated twice. Pellets were resuspended in 5 ml of ice-cold 10% glycerol and centrifuged at 12000 RCF for 10 min at 4ºC. 50 µL of electrocompetent cells were aliquoted in 600 µl tubes that were pre-chilled on ice. Electrocompetent cells were electroporated directly or frozen in liquid nitrogen and stored at -80ºC.

5.2.4.3 Transformation

5.2.4.3.1 Transformation of *E. coli* by heat shock

A tube of competent *E. coli* cells (see preparation of chemically competent *E. coli* in section 5.2.4.2.1) was thawed on ice. 1 µL of circular plasmid (see information about the plasmids in Table 6) or 5 µL of Gibson assembly reaction was pipetted into the tube and mixed well with the cell. The cells were incubated for 30 min on ice. The tube was transferred to a water bath at 42 ºC for 45 s and put back on ice subsequently for 2 min. 1 mL of LB was added to the tube, mixed well, and incubated for 1 min at RT. The cells were incubated at 37ºC for 1 hr in a rotatory shaker. 100 µL of cells were pipetted onto an LB plate with the corresponding antibiotic (see the antibiotic concentration in section 5.2.2.1.2) and spread over the agar surface. The plate was incubated at 37ºC ON.

5.2.4.3.2 Electroporation of *E. coli* BTH101 for BACTH library screen

For the bacterial two-hybrid library screen, BTH101 was co-transformed with the pKNT25-*calP* and pUT18C-*Caulobacter* library by electroporation. The electroporator used was the Eppendorf Eporator set to 400 Ω and 1.5 kV. For an estimation of the total number of transformants 1 µL was mixed with 999 µL of SOC medium (see in the media section 5.2.2.1.1.2.2) and plated on LB medium with kanamycin and carbenicillin. The rest of the transformation was washed twice in the M63 medium (see buffers in section 5.2.2.1.3) and resuspended in 1 mL of the M63 medium. The whole volume of resuspended cells was plated on M63 minimal-medium plates (see M63 medium composition in section 5.2.2.1.1.2). Plates were incubated at 30 °C for 4 days.

5.2.4.3.3 Transformation of *C. crescentus* by electroporation

3 µL of the corresponding plasmid (see information about the plasmids in Table 6) were pipetted into each tube of 50 µL of electrocompetent *C. crescentus* WT or Δ*calP*. The mixture of cells and plasmid was transferred to electroporation cuvettes, ensuring that cells settled at the bottom with no bubbles. Cells were electroporated in the electroporator Eppendorf Eporator set to 400 Ω and 1.5 kV. 500 µL of PYE were immediately added to the cells in the cuvette after the electric pulse. The diluted cells were transferred to a fresh 50 mL tube and incubated at 30ºC for 2 hrs with rotatory shaking. Cells were plated on a PYE agar plate with 25 µg/mL kanamycin. The same spreader used to disseminate cells on the plate was used to spread the leftover cells on a new fresh plate. This second plate with a lower colony density allowed us to pick isolated colonies if the first plate had a very high density, which prevented a proper selection of the colonies. Plates were incubated for 48 hrs at 30ºC with 25 µg/mL kanamycin.

5.2.4.4 Double crossover in *C. crescentus*

The integrative plasmid pNTPS138 harbours *sacB* (see information about the plasmids in Table 6), a gene that produces the toxic compound levansucrase, which uses sucrose as a substrate. This is a counter-negative selection system used to choose cells that performed the double crossover, excising pNTPS138 and keeping

the inserted gene in the *C. crescentus* genome [735-737]. To do so, colonies grown from electroporated *C. crescentus* were selected and plated on PYE 3% (w/v) sucrose plates. Only double recombinants were able to grow in the presence of sucrose and some colonies were picked and transferred to a PYE 25 μg/mL kanamycin agarose plate. The genotype of these transformants was verified with a colony PCR (see section 5.2.6.1.3).

5.2.5 In vivo assays

5.2.5.1 Sub-inhibitory concentration determinations of toxic compounds

The sub-inhibitory concentration (SIC) of antibiotics (see information about the antibiotics in section 5.2.2.1.2) or other compounds was defined as the lowest concentration of a toxic compound at which some growth was observed for a given species or strain. The SIC of each toxic compound was determined experimentally. Cultures of *C. crescentus* were supplemented with increasing concentrations of each compound in a PYE liquid or a PYE solid agar media (Table 4). *E. coli* cells were only tested with increasing concentrations of MMC (Table 4.1). For the assessment of liquid medium cultures, the OD_{600} was measured every hour for 48 hrs. The value of absorbance at each time point was used to draw a line plot to observe the rise or drop of the cell population. The values of absorbance with no toxic compound and between different concentrations were compared. Plates were evaluated every day for 3 days after inoculation, comparing the number of colonies with no toxic compound added and with different concentrations of toxic compound. Concentrations that did not allow cell growth were rejected. Conversely, those concentrations that lightly affected cell growth, resembling the unsupplemented medium, were also ignored.

5.2.5.2 Sensitivity assays

5.2.5.2.1 Sensitivity assay in a liquid medium

Cells were grown to mid-exponential phase and cultures were diluted to an $OD_{600}=3.3\cdot10^{-4}$ before the appropriate DDA was added. 10 μL of culture were mixed with 140 μL PYE and supplemented with the SIC of each DDA (see the SIC

determination in section 5.2.5.1). Each liquid sensitivity assay was performed on a separated 96-well plate, and the outermost wells were filled with distilled water (dH_2O) to avoid aberrant measurements caused by evaporation. To further reduce evaporation, plates were also sealed with parafilm. Plates were incubated for 48 hrs at 30°C with rotatory shaking, and the OD_{600} was measured every hour. The plate reader used was manufactured by Biotech Instruments Ltd., and the data visualisation software used was Gen5 (versions/1.9/2.0.). The output was further analysed with the statistics and imaging software GraphPad Prism (versions 9.4.1/9.5.0).

5.2.5.2.2 Sensitivity assay on a solid medium

A single colony of each strain was picked from a PYE agar plate and supplemented with the corresponding SIC of each antibiotic (see information about antibiotics in section 5.2.2.1.2) or cytotoxic compound (Table 4) when necessary and streaked on a fresh PYE agar plate. Plates were supplemented or unsupplemented with the corresponding toxic compound and incubated for 48 hrs at 30°C.

5.2.5.2.3 Spotting assay

PYE agar plates were supplemented or unsupplemented with 6 µg/mL norfloxacin, 2 µg/mL ciprofloxacin, 0.25 µg/mL MMC, 1 µg/mL MMS, and 1.5 and 2 µL/mL CCCP (see information about the toxic compounds in Table 4). *C. crescentus* WT, *ΔrecA,* and *ΔcalP* (Table 5) were the strains tested in this assay. Cells were grown in a liquid PYE at 30°C ON and cultures were diluted to an OD_{600}=0.1. Diluted cultures were grown to mid-exponential phase at 30ºC, and 10-fold serially diluted. Drops of 5 µL of each diluted culture were spotted on the agar from the most concentrated on the right side to the most diluted on the left side (X-axis). Each new strain was pipetted below the previous one (Y-axis). Plates were incubated for 48 hrs at 30°C before the image was taken.

5.2.5.3 Bacterial two-hybrid assay

One-to-one BACTH assays were performed as described previously for the sensitivity assays on a solid medium (see sensitivity assay details in section

5.2.5.2.2) [12]. *E. coli* BTH101 (see strains in Table 5) was co-transformed (see the transformation process in section 5.2.4.3.1) with the plasmids pKNT25 and pUT18, or the plasmids pKT25 and pUT18C (see strains and plasmids in Tables 5, 6, respectively). These vectors were previously cloned with their corresponding fragments or were left empty (controls) (see strains in Table 6). The different combinations of plasmids that were co-transformed into BTH101 are summarised in Table 6. The transformants were streaked on a MacConkey agar medium and incubated at 30°C for 48 hrs. The red colonies were selected and inoculated in 10 mL LB and supplemented with carbenicillin (for pUT18/pUT18C plasmids) or kanamycin (for pKNT25/pKT25 plasmids) at 30°C ON (see information about the antibiotics in section 5.2.2.1.2).

5.2.5.4 Bacterial two-hybrid screen

BTH101 was co-transformed with the constructs pKNT25-*calP* and pUT18C-*C crescentus* library (see electroporation details in section 5.2.4.3.2). Blue colonies that grew in the M63 plates were streaked out onto MacConkey agar plates (see the media recipe in section 5.2.2.1.1.2). The red colonies were selected and inoculated in 10 mL LB and supplemented with carbenicillin at 30°C ON (see information about the antibiotics in section 5.2.2.1.2). To reveal the sequence of the insert, plasmids were isolated (see plasmid isolation in section 5.2.6.1.1.2) and the plasmid pUT18C-*C crescentus* library was sequenced using the oligos 1411 and 1412. Sequencing results were analysed with the DNA sequence annotator, visualiser, and analyser software Artemis (version 17.0.1) and Geneious Prime to reveal which constructs of the *C. crescentus* library interacted with CalP.

5.2.5.5 PhoA-LacZα assay

The PhoA-LacZα assay was performed as described previously for sensitivity assays on a solid medium [25]. The strains of *E. coli* used in this experiment were: DH5α+pKTOP::*ø*, DH5α+pKTOP::*calP,* and DH5α+pKTOP::*rsbN* (Table 5). The strains were streaked onto plates with LB dual-indicator agar medium and incubated at 30°C for 24 hrs.

5.2.5.6 Microscopy

5.2.5.6.1 Agarose pad preparation for time-lapse microscopy

UltraPure Agarose (Invitrogen/cat. no. 16500-100) was used to prepare 1% square agarose pads attached to a microscope slide. 0.18 g of agarose was dissolved in 5 mL of PYE medium and incubated in a water bath until it was completely melted. In the meantime, the microscopy slides were cleaned with EtOH and a square gene frame (Thermo-Fisher Scientific/cat. no. AB0577) was attached to the centre of each microscopy slide. A gene frame has an empty squared outline in the centre aimed at retaining the liquid agarose until it solidifies to form the pad. The microscopy slides with each gene frame and 666 µL PYE medium were heated at 70ºC in a heating block. 333 µL of melted agarose were pipetted and mixed with 666 µL from the pre-warmed PYE medium. 500 µL PYE agarose was separated and supplemented with 0.12 µg/mL MMC. 120 µL of each agarose-PYE mixture were quickly pipetted into a gene frame and covered with a cover slip while the microscopy slide was still in the heat block. The cover slip was moved around the liquid agarose pad to remove bubbles and make it flat. The pad was let dry for at least 20 min and the cover slip was subsequently withdrawn. The agarose pad was trimmed with a razor blade to a 3-5 mm wide agarose stripe.

5.2.5.6.2 Culture loading on pads and microscopy visualisation

For phase contrast microscopy, mid-exponential phase cultures of WT and *ΔcalP::*P_{calP}*-calP-yfp* (Table 5) were treated with 0.12 µg/mL MMC or left untreated and incubated for two hrs at 30°C. 2 µL of each strain were pipetted at the end of the stripe of a gene frame with PYE with or without 0.12 µg/mL MMC, which were tilted to let the culture move across the stripe. The culture was let dry for 2 min and covered with a standard large/medium cover slip. The cover slip was pressed along the outline of the gene frames to seal it properly. Images were acquired on a Zeiss Axio Observer Z1 inverted light microscope with a 100x objective (immersion oil added). The channels used were bright field and phase contrast with the 100X objective. The filter combination for fluorescence to visualise CalP-YFP was: 489-512 nm excitation range and 520-550 nm emission

range. The exposure was 150 ms, and the light intensity was 8 volts. The image editing software Fiji (Image J) was employed to process images.

5.2.5.7 Membrane accumulation assay

Four biological replicates from ON cultures of *C. crescentus* WT and *ΔcalP* (see strains in Table 5) were reinoculated to an OD_{600}=0.1 and incubated at 30ºC until reaching the OD=0.4. The OD_{600} of each culture was normalised according to the optical density of the culture with the lowest OD_{600}. 1 mL of each culture was pipetted into 1.5 mL microfuge tubes in duplicates. 1 µg (2 µL) of 0.5 mg/mL MMC-TRC (see details for the conjugation of MMC-TRC in section 5.2.6.3.2) was added to one duplicate, while the second duplicate remained unsupplemented. MMC-treated and untreated cultures were incubated for two hrs at 30°C with rotatory shaking. After 1 hr, the tubes were washed twice with phosphate-buffered saline (PBS) (see buffer section 5.2.2.1.3) at 12000 RCF for 1 min and resuspended in 350 mL PBS. The OD_{600} of cultures was measured in triplicate and the means were used to normalise cultures based on the lowest OD_{600} value. A calculated volume of PBS was added to compensate for the excess of cells in comparison to the sample with the lowest optical density. 150 µL of each culture and 150 µL of plain PBS to make the blank (in triplicates) were added into each black flat bottom 96-well plate (Corning/cat. no. 4580). The excitation of MMC-TRC is 586 nm and the emission is 605 nm. The plate reader used to measure the fluorescence was the fluorometer FLUOstar Omega (BMG Labtech). The settings of excitation and emission of the fluorometer monochromators were 470-20 and 630-40 nm, respectively, selected from the Texas-Red endpoint program. The statistics and imaging software GraphPad Prism 10 was used to analyse the data results, draw line plots, and elaborate the statistical T-test. To assess the statistical significance of the mean between the fluorometric measurements, an unpaired t-test with Welch´s correction was conducted using the statistical and graphical software GraphPad Prism (see details of the t-test in Table A2, Fig. A19).

5.2.6 In vitro assays

5.2.6.1 Nucleic acid manipulation

5.2.6.1.1 Nucleic acid isolation

1.4.1.1.1.5 Genomic DNA isolation

C. crescentus WT (see strains in Table 5) cells were incubated ON at 30ºC in a PYE medium. 1 mL of the ON culture was centrifuged in a microfuge tube at 12000 RCF for 2 min. This process can be repeated with as many samples as desired to increase the yield. The cell pellet was resuspended in 600 µL of cell lysis solution (Qiagen/cat. no. 158113) and incubated at 50ºC for 5 min to lyse cells. 4 µL of RNase (10 mg/mL) was added to the solution, which was incubated at 37ºC for 30 min. The mixture was cooled to RT and 200 µL of protein precipitation solution (Qiagen/cat. no. 158123) was added. The solution was vortexed for 30 s and chilled on ice for 10 min. The mixture was centrifuged at 12000 RCF for 5 min. The supernatant was transferred to a clean microfuge tube and mixed with 600 µL of isopropanol (Thermo-Fisher Scientific) by inverting the tube 50 times. The solution was centrifuged at 12000 RFC for 1 min and a small white pellet was formed at the bottom of the tube. The supernatant was discarded, and the leftover liquid was removed with paper, preventing the pellet from coming out of the tube. The pellet was washed with 600 µL of 70% EtOH (VWR chemicals/cat. no. 20821.330) by inverting the tube 3 times. The solution was centrifuged at 12000 RCF and the supernatant was carefully discarded, preventing the pellet from being drained out. Centrifuge again with the same speed to remove the leftover supernatant and carefully pipette it out of the tube. The pellet was resuspended in dH_2O and left at RT ON for the genomic DNA to untangle and resuspend. The yield should be ~200 ng/µL.

1.4.1.1.1.6 Plasmid isolation

E. coli DH5α strains (see strains in Table 5) harbouring the plasmid of interest (see plasmids in Table 6) cultured in an LB medium were incubated ON at 37ºC with the corresponding antibiotic (see the antibiotic concentration in Table 4). ON cultures were transferred to 2 mL microfuge tubes and centrifuged at 12000 RCF to

pellet cells. The supernatant was discarded, and more culture was added to the microfuge tube. This step was repeated twice to accumulate more cells and enhance the plasmid yield. Following this step, a commercial Miniprep Kit for plasmid DNA purification was used (Qiagen/cat. no. 27104). The elution of the plasmids was done with dH2O in 30 µL to increase the plasmid concentration.

1.4.1.1.1.7 Total RNA isolation

ON cultures of *C. crescentus* WT and *ΔcalP* (see strains in Table 5) were diluted in a liquid PYE to an OD_{600}=0.01 and treated with 3 µg/mL MMC or left untreated for approximately 1 hr or until they reached the OD_{600}=0.15. 6 mL of culture was centrifuged and washed with 1 mL PBS (see buffer section 5.2.2.1.3) and pellets were frozen with liquid nitrogen and stored at -80ºC. For the extraction of the total RNA, an RNA isolation kit was used (Zymo Research/ cat. no. R2050). To break cells, pellets were mixed with 400 µL of hot Trizol (Zymo Research/ cat. no. R2050) at 65ºC. Pellets were vortexed and the tubes were placed in the thermomixer at 65ºC for 10 min at 270 RCF. Tubes were placed at -80ºC again to freeze the cells and Trizol for at least 10 min. Pellets were left at RT to thaw, and tubes were centrifuged at 11300 RCF for 30 s. The flow-through was discarded and the PreWash step was repeated. 700 µL of RNA Wash Buffer (Zymo Research/ cat. no. R2050) was added to the column and tubes were centrifuged for 30 s. Tubes were centrifuged for another 2 min to remove the residual buffer. Columns were transferred to fresh 1.5 µL microfuge tubes and 30-50 µL of nuclease-free dH_2O was added to the column (depending on how concentrated the sample is desired). Columns were incubated at RT for at least 2 min and centrifuged for 1 min at 6700 g. The elution was transferred again to the column and the elution process was repeated to capture the highest amount of total RNA as possible.

5.2.6.1.2 DNA and RNA measurement by NanoDrop

To prevent sample contamination, the spectrophotometer (Thermo-Fisher Scientific/NanoDrop 2000) sample base must be cleaned with bi-distilled water and a thin microfiber paper tissue before measuring nucleic acids. Before performing the measurements, it was required to calibrate the machine with the same buffer

that the sample was dissolved in. In this project, all nucleic acids were dissolved in Mili-Q water, so 1.5 µL of Mili-Q water was pipetted on the NanoDrop sample base to calibrate the machine. Following calibration, the NanoDrop sample base was cleaned and another 1.5 µL of Mili-Q water was added to the base to measure the blank or zero sample. The base was cleaned again and 1.5 µL of DNA or RNA isolation was pipetted onto the NanoDrop sample base, and the nucleic acid concentration was measured at 260 nm. To ensure the quality of the DNA or RNA was good, the ratio 260/280 must be between 1.8-2 and the ratio 260/230 between 2-2.2 (the lower, the worse for both ratios). For each mL of the culture of *C. crescentus* at OD_{600}=0.15, at least 10 µg of total RNA should be isolated.

5.2.6.1.3 Polymerase chain reaction (PCR)

PCR was performed with Phusion HF DNA polymerase (Thermo-Fisher Scientific/F630L). Each reaction contained the following components:

10 µl buffer (from a 10X stock)
1 µl (10 mM) dNTPs, 1 µl DMSO
0.25 µL (100 µM) forward oligo (Table 8)
0.25 µL (100 µM) reverse oligo (Table 8)
50 ng DNA template
0.5 µl DNA polymerase
Nuclease-free dH_2O (up to 50 µl)

Two-step cycling was performed as follows:

Initial denaturation: 98°C for 30 s
Denaturation: 98ºC for 10s
Annealing: 72ºC for 30s
Extension: 72º for 10s
Repeat the previous steps 29X
Final extension 72 for 5 min

For a standard PCR, isolated genomic DNA (see genomic DNA isolation in section 5.2.6.1.1.1), plasmid DNA (see genomic DNA isolation in section 5.2.6.1.1.2), or other PCR fragments were used. For a colony PCR, a colony was picked from a plate with a small pipette tip and dissolved in the master mix after all other reagents were added. The initial denaturation of the thermocycling steps was slightly modified. The temperature changed from 10 sec to 3 min to give enough time for membranes to denature and release the genomic DNA of cells.

PCR products were run in an agarose gel (see section 5.2.6.1.4.1 for DNA migration in an agarose gel electrophoresis) and gel-purified (see section 5.2.6.1.4.1.1 for isolation of DNA from an agarose gel) to be used in subsequent cloning rounds if necessary.

5.2.6.1.4 Agarose gel electrophoresis

1.4.1.1.1.8 Agarose gel electrophoresis of DNA

1% w/v of agarose powder (Melford laboratories/cat. no. A20080) was added to the TAE buffer (Formedium/cat. no. TAE5000). The blend was heated until it was completely homogeneous. It was left to cool down and 0.5% µg/mL of ethidium bromide was added and swirled to dissolve the dye. The mixture was poured into a gel tray and a comb was shrunk into one of the poles of the tray to form the lanes. The agarose blend was left to solidify at RT. The comb was withdrawn after the gel was solidified and the DNA ladder was loaded into a lane. The gel tray was put into the electrophoresis tank and 1x TAE (Formedium/ cat. no. TAE5000) was poured on it until the liquid covered the top of the agarose gel. DNA samples were mixed with DNA loading dye (NEB/cat. no. B7024S) in a 6:1 (v/v) ratio to make the bands denser and visible. Each sample was loaded into a lane of the agarose gel. The volume loaded depends on the size of the lane. The cap of the tank was set, and the gel was electrophoresed at 120 V for approximately 40 min. The gel was taken out of the tank and the bands were visualised by UV transillumination.

1.4.1.1.1.9 Isolation of DNA from agarose gel

The extraction of the electrophoresed DNA from the agarose gel (see the agarose electrophoresis of DNA in section 5.2.6.1.4.1) started by cutting the agarose gel with a razor blade to create a square around the desired DNA band. The selected pieces of agarose gel were excised and introduced in a pre-weighted microfuge tube. The tube with the agarose fragment was weighed again and the value was subtracted from the weight of the tube without the fragment to know the weight of each DNA-containing agarose fragment. The weight of the agarose piece was used to calculate the corresponding volume of the agarose melting buffer. The next steps were performed following the manufacturer´s protocol (Qiagen/cat. no. 28706).

1.4.1.1.1.10 Sodium hypochlorite agarose gel electrophoresis for total RNA integrity verification

The preparation of the agarose gel for RNA mainly proceeded as described for agarose gel electrophoresis of DNA (see the information about the agarose electroporation of DNA in section 5.2.6.1.4.2), with some exceptions. The electrophoresis tank, gel tray, and comb(s) had to be pre-cleaned with RNase (Thermo-Fisher Scientific/cat. no. AM9780) to prevent RNA degradation during the electrophoresis. 1% v/v of hydrogen peroxide was added to the agarose and TAE blend after heating to dissolve the agar. The presence of hydrogen peroxide in the solution deactivates the RNases, preventing the degradation of the total RNA [738]. 1 µL of each sample of RNA was mixed with RNA loading dye (New England Biolabs/cat. no. B0363S) in a 1:1 (v/v) ratio and heated at 70ºC for 10 min. The RNA samples with loading dye were loaded into the gel at 100 V for 15 min. The bands for 23S and 16S rRNA should appear clearly when the integrity of the RNA is good. The band of 23S rRNA should be brighter than the band of 16S rRNA.

5.2.6.1.5 Gibson cloning

The PCR was run with oligonucleotides carrying complementary sequences to fragments that were intended to ligate in a subsequent Gibson assembly reaction [739]. 4 µL of PCR-amplified DNA product (one or more fragments) was mixed with 1 µL of plasmid (diluted in dH_20) and 5 µL of Gibson assembly master mix (NEB/cat. no. E25611S). The mixture was incubated at 50ºC for 1 h.

5.2.6.1.6 Degradation of the DNA from the total RNA samples with DNase I

DNA traces were accumulated during total RNA isolation (see the total RNA isolation procedure in section 5.2.6.1.1.3), so it was necessary to eliminate all DNA in the samples to prevent amplifying the wrong DNA during the qPCR process. To eliminate DNA from the solution of the total RNA, 10 µg of total RNA from each sample was treated with DNAse I (1U/µL) (Thermo-Fisher Scientific/cat. no. 18068015) to degrade DNA. Before the addition of 5 µL of Turbo DNAse I, 10 µL of Turbo DNAse I buffer (Thermo-Fisher Scientific/cat. no. 18068015) was added to the solution and was topped up to 100 µL. The mixture was incubated at 37ºC for 30 min. To ensure the complete removal of DNA, the process was repeated by adding 5 µL of DNAse I followed by another incubation at 37ºC for 30 min.

1.4.1.1.1.11 Total RNA cleaning

To remove DNAse I and impurities from the total RNA samples (see degradation of DNA with DNase I from the total RNA in section 5.2.6.1.6), a commercial Clean Up and Concentrator kit from Zymo Research/cat no. R1013) was used. The process was performed following the manufacturer´s instructions and the total RNA was eluted in 30 µL of nuclease-free dH_2O.

5.2.6.1.7 cDNA conversion

The total RNA to cDNA conversion (see the total RNA isolation procedure in section 5.2.6.1.1.3) was done with the SuperScript III reverse transcriptase (Invitrogen/cat. no. 11752-050) according to the manufacturer's instructions. Before the conversion, the RNA had to be quantified to calculate the amount to add to the reaction. A total of 1 µg of total RNA from each sample was added to the reaction to be converted into cDNA. The volume to add to the reaction needs to be calculated according to the concentration of each sample. The sample having the lowest concentration was not diluted with nuclease-free dH_2O. The rest of the samples were normalised according to the lowest-concentrated sample by adding an equivalent volume of nuclease-free dH_2O. Once the reaction was set, it was placed

in a PCR thermocycler with the following setup, which was a modification of the manufacturer´s protocol (Invitrogen/cat. no. 11752-050):

25ºC for 10 min
42ºC for 120 min
50ºC for 30 min
55ºC for 30 min
85ºC for 5 min

Following the thermocycler incubation, 1 µL of *E. coli* RNase H (Invitrogen/cat. no. 11752-050) was added to each sample to stop the reaction. *E. coli* RNase H acted by separating the RNA template from the cDNA. Each reaction was incubated at 37ºC for 20 min. The samples were chilled and stored at 4ºC or used for the RT-qPCR analysis.

5.2.6.1.8 Reverse transcription-quantitative polymerase chain reaction (RT-qPCR) analysis

21 µL of cDNA was diluted in nuclease-free dH_2O (Thermo-Fisher Scientific/cat. no. 11752-050) in a 2:1 ratio. The SYBR Green JumpStart Taq ReadyMix (Sigma-Aldrich/cat. no. S4438) was used to amplify the cDNA (see the protocol for cDNA conversion in section 5.2.6.1.7). To know the volume needed to prepare the master mix for all reactions, the next formula was applied: N·3.5+3.5=X (N=number of samples, X=factor to multiply each reaction to make the master mix). N is determined by the number of samples, which are given by the number of conditions (C), and the number of biological or technical replicates (R): N=C·R. The components of the RT-qPCR reaction were:

10 µL SYBR green Taq polymerase
0.2 µL primer 1
0.2 µL primer 2
7.6 µL nuclease-free dH_2O

Each component of the RT-qPCR reaction was multiplied by the X factor to know the volume to add to the master mix. Two different master mixes with an equal number of samples and volumes were prepared per pair of primers following the previous formula and indications. The first master mix contained the primers q141.calPF1 and q142.calPR1 (Table 8) to quantify *calP* transcription. The second pair of primers, 2740F and 2741R (Table 8), were used as a control for the quantification of the transcription of the housekeeping gene RpoD. Finally, 18 µL of each master mix was mixed with 2 µL of the diluted cDNA in triplicates (3 replicates with the same cDNA with each master mix of pair of primers). Each 20 µL final reaction was pipetted in an RT-qPCR 96-well plate (with a V bottom) and covered with parafilm to prevent evaporation. The 96-plate was centrifuged to settle samples on the bottom of the well at 2900 RCF for 10 sec. The 96-plate was placed in the RT-qPCR thermocycler to start the analysis.

The RT-qPCR cycling was performed as described in the technical bulletin of the SYBR Green JumpStart Taq ReadyMix (Sigma-Aldrich/cat. no. S4438). The thermocycler used for the RT-qPCR was Bio-Rad/model no. CFX96 C1000 Touch. Relative expression values were calculated by using the comparative Ct method (ΔΔCt) and were the average of two biological replicates. Error bars represent the relative expression values calculated from plus or minus 1 standard deviation from the mean ΔΔCt values.

5.2.6.2 Protein manipulation

5.2.6.2.1 Cell sonication

750 µL of buffered-resuspended cells (cell fractionation resuspension buffer (CFRB) or protein lysis buffer; see buffer composition in section 5.2.2.1.3) were sonicated in a 1.5 µL microfuge tube. The sonication finger (Sanyo/model no. Soniprep 150) was introduced into the tube and subjected to ultrasound at 10 microns for 15 sec. This process was repeated 5 cycles with 15-sec gaps between cycles. During the process, the tube was kept on ice and the sonication finger was

cleaned with 70% ethanol (EtOH) (VWR chemicals/cat. no. 20821.330) and paper between different samples.

5.2.6.2.2 Cell fractionation

Cell fractionation was performed following a modified version of the indications from the Model et al. (2014) cell fractionation protocol. The cell pellets of *C. crescentus* or *E. coli*) were resuspended in 750 µL of CFRB. Cells were broken by sonication (see the protocol for sonication in section 5.2.6.2.1) and the cell lysate was centrifuged at 7000 RCF in the centrifuge (Heraeus/model No. Primo Fresco) at 4ºC for 15 min. 70 mL of supernatant (input) were set apart to be used as a whole cell extract control. The protein content was measured in the whole-cell fraction with the Bradford method (see protein quantification by Bradford method in section 5.2.6.2.4.2) and normalised within samples [740]. The remaining supernatant was transferred to the ultracentrifugation tubes (Beckman Coulter/cat. no. 349622) and ultracentrifuged at 194000 RCF (Beckman Coulter/model No. Optima MAX-E/TLA-100.3 rotor) for 1 hr at 4 ºC. 500 µL of the top layer of the soluble fraction was transferred to a clean tube and the remaining 250 µL were discarded from the bottom layer. 750 µL of CFRB were discarded into the conical centrifugation tube to wash the membranes, preventing them from detaching from the tube. The washing step to remove traces of the soluble fraction was repeated, and the membrane fraction was resuspended in 750 µL of CFRB. The volume of sample calculated in the normalisation to add in each well compares the different protein concentrations within samples (although within fractions (soluble, membrane, and whole cell), the volume to take was the same for the three samples). 2.5 µL of protein loading dye (New England Biolabs/cat. no. B7703S) were added to 12.5 µL of every sample. Samples were run in a 4-20% Tris-Glycine SDS-PAGE and incubated with an anti-FLAG antibody to highlight CalP-FLAG (see indications for SDS-PAGE in section 5.2.6.2.4).

5.2.6.2.3 Protein isolation

Purified proteins were used for western blot, MS/MS, and MP analysis. Two biological replicates of the *C. crescentus ΔcalP::*P_{calP}*-calP-flag* strain were purified

and two biological replicates of the untagged *C. crescentus* WT were purified as an untagged control. Cultures of *C. crescentus* WT and *ΔcalP::*P_{calP}*-calP-flag* were grown in a PYE liquid medium and treated with 0.125 µg/mL MMC or left untreated. Mid-exponential phase cultures were washed twice at 9000 RCF with 40 mL of ice-cold PBS. Cells were transferred to 2 mL microfuge tubes and washed once more at 12000 RCF with 2 mL of ice-cold PBS. Pellets were frozen with liquid nitrogen and stored at -80ºC to continue the next day. Pellets were resuspended in 0.75 mL of protein lysis buffer and cells were broken by sonication (see the sonication section 5.2.6.2.1). The cell lysates were centrifuged at 12000 RCF and the supernatants were transferred to clean 1.5 microfuge tubes. The tubes were centrifuged again, and the supernatants were pipetted into new 1.5 mL tubes. 50 µL of each sample was pipetted into tubes and these samples were put aside as a pre-isolation sample. 50 µL of anti-FLAG antibody conjugated with magnetic beads (Miltenyi Biotec/cat. no. 130-101-591) was added to each tube (except for the pre-isolation samples). Tubes were incubated with a rotatory shake at 4 °C for 1 hr. To purify CalP, the µMACS DYKDDDDK isolation kit (Miltenyi Biotec/cat. no. 130-101-591) was used. This kit enabled the purification of FLAG-tagged proteins that were attached to an anti-FLAG monoclonal antibody, which was fused to magnetic beads inserted into the purification column. Purification columns of the isolation kit were activated by pipetting 200 µL of the lysis buffer. The cell lysate was applied to the columns and allowed to run through. Columns were rinsed with 200 µL of Wash Buffer 1 (Miltenyi Biotec/cat. no. 130-101-591) four times and once with 100 µL of Wash Buffer 2 (Miltenyi Biotec/cat. no. 130-101-591). 20 µL of 0.1 M triethylamine (TEA) (Sigma-Aldrich/471283-100ML) was applied to each column, which was incubated for 5 min at RT. 50 µL of 0.1 M TEA was applied to the column to elute CalP-FLAG. Each eluate was collected in a tube containing 3 µL of 1 M MES (pH 3) for neutralisation. A second elution by applying another 50 µL of 0.1 M TEA to the column was performed and was collected in a tube with 3 µL MES (pH 3). The second eluate was mixed with the first eluate if the yield was low. One of the biological replicates was eluted in a 0.1 M TEA buffer with 0.1 M Triton-X (Merck/cat. no. 1086031000) (for MS/MS) and another one in a TEA buffer

without Triton-X (to be used in the MP assay; see the indications for the MP analysis in section 5.2.6.3.3).

5.2.6.2.4 Protein quantification

1.4.1.1.1.12 Lowry method

The Lowry method colours proteins and allows for the determination of the protein content of WT and CalP-FLAG. To do so, the samples were mixed with the DC protein assay (Bio-Rad/cat. no. 5000111) and the OD_{600} was measured. The DC protein assay is comprised of three different reagents: reagent A, reagent B, and reagent S. The reagent A' was prepared by adding 20 µl of reagent S to each ml of reagent A needed for the run. 20 µl of the sample was pipetted (concentration should be from 0.2 mg/ml to about 1.5 mg/ml) to 100 µl of reagent A'. 800 µl of reagent B was added to the mixture of sample and reagent A' and mixed. The mix was incubated at RT for at least 15 min and the absorbance was measured at OD_{750}. Parallel to the spectrophotometric measurement of samples, increasing volumes of bovine serum albumin (BSA) were also measured. 1, 5, 8, 10, 15, and 20 µL of 2 µg/µL BSA were added to the DC protein assay kit to be measured at OD_{750}. A calibration curve was done with the absorbance values of the BSA. The absorbance values of WT or CalP-FLAG were used to substitute the "x" value from the calibration curve equation to infer the concentration of proteins in the sample.

1.4.1.1.1.13 Bradford method

The Bradford method [740] was used for determining the relative protein content in each sample compared to other samples. To do so, 1 µL of the centrifuged cell lysate supernatant was mixed with 999 mL 1X Bradford dye (Bio-Rad/cat. no. 5000006) to colour the proteins. The OD_{600} of Bradford dye with no protein was measured to set the blank. The OD_{600} of each sample mixed with Bradford dye was measured and the absorbance was annotated. The absorbance value is used to compare the relative protein content in each sample. The sample with the minimum absorbance value is divided by the absorbance value of the rest of the samples to obtain a dilution factor. The volume of cell lysate supernatant to add to normalise the samples is obtained by multiplying each cell lysate´s dilution factor by the

maximum volume of sample required for a subsequent SDS-PAGE. The result of the multiplication of each sample is subtracted from the maximum volume of sample required and the result is the volume of dH_2O to add, to top up the required volume. After sample normalisation, all samples must have a similar protein content.

5.2.6.2.5 Sodium dodecyl sulphate-polyacrylamide gel electrophoresis (SDS-PAGE)

ON cultures of *C. crescentus* or *E. coli* cells were diluted to the OD_{600}=0.1 and treated with either 0.12 µg/mL MMC, with increasing MMC concentrations or other DDA. Cells were grown to mid-exponential phase at 30°C for 2 hrs. Cultures were centrifuged and resuspended in protein lysis buffer (see buffer section 5.2.2.1.3). Cells were sonicated (see the sonication details in section 5.2.6.2.1) and centrifuged at 12000 RCF for 20 min. 200 µL of supernatant was collected and the total protein content was quantified by applying the Bradford method (see Bradford method for protein determination in section 5.2.6.2.4.2). Proteins in the sample were denatured by mixing them with protein loading dye (New England Biolabs/cat. no. B7703S) and incubating them at RT for 30 min. Samples were centrifuged and loaded on a precast Novex WedgeWell 4-20% Tris-Glycine gel (Invitrogen-Thermo-Fisher Scientific/cat. no. XP04202BOX). The gel was run in an Invitrogen® Mini Gel Tank (Invitrogen/cat. no. A25977) at 150 V for 45 min to separate the proteins. The same procedure of loading and running in the SDS PAGE was followed for immunoprecipitated isolated CalP and CalP derivative mutants (see protein isolation protocol in section 5.2.6.2.3).

1.4.1.1.1.14 Coomassie-stained polyacrylamide gel

The polyacrylamide gel was stained with 100 mL Coomassie brilliant blue (Abcam/cat. no. ab119211) and incubated at RT for 1 hr with rotatory shaking. Only the immunoprecipitated CalP or CalP derivative mutants were visualised in a Coomassie-stained polyacrylamide gel (see protein isolation protocol in section 5.2.6.2.3) The gel was discoloured with dH_2O for 15 min three times with rotatory

shaking (only the protein bands remained coloured). Protein-stained bands were visualised on the polyacrylamide gels in a transilluminator.

1.4.1.1.1.15 Immunoblot analysis

As an alternative to Coomassie dye staining, CalP and CalP derivative mutants were immunoblotted with antibodies. Following the protein migration in an SDS-PAGE (see the protocol information in section 5.2.6.2.4), the polyacrylamide gel was transferred to a tray with 10 mL of transfer buffer (Thermo-Fisher Scientific/cat. no. LC3675) with MeOH (Thermo-Fisher Scientific/cat. no. 325740025) (1:3 ratio; v/v) and was incubated at RT for 10 min with rotatory shaking. The resolved proteins were transferred to a polyvinylidene fluoride membrane (Trans-Blot Turbo Mini 0.2 µm PDFV Transfer Packs) (Bio-Rad/cat. no. 1704156). The Trans-Blot Turbo Transfer System (Bio-Rad/cat. no. 1704150) with the Turbo and MiniGel program set was used to force the transference from the polyacrylamide gel to the membrane for 5 min. The membrane with the proteins was incubated for 1 hr in a small tray filled with 10 mL TBS-Tween (TBST) (see the composition of the buffer in section 5.2.2.1.3). The TBST was removed, and the membrane was shrunk in 10 mL of fresh TBST that was mixed with an antibody in the following proportions: 1:10000 dilution of α-FLAG HRP-conjugated antibody (Sigma-Aldrich/cat. no. A8592), 1:1000 dilution of α-T18 HRP-conjugated antibody (Abcam/cat. no. ab277790), or 1:10000 dilution of α-GFP antibody (Abcam/cat. no. 5450). The membranes were incubated with TBST with a conjugated antibody for 1 hr and with non-conjugated antibodies for 2 hrs (1 hr for the primary antibody and 1 hr for the secondary antibody). The membrane was washed three times for 5 min with TBS. 150 µL of chemiluminescence substrate (Thermo-Fisher Scientific/cat. no. 37070) was added to the membrane to detect the luminescence signal of immunoblotted proteins. Blots were imaged using the chemiluminescence measurer instrument Amersham Imager 600 (GE Healthcare).

1.4.1.1.1.16 Automated immunoblot analysis

The automated western blot was performed in the WES instrument (ProteinSimple) to visualize CalP. This assay is a hybrid system that combines protein migration like an SDS-PAGE and an immunoblot assay to highlight proteins with an antibody. Cells expressing CalP-FLAG and a WT control were grown to mid-exponential phase ON at 30ºC. Cell pellets were re-inoculated at OD_{600}=0.1 and cells were treated with 0.12 µg/mL MMC or left untreated. Cell pellets were resuspended in TE buffer with Triton-X (to enhance the resuspension of CalP). Resuspended cells were sonicated (see sonication procedure in section 5.2.6.2.1). One replicate of the cell lysate was heated at 100 °C for 5 minutes, and the other replicate remained at RT. The total protein content was estimated with the Lowry method (see protein quantification in section 5.2.6.2.4.1). 0.25, 0.5, and 1 µg/mL of CalP-FLAG were loaded into the WES plate. Two concentrations of anti-FLAG antibody were loaded in the plate: 1/50 and 1/100 to highlight CalP-FLAG with two different intensities. The samples loading into the WES plate and the running indications were done according to the manufacturer´s indications.

5.2.6.3 Biophysical and biochemical analysis

5.2.6.3.1 Mass spectrometry

1.4.1.1.1.17 Preparation of a handcasting SDS-PAGE gel

The separation of protein bands following CalP purification before MS/MS analysis requires a resolving gel without a stacking gel. To prepare a handcasting polyacrylamide gel without the stacking gel, it was required to set two rectangular glass plates in front of each other, leaving a gap to introduce the gel. The bottom must be pressed against the base to prevent leaking. To prepare 10 mL of a 10% polyacrylamide gel, the next reagents must be mixed and poured in between the two glass plates:

30% acrylamide bis (Severn Biotech/Cat. No. 20-9001-10)	5 mL
1.5 M Tris-HCl, pH 8.8 (Merck/cat. no. 648317)	3,75 mL
10% SDS (Severn Biotech/cat. no. 20-4000-10)	150 µL

dH_2O	6.03 mL
TEMED (Merck/cat. no. 110732)	7.5 µL
10% APS (Merck/cat. no. A3678)	75 µL

Following the pouring of the liquid gel, the comb was added, trying to remove all bubbles from the gel. The gel must dry for at least 2 hrs to be completely solidified before loading the protein samples. After 2 hrs, the comb was removed and the solidified handcasting SDS-PAGE gel was disassembled from the holder. The gel was transferred to a running tank and the cuvette was filled with 500 mL of Novex Tris-Glycine buffer (Thermo-Fisher Scientific/cat. no. LC26754). To make the sample visible and denser in the cell of the gel, 2.5 µL of protein loading dye (NEB/cat. no. B7703S) was mixed with 10 µL of each protein sample and 12.5 µL of each sample was loaded on each well. The voltage applied by the power supplier (Bio-Rad/cat. no. 1645050) was 150V for no more than 10 min or until the blue bands entered the gel.

1.4.1.1.1.18 Preparation of trypsin digestion

The blue bands of each cell of the handcasting SDS-PAGE (see the procedure for preparing and running a stacking gel-free polyacrylamide gel in section 5.2.6.3.1.1) were cut and transferred to a microfuge tube. Gel slices containing CalP were prepared according to standard procedures adapted from Shevchenko et al. (2007) [741]. 1.5 µL of 30% EtOH (VWR chemicals/cat. no. 20821.330) was pipetted into each tube and incubated at 65ºC for 30 min to discolour the protein loading dye (NEB/cat. no. B7703S). The EtOH was removed and 1.5 µL of 10 mM dithiothreitol (DTT) (Sigma-Aldrich/cat. no. D0632) dissolved in 50 mM triethylammonium bicarbonate buffer (TEAB) (Sigma-Aldrich/cat. no. 140023) was added to the solution. The solution was incubated for 30 min at 55ºC and DTT was removed from the tube. 1.5 µL of 30 mM iodoacetamide (IAA) (Sigma-Aldrich/cat. no. I6125) dissolved in 50 mM TEAB buffer was added to the tube and incubated at RT for 30 min in a dark tube to prevent dark damaging the reagent. The tube was vortexed every 5 min to homogenise the mixture and the IAA was removed. 1.5 µL of 50 mM TEAB buffer mixed with 50% acetonitrile (Thermo-Fisher Scientific/

cat. no. 268260025) (in 50% dH_2O) (TEAB/50%/ACN) was added to the tube and vortexed to wash the piece of the gel. TEAB/50%/ACN was removed from the tube, and 1.5 µL of 50 mM TEAB was added and vortexed. TEAB was removed and the slice of gel was cut into pieces of 1x1 mm on a Petri dish with a scalpel. A drop of TEAB was used to make the cutting process easier. Every fragment of the gel was transferred to a low-binding tube (Eppendorf) and the name of the sample and size of the fragment were written on the side of the tube, but not on the lid. 1.5 µL of TEAB/50%/ACN was added to the fragments and vortexed for 20 min to wash them. 1.5 µL of TEAB/50%/ACN was removed and substituted by 100% acetonitrile (Thermo-Fisher Scientific/268260025), making the gel hard and white. The acetonitrile was substituted by another 1.5 µL of fresh 100% acetonitrile to re-wash the samples and finally removed completely to start the freeze-drying step. The lid of the tube was closed, and one small hole was made in the lid of each tube with a needle. The tubes were placed in the speed vacuum (GeneVac EZ-2 Plus SpeedVac Concentrator) for 30 min with the OH^- program selected to dehydrate the gel fragments. Eventually, fragments were sent for MS/MS analysis (see tandem MS/MS analysis details in section 5.2.6.3.1.3).

1.4.1.1.1.19 Tandem mass spectrometry analysis

The purified proteins of WT and *ΔcalP::*P_{calP}*-calP-flag* strains required a preparatory process before being apt for MS/MS analysis. Once the gel fragments were washed and dehydrated with acetonitrile (Thermo-Fisher Scientific/cat. no. 268260025) to finish the preparatory process (see the preparation of gel fragments for trypsin digestion in section 5.2.6.3.1.3), fragments were sent for MS/MS analysis. The screening for interacting partners of CalP in WT and *ΔcalP::*P_{calP}*-calP-flag* with and without MMC was done by Dr Carlo Martins and Dr Gerhard Saalbach from the Proteomics Facility of the JIC.

Before the MS/MS analysis, the gels were soaked with 50 mM TEAB containing 10 ng/µl of Sequencing Grade Trypsin (Promega/cat. no. V5111) and incubated at 40 °C for 8 h. The extracted peptide solution was dried down, and the peptides were dissolved in 3% acetonitrile (Thermo-Fisher Scientific/cat. no. 268260025) and

0.1% trifluoroacetic acid (TFA) (Thermo-Fisher Scientific/cat. no. 10723857). Aliquots were analysed by nanoLC-MS/MS on an Orbitrap Eclipse™ Tribrid™ mass spectrometer coupled to an UltiMate® 3000 RSLCnano LC system (Thermo-Fisher Scientific, Hemel Hempstead, UK). The samples were loaded and trapped using a pre-column with 0.1% TFA at 15 µl min^{-1} for 4 min. The trap column was then switched in line with the analytical column (nanoEase M/Z column, HSS C18 T3, 100 Å, 1.8 µm; Waters, Wilmslow, UK) for separation using the following gradient of solvents A (water, 0.1% formic acid (Sigma-Aldrich/cat. no. 85178)) and B (80% acetonitrile, 0.1% formic acid) at a flow rate of 0.2 µl min^{-1}:0-3 min 3% B (parallel to trapping); 4-10 min linear increase B to 9%; 10-70 min increase B to 40%; 70-90 min increase B to 60%; followed by a ramp to 99% B and re-equilibration to 3% B [1,2]. Data were acquired with the following mass spectrometer settings in positive ion mode: MS1/Orbitrap (OT): resolution 120K, profile mode, mass range *m/z* 300-1800, normalised. Automated Gain Control (AGC) target 100%, maximum fill time 50 ms; MS2/Ion Trap (IT): data-dependent analysis was performed using Higher-energy C-trap Dissociation (HCD) fragmentation with the following parameters: top 20 in IT turbo mode, centroid mode, isolation window 1.0 Da, charge states 2-5, threshold $1.0e^4$, CE=33, AGC target $1e^4$, max. inject time 35 ms, dynamic exclusion 1 count, 15 s exclusion, exclusion mass window ±10 ppm [3].

Peak lists were generated from the MS raw files with MSConvert v2.0, from Proteowizard [742]. The final search was performed using in-house Mascot Server 2.7.0.1 (Matrixscience, London, UK) on the *Caulobacter vibrioides* protein sequence (Uniprot, 17/09/2020, 3859 entries) and the MaxQuant contaminants database (250 entries) [4]. For this search, a precursor tolerance of 6 ppm and a fragment tolerance of 0.6 Da were used. The enzyme was set to trypsin with a maximum of 2 allowed missed cleavages. Oxidation (M), deamidation (N/Q) and acetylation (protein N-terminus) were set as variable modifications and carbamidomethylation (CAM) of cysteine as fixed modification. The Mascot search results were imported into Scaffold 4.11.0 for visualization.

Annotations

1) For the MS/MS experiment, the gradient was as follows:
0-4 min 3% B (parallel to trapping); 4-10 min linear increase B to 8%; 10-60 min increase B to 25%; 60-80 min increase B to 38%; 80-90 min increase B to 60% followed by a ramp to 99% B and re-equilibration to 3% B, for a total of 118 min.

2) For the MS/MS experiment, the gradient was:
0-4 min 3% B (parallel to trapping); 4-10 min linear increase B to 7%; 10-70 min increase B to 37%; 70-90 min increase B to 55%; followed by a ramp to 99% B and re-equilibration to 3% B, for a total of 122 min.

3) For the MS/MS experiment, the mass spectrometry conditions were:
MS1/Orbitrap (OT): resolution 120K, profile mode, mass range *m/z* 300-1800, normalised. Automated Gain Control (AGC) target 50%, maximum fill time 50 ms; MS2/Orbitrap (OT): 15 K resolution, data-dependent analysis was performed using Higher-energy C-trap Dissociation (HCD) fragmentation with the following parameters: Top 20 in OT mode, centroid mode, isolation window 2.0 Da, charge states 2-5, threshold $1.0e^4$, CE=30, AGC target $1e^4$, max. inject time 22 ms, dynamic exclusion 1 count, 15 s exclusion, exclusion mass window ±5 ppm.

4) For the MS/MS experiment the specific sequences were added to the search.

5.2.6.3.2 High-performance liquid chromatography (HPLC) and MS/MS for the MMC-TR conjugation

The conjugation of compounds to generate MMC-TRC started with two precursors: MMA (Toronto Research Chemicals/cat. no. M371890) and TRC (AAT/cat. no. 482). The reagents needed for the conjugation were:

MMA (MW: 349.13; 2.5 mg, 7.2 µmol, 1 equimolar)
TRC 5.0 mg, 7.24 µmol, 1.01 equimolar)
TEA (1.03 mg, 10.7 µmol, 1.49 equimolar)
MeOH (0.5 ml)

The reaction was performed in an amber HPLC vial (2 ml). TRC was dissolved in 250 µL MeOH (Thermo-Fisher Scientific/cat. no. 325740025) and TEA (?) was added in 3 portions: 3 x 1.43 µl. 10 µl of TRC was put aside to be used as a standard. 2.5 mg MMA was dissolved in 250 µl MeOH. 10 µl of MMA was put aside to be used as a standard). The solutions were combined and stirred at ambient temperature. The reaction progress was monitored by TLC (SiO2, 20% EtOH in CH_2Cl_2). When MMA was consumed after 24 h, the mixture was purified by C18-RP HPLC using a gradient of acetonitrile (Thermo-Fisher Scientific/cat. no. 268260025) against the water with UV detection at 500 nm.

HPLC Instrument: Dionex Ultimate 3000, Rheodyne injection valve, loop 500 µl.
Column: Phenomenex, Gemini NX-C18 110 A, axial compression, particle size 5 µm, dimension 150 x 21.2 mm (CV=53 ml, VV=40 ml). Part Number: 00F-4454-P0-AX.

Solvent A: water
Solvent B: acetonitrile

HPLC Method: at a flow rate of 20 ml/min, 5% B for 2 min. The gradient was increased to 100% B over 20 min and held for 2 min. The gradient was reduced again to 5% B over 1 min and equilibrated for 4 min with UV detection at 500 nm. Five fractions were collected (MRC63-1 to MRC63-5). The solvent was evaporated by the freeze-drying method (Genevac) and the residue was stored in the dark at -20^{o}C. HR-MS (Synapt G2 Si) indicated the presence of the target analyte in the sample MRC63-4 (blue solid). Martin Rejzek did the HPLC analysis of MMC-TRC from the JIC Biochemistry Facility.

5.2.6.3.3 Mass photometry analysis

CalP was isolated by immunoprecipitation as described in the protein isolation section 5.2.6.2.3. The use of the Triton-X (Merck/cat. no. 1086031000) detergent may distort the analysis of the protein mass. Because of this, the cell breakage and the elution from the precipitation columns were done by omitting the addition of

Triton-X to the lysis and elution buffer (Miltenyi Biotec/cat. no. 130-101-591). 100 nM of CalP in a TAE buffer (without Triton-X) was sent for analysis. All mass photometric measurements were recorded at 25°C using the Refeyn OneMP mass photometer (Refeyn). The instrument was calibrated with a native marker unstained protein standard mixture (Thermo-Fisher Scientific/cat. no. LC0725), containing proteins from 20 to 1200 KDa. The following masses were used to generate a standard calibration curve: 146, 480, and 1,048 KDa. PEP was purified in TEA buffer (Formedium/cat. no. TAE5000) as described above and concentrated to 130 nM. 2 µL of PEP was applied to 8 µL buffer on a coverslip, resulting in a final concentration of ~25 nM. Movies were recorded using AcquireMP software (version R1) for 60 sec with a frame rate of 60 per sec and using a large field of view. The data were processed using DiscoverMP software (version R1.2). The mass of the PEP complex was estimated by fitting a Gaussian distribution into mass histograms and taking the value at the mode of the distribution. Dr Abbas Maqbool and Julia Mundy from the Biophysical Analysis Facility of the JIC did the MP analysis of WT and *ΔcalP*::P_{calP}-*calP-flag* strains.

Appendix

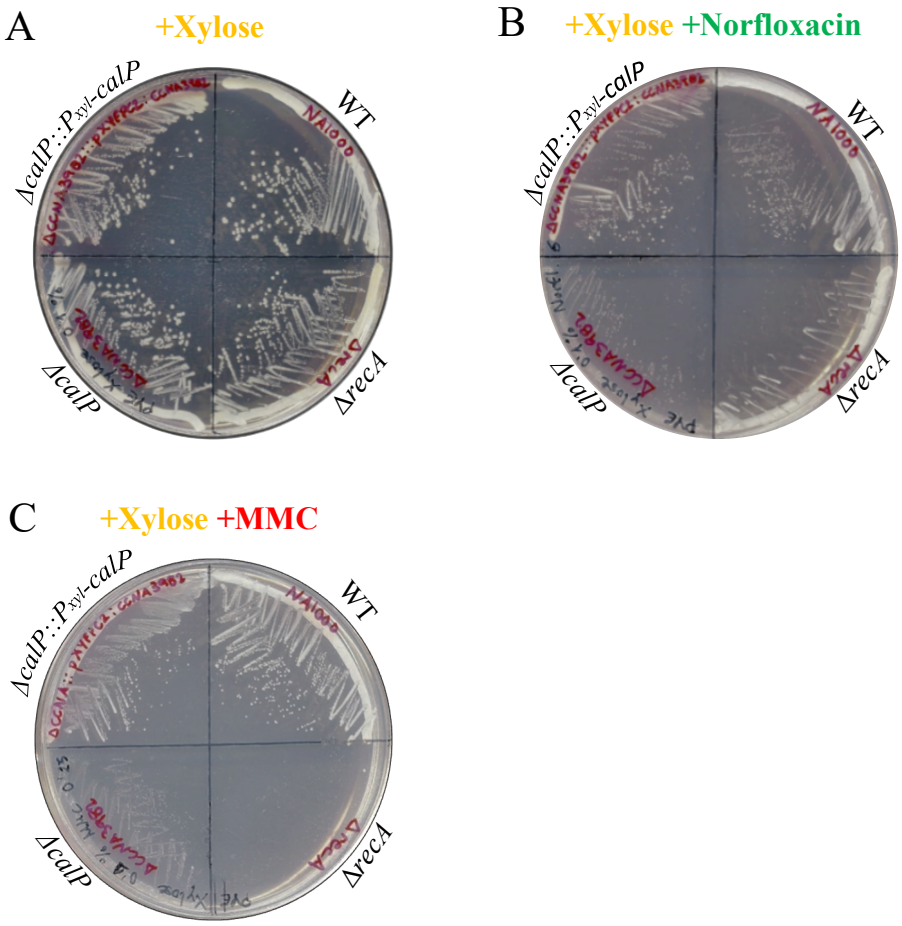

Fig. A1. *ΔcalP* was successfully complemented in a solid medium upon treatment with MMC. The plates shown in the figure assess the complementation of the WT phenotype after the insertion of *calP* back into the Δ*calP* background when the medium was supplemented with MMC or unsupplemented. Cells were grown to mid-exponential phase and cultures were diluted to an $OD_{600}=3.3\cdot10^{-4}$. Cells were streaked onto PYE agar plates supplemented with (A) 0.3% xylose, (B) 0.3% xylose and 6 µg/mL norfloxacin, and (C) 0.3% xylose and 0.25 µg/mL MMC. Plates were incubated for 48 hrs at 30°C. The strains WT, *ΔrecA*, and Δ*calP* were included as controls. Plates were divided into four sectors and each strain was streaked out as follows: *ΔcalP*::P_{xyl}-*calP* (top left), WT (top right), *ΔrecA* (bottom right), and *ΔcalP* (bottom left).

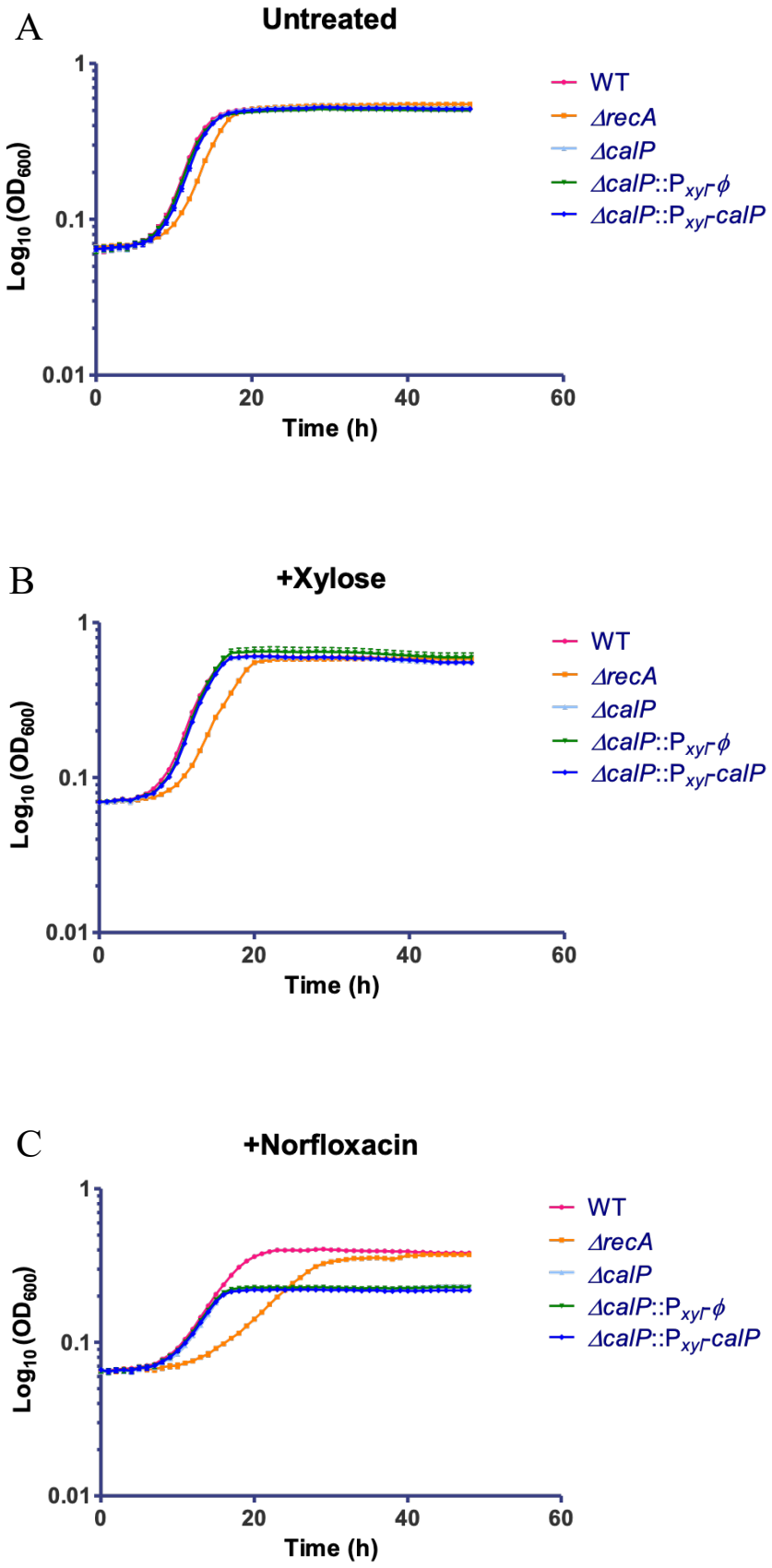
A
Untreated
Log10 (OD600)
1
0.1
0.01
0
20
40
60
Time (h)
WT
ΔrecA
ΔcalP
ΔcalP::Pxyl-ϕ
ΔcalP::Pxyl-calP
B
+Xylose
Log10 (OD600)
1
0.1
0.01
0
20
40
60
Time (h)
WT
ΔrecA
ΔcalP
ΔcalP::Pxyl-ϕ
ΔcalP::Pxyl-calP
C
+Norfloxacin
Log10 (OD600)
1
0.1
0.01
0
20
40
60
Time (h)
WT
ΔrecA
ΔcalP
ΔcalP::Pxyl-ϕ
ΔcalP::Pxyl-calP

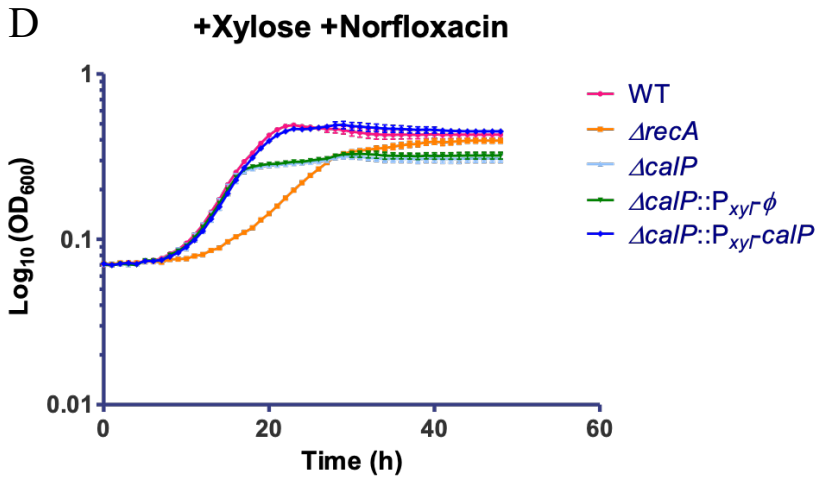

Fig. A2. An ectopic expression of *calP* restored the tolerance of the *ΔcalP* strain to norfloxacin. Growth curves testing the complementation of *ΔcalP*::P_{xyl}-*calP* in the presence and absence of 6 µg/mL norfloxacin in a liquid medium. The WT, *ΔrecA, ΔcalP,* and *ΔcalP*::P_{xyl}-*ø* strains were used as controls. To induce *calP* expression, (under a xylose-inducible promoter) in strains carrying the pXYFPC- 2 vector, the medium was supplemented with 0.1% xylose when necessary. Cells were grown to mid-exponential phase in a PYE medium to an OD_{600}=0.5 and cultures were diluted to an $OD_{600}=3.3\cdot10^{-4}$. Cells were mixed with 6 µg/mL norfloxacin when needed and incubated for 48 hrs at 30°C before the OD_{600} was measured hourly in an automated plate reader. Three technical replicates were used to calculate the OD_{600} mean. Plot lines correspond to a medium with (A) no additives, (B) supplemented with 0.1% xylose, (C) supplemented with 6 µg/mL norfloxacin, or (D) supplemented with 0.1% xylose and 6 µg/mL norfloxacin.

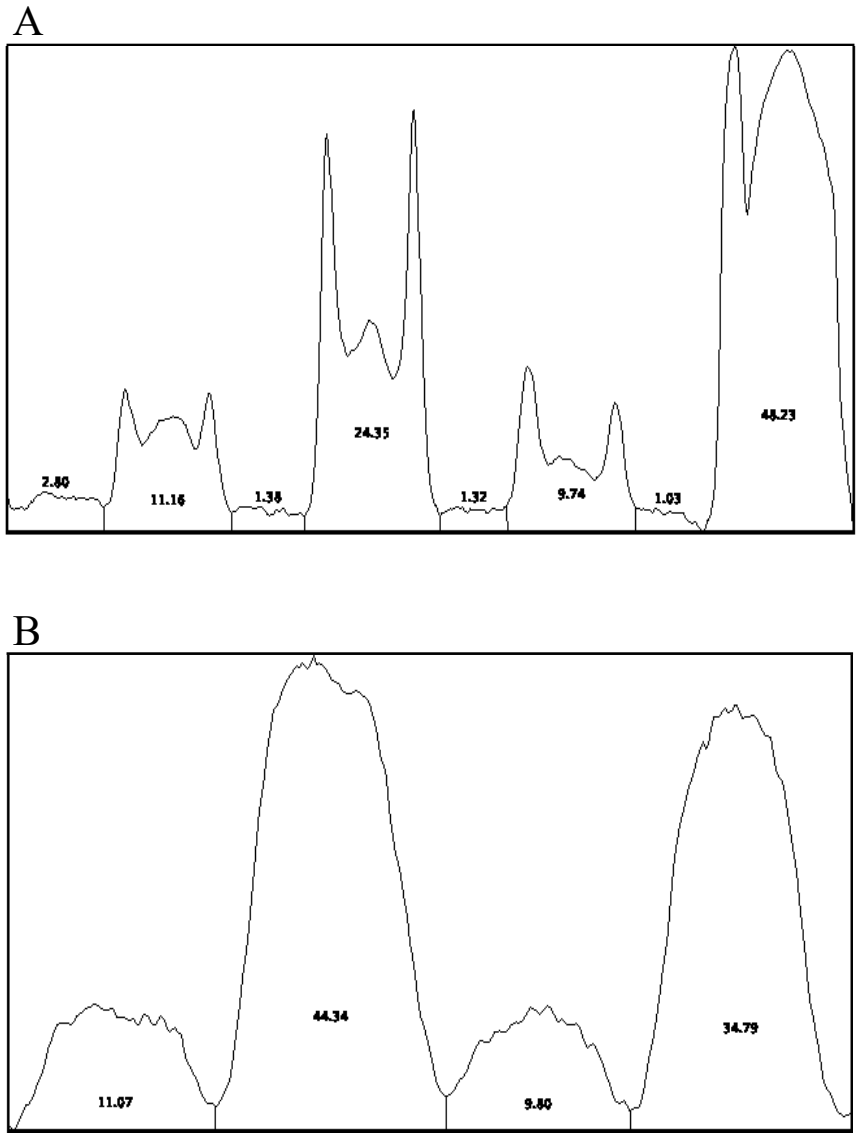

Fig. A3. *calP* shows a different polymerisation pattern when expressed under different promoters. Intensity measurement of CalP-FLAG bands in an immunoblot assay when *C. crescentus* was challenged or not with MMC. The graphs show the peak areas representing different protein band intensities of the immunoblots shown in Fig. 15 (Fig. 15A corresponds to Fig. A3A and Fig. 15C corresponds to Fig. A3B). The percentage exhibited in each peak area is represented in a bar chart in Fig. 15 (Fig. 15B correspond to Fig. A3A and Fig. 15D corresponds to Fig. A3B). The numbers represent the relative percentage of band intensity compared to other bands in the sample. A higher peak indicates a higher intensity of the CalP band. (A) The four peaks on the left side of the graph represent *ΔcalP*::P_{xyl}*-calP-flag* bands and the four peaks on the right correspond to *ΔcalP*::P_{xyl}*-scrambled calP-flag*

bands. The protein bands of both strains which are represented with each peak area were isolated from cells grown in a medium with (from left to right) no additives, supplemented with 0.1% xylose, supplemented with 0.12 μg/mL MMC, or supplemented with 0.1% xylose and 0.12 μg/mL MMC. (B) The two peaks on the left of the graph belong to *ΔcalP*::P_{calP}-*calP-flag* bands and the two peaks on the right belong to *ΔcalP*::P_{calP}-*scrambled calP-flag* bands. Each strain was (from left to right) unsupplemented or supplemented with 0.12 μg/mL MMC.

A

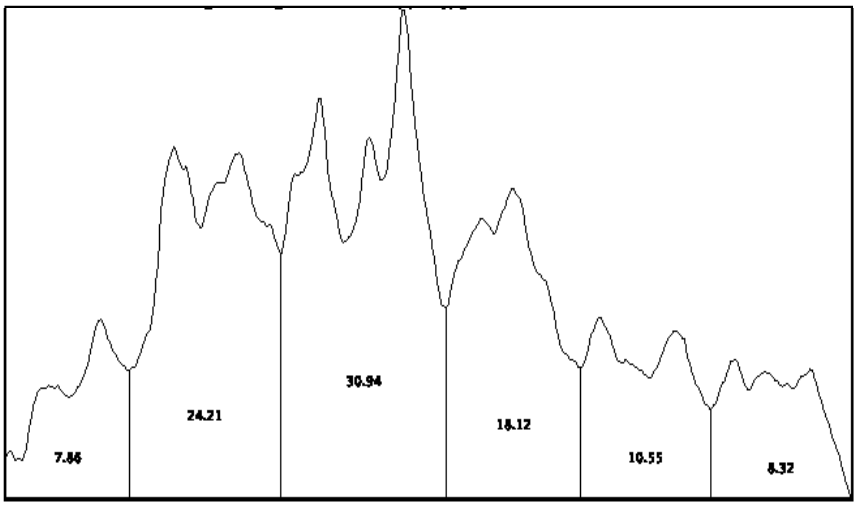
7.86
24.21
30.94
18.12
10.55
8.32

B

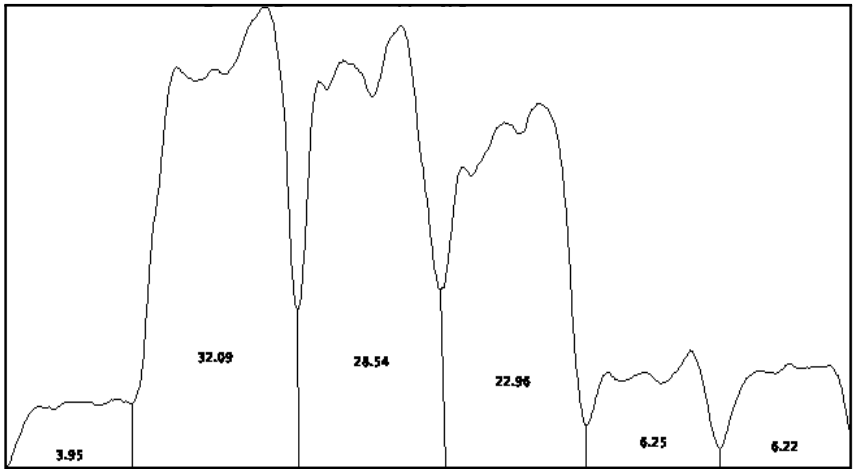
3.95
32.09
28.54
22.96
6.25
6.22

C

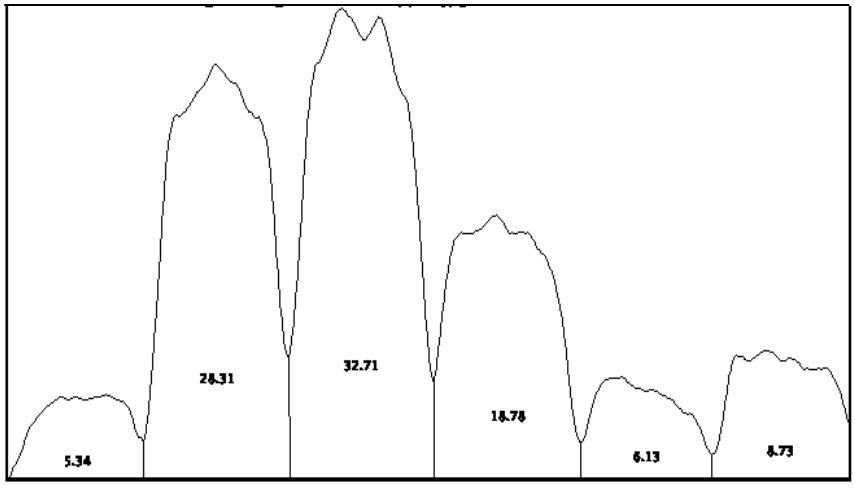
5.34
28.31
32.71
18.78
6.13
8.73

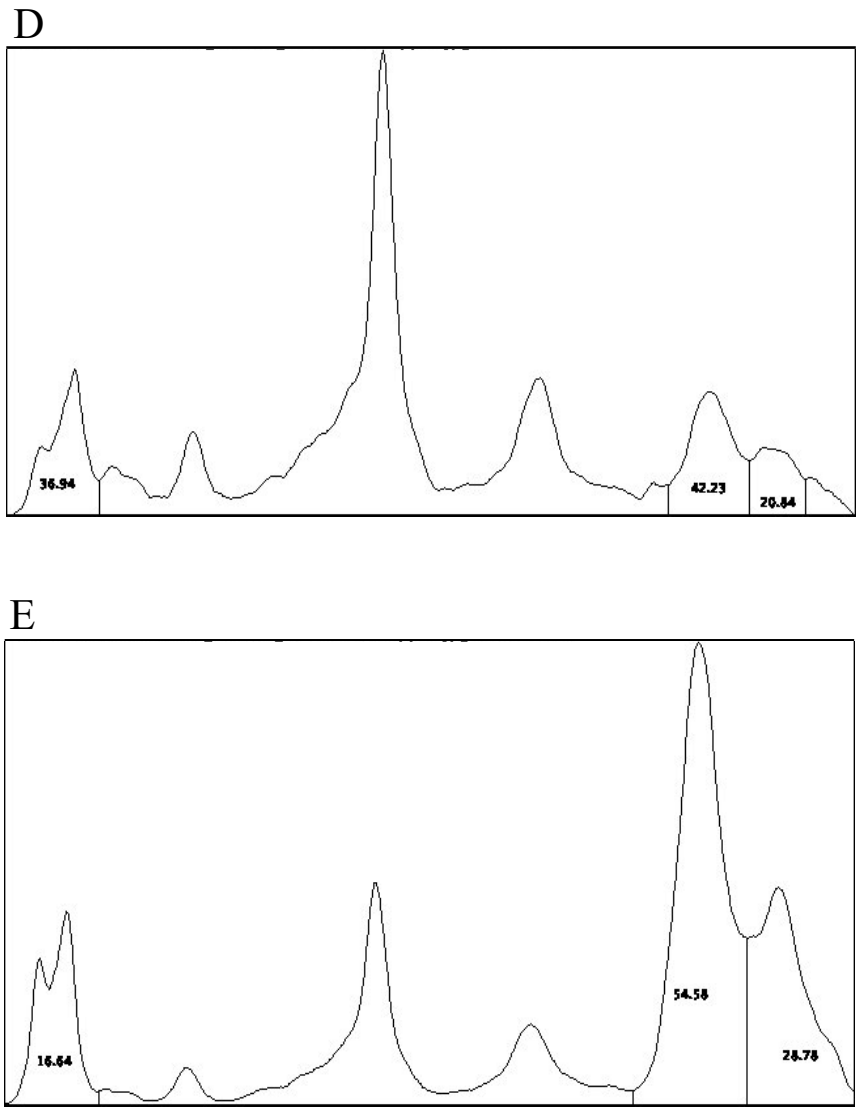

Fig. A4. *C. crescentus* increases CalP production when exposed to DDA. Intensity measurement of CalP-FLAG bands in an immunoblot assay when *C. crescentus ΔcalP*::P$_{calP}$-*calP-flag* was challenged or not with DDA. The graph shows the peak areas of different protein bands in a western blot shown in Fig. 16A. The numbers represent the relative percentage of band intensities compared to other bands in the sample. The percentage exhibited in each peak area is represented in a bar chart in Fig. 16. Each band corresponded to the band intensity of CalP-FLAG when cells were treated with a distinct DDA. A higher peak indicates a higher intensity of the CalP band. (A) 8 KDa monomeric CalP bands. Each peak area corresponds to a protein band isolated from cells grown in (from left to right) an unsupplemented medium or a medium supplemented with 0.12 μg/mL MMC, 1.5 mM MMS, 4 μg/mL norfloxacin, 15 mM HU, or 0.5 μg/mL novobiocin. The percentage value of

this figure is represented in the bar chart in Fig. 16B. (B) 60 KDa multimeric CalP bands. The order of the peak areas as in A. The percentage value of this figure is represented in the bar chart in Fig. 16C. (C) 75 KDa multimeric CalP bands. The order of the peak areas as in B. The percentage value of this figure is represented in the bar chart in Fig. 16D. (D) Untreated CalP-FLAG bands. The peak areas (from left to right) correspond to 8 KDa, 60 KDa, and 75 KDa. The percentage value of this figure is represented in the bar chart in Fig. 16E. (E) MMC-treated CalP-FLAG bands. The order of the peak areas as in D. The percentage value of this figure is represented in the bar chart in Fig. 16F.

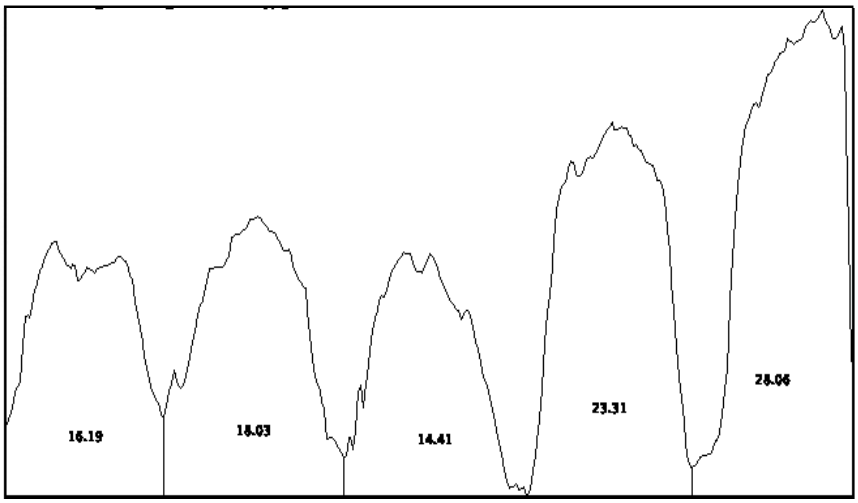

Fig. A5. CalP production in *C. crescentus* increases proportionally to the MMC concentration. Intensity measurement of CalP-FLAG bands in an immunoblot assay when *C. crescentus ΔcalP*::P$_{calP}$-*calP-flag* was challenged by increasing concentrations of MMC. The graph shows the peak areas of different protein bands in a western blot shown in Fig. 17A. The numbers into the peak area represent the relative percentage of band intensity compared to other bands in the sample. The percentage exhibited in each peak area is represented in a bar chart in Fig. 17B. Each peak corresponds to a CalP-FLAG band isolated from cells treated with 0, 0.05, 0.1, 0.25, or 0.5 μg/mL MMC from left to right. A higher peak indicates a higher intensity of the CalP band. The percentage value of this figure is represented in the bar chart in Fig. 17B.

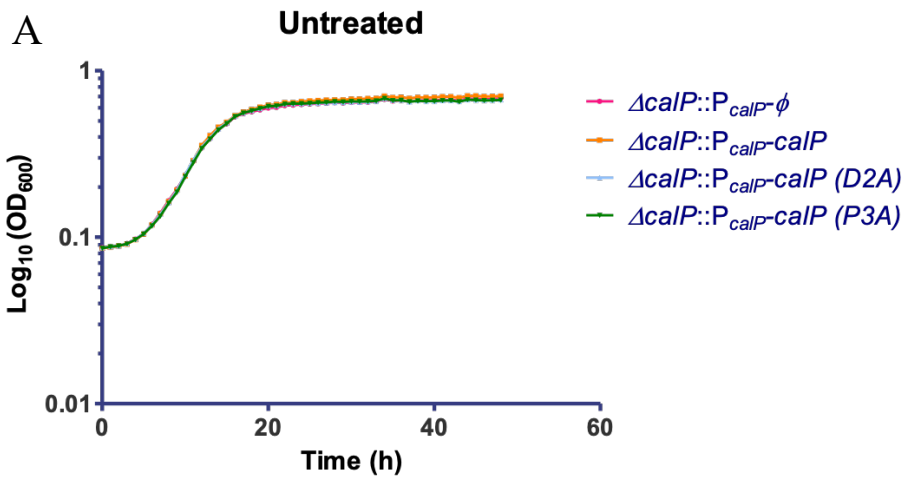
A
Untreated
1
0.1
0.01
Log10(OD600)
0
20
40
60
Time (h)
ΔcalP::PcalP-ϕ
ΔcalP::PcalP-calP
ΔcalP::PcalP-calP (D2A)
ΔcalP::PcalP-calP (P3A)

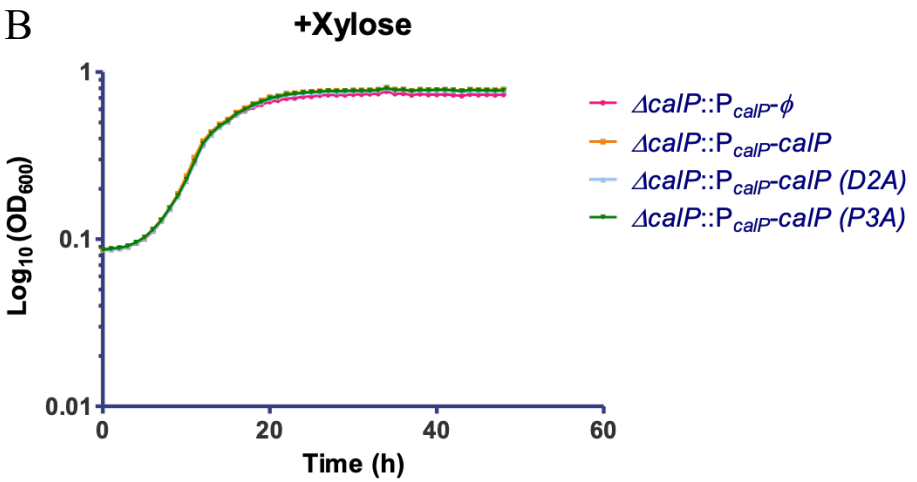
B
+Xylose
1
0.1
0.01
Log10(OD600)
0
20
40
60
Time (h)
ΔcalP::PcalP-ϕ
ΔcalP::PcalP-calP
ΔcalP::PcalP-calP (D2A)
ΔcalP::PcalP-calP (P3A)

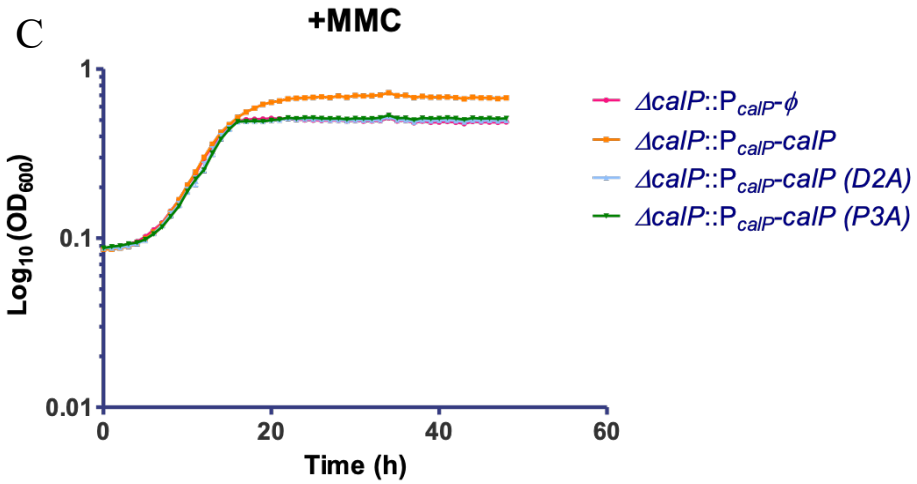
C
+MMC
1
0.1
0.01
Log10(OD600)
0
20
40
60
Time (h)
ΔcalP::PcalP-ϕ
ΔcalP::PcalP-calP
ΔcalP::PcalP-calP (D2A)
ΔcalP::PcalP-calP (P3A)

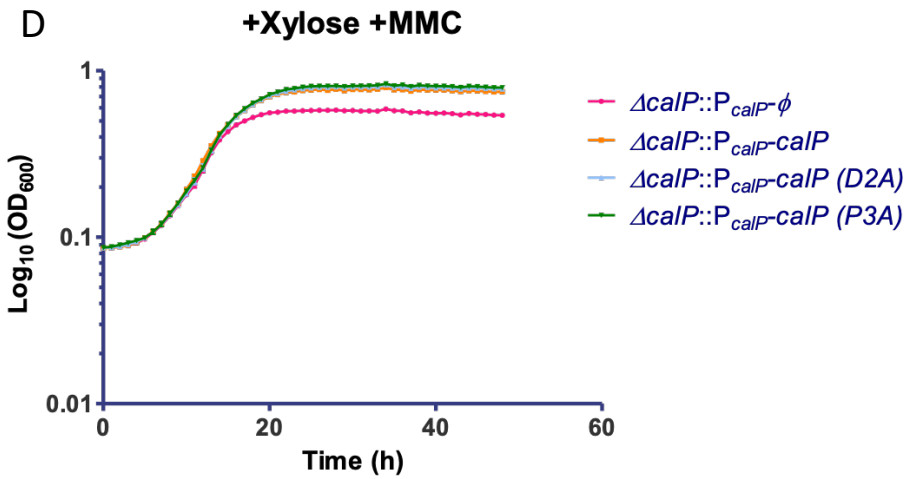

Fig. A6. *ΔcalP* complementation with *calP* derivative mutants restored the WT phenotype of every *C. crescentus* strain except the 2nd, and 3rd amino acid derivative mutants when challenged with MMC to tolerate MMC. Plot showing the *ΔcalP* complementation test with *calP* derivative mutants when exposed to MMC. Each *calP* derivative was ectopically expressed from the xylose-inducible promoter (P_{xyl}) harboured in the integrative plasmid pXYFPC-2 in a *C. crescentus ΔcalP* background. Mutant strains were grown in a PYE liquid medium to mid-exponential phase at 30ºC and diluted to $3.3x10^{-4}$. Cultures contained (A) no additives, (B) 0.1% xylose, (C) 0.12 µg/mL MMC, (D) or 0.1% xylose and 0.12 µg/mL MMC. Strains of each growth curve are *ΔcalP*::P_{xyl}-*ø* (magenta line), *ΔcalP*::P_{xyl}-*calP-flag* (orange line), *ΔcalP*::P_{xyl}-*calP (D2A)-flag* (light-blue line), and *ΔcalP*::P_{xyl}-*calP (P3A)-flag* (green line). 96-well plates were incubated at 30 °C for 48 hrs in an automated plate reader. The OD_{600} was measured hourly and the average of three cultures was taken to generate the plot.

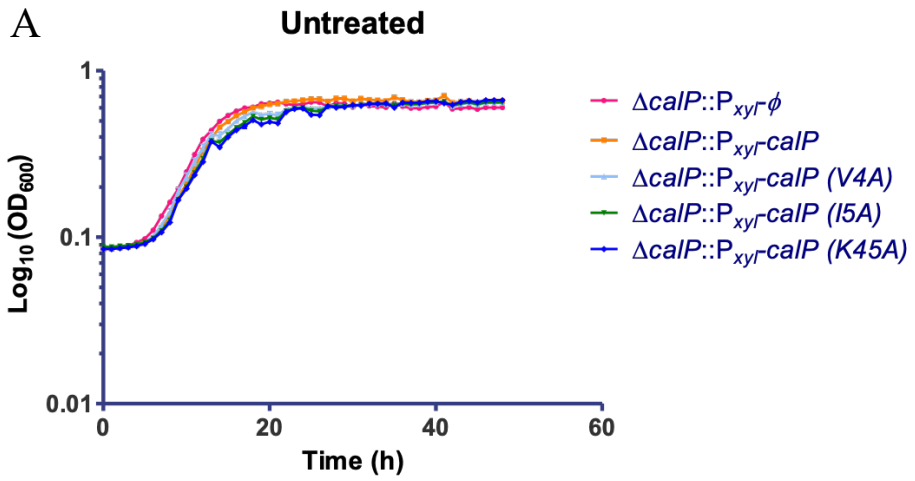
A
Untreated
1
0.1
0.01
Log10 (OD600)
0
20
40
60
Time (h)
ΔcalP::Pxyl-ϕ
ΔcalP::Pxyl-calP
ΔcalP::Pxyl-calP (V4A)
ΔcalP::Pxyl-calP (I5A)
ΔcalP::Pxyl-calP (K45A)

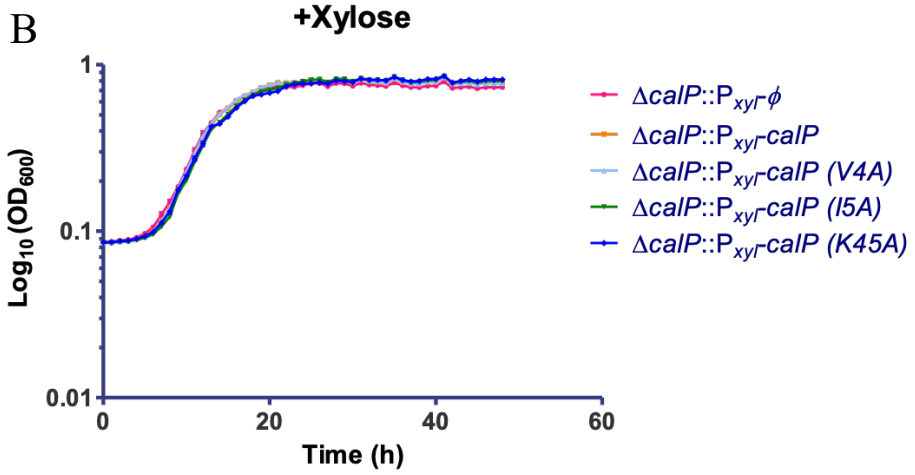
B
+Xylose
1
0.1
0.01
Log10 (OD600)
0
20
40
60
Time (h)
ΔcalP::Pxyl-ϕ
ΔcalP::Pxyl-calP
ΔcalP::Pxyl-calP (V4A)
ΔcalP::Pxyl-calP (I5A)
ΔcalP::Pxyl-calP (K45A)

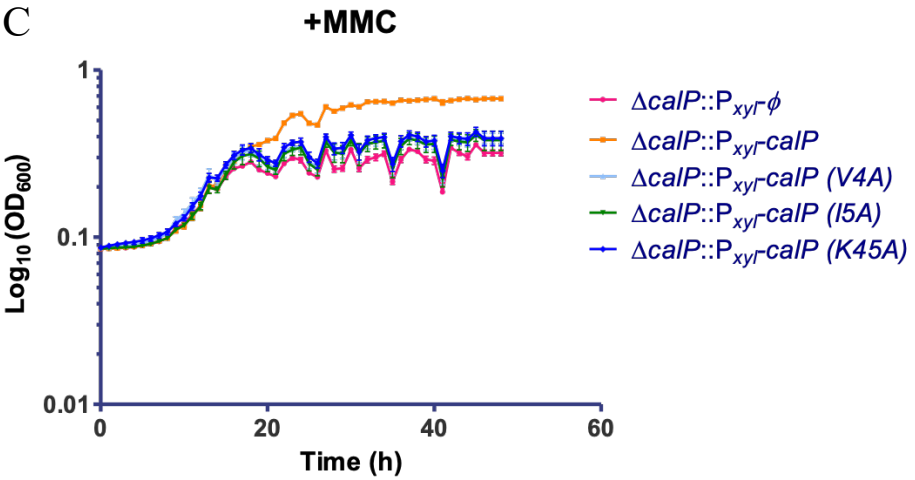
C
+MMC
1
0.1
0.01
Log10 (OD600)
0
20
40
60
Time (h)
ΔcalP::Pxyl-ϕ
ΔcalP::Pxyl-calP
ΔcalP::Pxyl-calP (V4A)
ΔcalP::Pxyl-calP (I5A)
ΔcalP::Pxyl-calP (K45A)

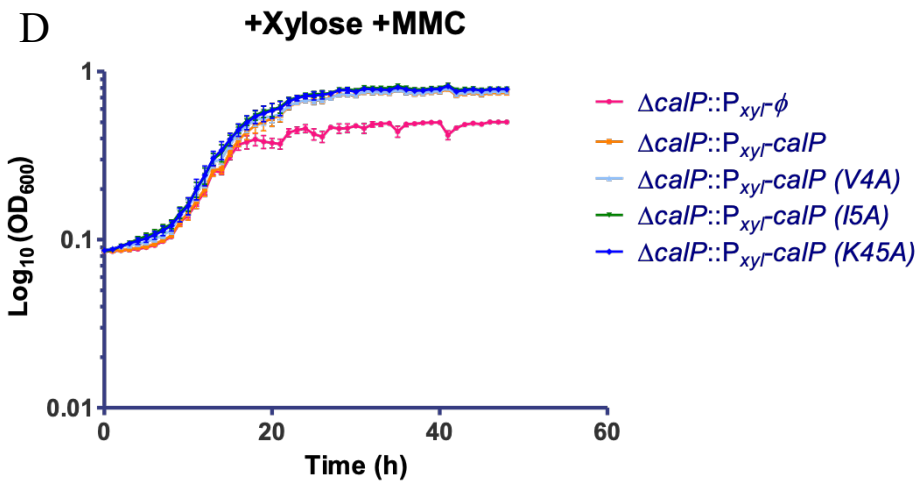

Fig. A7. *ΔcalP* complementation with *calP* derivative mutants restored the WT phenotype of every *C. crescentus* strain except the 4th, 5th, and 45th amino acid mutants when challenged with MMC. Plot showing the *ΔcalP* complementation test with truncated *calP* derivatives when challenged with MMC. *calP* mutant derivatives were ectopically expressed from the xylose-inducible promoter (P_{xyl}) harboured in the integrative plasmid pXYFPC-2 in the *ΔcalP* background of *C. crescentus*. Complemented *C. crescentus ΔcalP* cells were grown in a liquid PYE medium to mid-exponential phase at 30ºC and diluted to $3.3x10^{-4}$. Culture contained (A) no additives, (B) 0.1% xylose, (C) 0.12 µg/mL of MMC, (D) or 0.1% xylose and 0.12 µg/mL of MMC. Strains of each growth curve are *ΔcalP*::P_{xyl}-*ø* (magenta line), *ΔcalP*::P_{xyl}-*calP-flag* (orange line), *ΔcalP*::P_{xyl}-*calP (V4A)-flag* (light-blue line), and *ΔcalP*::P_{xyl}-*calP (I5A)-flag* (green line), *ΔcalP*::P_{xyl}-*calP (K45A)-flag* (purple line). 96-well plates were incubated at 30 °C for 48 hrs with orbital shaking. The OD_{600} was measured at the indicated times, and the average of three cultures was taken.

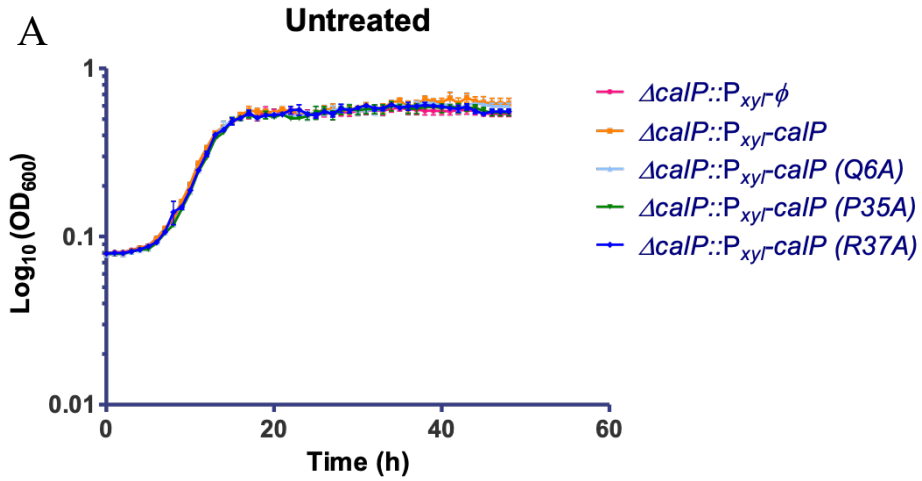
A
Untreated
Log10 (OD600)
1
0.1
0.01
0
20
40
60
Time (h)
ΔcalP::Pxyl-ϕ
ΔcalP::Pxyl-calP
ΔcalP::Pxyl-calP (Q6A)
ΔcalP::Pxyl-calP (P35A)
ΔcalP::Pxyl-calP (R37A)

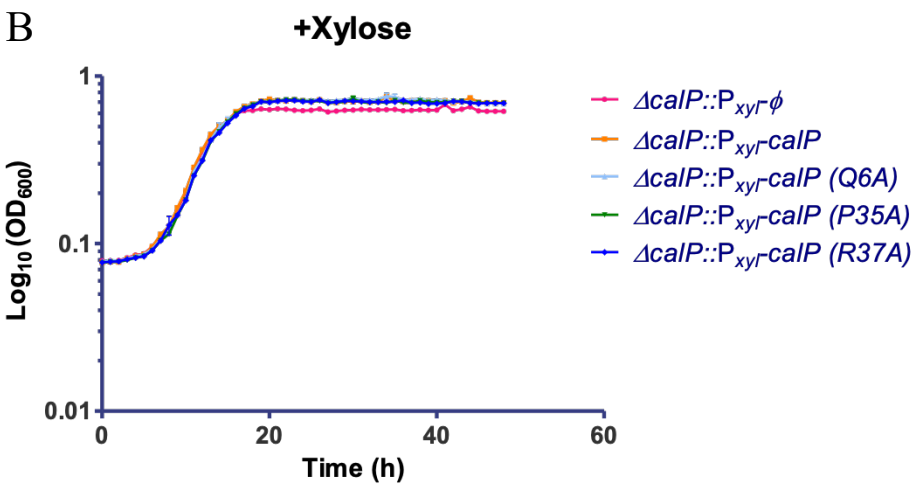
B
+Xylose
Log10 (OD600)
1
0.1
0.01
0
20
40
60
Time (h)
ΔcalP::Pxyl-ϕ
ΔcalP::Pxyl-calP
ΔcalP::Pxyl-calP (Q6A)
ΔcalP::Pxyl-calP (P35A)
ΔcalP::Pxyl-calP (R37A)

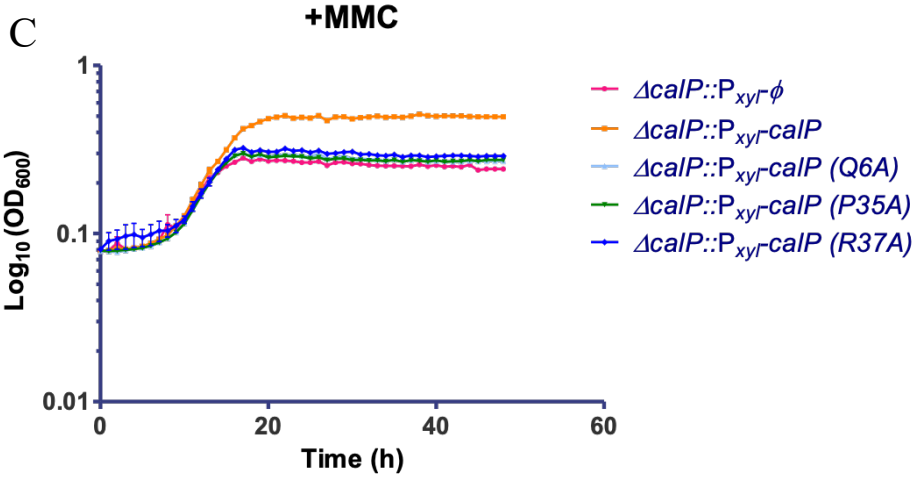
C
+MMC
Log10 (OD600)
1
0.1
0.01
0
20
40
60
Time (h)
ΔcalP::Pxyl-ϕ
ΔcalP::Pxyl-calP
ΔcalP::Pxyl-calP (Q6A)
ΔcalP::Pxyl-calP (P35A)
ΔcalP::Pxyl-calP (R37A)

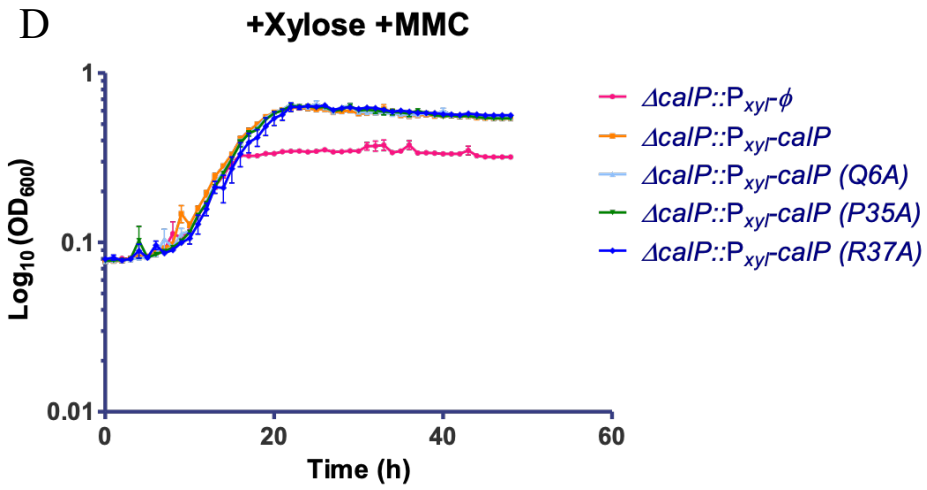

Fig. A8. *ΔcalP* complementation with *calP* derivative mutants restored the WT phenotype of every *C. crescentus* strain except the 6th, 35th, and 37th amino acid mutants when challenged with MMC. Plot showing the *ΔcalP* complementation test with truncated *calP* derivatives when exposed to MMC. *calP* mutant derivatives were ectopically expressed from the xylose-inducible promoter (P_{xyl}) harboured in the integrative plasmid pXYFPC-2 in the *ΔcalP* background of *C. crescentus*. Complemented *ΔcalP C. crescentus* cells were grown in a liquid PYE medium to mid-exponential phase at 30ºC and diluted to $3.3x10^{-4}$. Cultures contained (A) no additives, (B) 0.1% xylose, (C) 0.12 µg/mL of MMC, (D) or 0.1% xylose and 0.12 µg/mL of MMC. Strains of each growth curve are *ΔcalP*::P_{xyl}-*ø* (magenta line), *ΔcalP*::P_{xyl}-*calP-flag* (orange line), *ΔcalP*::P_{xyl}-*calP (Q6A)-flag* (light-blue line), and *ΔcalP*::P_{xyl}-*calP (P35A)-flag* (green line), *ΔcalP*::P_{xyl}-*calP (R37A)-flag* (purple line). 96-well plates were incubated at 30 °C for 48 hrs with orbital shaking. The OD_{600} was measured at the indicated times, and the average of three cultures was taken.

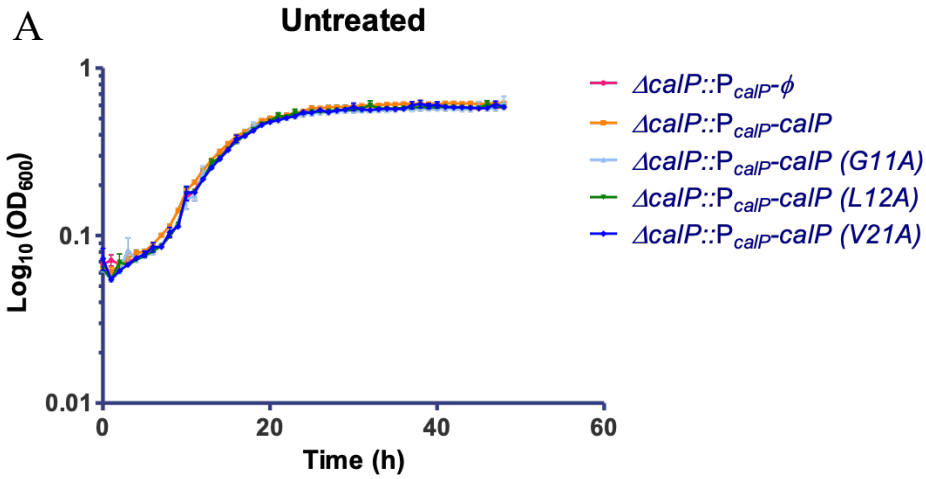
A
Untreated
1
0.1
0.01
Log10 (OD600)
0
20
40
60
Time (h)
ΔcalP::PcalP-ϕ
ΔcalP::PcalP-calP
ΔcalP::PcalP-calP (G11A)
ΔcalP::PcalP-calP (L12A)
ΔcalP::PcalP-calP (V21A)

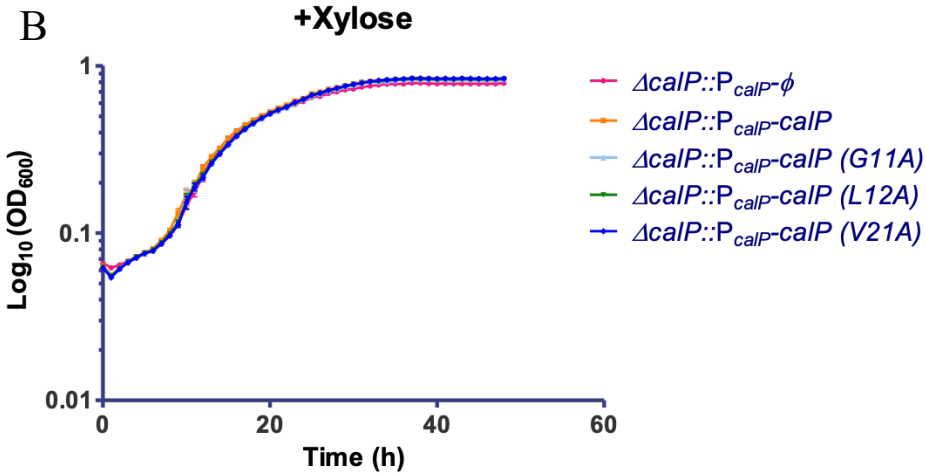
B
+Xylose
1
0.1
0.01
Log10 (OD600)
0
20
40
60
Time (h)
ΔcalP::PcalP-ϕ
ΔcalP::PcalP-calP
ΔcalP::PcalP-calP (G11A)
ΔcalP::PcalP-calP (L12A)
ΔcalP::PcalP-calP (V21A)

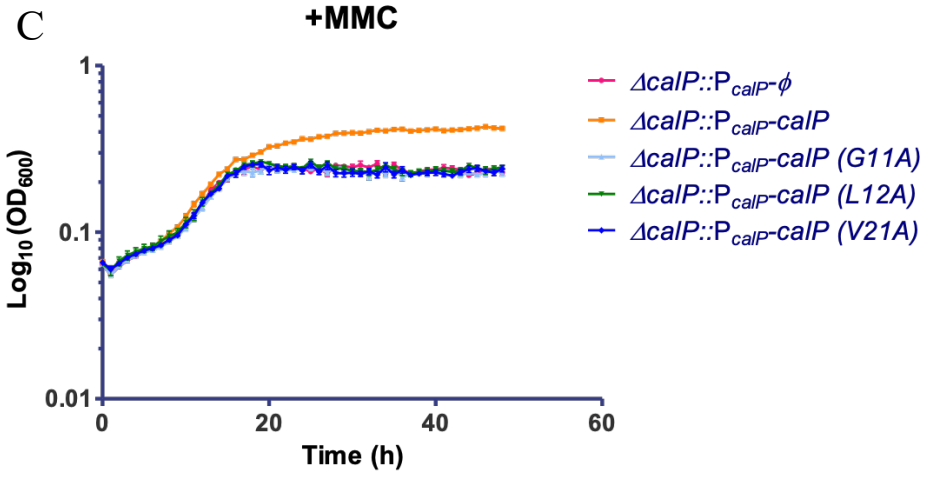
C
+MMC
1
0.1
0.01
Log10 (OD600)
0
20
40
60
Time (h)
ΔcalP::PcalP-ϕ
ΔcalP::PcalP-calP
ΔcalP::PcalP-calP (G11A)
ΔcalP::PcalP-calP (L12A)
ΔcalP::PcalP-calP (V21A)

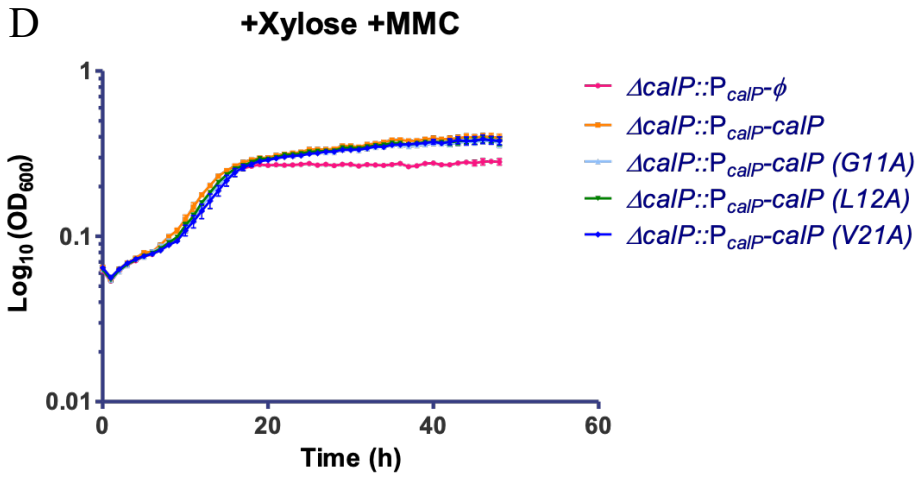

Fig. A9. *ΔcalP* complementation with *calP* derivative mutants restored the WT phenotype of every *C. crescentus* strain except the 11th, 12th, and 21st amino acid mutants when challenged with MMC. Plot showing the *ΔcalP* complementation test with truncated *calP* derivatives when exposed to MMC. *calP* mutant derivatives were ectopically expressed from the xylose-inducible promoter (P_{xyl}) harboured in the integrative plasmid pXYFPC-2 in *C. crescentus ΔcalP* background. Complemented *ΔcalP C. crescentus* cells were grown in a liquid PYE medium to mid-exponential phase at 30ºC and diluted to $3.3x10^{-4}$. Cultures contained (A) no additives, (B) 0.1% xylose, (C) 0.12 µg/mL of MMC, (D) or 0.1% xylose and 0.12 µg/mL of MMC. Strains of each growth curve are *ΔcalP*::P_{xyl}-*ø* (magenta line), *ΔcalP*::P_{xyl}-*calP-flag* (orange line), *ΔcalP*::P_{xyl}-*calP (G11A)-flag* (light-blue line), and *ΔcalP*::P_{xyl}-*calP (L12A)-flag* (green line), *ΔcalP*::P_{xyl}-*calP (V21A)-flag* (purple line). 96-well plates were incubated at 30 °C for 48 hrs with orbital shaking. The OD_{600} was measured at the indicated times, and the average of three cultures was taken.

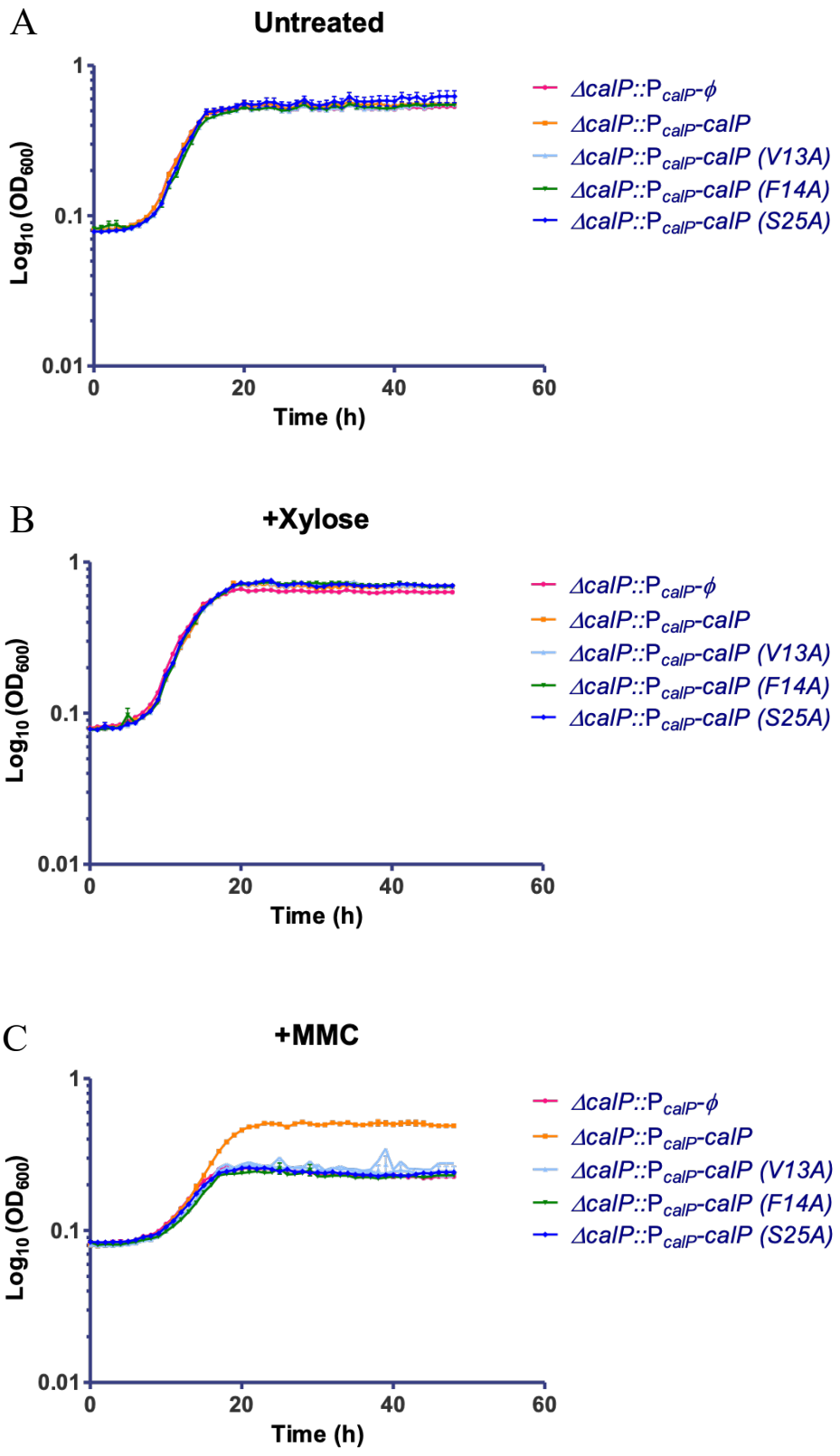
A
Untreated
1
0.1
0.01
Log10 (OD600)
0
20
40
60
Time (h)
ΔcalP::PcalP-ϕ
ΔcalP::PcalP-calP
ΔcalP::PcalP-calP (V13A)
ΔcalP::PcalP-calP (F14A)
ΔcalP::PcalP-calP (S25A)
B
+Xylose
1
0.1
0.01
Log10 (OD600)
0
20
40
60
Time (h)
ΔcalP::PcalP-ϕ
ΔcalP::PcalP-calP
ΔcalP::PcalP-calP (V13A)
ΔcalP::PcalP-calP (F14A)
ΔcalP::PcalP-calP (S25A)
C
+MMC
1
0.1
0.01
Log10 (OD600)
0
20
40
60
Time (h)
ΔcalP::PcalP-ϕ
ΔcalP::PcalP-calP
ΔcalP::PcalP-calP (V13A)
ΔcalP::PcalP-calP (F14A)
ΔcalP::PcalP-calP (S25A)

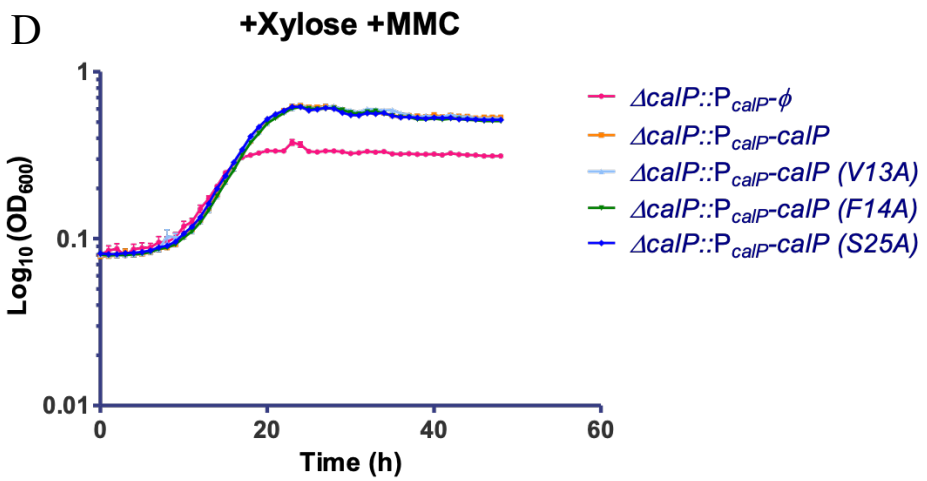

Fig. A10. *ΔcalP* complementation with *calP* derivative mutants restored the WT phenotype of every *C. crescentus* strain except the 13th, 14th, and 25th amino acid mutants when challenged with MMC. Plot showing the *ΔcalP* complementation test with truncated *calP* derivatives when exposed to MMC. *calP* mutant derivatives were ectopically expressed from the xylose-inducible promoter (P_{xyl}) harboured in the integrative plasmid pXYFPC-2 in the *ΔcalP* background of *C. crescentus*. Complemented *ΔcalP C. crescentus* cells were grown in a liquid PYE medium to mid-exponential phase at 30ºC and diluted to $3.3x10^{-4}$. Cultures contained (A) no additives, (B) 0.1% xylose, (C) 0.12 µg/mL of MMC, (D) or 0.1% xylose and 0.12 µg/mL of MMC. Strains of each growth curve are *ΔcalP*::P_{xyl}-*ø* (magenta line), *ΔcalP*::P_{xyl}-*calP-flag* (orange line), *ΔcalP*::P_{xyl}-*calP (V13A)-flag* (light-blue line), *ΔcalP*::P_{xyl}-*calP (F14A)-flag* (green line), and *ΔcalP*::P_{xyl}-*calP (S25A)-flag* (purple line). 96-well plates were incubated at 30 °C for 48 hrs with orbital shaking. The OD_{600} was measured at the indicated times, and the average of three cultures was taken.

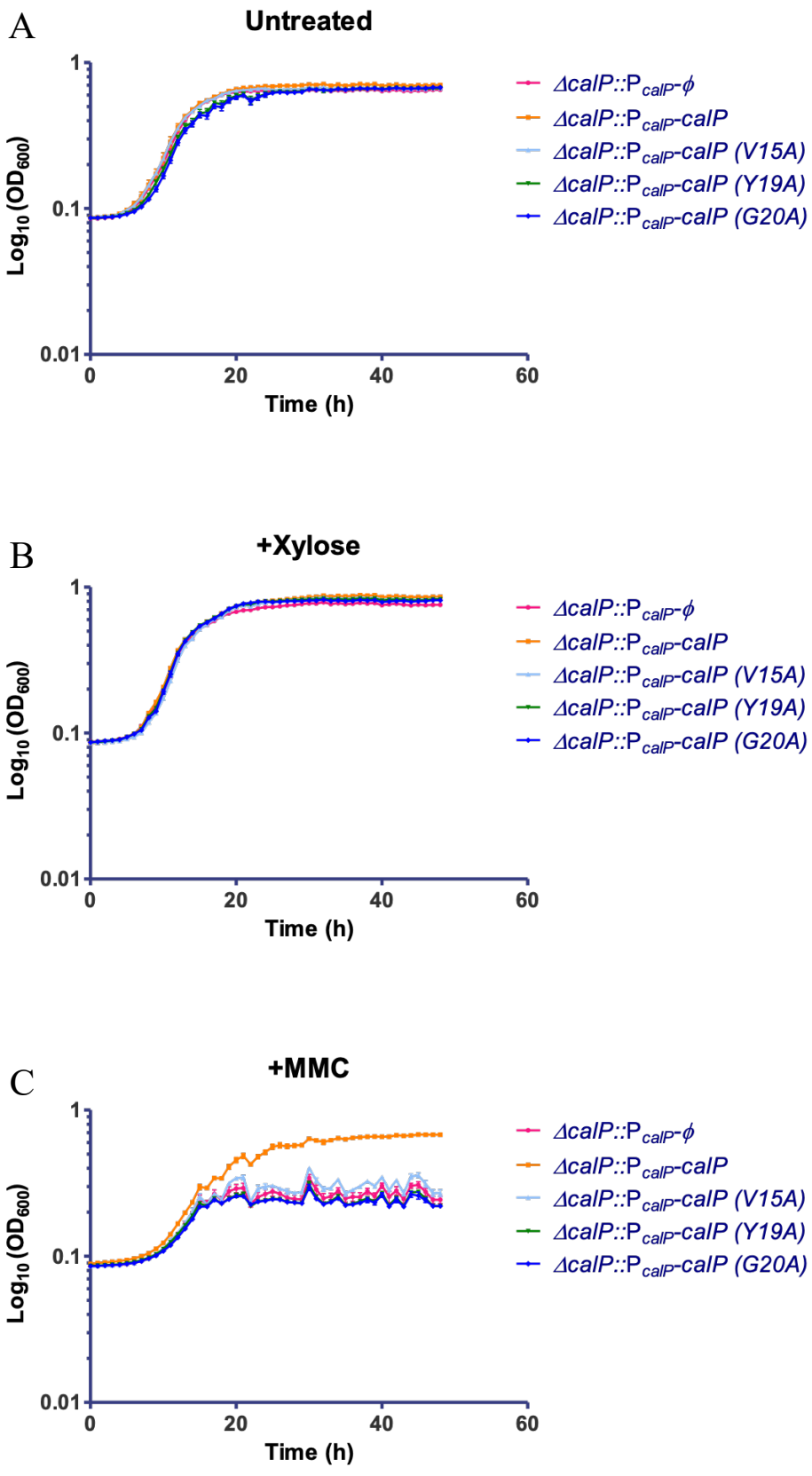
A
Untreated
Log10 (OD600)
1
0.1
0.01
0
20
40
60
Time (h)
ΔcalP::PcalP-ϕ
ΔcalP::PcalP-calP
ΔcalP::PcalP-calP (V15A)
ΔcalP::PcalP-calP (Y19A)
ΔcalP::PcalP-calP (G20A)
B
+Xylose
Log10 (OD600)
1
0.1
0.01
0
20
40
60
Time (h)
ΔcalP::PcalP-ϕ
ΔcalP::PcalP-calP
ΔcalP::PcalP-calP (V15A)
ΔcalP::PcalP-calP (Y19A)
ΔcalP::PcalP-calP (G20A)
C
+MMC
Log10 (OD600)
1
0.1
0.01
0
20
40
60
Time (h)
ΔcalP::PcalP-ϕ
ΔcalP::PcalP-calP
ΔcalP::PcalP-calP (V15A)
ΔcalP::PcalP-calP (Y19A)
ΔcalP::PcalP-calP (G20A)

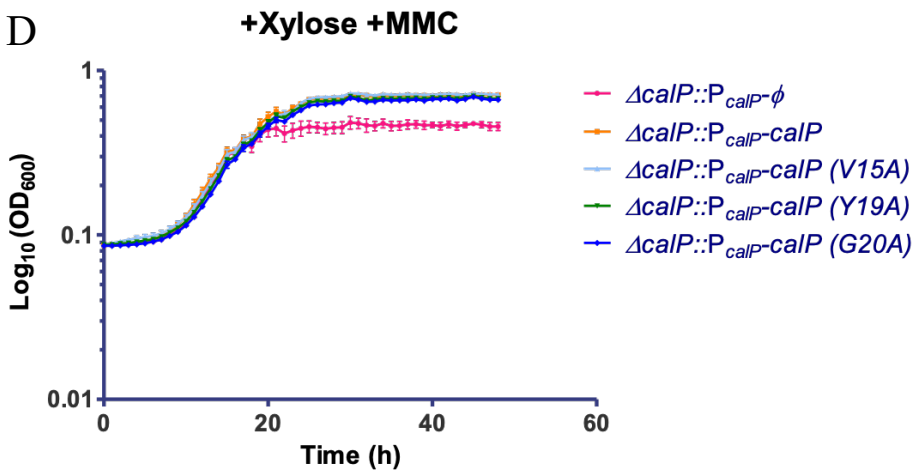

Fig. A11. *ΔcalP* complementation with *calP* derivative mutants restored the WT phenotype of every *C. crescentus* strain except the 15th, 19th, and 20th amino acid mutants when challenged with MMC. Plot showing the *ΔcalP* complementation test with truncated *calP* derivatives when exposed to MMC. *calP* mutant derivatives were ectopically expressed from the xylose-inducible promoter (P_{xyl}) harboured in the integrative plasmid pXYFPC-2 in the *ΔcalP* background of *C. crescentus*. Complemented *ΔcalP C. crescentus* cells were grown in a liquid PYE medium to mid-exponential phase at 30ºC and diluted to $3.3x10^{-4}$. Cultures contained (A) no additives, (B) 0.1% xylose, (C) 0.12 µg/mL of MMC, (D) or 0.1% xylose and 0.12 µg/mL of MMC. Strains of each growth curve are *ΔcalP*::P_{xyl}-*ø* (magenta line), *ΔcalP*::P_{xyl}-*calP-flag* (orange line), *ΔcalP*::P_{xyl}-*calP (V15A)-flag* (light-blue line), *ΔcalP*::P_{xyl}-*calP (Y19A)-flag* (green line), and *ΔcalP*::P_{xyl}-*calP (G20A)-flag* (purple line). 96-well plates were incubated at 30 °C for 48 hrs with orbital shaking. OD_{600} was measured at the indicated times, and the average of three cultures was taken.

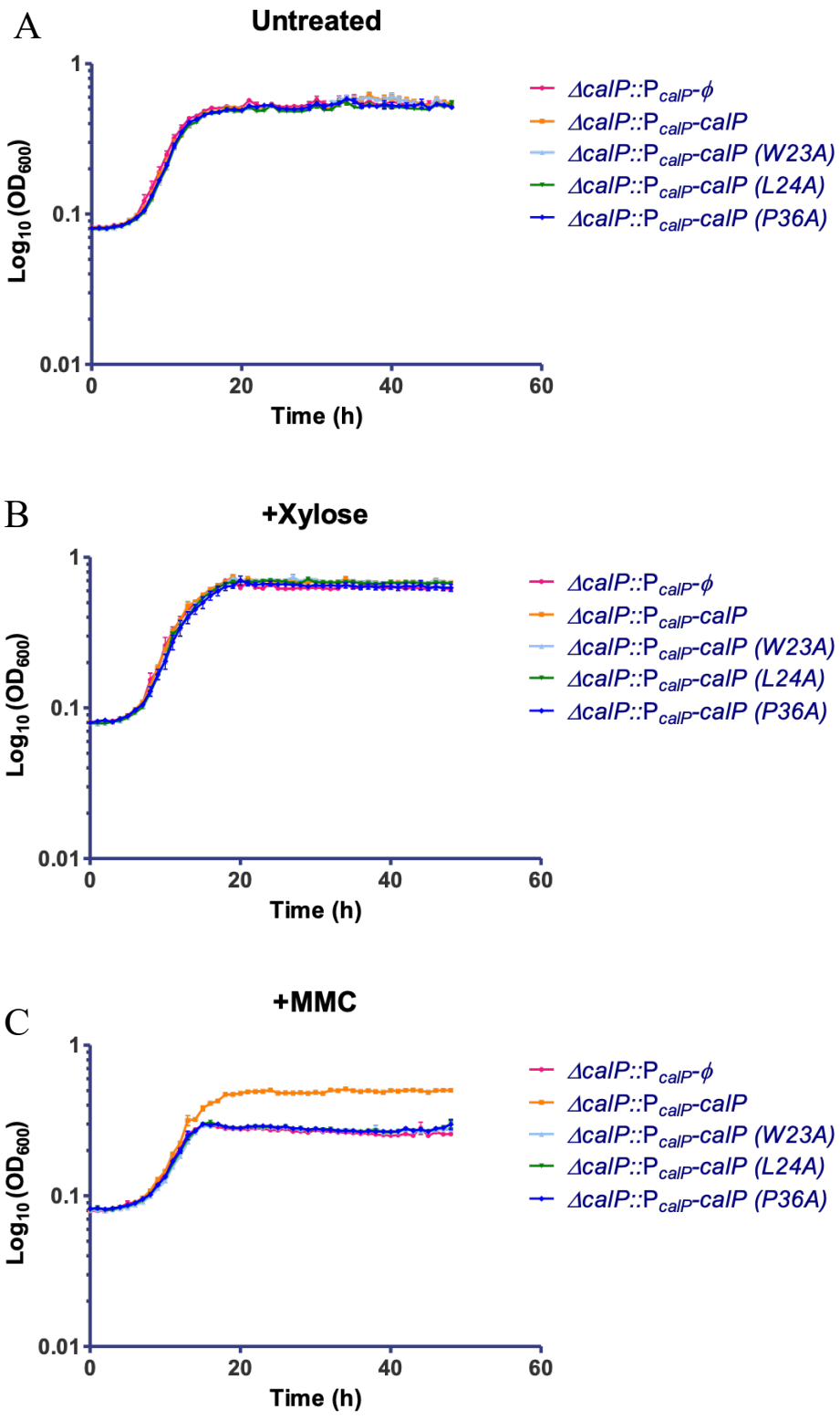
A
Untreated
Log10 (OD600)
1
0.1
0.01
0
20
40
60
Time (h)
ΔcalP::PcalP-ϕ
ΔcalP::PcalP-calP
ΔcalP::PcalP-calP (W23A)
ΔcalP::PcalP-calP (L24A)
ΔcalP::PcalP-calP (P36A)
B
+Xylose
Log10 (OD600)
1
0.1
0.01
0
20
40
60
Time (h)
ΔcalP::PcalP-ϕ
ΔcalP::PcalP-calP
ΔcalP::PcalP-calP (W23A)
ΔcalP::PcalP-calP (L24A)
ΔcalP::PcalP-calP (P36A)
C
+MMC
Log10 (OD600)
1
0.1
0.01
0
20
40
60
Time (h)
ΔcalP::PcalP-ϕ
ΔcalP::PcalP-calP
ΔcalP::PcalP-calP (W23A)
ΔcalP::PcalP-calP (L24A)
ΔcalP::PcalP-calP (P36A)

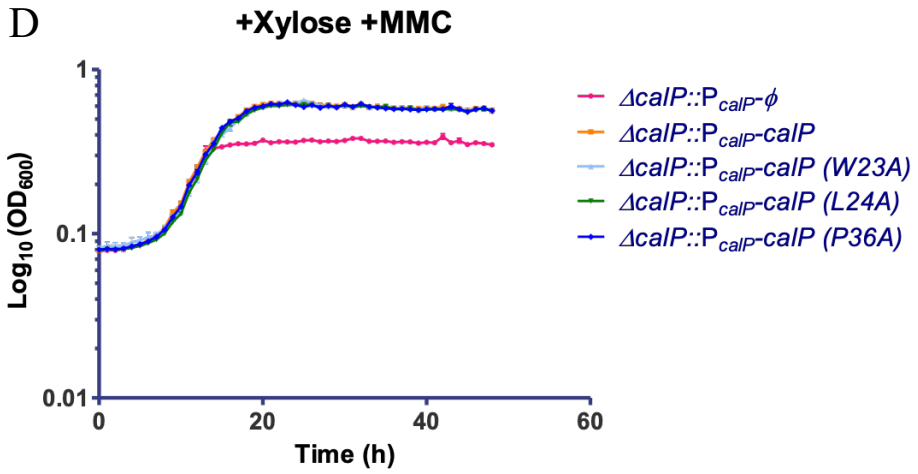

Fig. A12. *ΔcalP* complementation with *calP* derivative mutants restored the WT phenotype of every *C. crescentus* strain except the 23rd, 24th, and 36th amino acid mutants when challenged with MMC. Growth curves showing the *ΔcalP* complementation test with truncated *calP* derivatives when exposed to MMC. *calP* mutant derivatives were ectopically expressed from the xylose-inducible promoter (P_{xyl}) harboured in the integrative plasmid pXYFPC-2 in the *ΔcalP* background of *C. crescentus*. Complemented *ΔcalP C. crescentus* cells were grown in a liquid PYE medium to mid-exponential phase at 30ºC and diluted to 3.3x10^{-4}. Cultures contained (A) no additives, (B) 0.1% xylose, (C) 0.12 µg/mL of MMC, (D) or 0.1% xylose and 0.12 µg/mL of MMC. Strains of each growth curve are *ΔcalP*::P_{xyl}-*ø* (magenta line), *ΔcalP*::P_{xyl}-*calP-flag* (orange line), *ΔcalP*::P_{xyl}-*calP (W23A)-flag* (light-blue line), *ΔcalP*::P_{xyl}-*calP (L24A)-flag* (green line), and *ΔcalP*::P_{xyl}-*calP (P36A)-flag* (purple line). 96-well plates were incubated at 30 °C for 48 hrs with orbital shaking. The OD_{600} was measured at the indicated times, and the average of three cultures was taken.

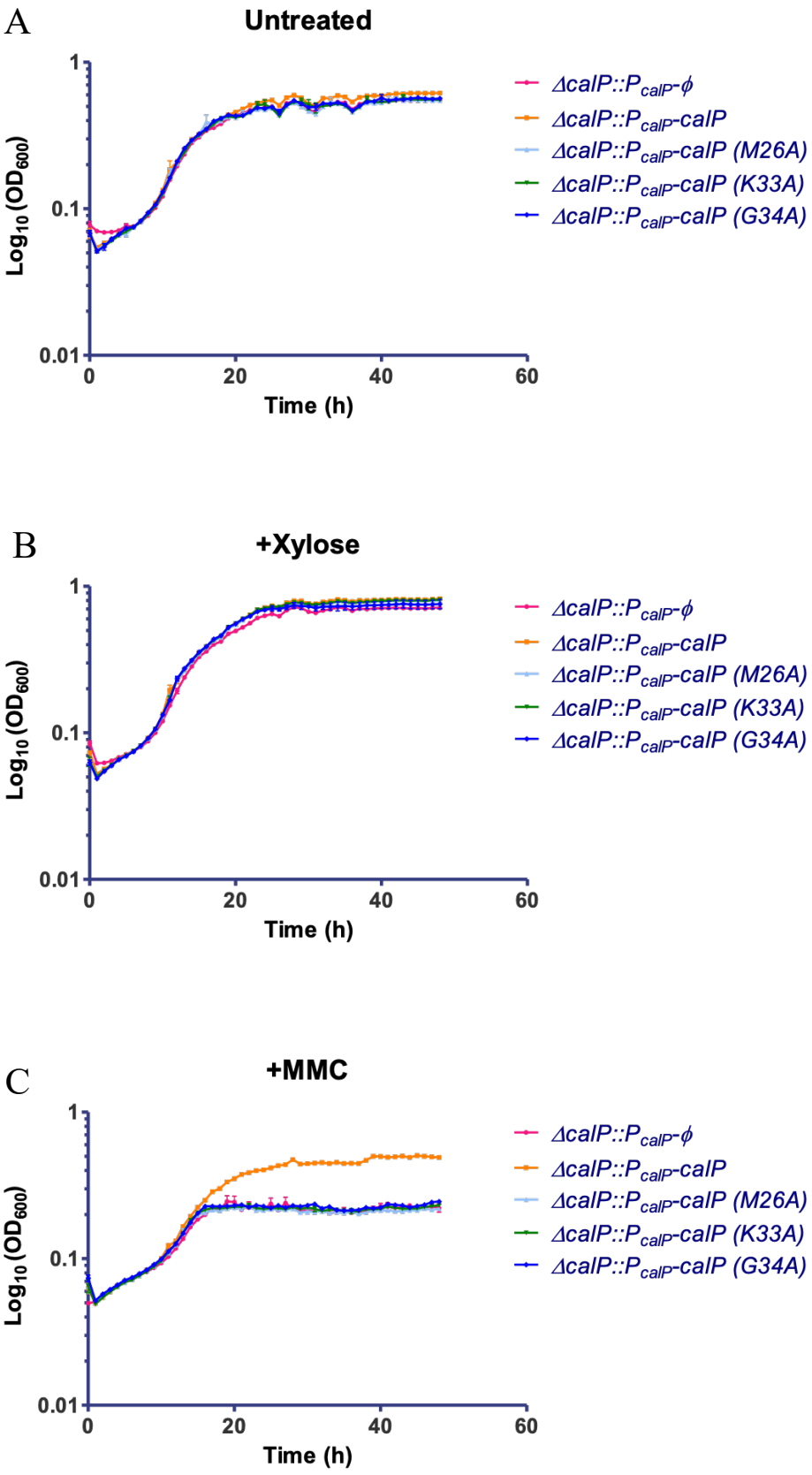
A
Untreated
B
+Xylose
C
+MMC
Log10 (OD600)
1
0.1
0.01
0
20
40
60
Time (h)
ΔcalP::PcalP-ϕ
ΔcalP::PcalP-calP
ΔcalP::PcalP-calP (M26A)
ΔcalP::PcalP-calP (K33A)
ΔcalP::PcalP-calP (G34A)

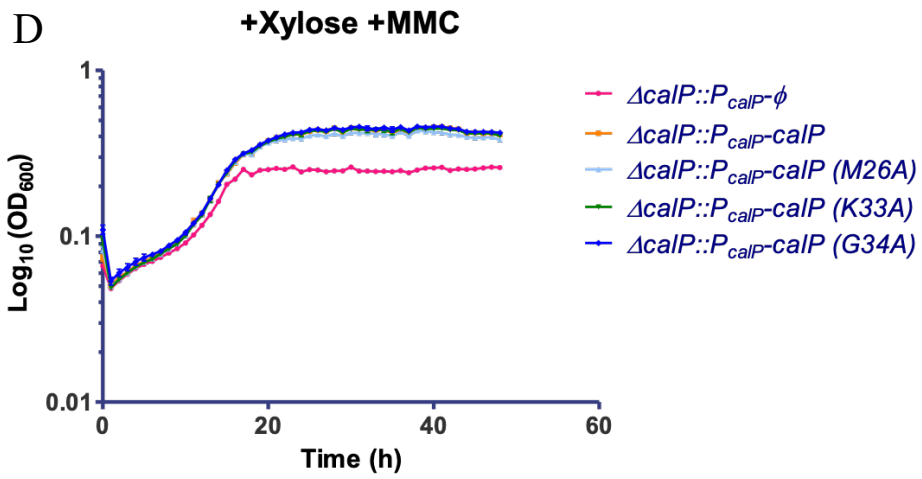

Fig. A13. *ΔcalP* complementation with *calP* derivative mutants restored the WT phenotype of every *C. crescentus* strain except the 26th, 33rd, and 34th amino acid mutants when challenged with MMC. Plot showing the *ΔcalP* complementation test with truncated *calP* derivatives when exposed to MMC. *calP* mutant derivatives were ectopically expressed from the xylose-inducible promoter (P_{xyl}) harboured in the integrative plasmid pXYFPC-2 in the *ΔcalP* background of *C. crescentus*. Complemented *ΔcalP C. crescentus* cells were grown in a liquid PYE medium to mid-exponential phase at 30ºC and diluted to $3.3x10^{-4}$. Cultures contained (A) no additives, (B) 0.1% xylose, (C) 0.12 µg/mL of MMC, (D) or 0.1% xylose and 0.12 µg/mL of MMC. Strains of each growth curve are *ΔcalP*::P_{xyl}-*ø* (magenta line), *ΔcalP*::P_{xyl}-*calP-flag* (orange line), *ΔcalP*::P_{xyl}-*calP (M26A)-flag* (light-blue line), *ΔcalP*::P_{xyl}-*calP (K33A)-flag* (green line), and *ΔcalP*::P_{xyl}-*calP (G34A)-flag* (purple line). 96-well plates were incubated at 30 °C for 48 hrs with orbital shaking. The OD_{600} was measured at the indicated times, and the average of three cultures was taken.

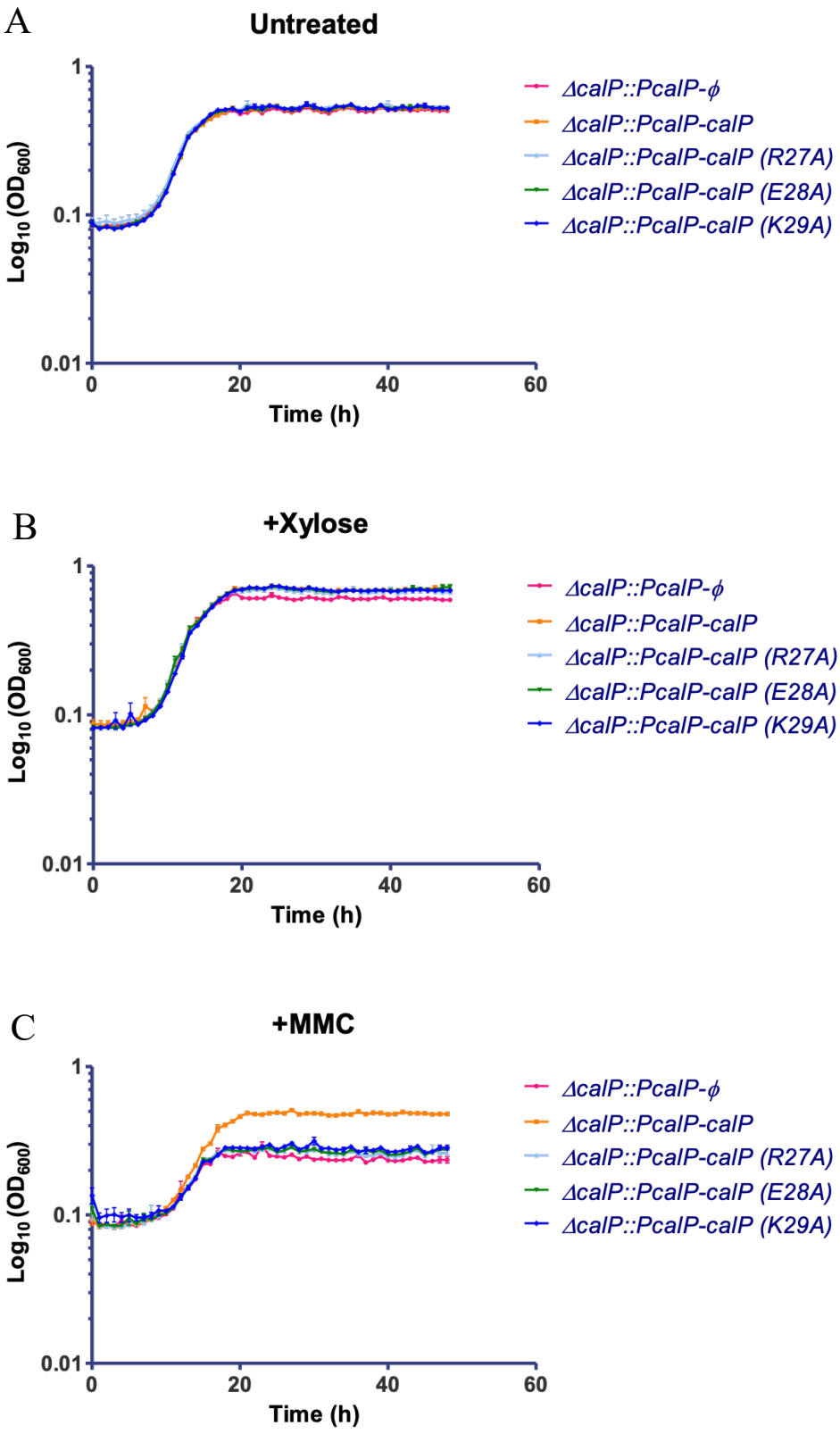
A
Untreated
Log10 (OD600)
1
0.1
0.01
0
20
40
60
Time (h)
ΔcalP::PcalP-ϕ
ΔcalP::PcalP-calP
ΔcalP::PcalP-calP (R27A)
ΔcalP::PcalP-calP (E28A)
ΔcalP::PcalP-calP (K29A)
B
+Xylose
Log10 (OD600)
1
0.1
0.01
0
20
40
60
Time (h)
ΔcalP::PcalP-ϕ
ΔcalP::PcalP-calP
ΔcalP::PcalP-calP (R27A)
ΔcalP::PcalP-calP (E28A)
ΔcalP::PcalP-calP (K29A)
C
+MMC
Log10 (OD600)
1
0.1
0.01
0
20
40
60
Time (h)
ΔcalP::PcalP-ϕ
ΔcalP::PcalP-calP
ΔcalP::PcalP-calP (R27A)
ΔcalP::PcalP-calP (E28A)
ΔcalP::PcalP-calP (K29A)

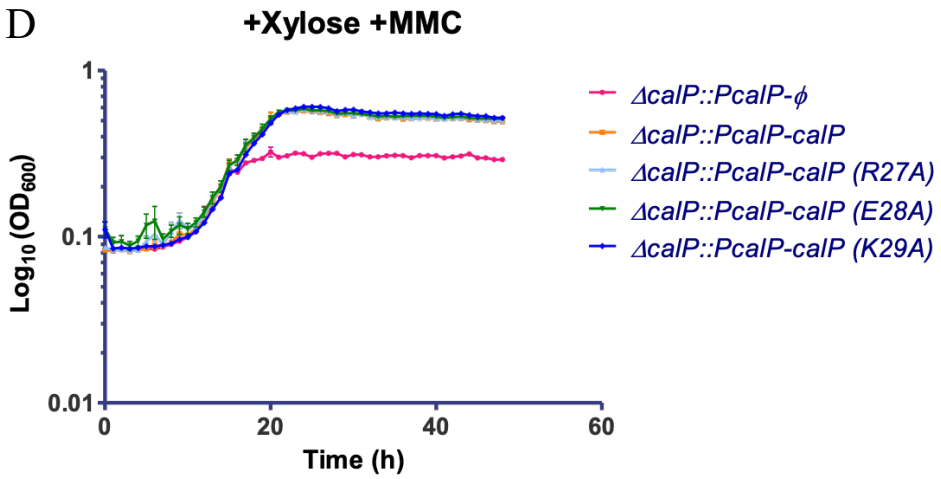

Fig. A14. *ΔcalP* complementation with *calP* derivative mutants restored the WT phenotype of every *C. crescentus* strain except the 27th, 28th, and 29th amino acid mutants when challenged with MMC. Plot showing the *ΔcalP* complementation test with truncated *calP* derivatives when exposed to MMC. *calP* mutant derivatives were ectopically expressed from the xylose-inducible promoter (P_{xyl}) harboured in the integrative plasmid pXYFPC-2 in the *ΔcalP* background of *C. crescentus*. Complemented *ΔcalP C. crescentus* cells were grown in a liquid PYE medium to mid-exponential phase at 30ºC and diluted to $3.3x10^{-4}$. Cultures contained (A) no additives, (B) 0.1% xylose, (C) 0.12 µg/mL of MMC, (D) or 0.1% xylose and 0.12 µg/mL of MMC. Strains of each growth curve are *ΔcalP*::P_{xyl}-*ø* (magenta line), *ΔcalP*::P_{xyl}-*calP-flag* (orange line), *ΔcalP*::P_{xyl}-*calP (R27A)-flag* (light-blue line), *ΔcalP*::P_{xyl}-*calP (E28A)-flag* (green line), and *ΔcalP*::P_{xyl}-*calP (K29A)-flag* (purple line). 96-well plates were incubated at 30 °C for 48 hrs with orbital shaking. The OD_{600} was measured at the indicated times, and the average of three cultures was taken.

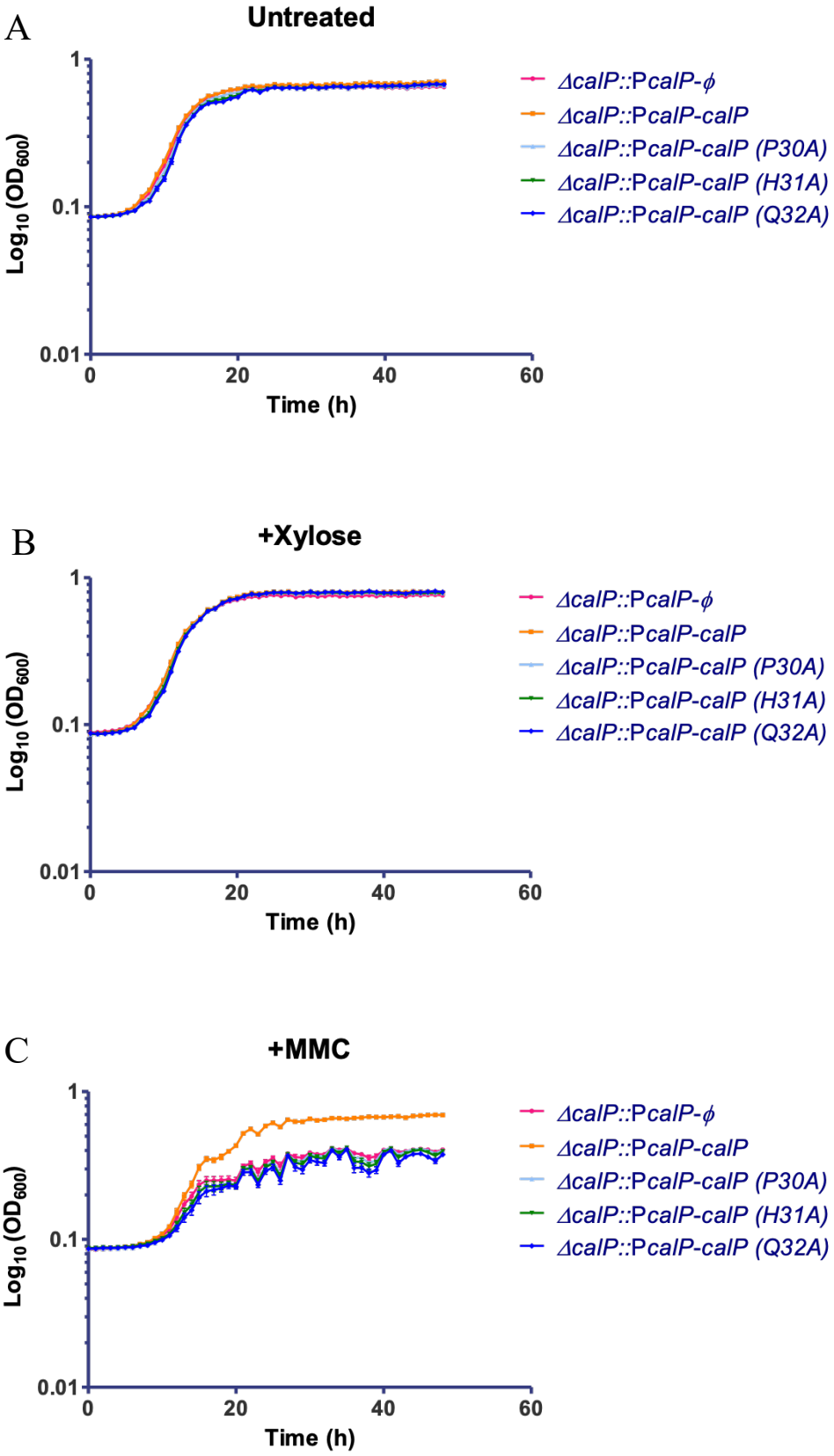
A
Untreated
Log10 (OD600)
1
0.1
0.01
0
20
40
60
Time (h)
ΔcalP::PcalP-ϕ
ΔcalP::PcalP-calP
ΔcalP::PcalP-calP (P30A)
ΔcalP::PcalP-calP (H31A)
ΔcalP::PcalP-calP (Q32A)
B
+Xylose
Log10 (OD600)
1
0.1
0.01
0
20
40
60
Time (h)
ΔcalP::PcalP-ϕ
ΔcalP::PcalP-calP
ΔcalP::PcalP-calP (P30A)
ΔcalP::PcalP-calP (H31A)
ΔcalP::PcalP-calP (Q32A)
C
+MMC
Log10 (OD600)
1
0.1
0.01
0
20
40
60
Time (h)
ΔcalP::PcalP-ϕ
ΔcalP::PcalP-calP
ΔcalP::PcalP-calP (P30A)
ΔcalP::PcalP-calP (H31A)
ΔcalP::PcalP-calP (Q32A)

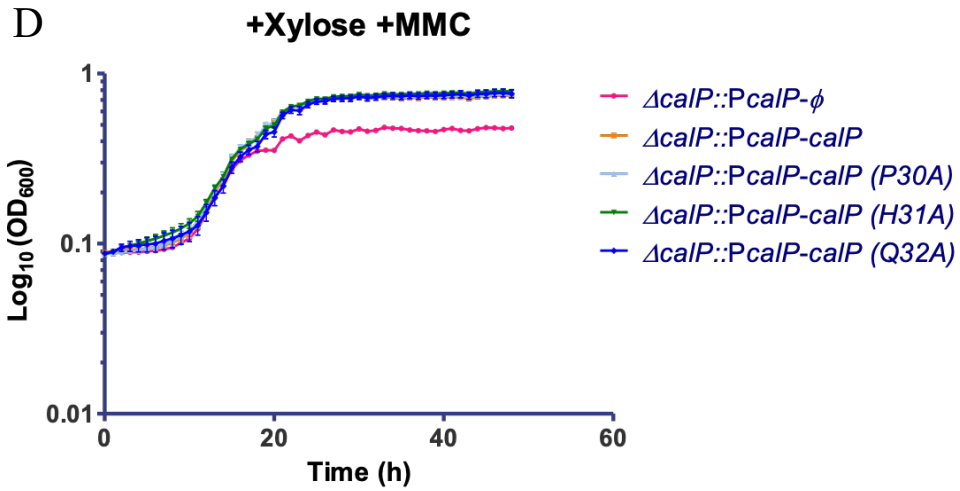

Fig. A15. *ΔcalP* complementation with *calP* derivative mutants restored the WT phenotype of every *C. crescentus* strain except the 30th, 31st, and 32nd amino acid mutants when challenged with MMC. Plot showing the *ΔcalP* complementation test with truncated *calP* derivatives when exposed to MMC. *calP* mutant derivatives were ectopically expressed from the xylose-inducible promoter (P_{xyl}) harboured in the integrative plasmid pXYFPC-2 in the *ΔcalP* background of *C. crescentus*. Complemented *ΔcalP C. crescentus* cells were grown in a liquid PYE medium to mid-exponential phase at 30ºC and diluted to 3.3x10^{-4}. Cultures contained (A) no additives, (B) 0.1% xylose, (C) 0.12 µg/mL MMC (D) or 0.1% xylose and 0.12 µg/mL MMC. Strains of each growth curve are *ΔcalP*::P_{xyl}-*ø* (magenta line), *ΔcalP*::P_{xyl}-*calP-flag* (orange line), *ΔcalP*::P_{xyl}-*calP (P30A)-flag* (light-blue line), *ΔcalP*::P_{xyl}-*calP (H31A)-flag* (green line), and *ΔcalP*::P_{xyl}-*calP (Q32A)-flag* (purple line). 96-well plates were incubated at 30 °C for 48 hrs with orbital shaking. The OD_{600} was measured at the indicated times, and the average of three cultures was taken.

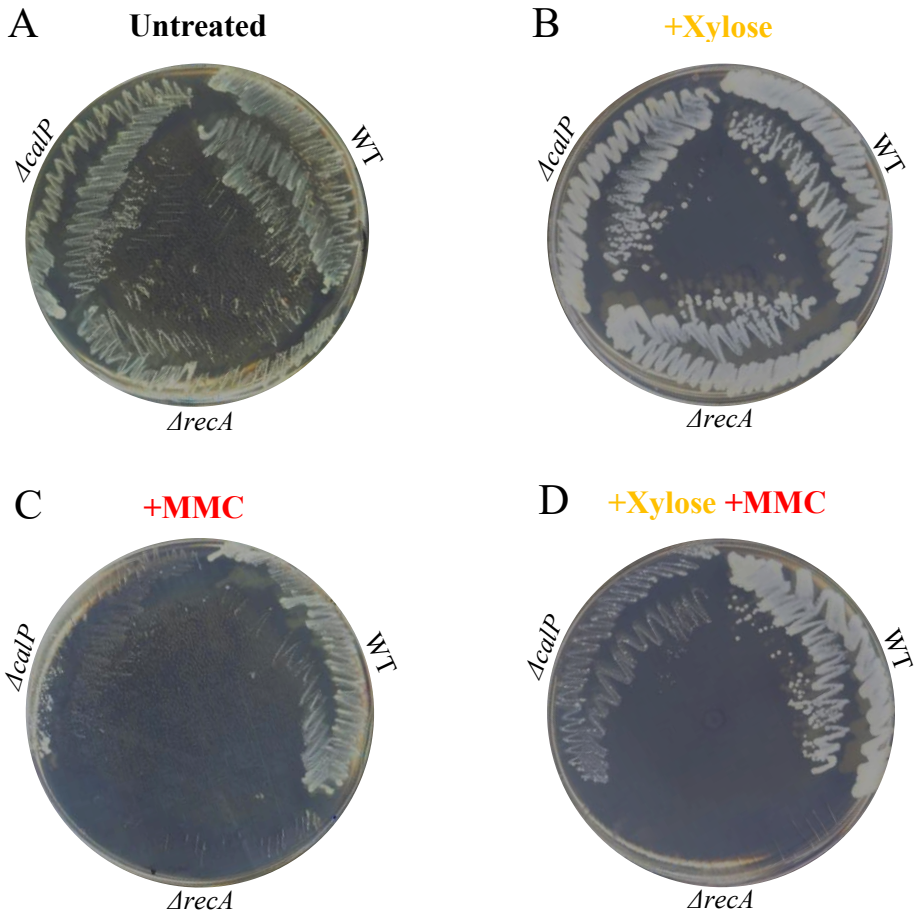

Fig. A16. The complementation of *ΔcalP* with *calP (A16P)*, *calP (A18P),* and *calP (F22A)* did not restore the WT phenotype in *C. crescentus* following MMC treatment. *C. crescentus* WT, *ΔrecA,* and *ΔcalP* growing on plates with a PYE agar medium. Cultures contained (A) no additives (dark letters), (B) 0.3% xylose (yellow letters), (C) 0.25 µg/mL MMC (red letters), or (D) 0.3% xylose and 0.25 µg/mL MMC. Plates were incubated at 30°C for 48 hrs.

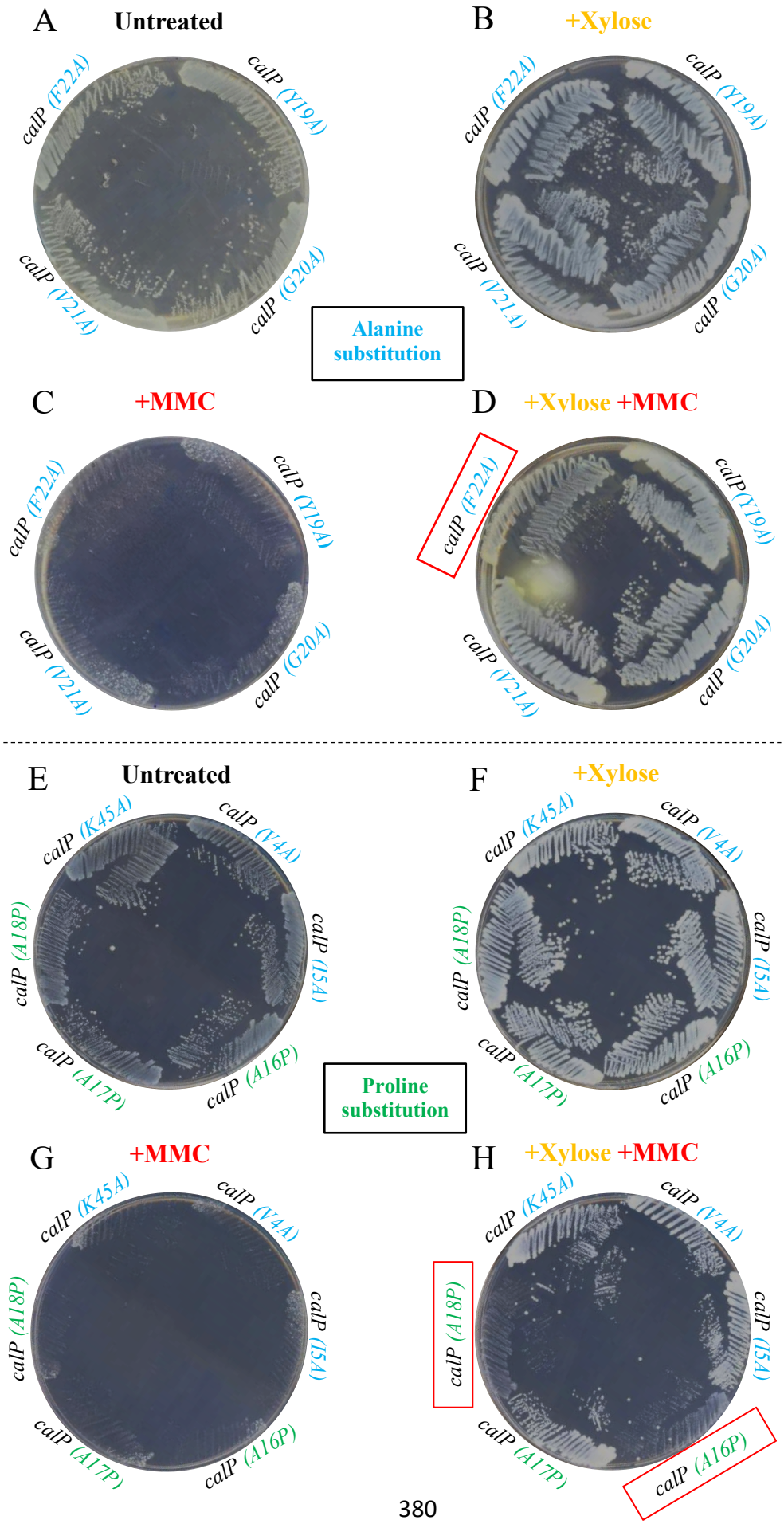
A
Untreated
calP (F22A)
calP (Y19A)
calP (V21A)
calP (G20A)
B
+Xylose
calP (F22A)
calP (Y19A)
calP (V21A)
calP (G20A)
Alanine substitution
C
+MMC
calP (F22A)
calP (Y19A)
calP (V21A)
calP (G20A)
D
+Xylose +MMC
calP (F22A)
calP(Y19A)
calP (V21A)
calP (G20A)
E
Untreated
calP (K45A)
calP (V4A)
calP (A18P)
calP (I5A)
calP (A17P)
calP (A16P)
F
+Xylose
calP (K45A)
calP (V4A)
calP (A18P)
calP (I5A)
calP (A17P)
calP (A16P)
Proline substitution
G
+MMC
calP (K45A)
calP (V4A)
calP (A18P)
calP (I5A)
calP (A17P)
calP (A16P)
H
+Xylose +MMC
calP (K45A)
calP (V4A)
calP (A18P)
calP (I5A)
calP (A17P)
calP (A16P)

Fig. A17. The complementation of *ΔcalP* with *calP (A16P)*, *calP (A18P),* and *calP (F22A)* could not rescue the WT phenotype in *C. crescentus* upon treatment with MMC. When challenged with MMC, a solid medium assay showed ΔcalP complementation with truncated calP derivatives. Truncated c*alP* mutants were ectopically expressed from a P_{xyl} promoter in the *C. crescentus ΔcalP* background. Complemented *C. crescentus ΔcalP* strains were grown on a PYE agar medium containing (A, E) no additives (dark uppercase letters), (B, F) 0.3% xylose (yellow letters), (C, G) 0.25 µg/mL MMC (red letters), (D, H) or 0.3% xylose and 0.25 µg/mL MMC. Plates were incubated at 30°C for 48 hrs. (A-D) *ΔcalP::*P_{xyl}*-calP (Y19A)-flag, ΔcalP::*P_{xyl}*-calP (G20A)-flag, ΔcalP::*P_{xyl}*-calP (V21A)-flag*, and *ΔcalP::*P_{xyl}*-calP (F22A)-flag.* (E-H) *ΔcalP::*P_{xyl}*-calP (V4A)-flag, ΔcalP::*P_{xyl}*-calP (I5A)-flag, ΔcalP::*P_{xyl}*-calP (A16P)-flag*, *ΔcalP::*P_{xyl}*-calP (A17P)-flag, ΔcalP::*P_{xyl}*-calP (A18P)-flag*, and *ΔcalP::*P_{xyl}*-calP (K45A)-flag*. Blue letters indicate alanine substitutions and green letters indicate proline substitutions. Mutants showing sensitivity are surrounded by a red square.

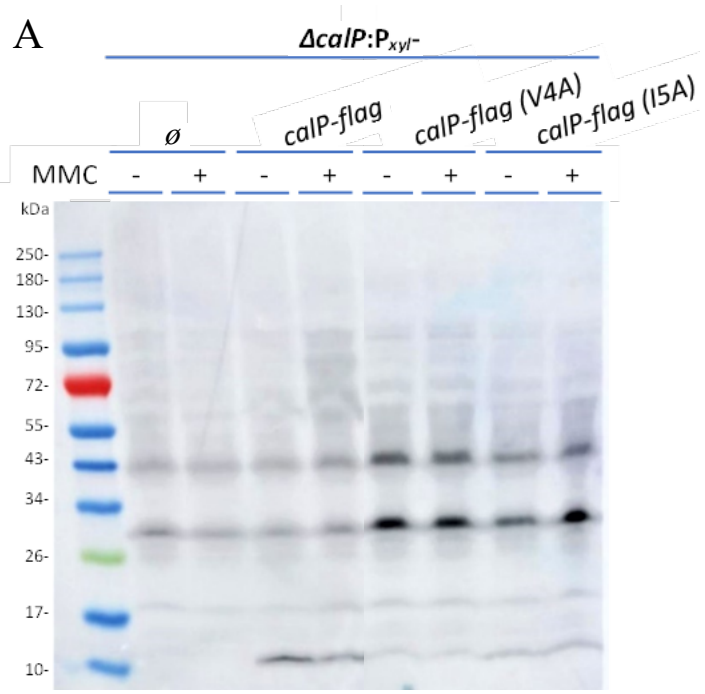
A
ΔcalP:Pxyl-
ø
calP-flag
calP-flag (V4A)
calP-flag (I5A)
MMC
- + - + - + - +
kDa
250-
180-
130-
95-
72-
55-
43-
34-
26-
17-
10-

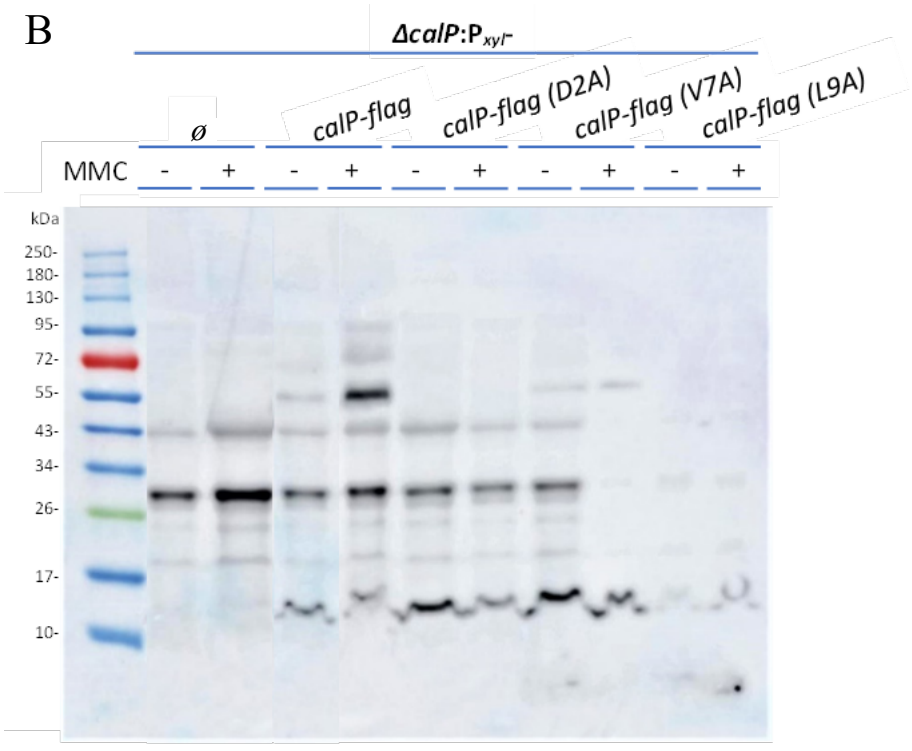
B
ΔcalP:Pxyl-
ø
calP-flag
calP-flag (D2A)
calP-flag (V7A)
calP-flag (L9A)
MMC
- + - + - + - + - +
kDa
250-
180-
130-
95-
72-
55-
43-
34-
26-
17-
10-

C

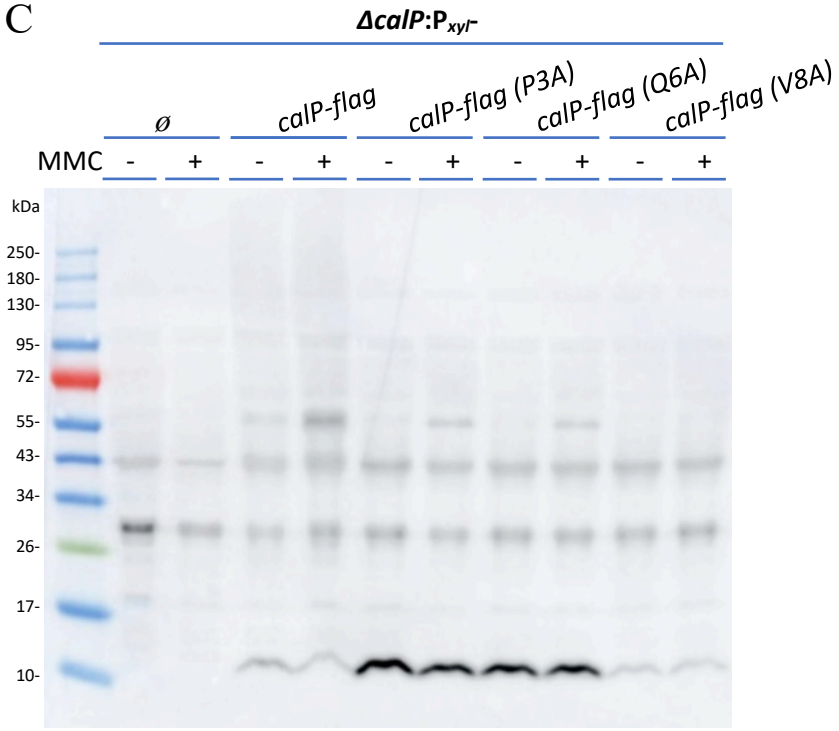
ΔcalP:P$_{xyl}$-
Ø
calP-flag
calP-flag (P3A)
calP-flag (Q6A)
calP-flag (V8A)
MMC - + - + - + - + - +
kDa
250-
180-
130-
95-
72-
55-
43-
34-
26-
17-
10-

D

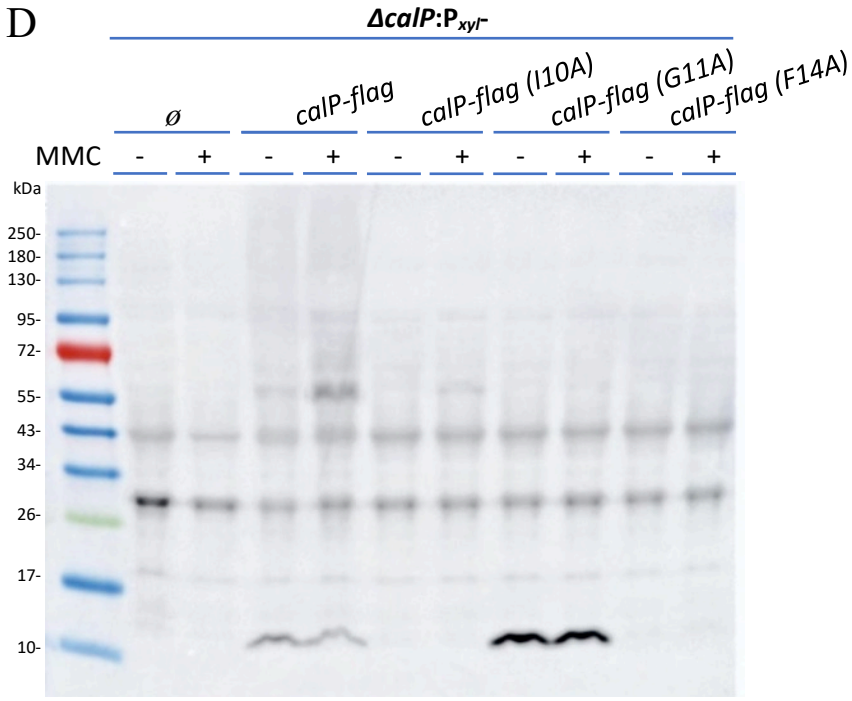
ΔcalP:P$_{xyl}$-
Ø
calP-flag
calP-flag (I10A)
calP-flag (G11A)
calP-flag (F14A)
MMC - + - + - + - + - +
kDa
250-
180-
130-
95-
72-
55-
43-
34-
26-
17-
10-

E

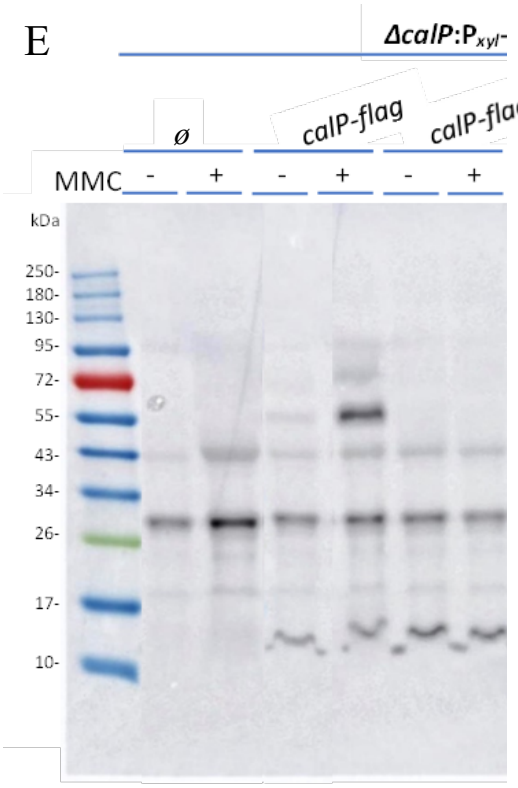
ΔcalP:Pxyl-
ø
calP-flag
calP-flag (L12A)
MMC - + - + - +
kDa
250-
180-
130-
95-
72-
55-
43-
34-
26-
17-
10-

F

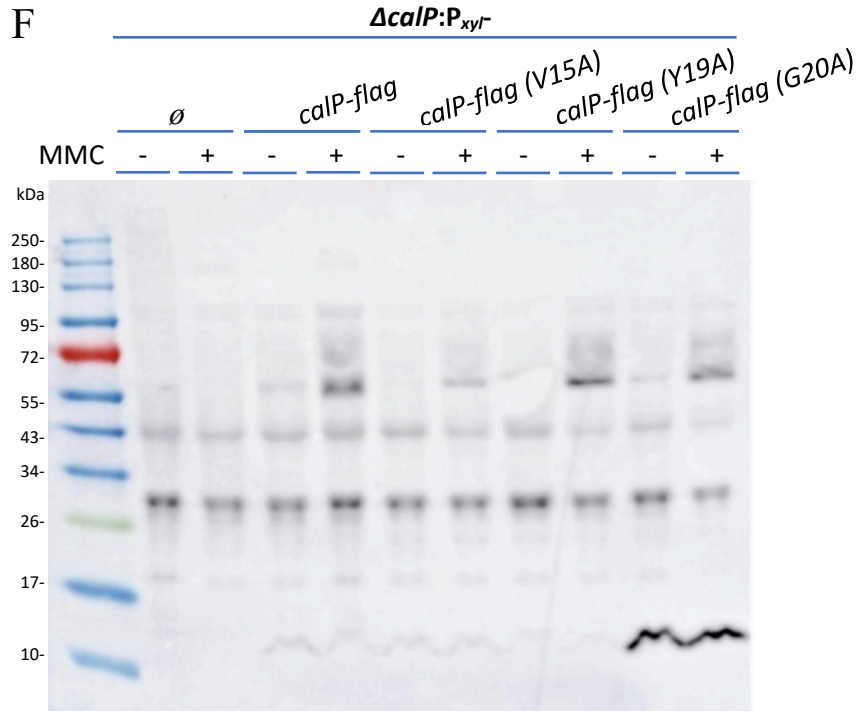
ΔcalP:Pxyl-
ø
calP-flag
calP-flag (V15A)
calP-flag (Y19A)
calP-flag (G20A)
MMC - + - + - + - + - +
kDa
250-
180-
130-
95-
72-
55-
43-
34-
26-
17-
10-

G

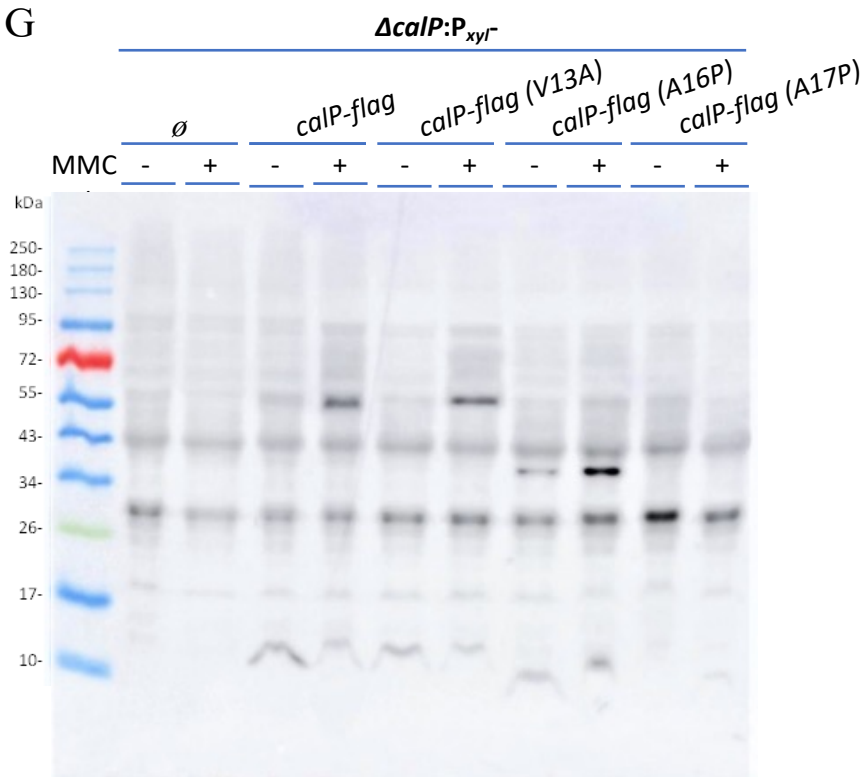
ΔcalP:P$_{xyl}$-
Ø
calP-flag
calP-flag (V13A)
calP-flag (A16P)
calP-flag (A17P)
MMC - + - + - + - + - +
kDa
250-
180-
130-
95-
72-
55-
43-
34-
26-
17-
10-

H

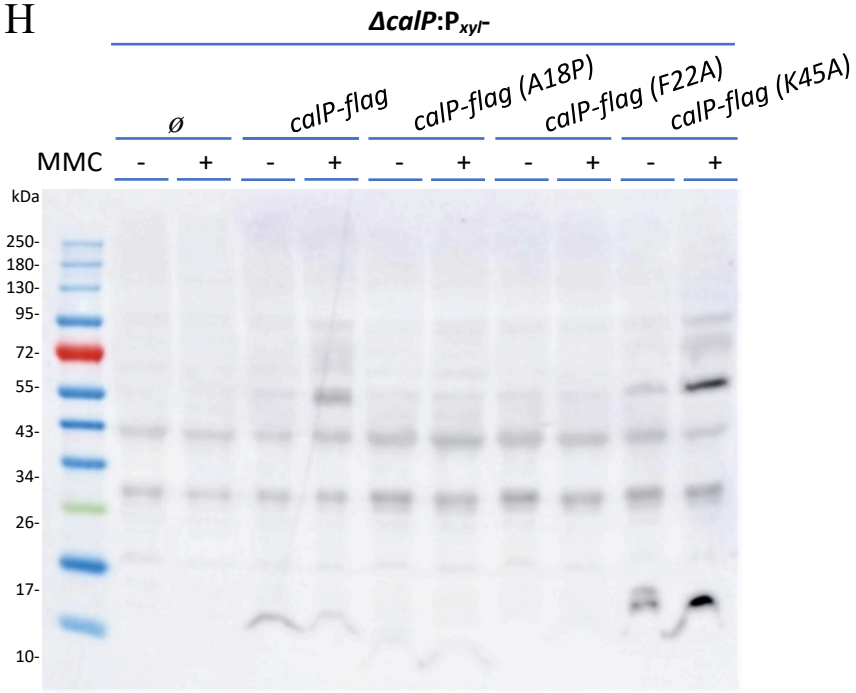
ΔcalP:P$_{xyl}$-
Ø
calP-flag
calP-flag (A18P)
calP-flag (F22A)
calP-flag (K45A)
MMC - + - + - + - + - +
kDa
250-
180-
130-
95-
72-
55-
43-
34-
26-
17-
10-

I

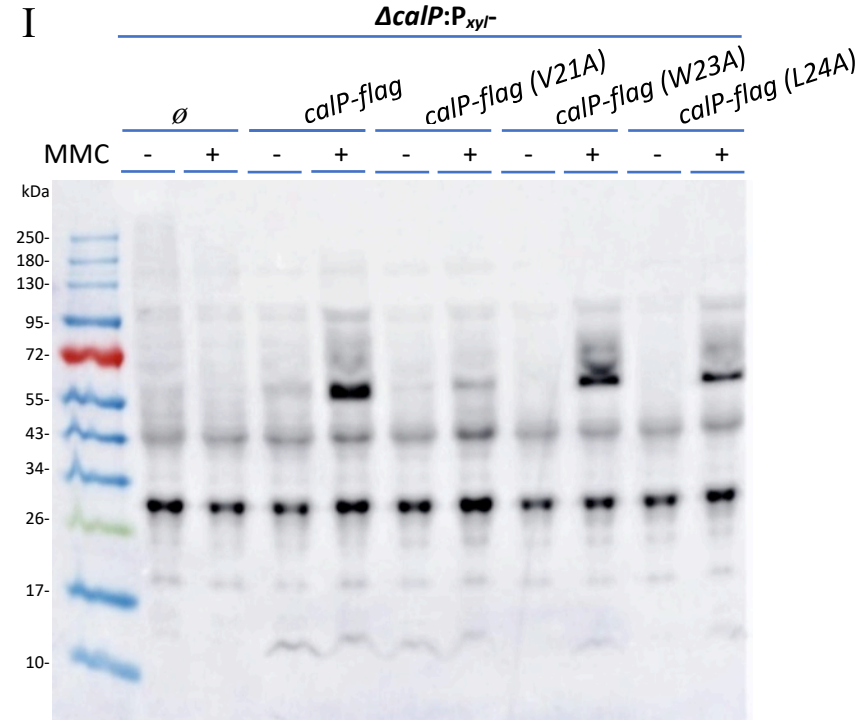
ΔcalP:Pxyl-
ø
calP-flag
calP-flag (V21A)
calP-flag (W23A)
calP-flag (L24A)
MMC
- + - + - + - + - +
kDa
250-
180-
130-
95-
72-
55-
43-
34-
26-
17-
10-

J

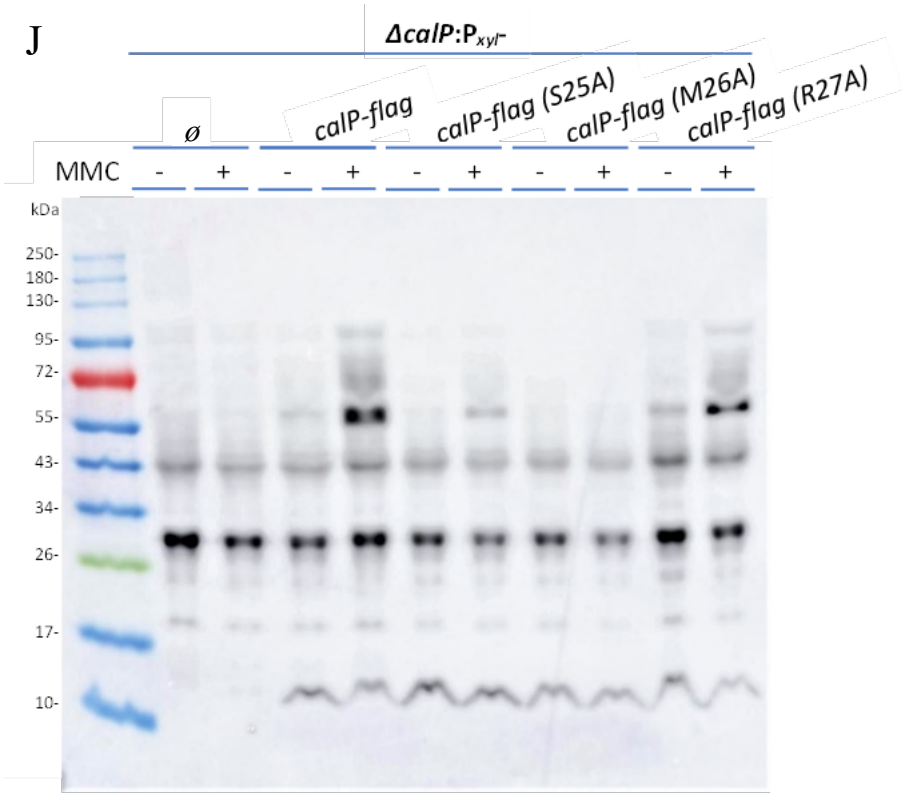
ΔcalP:Pxyl-
ø
calP-flag
calP-flag (S25A)
calP-flag (M26A)
calP-flag (R27A)
MMC
- + - + - + - + - +
kDa
250-
180-
130-
95-
72-
55-
43-
34-
26-
17-
10-

K

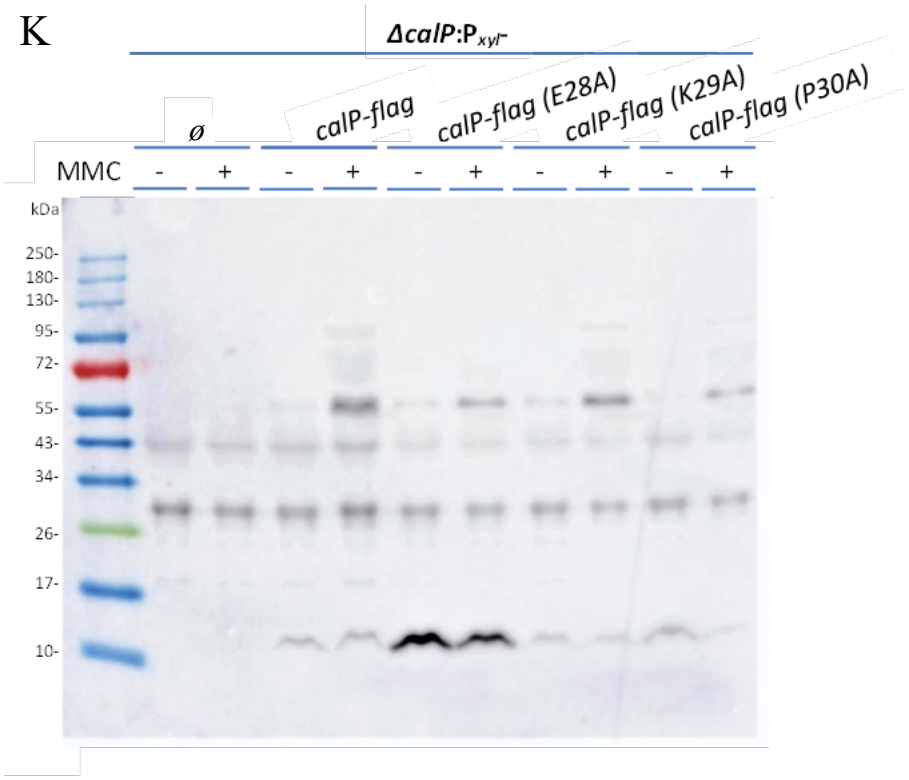
ΔcalP:Pxyl-
ø
calP-flag
calP-flag (E28A)
calP-flag (K29A)
calP-flag (P30A)
MMC
- + - + - + - + - +
kDa
250-
180-
130-
95-
72-
55-
43-
34-
26-
17-
10-

L

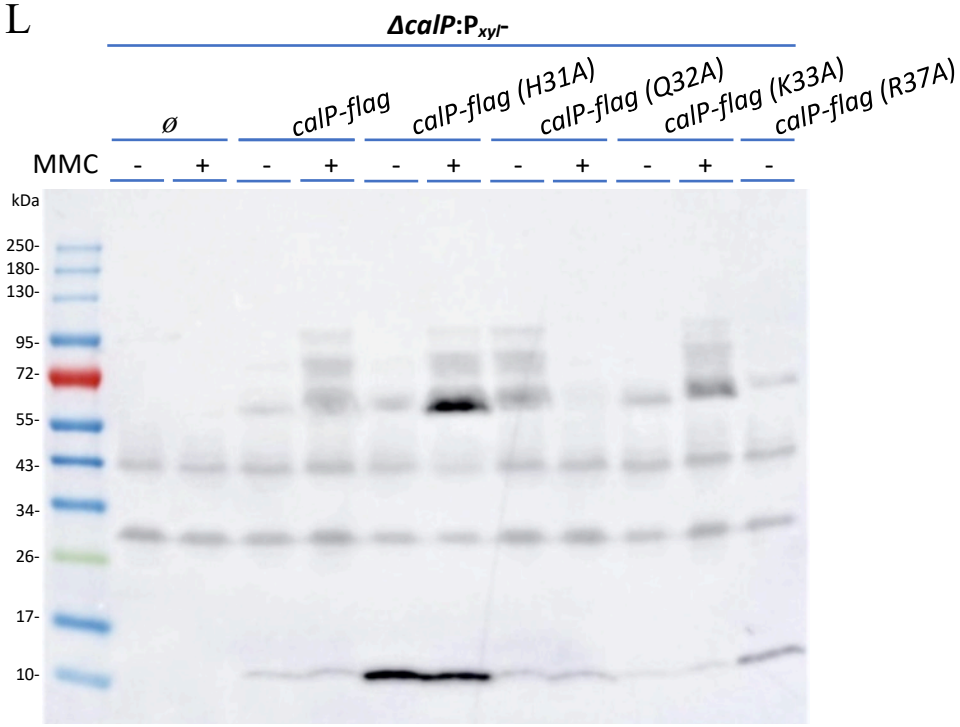
ΔcalP:Pxyl-
ø
calP-flag
calP-flag (H31A)
calP-flag (Q32A)
calP-flag (K33A)
calP-flag (R37A)
MMC
- + - + - + - + - + -
kDa
250-
180-
130-
95-
72-
55-
43-
34-
26-
17-
10-

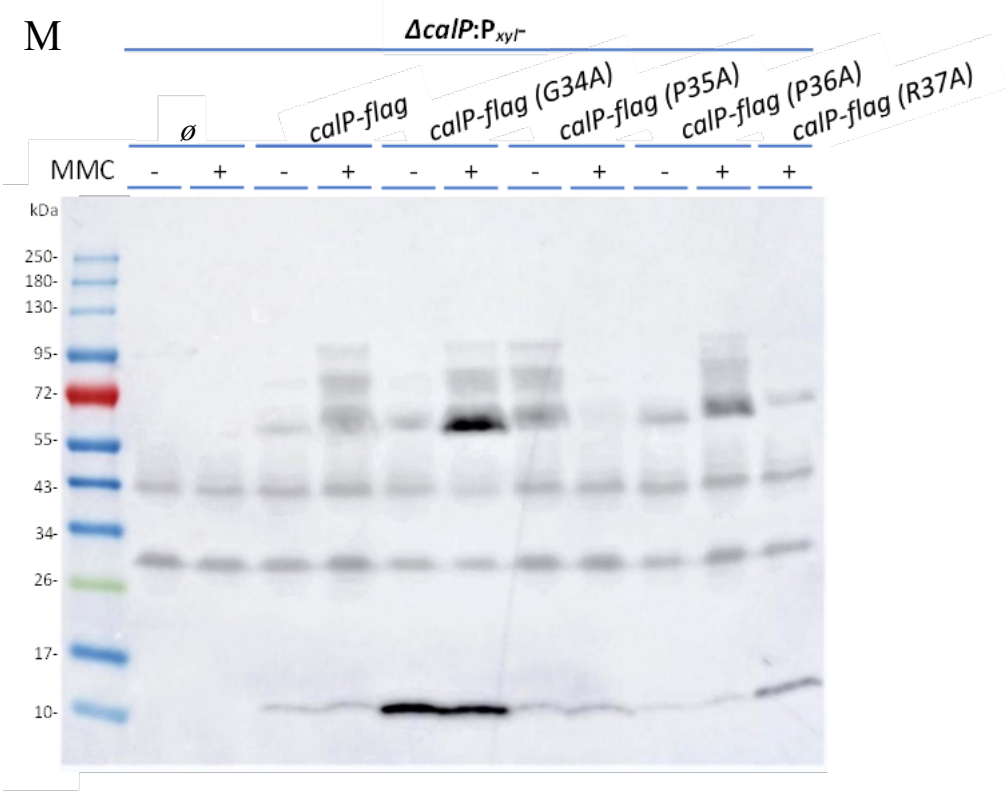

Fig. A18 (A-M). Alanine substitutions in CalP amino acids show different multimerisation patterns. Western blot assay displaying truncated versions of CalP when treated with MMC or left untreated. *calP* mutants were ectopically expressed from the xylose-inducible promoter (P_{xyl}) in a *C. crescentus ΔcalP* background. Cells were grown ON to mid-exponential phase in a PYE medium at 30ºC. Cells were sub-inoculated to an OD_{600} =0.1 and grown for 3 hrs in PYE medium. Cultures were incubated for 2 hrs with 0.1% xylose and 0.12 µg/mL MMC or without MMC. Cell lysates were mixed with anti-FLAG antibody conjugated with magnetic beads and passed through a purification column to retain C-terminally *flag*-tagged CalP. Eluates were run in a 4-20% Tris-glycine SDS-PAGE and blotted with 1:10000 α-FLAG/M2 antibodies to highlight desired bands. From left to right on the SDS-PAGE: (A) *ΔcalP*::P_{xyl}-*calP-φ, ΔcalP*::P_{xyl}-*calP-flag, ΔcalP*::P_{xyl}-*calP* (*V4A*)-*flag*, and *ΔcalP*::P_{xyl}-*calP* (*I5A*)-*flag*. (B) *ΔcalP*::P_{xyl}-*calP-ø, ΔcalP*::P_{xyl}-*calP-flag, ΔcalP*::P_{xyl}-*calP* (*D2A*)-*flag, ΔcalP*::P_{xyl}-*calP* (*V7A*)-*flag* and *ΔcalP*::P_{xyl}-*calP* (*L9A*)-*flag*. (C) *ΔcalP*::P_{xyl}-*calP- ø, ΔcalP*::P_{xyl}-*calP-flag, ΔcalP*::P_{xyl}-*calP* (*P3A*)-

flag, ΔcalP::P$_{xyl}$*-calP* (Q6*A*)*-flag*, and *ΔcalP*::P$_{xyl}$*-calP* (*V8A)-flag*. (D) *ΔcalP*::P$_{xyl}$*-calP-ø, ΔcalP*::P$_{xyl}$*-calP-flag, ΔcalP*::P$_{xyl}$*-calP* (*I10A*)*-flag, ΔcalP*::P$_{xyl}$*-calP* (*G11A*)*-flag*, and *ΔcalP*::P$_{xyl}$*-calP* (*F14A)-flag*. (E) *ΔcalP*::P$_{xyl}$*-calP- ø, ΔcalP*::P$_{xyl}$*-calP-flag*, *and ΔcalP*::P$_{xyl}$*-calP* (*L12A*)*-flag.* (F) *ΔcalP*::P$_{xyl}$*-calP- ø, ΔcalP*::P$_{xyl}$*-calP-flag, ΔcalP*::P$_{xyl}$*-calP* (*V15A*)*-flag, ΔcalP*::P$_{xyl}$*-calP* (*Y19A*)*-flag*, and *ΔcalP*::P$_{xyl}$*-calP* (*G20A)-flag*. (G) *ΔcalP*::P$_{xyl}$*-calP-ø, ΔcalP*::P$_{xyl}$*-calP-flag, ΔcalP*::P$_{xyl}$*-calP* (*V13A*)*-flag, ΔcalP*::P$_{xyl}$*-calP* (*A16P*)*-flag*, and *ΔcalP*::P$_{xyl}$*-calP* (*A17P)-flag*. (H) *ΔcalP*::P$_{xyl}$*-calP-ø*, *ΔcalP*::P$_{xyl}$*-calP-flag, ΔcalP*::P$_{xyl}$*-calP (A18P)-flag, ΔcalP*::P$_{xyl}$*-calP (F22A)-flag*, and *ΔcalP*::P$_{xyl}$*-calP (K45A)-flag*. (I) *ΔcalP*::P$_{xyl}$*-calP-ø*, *ΔcalP*::P$_{xyl}$*-calP-flag, ΔcalP*::P$_{xyl}$*-calP* (*V21A*)*-flag, ΔcalP*::P$_{xyl}$*-calP* (*W23A*)*-flag*, and *ΔcalP*::P$_{xyl}$*-calP* (*L24A)-flag*. (J) *ΔcalP*::P$_{xyl}$*-calP-ø*, *ΔcalP*::P$_{xyl}$*-calP-flag, ΔcalP*::P$_{xyl}$*-calP (S25A)-flag, ΔcalP*::P$_{xyl}$*-calP (M26A)-flag*, and *ΔcalP*::P$_{xyl}$*-calP (R27A)-flag.* (K) *ΔcalP*::P$_{xyl}$*-calP-ø*, *ΔcalP*::P$_{xyl}$*-calP-flag, ΔcalP*::P$_{xyl}$*-calP (E28A)-flag, ΔcalP*::P$_{xyl}$*-calP (K29A)-flag*, and *ΔcalP*::P$_{xyl}$*-calP (P30A)-flag.* (L) *ΔcalP*::P$_{xyl}$*-calP-ø*, *ΔcalP*::P$_{xyl}$*-calP-flag, ΔcalP*::P$_{xyl}$*-calP (H31A)-flag, ΔcalP*::P$_{xyl}$*-calP (Q32A)-flag*, *ΔcalP*::P$_{xyl}$*-calP (K33A)-flag*, and *ΔcalP*::P$_{xyl}$*-calP (R37A)-flag* (only the untreated sample). (M) *ΔcalP*::P$_{xyl}$*-calP-ø*, *ΔcalP*::P$_{xyl}$*-calP-flag, ΔcalP*::P$_{xyl}$*-calP (G34A)-flag, ΔcalP*::P$_{xyl}$*-calP (P35A)-flag*, *ΔcalP*::P$_{xyl}$*-calP (P36A)-flag,* and *ΔcalP*::P$_{xyl}$*-calP (R37A)-flag* (only the MMC-treated sample).

```
>svd:CP969_20525 stress protein
Length=585

 Score = 42.8 bits (46),  Expect = 0.28
 Identities = 23/23 (100%), Gaps = 0/23 (0%)
 Strand=Plus/Plus

Query  35   TCGTGTTCGTCGCCGCCGCCTAC  57
            |||||||||||||||||||||||
Sbjct  323  TCGTGTTCGTCGCCGCCGCCTAC  345
```

```
>spra:CP972_05265 stress protein
Length=585

 Score = 42.8 bits (46),  Expect = 0.28
 Identities = 23/23 (100%), Gaps = 0/23 (0%)
 Strand=Plus/Plus

Query  35   TCGTGTTCGTCGCCGCCGCCTAC  57
            |||||||||||||||||||||||
Sbjct  323  TCGTGTTCGTCGCCGCCGCCTAC  345
```

```
>sfug:CNQ36_18160 stress protein
Length=585

 Score = 42.8 bits (46),  Expect = 0.28
 Identities = 23/23 (100%), Gaps = 0/23 (0%)
 Strand=Plus/Plus

Query  35   TCGTGTTCGTCGCCGCCGCCTAC  57
            |||||||||||||||||||||||
Sbjct  323  TCGTGTTCGTCGCCGCCGCCTAC  345
```

```
>spav:Spa2297_30475 stress protein
Length=585

 Score = 42.8 bits (46),  Expect = 0.28
 Identities = 23/23 (100%), Gaps = 0/23 (0%)
 Strand=Plus/Plus

Query  35   TCGTGTTCGTCGCCGCCGCCTAC  57
            |||||||||||||||||||||||
Sbjct  323  TCGTGTTCGTCGCCGCCGCCTAC  345
```

```
>ssx:SACTE_0325 stress protein
Length=585

 Score = 42.8 bits (46),  Expect = 0.28
 Identities = 23/23 (100%), Gaps = 0/23 (0%)
 Strand=Plus/Plus

Query  35   TCGTGTTCGTCGCCGCCGCCTAC  57
            |||||||||||||||||||||||
Sbjct  323  TCGTGTTCGTCGCCGCCGCCTAC  345
```

```
>noz:DMB37_09820 peptidase
Length=525

 Score = 42.8 bits (46),  Expect = 0.28
 Identities = 23/23 (100%), Gaps = 0/23 (0%)
 Strand=Plus/Plus

Query  19   GTCGTCCTGATCGGTCTCGTGTT  41
            |||||||||||||||||||||||
Sbjct  28   GTCGTCCTGATCGGTCTCGTGTT  50
```

```
>strc:AA958_27815 ABC transporter permease
Length=1326

 Score = 41.0 bits (44),  Expect = 0.97
 Identities = 22/22 (100%), Gaps = 0/22 (0%)
 Strand=Plus/Plus

Query  42   CGTCGCCGCCGCCTACGGCGTG  63
            ||||||||||||||||||||||
Sbjct  657  CGTCGCCGCCGCCTACGGCGTG  678
```

```
>ddz:DSYM_14180 RNA-splicing ligase RtcB
Length=1428

 Score = 41.0 bits (44),  Expect = 0.97
 Identities = 22/22 (100%), Gaps = 0/22 (0%)
 Strand=Plus/Plus

Query  42   CGTCGCCGCCGCCTACGGCGTG  63
            ||||||||||||||||||||||
Sbjct  648  CGTCGCCGCCGCCTACGGCGTG  669
```

```
>sata:C5746_41955 stress protein
Length=585

 Score = 39.2 bits (42),  Expect = 3.4
 Identities = 21/21 (100%), Gaps = 0/21 (0%)
 Strand=Plus/Plus

Query  37   GTGTTCGTCGCCGCCGCCTAC  57
            |||||||||||||||||||||
Sbjct  325  GTGTTCGTCGCCGCCGCCTAC  345
```

```
>sphw:NFX46_23040 TerD family protein
Length=585

 Score = 39.2 bits (42),  Expect = 3.4
 Identities = 21/21 (100%), Gaps = 0/21 (0%)
 Strand=Plus/Plus

Query  35   TCGTGTTCGTCGCCGCCGCCT  55
            |||||||||||||||||||||
Sbjct  323  TCGTGTTCGTCGCCGCCGCCT  343
```

```
>ldn:H9L06_07705 FUSC family protein
Length=1059

 Score = 39.2 bits (42),  Expect = 3.4
 Identities = 21/21 (100%), Gaps = 0/21 (0%)
 Strand=Plus/Plus

Query  27   GATCGGTCTCGTGTTCGTCGC  47
            |||||||||||||||||||||
Sbjct  321  GATCGGTCTCGTGTTCGTCGC  341
```

```
>cdon:KKR89_16740 MFS transporter
Length=1263

 Score = 41.0 bits (44),  Expect = 0.97
 Identities = 24/25 (96%), Gaps = 0/25 (0%)
 Strand=Plus/Plus

Query  29   TCGGTCTCGTGTTCGTCGCCGCCGC  53
            ||||||||| ||||||||||||||||
Sbjct  254  TCGGTCTCGCGTTCGTCGCCGCCGC  278
```

```
>haln:B4589_008335 MATE family efflux transporter
Length=1398

 Score = 41.0 bits (44),  Expect = 0.97
 Identities = 24/25 (96%), Gaps = 0/25 (0%)
 Strand=Plus/Plus

Query  29   TCGGTCTCGTGTTCGTCGCCGCCGC  53
            ||||||||||||||||||| |||||
Sbjct  1010 TCGGTCTCGTGTTCGTCGCCGACGC  1034
```

```
>amv:ACMV_17410 methyl-accepting chemotaxis protein
Length=1653

 Score = 41.0 bits (44),  Expect = 0.97
 Identities = 24/25 (96%), Gaps = 0/25 (0%)
 Strand=Plus/Plus

Query  46  GCCGCCGCCTACGGCGTGTTCTGGC  70
           ||||||||||||||| ||||||||
Sbjct  70  GCCGCCGCCTACGGCGAGTTCTGGC  94
```

Table A1. Table summarising proteins found in a nucleotide homology test (BLASTN) of *calP* in the NCBI platform. Genes are shown from top to bottom in descendent order of identity with *calP* (in percentage). Only proteins with an identity greater than 95% were selected and summarised in the table. The blue names indicate the initials of the species that harbour the gene (left side of the colon) and the gene name (right side of the colon). The annotation on top of each image indicates the predicted function of the protein encoded by the gene and/or the protein family. The length indicates the number of nucleotides in each gene. The identity shows the relative number of nucleotides that correspond to the subject gene and *calP* (query) and the result of this ratio (in percentage). Gaps represent the number of nucleotide insertions that make the sequence non-consecutive for the alignment (represented in a ratio of nucleotides shifted and non-shifted and the result of this ratio (in percentage). The alignment shows two sequences, one on top called the query (*calP*) and another at the bottom called the subject (protein candidate found in the homology screening).

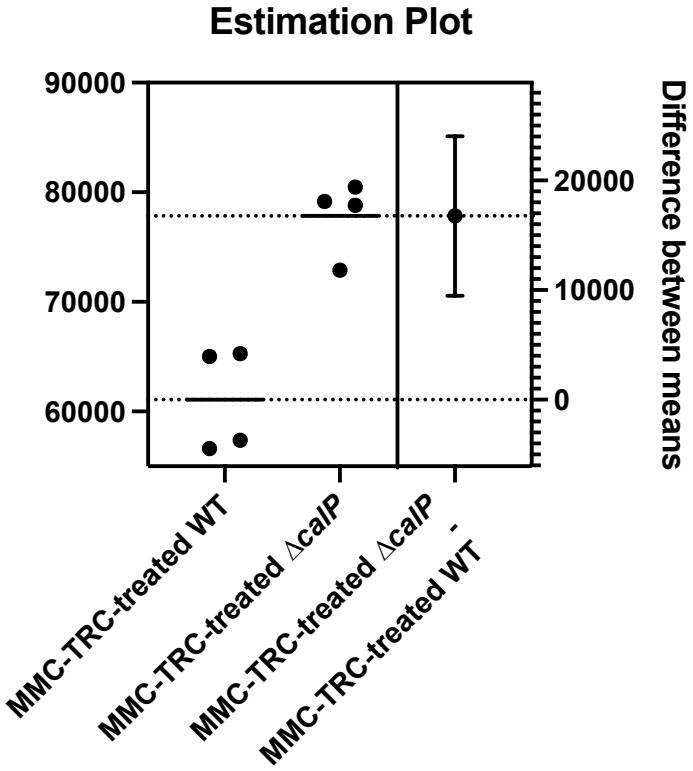

Fig. A19. The mean of the fluorescence values from MMC-TRC in WT and *ΔcalP* is significantly different. Estimation plot of Welch's t-test. The estimation plot compares the distribution of the fluorescence values of the accumulated MMC-TRC in WT and *ΔcalP* cells. The dots indicate the numerical value in which the accumulation was situated. The numbers on the left Y-axis indicate the fluorescence. The numbers on the right Y-axis show the difference between means. On the X-axis are indicated the different strains tested in the assay.

Unpaired t-test with Welch's correction	
P value	0.0017
P value summary	**
Significantly different (P < 0.05)?	Yes
One- or two-tailed P value?	Two-tailed
Welch-corrected t, df	t=5.781, df=5.428
How big ws the difference?	
Mean of column C	61077
Mean of column D	77841
Difference between means (D - C) ± SEM	16764 ± 2900
95% confidence interval	9483 to 24045
R squared (eta squared)	0.8603
F test to compare variances	
F, DFn, Dfd	1.962, 3, 3
P value	0.5939
P value summary	ns
Significantly different (P < 0.05)?	No
Data analysed	
Sample size, column C	4
Sample size, column D	4

Table A2. The different means of the fluorescence values of WT and *ΔcalP* in MMC-TRC are statistically significant. Table summarising the T-test calculations for the accumulation test values of WT and *ΔcalP* with MMC-TRC. The t-test with Welch´s correction was performed using the means of WT and *ΔcalP* values, employing GraphPad Prism statistical software (version 10.1.0).

Bibliography

1. Jones, M., *A peculiar microorganism showing rosette formation.* Zentralbl. Bakteriol. Parasitenkd. Abt. II, 1905. **14**: p. 459-463.
2. Henrici, A.T. and D.E. Johnson, *Studies of Freshwater Bacteria: II. Stalked Bacteria, a New Order of Schizomycetes.* J Bacteriol, 1935. **30**(1): p. 61-93.
3. Henrici, A.T., *Studies of Freshwater Bacteria: I. A Direct Microscopic Technique.* J Bacteriol, 1932. **25**(3): p. 277-87.
4. Stove, J. and R. Stanier, *Cellular differentiation in stalked bacteria.* Nature, 1962. **196**(4860): p. 1189-1192.
5. Poindexter, J.S., *Biological properties and classification of the Caulobacter group.* Bacteriol Rev, 1964. **28**(3): p. 231-95.
6. Houwink, A.L. and I.W. van, *Electron microscopical observations on bacterial cytology; a study on flagellation.* Biochim Biophys Acta, 1950. **5**(1): p. 10-44.
7. Houwink, A.L., *Caulobacter versus Bacillus spec. div.* Nature, 1951. **168**(4276): p. 654-5.
8. Houwink, A.L., *Caulobacter; its morphogenesis, taxonomy and parasitism.* Antonie Van Leeuwenhoek, 1955. **21**(1): p. 49-64.
9. Bowers, L.E., et al., *Studies on a strain of Caulobacter from water. I. Isolation and identification as Caulobacter vibrioides Henrici and Johnson with emended description.* J Bacteriol, 1954. **68**(2): p. 194-200.
10. Nierman, W.C., et al., *Complete genome sequence of Caulobacter crescentus.* Proc Natl Acad Sci U S A, 2001. **98**(7): p. 4136-41.
11. Kunkel, T.A., *DNA replication fidelity.* J Biol Chem, 2004. **279**(17): p. 16895-8.
12. Chatterjee, N. and G.C. Walker, *Mechanisms of DNA damage, repair, and mutagenesis.* Environ Mol Mutagen, 2017. **58**(5): p. 235-263.
13. Bos, J., A.A. Yakhnina, and Z. Gitai, *BapE DNA endonuclease induces an apoptotic-like response to DNA damage in Caulobacter</em&gt.* Proceedings of the National Academy of Sciences, 2012. **109**(44): p. 18096.
14. Dwyer, D.J., et al., *Antibiotic-induced bacterial cell death exhibits physiological and biochemical hallmarks of apoptosis.* Mol Cell, 2012. **46**(5): p. 561-72.

15. Ganai, R.A. and E. Johansson, *DNA Replication-A Matter of Fidelity.* Mol Cell, 2016. **62**(5): p. 745-55.
16. Cadet, J. and J.R. Wagner, *DNA base damage by reactive oxygen species, oxidizing agents, and UV radiation.* Cold Spring Harb Perspect Biol, 2013. **5**(2).
17. Sen, A. and J.A. Imlay, *How Microbes Defend Themselves From Incoming Hydrogen Peroxide.* Frontiers in Immunology, 2021. **12**.
18. Imlay, J.A., *Cellular defenses against superoxide and hydrogen peroxide.* Annu Rev Biochem, 2008. **77**: p. 755-76.
19. Schroeder, J.W., et al., *The Effect of Local Sequence Context on Mutational Bias of Genes Encoded on the Leading and Lagging Strands.* Curr Biol, 2016. **26**(5): p. 692-7.
20. Akashi, M. and H. Yoshikawa, *Relevance of GC content to the conservation of DNA polymerase III/mismatch repair system in Gram-positive bacteria.* Frontiers in Microbiology, 2013. **4**.
21. Schaaper, R.M., *Base selection, proofreading, and mismatch repair during DNA replication in Escherichia coli.* J Biol Chem, 1993. **268**(32): p. 23762-5.
22. Kunkel, T.A., *Evolving views of DNA replication (in)fidelity.* Cold Spring Harb Symp Quant Biol, 2009. **74**: p. 91-101.
23. Loeb, L.A. and R.J. Monnat, Jr., *DNA polymerases and human disease.* Nat Rev Genet, 2008. **9**(8): p. 594-604.
24. Fuchs, R.P. and S. Fujii, *Translesion DNA synthesis and mutagenesis in prokaryotes.* Cold Spring Harbor perspectives in biology, 2013. **5**(12): p. a012682-a012682.
25. Tashjian, T.F., et al., *Residues in the fingers domain of the translesion DNA polymerase DinB enable its unique participation in error-prone double-strand break repair.* J Biol Chem, 2019. **294**(19): p. 7588-7600.
26. Santos-Escobar, F., et al., *Roles of Bacillus subtilis RecA, Nucleotide Excision Repair, and Translesion Synthesis Polymerases in Counteracting Cr(VI)-Promoted DNA Damage.* J Bacteriol, 2019. **201**(8).

27. Kreuzer, K.N., *DNA damage responses in prokaryotes: regulating gene expression, modulating growth patterns, and manipulating replication forks.* Cold Spring Harb Perspect Biol, 2013. **5**(11): p. a012674.
28. Andersen, S., et al., *Incorporation of dUMP into DNA is a major source of spontaneous DNA damage, while excision of uracil is not required for cytotoxicity of fluoropyrimidines in mouse embryonic fibroblasts.* Carcinogenesis, 2005. **26**(3): p. 547-55.
29. Vértessy, B.G. and J. Tóth, *Keeping uracil out of DNA: physiological role, structure and catalytic mechanism of dUTPases.* Acc Chem Res, 2009. **42**(1): p. 97-106.
30. Kumar, D., et al., *Mechanisms of mutagenesis in vivo due to imbalanced dNTP pools.* Nucleic Acids Res, 2011. **39**(4): p. 1360-71.
31. Clausen, A.R., et al., *Ribonucleotide incorporation, proofreading and bypass by human DNA polymerase δ.* DNA Repair (Amst), 2013. **12**(2): p. 121-7.
32. Buckland, R.J., et al., *Increased and imbalanced dNTP pools symmetrically promote both leading and lagging strand replication infidelity.* PLoS Genet, 2014. **10**(12): p. e1004846.
33. Potenski, C.J. and H.L. Klein, *How the misincorporation of ribonucleotides into genomic DNA can be both harmful and helpful to cells.* Nucleic Acids Res, 2014. **42**(16): p. 10226-34.
34. Staker, B.L., et al., *The mechanism of topoisomerase I poisoning by a camptothecin analog.* Proc Natl Acad Sci U S A, 2002. **99**(24): p. 15387-92.
35. Han, H.-J., et al., *Natural Inhibitors of DNA Topoisomerase I with Cytotoxicities.* Chemistry & Biodiversity, 2008. **5**(7): p. 1364-1368.
36. Cheng, G., et al., *Antibacterial action of quinolones: from target to network.* Eur J Med Chem, 2013. **66**: p. 555-62.
37. Maxwell, A., *DNA gyrase as a drug target.* Trends in Microbiology, 1997. **5**(3): p. 102-109.
38. Maxwell, A., *DNA gyrase as a drug target.* Biochem Soc Trans, 1999. **27**(2): p. 48-53.

39. Heeb, S., et al., *Quinolones: from antibiotics to autoinducers.* Fems Microbiology Reviews, 2011. **35**(2): p. 247-274.
40. Drlica, K. and X. Zhao, *DNA gyrase, topoisomerase IV, and the 4-quinolones.* Microbiol Mol Biol Rev, 1997. **61**(3): p. 377-92.
41. Pommier, Y., et al., *DNA Topoisomerases and Their Poisoning by Anticancer and Antibacterial Drugs.* Chemistry & Biology, 2010. **17**(5): p. 421-433.
42. Cabral, J.H.M., et al., *Crystal structure of the breakage-reunion domain of DNA gyrase.* Nature, 1997. **388**(6645): p. 903-906.
43. Pourquier, P. and Y. Pommier, *Topoisomerase I-mediated DNA damage.* Adv Cancer Res, 2001. **80**: p. 189-216.
44. Burgin, A.B., Jr., B.N. Huizenga, and H.A. Nash, *A novel suicide substrate for DNA topoisomerases and site-specific recombinases.* Nucleic Acids Res, 1995. **23**(15): p. 2973-9.
45. Chen, H. and B.R. Shaw, *Kinetics of bisulfite-induced cytosine deamination in single-stranded DNA.* Biochemistry, 1993. **32**(14): p. 3535-9.
46. Lindahl, T., *Instability and decay of the primary structure of DNA.* Nature, 1993. **362**(6422): p. 709-15.
47. Yonekura, S., et al., *Generation, biological consequences and repair mechanisms of cytosine deamination in DNA.* J Radiat Res, 2009. **50**(1): p. 19-26.
48. Lindahl, T., *DNA glycosylases, endonucleases for apurinic/apyrimidinic sites, and base excision-repair.* Prog Nucleic Acid Res Mol Biol, 1979. **22**: p. 135-92.
49. Goff, S.P., *Death by deamination: a novel host restriction system for HIV-1.* Cell, 2003. **114**(3): p. 281-3.
50. Chandra, V., A. Bortnick, and C. Murre, *AID targeting: old mysteries and new challenges.* Trends Immunol, 2015. **36**(9): p. 527-35.
51. Moyer, R., et al., *Echinomycin, a bis-intercalating agent, induces C-->T mutations via cytosine deamination.* Mutat Res, 1993. **288**(2): p. 291-300.
52. Pfeifer, G.P., Y.H. You, and A. Besaratinia, *Mutations induced by ultraviolet light.* Mutat Res, 2005. **571**(1-2): p. 19-31.

53. d'Ischia, M., et al., *Secondary targets of nitrite-derived reactive nitrogen species: nitrosation/nitration pathways, antioxidant defense mechanisms and toxicological implications.* Chem Res Toxicol, 2011. **24**(12): p. 2071-92.
54. Lindahl, T. and D.E. Barnes, *Repair of endogenous DNA damage.* Cold Spring Harb Symp Quant Biol, 2000. **65**: p. 127-33.
55. Tropp, B., *Molecular biology, From gene to protein.* Jones & Bartlett Learning. Vol. 4. 2011.
56. Bailly, V. and W.G. Verly, *Possible roles of beta-elimination and delta-elimination reactions in the repair of DNA containing AP (apurinic/apyrimidinic) sites in mammalian cells.* Biochem J, 1988. **253**(2): p. 553-9.
57. Waters, L.S. and G.C. Walker, *The critical mutagenic translesion DNA polymerase Rev1 is highly expressed during G(2)/M phase rather than S phase.* Proc Natl Acad Sci U S A, 2006. **103**(24): p. 8971-6.
58. Chan, K., M.A. Resnick, and D.A. Gordenin, *The choice of nucleotide inserted opposite abasic sites formed within chromosomal DNA reveals the polymerase activities participating in translesion DNA synthesis.* DNA Repair (Amst), 2013. **12**(11): p. 878-89.
59. Henle, E.S. and S. Linn, *Formation, prevention, and repair of DNA damage by iron/hydrogen peroxide.* J Biol Chem, 1997. **272**(31): p. 19095-8.
60. Friedberg, E.C., GCW, Siede, Wolfram, Wood, Richard D., Schultz, Roger A., Ellenberger, Tom., *DNA repair and mutagenesis (2nd ed.)*. The Quarterly Review of Biology. Vol. 81. 2006: ASM Press. 1089.
61. Segal, A.W., *How neutrophils kill microbes.* Annu Rev Immunol, 2005. **23**: p. 197-223.
62. Malle, E., et al., *Myeloperoxidase: a target for new drug development?* Br J Pharmacol, 2007. **152**(6): p. 838-54.
63. Bjelland, S. and E. Seeberg, *Mutagenicity, toxicity and repair of DNA base damage induced by oxidation.* Mutat Res, 2003. **531**(1-2): p. 37-80.
64. Cadet, J., T. Douki, and J.L. Ravanat, *Oxidatively generated base damage to cellular DNA.* Free Radic Biol Med, 2010. **49**(1): p. 9-21.

65. Cadet, J., T. Douki, and J.L. Ravanat, *Measurement of oxidatively generated base damage in cellular DNA.* Mutat Res, 2011. **711**(1-2): p. 3-12.
66. Cadet, J., et al., *Oxidatively generated complex DNA damage: tandem and clustered lesions.* Cancer Lett, 2012. **327**(1-2): p. 5-15.
67. Cadet, J. and J.R. Wagner, *Oxidatively generated base damage to cellular DNA by hydroxyl radical and one-electron oxidants: similarities and differences.* Arch Biochem Biophys, 2014. **557**: p. 47-54.
68. Ravanat, J.L., J. Cadet, and T. Douki, *Oxidatively generated DNA lesions as potential biomarkers of in vivo oxidative stress.* Curr Mol Med, 2012. **12**(6): p. 655-71.
69. Imlay, J.A., S.M. Chin, and S. Linn, *Toxic DNA damage by hydrogen peroxide through the Fenton reaction in vivo and in vitro.* Science, 1988. **240**(4852): p. 640-2.
70. Dizdaroglu, M., et al., *Damage to the DNA bases in mammalian chromatin by hydrogen peroxide in the presence of ferric and cupric ions.* Arch Biochem Biophys, 1991. **285**(2): p. 317-24.
71. Breen, A.P. and J.A. Murphy, *Reactions of oxyl radicals with DNA.* Free Radic Biol Med, 1995. **18**(6): p. 1033-77.
72. Winterbourn, C.C., *Reconciling the chemistry and biology of reactive oxygen species.* Nat Chem Biol, 2008. **4**(5): p. 278-86.
73. Giloni, L., et al., *Bleomycin-induced strand-scission of DNA. Mechanism of deoxyribose cleavage.* J Biol Chem, 1981. **256**(16): p. 8608-15.
74. Henner, W.D., S.M. Grunberg, and W.A. Haseltine, *Enzyme action at 3' termini of ionizing radiation-induced DNA strand breaks.* J Biol Chem, 1983. **258**(24): p. 15198-205.
75. Henner, W.D., et al., *gamma Ray induced deoxyribonucleic acid strand breaks. 3' Glycolate termini.* J Biol Chem, 1983. **258**(2): p. 711-3.
76. Marnett, L.J., *Oxyradicals and DNA damage.* Carcinogenesis, 2000. **21**(3): p. 361-70.
77. Plastaras, J.P., et al., *Reactivity and mutagenicity of endogenous DNA oxopropenylating agents: base propenals, malondialdehyde, and*

N(epsilon)-oxopropenyllysine. Chem Res Toxicol, 2000. **13**(12): p. 1235-42.

78. VanderVeen, L.A., et al., *Evaluation of the mutagenic potential of the principal DNA adduct of acrolein.* J Biol Chem, 2001. **276**(12): p. 9066-70.
79. Larson, K., et al., *Methylation-induced blocks to in vitro DNA replication.* Mutat Res, 1985. **150**(1-2): p. 77-84.
80. De Bont, R. and N. van Larebeke, *Endogenous DNA damage in humans: a review of quantitative data.* Mutagenesis, 2004. **19**(3): p. 169-85.
81. Loechler, E.L., C.L. Green, and J.M. Essigmann, *In vivo mutagenesis by O6-methylguanine built into a unique site in a viral genome.* Proc Natl Acad Sci U S A, 1984. **81**(20): p. 6271-5.
82. Preston, B.D., B. Singer, and L.A. Loeb, *Mutagenic potential of O4-methylthymine in vivo determined by an enzymatic approach to site-specific mutagenesis.* Proc Natl Acad Sci U S A, 1986. **83**(22): p. 8501-5.
83. Preston, B.D., B. Singer, and L.A. Loeb, *Comparison of the relative mutagenicities of O-alkylthymines site-specifically incorporated into phi X174 DNA.* J Biol Chem, 1987. **262**(28): p. 13821-7.
84. Singer, B., et al., *Effect of 3' flanking neighbors on kinetics of pairing of dCTP or dTTP opposite O6-methylguanine in a defined primed oligonucleotide when Escherichia coli DNA polymerase I is used.* Proc Natl Acad Sci U S A, 1989. **86**(21): p. 8271-4.
85. Fronza, G. and B. Gold, *The biological effects of N3-methyladenine.* J Cell Biochem, 2004. **91**(2): p. 250-7.
86. Monti, P., et al., *Mutagenicity of N3-methyladenine: a multi-translesion polymerase affair.* Mutat Res, 2010. **683**(1-2): p. 50-6.
87. Rydberg, B. and T. Lindahl, *Nonenzymatic methylation of DNA by the intracellular methyl group donor S-adenosyl-L-methionine is a potentially mutagenic reaction.* Embo j, 1982. **1**(2): p. 211-6.
88. O'Connor, T.R., S. Boiteux, and J. Laval, *Ring-opened 7-methylguanine residues in DNA are a block to in vitro DNA synthesis.* Nucleic Acids Res, 1988. **16**(13): p. 5879-94.

89. Tudek, B., S. Boiteux, and J. Laval, *Biological properties of imidazole ring-opened N7-methylguanine in M13mp18 phage DNA.* Nucleic Acids Res, 1992. **20**(12): p. 3079-84.
90. O'Driscoll, M., et al., *The cytotoxicity of DNA carboxymethylation and methylation by the model carboxymethylating agent azaserine in human cells.* Carcinogenesis, 1999. **20**(9): p. 1855-62.
91. Zhao, C., et al., *Endogenous and background DNA adducts by methylating and 2-hydroxyethylating agents.* Mutat Res, 1999. **424**(1-2): p. 117-25.
92. Sakumi, K. and M. Sekiguchi, *Structures and functions of DNA glycosylases.* Mutat Res, 1990. **236**(2-3): p. 161-72.
93. Huang, J.C., et al., *Substrate spectrum of human excinuclease: repair of abasic sites, methylated bases, mismatches, and bulky adducts.* Proc Natl Acad Sci U S A, 1994. **91**(25): p. 12213-7.
94. Zak, P., K. Kleibl, and F. Laval, *Repair of O6-methylguanine and O4-methylthymine by the human and rat O6-methylguanine-DNA methyltransferases.* J Biol Chem, 1994. **269**(1): p. 730-3.
95. Ye, N., G.P. Holmquist, and T.R. O'Connor, *Heterogeneous repair of N-methylpurines at the nucleotide level in normal human cells.* J Mol Biol, 1998. **284**(2): p. 269-85.
96. Desouky, O.S., N. Ding, and G. Zhou, *Targeted and non-targeted effects of ionizing radiation.* Journal of Radiation Research and Applied Sciences, 2015. **8**: p. 247 - 254.
97. Wardman, P., *The importance of radiation chemistry to radiation and free radical biology (The 2008 Silvanus Thompson Memorial Lecture).* Br J Radiol, 2009. **82**(974): p. 89-104.
98. Vignard, J., G. Mirey, and B. Salles, *Ionizing-radiation induced DNA double-strand breaks: a direct and indirect lighting up.* Radiother Oncol, 2013. **108**(3): p. 362-9.
99. Henner, W.D., S.M. Grunberg, and W.A. Haseltine, *Sites and structure of gamma radiation-induced DNA strand breaks.* J Biol Chem, 1982. **257**(19): p. 11750-4.

100. Obe, G., C. Johannes, and D. Schulte-Frohlinde, *DNA double-strand breaks induced by sparsely ionizing radiation and endonucleases as critical lesions for cell death, chromosomal aberrations, mutations and oncogenic transformation.* Mutagenesis, 1992. **7**(1): p. 3-12.
101. Iliakis, G., *The role of DNA double strand breaks in ionizing radiation-induced killing of eukaryotic cells.* Bioessays, 1991. **13**(12): p. 641-8.
102. Hutchinson, F., *Chemical changes induced in DNA by ionizing radiation.* Prog Nucleic Acid Res Mol Biol, 1985. **32**: p. 115-54.
103. Lomax, M.E., L.K. Folkes, and P. O'Neill, *Biological consequences of radiation-induced DNA damage: relevance to radiotherapy.* Clin Oncol (R Coll Radiol), 2013. **25**(10): p. 578-85.
104. Davies, R.J., *Royal Irish Academy Medal Lecture. Ultraviolet radiation damage in DNA.* Biochem Soc Trans, 1995. **23**(2): p. 407-18.
105. Varghese, A.J., *Photochemistry of nucleic acids and their constituents.* Photophysiology, 1972(7): p. 207-74.
106. Mitchell, D.L. and R.S. Nairn, *The biology of the (6-4) photoproduct.* Photochem Photobiol, 1989. **49**(6): p. 805-19.
107. Goosen, N. and G.F. Moolenaar, *Repair of UV damage in bacteria.* DNA Repair (Amst), 2008. **7**(3): p. 353-79.
108. Demple, B. and S. Linn, *5,6-Saturated thymine lesions in DNA: production by ultraviolet light or hydrogen peroxide.* Nucleic Acids Res, 1982. **10**(12): p. 3781-9.
109. Bose, S.N., et al., *Formation of an adenine-thymine photoadduct in the deoxydinucleoside monophosphate d(TpA) and in DNA.* Science, 1983. **220**(4598): p. 723-5.
110. Kumar, S., et al., *Adenine photodimerization in deoxyadenylate sequences: elucidation of the mechanism through structural studies of a major d(ApA) photoproduct.* Nucleic Acids Res, 1991. **19**(11): p. 2841-7.
111. Mitchell, D.L., J. Jen, and J.E. Cleaver, *Relative induction of cyclobutane dimers and cytosine photohydrates in DNA irradiated in vitro and in vivo with ultraviolet-C and ultraviolet-B light.* Photochem Photobiol, 1991. **54**(5): p. 741-6.

112. Peak, M.J. and J.G. Peak, *DNA-to-protein crosslinks and backbone breaks caused by far- and near-ultraviolet, and visible light radiations in mammalian cells.* Basic Life Sci, 1986. **38**: p. 193-202.
113. Sancar, A., *DNA excision repair.* Annu Rev Biochem, 1996. **65**: p. 43-81.
114. Eppink, B., et al., *The response of mammalian cells to UV-light reveals Rad54-dependent and independent pathways of homologous recombination.* DNA Repair (Amst), 2011. **10**(11): p. 1095-105.
115. Singer, B., *O-alkyl pyrimidines in mutagenesis and carcinogenesis: occurrence and significance.* Cancer Res, 1986. **46**(10): p. 4879-85.
116. Singer, B. and J.T. Kuśmierek, *Chemical mutagenesis.* Annu Rev Biochem, 1982. **51**: p. 655-93.
117. Naegeli, H. *DNA Structure: Inherent Instability and Genotoxic Reactions*. 1997.
118. Loechler, E.L., *A violation of the Swain-Scott principle, and not SN1 versus SN2 reaction mechanisms, explains why carcinogenic alkylating agents can form different proportions of adducts at oxygen versus nitrogen in DNA.* Chem Res Toxicol, 1994. **7**(3): p. 277-80.
119. Mielecki, D. and E. Grzesiuk, *Ada response - a strategy for repair of alkylated DNA in bacteria.* Fems Microbiology Letters, 2014. **355**(1): p. 1-11.
120. Beranek, D.T., *Distribution of methyl and ethyl adducts following alkylation with monofunctional alkylating agents.* Mutat Res, 1990. **231**(1): p. 11-30.
121. Wyatt, M.D. and D.L. Pittman, *Methylating agents and DNA repair responses: Methylated bases and sources of strand breaks.* Chem Res Toxicol, 2006. **19**(12): p. 1580-94.
122. Lawley, P.D., *Effects of some chemical mutagens and carcinogens on nucleic acids.* Prog Nucleic Acid Res Mol Biol, 1966. **5**: p. 89-131.
123. Pegg, A.E., *DNA Repair and Carcinogenesis by Alkylating Agents*, in *Chemical Carcinogenesis and Mutagenesis II*, C.S. Cooper and P.L. Grover, Editors. 1990, Springer Berlin Heidelberg: Berlin, Heidelberg. p. 103-131.

124. Sikora, A., et al., *Lethal and mutagenic properties of MMS-generated DNA lesions in Escherichia coli cells deficient in BER and AlkB-directed DNA repair.* Mutagenesis, 2009. **25**(2): p. 139-147.
125. Hammons, G.J., et al., *Metabolism of carcinogenic heterocyclic and aromatic amines by recombinant human cytochrome P450 enzymes.* Carcinogenesis, 1997. **18**(4): p. 851-4.
126. Kriek, E., *Fifty years of research on N-acetyl-2-aminofluorene, one of the most versatile compounds in experimental cancer research.* J Cancer Res Clin Oncol, 1992. **118**(7): p. 481-9.
127. Heflich, R.H. and R.E. Neft, *Genetic toxicity of 2-acetylaminofluorene, 2-aminofluorene and some of their metabolites and model metabolites.* Mutat Res, 1994. **318**(2): p. 73-114.
128. Shibutani, S., et al., *Influence of flanking sequence context on the mutagenicity of acetylaminofluorene-derived DNA adducts in mammalian cells.* Biochemistry, 2001. **40**(12): p. 3717-22.
129. Mah, M.C., et al., *Mutations induced by aminofluorene-DNA adducts during replication in human cells.* Carcinogenesis, 1989. **10**(12): p. 2321-8.
130. Eckel, L.M. and T.R. Krugh, *2-Aminofluorene modified DNA duplex exists in two interchangeable conformations.* Nat Struct Biol, 1994. **1**(2): p. 89-94.
131. Eckel, L.M. and T.R. Krugh, *Structural characterization of two interchangeable conformations of a 2-aminofluorene-modified DNA oligomer by NMR and energy minimization.* Biochemistry, 1994. **33**(46): p. 13611-24.
132. Mu, H., et al., *Nucleotide excision repair of 2-acetylaminofluorene- and 2-aminofluorene-(C8)-guanine adducts: molecular dynamics simulations elucidate how lesion structure and base sequence context impact repair efficiencies.* Nucleic Acids Res, 2012. **40**(19): p. 9675-90.
133. Sugimura, T., *Past, present, and future of mutagens in cooked foods.* Environ Health Perspect, 1986. **67**: p. 5-10.
134. Skipper, P.L., et al., *Monocyclic aromatic amines as potential human carcinogens: old is new again.* Carcinogenesis, 2010. **31**(1): p. 50-8.

135. *A Review of: "Polycyclic Aromatic Hydrocarbons: Chemistry and Carcinogenicity".* Polycyclic Aromatic Compounds, 1993. **3**(4): p. 279-280.
136. Butlin, H.T., *THREE LECTURES on CANCER of the SCROTUM in CHIMNEY-SWEEPS and OTHERS: Delivered at the Royal College of Surgeons of England.* British medical journal, 1892. **1**(1643): p. 1341-1346.
137. Phillips, D.H., *Fifty years of benzo(a)pyrene.* Nature, 1983. **303**(5917): p. 468-72.
138. Fujiki, H., *Gist of Dr. Katsusaburo Yamagiwa's papers entitled "Experimental study on the pathogenesis of epithelial tumors" (I to VI reports).* Cancer Sci, 2014. **105**(2): p. 143-9.
139. Strniste, G.F., et al., *Photo-induced reactions of benzo(a)pyrene with DNA in vitro.* Cancer Res, 1980. **40**(2): p. 245-52.
140. Fu, P.P., *Metabolism of nitro-polycyclic aromatic hydrocarbons.* Drug Metab Rev, 1990. **22**(2-3): p. 209-68.
141. Rogan, E.G., et al., *Identification and quantitation of benzo[a]pyrene-DNA adducts formed in mouse skin.* Chem Res Toxicol, 1993. **6**(3): p. 356-63.
142. RamaKrishna, N.V., et al., *Mechanism of metabolic activation of the potent carcinogen 7,12-dimethylbenz[a]anthracene.* Chem Res Toxicol, 1992. **5**(2): p. 220-6.
143. Flowers, L., S.T. Ohnishi, and T.M. Penning, *DNA strand scission by polycyclic aromatic hydrocarbon o-quinones: role of reactive oxygen species, Cu(II)/Cu(I) redox cycling, and o-semiquinone anion radicals.* Biochemistry, 1997. **36**(28): p. 8640-8.
144. Penning, T.M., et al., *Dihydrodiol dehydrogenases and polycyclic aromatic hydrocarbon activation: generation of reactive and redox active o-quinones.* Chem Res Toxicol, 1999. **12**(1): p. 1-18.
145. Yu, H., *Environmental carcinogenic polycyclic aromatic hydrocarbons: photochemistry and phototoxicity.* J Environ Sci Health C Environ Carcinog Ecotoxicol Rev, 2002. **20**(2): p. 149-83.

146. Cosman, M., et al., *Solution conformation of the major adduct between the carcinogen (+)-anti-benzo[a]pyrene diol epoxide and DNA.* Proc Natl Acad Sci U S A, 1992. **89**(5): p. 1914-8.
147. Geacintov, N.E., *Is intercalation a critical factor in the covalent binding of mutagenic and tumorigenic polycyclic aromatic diol epoxides to DNA?* Carcinogenesis, 1986. **7**(5): p. 759-66.
148. Gräslund, A. and B. Jernström, *DNA-carcinogen interaction: covalent DNA-adducts of benzo(a)pyrene 7,8-dihydrodiol 9,10-epoxides studied by biochemical and biophysical techniques.* Q Rev Biophys, 1989. **22**(1): p. 1-37.
149. Schoket, B., *DNA damage in humans exposed to environmental and dietary polycyclic aromatic hydrocarbons.* Mutat Res, 1999. **424**(1-2): p. 143-53.
150. Braithwaite, E., X. Wu, and Z. Wang, *Repair of DNA lesions induced by polycyclic aromatic hydrocarbons in human cell-free extracts: involvement of two excision repair mechanisms in vitro.* Carcinogenesis, 1998. **19**(7): p. 1239-46.
151. Jha, V., et al., *Structure and mechanism of error-free replication past the major benzo[a]pyrene adduct by human DNA polymerase κ.* Nucleic Acids Res, 2016. **44**(10): p. 4957-67.
152. Ames, B.N., M. Profet, and L.S. Gold, *Dietary pesticides (99.99% all natural).* Proc Natl Acad Sci U S A, 1990. **87**(19): p. 7777-81.
153. López, C., et al., *Aflatoxin B1 content in patients with hepatic diseases.* Medicina (B Aires), 2002. **62**(4): p. 313-6.
154. Essigmann, J.M., et al., *Structural identification of the major DNA adduct formed by aflatoxin B1 in vitro.* Proc Natl Acad Sci U S A, 1977. **74**(5): p. 1870-4.
155. Smela, M.E., et al., *The chemistry and biology of aflatoxin B(1): from mutational spectrometry to carcinogenesis.* Carcinogenesis, 2001. **22**(4): p. 535-45.
156. Gregory, C.D. and A.E. Milner, *Regulation of cell survival in Burkitt lymphoma: implications from studies of apoptosis following cold-shock treatment.* Int J Cancer, 1994. **57**(3): p. 419-26.

157. Gafter-Gvili, A., et al., *Oxidative stress-induced DNA damage and repair in human peripheral blood mononuclear cells: protective role of hemoglobin.* PLoS One, 2013. **8**(7): p. e68341.

158. Luoto, K.R., R. Kumareswaran, and R.G. Bristow, *Tumor hypoxia as a driving force in genetic instability.* Genome Integr, 2013. **4**(1): p. 5.

159. Neutelings, T., et al., *Effects of mild cold shock (25°C) followed by warming up at 37°C on the cellular stress response.* PLoS One, 2013. **8**(7): p. e69687.

160. Kantidze, O.L., et al., *Heat Stress-Induced DNA Damage.* Acta Naturae, 2016. **8**(2): p. 75-8.

161. Chatterjee, N., et al., *Environmental stress induces trinucleotide repeat mutagenesis in human cells.* Proc Natl Acad Sci U S A, 2015. **112**(12): p. 3764-9.

162. Chatterjee, N., et al., *Environmental Stress Induces Trinucleotide Repeat Mutagenesis in Human Cells by Alt-Nonhomologous End Joining Repair.* J Mol Biol, 2016. **428**(15): p. 2978-80.

163. Calhoun, C., H.R. Wermuth, and G.A. Hall, *Antibiotics*, in *StatPearls*. 2022: Treasure Island (FL).

164. Chopra, I. and M. Roberts, *Tetracycline antibiotics: mode of action, applications, molecular biology, and epidemiology of bacterial resistance.* Microbiol Mol Biol Rev, 2001. **65**(2): p. 232-60 ; second page, table of contents.

165. Gomes, C.F., J.H. Gomes, and E.F. da Silva, *Bacteriostatic and bactericidal clays: an overview.* Environmental Geochemistry and Health, 2020. **42**(11): p. 3507-3527.

166. Pankey, G.A. and L.D. Sabath, *Clinical relevance of bacteriostatic versus bactericidal mechanisms of action in the treatment of Gram-positive bacterial infections.* Clin Infect Dis, 2004. **38**(6): p. 864-70.

167. Nemeth, J., G. Oesch, and S.P. Kuster, *Bacteriostatic versus bactericidal antibiotics for patients with serious bacterial infections: systematic review and meta-analysis.* J Antimicrob Chemother, 2015. **70**(2): p. 382-95.

168. Silva, F., et al., *Bacteriostatic versus bactericidal activity of ciprofloxacin in Escherichia coli assessed by flow cytometry using a novel far-red dye.* The Journal of Antibiotics, 2011. **64**(4): p. 321-325.

169. Bonev, B., J. Hooper, and J. Parisot, *Principles of assessing bacterial susceptibility to antibiotics using the agar diffusion method.* J Antimicrob Chemother, 2008. **61**(6): p. 1295-301.

170. Muller, A.U., F. Imkamp, and E. Weber-Ban, *The Mycobacterial LexA/RecA-Independent DNA Damage Response Is Controlled by PafBC and the Pup-Proteasome System.* Cell Rep, 2018. **23**(12): p. 3551-3564.

171. Tomasz, M., *Mitomycin C: small, fast and deadly (but very selective).* Chemistry & Biology, 1995. **2**(9): p. 575-579.

172. Dronkert, M.L.G. and R. Kanaar, *Repair of DNA interstrand cross-links.* Mutation Research/DNA Repair, 2001. **486**(4): p. 217-247.

173. Lopes-Kulishev, C.O., et al., *Functional characterization of two SOS-regulated genes involved in mitomycin C resistance in Caulobacter crescentus.* DNA Repair (Amst), 2015. **33**: p. 78-89.

174. Sinawe, H. and D. Casadesus, *Mitomycin*, in *StatPearls*. 2022, StatPearls Publishing

Copyright © 2022, StatPearls Publishing LLC.: Treasure Island (FL).

175. Dumbrăveanu, L., V. Cușnir, and D. Bobescu, *A review of neovascular glaucoma. Etiopathogenesis and treatment.* Rom J Ophthalmol, 2021. **65**(4): p. 315-329.

176. Agency, E.M., *Disabling and potentially permanent side effects lead to suspension or restrictions of quinolone and fluoroquinolone antibiotics*, E.M. Agency, Editor. 2019. p. 4.

177. Adams, D.E., et al., *The role of topoisomerase IV in partitioning bacterial replicons and the structure of catenated intermediates in DNA replication.* Cell, 1992. **71**(2): p. 277-88.

178. Peng, H. and K.J. Marians, *Escherichia coli topoisomerase IV. Purification, characterization, subunit structure, and subunit interactions.* J Biol Chem, 1993. **268**(32): p. 24481-90.

179. Hoshino, K., et al., *Comparison of inhibition of Escherichia coli topoisomerase IV by quinolones with DNA gyrase inhibition.* Antimicrob Agents Chemother, 1994. **38**(11): p. 2623-7.
180. Chen, C.R., et al., *DNA gyrase and topoisomerase IV on the bacterial chromosome: quinolone-induced DNA cleavage.* J Mol Biol, 1996. **258**(4): p. 627-37.
181. Kato, J., et al., *New topoisomerase essential for chromosome segregation in E. coli.* Cell, 1990. **63**(2): p. 393-404.
182. Kato, J., H. Suzuki, and H. Ikeda, *Purification and characterization of DNA topoisomerase IV in Escherichia coli.* J Biol Chem, 1992. **267**(36): p. 25676-84.
183. Laponogov, I., et al., *Structural insight into the quinolone-DNA cleavage complex of type IIA topoisomerases.* Nat Struct Mol Biol, 2009. **16**(6): p. 667-9.
184. Blanche, F., et al., *Differential behaviors of Staphylococcus aureus and Escherichia coli type II DNA topoisomerases.* Antimicrob Agents Chemother, 1996. **40**(12): p. 2714-20.
185. Muñoz, R. and A.G. De La Campa, *ParC subunit of DNA topoisomerase IV of Streptococcus pneumoniae is a primary target of fluoroquinolones and cooperates with DNA gyrase A subunit in forming resistance phenotype.* Antimicrob Agents Chemother, 1996. **40**(10): p. 2252-7.
186. Pan, X.S., et al., *Involvement of topoisomerase IV and DNA gyrase as ciprofloxacin targets in Streptococcus pneumoniae.* Antimicrob Agents Chemother, 1996. **40**(10): p. 2321-6.
187. Beranek, D.T., *Distribution of methyl and ethyl adducts following alkylation with monofunctional alkylating agents.* Mutation research, 1990. **231 1**: p. 11-30.
188. Lundin, C., et al., *Methyl methanesulfonate (MMS) produces heat-labile DNA damage but no detectable in vivo DNA double-strand breaks.* Nucleic Acids Res, 2005. **33**(12): p. 3799-811.
189. Ghosh, S., *Cisplatin: The first metal based anticancer drug.* Bioorg Chem, 2019. **88**: p. 102925.

190. Nowosielska, A. and M.G. Marinus, *Cisplatin induces DNA double-strand break formation in Escherichia coli dam mutants.* DNA Repair, 2005. **4**(7): p. 773-781.

191. Eastman, A., *Characterization of the adducts produced in DNA by cis-diamminedichloroplatinum(II) and cis-dichloro(ethylenediamine)platinum(II).* Biochemistry, 1983. **22**(16): p. 3927-33.

192. Keller, K.L., T.L. Overbeck-Carrick, and D.J. Beck, *Survival and induction of SOS in Escherichia coli treated with cisplatin, UV-irradiation, or mitomycin C are dependent on the function of the RecBC and RecFOR pathways of homologous recombination.* Mutat Res, 2001. **486**(1): p. 21-9.

193. Sinha, N.K. and D.P. Snustad, *Mechanism of Inhibition of Deoxyribonucleic Acid Synthesis in Escherichia coli by Hydroxyurea.* Journal of Bacteriology, 1972. **112**(3): p. 1321-1334.

194. Zimanyi, C.M., et al., *Molecular basis for allosteric specificity regulation in class Ia ribonucleotide reductase from Escherichia coli.* eLife, 2016. **5**: p. e07141.

195. Tanaka, T., et al., *Cytometry of ATM activation and histone H2AX phosphorylation to estimate extent of DNA damage induced by exogenous agents.* Cytometry A, 2007. **71**(9): p. 648-61.

196. Koç, A., et al., *Hydroxyurea arrests DNA replication by a mechanism that preserves basal dNTP pools.* J Biol Chem, 2004. **279**(1): p. 223-30.

197. Singh, A. and Y.-J. Xu, *The Cell Killing Mechanisms of Hydroxyurea.* Genes, 2016. **7**(11): p. 99.

198. Rosenkranz, H.S., et al., *Studies with Hydroxyurea VII. Hydroxyurea and the Synthesis of Functional Proteins.* Journal of Bacteriology, 1967. **94**(4): p. 1025-1033.

199. Silva, L.G., et al., *OxyR and the hydrogen peroxide stress response in Caulobacter crescentus.* Gene, 2019. **700**: p. 70-84.

200. Seaver, L.C. and J.A. Imlay, *Hydrogen peroxide fluxes and compartmentalization inside growing Escherichia coli.* J Bacteriol, 2001. **183**(24): p. 7182-9.

201. Aslund, F., et al., *Regulation of the OxyR transcription factor by hydrogen peroxide and the cellular thiol-disulfide status.* Proc Natl Acad Sci U S A, 1999. **96**(11): p. 6161-5.

202. Cabiscol, E., J. Tamarit, and J. Ros, *Oxidative stress in bacteria and protein damage by reactive oxygen species.* Int Microbiol, 2000. **3**(1): p. 3-8.

203. Masip, L., K. Veeravalli, and G. Georgiou, *The many faces of glutathione in bacteria.* Antioxid Redox Signal, 2006. **8**(5-6): p. 753-62.

204. Maxwell, A., *The interaction between coumarin drugs and DNA gyrase.* Molecular Microbiology, 1993. **9**(4): p. 681-686.

205. Schröder, W., C. Goerke, and C. Wolz, *Opposing effects of aminocoumarins and fluoroquinolones on the SOS response and adaptability in Staphylococcus aureus.* Journal of Antimicrobial Chemotherapy, 2012. **68**(3): p. 529-538.

206. Jara, L.M., et al., *Novobiocin Inhibits the Antimicrobial Resistance Acquired through DNA Damage-Induced Mutagenesis in Acinetobacter baumannii.* Antimicrob Agents Chemother, 2016. **60**(1): p. 637-9.

207. Byun, K.-H., et al., *Efficacy of chlorine-based disinfectants (sodium hypochlorite and chlorine dioxide) on Salmonella Enteritidis planktonic cells, biofilms on food contact surfaces and chicken skin.* Food Control, 2021. **123**: p. 107838.

208. Wojtowicz, J.A. *Chlorine Oxygen Acids and Salts, Dichlorine Monoxide, Hypochlorous Acid, and Hypochlorites*. 2000.

209. Fukuzaki, S., *Mechanisms of Actions of Sodium Hypochlorite in Cleaning and Disinfection Processes.* Biocontrol Science, 2006. **11**(4): p. 147-157.

210. Lee, N.Y., S.W. Kim, and S.D. Ha, *Synergistic effects of ultrasound and sodium hypochlorite (NaOCl) on reducing Listeria monocytogenes ATCC19118 in broth, stainless steel, and iceberg lettuce.* Foodborne Pathog Dis, 2014. **11**(7): p. 581-7.

211. Bang, J., et al., *Inactivation of Escherichia coli O157:H7 in biofilm on food-contact surfaces by sequential treatments of aqueous chlorine dioxide and drying.* Int J Food Microbiol, 2014. **191**: p. 129-34.

212. Ristuccia, A.M. and B.A. Cunha, *The aminoglycosides.* Med Clin North Am, 1982. **66**(1): p. 303-12.
213. Garneau-Tsodikova, S. and K.J. Labby, *Mechanisms of Resistance to Aminoglycoside Antibiotics: Overview and Perspectives.* Medchemcomm, 2016. **7**(1): p. 11-27.
214. Zhuang, Y., et al., *Short-Term Pretreatment of Sub-Inhibitory Concentrations of Gentamycin Inhibits the Swarming Motility of Escherichia Coli by Down-Regulating the Succinate Dehydrogenase Gene.* Cell Physiol Biochem, 2016. **39**(4): p. 1307-16.
215. Schnappinger, D. and W. Hillen, *Tetracyclines: antibiotic action, uptake, and resistance mechanisms.* Arch Microbiol, 1996. **165**(6): p. 359-69.
216. Chopra, I., P.M. Hawkey, and M. Hinton, *Tetracyclines, molecular and clinical aspects.* J Antimicrob Chemother, 1992. **29**(3): p. 245-77.
217. Mason, D.J., A. Dietz, and R.M. Smith, *Actinospectacin, a new antibiotic. I. Discovery and biological properties.* Antibiot Chemother (Northfield), 1961. **11**: p. 118-22.
218. Bergy, M.E., T.E. Eble, and R.R. Herr, *Actinospectacin, a new antibiotic. IV. Isolation, purification, and chemical properties.* Antibiot Chemother (Northfield), 1961. **11**: p. 661-4.
219. Galimand, M., G. Gerbaud, and P. Courvalin, *Spectinomycin resistance in Neisseria spp. due to mutations in 16S rRNA.* Antimicrob Agents Chemother, 2000. **44**(5): p. 1365-6.
220. Kanchugal, P.S. and M. Selmer, *Structural Recognition of Spectinomycin by Resistance Enzyme ANT(9) from Enterococcus faecalis.* Antimicrob Agents Chemother, 2020. **64**(6).
221. Sandvang, D., *Novel streptomycin and spectinomycin resistance gene as a gene cassette within a class 1 integron isolated from Escherichia coli.* Antimicrob Agents Chemother, 1999. **43**(12): p. 3036-8.
222. Balganesh, M., et al., *Efflux pumps of Mycobacterium tuberculosis play a significant role in antituberculosis activity of potential drug candidates.* Antimicrob Agents Chemother, 2012. **56**(5): p. 2643-51.

223. Ramon-Garcia, S., et al., *Contribution of the Rv2333c efflux pump (the Stp protein) from Mycobacterium tuberculosis to intrinsic antibiotic resistance in Mycobacterium bovis BCG.* J Antimicrob Chemother, 2007. **59**(3): p. 544-7.
224. Wozniak, K.J. and L.A. Simmons, *Bacterial DNA excision repair pathways.* Nat Rev Microbiol, 2022. **20**(8): p. 465-477.
225. Iyer, R.R., et al., *DNA Mismatch Repair: Functions and Mechanisms.* Chemical Reviews, 2006. **106**(2): p. 302-323.
226. Fishel, R., *Mismatch repair.* J Biol Chem, 2015. **290**(44): p. 26395-403.
227. Tiraby, J.G. and M.S. Fox, *Marker discrimination in transformation and mutation of pneumococcus.* Proc Natl Acad Sci U S A, 1973. **70**(12): p. 3541-5.
228. Siegel, E.C. and V. Bryson, *Mutator gene of Escherichia coli B.* J Bacteriol, 1967. **94**(1): p. 38-47.
229. Guarné, A., *The functions of MutL in mismatch repair: the power of multitasking.* Prog Mol Biol Transl Sci, 2012. **110**: p. 41-70.
230. McHugh, P.J., V.J. Spanswick, and J.A. Hartley, *Repair of DNA interstrand crosslinks: molecular mechanisms and clinical relevance.* Lancet Oncol, 2001. **2**(8): p. 483-90.
231. Eastman, A., *The formation, isolation and characterization of DNA adducts produced by anticancer platinum complexes.* Pharmacol Ther, 1987. **34**(2): p. 155-66.
232. Bellon, S., et al., *Guanine-thymine intrastrand cross-linked lesion containing oligonucleotides: from chemical synthesis to in vitro enzymatic replication.* Org Biomol Chem, 2006. **4**(20): p. 3831-7.
233. Jiang, Y., et al., *In vivo formation and in vitro replication of a guanine-thymine intrastrand cross-link lesion.* Biochemistry, 2007. **46**(44): p. 12757-63.
234. Kuzminov, A., *Recombinational repair of DNA damage in Escherichia coli and bacteriophage lambda.* Microbiol Mol Biol Rev, 1999. **63**(4): p. 751-813, table of contents.

235. Cole, R.S., *Repair of DNA containing interstrand crosslinks in Escherichia coli: sequential excision and recombination.* Proc Natl Acad Sci U S A, 1973. **70**(4): p. 1064-8.

236. Suzuki, H., et al., *On the mechanism of action of bleomycin: scission of DNA strands in vitro and in vivo.* J Antibiot (Tokyo), 1969. **22**(9): p. 446-8.

237. Spies, M. and S.C. Kowalczykowski, *Homologous Recombination by the RecBCD and RecF Pathways*, in *The Bacterial Chromosome*. 2005. p. 389-403.

238. Rothkamm, K., et al., *DNA damage foci: Meaning and significance.* Environ Mol Mutagen, 2015. **56**(6): p. 491-504.

239. Wigley, D.B., *Bacterial DNA repair: recent insights into the mechanism of RecBCD, AddAB and AdnAB.* Nature Reviews Microbiology, 2013. **11**(1): p. 9-13.

240. Pfeiffer, P., W. Goedecke, and G. Obe, *Mechanisms of DNA double-strand break repair and their potential to induce chromosomal aberrations.* Mutagenesis, 2000. **15**(4): p. 289-302.

241. Maslowska, K.H., K. Makiela-Dzbenska, and I.J. Fijalkowska, *The SOS system: A complex and tightly regulated response to DNA damage.* Environ Mol Mutagen, 2019. **60**(4): p. 368-384.

242. Carusillo, A. and C. Mussolino, *DNA Damage: From Threat to Treatment.* Cells, 2020. **9**(7).

243. Dalhus, B., et al., *DNA base repair--recognition and initiation of catalysis.* FEMS Microbiol Rev, 2009. **33**(6): p. 1044-78.

244. Kurthkoti, K., et al., *Base excision repair pathways of bacteria: new promise for an old problem.* Future Med Chem, 2020. **12**(4): p. 339-355.

245. Wallace, S.S., *Base excision repair: a critical player in many games.* DNA Repair (Amst), 2014. **19**: p. 14-26.

246. Stivers, J.T. and Y.L. Jiang, *A mechanistic perspective on the chemistry of DNA repair glycosylases.* Chem Rev, 2003. **103**(7): p. 2729-59.

247. Labahn, J., et al., *Structural basis for the excision repair of alkylation-damaged DNA.* Cell, 1996. **86**(2): p. 321-9.

248. Krokan, H.E. and M. Bjørås, *Base excision repair.* Cold Spring Harb Perspect Biol, 2013. **5**(4): p. a012583.

249. Baute, J. and A. Depicker, *Base excision repair and its role in maintaining genome stability.* Crit Rev Biochem Mol Biol, 2008. **43**(4): p. 239-76.

250. Hollis, T., Y. Ichikawa, and T. Ellenberger, *DNA bending and a flip-out mechanism for base excision by the helix-hairpin-helix DNA glycosylase, Escherichia coli AlkA.* Embo j, 2000. **19**(4): p. 758-66.

251. Grøsvik, K., et al., *The Escherichia coli alkA Gene Is Activated to Alleviate Mutagenesis by an Oxidized Deoxynucleoside.* Front Microbiol, 2020. **11**: p. 263.

252. Aravind, L. and E.V. Koonin, *The DNA-repair protein AlkB, EGL-9, and leprecan define new families of 2-oxoglutarate- and iron-dependent dioxygenases.* Genome Biol, 2001. **2**(3): p. Research0007.

253. Delaney, J.C. and J.M. Essigmann, *Mutagenesis, genotoxicity, and repair of 1-methyladenine, 3-alkylcytosines, 1-methylguanine, and 3-methylthymine in alkB Escherichia coli.* Proc Natl Acad Sci U S A, 2004. **101**(39): p. 14051-6.

254. Margison, G.P., D.P. Cooper, and P.M. Potter, *The E. coli ogt gene.* Mutation Research/Fundamental and Molecular Mechanisms of Mutagenesis, 1990. **233**(1): p. 15-21.

255. Vidal, A., N. Abril, and C. Pueyo, *The influence of DNA repair by Ogt alkyltransferase on the distribution of alkylnitrosourea-induced mutations in Escherichia coli.* Environ Mol Mutagen, 1997. **29**(2): p. 180-8.

256. Abril, N., et al., *The effectiveness of the O(6)-alkylguanine-DNA alkyltransferase encoded by the ogt(ST) gene from S. typhimurium in protection against alkylating drugs, resistance to O(6)-benzylguanine and sensitisation to dibromoalkane genotoxicity.* Mutat Res, 2001. **497**(1-2): p. 111-21.

257. Rippa, V., et al., *Preferential DNA damage prevention by the E. coli AidB gene: A new mechanism for the protection of specific genes.* DNA Repair (Amst), 2011. **10**(9): p. 934-41.

258. Sancar, A. and J.T. Reardon, *Nucleotide Excision Repair in E. Coli and Man*, in *Advances in Protein Chemistry*. 2004, Academic Press. p. 43-71.
259. Puumalainen, M.R., et al., *Xeroderma pigmentosum group C sensor: unprecedented recognition strategy and tight spatiotemporal regulation.* Cell Mol Life Sci, 2016. **73**(3): p. 547-66.
260. Spivak, G., *Nucleotide excision repair in humans.* DNA Repair (Amst), 2015. **36**: p. 13-18.
261. Schärer, O.D., *Nucleotide excision repair in eukaryotes.* Cold Spring Harb Perspect Biol, 2013. **5**(10): p. a012609.
262. Mellon, I. and P.C. Hanawalt, *Induction of the Escherichia coli lactose operon selectively increases repair of its transcribed DNA strand.* Nature, 1989. **342**(6245): p. 95-8.
263. Boyce, R.P. and P. Howard-Flanders, *RELEASE OF ULTRAVIOLET LIGHT-INDUCED THYMINE DIMERS FROM DNA IN E. COLI K-12.* Proceedings of the National Academy of Sciences, 1964. **51**(2): p. 293-300.
264. Howard-Flanders, P., R.P. Boyce, and L. Theriot, *THREE LOCI IN ESCHERICHIA COLI K-12 THAT CONTROL THE EXCISION OF PYRIMIDINE DIMERS AND CERTAIN OTHER MUTAGEN PRODUCTS FROM DNA.* Genetics, 1966. **53**(6): p. 1119-1136.
265. Sancar, A. and W.D. Rupp, *A novel repair enzyme: UVRABC excision nuclease of Escherichia coli cuts a DNA strand on both sides of the damaged region.* Cell, 1983. **33**(1): p. 249-260.
266. Truglio, J.J., et al., *Prokaryotic Nucleotide Excision Repair: The UvrABC System.* Chemical Reviews, 2006. **106**(2): p. 233-252.
267. Pakotiprapha, D., et al., *Structure and mechanism of the UvrA–UvrB DNA damage sensor.* Nature Structural & Molecular Biology, 2012. **19**(3): p. 291-298.
268. Kad, N.M., et al., *Collaborative Dynamic DNA Scanning by Nucleotide Excision Repair Proteins Investigated by Single- Molecule Imaging of Quantum-Dot-Labeled Proteins.* Molecular Cell, 2010. **37**(5): p. 702-713.
269. Stracy, M., et al., *Single-molecule imaging of UvrA and UvrB recruitment to DNA lesions in living Escherichia coli.* Nat Commun, 2016. **7**: p. 12568.

270. Yokota, H., *Roles of the C-Terminal Amino Acids of Non-Hexameric Helicases: Insights from Escherichia coli UvrD.* Int J Mol Sci, 2021. **22**(3).
271. Johnson, S.J. and L.S. Beese, *Structures of mismatch replication errors observed in a DNA polymerase.* Cell, 2004. **116**(6): p. 803-16.
272. Su, S.S., et al., *Mispair specificity of methyl-directed DNA mismatch correction in vitro.* J Biol Chem, 1988. **263**(14): p. 6829-35.
273. Modrich, P., *Methyl-directed DNA mismatch correction.* J Biol Chem, 1989. **264**(12): p. 6597-600.
274. Lenhart, J.S., et al., *Mismatch repair in Gram-positive bacteria.* Res Microbiol, 2016. **167**(1): p. 4-12.
275. Putnam, C.D., *Evolution of the methyl directed mismatch repair system in Escherichia coli.* DNA Repair (Amst), 2016. **38**: p. 32-41.
276. Liao, Y., et al., *Single-molecule motions and interactions in live cells reveal target search dynamics in mismatch repair.* Proc Natl Acad Sci U S A, 2015. **112**(50): p. E6898-906.
277. Chai, T., C. Terrettaz, and J. Collier, *Spatial coupling between DNA replication and mismatch repair in Caulobacter crescentus.* Nucleic Acids Res, 2021. **49**(6): p. 3308-3321.
278. López de Saro, F.J. and M. O'Donnell, *Interaction of the beta sliding clamp with MutS, ligase, and DNA polymerase I.* Proc Natl Acad Sci U S A, 2001. **98**(15): p. 8376-80.
279. Dalrymple, B.P., et al., *A universal protein-protein interaction motif in the eubacterial DNA replication and repair systems.* Proc Natl Acad Sci U S A, 2001. **98**(20): p. 11627-32.
280. Simmons, L.A., et al., *Beta clamp directs localization of mismatch repair in Bacillus subtilis.* Mol Cell, 2008. **29**(3): p. 291-301.
281. Ishino, S., et al., *Identification of a mismatch-specific endonuclease in hyperthermophilic Archaea.* Nucleic Acids Res, 2016. **44**(7): p. 2977-86.
282. Castañeda-García, A., et al., *A non-canonical mismatch repair pathway in prokaryotes.* Nat Commun, 2017. **8**: p. 14246.

283. Ishino, S., et al., *Activation of the mismatch-specific endonuclease EndoMS/NucS by the replication clamp is required for high fidelity DNA replication.* Nucleic Acids Res, 2018. **46**(12): p. 6206-6217.

284. Takemoto, N., et al., *Bacterial EndoMS/NucS acts as a clamp-mediated mismatch endonuclease to prevent asymmetric accumulation of replication errors.* Nucleic Acids Res, 2018. **46**(12): p. 6152-6165.

285. Nakae, S., et al., *Structure of the EndoMS-DNA Complex as Mismatch Restriction Endonuclease.* Structure, 2016. **24**(11): p. 1960-1971.

286. Persky, N.S. and S.T. Lovett, *Mechanisms of recombination: lessons from E. coli.* Crit Rev Biochem Mol Biol, 2008. **43**(6): p. 347-70.

287. Horii, Z. and A.J. Clark, *Genetic analysis of the recF pathway to genetic recombination in Escherichia coli K12: isolation and characterization of mutants.* J Mol Biol, 1973. **80**(2): p. 327-44.

288. Wang, T.V. and K.C. Smith, *recF-dependent and recF recB-independent DNA gap-filling repair processes transfer dimer-containing parental strands to daughter strands in Escherichia coli K-12 uvrB.* J Bacteriol, 1984. **158**(2): p. 727-9.

289. Tseng, Y.C., J.L. Hung, and T.C. Wang, *Involvement of RecF pathway recombination genes in postreplication repair in UV-irradiated Escherichia coli cells.* Mutat Res, 1994. **315**(1): p. 1-9.

290. Kowalczykowski, S.C., *Initiation of genetic recombination and recombination-dependent replication.* Trends Biochem Sci, 2000. **25**(4): p. 156-65.

291. Lloyd, R.G. and C. Buckman, *Identification and genetic analysis of sbcC mutations in commonly used recBC sbcB strains of Escherichia coli K-12.* J Bacteriol, 1985. **164**(2): p. 836-44.

292. Kowalczykowski, S.C., et al., *Biochemistry of homologous recombination in Escherichia coli.* Microbiol Rev, 1994. **58**(3): p. 401-65.

293. Rocha, E.P., E. Cornet, and B. Michel, *Comparative and evolutionary analysis of the bacterial homologous recombination systems.* PLoS Genet, 2005. **1**(2): p. e15.

294. Morimatsu, K. and S.C. Kowalczykowski, *RecQ helicase and RecJ nuclease provide complementary functions to resect DNA for homologous recombination.* Proc Natl Acad Sci U S A, 2014. **111**(48): p. E5133-42.

295. Handa, N., et al., *Reconstitution of initial steps of dsDNA break repair by the RecF pathway of E. coli.* Genes Dev, 2009. **23**(10): p. 1234-45.

296. Harmon, F.G., J.P. Brockman, and S.C. Kowalczykowski, *RecQ helicase stimulates both DNA catenation and changes in DNA topology by topoisomerase III.* J Biol Chem, 2003. **278**(43): p. 42668-78.

297. Lovett, S.T. and A.J. Clark, *Genetic analysis of the recJ gene of Escherichia coli K-12.* J Bacteriol, 1984. **157**(1): p. 190-6.

298. Corrette-Bennett, S.E. and S.T. Lovett, *Enhancement of RecA strand-transfer activity by the RecJ exonuclease of Escherichia coli.* J Biol Chem, 1995. **270**(12): p. 6881-5.

299. Umezu, K., K. Nakayama, and H. Nakayama, *Escherichia coli RecQ protein is a DNA helicase.* Proc Natl Acad Sci U S A, 1990. **87**(14): p. 5363-7.

300. Harmon, F.G. and S.C. Kowalczykowski, *Biochemical characterization of the DNA helicase activity of the escherichia coli RecQ helicase.* J Biol Chem, 2001. **276**(1): p. 232-43.

301. Harmon, F.G., R.J. DiGate, and S.C. Kowalczykowski, *RecQ helicase and topoisomerase III comprise a novel DNA strand passage function: a conserved mechanism for control of DNA recombination.* Mol Cell, 1999. **3**(5): p. 611-20.

302. Sanchez, H. and J.C. Alonso, *Bacillus subtilis RecN binds and protects 3'-single-stranded DNA extensions in the presence of ATP.* Nucleic Acids Res, 2005. **33**(7): p. 2343-50.

303. Sanchez, H., et al., *Recruitment of Bacillus subtilis RecN to DNA double-strand breaks in the absence of DNA end processing.* J Bacteriol, 2006. **188**(2): p. 353-60.

304. Alonso, J.C., et al., *Early steps of double-strand break repair in Bacillus subtilis.* DNA Repair (Amst), 2013. **12**(3): p. 162-76.

305. Morimatsu, K. and S.C. Kowalczykowski, *RecFOR proteins load RecA protein onto gapped DNA to accelerate DNA strand exchange: a universal step of recombinational repair.* Mol Cell, 2003. **11**(5): p. 1337-47.
306. Umezu, K., N.W. Chi, and R.D. Kolodner, *Biochemical interaction of the Escherichia coli RecF, RecO, and RecR proteins with RecA protein and single-stranded DNA binding protein.* Proc Natl Acad Sci U S A, 1993. **90**(9): p. 3875-9.
307. Umezu, K. and R.D. Kolodner, *Protein interactions in genetic recombination in Escherichia coli. Interactions involving RecO and RecR overcome the inhibition of RecA by single-stranded DNA-binding protein.* J Biol Chem, 1994. **269**(47): p. 30005-13.
308. Seigneur, M., et al., *RuvAB acts at arrested replication forks.* Cell, 1998. **95**(3): p. 419-30.
309. Flores, M.J., et al., *Impairment of lagging strand synthesis triggers the formation of a RuvABC substrate at replication forks.* Embo j, 2001. **20**(3): p. 619-29.
310. Briggs, G.S., et al., *Interplay between DNA replication, recombination and repair based on the structure of RecG helicase.* Philos Trans R Soc Lond B Biol Sci, 2004. **359**(1441): p. 49-59.
311. Howard-Flanders, P., *Repair by genetic recombination in bacteria: overview.* Basic Life Sci, 1975. **5a**: p. 265-74.
312. Pagès, V., *Single-strand gap repair involves both RecF and RecBCD pathways.* Curr Genet, 2016. **62**(3): p. 519-21.
313. Wang, B.B., et al., *Review of DNA repair enzymes in bacteria: With a major focus on AddAB and RecBCD.* DNA Repair (Amst), 2022. **118**: p. 103389.
314. Lam, S.T., et al., *Rec-mediated recombinational hot spot activity in bacteriophage lambda. II. A mutation which causes hot spot activity.* Genetics, 1974. **77**(3): p. 425-33.
315. Halpern, D., et al., *Identification of DNA motifs implicated in maintenance of bacterial core genomes by predictive modeling.* PLoS Genet, 2007. **3**(9): p. 1614-21.

316. Liu, B., R.J. Baskin, and S.C. Kowalczykowski, *DNA unwinding heterogeneity by RecBCD results from static molecules able to equilibrate.* Nature, 2013. **500**(7463): p. 482-485.

317. Taylor, A.F. and G.R. Smith, *RecBCD enzyme is a DNA helicase with fast and slow motors of opposite polarity.* Nature, 2003. **423**(6942): p. 889-93.

318. Dillingham, M.S., M. Spies, and S.C. Kowalczykowski, *RecBCD enzyme is a bipolar DNA helicase.* Nature, 2003. **423**(6942): p. 893-7.

319. Dixon, D.A. and S.C. Kowalczykowski, *The recombination hotspot chi is a regulatory sequence that acts by attenuating the nuclease activity of the E. coli RecBCD enzyme.* Cell, 1993. **73**(1): p. 87-96.

320. Bianco, P.R. and S.C. Kowalczykowski, *The recombination hotspot Chi is recognized by the translocating RecBCD enzyme as the single strand of DNA containing the sequence 5'-GCTGGTGG-3'.* Proc Natl Acad Sci U S A, 1997. **94**(13): p. 6706-11.

321. Kidane , D. and P.L. Graumann *Dynamic formation of RecA filaments at DNA double strand break repair centers in live cells.* Journal of Cell Biology, 2005. **170**(3): p. 357-366.

322. Vlašić, I., et al., *Bacillus subtilis RecA and its accessory factors, RecF, RecO, RecR and RecX, are required for spore resistance to DNA double-strand break.* Nucleic Acids Res, 2014. **42**(4): p. 2295-307.

323. Ayora, S., et al., *Double-strand break repair in bacteria: a view from Bacillus subtilis.* FEMS Microbiol Rev, 2011. **35**(6): p. 1055-81.

324. Spies, M. and S.C. Kowalczykowski, *The RecA binding locus of RecBCD is a general domain for recruitment of DNA strand exchange proteins.* Mol Cell, 2006. **21**(4): p. 573-80.

325. Chédin, F., et al., *A five-nucleotide sequence protects DNA from exonucleolytic degradation by AddAB, the RecBCD analogue of Bacillus subtilis.* Mol Microbiol, 1998. **29**(6): p. 1369-77.

326. Yeeles, J.T. and M.S. Dillingham, *A dual-nuclease mechanism for DNA break processing by AddAB-type helicase-nucleases.* J Mol Biol, 2007. **371**(1): p. 66-78.

327. Chédin, F., et al., *The AddAB helicase/nuclease forms a stable complex with its cognate chi sequence during translocation.* J Biol Chem, 2006. **281**(27): p. 18610-7.

328. Sinha, K.M., et al., *AdnAB: a new DSB-resecting motor-nuclease from mycobacteria.* Genes Dev, 2009. **23**(12): p. 1423-37.

329. Unciuleac, M.C. and S. Shuman, *Double strand break unwinding and resection by the mycobacterial helicase-nuclease AdnAB in the presence of single strand DNA-binding protein (SSB).* J Biol Chem, 2010. **285**(45): p. 34319-29.

330. Jia, N., et al., *Structures and single-molecule analysis of bacterial motor nuclease AdnAB illuminate the mechanism of DNA double-strand break resection.* Proceedings of the National Academy of Sciences, 2019. **116**(49): p. 24507-24516.

331. Krajewski, W.W., et al., *Structural basis for translocation by AddAB helicase–nuclease and its arrest at χ sites.* Nature, 2014. **508**(7496): p. 416-419.

332. Unciuleac, M.-C. and S. Shuman, *Characterization of the Mycobacterial AdnAB DNA Motor Provides Insights into the Evolution of Bacterial Motor-Nuclease Machines*.* Journal of Biological Chemistry, 2010. **285**(4): p. 2632-2641.

333. Kushner, S.R., H. Nagaishi, and A.J. Clark, *Indirect suppression of recB and recC mutations by exonuclease I deficiency.* Proc Natl Acad Sci U S A, 1972. **69**(6): p. 1366-70.

334. Gibson, F.P., D.R. Leach, and R.G. Lloyd, *Identification of sbcD mutations as cosuppressors of recBC that allow propagation of DNA palindromes in Escherichia coli K-12.* J Bacteriol, 1992. **174**(4): p. 1222-8.

335. Makarova, K.S., et al., *Genome of the extremely radiation-resistant bacterium Deinococcus radiodurans viewed from the perspective of comparative genomics.* Microbiol Mol Biol Rev, 2001. **65**(1): p. 44-79.

336. Xu, G., et al., *RecO is essential for DNA damage repair in Deinococcus radiodurans.* J Bacteriol, 2008. **190**(7): p. 2624-8.

337. Makharashvili, N., et al., *RecR-mediated modulation of RecF dimer specificity for single- and double-stranded DNA.* J Biol Chem, 2009. **284**(3): p. 1425-34.
338. Nowosielska, A., *Bacterial DNA repair genes and their eukaryotic homologues: 5. The role of recombination in DNA repair and genome stability.* Acta Biochim Pol, 2007. **54**(3): p. 483-94.
339. Kowalczykowski, S.C., *An Overview of the Molecular Mechanisms of Recombinational DNA Repair.* Cold Spring Harb Perspect Biol, 2015. **7**(11).
340. Galletto, R. and S.C. Kowalczykowski, *RecA.* Curr Biol, 2007. **17**(11): p. R395-7.
341. Lee, J.Y., Z. Qi, and E.C. Greene, *ATP hydrolysis Promotes Duplex DNA Release by the RecA Presynaptic Complex.* J Biol Chem, 2016. **291**(42): p. 22218-22230.
342. Hsieh, P., C.S. Camerini-Otero, and R.D. Camerini-Otero, *The synapsis event in the homologous pairing of DNAs: RecA recognizes and pairs less than one helical repeat of DNA.* Proc Natl Acad Sci U S A, 1992. **89**(14): p. 6492-6.
343. Danilowicz, C., et al., *The poor homology stringency in the heteroduplex allows strand exchange to incorporate desirable mismatches without sacrificing recognition in vivo.* Nucleic Acids Res, 2015. **43**(13): p. 6473-85.
344. Bazemore, L.R., et al., *RecA tests homology at both pairing and strand exchange.* Proc Natl Acad Sci U S A, 1997. **94**(22): p. 11863-8.
345. Greene, E.C., *DNA Sequence Alignment during Homologous Recombination.* J Biol Chem, 2016. **291**(22): p. 11572-80.
346. Rosselli, W. and A. Stasiak, *The ATPase activity of RecA is needed to push the DNA strand exchange through heterologous regions.* Embo j, 1991. **10**(13): p. 4391-6.
347. Bianco, P.R., *I came to a fork in the DNA and there was RecG.* Prog Biophys Mol Biol, 2015. **117**(2-3): p. 166-173.
348. Del Val, E., et al., *RecA and DNA recombination: a review of molecular mechanisms.* Biochem Soc Trans, 2019. **47**(5): p. 1511-1531.

349. Bell, J.C. and S.C. Kowalczykowski, *RecA: Regulation and Mechanism of a Molecular Search Engine.* Trends Biochem Sci, 2016. **41**(6): p. 491-507.
350. Little, J.W. and D.W. Mount, *The SOS regulatory system of Escherichia coli.* Cell, 1982. **29**(1): p. 11-22.
351. Blanchard, L. and A. de Groot, *Coexistence of SOS-Dependent and SOS-Independent Regulation of DNA Repair Genes in Radiation-Resistant Deinococcus Bacteria.* Cells, 2021. **10**(4).
352. Butala, M., D. Zgur-Bertok, and S.J. Busby, *The bacterial LexA transcriptional repressor.* Cell Mol Life Sci, 2009. **66**(1): p. 82-93.
353. Sassanfar, M. and J.W. Roberts, *Nature of the SOS-inducing signal in Escherichia coli. The involvement of DNA replication.* J Mol Biol, 1990. **212**(1): p. 79-96.
354. Cox, M.M., *Why does RecA protein hydrolyse ATP?* Trends Biochem Sci, 1994. **19**(5): p. 217-22.
355. Menetski, J.P. and S.C. Kowalczykowski, *Interaction of recA protein with single-stranded DNA. Quantitative aspects of binding affinity modulation by nucleotide cofactors.* J Mol Biol, 1985. **181**(2): p. 281-95.
356. Kim, J.I., M.M. Cox, and R.B. Inman, *On the role of ATP hydrolysis in RecA protein-mediated DNA strand exchange. II. Four-strand exchanges.* J Biol Chem, 1992. **267**(23): p. 16444-9.
357. Roman, L.J. and S.C. Kowalczykowski, *Characterization of the adenosinetriphosphatase activity of the Escherichia coli RecBCD enzyme: relationship of ATP hydrolysis to the unwinding of duplex DNA.* Biochemistry, 1989. **28**(7): p. 2873-81.
358. Roman, L.J. and S.C. Kowalczykowski, *Characterization of the helicase activity of the Escherichia coli RecBCD enzyme using a novel helicase assay.* Biochemistry, 1989. **28**(7): p. 2863-73.
359. Deng, Y., et al., *Measuring and modeling energy and power consumption in living microbial cells with a synthetic ATP reporter.* BMC Biology, 2021. **19**(1): p. 101.

360. Reuter, M., et al., *Single-molecule imaging of Bacteroides fragilis AddAB reveals the highly processive translocation of a single motor helicase.* Nucleic Acids Res, 2010. **38**(11): p. 3721-31.

361. Velankar, S.S., et al., *Crystal structures of complexes of PcrA DNA helicase with a DNA substrate indicate an inchworm mechanism.* Cell, 1999. **97**(1): p. 75-84.

362. Lee, J.Y. and W. Yang, *UvrD helicase unwinds DNA one base pair at a time by a two-part power stroke.* Cell, 2006. **127**(7): p. 1349-60.

363. Dillingham, M.S., D.B. Wigley, and M.R. Webb, *Demonstration of unidirectional single-stranded DNA translocation by PcrA helicase: measurement of step size and translocation speed.* Biochemistry, 2000. **39**(1): p. 205-12.

364. Bertrand, C., et al., *Bacterial NHEJ: a never ending story.* Mol Microbiol, 2019. **111**(5): p. 1139-1151.

365. Pitcher, R.S., N.C. Brissett, and A.J. Doherty, *Nonhomologous end-joining in bacteria: a microbial perspective.* Annu Rev Microbiol, 2007. **61**: p. 259-82.

366. Zhang, X., et al., *Deletion of ku homologs increases gene targeting frequency in Streptomyces avermitilis.* J Ind Microbiol Biotechnol, 2012. **39**(6): p. 917-25.

367. Hoff, G., et al., *Multiple and Variable NHEJ-Like Genes Are Involved in Resistance to DNA Damage in Streptomyces ambofaciens.* Front Microbiol, 2016. **7**: p. 1901.

368. Raguse, M., et al., *Bacillus subtilis DisA helps to circumvent replicative stress during spore revival.* DNA Repair (Amst), 2017. **59**: p. 57-68.

369. Dupuy, P., L. Sauviac, and C. Bruand, *Stress-inducible NHEJ in bacteria: function in DNA repair and acquisition of heterologous DNA.* Nucleic Acids Res, 2019. **47**(3): p. 1335-1349.

370. Cytryn, E.J., et al., *Transcriptional and physiological responses of Bradyrhizobium japonicum to desiccation-induced stress.* J Bacteriol, 2007. **189**(19): p. 6751-62.

371. Alexandre, A., M. Laranjo, and S. Oliveira, *Global transcriptional response to heat shock of the legume symbiont Mesorhizobium loti MAFF303099 comprises extensive gene downregulation.* DNA Res, 2014. **21**(2): p. 195-206.

372. McGovern, S., et al., *C-terminal region of bacterial Ku controls DNA bridging, DNA threading and recruitment of DNA ligase D for double strand breaks repair.* Nucleic Acids Res, 2016. **44**(10): p. 4785-4806.

373. Chayot, R., et al., *An end-joining repair mechanism in Escherichia coli.* Proc Natl Acad Sci U S A, 2010. **107**(5): p. 2141-6.

374. Gong, C., et al., *Biochemical and genetic analysis of the four DNA ligases of mycobacteria.* J Biol Chem, 2004. **279**(20): p. 20594-606.

375. Gong, C., et al., *Mechanism of nonhomologous end-joining in mycobacteria: a low-fidelity repair system driven by Ku, ligase D and ligase C.* Nat Struct Mol Biol, 2005. **12**(4): p. 304-12.

376. Aniukwu, J., M.S. Glickman, and S. Shuman, *The pathways and outcomes of mycobacterial NHEJ depend on the structure of the broken DNA ends.* Genes Dev, 2008. **22**(4): p. 512-27.

377. Pitcher, R.S., et al., *Mycobacteriophage exploit NHEJ to facilitate genome circularization.* Mol Cell, 2006. **23**(5): p. 743-8.

378. Wilson, T.E., L.M. Topper, and P.L. Palmbos, *Non-homologous end-joining: bacteria join the chromosome breakdance.* Trends Biochem Sci, 2003. **28**(2): p. 62-6.

379. Malyarchuk, S., et al., *Expression of Mycobacterium tuberculosis Ku and Ligase D in Escherichia coli results in RecA and RecB-independent DNA end-joining at regions of microhomology.* DNA Repair (Amst), 2007. **6**(10): p. 1413-24.

380. Van Houten, B., *Nucleotide excision repair in Escherichia coli.* Microbiol Rev, 1990. **54**(1): p. 18-51.

381. Sladek, F.M., et al., *In vitro repair of psoralen-DNA cross-links by RecA, UvrABC, and the 5'-exonuclease of DNA polymerase I.* J Biol Chem, 1989. **264**(12): p. 6755-65.

382. Cole, R.S., D. Levitan, and R.R. Sinden, *Removal of psoralen interstrand cross-links from DNA of Escherichia coli: mechanism and genetic control.* J Mol Biol, 1976. **103**(1): p. 39-59.

383. Cheng, S., A. Sancar, and J.E. Hearst, *RecA-dependent incision of psoralen-crosslinked DNA by (A)BC excinuclease.* Nucleic Acids Res, 1991. **19**(3): p. 657-63.

384. Li, X. and W.D. Heyer, *Homologous recombination in DNA repair and DNA damage tolerance.* Cell Res, 2008. **18**(1): p. 99-113.

385. Shah Punatar, R., et al., *Resolution of single and double Holliday junction recombination intermediates by GEN1*. Proceedings of the National Academy of Sciences, 2017. **114**(3): p. 443-450.

386. Van Houten, B., et al., *Action mechanism of ABC excision nuclease on a DNA substrate containing a psoralen crosslink at a defined position.* Proc Natl Acad Sci U S A, 1986. **83**(21): p. 8077-81.

387. Berardini, M., P.L. Foster, and E.L. Loechler, *DNA polymerase II (polB) is involved in a new DNA repair pathway for DNA interstrand cross-links in Escherichia coli.* J Bacteriol, 1999. **181**(9): p. 2878-82.

388. Walker, G.C., *Mutagenesis and inducible responses to deoxyribonucleic acid damage in Escherichia coli.* Microbiol Rev, 1984. **48**(1): p. 60-93.

389. Echols, H. and M.F. Goodman, *Mutation induced by DNA damage: a many protein affair.* Mutation Research/DNA Repair, 1990. **236**(2): p. 301-311.

390. Cheo, D.L., K.W. Bayles, and R.E. Yasbin, *Cloning and characterization of DNA damage-inducible promoter regions from Bacillus subtilis.* Journal of Bacteriology, 1991. **173**(5): p. 1696-1703.

391. Au, N., et al., *Genetic Composition of the Bacillus subtilis SOS System.* Journal of Bacteriology, 2005. **187**(22): p. 7655-7666.

392. Goranov, A.I., et al., *Characterization of the Global Transcriptional Responses to Different Types of DNA Damage and Disruption of Replication in Bacillus subtilis.* Journal of Bacteriology, 2006. **188**(15): p. 5595-5605.

393. Smith, B.T. and G.C. Walker, *Mutagenesis and more: umuDC and the Escherichia coli SOS response.* Genetics, 1998. **148**(4): p. 1599-610.

394. Woodgate, R. and S.G. Sedgwick, *Mutagenesis induced by bacterial UmuDC proteins and their plasmid homologues.* Mol Microbiol, 1992. **6**(16): p. 2213-8.

395. Sommer, S., et al., *Induction of only one SOS operon, umuDC, is required for SOS mutagenesis in Escherichia coli.* Mol Gen Genet, 1993. **239**(1-2): p. 137-44.

396. Bagg, A., C.J. Kenyon, and G.C. Walker, *Inducibility of a gene product required for UV and chemical mutagenesis in Escherichia coli.* Proc Natl Acad Sci U S A, 1981. **78**(9): p. 5749-53.

397. Bailone, A., et al., *A RecA protein mutant deficient in its interaction with the UmuDC complex.* Biochimie, 1991. **73**(4): p. 479-84.

398. Burckhardt, S.E., et al., *UmuD mutagenesis protein of Escherichia coli: overproduction, purification, and cleavage by RecA.* Proc Natl Acad Sci U S A, 1988. **85**(6): p. 1811-5.

399. Rajagopalan, M., et al., *Activity of the purified mutagenesis proteins UmuC, UmuD', and RecA in replicative bypass of an abasic DNA lesion by DNA polymerase III.* Proc Natl Acad Sci U S A, 1992. **89**(22): p. 10777-81.

400. Tang, M., et al., *Biochemical basis of SOS-induced mutagenesis in Escherichia coli: reconstitution of in vitro lesion bypass dependent on the UmuD'2C mutagenic complex and RecA protein.* Proc Natl Acad Sci U S A, 1998. **95**(17): p. 9755-60.

401. Kim, S.R., et al., *Roles of chromosomal and episomal dinB genes encoding DNA pol IV in targeted and untargeted mutagenesis in Escherichia coli.* Mol Genet Genomics, 2001. **266**(2): p. 207-15.

402. Cafarelli, T.M., T.J. Rands, and V.G. Godoy, *The DinB•RecA complex of Escherichia coli mediates an efficient and high-fidelity response to ubiquitous alkylation lesions.* Environ Mol Mutagen, 2014. **55**(2): p. 92-102.

403. Benson, R.W., et al., *An active site aromatic triad in Escherichia coli DNA Pol IV coordinates cell survival and mutagenesis in different DNA damaging agents.* PLoS One, 2011. **6**(5): p. e19944.

404. Jarosz, D.F., et al., *A single amino acid governs enhanced activity of DinB DNA polymerases on damaged templates.* Nature, 2006. **439**(7073): p. 225-228.

405. Jarosz, D.F., V.G. Godoy, and G.C. Walker, *Proficient and accurate bypass of persistent DNA lesions by DinB DNA polymerases.* Cell Cycle, 2007. **6**(7): p. 817-22.

406. Yuan, B., et al., *Efficient and accurate bypass of N²-(1-carboxyethyl)-2′-deoxyguanosine by DinB DNA polymerase in vitro and in vivo.* Proceedings of the National Academy of Sciences, 2008. **105**(25): p. 8679-8684.

407. Bjedov, I., et al., *Involvement of Escherichia coli DNA polymerase IV in tolerance of cytotoxic alkylating DNA lesions in vivo.* Genetics, 2007. **176**(3): p. 1431-40.

408. Cafarelli, T.M., et al., *A Single Residue Unique to DinB-Like Proteins Limits Formation of the Polymerase IV Multiprotein Complex in Escherichia coli.* Journal of Bacteriology, 2013. **195**(6): p. 1179-1193.

409. Friedberg, E.C., P.L. Fischhaber, and C. Kisker, *Error-prone DNA polymerases: novel structures and the benefits of infidelity.* Cell, 2001. **107**(1): p. 9-12.

410. Yang, W., *Damage repair DNA polymerases Y.* Current Opinion in Structural Biology, 2003. **13**(1): p. 23-30.

411. Kim, S.R., et al., *Roles of chromosomal and episomal dinB genes encoding DNA pol IV in targeted and untargeted mutagenesis in Escherichia coli.* Molecular Genetics and Genomics, 2001. **266**(2): p. 207-215.

412. Nohmi, T., *Environmental Stress and Lesion-Bypass DNA Polymerases.* Annual Review of Microbiology, 2006. **60**(1): p. 231-253.

413. Duigou, S., et al., *Distinctive genetic features exhibited by the Y-family DNA polymerases in Bacillus subtilis.* Molecular Microbiology, 2004. **54**(2): p. 439-451.

414. Rivas-Castillo, A.M., et al., *Role of the Y-Family DNA Polymerases YqjH and YqjW in Protecting Sporulating Bacillus subtilis Cells from DNA Damage.* Current Microbiology, 2010. **60**(4): p. 263-267.

415. Galhardo, R.S., et al., *An SOS-regulated operon involved in damage-inducible mutagenesis in Caulobacter crescentus.* Nucleic Acids Res, 2005. **33**(8): p. 2603-14.

416. Erill, I., et al., *Dispersal and regulation of an adaptive mutagenesis cassette in the bacteria domain.* Nucleic Acids Res, 2006. **34**(1): p. 66-77.

417. Alves, I.R., et al., *Effect of SOS-induced levels of imuABC on spontaneous and damage-induced mutagenesis in Caulobacter crescentus.* DNA Repair, 2017. **59**: p. 20-26.

418. Martins-Pinheiro, M., R.C. Marques, and C.F. Menck, *Genome analysis of DNA repair genes in the alpha proteobacterium Caulobacter crescentus.* BMC Microbiol, 2007. **7**: p. 17.

419. Bruck, I., M.F. Goodman, and M. O'Donnell, *The essential C family DnaE polymerase is error-prone and efficient at lesion bypass.* J Biol Chem, 2003. **278**(45): p. 44361-8.

420. Le Chatelier, E., et al., *Involvement of DnaE, the second replicative DNA polymerase from Bacillus subtilis, in DNA mutagenesis.* J Biol Chem, 2004. **279**(3): p. 1757-67.

421. Foster, P.L., *Stress-induced mutagenesis in bacteria.* Crit Rev Biochem Mol Biol, 2007. **42**(5): p. 373-97.

422. Podlesek, Z. and D. Žgur Bertok, *The DNA Damage Inducible SOS Response Is a Key Player in the Generation of Bacterial Persister Cells and Population Wide Tolerance.* Frontiers in Microbiology, 2020. **11**.

423. Goormaghtigh, F. and L. Van Melderen, *Single-cell imaging and characterization of Escherichia coli persister cells to ofloxacin in exponential cultures.* Sci Adv, 2019. **5**(6): p. eaav9462.

424. Dorr, T., K. Lewis, and M. Vulic, *SOS response induces persistence to fluoroquinolones in Escherichia coli.* PLoS Genet, 2009. **5**(12): p. e1000760.

425. Trastoy, R., et al., *Mechanisms of Bacterial Tolerance and Persistence in the Gastrointestinal and Respiratory Environments.* Clin Microbiol Rev, 2018. **31**(4).

426. Molina-Quiroz, R.C., et al., *Cyclic AMP Regulates Bacterial Persistence through Repression of the Oxidative Stress Response and SOS-Dependent DNA Repair in Uropathogenic Escherichia coli.* mBio, 2018. **9**(1).
427. Fall, S., et al., *Horizontal Gene Transfer Regulation in Bacteria as a "Spandrel" of DNA Repair Mechanisms.* Plos One, 2007. **2**(10).
428. Kwan, B.W., et al., *Arrested protein synthesis increases persister-like cell formation.* Antimicrob Agents Chemother, 2013. **57**(3): p. 1468-73.
429. Harms, A., E. Maisonneuve, and K. Gerdes, *Mechanisms of bacterial persistence during stress and antibiotic exposure.* Science, 2016. **354**(6318).
430. *The SOS Responses of Prokaryotes to DNA Damage*, in *DNA Repair and Mutagenesis*. 2005. p. 463-508.
431. da Rocha, R.P., et al., *Characterization of the SOS regulon of Caulobacter crescentus.* J Bacteriol, 2008. **190**(4): p. 1209-18.
432. Fonseca, L.S., et al., *Leptospira interrogans serovar copenhageni harbors two lexA genes involved in SOS response.* PLoS One, 2013. **8**(10): p. e76419.
433. Cirz, R.T., et al., *Complete and SOS-mediated response of Staphylococcus aureus to the antibiotic ciprofloxacin.* J Bacteriol, 2007. **189**(2): p. 531-9.
434. Matic, I., F. Taddei, and M. Radman, *Survival versus maintenance of genetic stability: a conflict of priorities during stress.* Res Microbiol, 2004. **155**(5): p. 337-41.
435. Erill, I., S. Campoy, and J. Barbe, *Aeons of distress: an evolutionary perspective on the bacterial SOS response.* Fems Microbiology Reviews, 2007. **31**(6): p. 637-656.
436. Butala, M., D. Zgur-Bertok, and S.J.W. Busby, *The bacterial LexA transcriptional repressor.* Cellular and Molecular Life Sciences, 2009. **66**(1): p. 82-93.
437. Erill, I., et al., *Differences in LexA regulon structure among Proteobacteria through in vivo assisted comparative genomics.* Nucleic Acids Res, 2004. **32**(22): p. 6617-26.

438. Au, N., et al., *Genetic composition of the Bacillus subtilis SOS system.* J Bacteriol, 2005. **187**(22): p. 7655-66.

439. Goranov, A.I., et al., *Characterization of the global transcriptional responses to different types of DNA damage and disruption of replication in Bacillus subtilis.* J Bacteriol, 2006. **188**(15): p. 5595-605.

440. Courcelle, J., et al., *Comparative gene expression profiles following UV exposure in wild-type and SOS-deficient Escherichia coli.* Genetics, 2001. **158**(1): p. 41-64.

441. Friedberg, E.C., *DNA repair and mutagenesis (2nd ed.)*. ASM Press. Vol. ISBN 978-1-55581-319-2. (2006).

442. Galhardo, R.S., et al., *An SOS-regulated operon involved in damage-inducible mutagenesis in Caulobacter crescentus.* Nucleic Acids Research, 2005. **33**(8): p. 2603-2614.

443. Modell, J.W., A.C. Hopkins, and M.T. Laub, *A DNA damage checkpoint in Caulobacter crescentus inhibits cell division through a direct interaction with FtsW (vol 25, pg 1328, 2011).* Genes & Development, 2011. **25**(15): p. 1662-1662.

444. Frohlich, K.S., K.U. Forstner, and Z. Gitai, *Post-transcriptional gene regulation by an Hfq-independent small RNA in Caulobacter crescentus.* Nucleic Acids Research, 2018. **46**(20): p. 10969-10982.

445. Janion, C., *Inducible SOS response system of DNA repair and mutagenesis in Escherichia coli.* Int J Biol Sci, 2008. **4**(6): p. 338-44.

446. López, E., et al., *Antibiotic-mediated recombination: ciprofloxacin stimulates SOS-independent recombination of divergent sequences in Escherichia coli.* Mol Microbiol, 2007. **64**(1): p. 83-93.

447. Prudhomme, M., et al., *Antibiotic stress induces genetic transformability in the human pathogen Streptococcus pneumoniae.* Science, 2006. **313**(5783): p. 89-92.

448. Dorer, M.S., T.H. Sessler, and N.R. Salama, *Recombination and DNA repair in Helicobacter pylori.* Annu Rev Microbiol, 2011. **65**: p. 329-48.

449. Modell, J.W., et al., *A DNA Damage-Induced, SOS-Independent Checkpoint Regulates Cell Division in Caulobacter crescentus.* Plos Biology, 2014. **12**(10).

450. Gozzi, K., et al., *ssDNA is an allosteric regulator of the C. crescentus SOS-independent DNA damage response transcription activator, DriD.* Genes & Development, 2022. **36**.

451. Steinberg, R. and H.-G. Koch, *The largely unexplored biology of small proteins in pro- and eukaryotes.* FEBS J., 2021. **288: 7002-7024**(3).

452. Storz, G., Y.I. Wolf, and K.S. Ramamurthi, *Small Proteins Can No Longer Be Ignored.* Annual Review of Biochemistry, Vol 83, 2014. **83**: p. 753-+.

453. Hemm, M.R., et al., *Small membrane proteins found by comparative genomics and ribosome binding site models.* Mol Microbiol, 2008. **70**(6): p. 1487-501.

454. Fontaine, F., R.T. Fuchs, and G. Storz, *Membrane localization of small proteins in Escherichia coli.* J Biol Chem, 2011. **286**(37): p. 32464-74.

455. Steinberg, R., et al., *Posttranslational insertion of small membrane proteins by the bacterial signal recognition particle.* PLoS Biol, 2020. **18**(9): p. e3000874.

456. Hobbs, E.C., et al., *An expanding universe of small proteins.* Current Opinion in Microbiology, 2011. **14**(2): p. 167-173.

457. Fontaine, F., R.T. Fuchs, and G. Storz, *Membrane Localization of Small Proteins in Escherichia coli.* Journal of Biological Chemistry, 2011. **286**(37): p. 32464-32474.

458. Steinberg, R., et al., *Posttranslational insertion of small membrane proteins by the bacterial signal recognition particle.* PLOS Biology, 2020. **18**(9): p. e3000874.

459. Maggi, S., et al., *Functional characterization of the type I toxin Lpt from Lactobacillus rhamnosus by fluorescence and atomic force microscopy.* Sci Rep, 2019. **9**(1): p. 15208.

460. Yang, X., et al., *Discovery and annotation of small proteins using genomics, proteomics, and computational approaches.* Genome research, 2011. **21**(4): p. 634-641.

461. Bartholomaus, A., et al., *smORFer: a modular algorithm to detect small ORFs in prokaryotes.* Nucleic Acids Res, 2021. **49**(15): p. e89.
462. Li, L. and Y. Chao, *sPepFinder expedites genome-wide identification of small proteins in bacteria.* bioRxiv, 2020: p. 2020.05.05.079178.
463. Samayoa, J., F.H. Yildiz, and K. Karplus, *Identification of prokaryotic small proteins using a comparative genomic approach.* Bioinformatics, 2011. **27**(13): p. 1765-1771.
464. Impens, F., et al., *N-terminomics identifies Prli42 as a membrane miniprotein conserved in Firmicutes and critical for stressosome activation in Listeria monocytogenes.* Nature Microbiology, 2017. **2**(5): p. 17005.
465. Slavoff, S.A., et al., *Peptidomic discovery of short open reading frame–encoded peptides in human cells.* Nature Chemical Biology, 2013. **9**(1): p. 59-64.
466. Shen, Y., et al., *Improved PEP-FOLD Approach for Peptide and Miniprotein Structure Prediction.* Journal of Chemical Theory and Computation, 2014. **10**(10): p. 4745-4758.
467. Vishnepolsky, B. and M. Pirtskhalava, *Prediction of Linear Cationic Antimicrobial Peptides Based on Characteristics Responsible for Their Interaction with the Membranes.* Journal of Chemical Information and Modeling, 2014. **54**(5): p. 1512-1523.
468. Aspden, J.L., et al., *Extensive translation of small Open Reading Frames revealed by Poly-Ribo-Seq.* eLife, 2014. **3**: p. e03528.
469. Hao, Y., et al., *SmProt: a database of small proteins encoded by annotated coding and non-coding RNA loci.* Brief Bioinform, 2018. **19**(4): p. 636-643.
470. Gusic, M. and H. Prokisch, *ncRNAs: New Players in Mitochondrial Health and Disease?* Frontiers in Genetics, 2020. **11**(95).
471. Makarewich, C.A., *The hidden world of membrane microproteins.* Experimental cell research, 2020. **388**(2): p. 111853-111853.
472. Chu, Q., et al., *Regulation of the ER stress response by a mitochondrial microprotein.* Nat Commun, 2019. **10**(1): p. 4883.
473. Wang, F., et al., *A systematic survey of mini-proteins in bacteria and archaea.* PLoS One, 2008. **3**(12): p. e4027.

474. Khitun, A., T.J. Ness, and S.A. Slavoff, *Small open reading frames and cellular stress responses.* Mol Omics, 2019. **15**(2): p. 108-116.
475. Zickermann, V., et al., *Small single transmembrane domain (STMD) proteins organize the hydrophobic subunits of large membrane protein complexes.* FEBS Lett, 2010. **584**(12): p. 2516-25.
476. Duval, M. and P. Cossart, *Small bacterial and phagic proteins: an updated view on a rapidly moving field.* Current Opinion in Microbiology, 2017. **39**: p. 81-88.
477. Denks, K., et al., *The Sec translocon mediated protein transport in prokaryotes and eukaryotes.* Mol Membr Biol, 2014. **31**(2-3): p. 58-84.
478. Balchin, D., M. Hayer-Hartl, and F.U. Hartl, *Recent advances in understanding catalysis of protein folding by molecular chaperones.* FEBS Lett, 2020. **594**(17): p. 2770-2781.
479. Zimmermann, R., et al., *Protein translocation across the ER membrane.* Biochim Biophys Acta, 2011. **1808**(3): p. 912-24.
480. Hemm, M.R., J. Weaver, and G. Storz, *Escherichia coli Small Proteome.* EcoSal Plus, 2020. **9**(1).
481. VanOrsdel, C.E., et al., *Identifying New Small Proteins in Escherichia coli.* Proteomics, 2018. **18**(10): p. e1700064-e1700064.
482. Hemm, M.R., et al., *Small stress response proteins in Escherichia coli: proteins missed by classical proteomic studies.* J Bacteriol, 2010. **192**(1): p. 46-58.
483. Alix, E. and A.-B. Blanc-Potard, *Hydrophobic peptides: novel regulators within bacterial membrane.* Molecular Microbiology, 2009. **72**(1): p. 5-11.
484. Lloyd, C.R., et al., *The Small Protein SgrT Controls Transport Activity of the Glucose-Specific Phosphotransferase System.* J Bacteriol, 2017. **199**(11).
485. Gassel, M., et al., *The KdpF subunit is part of the K+-translocating Kdp complex of Escherichia coli and is responsible for stabilization of the complex in vitro.* Journal of Biological Chemistry, 1999. **274**(53): p. 37901-37907.

486. Miyashiro, T. and M. Goulian, *Stimulus-dependent differential regulation in the Escherichia coli PhoQ PhoP system.* Proc Natl Acad Sci U S A, 2007. **104**(41): p. 16305-10.

487. Lippa, A.M. and M. Goulian, *Feedback inhibition in the PhoQ/PhoP signaling system by a membrane peptide.* PLoS Genet, 2009. **5**(12): p. e1000788.

488. Burkholder, W.F., I. Kurtser, and A.D. Grossman, *Replication initiation proteins regulate a developmental checkpoint in Bacillus subtilis.* Cell, 2001. **104**(2): p. 269-279.

489. Gassel, M., et al., *The KdpF subunit is part of the K(+)-translocating Kdp complex of Escherichia coli and is responsible for stabilization of the complex in vitro.* J Biol Chem, 1999. **274**(53): p. 37901-7.

490. Alix, E. and A.B. Blanc-Potard, *Peptide-assisted degradation of the Salmonella MgtC virulence factor.* Embo Journal, 2008. **27**(3): p. 546-557.

491. Martin, J.E., et al., *The Escherichia coli small protein MntS and exporter MntP optimize the intracellular concentration of manganese.* PLoS Genet, 2015. **11**(3): p. e1004977.

492. Hobbs, E.C., et al., *Conserved small protein associates with the multidrug efflux pump AcrB and differentially affects antibiotic resistance.* Proc Natl Acad Sci U S A, 2012. **109**(41): p. 16696-701.

493. Brielle, R., M.-L. Pinel-Marie, and B. Felden, *Linking bacterial type I toxins with their actions.* Current Opinion in Microbiology, 2016. **30**: p. 114-121.

494. Fozo, E.M., M.R. Hemm, and G. Storz, *Small toxic proteins and the antisense RNAs that repress them.* Microbiol Mol Biol Rev, 2008. **72**(4): p. 579-89, Table of Contents.

495. Brantl, S. and N. Jahn, *sRNAs in bacterial type I and type III toxin-antitoxin systems.* FEMS Microbiology Reviews, 2015. **39**(3): p. 413-427.

496. Sayed, N., et al., *Functional and Structural Insights of a Staphylococcus aureus Apoptotic-like Membrane Peptide from a Toxin-Antitoxin Module*.* Journal of Biological Chemistry, 2012. **287**(52): p. 43454-43463.

497. Karplus, M., *Behind the folding funnel diagram.* Nat Chem Biol, 2011. **7**(7): p. 401-4.

498. Neidigh, J.W., R.M. Fesinmeyer, and N.H. Andersen, *Designing a 20-residue protein.* Nature Structural Biology, 2002. **9**(6): p. 425-430.
499. Gellman, S.H. and D.N. Woolfson, *Mini-proteins Trp the light fantastic.* Nat Struct Biol, 2002. **9**(6): p. 408-10.
500. Rocklin, G.J., et al., *Global analysis of protein folding using massively parallel design, synthesis, and testing.* Science, 2017. **357**(6347): p. 168-175.
501. Kubatova, N., et al., *Rapid Biophysical Characterization and NMR Spectroscopy Structural Analysis of Small Proteins from Bacteria and Archaea.* Chembiochem : a European journal of chemical biology, 2020. **21**(8): p. 1178-1187.
502. Zhang, L.-j. and R.L. Gallo, *Antimicrobial peptides.* Current Biology, 2016. **26**(1): p. R14-R19.
503. Bechinger, B., *Insights into the mechanisms of action of host defence peptides from biophysical and structural investigations.* J Pept Sci, 2011. **17**(5): p. 306-14.
504. Bechinger, B. and C. Aisenbrey, *The polymorphic nature of membrane-active peptides from biophysical and structural investigations.* Curr Protein Pept Sci, 2012. **13**(7): p. 602-10.
505. Salinas, N., et al., *The amphibian antimicrobial peptide uperin 3.5 is a cross-α/cross-β chameleon functional amyloid.* Proc Natl Acad Sci U S A, 2021. **118**(3).
506. Boyd, D., C. Manoil, and J. Beckwith, *Determinants of membrane protein topology.* Proc Natl Acad Sci U S A, 1987. **84**(23): p. 8525-9.
507. Kuhn, A., H.G. Koch, and R.E. Dalbey, *Targeting and Insertion of Membrane Proteins.* EcoSal Plus, 2017. **7**(2).
508. Haßdenteufel, S., et al., *ER import of small human presecretory proteins: components and mechanisms.* FEBS Letters, 2019. **593**(18): p. 2506-2524.
509. Müller, M., et al., *Protein traffic in bacteria: multiple routes from the ribosome to and across the membrane.* Prog Nucleic Acid Res Mol Biol, 2001. **66**: p. 107-57.

510. Hizlan, D., et al., *Structure of the SecY complex unlocked by a preprotein mimic.* Cell Rep, 2012. **1**(1): p. 21-8.
511. Park, E. and T.A. Rapoport, *Mechanisms of Sec61/SecY-mediated protein translocation across membranes.* Annu Rev Biophys, 2012. **41**: p. 21-40.
512. Voorhees, R.M. and R.S. Hegde, *Structure of the Sec61 channel opened by a signal sequence.* Science, 2016. **351**(6268): p. 88-91.
513. Jung, S., et al., *SecY-mediated quality control prevents the translocation of non-gated porins.* Sci Rep, 2020. **10**(1): p. 16347.
514. Herranz, C. and A.J. Driessen, *Sec-mediated secretion of bacteriocin enterocin P by Lactococcus lactis.* Appl Environ Microbiol, 2005. **71**(4): p. 1959-63.
515. van den Berg van Saparoea, H.B., et al., *Distinct Contributions of the Nisin Biosynthesis Enzymes NisB and NisC and Transporter NisT to Prenisin Production by Lactococcus lactis*. Applied and Environmental Microbiology, 2008. **74**(17): p. 5541-5548.
516. Beis, K. and S. Rebuffat, *Multifaceted ABC transporters associated to microcin and bacteriocin export.* Res Microbiol, 2019. **170**(8): p. 399-406.
517. Hassan, M., et al., *Natural antimicrobial peptides from bacteria: characteristics and potential applications to fight against antibiotic resistance.* J Appl Microbiol, 2012. **113**(4): p. 723-36.
518. Baumgartner, D., et al., *Small proteins in cyanobacteria provide a paradigm for the functional analysis of the bacterial micro-proteome.* BMC Microbiology, 2016. **16**(1): p. 285.
519. Smets, D., et al., *Protein Transport Across the Bacterial Plasma Membrane by the Sec Pathway.* Protein J, 2019. **38**(3): p. 262-273.
520. Kusters, I. and A.J.M. Driessen, *SecA, a remarkable nanomachine.* Cellular and molecular life sciences : CMLS, 2011. **68**(12): p. 2053-2066.
521. Matsumoto, G., T. Yoshihisa, and K. Ito, *SecY and SecA interact to allow SecA insertion and protein translocation across the Escherichia coli plasma membrane.* The EMBO Journal, 1997. **16**(21): p. 6384-6393.
522. Beckwith, J., *The Sec-dependent pathway.* Res Microbiol, 2013. **164**(6): p. 497-504.

523. Knüpffer, L., et al., *Molecular Mimicry of SecA and Signal Recognition Particle Binding to the Bacterial Ribosome.* mBio, 2019. **10**(4): p. e01317-19.

524. Origi, A., et al., *Yet another job for the bacterial ribosome.* Microb Cell, 2019. **6**(11): p. 524-526.

525. Huber, D., et al., *SecA interacts with ribosomes in order to facilitate posttranslational translocation in bacteria.* Mol Cell, 2011. **41**(3): p. 343-53.

526. Saraogi, I. and S.O. Shan, *Co-translational protein targeting to the bacterial membrane.* Biochim Biophys Acta, 2014. **1843**(8): p. 1433-41.

527. Cranford-Smith, T. and D. Huber, *The way is the goal: how SecA transports proteins across the cytoplasmic membrane in bacteria.* FEMS Microbiol Lett, 2018. **365**(11).

528. Steinberg, R., et al., *Co-translational protein targeting in bacteria.* FEMS Microbiology Letters, 2018. **365**(11).

529. Denks, K., et al., *The signal recognition particle contacts uL23 and scans substrate translation inside the ribosomal tunnel.* Nat Microbiol, 2017. **2**: p. 16265.

530. Josefsson, L.G. and L.L. Randall, *Different exported proteins in E. coli show differences in the temporal mode of processing in vivo.* Cell, 1981. **25**(1): p. 151-7.

531. Josefsson, L.G. and L.L. Randall, *Processing in vivo of precursor maltose-binding protein in Escherichia coli occurs post-translationally as well as co-translationally.* J Biol Chem, 1981. **256**(5): p. 2504-7.

532. Randall, L.L., *Translocation of domains of nascent periplasmic proteins across the cytoplasmic membrane is independent of elongation.* Cell, 1983. **33**(1): p. 231-40.

533. Lee, H.C. and H.D. Bernstein, *The targeting pathway of Escherichia coli presecretory and integral membrane proteins is specified by the hydrophobicity of the targeting signal.* Proc Natl Acad Sci U S A, 2001. **98**(6): p. 3471-6.

534. Schierle, C.F., et al., *The DsbA signal sequence directs efficient, cotranslational export of passenger proteins to the Escherichia coli periplasm via the signal recognition particle pathway.* J Bacteriol, 2003. **185**(19): p. 5706-13.

535. Oliver, D.B. and J. Beckwith, *Identification of a new gene (secA) and gene product involved in the secretion of envelope proteins in Escherichia coli.* J Bacteriol, 1982. **150**(2): p. 686-91.

536. Oliver, D.B. and J. Beckwith, *Regulation of a membrane component required for protein secretion in Escherichia coli.* Cell, 1982. **30**(1): p. 311-9.

537. Oliver, D.B. and J. Beckwith, *E. coli mutant pleiotropically defective in the export of secreted proteins.* Cell, 1981. **25**(3): p. 765-72.

538. Huber, D., et al., *Use of thioredoxin as a reporter to identify a subset of Escherichia coli signal sequences that promote signal recognition particle-dependent translocation.* J Bacteriol, 2005. **187**(9): p. 2983-91.

539. van der Sluis, E.O. and A.J. Driessen, *Stepwise evolution of the Sec machinery in Proteobacteria.* Trends Microbiol, 2006. **14**(3): p. 105-8.

540. Antunes, L.C.M., et al., *Quorum sensing in bacterial virulence.* Microbiology (Reading), 2010. **156**(Pt 8): p. 2271-2282.

541. Castillo-Juárez, I., et al., *Role of quorum sensing in bacterial infections.* World J Clin Cases, 2015. **3**(7): p. 575-98.

542. Rutherford, S.T. and B.L. Bassler, *Bacterial quorum sensing: its role in virulence and possibilities for its control.* Cold Spring Harb Perspect Med, 2012. **2**(11).

543. Cook, L.C. and M.J. Federle, *Peptide pheromone signaling in Streptococcus and Enterococcus.* FEMS Microbiol Rev, 2014. **38**(3): p. 473-92.

544. Mookherjee, N., et al., *Antimicrobial host defence peptides: functions and clinical potential.* Nat Rev Drug Discov, 2020. **19**(5): p. 311-332.

545. Florin, T., et al., *An antimicrobial peptide that inhibits translation by trapping release factors on the ribosome.* Nat Struct Mol Biol, 2017. **24**(9): p. 752-757.

546. Bahar, A.A. and D. Ren, *Antimicrobial peptides.* Pharmaceuticals (Basel), 2013. **6**(12): p. 1543-75.
547. Kumariya, R., et al., *Bacteriocins: Classification, synthesis, mechanism of action and resistance development in food spoilage causing bacteria.* Microb Pathog, 2019. **128**: p. 171-177.
548. Cotter, P.D., R.P. Ross, and C. Hill, *Bacteriocins — a viable alternative to antibiotics?* Nature Reviews Microbiology, 2013. **11**(2): p. 95-105.
549. Yount, N.Y. and M.R. Yeaman, *Peptide antimicrobials: cell wall as a bacterial target.* Ann N Y Acad Sci, 2013. **1277**: p. 127-38.
550. Guha, S., et al., *Mechanistic Landscape of Membrane-Permeabilizing Peptides.* Chem Rev, 2019. **119**(9): p. 6040-6085.
551. Breukink, E., et al., *Use of the cell wall precursor lipid II by a pore-forming peptide antibiotic.* Science, 1999. **286**(5448): p. 2361-4.
552. Brötz, H., et al., *The lantibiotic mersacidin inhibits peptidoglycan synthesis by targeting lipid II.* Antimicrob Agents Chemother, 1998. **42**(1): p. 154-60.
553. Piers, K.L., M.H. Brown, and R.E. Hancock, *Improvement of outer membrane-permeabilizing and lipopolysaccharide-binding activities of an antimicrobial cationic peptide by C-terminal modification.* Antimicrobial agents and chemotherapy, 1994. **38**(10): p. 2311-2316.
554. Piers, K.L. and R.E. Hancock, *The interaction of a recombinant cecropin/melittin hybrid peptide with the outer membrane of Pseudomonas aeruginosa.* Mol Microbiol, 1994. **12**(6): p. 951-8.
555. Quereda, J.J., et al., *Listeriolysin S: A bacteriocin from epidemic Listeria monocytogenes strains that targets the gut microbiota.* Gut Microbes, 2017. **8**(4): p. 384-391.
556. Cogen, A.L., et al., *Staphylococcus epidermidis Antimicrobial δ-Toxin (Phenol-Soluble Modulin-γ) Cooperates with Host Antimicrobial Peptides to Kill Group A Streptococcus.* PLOS ONE, 2010. **5**(1): p. e8557.
557. Sassone-Corsi, M., et al., *Microcins mediate competition among Enterobacteriaceae in the inflamed gut.* Nature, 2016. **540**(7632): p. 280-283.

558. Quereda, J.J., et al., *Bacteriocin from epidemic Listeria strains alters the host intestinal microbiota to favor infection.* Proceedings of the National Academy of Sciences, 2016. **113**(20): p. 5706-5711.
559. Quereda, J.J., et al., *Listeriolysin S Is a Streptolysin S-Like Virulence Factor That Targets Exclusively Prokaryotic Cells In Vivo.* mBio, 2017. **8**(2): p. e00259-17.
560. Wladyka, B., et al., *A peptide factor secreted by Staphylococcus pseudintermedius exhibits properties of both bacteriocins and virulence factors.* Scientific Reports, 2015. **5**(1): p. 14569.
561. Ghequire, M.G. and R. De Mot, *Ribosomally encoded antibacterial proteins and peptides from Pseudomonas.* FEMS Microbiol Rev, 2014. **38**(4): p. 523-68.
562. Cascales, E., et al., *Colicin biology.* Microbiol Mol Biol Rev, 2007. **71**(1): p. 158-229.
563. Telhig, S., et al., *Bacteriocins to Thwart Bacterial Resistance in Gram Negative Bacteria.* Frontiers in Microbiology, 2020. **11**(2807).
564. Li, Y. and S. Rebuffat, *The manifold roles of microbial ribosomal peptide-based natural products in physiology and ecology.* The Journal of biological chemistry, 2020. **295**(1): p. 34-54.
565. Zhao, Z., et al., *Genome-Wide Screening Identifies Six Genes That Are Associated with Susceptibility to Escherichia coli Microcin PDI.* Appl Environ Microbiol, 2015. **81**(20): p. 6953-63.
566. Metlitskaya, A., et al., *Aspartyl-tRNA synthetase is the target of peptide nucleotide antibiotic Microcin C.* J Biol Chem, 2006. **281**(26): p. 18033-42.
567. Kidane, D., et al., *Visualization of DNA double-strand break repair in live bacteria reveals dynamic recruitment of Bacillus subtilis RecF, RecO and RecN proteins to distinct sites on the nucleoids.* Molecular Microbiology, 2004. **52**(6): p. 1627-1639.
568. Cox, M.M., et al., *The importance of repairing stalled replication forks.* Nature, 2000. **404**(6773): p. 37-41.

569. Fichtinger-Schepman, A.M., et al., *Adducts of the antitumor drug cis-diamminedichloroplatinum(II) with DNA: formation, identification, and quantitation.* Biochemistry, 1985. **24**(3): p. 707-13.

570. Pinto, A.L. and S.J. Lippard, *Binding of the antitumor drug cis-diamminedichloroplatinum(II) (cisplatin) to DNA.* Biochim Biophys Acta, 1985. **780**(3): p. 167-80.

571. Miller, S., et al., *The accessible surface area and stability of oligomeric proteins.* Nature, 1987. **328**(6133): p. 834-6.

572. Permana, D., H.E. Putra, and D. Djaenudin, *Designed protein multimerization and polymerization for functionalization of proteins.* Biotechnology Letters, 2022. **44**(3): p. 341-365.

573. Hashimoto, K., et al., *Caught in self-interaction: evolutionary and functional mechanisms of protein homooligomerization.* Phys Biol, 2011. **8**(3): p. 035007.

574. Lukatsky, D.B., et al., *Structural similarity enhances interaction propensity of proteins.* J Mol Biol, 2007. **365**(5): p. 1596-606.

575. Andre, I., et al., *Emergence of symmetry in homooligomeric biological assemblies.* Proc Natl Acad Sci U S A, 2008. **105**(42): p. 16148-52.

576. Wright, C.F., et al., *The importance of sequence diversity in the aggregation and evolution of proteins.* Nature, 2005. **438**(7069): p. 878-81.

577. Cornish-Bowden, A.J. and D.E. Koshland, Jr., *The quaternary structure of proteins composed of identical subunits.* J Biol Chem, 1971. **246**(10): p. 3092-102.

578. Blundell, T.L. and N. Srinivasan, *Symmetry, stability, and dynamics of multidomain and multicomponent protein systems.* Proc Natl Acad Sci U S A, 1996. **93**(25): p. 14243-8.

579. Dayhoff, J.E., et al., *Evolution of protein binding modes in homooligomers.* J Mol Biol, 2010. **395**(4): p. 860-70.

580. Chen, C.P., et al., *Specificity of cell-cell adhesion by classical cadherins: Critical role for low-affinity dimerization through beta-strand swapping.* Proc Natl Acad Sci U S A, 2005. **102**(24): p. 8531-6.

581. Hashimoto, K. and A.R. Panchenko, *Mechanisms of protein oligomerization, the critical role of insertions and deletions in maintaining different oligomeric states.* Proceedings of the National Academy of Sciences, 2010. **107**(47): p. 20352-20357.
582. Grueninger, D., et al., *Designed protein-protein association.* Science, 2008. **319**(5860): p. 206-9.
583. Nishi, H. and M. Ota, *Amino acid substitutions at protein-protein interfaces that modulate the oligomeric state.* Proteins, 2010. **78**(6): p. 1563-74.
584. Bertolini, M., et al., *Interactions between nascent proteins translated by adjacent ribosomes drive homomer assembly.* Science, 2021. **371**(6524): p. 57-64.
585. Price, M.N., et al., *Mutant phenotypes for thousands of bacterial genes of unknown function.* Nature, 2018. **557**(7706): p. 503-509.
586. Thanbichler, M., A.A. Iniesta, and L. Shapiro, *A comprehensive set of plasmids for vanillate- and xylose-inducible gene expression in Caulobacter crescentus.* Nucleic Acids Research, 2007. **35**(20).
587. Karimova, G., et al., *Protein-Protein Interaction: Bacterial Two-Hybrid.* Methods Mol Biol, 2017. **1615**: p. 159-176.
588. Varadi, M., et al., *AlphaFold Protein Structure Database: massively expanding the structural coverage of protein-sequence space with high-accuracy models.* Nucleic Acids Research, 2021. **50**(D1): p. D439-D444.
589. Jumper, J., et al., *Highly accurate protein structure prediction with AlphaFold.* Nature, 2021. **596**(7873): p. 583-589.
590. Krogh, A., et al., *Predicting transmembrane protein topology with a hidden Markov model: application to complete genomes.* J Mol Biol, 2001. **305**(3): p. 567-80.
591. Sonnhammer, E.L., G. von Heijne, and A. Krogh, *A hidden Markov model for predicting transmembrane helices in protein sequences.* Proc Int Conf Intell Syst Mol Biol, 1998. **6**: p. 175-82.
592. Karimova, G. and D. Ladant, *Defining Membrane Protein Topology Using pho-lac Reporter Fusions.* Methods Mol Biol, 2017. **1615**: p. 129-142.

593. Schumacher, M.A., et al., *The crystal structure of the RsbN-sigmaBldN complex from Streptomyces venezuelae defines a new structural class of anti-sigma factor.* Nucleic Acids Res, 2018. **46**(14): p. 7405-7417.
594. Phillips, D.H. and V.M. Arlt, *Genotoxicity: damage to DNA and its consequences.* Exs, 2009. **99**: p. 87-110.
595. Zhou, Z., et al., *Codon usage is an important determinant of gene expression levels largely through its effects on transcription.* Proceedings of the National Academy of Sciences, 2016. **113**(41): p. E6117-E6125.
596. Shieh, Y.W., et al., *Operon structure and cotranslational subunit association direct protein assembly in bacteria.* Science, 2015. **350**(6261): p. 678-80.
597. Carabetta, V.J. and J. Hardouin, *Editorial: Bacterial Post-translational Modifications.* Frontiers in Microbiology, 2022. **13**.
598. Macek, B., et al., *Protein post-translational modifications in bacteria.* Nature Reviews Microbiology, 2019. **17**(11): p. 651-664.
599. Cassidy, L., et al., *Multidimensional separation schemes enhance the identification and molecular characterization of low molecular weight proteomes and short open reading frame-encoded peptides in top-down proteomics.* J Proteomics, 2021. **230**: p. 103988.
600. von Heijne, G., *Signals for protein targeting into and across membranes.* Subcell Biochem, 1994. **22**: p. 1-19.
601. Briat, J.-F., *Iron assimilation storage in prokaryotes.* Microbiology, 1992. **138**(12): p. 2475-2483.
602. Ferguson, A.D. and J. Deisenhofer, *TonB-dependent receptors—structural perspectives.* Biochimica et Biophysica Acta (BBA) - Biomembranes, 2002. **1565**(2): p. 318-332.
603. Neilands, J.B., *Siderophores: structure and function of microbial iron transport compounds.* J Biol Chem, 1995. **270**(45): p. 26723-6.
604. Bradbeer, C., *The proton motive force drives the outer membrane transport of cobalamin in Escherichia coli.* J Bacteriol, 1993. **175**(10): p. 3146-50.
605. Llamas, M.A., et al., *Cell-surface signaling in Pseudomonas: stress responses, iron transport, and pathogenicity.* FEMS Microbiology Reviews, 2014. **38**(4): p. 569-597.

606. Braun, V. and F. Endriss, *Energy-coupled outer membrane transport proteins and regulatory proteins.* Biometals, 2007. **20**(3-4): p. 219-31.
607. Krewulak, K.D. and H.J. Vogel, *Structural biology of bacterial iron uptake.* Biochim Biophys Acta, 2008. **1778**(9): p. 1781-804.
608. Noinaj, N., et al., *TonB-dependent transporters: regulation, structure, and function.* Annu Rev Microbiol, 2010. **64**: p. 43-60.
609. Li, X.Z., P. Plésiat, and H. Nikaido, *The challenge of efflux-mediated antibiotic resistance in Gram-negative bacteria.* Clin Microbiol Rev, 2015. **28**(2): p. 337-418.
610. Uddin, T.M., et al., *Antibiotic resistance in microbes: History, mechanisms, therapeutic strategies and future prospects.* J Infect Public Health, 2021. **14**(12): p. 1750-1766.
611. Pang, Z., et al., *Antibiotic resistance in Pseudomonas aeruginosa: mechanisms and alternative therapeutic strategies.* Biotechnol Adv, 2019. **37**(1): p. 177-192.
612. Abushaheen, M.A., et al., *Antimicrobial resistance, mechanisms and its clinical significance.* Dis Mon, 2020. **66**(6): p. 100971.
613. Nikaido, H., *Multidrug efflux pumps of gram-negative bacteria.* J Bacteriol, 1996. **178**(20): p. 5853-9.
614. Zgurskaya, H.I. and H. Nikaido, *Multidrug resistance mechanisms: drug efflux across two membranes.* Mol Microbiol, 2000. **37**(2): p. 219-25.
615. Alcalde-Rico, M., et al., *Multidrug Efflux Pumps at the Crossroad between Antibiotic Resistance and Bacterial Virulence.* Front Microbiol, 2016. **7**: p. 1483.
616. Juliano, R.L. and V. Ling, *A surface glycoprotein modulating drug permeability in Chinese hamster ovary cell mutants.* Biochim Biophys Acta, 1976. **455**(1): p. 152-62.
617. Paulsen, I.T., et al., *Microbial genome analyses: comparative transport capabilities in eighteen prokaryotes.* J Mol Biol, 2000. **301**(1): p. 75-100.
618. Nishino, K. and A. Yamaguchi, *Analysis of a complete library of putative drug transporter genes in Escherichia coli.* J Bacteriol, 2001. **183**(20): p. 5803-12.

619. Nishino, K., T. Latifi, and E.A. Groisman, *Virulence and drug resistance roles of multidrug efflux systems of Salmonella enterica serovar Typhimurium.* Mol Microbiol, 2006. **59**(1): p. 126-41.

620. Villagra, N.A., et al., *SmvA, and not AcrB, is the major efflux pump for acriflavine and related compounds in Salmonella enterica serovar Typhimurium.* J Antimicrob Chemother, 2008. **62**(6): p. 1273-6.

621. Yamasaki, S., et al., *Phenotype microarray analysis of the drug efflux systems in Salmonella enterica serovar Typhimurium.* J Infect Chemother, 2016. **22**(11): p. 780-784.

622. Du, D., et al., *Multidrug efflux pumps: structure, function and regulation.* Nature Reviews Microbiology, 2018. **16**(9): p. 523-539.

623. Nichols, R.J., et al., *Phenotypic landscape of a bacterial cell.* Cell, 2011. **144**(1): p. 143-56.

624. Lee, A., et al., *Interplay between efflux pumps may provide either additive or multiplicative effects on drug resistance.* J Bacteriol, 2000. **182**(11): p. 3142-50.

625. Tal, N. and S. Schuldiner, *A coordinated network of transporters with overlapping specificities provides a robust survival strategy.* Proc Natl Acad Sci U S A, 2009. **106**(22): p. 9051-6.

626. Whittle, E.E., et al., *Efflux Impacts Intracellular Accumulation Only in Actively Growing Bacterial Cells.* mBio, 2021. **0**(0): p. e02608-21.

627. Pu, Y., et al., *Enhanced Efflux Activity Facilitates Drug Tolerance in Dormant Bacterial Cells.* Mol Cell, 2016. **62**(2): p. 284-294.

628. Alav, I., J.M. Sutton, and K.M. Rahman, *Role of bacterial efflux pumps in biofilm formation.* J Antimicrob Chemother, 2018. **73**(8): p. 2003-2020.

629. Putman, M., H.W. van Veen, and W.N. Konings, *Molecular properties of bacterial multidrug transporters.* Microbiol Mol Biol Rev, 2000. **64**(4): p. 672-93.

630. Nishino, K., E. Nikaido, and A. Yamaguchi, *Regulation and physiological function of multidrug efflux pumps in Escherichia coli and Salmonella.* Biochim Biophys Acta, 2009. **1794**(5): p. 834-43.

631. Hassan, K.A., et al., *Homologs of the Acinetobacter baumannii AceI transporter represent a new family of bacterial multidrug efflux systems.* mBio, 2015. **6**(1).

632. Kornelsen, V. and A. Kumar, *Update on Multidrug Resistance Efflux Pumps in Acinetobacter spp.* Antimicrob Agents Chemother, 2021. **65**(7): p. e0051421.

633. Hassan, K.A., et al., *Transcriptomic and biochemical analyses identify a family of chlorhexidine efflux proteins.* Proc Natl Acad Sci U S A, 2013. **110**(50): p. 20254-9.

634. Zwama, M. and A. Yamaguchi, *Molecular mechanisms of AcrB-mediated multidrug export.* Res Microbiol, 2018. **169**(7-8): p. 372-383.

635. Weston, N., et al., *Regulation of the AcrAB-TolC efflux pump in Enterobacteriaceae.* Res Microbiol, 2018. **169**(7-8): p. 425-431.

636. Müller, R.T. and K.M. Pos, *The assembly and disassembly of the AcrAB-TolC three-component multidrug efflux pump.* Biol Chem, 2015. **396**(9-10): p. 1083-9.

637. Schuldiner, S., *The Escherichia coli effluxome.* Res Microbiol, 2018. **169**(7-8): p. 357-362.

638. Kirkpatrick, C.L. and P.H. Viollier, *Synthetic Interaction between the TipN Polarity Factor and an AcrAB-Family Efflux Pump Implicates Cell Polarity in Bacterial Drug Resistance.* Chemistry & Biology, 2014. **21**(5): p. 657-665.

639. Marcos-Torres, F.J., et al., *Mechanisms of Action of Non-Canonical ECF Sigma Factors.* Int J Mol Sci, 2022. **23**(7).

640. Davis, M.C., et al., *The essential activities of the bacterial sigma factor.* Can J Microbiol, 2017. **63**(2): p. 89-99.

641. Murakami, K.S. and S.A. Darst, *Bacterial RNA polymerases: the wholo story.* Current Opinion in Structural Biology, 2003. **13**(1): p. 31-39.

642. Feklístov, A., et al., *Bacterial Sigma Factors: A Historical, Structural, and Genomic Perspective.* Annual Review of Microbiology, 2014. **68**(1): p. 357-376.

643. Juang, Y.L. and J.D. Helmann, *A promoter melting region in the primary sigma factor of Bacillus subtilis. Identification of functionally important aromatic amino acids.* J Mol Biol, 1994. **235**(5): p. 1470-88.

644. Panaghie, G., et al., *Aromatic amino acids in region 2.3 of Escherichia coli sigma 70 participate collectively in the formation of an RNA polymerase-promoter open complex11Edited by R. Ebright.* Journal of Molecular Biology, 2000. **299**(5): p. 1217-1230.

645. DeHaseth, P.L. and J.D. Helmann, *Open complex formation by Escherichia coli RNA polymerase: the mechanism of polymerase-induced strand separation of double helical DNA.* Molecular Microbiology, 1995. **16**(5): p. 817-824.

646. Paget, M.S., *Bacterial Sigma Factors and Anti-Sigma Factors: Structure, Function and Distribution.* Biomolecules, 2015. **5**(3): p. 1245-65.

647. Zhang, N. and M. Buck, *A Perspective on the Enhancer Dependent Bacterial RNA Polymerase.* Biomolecules, 2015. **5**(2): p. 1012-1019.

648. Paget, M.S.B. and J.D. Helmann, *The σ70family of sigma factors.* Genome Biology, 2003. **4**(1): p. 203.

649. Zhang, N. and M. Buck, *A perspective on the enhancer dependent bacterial RNA polymerase.* Biomolecules, 2015. **5**(2): p. 1012-9.

650. Missiakas, D. and S. Raina, *The extracytoplasmic function sigma factors: role and regulation.* Molecular Microbiology, 1998. **28**(6): p. 1059-1066.

651. Lonetto, M., M. Gribskov, and C.A. Gross, *The sigma 70 family: sequence conservation and evolutionary relationships.* Journal of Bacteriology, 1992. **174**(12): p. 3843-3849.

652. Gruber, T.M. and C.A. Gross, *Multiple Sigma Subunits and the Partitioning of Bacterial Transcription Space.* Annual Review of Microbiology, 2003. **57**(1): p. 441-466.

653. Zhou, B., et al., *The Global Regulatory Architecture of Transcription during the Caulobacter Cell Cycle.* PLOS Genetics, 2015. **11**(1): p. e1004831.

654. Malakooti, J. and B. Ely, *Principal sigma subunit of the Caulobacter crescentus RNA polymerase.* J Bacteriol, 1995. **177**(23): p. 6854-60.

655. Campbell, E.A., L.F. Westblade, and S.A. Darst, *Regulation of bacterial RNA polymerase sigma factor activity: a structural perspective.* Curr Opin Microbiol, 2008. **11**(2): p. 121-7.

656. Campbell, E.A., et al., *A conserved structural module regulates transcriptional responses to diverse stress signals in bacteria.* Mol Cell, 2007. **27**(5): p. 793-805.

657. Staron, A., et al., *The third pillar of bacterial signal transduction: classification of the extracytoplasmic function (ECF) sigma factor protein family.* Molecular Microbiology, 2009. **74**(3): p. 557-581.

658. Jogler, C., et al., *Identification of proteins likely to be involved in morphogenesis, cell division, and signal transduction in Planctomycetes by comparative genomics.* J Bacteriol, 2012. **194**(23): p. 6419-30.

659. Grage, S.L., et al., *Membrane Thinning and Thickening Induced by Membrane-Active Amphipathic Peptides.* Front Cell Dev Biol, 2016. **4**: p. 65.

660. Shigapova, N., et al., *Membrane fluidization triggers membrane remodeling which affects the thermotolerance in Escherichia coli.* Biochem Biophys Res Commun, 2005. **328**(4): p. 1216-23.

661. Horváth, I., et al., *Membrane physical state controls the signaling mechanism of the heat shock response in Synechocystis PCC 6803: identification of hsp17 as a "fluidity gene".* Proc Natl Acad Sci U S A, 1998. **95**(7): p. 3513-8.

662. Riffaud, C., M.L. Pinel-Marie, and B. Felden, *Cross-Regulations between Bacterial Toxin-Antitoxin Systems: Evidence of an Interconnected Regulatory Network?* Trends Microbiol, 2020. **28**(10): p. 851-866.

663. Alix, E. and A.B. Blanc-Potard, *Hydrophobic peptides: novel regulators within bacterial membrane.* Mol Microbiol, 2009. **72**(1): p. 5-11.

664. Edelmann, D. and B.A. Berghoff, *Type I toxin-dependent generation of superoxide affects the persister life cycle of Escherichia coli.* Sci Rep, 2019. **9**(1): p. 14256.

665. Edelmann, D., et al., *Post-transcriptional deregulation of the tisB/istR-1 toxin-antitoxin system promotes SOS-independent persister formation in Escherichia coli.* Environ Microbiol Rep, 2021. **13**(2): p. 159-168.

666. Berghoff, B.A., et al., *Two regulatory RNA elements affect TisB-dependent depolarization and persister formation.* Mol Microbiol, 2017. **103**(6): p. 1020-1033.

667. Boto, L., *Horizontal gene transfer in evolution: facts and challenges.* Proc Biol Sci, 2010. **277**(1683): p. 819-27.

668. Nasvall, J., et al., *Real-time evolution of new genes by innovation, amplification, and divergence.* Science, 2012. **338**(6105): p. 384-7.

669. Ruiz-Orera, J., et al., *Translation of neutrally evolving peptides provides a basis for de novo gene evolution.* Nat Ecol Evol, 2018. **2**(5): p. 890-896.

670. Wilson, B.A. and J. Masel, *Putatively Noncoding Transcripts Show Extensive Association with Ribosomes.* Genome Biology and Evolution, 2011. **3**: p. 1245-1252.

671. Dornenburg, J.E., et al., *Widespread Antisense Transcription in Escherichia coli.* mBio, 2010. **1**(1): p. e00024-10.

672. Wade, J.T. and D.C. Grainger, *Pervasive transcription: illuminating the dark matter of bacterial transcriptomes.* Nature Reviews Microbiology, 2014. **12**(9): p. 647-653.

673. Olexiouk, V., W. Van Criekinge, and G. Menschaert, *An update on sORFs.org: a repository of small ORFs identified by ribosome profiling.* Nucleic Acids Research, 2017. **46**(D1): p. D497-D502.

674. Knopp, M., et al., *De Novo Emergence of Peptides That Confer Antibiotic Resistance.* mBio, 2019. **10**(3): p. e00837-19.

675. Cassidy, L., et al., *Bottom-up and top-down proteomic approaches for the identification, characterization, and quantification of the low molecular weight proteome with focus on short open reading frame-encoded peptides.* PROTEOMICS, 2021. **21**(23-24): p. 2100008.

676. Tirumalai, R.S., et al., *Characterization of the low molecular weight human serum proteome.* Mol Cell Proteomics, 2003. **2**(10): p. 1096-103.

677. Carr, S., et al., *The need for guidelines in publication of peptide and protein identification data: Working Group on Publication Guidelines for Peptide and Protein Identification Data.* Mol Cell Proteomics, 2004. **3**(6): p. 531-3.

678. Kaulich, P.T., et al., *Multi-protease Approach for the Improved Identification and Molecular Characterization of Small Proteins and Short Open Reading Frame-Encoded Peptides.* J Proteome Res, 2021. **20**(5): p. 2895-2903.

679. Kaulich, P.T., et al., *Complementarity of Different SDS-PAGE Gel Staining Methods for the Identification of Short Open Reading Frame-Encoded Peptides.* PROTEOMICS, 2020. **20**(19-20): p. 2000084.

680. Cardon, T., et al., *Optimized Sample Preparation Workflow for Improved Identification of Ghost Proteins.* Anal Chem, 2020. **92**(1): p. 1122-1129.

681. Cassidy, L., P.T. Kaulich, and A. Tholey, *Depletion of High-Molecular-Mass Proteins for the Identification of Small Proteins and Short Open Reading Frame Encoded Peptides in Cellular Proteomes.* J Proteome Res, 2019. **18**(4): p. 1725-1734.

682. Greening, D.W. and R.J. Simpson, *A centrifugal ultrafiltration strategy for isolating the low-molecular weight (<or=25K) component of human plasma proteome.* J Proteomics, 2010. **73**(3): p. 637-48.

683. Cassidy, L., et al., *Combination of Bottom-up 2D-LC-MS and Semi-top-down GelFree-LC-MS Enhances Coverage of Proteome and Low Molecular Weight Short Open Reading Frame Encoded Peptides of the Archaeon Methanosarcina mazei.* Journal of Proteome Research, 2016. **15**(10): p. 3773-3783.

684. Harney, D.J., et al., *Small-protein Enrichment Assay Enables the Rapid, Unbiased Analysis of Over 100 Low Abundance Factors from Human Plasma.* Mol Cell Proteomics, 2019. **18**(9): p. 1899-1915.

685. Petruschke, H., et al., *Enrichment and identification of small proteins in a simplified human gut microbiome.* Journal of Proteomics, 2020. **213**: p. 103604.

686. Ma, J., et al., *Improved Identification and Analysis of Small Open Reading Frame Encoded Polypeptides.* Anal Chem, 2016. **88**(7): p. 3967-75.

687. D'Lima, N.G., et al., *Comparative Proteomics Enables Identification of Nonannotated Cold Shock Proteins in E. coli.* Journal of Proteome Research, 2017. **16**(10): p. 3722-3731.

688. Khitun, A. and S.A. Slavoff, *Proteomic Detection and Validation of Translated Small Open Reading Frames.* Curr Protoc Chem Biol, 2019. **11**(4): p. e77.

689. Cassidy, L., et al., *Combination of Bottom-up 2D-LC-MS and Semi-top-down GelFree-LC-MS Enhances Coverage of Proteome and Low Molecular Weight Short Open Reading Frame Encoded Peptides of the Archaeon Methanosarcina mazei.* J Proteome Res, 2016. **15**(10): p. 3773-3783.

690. Li, W., et al., *Separation and identification of mouse brain tissue microproteins using top-down method with high resolution nanocapillary liquid chromatography mass spectrometry.* Proteomics, 2017. **17**(12).

691. Sassanfar, M. and J.W. Roberts, *Nature of the SOS-inducing signal in Escherichia coli: The involvement of DNA replication.* Journal of Molecular Biology, 1990. **212**(1): p. 79-96.

692. Sanchez-Carbonel, A., et al., *The effect of the efflux pump inhibitor Carbonyl Cyanide m-Chlorophenylhydrazone (CCCP) on the susceptibility to imipenem and cefepime in clinical strains of Acinetobacter baumannii.* PLoS One, 2021. **16**(12): p. e0259915.

693. Altschul, S.F., et al., *Gapped BLAST and PSI-BLAST: a new generation of protein database search programs.* Nucleic Acids Res, 1997. **25**(17): p. 3389-402.

694. Schäffer, A.A., et al., *Improving the accuracy of PSI-BLAST protein database searches with composition-based statistics and other refinements.* Nucleic Acids Res, 2001. **29**(14): p. 2994-3005.

695. Mehla, J., et al., *A Comparison of Two-Hybrid Approaches for Detecting Protein-Protein Interactions.* Methods Enzymol, 2017. **586**: p. 333-358.

696. Choudhury, H.G., et al., *Structure of an antibacterial peptide ATP-binding cassette transporter in a novel outward occluded state.* Proc Natl Acad Sci U S A, 2014. **111**(25): p. 9145-50.

697. Dawson, R.J.P. and K.P. Locher, *Structure of a bacterial multidrug ABC transporter.* Nature, 2006. **443**(7108): p. 180-185.

698. Bountra, K., et al., *Structural basis for antibacterial peptide self-immunity by the bacterial ABC transporter McjD.* Embo j, 2017. **36**(20): p. 3062-3079.

699. Lu, M., et al., *Structural insights into H+-coupled multidrug extrusion by a MATE transporter.* Nature Structural & Molecular Biology, 2013. **20**(11): p. 1310-1317.

700. Tanaka, Y., et al., *Structural basis for the drug extrusion mechanism by a MATE multidrug transporter.* Nature, 2013. **496**(7444): p. 247-51.

701. Radchenko, M., et al., *Structural basis for the blockade of MATE multidrug efflux pumps.* Nature Communications, 2015. **6**(1): p. 7995.

702. Sharma, P., et al., *The multiple antibiotic resistance operon of enteric bacteria controls DNA repair and outer membrane integrity.* Nature Communications, 2017. **8**(1): p. 1444.

703. Singh, M., et al., *Effect of efflux pump inhibitors on drug susceptibility of ofloxacin resistant Mycobacterium tuberculosis isolates.* Indian J Med Res, 2011. **133**(5): p. 535-40.

704. Baek, J., et al., *Identification of Unannotated Small Genes in Salmonella.* G3 Genes|Genomes|Genetics, 2017. **7**(3): p. 983-989.

705. Cdc, *Antibiotic / Antimicrobial Resistance.* Centers for Disease Control and Prevention, 2019.

706. Karam, G., et al., *Antibiotic strategies in the era of multidrug resistance.* Crit Care, 2016. **20**(1): p. 136.

707. Fisher, R.A., B. Gollan, and S. Helaine, *Persistent bacterial infections and persister cells.* Nat Rev Microbiol, 2017. **15**(8): p. 453-464.

708. Bhardwaj, S., et al., *Antibiotics and Antibiotic Resistance- Flipsides of the Same Coin.* Curr Pharm Des, 2022. **28**(28): p. 2312-2329.

709. Hughes, D. and D.I. Andersson, *Environmental and genetic modulation of the phenotypic expression of antibiotic resistance.* FEMS Microbiology Reviews, 2017. **41**(3): p. 374-391.

710. Kabra, R., et al., *Efflux pumps and antimicrobial resistance: Paradoxical components in systems genomics.* Prog Biophys Mol Biol, 2019. **141**: p. 15-24.
711. Otsuji, N., *Properties of mitomycin C-sensitive mutants of Escherichia coli K-12.* J Bacteriol, 1968. **95**(2): p. 540-5.
712. Fudrini Olivencia, B., et al., *Mycobacterium smegmatis PafBC is involved in regulation of DNA damage response.* Sci Rep, 2017. **7**(1): p. 13987.
713. Muller, A.U., et al., *Structure and functional implications of WYL domain-containing bacterial DNA damage response regulator PafBC.* Nat Commun, 2019. **10**(1): p. 4653.
714. Shah, P.M., *The need for new therapeutic agents: what is the pipeline?* Clin Microbiol Infect, 2005. **11 Suppl 3**: p. 36-42.
715. Dinos, G.P., *The macrolide antibiotic renaissance.* Br J Pharmacol, 2017. **174**(18): p. 2967-2983.
716. Pasberg-Gauhl, C., *A need for new generation antibiotics against MRSA resistant bacteria.* Drug Discov Today Technol, 2014. **11**: p. 109-16.
717. Dubin, A., et al., *New generation of peptide antibiotics.* Acta Biochim Pol, 2005. **52**(3): p. 633-8.
718. Hutchings, M.I., A.W. Truman, and B. Wilkinson, *Antibiotics: past, present and future.* Curr Opin Microbiol, 2019. **51**: p. 72-80.
719. Gutierrez, B. and P. Domingo-Calap, *Phage Therapy in Gastrointestinal Diseases.* Microorganisms, 2020. **8**(9).
720. Cunha, B.A., *Antibiotic side effects.* Med Clin North Am, 2001. **85**(1): p. 149-85.
721. Kashino, Y., et al., *Proteomic analysis of a highly active photosystem II preparation from the cyanobacterium Synechocystis sp. PCC 6803 reveals the presence of novel polypeptides.* Biochemistry, 2002. **41**(25): p. 8004-12.
722. Guskov, A., et al., *Cyanobacterial photosystem II at 2.9-Å resolution and the role of quinones, lipids, channels and chloride.* Nature Structural & Molecular Biology, 2009. **16**(3): p. 334-342.

723. Andrews, S.J. and J.A. Rothnagel, *Emerging evidence for functional peptides encoded by short open reading frames.* Nature Reviews Genetics, 2014. **15**(3): p. 193-204.

724. Yadavalli, S.S. and J. Yuan, *Bacterial small membrane proteins: the Swiss army knife of regulators at the lipid bilayer.* Journal of Bacteriology. **0**(ja): p. JB.00344-21.

725. Liebthal, M., et al., *Single molecule mass photometry reveals the dynamic oligomerization of human and plant peroxiredoxins.* iScience, 2021. **24**(11): p. 103258.

726. Lasker, K., et al., *CauloBrowser: A systems biology resource for Caulobacter crescentus.* Nucleic Acids Res, 2016. **44**(D1): p. D640-5.

727. Hottes, A.K., et al., *Transcriptional profiling of Caulobacter crescentus during growth on complex and minimal media.* J Bacteriol, 2004. **186**(5): p. 1448-61.

728. Marks, M.E., et al., *The genetic basis of laboratory adaptation in Caulobacter crescentus.* J Bacteriol, 2010. **192**(14): p. 3678-88.

729. Bertani, G., *Studies on lysogenesis. I. The mode of phage liberation by lysogenic Escherichia coli.* J Bacteriol, 1951. **62**(3): p. 293-300.

730. Sambrook, J., *Molecular cloning : a laboratory manual / Joseph Sambrook, David W. Russell*, ed. D.W. Russell and L. Cold Spring Harbor. 2001, Cold Spring Harbor, N.Y: Cold Spring Harbor Laboratory.

731. *Common buffers, media, and stock solutions.* Curr Protoc Hum Genet, 2001. **Appendix 2**: p. Appendix 2D.

732. Asuquo, A.E. and L.J. Piddock, *Accumulation and killing kinetics of fifteen quinolones for Escherichia coli, Staphylococcus aureus and Pseudomonas aeruginosa.* J Antimicrob Chemother, 1993. **31**(6): p. 865-80.

733. Kanchan, K., et al., *Transmembrane signaling in chimeras of the Escherichia coli aspartate and serine chemotaxis receptors and bacterial class III adenylyl cyclases.* J Biol Chem, 2010. **285**(3): p. 2090-9.

734. Dewitt, S.K. and E.A. Adelberg, *The Occurrence of a Genetic Transposition in a Strain of Escherichia Coli.* Genetics, 1962. **47**(5): p. 577-85.

735. Blomfield, I.C., et al., *Allelic exchange in Escherichia coli using the Bacillus subtilis sacB gene and a temperature-sensitive pSC101 replicon.* Mol Microbiol, 1991. **5**(6): p. 1447-57.

736. Reyrat, J.M., et al., *Counterselectable markers: untapped tools for bacterial genetics and pathogenesis.* Infect Immun, 1998. **66**(9): p. 4011-7.

737. Li, X.T., et al., *Positive and negative selection using the tetA-sacB cassette: recombineering and P1 transduction in Escherichia coli.* Nucleic Acids Res, 2013. **41**(22): p. e204.

738. Aranda, P.S., D.M. LaJoie, and C.L. Jorcyk, *Bleach gel: a simple agarose gel for analyzing RNA quality.* Electrophoresis, 2012. **33**(2): p. 366-9.

739. Gibson, D.G., *Enzymatic assembly of overlapping DNA fragments.* Methods Enzymol, 2011. **498**: p. 349-61.

740. Bradford, M.M., *A rapid and sensitive method for the quantitation of microgram quantities of protein utilizing the principle of protein-dye binding.* Anal Biochem, 1976. **72**: p. 248-54.

741. Shevchenko, A., et al., *In-gel digestion for mass spectrometric characterization of proteins and proteomes.* Nat Protoc, 2006. **1**(6): p. 2856-60.

742. Chambers, M.C., et al., *A cross-platform toolkit for mass spectrometry and proteomics.* Nat Biotechnol, 2012. **30**(10): p. 918-20.